NASA TECHNICAL TRANSLATION

NASA TT F-411

LOAN: AFWL (WLIL KIRTLAND

TECH LIBRARY KAFB, NM
0068848

NASA TT F-411

PROBLEMS IN REACTOR SHIELDING PHYSICS

COLLECTION OF ARTICLES

D. L. Broder, et al., Editors

Gosatomizdat,
Moscow, 1963

NATIONAL AERONAUTICS AND SPACE ADMINISTRATION • WASHINGTON, D. C. • JUNE 1967

TECH LIBRARY KAFB, NM
0068848
.1

PROBLEMS IN REACTOR SHIELDING PHYSICS

COLLECTION OF ARTICLES

Edited by D. L. Broder, A. P. Veselkin, Yu. A. Yegorov,
V. V. Orlov, and S. G. Tsypin

Translation of "Voprosy fiziki zashchity reaktorov. Sbornik statey."
Gosatomizdat, Moscow, 1963

NATIONAL AERONAUTICS AND SPACE ADMINISTRATION

For sale by the Clearinghouse for Federal Scientific and Technical Information
Springfield, Virginia 22151 – CFSTI price $3.00

NATIONAL AERONAUTICS AND SPACE ADMINISTRATION

TECHNICAL TRANSLATION EVALUATION

Budget Bureau No. 104-R037
Approval Expires: Sept. 30, 1969

NASA TTF NO. 411

TO: THE USERS OF THIS TRANSLATION

MAINTAINING THE QUALITY OF NASA TRANSLATIONS REQUIRES A CONTINUOUS EVALUATION PROGRAM. PLEASE COMPLETE AND MAIL THIS FORM TO AID IN THE EVALUATION OF THE USEFULNESS AND QUALITY OF THE TRANSLATING SERVICE.

THIS PUBLICATION *(Check one or more)*

- ☐ FURNISHED VALUABLE NEW DATA OR A NEW APPROACH TO RESEARCH.
- ☐ VERIFIED INFORMATION AVAILABLE FROM OTHER SOURCES.
- ☐ FURNISHED INTERESTING BACKGROUND INFORMATION.
- ☐ OTHER *(Explain)*: _____

FOLD LINE FOLD LINE

TRANSLATION TEXT *(Check one)*

- ☐ IS TECHNICALLY ACCURATE.
- ☐ IS SUFFICIENTLY ACCURATE FOR OUR PURPOSE.
- ☐ IS SATISFACTORY, BUT CONTAINS MINOR ERRORS.
- ☐ IS UNSATISFACTORY BECAUSE OF *(Check one or more)*:
  - ☐ POOR TERMINOLOGY.
  - ☐ NUMERICAL INACCURACIES.
  - ☐ INCOMPLETE TRANSLATION.
  - ☐ ILLEGIBLE SYMBOLS, TABULATIONS OR CURVES.
  - ☐ OTHER *(Explain)*: _____

FOLD LINE FOLD LINE

REMARKS

FROM

DATE

NOTE: REMOVE THIS SHEET FROM THE PUBLICATION, FOLD AS INDICATED, STAPLE OR TAPE, AND MAIL. NO POSTAGE NECESSARY.

NASA Form 1332 AUG 66

GPO 915-777

CUT ALONG THIS LINE

CUT ALONG THIS LINE

ANNOTATION

This collection of articles includes works which are concerned with the experimental and theoretical investigation of the biological shielding of nuclear reactors as well as works on the methodology and instruments for studying the shielding.

The works consider different analytical methods which make it possible to determine the three-dimensional energy and angular distribution of radiations in the shielding, the results of many experiments with radiations penetrating through homogeneous and multilayer shieldings through shieldings with heterogeneities and others.

Some of the works describe various devices to determine the fluxes and the spectral radiation distribution beyond the shielding and inside the shielding. These works also consider the method of analyzing the characteristics of devices and the process of measurement results.

This collection will be useful to a wide circle of readers concerned with the analysis and design of biological shielding of reactors and to specialists interested in the transmission of radiations through a substance, as well as to those working in the field of experimental nuclear physics.

PREFACE

The collection of articles presented to the attention of the reader covers the works of Soviet authors dedicated to the theoretical and experimental investigation and analysis of reactor shielding against penetrating radiation.

Practical requirements arising in connection with the intense application of atomic energy in various branches of engineering make it necessary for us to study an ever-increasing group of problems on the penetration of radiation into matter and the development of more accurate methods of analysis. This is particularly important in the construction of nuclear installations of small dimensions. For this purpose it is insufficient to study only the basic characteristics of protected materials--relaxation length, absorption coefficients, removal cross section, buildup factors for an infinite medium. It becomes absolutely necessary to have more detailed information on the energy, angular and three-dimensional distribution of radiations in infinite and in bounded media. Necessary data of this type can be obtained only by using new experimental devices and new methods of analysis. The works included in this volume are basically concerned with the investigation of such detailed characteristics of shielding and the description of experimental methods.

The entire material in this volume is divided into three parts: theory and method of analysis; experimental investigations and the descriptions of new experimental methods. The last division also includes articles which present results on the investigation of the properties of concretes.

This arrangement of the material is arbitrary to some extent, because some of the articles in the first division also contain descriptions of experiments used to obtain certain constants necessary for analysis, as well as data on the limits of application of the design methods and their accuracy. On the other hand, the experimental articles of the second division have been called upon to refine the methods of analysis.

The collected works start with the article by A. A. Abagyan, V. V. Orlov and G. I. Rodionov, which proposes a method of analysis based on the utilization of conjugate equations and functions and the theory of perturbations in shielding theory. The effectiveness functions of various materials in shielding, whose method of calculation is presented in this work, may be utilized for selecting the optimum shielding compositions. The same problem of applying conjugate equations to the analysis of shielding from radiation is considered in the article by G. I. Marchuk and Zh. N. Bel'skaya.

The work of Sh. S. Nikolayshvili, which is concerned with the analysis of the three-dimensional energy distributions from sources of monoenergetic neutrons in hydrogen, presents the basic quantities necessary to solve certain

practical problems. For example, by utilizing the neutron distributions in hydrogen, as computed in this work, and the known values of the "removal cross section" of various elements, we can carry out the analysis of three-dimensional distributions of neutrons in homogeneous and multilayer hydrogen contained in shields.

Although the analysis of neutron distribution in hydrogen contained in shieldings has been covered in many earlier works, the methods of designing shieldings which do not contain hydrogen have been developed to a lesser degree. The analytical methods and methods for determining the values of constants applied in the analysis of such shieldings are considered in the works of D. L. Broder, A. A Kutuzov, V. V. Levin and V. V. Frolov, in the works of B. I. Sinitsyn and S. G. Tsypin and in the work of B. R. Bergel'son. The problem of analyzing shieldings which do not contain hydrogen or which contain it in small quantities, which has been considered earlier in the Soviet periodic literature, has aroused a great deal of interest, particularly in the case of producing shieldings for high temperature installations where hydrogen-containing materials are frequently inapplicable.

The multiple group methods of analyzing three-dimensional energy distribution of neutrons have found wide application in the design of reactors. Recently several multiple group methods have been proposed for the analysis of shieldings which, in a certain sense, are analogous to those used in the design of reactors. Two such methods are described in the article by D. L. Broder, A. P. Kondrashov, A. A. Kutuzov, V. A. Naumov and others. In these methods the neutron flux is broken down into seven and ten energy groups.

The recently applied method of investigating the shielding properties of materials utilizing unidirectional beams of radiation are rather promising. By using this method it is possible to compute or measure the distribution of radiation fluxes, and to find the influence functions for sources of various form and various angular distribution. This problem is treated in the theoretical work of A. P. Suvorov, Ye. B. Breshenkova; the theoretical work of V. V. Orlov and the experimental work of V. P. Mashkovich, V. K. Sakharov and S. G. Tsypin.

Similar problems were also investigated in the work of V. I. Kukhtevich and L. A. Trykov. The problem associated with the transmission of γ-rays during their inclined incidence on the shielding barrier also arouses great interest in the analysis of shieldings with complex geometry.

The analysis of the effect associated with the geometric form of sources on the magnitude of the dose or of the radiation flux behind the shielding and its angular distribution, carried out in the article by D. L. Broder, Ye. N. Goryanina and others, serves as a substantial aid in the understanding of inaccuracies which occur in the various approximate methods of analysis.

The special features associated with the transmission of radiation through nonhomogeneous media are investigated in the theoretical works of N. I. Laletin and G. Ya. Rumyantsev. Equations are obtained which make it possible to evaluate the effect of medium nonhomogeneity on its attenuation properties.

The pertinent calculations and measurements of the angular distributions of neutrons and γ-radiations in shieldings are presented in the works of A. V. Larichev, L. R. Kimel', V. A. Kon'shin. The work of V. A. Kon'shin gives particular attention to the analysis of three-dimensional and angular distributions at short distances from the source. Information on the angular distributions of radiation fluxes in shielding and beyond the shielding barrier is necessary not only to understand the mechanism of radiation retardation by the shielding, but for the design of various shadow shieldings.

In the practical solution of problems associated with the transmission of neutrons in a substance various approximations of the kinetic equation are usually utilized (the P_2-approximation of the method of spherical harmonics, age approximations and higher approximations, etc.).

The work of V. M. Veselov presents the spatial, angular and energy distributions of neutrons in an infinite medium, using various approximations, which makes it possible to evaluate their applicability to specific problems.

The basic shielding in stationary atomic installations utilizes concretes of various grades, so that the interest in the investigation of their properties has not decreased to the present day. The present volume also devotes attention to the investigation of the shielding and mechanical properties of concrete. This problem is treated in the work of V. N. Avayev, G. A. Vasil'yev and others. The two works by I. A. Arshinov are also concerned with this problem.

A detailed investigation of the spectra of neutrons and γ-quanta in the shielding makes it possible to extend our knowledge on the mechanism of retardation of these radiations substantially and to evaluate with a higher degree of reliability, than in the case of total measurements, the degree of accuracy and the limits of application of certain approximate methods of computation. Some works of Yu. A. Yegorov and V. N. Avayev and others, and the work of A. T. Bakov, S. P. Velov, Yu. A. Kazanskiy and others present results on the measurements of spectra of fast neutrons and γ-quanta. The last work is also interesting from the point of view of nuclear-physical concepts concerning the reactions associated with the radiation capture of neutrons.

As a result of experiments conducted by D. L. Broder, Yu. P. Kayurin and A. A. Kutuzov and described in the present volume, an empirical relationship is obtained for computing multiple layer shielding for γ-radiation, which describes the experimental results much better than the methods recommended earlier.

The calculation of the radiation effects of emanations on various structures of an installation has become one of the foremost problems because of the application of high-energy reactors. The methods of analyzing the thermal shielding of a reactor and the calculation of radiation heat releases in the reactor screens and vessel, as well as the experimental verification of these calculations, are presented in the works of D. L. Broder, A. P. Kondrashov, V. A. Naumov and others.

The selection and formulation of systems of initial constants are of great significance for the correct analysis of shielding. This includes the interaction cross sections of neutrons with the nucleus as well as the establishment of spectra for the γ-quanta and neutrons and the decay periods for the products of various nuclear reactions, etc. Therefore the compilers of this volume have deemed it useful to include the article by D. L. Broder, A. I. Lashuk and others, the article by V. I. Lebedev, P. Ye. Stepanov and also the article by V. P. Il'in and V. Kh. Tokhtarov.

The last part of this volume is concerned with the methods of investigating the shielding. The principal difficulty in measuring the radiation fluxes in shieldings is due to the presence of mixed fields of neutrons and γ-rays. Therefore, when measuring the neutron fluxes the experimenters pay special attention to the selection of a detector which is sufficiently insensitive to γ-radiation and, vice versa, when recording the γ-quanta an effort is made to utilize counters or dosimeters which are insensitive to neutrons. Special attention must also be paid to the spectral sensitivity of detectors. Thus, for example, in measuring the dose fields, it is desirable that the signal fed from the detector to the counter be proportional to the dose produced by a particle of a given type and given energy which generates this signal. It is quite difficult to construct spectrometers for γ-radiation and for neutrons which operate satisfactorily in intense radiation fields of another type. Detectors for this type of measurements are considered in some of the works contained in the present volume.

Thus a survey of existing methods of detection in experiments on shielding is given in the articles by V. A. Dulin, Yu. A. Kazanskiy, Ye. S. Matusevich and V. N. Avayev, G. A. Vasil'yev and others.

The articles by Yu. A. Yegorov, V. N. Avayev, Yu. V. Orlov, N. N. Chentsov, A. S. Frolov, Yu. V. Pankrat'yev consider different types of neutron and γ-spectrometers which can be used in experiments on the investigation of shielding, including measurements made on reactors. These works also discuss the methods of calculating the characteristics of spectrometers and processing the results of measurements. In the articles by V. N. Avayev and others and of V. P. Mashkovich, methodological data are presented on the application of radioactive indicators to measure neutron fluxes, in particular the application of the method for the isolation of the characteristic γ-line.

The work of S. G. Tsypin describes the B-2 installation, which is used to investigate shieldings by means of a rather promising method--with the aid of an unidirectional beam of neutrons, which makes it possible to obtain more detailed information.

This volume may be useful to many readers concerned with the analysis and design of biological shielding of reactor installations and to specialists interested in the problems associated with radiation transport in a substance.

The second and third parts of the volume will undoubtedly be of interest to experimental physicists, because some of the methods described there, including those using neutron and γ-spectrometers, may be applied to various investigations in other fields of experimental nuclear physics.

The Editors

CONTENTS

	Page
Annotation	iii
Preface	v
PART I. THE THEORY OF RADIATION PENETRATION AND METHODS OF ANALYZING SHIELDING	
The Neutron Danger Functions in the Analysis of Shielding From Radiation A. A. Abagyan, V. V. Orlov and G. I. Rodionov	1
Three-dimensional Energy Distribution of Fast Neutrons in Hydrogen Sh. S. Nikolayshvili	27
Three-dimensional Distribution of Neutrons in an Infinite Homogeneous Medium with a Point Unidirectional Source A. P. Suvorov, Ye. B. Breshenkova and V. V. Orlov	36
Application of the Method of "Removal Cross Sections" to Analysis of Shielding Without Hydrogen D. L. Broder, A. A. Kutuzov, V. V. Levin and V. V. Frolov	70
Experimental Justification for the Multiple Group Methods in the Computation of Biological Shielding D. L. Broder, A. P. Kondrashov, A. A. Kutuzov, V. A. Naumov, Yu. A. Sergeyev and A. V. Turusova	81
Application of Empirical Data to the Calculation of Shielding B. I. Sinitsyn and S. G. Tsypin	99
Computation of Neutron Diffusion in a Two-dimensional Problem by Means of the P_2-approximation G. Ya. Rumyantsev	117
Investigation of the Accuracy of Various Approximations in the Problem of Three-dimensional Energy and Angular Distribution of Neutrons V. M. Veselov	125

Page

Application of Conjugate Equations to the Calculation of Radiation Shielding 141
G. I. Marchuk and Zh. N. Bel'skaya

Attenuation of Fast Neutrons in Nonhydrogen Moderators 146
B. R. Bergel'son

Angular Distribution of Neutrons at Small Distances from the Source in an Isotropically Scattering Medium 152
V. A. Kon'shin

The Question of Radiation Source Geometry 161
D. L. Broder, Ye. N. Goryanina, G. M. Levis, K. K. Popkov and S. M. Rubanov

Attenuation of Radiation in Heterogeneous Shieldings 171
N. I. Laletin

Selection of a System of Functions for the Excitation of Levels During Elastic Scattering of Neutrons by Iron, Nickel and Niobium Nuclei 192
D. L. Broder, A. I. Lashuk, I. P. Sadokhin and A. P. Suvorov

Representation of Decay Curves for Fission Fragments by Functions of a Given Form (e^{bt}) 207
V. I. Lebedev, P. Ye. Stepanov

The Spectrum of Gamma-radiation Produced by the Products of Uranium Fission. Effective Absorption Coefficients for the Gamma-ray Spectrum and Their Utilization for the Computation of Shielding 211
V. P. Il'in

Average Cross Sections of the Reaction for the Gamma-spectrum of Fission Fragments 238
V. Kh. Tokhtarov

Application of the Monte Carlo Method for Computing Nuclear Radiation Shielding 247
V. G. Zolotukhin and S. M. Yermakov

PART II. THE EXPERIMENTAL INVESTIGATIONS OF SHIELDING

Three-dimensional Energy Distribution of Neutrons in Thick Iron Layers 263
V. P. Mashkovich, V. K. Sakharov and S. G. Tsypin

Deformation of Fast Neutron Spectrum in Concrete and Water 276
Yu. A. Yegorov

Page

Shielding Properties of Certain Types of Concretes 280
V. N. Avayev, G. A. Vasil'yev, A. P. Veselkin, Yu. A. Yegorov, A. D. Zhirnov, V. A. Kucheryayev, Yu. V. Orlov, Ye. A. Panov and Yu. V. Pankrat'yev

The Transmission of Gamma-radiation Through Heterogeneous Media 287
D. L. Broder, Yu. P. Kayurin, A. A. Kutuzov

The Gamma-spectrum of the Experimental Reactor 300
V. N. Avayev, Yu. A. Yegorov, I. Ya. Yemel'yanov, A. D. Zhirnov, Yu. V. Orlov and V. A. Remizov

The Inclined Incidence of Gamma-rays 304
V. I. Kukhtevich and L. A. Trykov

Investigation of the Spectral and Angular Distribution of Gamma-rays After Transmission Through Shielding Barriers 311
A. V. Larichev

Field Doses and the Angular Distribution of Gamma-radiation from the Surface of Isotropic Sources at the Boundary Separating two Media 316
L. P. Kimel'

The Three-dimensional Distribution of Scattered Energy from a Point Unidirectional Source 322
L. P. Kimel' and O. I. Leypunskiy

The Difference in the Spectra of Gamma-rays During Radiation Capture of Thermal Neutrons and of Neutrons with the Reactor Spectrum 331
A. T. Bakov, S. P. Belov, Yu. A. Kazanskiy and V. I. Popov

Transmission of Gamma-radiation Through a Flat Slit in Shielding 336
A. P. Veselkin, Yu. A. Yegorov and Ye. A. Panov

Heat Liberation in Reactor Screens and Vessels 344
D. L. Broder, A. P. Kondrashov, V. A. Naumov, K. K. Popkov and A. V. Turusova

PART III. EXPERIMENTAL METHODS OF INVESTIGATING SHIELDING AND SHIELDING MATERIALS

Investigation of Neutron Transmission Through Shielding by Means of Unidirectional Sources (the B-2 Installation) 357
S. G. Tsypin

Experimental Methods of Investigating Shielding (Radiation Detectors) 372
V. A. Dulin, Yu. A. Kazanskiy and Ye. S. Matusevich

Page

Counters and Dosimeters for Investigating Shielding and the Shielding Properties of Materials 385
V. N. Avayev, G. A. Vasil'yev, Yu. A. Yegorov, V. A. Kucheryayev, Yu. V. Orlov, Yu. V. Pankrat'yev and Ye. A. Panov

Application of Radioactive Tracers in the Investigation of Shielding 400
V. N. Avayev, Ye. V. Voskresenskiy, Yu. A. Yegorov and Yu. V. Orlov

Measurement of Fast Neutron Fluxes in Shielding when There is a Background of Intense Intermediate Neutron Fluxes 409
V. P. Mashkovich

Application of Random Sampling to the Computation of Spectrometer Characteristics for Gamma-radiation and fast Neutrons 415
V. N. Avayev, Yu. A. Yegorov and Yu. V. Orlov

Calculation and Analysis of the Characteristics of a Spectrometer with Boron-hydrogen Scintillator 428
V. N. Avayev, Yu. A. Yegorov, Yu. V. Orlov, A. S. Frolov and N. N. Chentsov

Single Crystal Fast Neutron Spectrometer for Measuring Continuous Spectra 451
Yu. A. Yegorov and Yu. V. Pankrat'yev

Permissible Gamma Background Radiation when Measuring Fast Neutrons with a Single Sensor Spectrometer 460
Yu. A. Yegorov, Yu. V. Orlov and Yu. V. Pankrat'yev

The Gamma-spectrometer Based on the Formation of Electron-positron Pairs 464
V. N. Avayev, Yu. A. Yegorov and Yu. V. Orlov

Application of a Single Crystal Gamma-spectrometer for Taking Measurements on a Nuclear Reactor 474
Yu. A. Yegorov and Yu. V. Orlov

Strength of Special Composition Concrete at High Temperatures (400-800°C) 486
I. A. Arshinov

Physical and Mechanical Properties of Concrete with Serpentine Fillers 500
I. A. Arshinov

PART I. THE THEORY OF RADIATION PENETRATION AND METHODS OF ANALYZING SHIELDING

THE NEUTRON DANGER FUNCTIONS IN THE ANALYSIS OF SHIELDING FROM RADIATION

A. A. Abagyan, V. V. Orlov and G. I. Rodionov

Introduction

The method of conjugate equations (refs. 1-4) has turned out to be /7* particularly useful in the analysis of nuclear reactors. The physical meaning of a conjugate function as the important feature of the neutron in a reactor is clarified most thoroughly in reference 1, which also derives a conjugate equation.

The theory of conjugate equations was further developed during the period 1957-1958 in the works of B. B. Kadomtsev (ref. 5) and G. I. Marchuk and V. V. Orlov (refs. 6 and 7). These works present the generalization for the case of nonhomogeneous equations and obtain the relationships of the theory of perturbations for arbitrary functionals which depend in a linear fashion on the neutron flux.

The present work presents the problems of the theory of conjugate equations, as they apply to the investigation and analysis of shielding from radiation.

The basic problems of analyzing a shielding involve the calculation of the following quantities:

(a) the flux of neutrons behind the shielding and the doses produced by them; (b) the flux and dose of the γ-quanta beyond the shielding; in this case both the γ-quanta generated in the reactor as well as the capture γ-quanta generated in the shielding as a result of neutron absorption are of interest; (c) integral neutron fluxes which fall on certain elements of reactor construction and shielding for the purpose of estimating the degree of radiation damage to material; (d) heat liberation in various elements of reactor construction and shielding (for example, in the vessel of the reactor), occurring as a result of γ-radiation absorption, and the moderation and absorption of neutrons.

---

*Numbers given in margin indicate pagination in original foreign text.

Unlike the universal conjugate function (value of neutrons) investigated during the analysis of reactors criticality, we shall require various conjugate functions, each of which refers to a specific quantity of interest to us.

As we have already pointed out, the conjugate function in a reactor has the sense of neutron value, and therefore each neutron determines a definite value. Depending on the conditions of injection, this value, i.e., the contribution of a neutron to the chain reaction, in power, will be different.

The situation is different in shielding. A neutron which has been injected into the shielding always represents a certain danger. This danger may be of a different type. The neutron is dangerous in itself and, depending on the conditions of injection, may produce a certain neutron dose. In the shielding a neutron may be dangerous from the point of view of generating secondary γ-radiation, heat liberation and radiation interaction with the materials, etc. Therefore it is expedient to utilize the term "neutron danger" in the shielding instead of the designation "conjugate function as the value of the neutron."

In computing the shielding of nuclear reactors we can distinguish two /8 stages. In the first stage we investigate the optimum composition of the shielding, the best arrangement of various structural elements, the best alternation of shielding layers. In the second stage, when the shielding has already been selected, it is necessary to carry out small changes dictated by constructional changes. Both in the first stage and in the second stage the method of conjugate functions and of the theory of perturbations may prove to be quite useful.

We should like to point out two of the possible applications of conjugate functions and of the theory of perturbations. In the first place, if we know the conjugate function, we can select the most rational arrangement of various materials in the shielding: moderators, neutron and γ-quanta absorbers; in the second place, it is possible for us to obtain the variations in the quantities of interest to us (doses, heat liberation, etc.), associated with certain changes in the construction and in the cross section of interaction. We can also obtain variations in quantities, due to effects not previously considered and without repeating the cumbersome calculations, by merely utilizing the relationships of the theory of perturbations.

It is true that in contrast to calculations of reactor criticality, where we are interested in rather small changes of reactivity, in the case of shielding analysis we are usually interested in large perturbations. Therefore, the utilization of the theory of perturbations in certain problems will give us qualitative rather than quantitative results. However, we know of a whole series of problems when the perturbations are additive to a substantial degree as illustrated, for example, by the utilization of the method of removal cross sections. In cases of this type the theory of perturbations may lead to results which are quantitatively correct even when the perturbations are large.

Theory of Conjugate Equations. Equations of the Perturbation Theory

Let us consider a flux of neutrons which satisfies the equation

$$\frac{1}{v}\cdot\frac{\partial\varphi}{\partial t}+\Omega\nabla\varphi+\Sigma(E)\varphi-\int d\Omega'\int dE'\varphi(\mathbf{r},\ \Omega',\ E',\ t)\,\Sigma(\Omega'\to\Omega,\ E'\to E)=q(\mathbf{r},\ \Omega,\ E,\ t), \tag{1}$$

where $\Sigma(E)$ is the total macroscopic cross section of interation; $\Sigma(\Omega' \to \Omega, E' \to E)$ is the differential cross section which characterizes the transfer of neutrons from the beam (Ω', E') to the beam (Ω, E) (here we take into account the elastic and inelastic transitions as well as fission); $q(r, \Omega, E, t)$ is the distribution of neutron sources. The medium in which we seek the solution of equation (1) covers a volume V which is bounded by surface S. If external radiation is absent, the natural boundary condition is

$$\varphi(\mathbf{r}_s,\ \Omega,\ E,\ t)=0 \quad \text{when} \quad (\Omega\mathbf{n})<0, \tag{2}$$

where n is the external normal to surface S.

However, we frequently encounter a situation in problems of shielding when a flux of neutrons falls on the boundary of the medium from the outside. In this case the boundary condition takes the form

$$\varphi(\mathbf{r}_s,\ \Omega,\ E,\ t)=f(\mathbf{r}_s,\ \Omega,\ E,\ t) \quad \text{when} \quad (\Omega\mathbf{n})<0. \tag{3}$$

In this case we can also utilize the boundary condition in form (2) by writing q (ref. 6) in equation (1) in the form

$$q\to q(\mathbf{r},\ \Omega,\ E',\ t)+(\Omega,\ \mathbf{n})\,f(\mathbf{r},\ \Omega,\ E,\ t)\,\delta(\mathbf{r}-\mathbf{r}_s) \quad \text{when} \quad (\Omega\mathbf{n})<0, \tag{4}$$

where $\delta(r-r_s)$ is the δ-function which transforms the volume integral into a surface integral. The point r_s in equality (2) should be interpreted as the limit $r_{s+\epsilon n}$ when $\epsilon \to 0$ $(\epsilon > 0)$. We shall first consider the following equation which is normally conjugated with (1)

$$-\frac{1}{v}\cdot\frac{\partial\varphi^+}{\partial t}-\Omega\nabla\varphi^+ +\Sigma(E)\varphi^+-\int d\Omega'\int dE'\varphi^+(\mathbf{r},\ \Omega',\ E't)\times \times\Sigma(\Omega\to\Omega',\ E\to E')=p(\mathbf{r},\ \Omega,\ E,\ t), \tag{5}$$

where p will be assumed to be an arbitrary function at this time.

For the sake of brevity we shall write equations (1) and (5) in the form

/9

$$\hat{L}\varphi_q(x) = q(x); \tag{6}$$

$$\hat{L}^*\varphi_p^+(x) = p(x). \tag{7}$$

We shall interpret x as the set of all variables. The operators $\hat{L}$ and $\hat{L}^+$ are linear and satisfy the relationship

$$\int f_1(x)\,\hat{L}f_2(x)\,dx = \int f_2(x)\,\hat{L}^*f_1(x)\,dx \tag{8}$$

for any two functions $f_1(x)$ and $f_2(x)$. We shall always be dealing with real operators and functions.

For functions $f_1(x)$ and $f_2(x)$ we may take the solutions of equations (1) and (5).

With equations (1) and (5) we introduce equations for the Green functions of the basic and conjugate equations

$$\hat{L}G(x,\ x_0) = \delta(x - x_0); \tag{9}$$

$$\hat{L}^*G^*(x,\ x_1) = \delta(x - x_1). \tag{10}$$

We shall prove the reciprocity theorem for the Green functions of the basic and conjugate equations. For this purpose we multiply equation (9) by $G^+(x,\ x_1)$ and equation (10) by $G(x,\ x_0)$. We integrate over the entire interval of values for the variable x and subtract one integral from the other (ref. 5)

$$\int G^*(x,\ x_1)\,LG(x,\ x_0)\,dx - \int G(x,\ x_0)\,L^*G^*(x,\ x_1)\,dx = \tag{11}$$
$$= G^*(x_0,\ x_1) - G(x_1,\ x_0).$$

Because the operators $\hat{L}$ and $\hat{L}^+$ conjugate, the left part of equation (11) becomes equal to zero. Consequently, if we designate x_1 by x, we obtain

$$G^*(x_0,\ x) = G(x,\ x_0). \tag{12}$$

We write the solution of equation (5) by means of the Green function

$$\varphi_p^+(x) = \int G^+(x,\ x_0),\ p(x_0)\,dx_0, \tag{13}$$

or by utilizing relationship (12),

$$\varphi_p^+(x) = \int G(x_0,\ x)\,p(x_0)\,dx_0. \tag{14}$$

Relationship (14) makes it possible for us to clarify the physical meaning of the solution for the conjugate equation (5). The function $G(x_0, x)$ may be interpreted to signify the flux of neutrons in x_0, if one neutron is admitted at point x.

Consequently, if $p(x_0)$ designates some characteristic of a process with neutrons, $G(x_0, x)\ p(x_0)$ is the number of acts of this process at the coordinate x_0, when one neutron is injected at point x. Then $\int G(x_0, x)\ p(x_0)\ dx_0$ gives us the total number of acts in some volume, if a neutron is injected at point x. For example, $\int_{V_0} G(x_0, x)\ \Sigma_a\ dx_0$ is the number of neutrons absorbed in the volume V_0, if one neutron is injected at point x.

Thus $\varphi_p^+(x)$ describes the variation in the total number of acts of a definite process with neutrons as a function of the conditions of neutron admission. The conjugate function tends to characterize the quality of the neutron with respect to a definite process, while the basic function gives us a quantitative characteristic of the neutron flux.

Proceeding from this interpretation of a conjugate function we formulate the boundary conditions for equation (5). If the neutrons which have left /10 the system cannot return and contribute to the given process, the boundary conditions for them will be

$$\varphi_p^+(\mathbf{r}_s,\ \Omega,\ E,\ t) = 0 \quad \text{when} \quad (\Omega\mathbf{n}) > 0 \tag{15}$$

For example, if $\varphi_p^+(x)$ characterizes the formation of capture γ-quanta, the neutrons which are directed from the medium into the vacuum at the boundary

cannot contribute to this process. Therefore their danger to the boundary will be equal to zero. In other cases, when the process is considered outside the given system, the boundary condition will have the form

$$\varphi_p^+(\mathbf{r}_s, \Omega, E, t) = f^+(\mathbf{r}_s, \Omega, E, t) \quad \text{when } (\Omega n) > 0. \tag{16}$$

This can happen, for example, if $\varphi_p^+(x)$ characterizes the contribution to the dose by neutrons which are measured at the surface of the shielding, depending on the conditions of neutron injection. Neutrons injected at the boundary and directed from the medium directly contribute to the dose in view of their biological effectiveness. As in the case of the basic equation, we can utilize the boundary condition in form (15), writing p in the form

$$p \to p(\mathbf{r}, \Omega, E, t) + (\Omega n) f^+(\mathbf{r}, \Omega, E, t)\, \delta(\mathbf{r} - \mathbf{r}_s) \quad \text{when} \quad (\Omega n) > 0. \tag{17}$$

In this case r_s in equation (15) should be interpreted as the limit $r_{s+\varepsilon n}$, when $\varepsilon \to 0$ ($\varepsilon > 0$).

G. I. Marchuk and V. V. Orlov (ref. 6) developed the theory of perturbations, assuming sources p(x) and q(x) in equations (1) and (5) to be constant. Let us consider the equations of the theory of perturbations for the general case, when in addition to the variation of the medium parameters there is also a variation in quantities p(x) and q(x). Such cases are frequently encountered in shielding. For example, quantity p(x) varies when we consider the variation in the intensity of the capture γ-radiation during the substitution of one material for another.

The functional characterizing a definite process with neutrons has the form

$$J_p = \int \varphi(x)\, p(x)\, dx. \tag{18}$$

Let us consider the functional

$$J_q = \int \varphi^+(x)\, q(x)\, dx. \tag{19}$$

In this case $\varphi(x)$ satisfies equation (1), while $\varphi^+(x)$ satisfies equation (5). We can show that $J_p = J_q$, in which case it is necessary to multiply equation

(1) by $\varphi^+(x)$ and equation (5) by $\varphi(x)$, and then to integrate equations (1) and (5) over x; subtracting one from the other, we obtain

$$\int \varphi^* \hat{L} \varphi \, dx - \int \varphi \hat{L}^* \varphi^* \, dx = - \int \varphi(x) \, p(x) \, dx + \int q(x) \, \varphi^*(x) \, dx. \tag{20}$$

Because the operators L and L^+ are conjugate, the left side of equality (20) is equal to zero. Consequently,

$$\int \varphi(x) \, p(x) \, dx = \int \varphi^*(x) \, q(x) \, dx \tag{21}$$

$$\text{and } J_p = J_q. \tag{22}$$

Let us assume that the variation in the parameters of the medium leads to a variation in the operators of equations (1) and (5) from $\hat{L}$ to $\hat{L}' = \hat{L} + \delta\hat{L}$ and $\hat{L}^+$ to $\hat{L}^{+'} = \hat{L}^+ + \delta\hat{L}^+$. In addition to this q(x) is replaced by $q'(x) = q(x) + \delta q(x)$ and p(x) is replaced by $p'(x) = p(x) + \delta p(x)$ in the right sides of equations (1) and (5).

The unperturbed system is described by equations

$$\left.\begin{aligned} \hat{L}\varphi(x) &= q(x); \\ \hat{L}^*\varphi^*(x) &= p(x). \end{aligned}\right\} \tag{23}$$

The perturbed system is described by equations <u>/11</u>

$$\left.\begin{aligned} (\hat{L} + \delta\hat{L})\,\varphi'(x) &= q(x) + \delta q(x); \\ (\hat{L}^* + \delta\hat{L}^*)\,\varphi^{*\prime}(x) &= p(x) + \delta p(x). \end{aligned}\right\} \tag{24}$$

The initial functional is equal to

$$J_p = \int \varphi(x) \, p(x) \, dx = J_q = \int \varphi^*(x) \, q(x) \, dx. \tag{25}$$

The perturbed functional is determined by expressions

$$J'_p = \int \varphi'(x) \, p'(x) \, dx = J'_q = \int \varphi^{*\prime}(x) \, q'(x) \, dx \tag{26}$$

and

$$\delta J_p = J'_p - J_p. \tag{27}$$

Let us establish a relationship between the variations in $\delta\hat{L}$, δp and δq and variations in the functional δJ_p. For this purpose we multiply the first equation of system (24) by $\varphi^+(x)$ and the second equation of system (23) by $\varphi'(x)$. Integrating and subtracting one from the other, we obtain

$$\int \varphi^+(x)\,\delta\hat{L}\varphi'(x)\,dx = \int q(x)\,\varphi^+(x)\,dx + \int \delta q(x)\,\varphi^+(x)\,dx -$$
$$- \int p(x)\,\varphi'(x)\,dx = \int q(x)\,\varphi^+(x)\,dx - \int [p(x)+\delta p(x)]\,\varphi'(x)\,dx +$$
$$+ \int \delta q(x)\,\varphi^+(x)\,dx + \int \delta p(x)\,\varphi'(x)\,dx.$$

By utilizing relationships (25-27) we obtain

$$\delta J_p = \int \delta p(x)\,\varphi'(x)\,dx + \int \delta q(x)\,\varphi^+(x)\,dx - \int \varphi^+(x)\,\delta\hat{L}\varphi'(x)\,dx. \tag{28}$$

In the same manner we obtain an equation for δJ_p in the form

$$\delta J_p = \int \delta p(x)\,\varphi(x)\,dx + \int \delta q(x)\,\varphi^{+\prime}(x)\,dx - \int \varphi(x)\,\delta\hat{L}^*\varphi^{+\prime}(x)\,dx. \tag{29}$$

We note that relationships (28) and (29) transform to the conventional equation of the theory of perturbations in cases when the perturbations of the quantities $p(x)$ and $q(x)$ are absent. In this case $\delta p = 0$, $\delta q = 0$,

$$\delta J_p = -\int \varphi(x)\,\delta\hat{L}^*\varphi^{+\prime}(x)\,dx. \tag{30}$$

We should note that the methods of conjugate functions and of the theory of perturbations presented in the present section are equally applicable to the γ-quanta.

The equations of the theory of small perturbations are obtained from equations (29) and (30) by replacing $\varphi'(x)$ with $\varphi(x)$ and $\varphi^{+\prime}(x)$ with $\varphi^+(x)$.

Certain Functionals in the Theory of Shielding

Let us write down the functionals which characterize the different quantities which are of interest to us during the calculation of the shielding. For simplicity we shall consider all of the functionals in one-dimensional plane geometry.

1. The functional which characterizes the formation and exit of capture γ-radiation (fig. 1) is

$$J_{n\gamma} = \sum_i k_i \beta_i \int\int\int \frac{\varphi(x, \mu, E)\,\Sigma_{n\gamma}(E)}{4\pi r_s^2} e^{-\sum_{k=0}^{n} \mu_k^i r_k} \cos\theta B_i\, d\mu\, dV\, dE, \qquad (31)$$

where k_i is the dose produced by a unit flux of γ-quanta with energy E_i; β_i is the output of γ-quanta with given energy E_i for each captured neutron; φ (x, μ, E) is the flux of neutrons; $\Sigma_{n\gamma}$ is the macroscopic neutron capture cross section when γ-quanta are formed; μ_k^i is the total coefficient of linear absorption for γ-quanta with an energy E_i; B_i is the dose factor for the buildup of γ-quanta with initial energy E_i. /12

Expression (31) describes the dose of γ-quanta leaving one cm^2 of the shielding surface. The intensity of γ-quanta dose at points which are close to the surface of the shielding is described by an expression similar to (31), but without the cos θ term under the integral sign.

If the dose buildup is represented in the form

$$B_i = A_i e^{-\alpha_1^i \sum_{k=0}^{n} \mu_k^i r_k} + (1 - A_i)\, e^{-\alpha_2^i \sum_{k=0}^{n} \mu_k^i r_k}, \qquad (32)$$

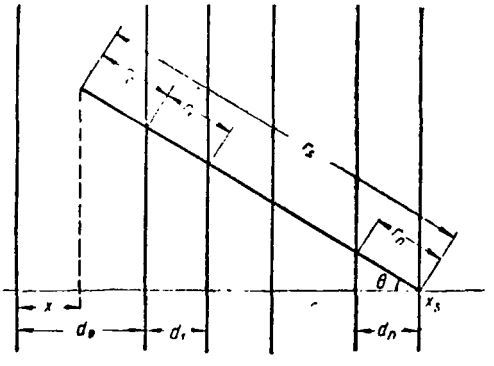

Figure 1. Analysis of capture γ-radiation.

we can integrate expression (31) over θ and φ and obtain

$$J_{n\gamma}=\frac{1}{2}\sum_i \beta_i k_i \int\int\int \varphi(x,\ \mu,\ E)\,\Sigma_{n\gamma}(E)\left\{A_i E_2\left[\mu_{01}^i(d_0-x)+\right.\right.$$
$$\left.\left.+\sum_{k=1}^{n}\mu_{k1}d_k\right]+(1-A_i)\,E_2\left[\mu_{02}^i(d_0-x)+\sum_{k=1}^{n}\mu_{k2}^i d_k\right]\right\}dx\,d\mu\,dE, \qquad (33)$$

where

$$\mu_{k1}^i=\mu_k^i(1+\alpha_1^i);\quad \mu_{k2}^i=\mu_k^i(1+\alpha_2^i);$$

d_0 is the thickness of the considered layer of material in which the γ-quanta are generated; d_k is the thickness of material layers which are situated behind the considered layer; $E_2=\int_1^\infty \frac{e^{-xt}}{t^2}\,dt$.

As we can see from equation (33), the function p is written in the following manner

$$p(x,\ E)=\sum_i \beta_i k_i \Sigma_{n\gamma}(E)\left\{A_i E_2\left[\mu_{01}^i(d_0-x)+\sum_{k=1}^{n}\mu_{k1}^i d_k\right]+\right.$$
$$\left.+(1-A_i)\,E_2\left[\mu_{02}^i(d_0-x)+\sum_{k=1}^{n}\mu_{2k}^i d_k\right]\right\}. \qquad (34)$$

The corresponding conjugate equation takes the form

$$\hat{L}^*\varphi^*=\sum_i k_i\beta_i\Sigma_{(n\gamma)}(E)\left\{A_i E_2\left[\mu_{01}^i(d_0-x)+\right.\right.$$
$$\left.\left.+\sum_{k=1}^{n}\mu_{k1}^i d_k\right]+(1-A_i)\,E_2\left[\mu_{02}^i(d_0-x)+\sum_{k=1}^{n}\mu_{k2}^i d_k\right]\right\}. \qquad (35)$$

The function $\varphi^+(x)$ describes the variation in the magnitude of the dose due to the capture γ-radiation on the surface of the shielding (and, generally speaking, at any point) depending on the condition of neutron admission, i.e., $\varphi^+(x)$ characterizes the danger of a neutron with respect to the formation and emission of the capture γ-radiation. This danger may be different, depending on the conditions under which the neutrons are injected. /13

2. The functional which characterizes the dose due to neutrons is

$$J_n = \int\int\int \varphi(x,\ \mu,\ E)\,\delta(x_s - x)\,f(E)\,d\mu\,dE\,dx, \tag{36}$$

where f(E) is a function characterizing the biological dose, produced by one neutron with energy E; $\delta\ (x_s - x)$ is the Dirac δ-function; x_s is a boundary point at which the dose due to neutrons is considered.

It follows from relationship (36) that

$$p\ (x,\ E) = f\ (E)\ \delta\ (x_s - x). \tag{37}$$

The corresponding conjugate equation is written in the form

$$\hat{L}^+\varphi^+ = f\ (E)\ \delta\ (x_s - x). \tag{38}$$

In accordance with the preceding section, equation (38) may be written in the form $\hat{L}^+\ \varphi^+ = 0$, with the boundary condition $\varphi^+\ (x_s) = f\ (E)$ when $(\Omega n) > 0$.

According to its physical meaning the function $\varphi^+\ (x)$ characterizes neutron danger from the point of view of the dose produced directly by the neutrons themselves.

3. The functional which characterizes the radiation interaction of neutrons with the material is

$$J_{Rad} = \int\int\int \varphi(x,\ \mu,\ E)\left\{g_1(E)\,\delta(x_s - x) + \sum_i g_2(E_i)\,\Sigma_{(n\gamma)}E \times \right.$$
$$\left. \times\ \beta_i B_{E_i} \frac{e^{-\mu_0^i r_s}}{4\pi r_s^2}\right\} dx\,d\mu\,dE, \tag{39}$$

where x_s is a point at which the radiation interaction with the material is considered; $x_s = r_s \cos\theta$; B_{E_i} is the energy buildup factor; $g_1\ (E)$ is a function which describes the measure of radiation interaction between the neutron and the material; $g_2\ (E_i)$ is a function which describes the measure of interaction between the substance and the γ-quanta with energy E_i.

The absolute value of functions $g_1\ (E)$ and $g_2\ (E_i)$ also depends on the illumination time. By making assumptions analogous to those presented in section 1 of this part, the function p (x, E) will have the following form after integration over Θ and φ

$$p(x,\ E)=g_1(E)\,\delta(x_s-x)+\sum_i \beta_i\Sigma_{(n\gamma)}(E)\,g_2(E_i)\times \\ \times\left[A_iE_1(\mu_{01}^i(x_s-x))+(1-A_i)\,E_1(\mu_{02}^i(x_s-x))\right]. \tag{40}$$

In this case the function $\varphi^+(x)$ characterizes the neutron danger from the point of view of radiation interaction due to a neutron, both directly as well as by means of the γ-quanta which it generates.

4. The functional which characterizes the contribution to heat liberation is

$$J_Q=\int\int\int \varphi(x,\ \mu,\ E)\left\{\left[\overline{\Delta E}\Sigma_s(E)+\Sigma_{n\alpha}(E)\,E_\alpha\right]\delta(x_s-x)+\right. \\ \left.+\sum_i \beta_i\mu_{\text{эн}}^i E_i\Sigma_{(n\gamma)}(E)\frac{e^{-\mu_0^i r_s}}{4\pi r_s^2}B_i+\sum_j \beta_j\mu_{\text{эн}}^j E_j\Sigma_{in}(E)\frac{e^{-\mu_0^j r_s}}{4\pi r_s^2}B_j\right\}dx\,d\mu\,dE, \tag{41}$$

(эн = en = energy)

where x_s is the point at which heat liberation is being considered; ΔE is the average energy loss of a neutron with energy E during a single collision; $\Sigma_s(E)$ is the macroscopic cross section of elastic scattering; $\Sigma_{n\alpha}(E)$ is the reaction cross section with the liberation of an α-particle or of some other charged particle; E_α is the energy of $(n\alpha)$-reaction; $\Sigma_{(n\gamma)}$ is the cross section of the radiation capture of neutrons; Σ_{in} is the cross section of inelastic scattering; μ_{en}^i is the energy coefficient for the attenuation of γ-quanta with energy E_i. If we represent the buildup factor B_i in the same manner as in sections 1 and 3, the function p (x, E) may be written in the form

/14

$$p(x,\ E)=(\overline{\Delta E}\Sigma_s(E)+\Sigma_{n\alpha}(E)\,E_\alpha)\,\delta(x_s-x)+ \\ +\Sigma\beta_iE_i\mu_{\text{эн}}^i\Sigma_{(n\gamma)}(E)\left[A_iE_1(\mu_{01}^i(x_s-x))+\right. \\ \left.+(1-A_i)\,E_1(\mu_{02}^i(x_s-x))\right]+ \\ +\sum_j \beta_jE_j\mu_{\text{эн}}^j\Sigma_{in}(E)\left[A_jE_1(\mu_{01}^j(x_s-x))+\right. \\ \left.+(1-A_j)\,E_1(\mu_{02}^j(x_s-x))\right]. \tag{42}$$

The first term in equation (42) takes into account the contribution by elastic scattering to heat liberation, while the second term is due to the reaction with the liberation of charged particles. The third term takes into

account the capture γ-radiation, and the fourth defines the contribution to heat liberation by γ-quanta formed during the inelastic scattering of neutrons.

If we are interested in heat liberation in a certain region of space, for example, in the reactor vessel, it is necessary to integrate expression (42) over x_s (fig. 2) within the limits of this space. Then the expression for p (x, E) will take the form

$$
\begin{aligned}
p(x,\ E) = \int_{x_1}^{x_2} p(x,\ x_s,\ E)\, dx_s = (\overline{\Delta E}\Sigma_s(E) + \Sigma_{n\alpha}E_\alpha) + \\
+ \sum_i \beta_i E_i \mu_{n1}^i \Sigma_{n\gamma}(E) \left\{ A_i \frac{1}{\mu_{01}^i} [E_2(\mu_{01}^i (x_1 - x)) - E_2(\mu_{01}^i (x_2 - x))] + \right. \\
\left. + (1 - A_i) \frac{1}{\mu_{02}^i} [E_2(\mu_{02}^i (x_1 - x)) - E_2(\mu_{02}^i (x_2 - x))] \right\} + \\
+ \sum_j \beta_j E_j \mu_{n1}^j \Sigma_{in}(E) \times \left\{ A_j \frac{1}{\mu_{01}^j} [E_2(\mu_{01}^j (x_1 - x)) - E_2(\mu_{01}^j (x_2 - x))] + \right. \\
\left. + (1 - A_j) \frac{1}{\mu_{02}^j} [E_2(\mu_{02}^j (x_1 - x)) - E_2(\mu_{02}^j (x_2 - x))] \right\}.
\end{aligned}
\tag{43}
$$

The terms $\overline{\Delta E}\Sigma_s$ (E) and $\Sigma_{n\alpha}E_\alpha$ become equal to zero when $x < x_1$ and $x > x_2$. In this case the thickness of the layer of the investigated material is $(x_2 - x_1)$, while the coefficient of linear attenuation for this layer is μ_0^i. The function φ^+ characterizes the contribution to heat liberation at a certain point x_s or in some region of space, depending on the conditions of neutron injection.

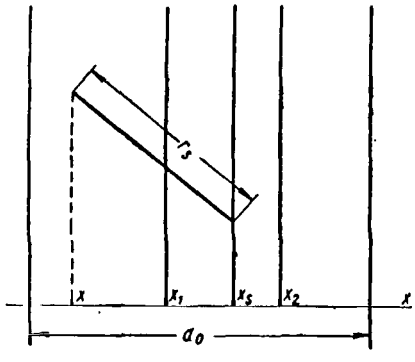

Figure 2. Calculation of heat liberation in a shielding.

If we have function $\varphi^+(x)$ which characterizes the neutron danger from the point of view of various processes, we can use equations (28) and (29) of the theory of perturbations to compute the effect of various factors on the dose due to capture radiation and due to neutrons, on heat liberation, etc.

Effectiveness Function of Shielding Materials

The various materials used in shielding have a different effect on the radiation flux beyond the shielding, and this effect depends to some degree on the position of this material in the shielding. For example, the effectiveness of boron materials is maximum when they are situated close to materials /15
which produce a strong secondary γ-radiation.

This variation in the effectiveness of a particular material on its location in the shielding may be described by a function $f_{Ap}(r)$, which we can call the effectiveness of the material A at the point r with respect to the quantity J_p. Obviously the function $f_{Ap}(r)$ may be different in different shielding compositions.

Quantitatively $f_{Ap}(r)$ is equal to the relative variation of the dose J_p when 1 g of material A is placed in 1 cm^3 near point r of the shielding.

If we know the flux distribution and the danger functions of neutrons in the shielding, we can compute this function by using equations (28) or (29) of the theory of perturbations.

$$f_{Ap}(\mathbf{r}) = \int_V d\mathbf{r}' \int_E dE \int d\Omega\, \delta p(\mathbf{r}, \mathbf{r}', E, \Omega)\, \varphi'(\mathbf{r}' E, \Omega) - \\ - \int dE \int d\Omega \varphi^+(\mathbf{r}, E, \Omega)\, \delta \hat{L}_A \varphi'(\mathbf{r}, E, \Omega) \ldots, \tag{44}$$

where $\delta\hat{L}_A$ and δp are due to the variation in the parameters of the medium and of the source in the conjugate equation due to the introduction of 1 g of material A at point r. This function makes it possible for us to select and arrange the material in the shielding correctly, in order to achieve a maximum increase in the shielding effectiveness. It is obvious that $f_{Ap}(r)$ gives us the effectiveness of material A only when its concentrations are small, when it does not substantially alter the spectrum of neutrons in the shielding. In order to find the optimum arrangement of materials, we must apparently use the method of successive approximations.

Investigation of Certain Effects in Shielding Made of Iron by Means of the Theory of Perturbations

As an example we present in the present division the calculation results for a two-dimensional shielding made of iron and of iron with 1 percent of boron by weight, with a thickness of 20 cm in both cases. We assume that the incident flux of neutrons is described by the fission spectrum χ (u). We shall consider the effect of boron and hydrogen introduced at various points of the shielding on the dose due to the capture γ-radiation and due to neutrons.

The three-dimensional energy distribution of the flux and of the neutron danger function is computed in the P_1-approximation by the multiple group method (26 groups). The system of constants and the breakdown into groups is shown in tables 1-4.

The system of equations for computing the neutron fluxes has the form (ref. 7)

$$\begin{gathered}\nabla\varphi_1^j+\Sigma_{\text{ув}}^j\varphi_0^j=\sum_{l=1}^{j-1}\Sigma_{in}^{l\to j}\varphi_0^l+\Sigma_{\text{зам}}^{j-1\to j}\varphi_0^{j-1};\\ \frac{1}{3}\nabla\varphi_0^j+\Sigma_{tr}^j\varphi_1^j=0.\end{gathered}\tag{45}$$

(ув = re = removal; зам = mod = moderation)

Here j = 1, 2, ..., 26, with conditions at the boundary

$$\frac{\varphi_1^j}{2}-\frac{\varphi_0^j}{4}=0\tag{46}$$

when $x = x_s$, x_s is the external boundary of the shielding; $\frac{\varphi_1^j}{2}+\frac{\varphi_0^j}{4}=\chi_j$ when $x = 0$ on the internal boundary of the shielding, where

$$\varphi_0^j=\int_{u_{j-1}}^{u_j}\varphi_0(u)\,du;\quad \varphi_1=\int_{u_{j-1}}^{u_j}\varphi_1(u)\,du.$$

Boundary conditions (46) mean that on the external boundary of the layer the neutron flux from without is absent, while on the internal boundary there is a flux from without of given intensity $\chi^j=\int_{u_{j-1}}^{u_j}\chi(u)\,du$. /18

TABLE 1. BREAKDOWN OF NEUTRON ENERGY ACCORDING TO GROUPS (j), CONSTANTS AND COEFFICIENTS OF CROSS SECTION BLOCKING FOR IRON.

j	E, eV	Δu	σ_c	σ_{mod}	σ_{re}	σ_{tr}	σ_{tot}	f_s	f_c	f_{tot}
1	$6{,}5\cdot10^6$—$10{,}5\cdot10^6$	0,48	0,035	0,0250	1,37	1,72	3,40	1,00	1,00	1,00
2	$4\cdot10^6$—$6{,}5\cdot10^6$	0,48	0,005	0,0508	1,35	2,04	3,80	0,98	0,97	0,96
3	$2{,}5\cdot10^6$—$4{,}0\cdot10^6$	0,48	0,002	0,0968	1,13	2,43	3,50	0,96	0,95	0,94
4	$1{,}4\cdot10^6$—$2{,}5\cdot10^6$	0,57	0,003	0,0960	0,90	2,57	3,30	0,87	0,90	0,74
5	$0{,}8\cdot10^6$—$1{,}4\cdot10^6$	0,57	0,004	0,120	0,484	2,29	2,90	0,79	0,79	0,61
6	$0{,}4\cdot10^6$—$0{,}8\cdot10^6$	0,69	0,005	0,161	0,166	3,16	3,80	0,68	0,63	0,45
7	$0{,}2\cdot10^6$—$0{,}4\cdot10^6$	0,69	0,006	0,142	0,148	3,76	3,00	0,77	0,62	0,55
8	$0{,}1\cdot10^6$—$0{,}2\cdot10^6$	0,69	0,006	0,181	0,187	3,52	3,70	0,66	0,50	0,39
9	$46{,}5\cdot10^3$—$100\cdot10^3$	0,77	0,007	0,237	0,234	5,12	5,30	0,60	0,53	0,34
10	$21{,}5\cdot10^3$—$46{,}5\cdot10^3$	0,77	0,017	0,657	0,674	14,21	14,50	0,07	0,39	0,03
11	$10\cdot10^3$—$21{,}5\cdot10^3$	0,77	0,005	0,183	0,188	3,96	4,00	1,00	0,75	1,00
12	$4{,}65\cdot10^3$—$10\cdot10^3$	0,77	0,004	0,385	0,389	8,32	8,40	0,76	0,60	0,86
13	$2{,}15\cdot10^3$—$4{,}65\cdot10^3$	0,77	0,011	0,270	0,281	5,85	5,90	1,00	0,77	1,00
14	$1\cdot10^3$—$2{,}15\cdot10^3$	0,77	0,106	0,338	0,444	7,43	7,50	1,00	0,37	1,00
15	465·1000	0,77	0,015	0,458	0,473	9,9	10,0	—	—	—
16	215·465	0,77	0,028	0,504	0,532	10,89	11,0	—	—	—
17	100·215	0,77	0,037	0,522	0,559	11,29	11,4	—	—	—
18	46,5·100	0,77	0,053	0,522	0,575	11,39	11,5	—	—	—
19	21,5·46,5	0,77	0,072	0,522	0,594	11,39	11,5	—	—	—
20	10·21,5	0,77	0,105	0,522	0,627	11,39	11,5	—	—	—
21	4,65·10	0,77	0,154	0,522	0,676	11,49	11,6	—	—	—
22	2,15·4,65	0,77	0,220	0,522	0,742	11,49	11,6	—	—	—
23	1,0·2,15	0,77	0,330	0,522	0,852	11,51	11,7	—	—	—
24	0,465·1,0	0,77	0,490	0,522	1,012	11,71	11,9	—	—	—
25	0,215·0,465	0,77	0,720	0,522	1,242	12,0	12,1	—	—	—
26	Thermal	—	2,53	—	2,53	13,79	13,9	—	—	—

NOTE: All commas in tables represent decimal points.

A system of equations for computing the neutron danger function with respect to the capture γ-radiation has the form

$$\left.\begin{aligned} &-\nabla\varphi_1^{+j}+\Sigma_{y_n}^{j}\varphi_0^{+j}=\sum_{l=j+1}^{m}\Sigma_{in}^{j\to l}\varphi_0^{+l}+\Sigma_{\text{вним}}^{j\to j+1}\varphi_0^{+(j+1)}+\\ &+\sum_i k_i\beta_i\Sigma_{(n\gamma)}\{A_iE_2[\mu_{01}^{i}(d_0-x)]+(1-A_i)\times\\ &\times E_2[\mu_{02}^{i}(d_0-x)]\};\quad -\frac{1}{3}\nabla\varphi_0^{+j}+\Sigma_{tr}^{j}\varphi_1^{+j}=0, \end{aligned}\right\} \qquad (47)$$

with the conditions at the boundary $\frac{\varphi_1^{+j}}{2}+\frac{\varphi_0^{+j}}{4}=0$ when $x=x_s$, i.e., at the external boundary; $\frac{\varphi_1^{+j}}{2}-\frac{\varphi_0^{+j}}{4}=0$ when $x=0$, i.e., on the internal boundary, where

$$\varphi_0^{+j} = \frac{\int_{u_{j-1}}^{u_j} \varphi_0^+(u)\,du}{\Delta u_j}\ ;\quad \varphi_1^{+j} = \frac{\int_{u_{j-1}}^{u_j} \varphi_1^+(u)\,du}{\Delta u_j}\ .$$

The physical meaning of such boundary conditions is obvious. The danger of neutrons which are directed from the medium into the vacuum at the boundary is equal to zero, because neutrons of this type cannot enter the medium and consequently cannot produce capture γ-radiation.

The system of equations for computing the danger function with respect to the neutron dose on the external surface of the shielding is written in the form

$$\left.\begin{aligned} &-\nabla\varphi_1^{+j} + \Sigma_{y.n}^j \varphi_n^{+j} = \sum_{l=j+1}^{m} \Sigma_{in}^{j\to l}\varphi_0^{+l} + \\ &+ \Sigma_{\text{зам}}^{j\to j+1}\varphi_n^{+(j+1)}\ ; \\ &-\frac{1}{3}\nabla\varphi_0^{+j} + \Sigma_{tr}^j \varphi_1^{+j} = 0 \end{aligned}\right\} \qquad (48)$$

TABLE 2. CROSS SECTION OF INELASTIC TRANSITION $\sigma_{in}^{l\to j}$ FOR IRON AND FOR BORON-10.

Iron

j \ l	1	2	3	4	5
2	0,08				
3	0,19	0,22			
4	0,40	0,31	0,60		
5	0,34	0,33	0,14	0,46	
6	0,22	0,23	0,13	0,25	0,15
7	0,08	0,10	0,05	0,03	0,15
8	0,04	0,03	0,03	0,01	0,05
9	0,01	0,01	0	0	0,01

Boron 10

j \ l	1	2	3	4
2	0,03			
3	0,07	0,03		
4	0,11	0,04	0,04	
5	0,06	0,04	0,01	0,03
6	0,03	0,01	0,01	0

TABLE 3. GROUP CROSS SECTIONS FOR BORON ISOTOPES B^{10} and B^{11}.

j	B^{10}					B^{11}			
	σ_c	σ_{mod}	σ_{re}	σ_{tr}	σ_{tot}	σ_{mod}	σ_{re}	σ_{tr}	σ_{tot}
1	0,15	0,185	0,635	1,04	1,50	0,184	0,594	1,00	1,50
2	0,30	0,235	0,655	1,16	1,60	0,244	0,394	1,04	1,55
3	0,25	0,416	0,726	1,34	1,90	0,406	0,436	1,17	1,65
4	0,30	0,425	0,755	1,53	2,00	0,563	0,563	1,76	2,00
5	0,22	0,645	0,865	2,05	2,50	0,619	0,619	1,91	2,20
6	0,50	0,967	1,47	3,81	4,10	0,592	0,592	2,240	2,80
7	0,90	1,09	1,99	4,62	4,90	0,739	0,739	3,22	3,50
8	1,60	0,869	2,47	4,58	4,80	0,782	0,782	3,20	3,70
9	2,40	0,584	2,98	4,63	4,80	0,836	0,836	3,53	3,80
10	3,60	0,487	4,08	5,46	5,60	0,846	0,846	3,57	3,80
11	5,20	0,560	5,76	7,34	7,50	0,846	0,846	3,57	3,80
12	7,70	0,633	8,33	10,1	10,3	0,846	0,846	3,57	3,80
13	11,20	0,706	11,91	13,9	14,1	0,846	0,846	3,57	3,80
14	16,60	0,755	17,35	19,4	19,7	0,846	0,846	3,57	3,80
15	24,30	0,779	25,08	27,1	27,5	0,846	0,846	3,57	3,80
16	35,70	0,803	36,5	38,5	39,0	0,846	0,846	3,57	3,80
17	52,50	0,803	53,3	55,3	55,8	0,846	0,846	3,57	3,80
18	77,0	0,803	77,8	79,8	80,3	0,846	0,846	3,57	3,80
19	112	0,803	112,8	114,8	115	0,846	0,846	3,57	3,80
20	166	0,803	116,8	169	169	0,846	0,846	3,57	3,80
21	243	0,803	243,8	246	246	0,846	0,846	3,57	3,80
22	357	0,803	358	360	360	0,846	0,846	3,57	3,80
23	525	0,803	526	528	528	0,846	0,846	3,57	3,80
24	770	0,803	771	773	773	0,846	0,846	3,57	3,80
25	1120	0,803	1121	1123	1123	0,846	0,846	3,57	3,80
26	4000	—	4001	4001	4003	—	—	3,57	3,80

with the boundary conditions

$$\frac{\varphi_1^{+j}}{2} + \frac{\varphi_1^{+j}}{4} = f^{+j} \quad \text{when } x = x_s;$$

$$\frac{\varphi_1^{+j}}{2} - \frac{\varphi_0^{+j}}{4} = 0 \quad \text{when } x = 0.$$

Indeed, the neutrons on the internal boundary of the shielding, which are directed from the medium into the vacuum, cannot contribute to the dose measured at the external boundary, and therefore their danger is equal to zero. A neutron on the external boundary, directed from the medium into the vacuum, contributes directly to the dose corresponding to the biological effectiveness f^{+j}.

Figures 3 and 4 show the neutron danger functions relative to the capture γ-radiation in iron and in iron with an addition of 1 percent boron by weight. These functions describe the variation in the dose due to the capture γ-radiation on the surface of the shielding as a function of the coordinate and of the energy at which the neutron is injected into the shielding.

TABLE 4. GROUP CONSTANTS FOR HYDROGEN.

l \ k	$\sigma^{l\to l+k}$ 1	2	3	4	5	6	7	8	9	10	σ_c	σ_s	σ_{re}
1	0,400	0,240	0.176	0,096	0,064	0,032	0,016	0,009	0,004	0,003	0	1,20	1,04
2	0,512	0,375	0,205	0,136	0,068	0,034	0,018	0,008	0,004	0,003	0	1,65	1,36
3	0,767	0,418	0,279	0,139	0,070	0,037	0,018	0,009	0,004	0,002	0	2,20	1,74
4	0,975	0,650	0,325	0,163	0,087	0,040	0,019	0,009	0,004	0,003	0	3,00	2,27
5	1,558	0,779	0,389	0,209	0,097	0,045	0,021	0,010	0,004	0,004	0	4,10	3,12
6	2,065	1,033	0,553	0,257	0,119	0,055	0,026	0,012	0,006	0,004	0	5,70	4,13
7	2,936	1,572	0,732	0,338	0,157	0,073	0,034	0,016	0,007	0,004	0	8,10	5,87
8	4,270	1,986	0,919	0,427	0,199	0,092	0,013	0,020	0,009	0,008	0	11,0	7,97
9	5,238	2,430	1,128	0,524	0,243	0,113	0,052	0,024	0,011	0,010	0	14,0	9,77
10	6,210	2,882	1,338	0,621	0,288	0,134	0,062	0,029	0,013	0,011	0	16,6	11,55
11	6,921	3,212	1,491	0,692	0,321	0,149	0,069	0,032	0,015	0,013	0	18,5	12,92
12	7,220	3,350	1,556	0,727	0,335	0,156	0,072	0,033	0,016	0,013	0	19,3	13,47
13	7,369	3,420	1,588	0,737	0,342	0,159	0,074	0,034	0,016	0,014	0,001	19,7	13,75
14	7,482	3,472	1,612	0,748	0,347	0,161	0,075	0,035	0,016	0,014	0,001	20,0	13,75
15	7,520	3,489	1,620	0,752	0,349	0,162	0,075	0,035	0,016	0,014	0,002	20,1	14,03
16	7,557	3,506	1,628	0,756	0,351	0,163	0,076	0,035	0,016	0,014	0,003	20,2	14,10
17	7,557	3,506	1,628	0,756	0,351	0,163	0,076	0,035	0,030		0,001	20,2	14,10
18	7,594	3,524	1,636	0,759	0,352	0,164	0,076	0,066			0,006	20,3	14,17
19	7,594	3,524	1,636	0,759	0,352	0,164	0,142				0,009	20,3	14,17
20	7,594	3,524	1,636	0,759	0,352	0,306					0,014	20,3	14,17
21	7,594	3,524	1,636	0,759	0,658						0,020	20,3	14,17
22	7,594	3,524	1,636	1,417							0,030	20,3	14,17
23	7,594	3,524	3,053								0,044	20,3	14,17
24	7,594	6,577									0,064	20,3	14,17
25	7,594										0,093	20,3	14,17
26	14,17										0,332	20,3	

As we can see from figure 3, the danger function has a maximum, during its variation, which is close to the external boundary of the shielding. /19 This variation of the curves is due to two reasons, a decrease in the probability of γ-quanta absorption as the edge of the shielding is approached and an increase in the probability of neutron leakage from the shielding without the formation of γ-quanta.

Therefore, the danger function increases up to certain points of the shielding where the leakage of neutrons is still small. Near the boundary where the neutron leakage effect becomes substantial, the danger function drops. The danger function decreases as the energy increases (fig. 3), because the formation of γ-radiation decreases due to a decrease in $\Sigma_{(n\gamma)}$.

When boron is introduced, there is a slight change in the distribution of the danger functions. In particular, neutrons of low energy in the shielding points situated far away from the external boundary have a smaller danger than neutrons of higher energy. In pure iron a neutron may diffuse over a /20 definite distance and only then be captured by the iron with the formation of the γ-quantum.

The addition of boron to iron leads to a decrease in the migration length of neutrons, particularly of those with small energy which are absorbed practically at the same place where they are bred. Therefore, the path traveled

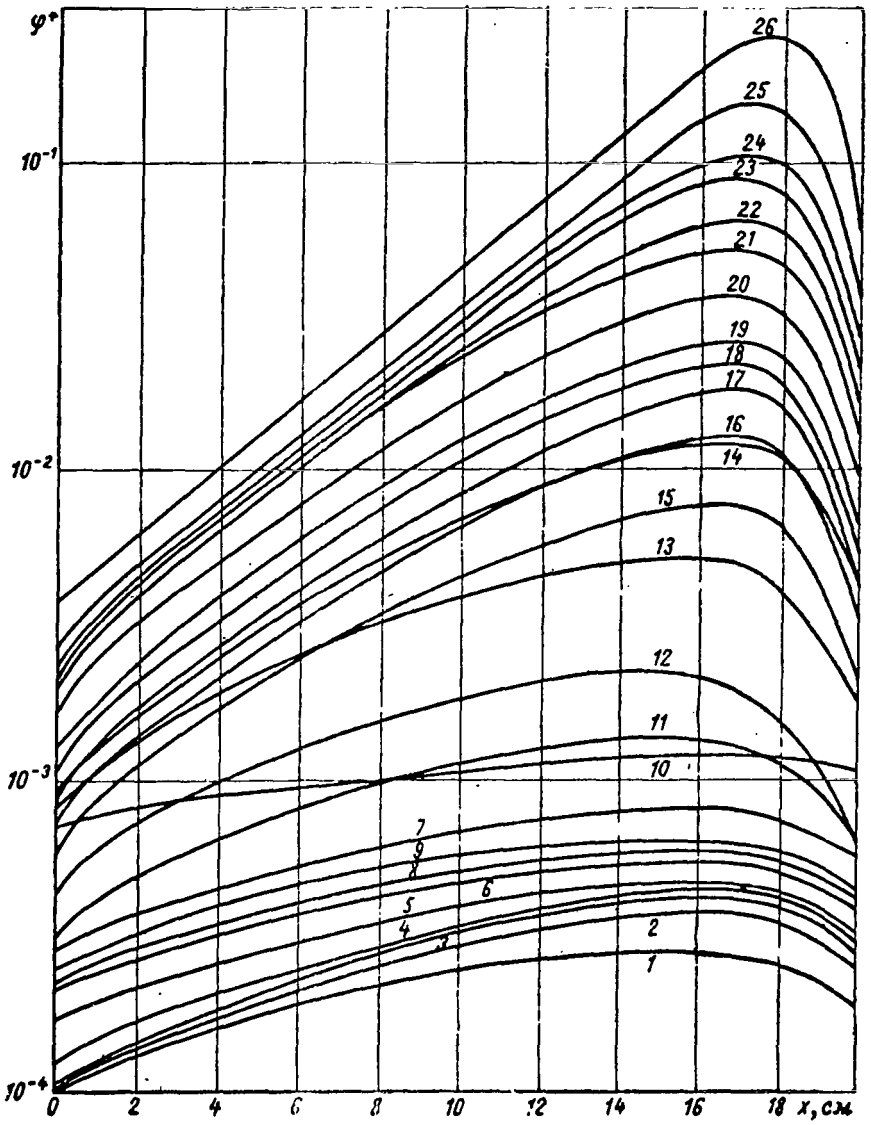

Figure 3. Danger function of neutrons with respect to capture γ-radiation in iron (numbers above curves designate numbers of energy groups; for breakdown of energy interval according to groups, see table 1).

by the γ-quanta to the surface of the shielding increases, which leads to a decrease in the danger function at points of the shielding away from the surface. The introduction of boron produces a decrease in the danger of soft neutron groups, also due to the occurrence of a competing process of neutron capture by boron nuclei without the generation of hard γ-radiation. In principle it is possible that with further addition of boron to iron the danger function of neutrons with low energy will be less over the entire thickness of the shielding.

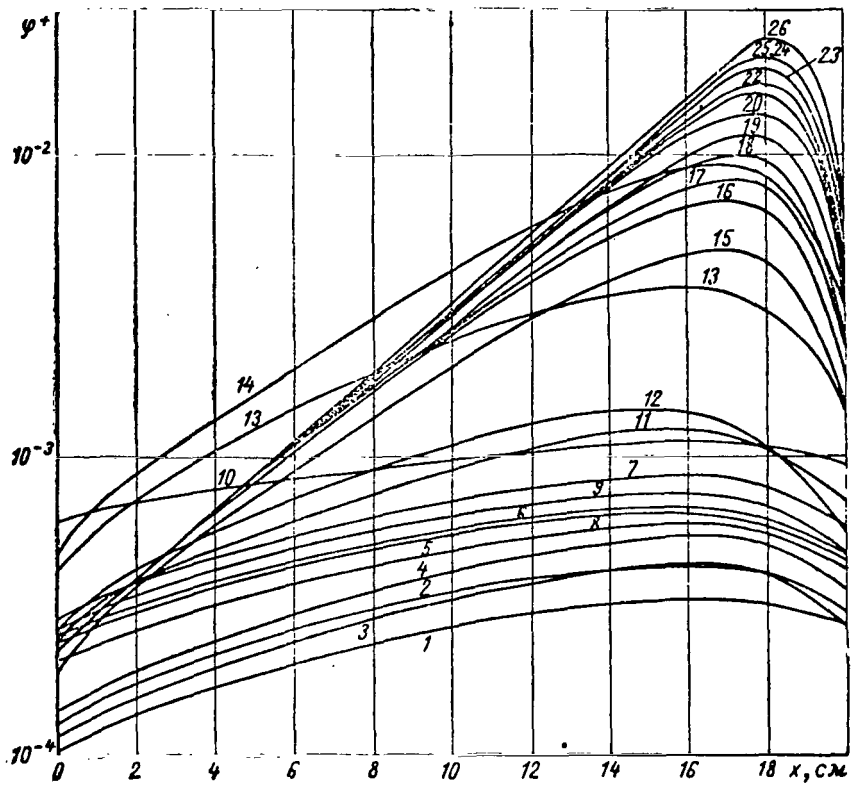

Figure 4. Neutron danger function with respect to capture γ-radiation in iron with addition of 1 percent boron by weight.

Figure 5 shows the danger function according to the neutron dose measured at the external surface of the shielding as a function of the coordinate and of the energy at which the neutrons are injected into the shielding. Such a function increases monotonically over the thickness, because as the neutron is injected closer to the surface, the probability of its leakage from the shielding increases, together with the possibility of its contribution to the dose.

The three-dimensional distribution of the danger function for neutrons of the 10th group with respect to the captured radiation and the neutron dose has a rather shallow nature. This is explained by the presence of a drop in the variation of the iron cross section in the 10th group, as a result of which a neutron of given energy diffuses freely over the entire thickness of the /21 iron. As a result the quantity of γ-quanta and the dosage due to neutrons on the surface of the shielding depend very little on the coordinate of the point where the neutrons are injected.

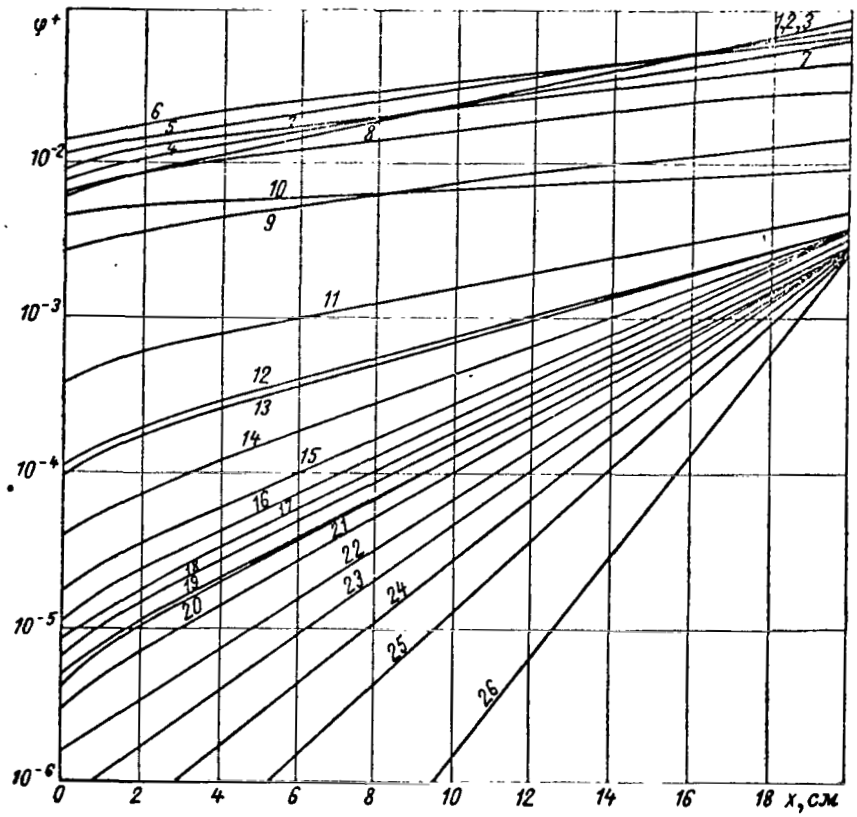

Figure 5. Danger function with respect to neutron dose measured on external surface of shielding.

To clarify the effect produced by the introduction of boron and hydrogen on the dose due to the capture γ-radiation and due to neutrons, we utilize the theory of perturbations. The equation of the theory of perturbations for a multiple group system of equations in the P_1-approximation has the form

$$\delta D = \int dx \left\{ \sum_{j=1}^{26} \left[\delta p^j \varphi_0^j - \delta \Sigma_c^j \varphi_0^{+j} \varphi_0^j + \delta \Sigma_{\text{зам}}^{j \to j+1} \varphi_0^j (\varphi_0^{+(j+1)} - \right.\right.$$
$$\left.\left. - \varphi_0^{+j}) + \varphi_0^j \sum_{l=j+1}^{26} \delta \Sigma_{in}^{j \to l} (\varphi_0^{+l} - \varphi_0^{+j}) - 3 \delta \Sigma_{tr}^j \varphi_1^j \varphi_1^{+j} \right] \right\} \qquad (49)$$

Integration is carried out within the limits of the region where perturbation takes place.

In the case when in the region from x_1 to x_2 (fig. 2) there is a variation in the attenuation properties with respect to γ-quanta and in the neutron

capture cross section $\Sigma_{(n\gamma)}$, the expression for $\delta p(x)$ in equation (49) assumes the following form when $0 \leq x \leq x_1$

$$\delta p^j(x) = \sum_i \beta_i k_i \Sigma^j_{(n\gamma)} \{[A_i E_2(\mu^i_{01}(d_0 - x) + \Delta\mu^i_{01}(x_2 - x_1)) + (1 - A_i) E_2(\mu^i_{02}(d_0 - x) + \Delta\mu^i_{02}(x_2 - x_1))] - [A_i E_2(\mu^i_{01}(d_0 - x)) + (1 - A_i) E_2(\mu^i_{02}(d_0 - x))]\}; \quad (50)$$

when $x_1 \leq x \leq x_2$ /22

$$\delta p^j(x) = \sum_i \beta_i k_i \{\Sigma^{j'}_{(n\gamma)} [A_i E_2(\mu^i_{01}(d_0 - x) + \Delta\mu^i_{01}(x_2 - x)) + (1 - A_i) E_2(\mu^i_{02}(d_0 - x) + \Delta\mu^i_{02}(x_2 - x))] - \Sigma^j_{(n\gamma)} [A_i E_2(\mu^i_{01}(d_0 - x)) + (1 - A_i) E_2(\mu^i_{02}(d_0 - x))]\}; \quad (51)$$

when $x > x_2$

$$\delta p^j(x) = 0, \quad (52)$$

$(x = x)$

where $\Delta\mu^i$ is the variation in the coefficient of linear γ-quanta attenuation with energy E_i, $\Delta\mu^i_{01} = \Delta\mu^i(1 + \alpha^i_1)$, $\Delta\mu^i = \mu^{i'} - \mu^i$.

We return to the consideration of plane shielding made of iron with a thickness of 20 cm, which is subjected to neutrons of the fission spectrum. As these neutrons are captured by the iron, they generate γ-quanta which produce a definite dose associated with γ-quanta as they exit to the external surface of the shielding. Let us investigate the variation of this dose as a function of the location where boron and hydrogen are introduced into the shielding. The three-dimensional energy distribution of neutrons in the iron layer is shown in figure 6.

Figure 7 shows the relative variation in the dose $\delta D/D$ as a function of the location where boron is introduced. Boron is introduced in place of iron in a layer with a thickness of 0.1 cm in the amount of 1 percent by weight. As we can see from the illustration, effectiveness of boron close to the edge of the shielding is approximately ten times greater than at the beginning of the layer.

The variation in $\delta D/D$ as a function of the point where hydrogen is introduced is shown in figure 8. Hydrogen is introduced in the quantity of 5 percent by volume in a layer of thickness 0.1 cm and a density of 0.111 g/cm^3. The curve $\delta D/D$, as shown in figure 8, has a maximum when $x \simeq 10$ cm.

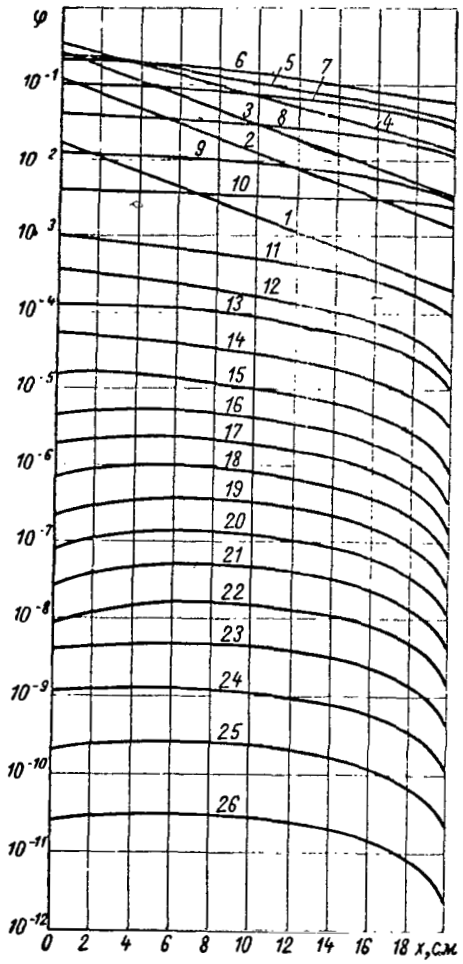

Figure 6. Neutron fluxes in iron shielding.

We should point out that the leakage of neutrons from the iron layer is rather high (approximately 96 percent), and the capture of a neutron takes place basically for fast neutrons with $E \simeq 50$ keV-1 MeV. In the first layers of iron some softening of the neutron spectrum takes place, as a result of which the action of hydrogen increases and the curve $\delta D/D$ increases. Beginning with $x \simeq 10$ cm, the effect of the boundary on the distribution of fast neutrons becomes more pronounced, while the variation of the spectrum practically ceases. Due to the effect of the boundary, the danger function of fast neutrons, which are primarily responsible for the capture, becomes shallow at first and then drops towards the edge of the shielding. The drop in $\delta D/D$ close to the external boundary, when iron is replaced by hydrogen, produces an effect which also decreases the quantity of the formed γ-quanta, due to the lowering of the value in the macroscopic neutron capture cross section

(the term $\delta p^j \varphi^j$). If iron is replaced by boron this further increases the negative action of boron.

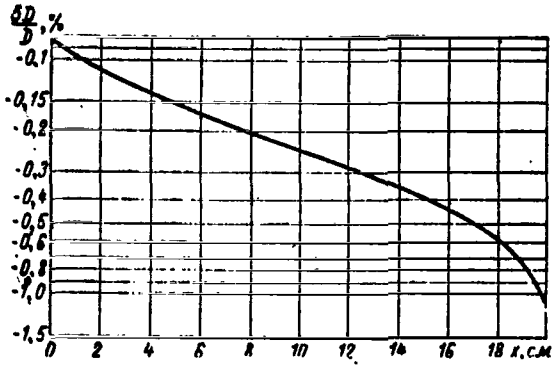

Figure 7. Relative variation of dose (δD/D) due to capture radiation as function of place where boron is introduced.

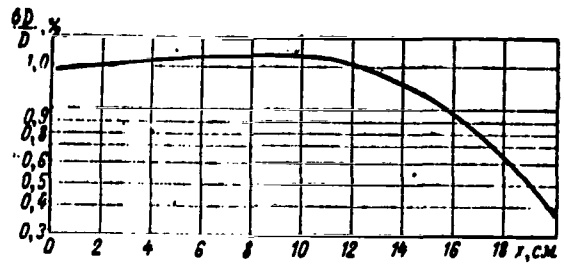

Figure 8. Relative variation in dose (δD/D) due to capture radiation as function of place where hydrogen is introduced.

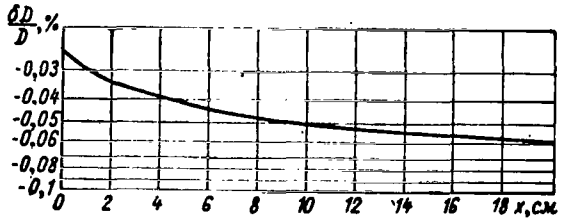

Figure 9. Relative variation of neutron dose (δD/D) as function of place where boron is introduced.

The variation in δD/D due to the neutron dose as a function of the place /24 where boron is introduced is shown in figure 9. Boron is introduced into a layer with a thickness of 0.1 cm in a quantity of 1 percent by weight. The action of boron (fig. 9) leads to a decrease in the dose due to neutrons. This is explained by the fact that the dose due to neutrons beyond the iron with a thickness of 20 cm primarily forms neutrons with an energy of approximately 500 keV, for which the action of boron is more pronounced than the action of iron. The increase in $\left|\frac{\delta D}{D}\right|$, as we move away from the internal edge of the shielding, is due to a certain softening of the neutron spectrum as a result of which the action of boron increases.

In conclusion we compute the variation in δD/D due to the capture radiation in the case when boron is introduced over the entire layer of iron. The calculations carried out with the exact equations of the theory of perturbations, utilizing the unperturbed flux and the perturbed danger function, give us a value δD/D = 75 percent. The effect computed by means of equations of

the theory of small perturbations utilizing an unperturbed flux and an unperturbed danger function give us a value $\delta D/D = 65$ percent. Consequently the equations of small perturbations in this case yield an acceptable accuracy.

The authors express their gratitude to A. I. Leypunskiy, V. Ya. Pupko and E. Ye. Petrov for useful advice and remarks.

REFERENCES

1. Usachev, L. N. Equations for the Value of Neutrons in a Kinetic Reactor and the Theory of Perturbations (Uravneniye dlya tsennosti neytronov kineticheskogo reaktora i teoriya vozmushcheniy). IN: Reactor Construction and Theory (Reaktorostroyeniye i teoriya reaktorov). Izd-vo AN SSSR, Moscow, 1955.

2. Weinberg, A. Am. J. Phys., Vol. 20, p. 401, 1952.

3. Glesston, S. and Edlund, M. The Basic Theory of Nuclear Reactors (Osnovy teorii yadernykh reaktorov). Izdatel'stvo Inostrannaya Literatura (I. L.), Moscow, p. 417, 1954.

4. Pupko, V. Ya. Physics and Heat Engineering of Reactors, Appendix No. 1, J. Atomic Energy (Fizika i teplotekhnika reaktorov, Prilozheniye No. 1 k zhurnalu Atomnaya energiya), 1958.

5. Kadomtsev, B. B. Dokl. AN SSSR, Vol. 113, p. 652, 1957.

6. Marchuk, G. I. and Orlov, V. V. IN: Neutron Physics (Neytronnaya fizika). Gosatomizdat, p. 30, 1961.

7. Marchuk, G. I. Methods of Calculating Nuclear Reactors (Metody rascheta yadernykh reaktorov). Gosatomizdat, Moscow, 1961.

THREE-DIMENSIONAL ENERGY DISTRIBUTION OF FAST NEUTRONS IN HYDROGEN

Sh. S. Nikolayshvili

An isotropic point source of monoenergetic neutrons in an infinite hydrogen medium is given. It is required to find the energy distribution of fast neutrons at various distances from the source. /24

For the spectral characteristic of the neutron field we utilize the neutron flux function $N_0(r, E)$ which is determined in the following manner.

If r is the distance of the considered point in space from the source, S is a sphere with a unit cross section of the large circle and with the center at this point, while E is the energy of the neutron in megaelectron volts, the total number of neutrons with energies within the interval (E, E + dE) intersecting the sphere S per unit time is equal to $N_0(r, E)\,dE$.

The problem of determining the function $N_0(r, E)$ is reduced to the solution of equation (refs. 1, 2 and 3).

$$\mu\frac{\partial\Phi}{\partial r}+\frac{1-\mu^2}{r}\cdot\frac{\partial\Phi}{\partial\mu}+\sigma\Phi=\frac{1}{2\pi}\int_0^u du'\sigma_s(u')\,e^{u'-u}\int_0^{2\pi}d\alpha\int_{-1}^{+1}d\mu'\delta(\mu_1-\\ -e^{\frac{u'-u}{2}})\Phi(r,\mu',u')+\frac{1}{2}\cdot\frac{\delta(r)\,\delta(u)}{4\pi r^2}, \tag{1}$$

where $\mu_1 = \mu\mu' + \sqrt{1-\mu^2}\sqrt{1-\mu'^2}\cos\alpha$. In the region of high energies /25 $\sigma(u) \equiv \sigma_s(u)$, while $\sigma_s(u)$ is obtained (ref. 4) by means of equation

$$\sigma_s(u)=\pi\left[\frac{3}{y^2+(0{,}089y^2-1{,}85)^2}+\frac{1}{y^2+(0{,}135y^2+0{,}422)^2}\right], \tag{2}$$

where $y^2 = 1.21\,e^{-u}$; E_0 is the initial energy of the neutrons; $u = \ln E_0/E$.

The unknown function $N_0(r, E)$ is determined from the relationship

$$N_0(r,\ E)=\frac{1}{E}\Phi_0(r,\ u), \tag{3}$$

where

$$\Phi_0(r,\ u)=\int_{-1}^{+1}\Phi(r,\ \mu,\ u)\,du, \tag{4}$$

while Φ (r, μ, u) is the solution of equation (1), which becomes equal to 0 when $r \to \infty$.

The approximate calculation of the function Φ_0 (r, u) is achieved by utilizing the method of moments (refs. 1 and 5), which consists of finding several first even moments of the function Φ_0 (r, u) from equation (1)

$$\Phi^0_{2n}(u)=\frac{1}{(2n)!}\int_0^{\infty}4\pi r^2\Phi_0(r,\ u)\,r^{2n}\,dr,\ n=0,\ 1,\ 2,\ \ldots, \tag{5}$$

and then constructing its approximate representation from the established moments of the function. In the present work this representation is constructed by means of the first three moments, utilizing a method described in reference 6.

The determination of the corresponding moments of the function, after the nonscattered part of the neutron field is eliminated, reduces to the solution of a system of six integral equations having a form

$$\sigma(u)\,y(u)=\int_0^{u}\sigma_s(u')\,Q_v\left(e^{\frac{u'-u}{2}}\right)y(u')\,du'+f(u), \tag{6}$$

where f (u) is a continuous function of u, while $Q_v\left(e^{\frac{u'-u}{2}}\right)$ is a polynomial of degree v with respect to $e^{\frac{u'-u}{2}}$

$$Q_v\left(e^{\frac{u'-u}{2}}\right)=\sum_{q=0}^{v}a_q e^{\frac{q}{2}(u'-u)}. \tag{7}$$

Equation (6) is easily solved by numerical integration. Below we describe the method. We lay out the points u_k, $u_k = kh$, $k = 0, 1/2, 1, 3/2, \ldots$, along the u axis, where h is a constant, and adopt the designation

$$y_k = y(u_k),\ \sigma_k = \sigma(u_k),\ \text{etc.} \tag{8}$$

If we introduce the new functions

$$A_q(u) = \int_0^u \sigma_s(u')\, e^{\frac{q}{2}(u'-u)} y(u')\, du', \tag{9}$$

equation (6) may be rewritten in the form

$$\sigma(u)\, y(u) = \sum_{q=0}^{\nu} a_q A_q(u) + f(u). \tag{10}$$

Assuming that $u = u_k$ in this equation, we obtain

$$\sigma_k y_k = \sum_{q=0}^{\nu} a_q A_{qk} + f_k. \tag{11}$$

Here, in view of the adopted designation

$$A_{qk} = \int_0^{u_k} \sigma_s(u')\, e^{\frac{q}{2}(u'-u_k)} y(u')\, du'. \tag{12}$$

Since $u_k = u_{k-1} + h$, the last expression may be written in the form /26

$$A_{qk} = e^{-\frac{qh}{2}} \int_0^{u_{k-1}} \sigma_s(u')\, e^{\frac{q}{2}(u'-u_{k-1})} y(u')\, du' + \int_{u_{k-1}}^{u_k} \sigma_s(u')\, e^{\frac{q}{2}(u'-u_{k-1})} y(u')\, du'$$

or

$$A_{qk} = e^{-\frac{qh}{2}} A_{q,\,k-1} + \int_{u_{k-1}}^{u_k} \sigma_s(u')\, e^{\frac{q}{2}(u'-u_{k-1})} y(u')\, du'.$$

We make use of the Simpson equation to compute the integral in the right side. In this case

$$A_{qk} = e^{-\frac{qh}{2}} A_{q,\,k-1} + \frac{h}{6}\left(\sigma_{s,\,k-1} e^{-\frac{qh}{2}} y_{k-1} + 4\sigma_{s,\,k-1/2} e^{-\frac{qh}{4}} y_{k-1/2} + \sigma_{sk} y_k\right). \tag{13}$$

Substituting the resulting expression A_{qk} into equation (10), we obtain the following equation for computing the values of y_k

$$\left(\sigma_k - \frac{\sigma_{sk} h}{6} \sum_{q=0}^{\nu}{}' a_q\right) y_k = \sum_{q=0}^{\nu}{}' a_q \left(e^{-\frac{qh}{2}} A_{q,\,k-1} + \frac{h}{6}\sigma_{s,\,k-1} \times \right.$$
$$\left. \times e^{-\frac{qh}{2}} y_{k-1} + \frac{4h}{6}\sigma_{s,\,k-1/2} e^{-\frac{qh}{4}} y_{k-1/2}\right). \tag{14}$$

Relationships (14) and (13) jointly yield an approximate solution of equation (6), if we know the values y_0, $y_{1/2}$, A_{q0}, $A_{q,1/2}$ (q = 0, 1, ..., v). When u = 0 we have

$$y_0 = \frac{f_0}{\sigma_0}; \quad A_{q0} = 0.$$

The values when $u = u_{1/2}$ may be obtained if we use the trapezoidal equation for computing the respective integrals.

After the moments Φ_0^0, Φ_2^0, Φ_4^0 have been established, the function Φ_0 (r, u) may be determined by means of the approximate equation

$$4\pi r^2 \Phi_0(r, u) = A r^{\nu} e^{-\alpha r} + e^{-\sigma r}\delta(u), \tag{15}$$

where

$$\nu = \frac{7p - 3 + \sqrt{1 + 14p + p^2}}{2(1-p)}; \quad p = \frac{(\Phi_2^0)^2}{6\Phi_0^0\Phi_4^0};$$

$$\alpha = \sqrt{\frac{(\nu+1)(\nu+2)}{2}\cdot\frac{\Phi_0^0}{\Phi_2^0}}; \quad A = \frac{\alpha^{\nu+1}\Phi_0^0}{2\Gamma(\nu+1)}; \quad \Gamma(\nu+1) = \int_0^{\infty} t^{\nu} e^{-t}\, dt.$$

To control the calculations it is useful to note that when u = 0, A = σ_{s0}, v = 1 and $\alpha = \sigma_0$.

TABLE 1

E_0 = 2 MeV

E, MeV \ r, см	10	20	30	40	50	60
2,000	0,9713	1,943	2,914	3,885	4,856	5,828
1,902	0,9929	2,011	3,052	4,115	5,203	6,311
1,810	1,015	2,079	3,188	4,346	5,541	6,797
1,638	1,063	2,222	3,465	4,791	6,208	7,717
1,482	1,116	2,373	3,747	5,237	6,850	8,587
1,341	1,171	2,531	4,035	5,681	7,477	9,350
1,213	1,232	2,696	4,331	6,128	8,095	10,24
1,098	1,296	2,869	4,636	6,581	8,710	11,02
0,993	1,362	3,050	4,950	7,040	9,322	11,79
0,899	1,433	3,238	5,274	7,298	9,939	12,55
0,813	1,507	3,434	5,609	7,980	10,56	13,33
0,736	1,584	3,639	5,955	8,481	11,20	14,09

TABLE 2

E_0 = 4 MeV

E, MeV \ r, см	10	20	30	60	90
4,000	0,3209	0,6419	0,9682	1,969	3,004
3,805	0,3237	0,6544	0,9922	2,049	3,299
3,619	0,3288	0,6677	1,017	2,124	3,600
3,275	0,3389	0,6967	1,070	2,276	4,226
2,963	0,3506	0,7286	1,126	2,430	5,088
2,681	0,3634	0,7635	1,188	2,588	5,598
2,426	0,3772	0,8011	1,253	2,749	6,357
2,195	0,3922	0,8416	1,323	2,916	7,177
1,797	0,4255	0,9306	1,475	3,270	9,035
1,472	0,4633	1,031	1,645	3,654	11,24
1,205	0,5064	1,153	1,833	4,072	13,90
0,986	0,5532	1,265	2,039	4,535	17,11

This method was used to compute the distribution of fast neutrons (with energies greater than 1 MeV) in pure hydrogen with a density equal to the density of the hydrogen nucleus in ordinary water, $n = \frac{2 \cdot 6.023 \cdot 10^{23}}{18} = 0.6692 \cdot 10^{23}$ nuclei of hydrogen per cubic centimeter.

It was assumed that we had an isotropic monoenergetic point source which emits one neutron with an energy E_0 every second. The initial energy /29 E_0 was assumed to be equal to 2, 4, 6, 8, 10, 12 and 14 MeV.

TABLE 3.

E_0 = 6 MeV

r, см / E, MeV	10	20	30	60	90
6,000	0,1586	0,3173	0,4759	0,9518	1,428
5,707	0,1603	0,3212	0,4827	0,9708	1,463
5,429	0,1620	0,3255	0,4900	0,9902	1,498
4,912	0,1659	0,3353	0,5066	1,031	1,566
4,445	0,1701	0,3463	0,5252	1,074	1,636
4,022	0,1748	0,3585	0,5459	1,121	1,708
3,639	0,1798	0,3721	0,5685	1,172	1,785
3,293	0,1857	0,3868	0,5932	1,227	1,866
2,980	0,1919	0,4029	0,6200	1,285	1,951
2,696	0,1985	0,4201	0,6489	1,349	2,046
2,207	0,2136	0,4588	0,7129	1,487	2,242
1,807	0,2309	0,5026	0,7856	1,644	2,467
1,480	0,2507	0,5521	0,8673	1,819	2,718
1,211	0,2730	0,6073	0,9580	2,013	2,997
0,992	0,2980	0,6684	1,058	2,228	3,307

TABLE 4

E_0 = 8 MeV

r, см / E, MeV	10	20	30	60	90
8,000	0,09278	0,1818	0,2671	0,5023	0,7085
7,610	0,09363	0,1834	0,2696	0,5073	0,7158
7,239	0,09440	0,1852	0,2723	0,5123	0,7223
6,550	0,09619	0,1892	0,2785	0,5244	0,7387
5,926	0,09816	0,1939	0,2859	0,5386	0,7574
5,363	0,1003	0,1991	0,2942	0,5549	0,7789
4,852	0,1028	0,2050	0,3036	0,5734	0,8032
4,390	0,1054	0,2115	0,3141	0,5939	0,8305
3,973	0,1084	0,2187	0,3255	0,6166	0,8608
3,595	0,1116	0,2266	0,3381	0,6414	0,8940
2,943	0,1189	0,2444	0,3665	0,6979	0,9699
2,410	0,1276	0,2650	0,3995	0,7635	1,058
1,973	0,1376	0,2888	0,4373	0,8386	1,160
1,615	0,1506	0,3158	0,4801	0,9235	1,276
1,322	0,1621	0,3460	0,5283	1,019	1,402
1,083	0,1769	0,3800	0,5816	1,124	1,548

TABLE 5

E_0 = 10 MeV

r, см / E, MeV	10	20	30	60	90
10,00	0,06253	0,1251	0,1876	0,3751	0,5621
9,512	0,06300	0,1259	0,1887	0,3765	0,5630
9,048	0,06346	0,1268	0,1901	0,3783	0,5641
8,187	0,06453	0,1290	0,1932	0,3833	0,5691
7,408	0,06563	0,1315	0,1969	0,3898	0,5766
6,703	0,06787	0,1343	0,2013	0,3980	0,5866
6,065	0,06819	0,1375	0,2062	0,4077	0,5994
5,488	0,06978	0,1411	0,2120	0,4188	0,6147
4,966	0,07146	0,1452	0,2184	0,4319	0,6322
4,493	0,07333	0,1495	0,2254	0,4460	0,6525
4,066	0,07537	0,1543	0,2331	0,4617	0,6742
3,679	0,07763	0,1596	0,2416	0,4792	0,6995
3,012	0,08262	0,1716	0,2608	0,5188	0,7559
2,466	0,08877	0,1857	0,2832	0,5657	0,8235
2,019	0,09578	0,2018	0,3089	0,6189	0,9005
1,653	0,1038	0,2202	0,3381	0,6798	0,9875
1,353	0,1129	0,2410	0,3710	0,7480	1,087
1,108	0,1232	0,2642	0,4076	0,8234	1,196

TABLE 6

E_0 = 12 MeV

r, см / E, MeV	10	20	30	60	90
12,00	0,04373	0,08745	0,1289	0,2512	0,3671
11,42	0,04403	0,08719	0,1295	0,2573	0,3657
10,86	0,04434	0,08773	0,1302	0,2517	0,3650
9,825	0,04499	0,08894	0,1318	0,2533	0,3649
8,890	0,04568	0,09033	0,1337	0,2560	0,3668
8,044	0,04647	0,09192	0,1360	0,2596	0,3705
7,278	0,04731	0,09374	0,1387	0,2645	0,3759
6,586	0,04827	0,09580	0,1418	0,2698	0,3828
5,959	0,04931	0,09809	0,1454	0,2763	0,3913
5,392	0,05047	0,1007	0,1493	0,2838	0,4013
4,879	0,05175	0,1035	0,1537	0,2923	0,4129
4,415	0,05316	0,1066	0,1585	0,3018	0,4259
3,614	0,05639	0,1138	0,1697	0,3239	0,4565
2,959	0,06023	0,1224	0,1830	0,3502	0,4933
2,423	0,06473	0,1323	0,1984	0,3806	0,5365
1,984	0,06993	0,1437	0,2162	0,4162	0,5863
1,624	0,07590	0,1568	0,2364	0,4562	0,6428
1,330	0,08266	0,1714	0,2591	0,5012	0,7046

TABLE 7

E_0 = 14 MeV

$\sigma_0 r$ / E, MeV	0,4	1,0	2,0	3,0	4,0
14,00	0,02857	0,07143	0,1429	0,2143	0,2857
11,46	0,02938	0,07294	0,1441	0,2135	0,2812
9,384	0,03030	0,07498	0,1471	0,2163	0,2823
7,683	0,03139	0,07766	0,1518	0,2222	0,2889
6,291	0,03270	0,08110	0,1585	0,2314	0,3000
5,150	0,03429	0,08540	0,1671	0,2438	0,3154
4,217	0,03621	0,09066	0,1777	0,2594	0,3354
3,452	0,03850	0,09695	0,1907	0,2784	0,3599
2,827	0,04119	0,1044	0,2060	0,3009	0,3891
2,314	0,04434	0,1130	0,2238	0,3273	0,4232
1,894	0,04797	0,1229	0,2442	0,3576	0,4624
1,551	0,05212	0,1342	0,2672	0,3918	0,5068
1,270	0,05680	0,1469	0,2932	0,4302	0,5568

The results of the calculations are shown on tables 1-7 and are presented in the form of the function $4\pi r^2 N_0 (r, E)$.[1]

The author expresses his deep gratitude to G. I. Marchuk for his valuable remarks and to T. I. Stavinskaya for the great deal of work she has performed in carrying out the numerical calculations.

REFERENCES

1. Gol'dshteyn, G. Principles of Reactor Shielding (Osnovy zashchity reaktorov). Gosatomizdat, Moscow, 1961.

2. Devison, B. The Theory of Neutron Transport (Teoriya perenosa neytronov). Atomizdat, Moscow, 1960.

[1] Analogous results for E_0 = 8.096 MeV are presented in reference 1. At substantial distances from the source these results vary significantly from the results of the present work. By extrapolating the function $4\pi r^2 N_0 (r, E)$, it was established that the value of σ_0 utilized in the computations of reference 1 was taken equal to 0.0784 cm, while in our calculations we assumed σ_0 = 0.0758 cm. The difference in the values of σ_0 completely explains this discrepancy.

3. Marchuk, G. I. Methods of Computing Nuclear Reactors (Metody rascheta yadernykh reaktorov). Gosatomizdat, Moscow, 1961.

4. Nuclear Reactors. Materials published by the Atomic Energy Commission, U.S.A. Part 1, Izd-vo, I. L., Moscow, 1956.

5. Ptitsyn, A. P. Atomnaya Energiya, Vol. 10, 1, 1961.

6. Nikolayshvili, Sh. S. Atomnaya Energiya, Vol. 10, 3, 1961.

THREE-DIMENSIONAL DISTRIBUTION OF NEUTRONS IN AN INFINITE HOMOGENEOUS MEDIUM WITH A POINT UNIDIRECTIONAL SOURCE

A. P. Suvorov, Ye. B. Breshenkova and V. V. Orlov

This work considers three-dimensional distribution of neutrons in an /30
infinite homogeneous medium with a point unidirectional source. The solution is carried out using a single velocity approximation. The determination of the three-dimensional distribution is reduced to the solution of the conjugate kinetic equation with an isotropic right part, which is solved by the method of moments.

A detailed examination is made of the physical meaning associated with the conjugate equation and its solution, the expediency of its utilization in the solution of specific problems. The distribution of fast neutrons in iron is computed and the results of the calculation are compared with experimental results.

Physical Meaning of Kinetic Conjugate Equation and its Solution

For the sake of brevity we write the kinetic equation, for an arbitrary distribution of sources, in the operational form, i.e., without writing out the left part of the kinetic equation in detail we designate it by LF (r, Ω, E) and obtain

$$LF(\mathbf{r}, \Omega, E) = q(\mathbf{r}, \Omega, E), \tag{1}$$

where L is a linear operator of the kinetic equation; F (r, Ω, E) is the radiation flux at the point r with velocity direction Ω and energy E from the distributed sources q (r, Ω, E); q (r, Ω, E) is a known source distribution function, i.e., the number of particles emitted every 1 sec at point r with energy E and with velocity direction Ω.

Any physical quantity, which is associated in a linear manner with the radiation flux F (r, Ω, E) from distributed sources q (r, Ω, E), may be expressed in the form of a triple integral over drdΩdE in the following manner

$$J_p = \int F(\mathbf{r}, \Omega, E)\, p(\mathbf{r}, \Omega, E)\, d\mathbf{r}\, d\Omega\, dE, \qquad (2)$$

where p (r, Ω, E) is a known function characterizing the relationship between quantity J_p and flux F, while the limits for the variation of variables associated with the observation point are determined from physical considerations. For example:

1. The radiation flux at an arbitrarily fixed point r' with a velocity direction Ω' and energy E' from the distributed sources is equal to

$$J_{\delta(\mathbf{r}-\mathbf{r}')\delta(\Omega-\Omega')\delta(E-E')}(\mathbf{r}', \Omega', E') = \int d\mathbf{r}\, d\Omega\, dE\, F(\mathbf{r}, \Omega, E)\, \delta(\mathbf{r}-\mathbf{r}')\delta(\Omega-\Omega')\, \delta(E-E'),$$

i.e., p (r, Ω, E) = δ (r-r') δ (Ω-Ω') δ (E-E') depends parametrically on r', Ω', E'.

2. The total radiation flux, i.e., the flux integrated over all possible velocity directions at an arbitrarily fixed point r' with energy E' from the distributed sources is equal to

$$J_{\delta(\mathbf{r}-\mathbf{r}')\delta(E-E')}(\mathbf{r}', E') = \int d\mathbf{r}\, d\Omega\, dE\, F(\mathbf{r}', \Omega', E')\, \delta(\mathbf{r}-\mathbf{r}')\, \delta(E-E'),$$

and depends parametrically on r' and E'; p (r, Ω, E) = δ (r-r') δ (E-E').

3. The number of collisions per 1 sec in an arbitrarily fixed point r' is equal to

$$J_{\Sigma(E)\delta(\mathbf{r}-\mathbf{r}')}(\mathbf{r}') = \int d\mathbf{r}\, d\Omega\, dE\, F(\mathbf{r}, \Omega, E)\, \Sigma(E)\, \delta(\mathbf{r}-\mathbf{r}'),$$

where Σ (E) is the total macroscopic cross section.

4. The count of a collimated detector per 1 sec at an arbitrarily fixed point r' during the collimation of the incident radiation in the direction Ω' is equal to /31

$$J_{\Sigma_D(E)\delta(\mathbf{r}-\mathbf{r}')\delta(\Omega-\Omega')}(\mathbf{r}', \Omega') = \int d\mathbf{r}\, d\Omega\, dE\, F(\mathbf{r}, \Omega, E)\, V\Sigma_D(E)\, \delta(\mathbf{r}-\mathbf{r}')\, \delta(\Omega-\Omega'),$$

where V is the volume of the detector; Σ_D (E) is the cross section of the detector.

5. The count of an isotropic detector at the point r' during 1 sec is equal to

$$J_{\Sigma_D(E)\delta(r-r')r'} = \int dr\, d\Omega\, dE\, F(r, \Omega, E)\, V\Sigma_D(E)\, \delta(r - r').$$

6. The dose at an arbitrarily fixed point r' from the distributed sources is equal to

$$J_{\delta(r-r')}(r') = \int dr\, d\Omega\, dE\, F(r, \Omega, E)\, \delta(r - r')\, D(E),$$

where D (E) is a dose corresponding to the unit radiation flux with energy E.

7. The integral dose from the distributed sources is equal to

$$J_D = \int dr\, d\Omega\, dE\, F(r, \Omega, E)\, D(E).$$

Let us consider the same physical quantity J_p not from the arbitrarily distributed sources q (r, Ω, E), but rather from an elementary source q (r, Ω, E) = δ (r-r_0) δ (Ω-Ω_0) δ (E-E_0), i.e., from a point unidirectional single energy source. Designating it by J_p^0, we obtain

$$J_p^0(r_0, \Omega_0, E_0) = \int dr\, d\Omega\, dE\, G(r, \Omega, E; r_0, \Omega_0, E_0)\, p(r, \Omega, E), \qquad (3)$$

where G (r, Ω, E; r_0, Ω_0, E_0) is the Green function of the kinetic equation (1), i.e., the radiation flux at the point r with the velocity direction Ω and energy E from a point unidirectional single energy source situated at the point r_0 with a beam direction Ω_0 and energy E_0. Let us call r, Ω, E the variables at the observation point, and r_0, Ω_0, E_0 the source variables. G (r, Ω, E; r_0, Ω_0, E_0) is determined as the solution of the following kinetic equation

$$LG(r, \Omega, E; r_0, \Omega_0, E_0) = \delta(r - r_0)\, \delta(\Omega - \Omega_0)\, \delta(E - E_0). \qquad (4)$$

The quantity J_p^0 (r_0, Ω_0, E_0) as well as the flux from the elementary source G (r, Ω, E; r_0, Ω_0, E_0) depend parametrically on the source variables r_0, Ω_0, and E_0 which are contained in the right side of equation identified as (4). We note that in the equations (1) and (4) the independent variables are the

variables at the observation point. We shall agree to consider r_0, Ω_0, E_0 in expression (3) as independent variables. Then $J_p^0(r_0, \Omega_0, E_0) = J_p^0(r, \Omega, E)$ as a function of the source variables is nothing more than the value of the physical quantity J_p when an elementary source with a beam direction Ω and energy E is situated at point r.

According to the principle of radiation superposition the value of the physical quantity J_p due to the arbitrarily distributed sources $q(r, \Omega, E)$ is equal to the total value of the physical quantities from all elementary sources, i.e.,

$$J_p = \int dr\, d\Omega\, dE\, J_p^0(r, \Omega, E)\, q(r, \Omega, E). \tag{5}$$

Let us show that $J_p^0(r, \Omega, E)$ as a function of source variables satisfies the conjugate kinetic equation whose right side is equal to $p(r, \Omega, E)$. We shall proceed in the following manner. We write down the conjugate kinetic equation in operational form with its right side equal to

$$\mathbf{L}^+F^+(r, \Omega, E) = p(r, \Omega, E). \tag{6}$$

The conjugate operator of the kinetic equation L^+ may be obtained from L by determining the conjugate nature of the linear operators /32

$$\begin{aligned} &\int dr\, d\Omega\, dE\, F^+(r, \Omega, E)\, \mathbf{L}G(r, \Omega, E; r_0, \Omega_0, E_0) = \\ &= \int dr\, d\Omega\, dE\, G(r, \Omega, E; r_0, \Omega_0, E_0)\, \mathbf{L}^+F^+(r, \Omega, E). \end{aligned} \tag{7}$$

According to (6) the expression (3) for $J_p^0(r_0, \Omega_0, E_0)$ may be rewritten in the following form

$$\begin{aligned} J_p^0(r_0, \Omega_0, E_0) &= \int dr\, d\Omega\, dE\, G(r, \Omega, E; r_0, \Omega_0, E_0)\, p(r, \Omega, E) = \\ &= \int dr\, d\Omega\, dE\, G(r, \Omega, E; r_0, \Omega_0, E_0)\, \mathbf{L}^+F^+(r, \Omega, E), \end{aligned}$$

from the conjugate property (7) it is equal to

$$\int dr\, d\Omega\, dE\, F^{*}(\mathbf{r}, \Omega, E) LG(\mathbf{r}, \Omega, E; \mathbf{r}_0, \Omega_0, E_0),$$

so that by using expression (4) we obtain

$$\int dr\, d\Omega\, dE\, F^{*}(\mathbf{r}, \Omega, E)\, \delta(\mathbf{r}-\mathbf{r}_0)\, \delta(\Omega-\Omega_0)\, \delta(E-E_0),$$

which, from the determination of the δ-function is equal to $F^{+}(r_0, \Omega_0, E_0)$. We have obtained the following

$$J_p^0(r_0, \Omega_0, E_0) = F^{*}(\mathbf{r}_0, \Omega_0, E_0). \tag{8}$$

It is obvious that equality (8) is valid for any values r_0, Ω_0, E_0. Consequently we maintain that $J_p^0(r, \Omega, E)$ as a function of the source variables, satisfies the conjugate kinetic equation (6), i.e.,

$$J_p^0(\mathbf{r}, \Omega, E) \equiv F^{*}(\mathbf{r}, \Omega, E). \tag{9}$$

According to the accepted terminology (refs. 1-4) $F^{+}(r, \Omega, E)$ is the value with respect to the linear functional of the flux J_p. Actually the value with respect to the given physical quantity is nothing more than the value of this quantity $J_p^0(r, \Omega, E) \equiv F^{+}(r, \Omega, E)$ when the elementary source r with beam direction Ω and energy E is situated at point r.

In the conjugate kinetic equation (6) the independent variables are the source variables; the variable observation points may enter parametrically into the right side of the equation with the corresponding form of the function $p(r, \Omega, E)$. For example, in the case of the entire radiation flux at an arbitrarily fixed point r' with energy E' from an elementary source, the right side of equation (6) $p(r, \Omega, E; r', E') = \delta(r-r')\,\delta(E-E')$ and consequently, the solution $F^{+}(r, \Omega, E; r', E')$ itself depends parametrically on the variables r' and E' of the observation point. According to (9), expression (5) may be written in the following manner

$$\begin{aligned} J_p &= \int dr\, d\Omega\, dE\, J_p^0(\mathbf{r}, \Omega, E)\, q(\mathbf{r}, \Omega, E) = \\ &= \int dr\, d\Omega\, dE\, F^{*}(\mathbf{r}, \Omega, E)\, q(\mathbf{r}, \Omega, E). \end{aligned} \tag{10}$$

On the other hand, according to equation (2)

$$J_p = \int F(\mathbf{r}, \Omega, E)\, p(\mathbf{r}, \Omega, E)\, d\mathbf{r}\, d\Omega\, dE.$$

Comparing expressions (2) and (10) we obtain

$$\begin{aligned} J_p &= \int F(\mathbf{r}, \Omega, E)\, p(\mathbf{r}, \Omega, E)\, d\mathbf{r}\, d\Omega\, dE = \\ &= \int d\mathbf{r}\, d\Omega\, dE\, F^{+}(\mathbf{r}, \Omega, E)\, q(\mathbf{r}, \Omega, E), \end{aligned} \tag{11}$$

i.e., the value of the physical quantity J_p for the arbitrarily distributed /33 $q(r, \Omega, E)$ is equal to the value of the same quantity $J_p^0(r, \Omega, E) \equiv F^+(r, \Omega, E)$ for an elementary source, multiplied by the distribution of sources $q(r, \Omega, E)$ and integrated over all source variables. From the physical standpoint equality (11) reflects the principle of radiation superposition. Equality (11) may be of great practical value in computing the physical quantity J_p. Frequently the solution of the kinetic equation (1) is associated with substantial mathematical difficulties, and in order to find the quantities J_p it becomes much more convenient to solve the conjugate kinetic equation (6) and then to utilize equality (11). Below, as an example, we consider the three-dimensional distribution of neutrons in an infinite homogeneous medium produced by a point unidirectional source. For this case we carry out detailed calculations since the problem is of interest by itself.

Three-dimensional Distribution of Neutrons in an Infinite Homogeneous Medium Due to a Point Unidirectional Source

Let us consider the three-dimensional distribution of neutrons in an infinite homogeneous medium from a point unidirectional monoenergetic source. We present the solution in a single velocity approximation. The kinetic equation for the transport of neutrons will then have the form

$$\begin{aligned} \Omega \operatorname{grad} G(\mathbf{r}, \Omega; \mathbf{r}_0, \Omega_0) + \Sigma G(\mathbf{r}, \Omega; \mathbf{r}_0, \Omega_0) - \Sigma_s \int d\Omega'\, G(\mathbf{r}, \Omega'; \mathbf{r}_0, \Omega_0) f(\Omega' \to \Omega) = \\ = \delta(\mathbf{r} - \mathbf{r}_0)\, \delta(\Omega - \Omega_0), \end{aligned} \tag{12}$$

where $G(r, \Omega; r_0, \Omega_0)$ is the flux of neutrons at point r with velocity direction Ω from an elementary source, situated at point r_0 with beam direction Ω_0; Σ_s is the macroscopic scattering cross section; Σ is the total macroscopic cross section; $f(\Omega' \to \Omega)$ is the relative probability for the variation in the

neutron velocity direction from Ω' to Ω as a result of collision. The quantity $f(\Omega' \to \Omega)$ depends only on $\mu_0 = (\Omega' \Omega)$, the cosine of the angle between directions Ω' and Ω, and consequently has the property of symmetry with respect to the substitution Ω' and Ω, i.e.,

$$f(\Omega' \to \Omega) = f(\Omega \to \Omega'). \tag{13}$$

We are interested in the three-dimensional distribution of neutrons. Let us consider the entire radiation flux at an arbitrarily fixed point r' from an elementary source situated at point r_0 with beam direction Ω_0, i.e., the quantity equal to

$$J^0_{\delta(r-r')}(r_0, \Omega_0; r') = \\ = \int G(r, \Omega; r_0, \Omega_0)\, \delta(r - r')\, dr\, d\Omega \equiv G_0(r'; r_0, \Omega_0).$$

According to expression (9) the entire flux at point r' from an elementary source G_0 (r'; r_0, Ω_0) as a function of the source variables r_0, Ω_0 satisfies the conjugate kinetic equation with an isotropic right part equal to δ (r-r'), i.e.,

$$G_0(r'; r, \Omega) = F^+(r, \Omega; r'),$$

where F^+ (r, Ω; r') is the solution of the following equation

$$L^+F^+(r, \Omega; r') = \delta(r - r'). \tag{14}$$

F^+ (r, Ω; r') is the entire radiation flux at point r' from an elementary source situated at point r with beam direction Ω. This is a function of source variables, while the variable observation point r' is considered a fixed parameter in the right side of the conjugate equation (14).

The kinetic equation (12) contains the independent variables as the variables of the observation point and contains the source variables as parameters in the anisotropic right side of the equation. A direct solution of equation (12) is associated with mathematical difficulties which occur due to the relatively large number of variables: the single directionality of the source leads to a three-dimensional relationship with cylindrical asymmetry, i.e., it gives two three-dimensional coordinates. The variation in the neutron flux with the velocity direction Ω gives two more variables--two angles. Thus the flux G (r, Ω; r_0, Ω_0) depends on four variables, which substantially complicates the calculations. /34

In the conjugate kinetic equation (14) the independent variables are the source variables, while the variable observation point r' is contained as a parameter in the right side of the equation. The isotropic property of the

right side of this equation leads to a solution having a spherical symmetry, which substantially simplifies the calculations.

Let us determine the form of the conjugate operator L^+ from condition (7). Let us consider the expression

$$\int dr\, d\Omega\, F^*(r, \Omega; r')\, LG(r, \Omega; r_0, \Omega_0).$$

We write the operator L in explicit form utilizing expression (12)

$$\begin{aligned} &\int dr\, d\Omega\, F^*(r, \Omega; r')(\Omega\nabla) G(r, \Omega; r_0, \Omega_0) + \\ &+ \Sigma \int dr\, d\Omega\, F^*(r, \Omega; r') G(r, \Omega; r_0, \Omega_0) - \\ &- \Sigma_s \int dr\, d\Omega\, F^*(r, \Omega; r') \int d\Omega' G(r, \Omega'; r_0, \Omega_0) f(\Omega' \to \Omega). \end{aligned} \tag{15}$$

Let us consider the following integral

$$\int dr\, (\Omega\nabla) F^*(r, \Omega; r') G(r, \Omega; r_0, \Omega_0).$$

According to the Gauss-Ostrogradskiy theorem it is equal to

$$\oint ds\, (\Omega n) F^*(r, \Omega; r') G(r, \Omega; r_0, \Omega_0).$$

If sources are absent at infinity, this integral is equal to zero, because from the physical meaning of $F^+(r, \Omega; r')$ and $G(r, \Omega; r_0, \Omega_0)$ it follows that on the surface of a sphere with infinite radius

$$G(r, \Omega; r_0, \Omega_0)|_{S\to\infty} = 0 \quad \text{for} \quad (\Omega n) < 0;$$

while

$$F^*(r, \Omega; r')|_{S\to\infty} = 0 \quad \text{for} \quad (\Omega n) > 0.$$

Thus

$$\begin{aligned} \int dr\, (\Omega\nabla) F^*(r, \Omega; r') G(r, \Omega; r_0, \Omega_0) &= \int dr\, F^*(r, \Omega; r')(\Omega\nabla) G(r, \Omega; r_0, \Omega_0) + \\ &+ \int dr\, G(r, \Omega; r_0, \Omega_0)(\Omega\nabla) F^*(r, \Omega; r') = 0. \end{aligned}$$

Consequently the first term of expression (15) may be written in the following manner

$$\int d\Omega\, dr\, F^+(r, \Omega; r')\,(\Omega\nabla)\,G(r, \Omega; r_0, \Omega_0) =$$
$$= -\int dr\, d\Omega\, G(r, \Omega; r_0, \Omega_0)\,(\Omega\nabla)\,F^+(r, \Omega; r').$$

If we replace the order of integration over the angles in the third term of expression (15), we obtain /35

$$-\Sigma_s \int dr \int d\Omega\, F^+(r, \Omega; r') \int d\Omega'\, G(r, \Omega'; r_0, \Omega_0)\, f(\Omega' \dashrightarrow \Omega) =$$
$$= -\Sigma_s \int dr \int d\Omega'\, G(r, \Omega'; r_0, \Omega_0) \int d\Omega\, F^+(r, \Omega; r')\, f(\Omega' \rightarrow \Omega);$$

taking into account the symmetric properties of the function $f(\Omega' \rightarrow \Omega)$ (13), we have

$$-\Sigma_s \int dr \int d\Omega'\, G(r, \Omega'; r_0, \Omega_0) \int d\Omega\, F^+(r, \Omega; r')\, f(\Omega \dashrightarrow \Omega');$$

if for convenience we redesignate the variables of integration respectively, we obtain

$$-\Sigma_s \int dr \int d\Omega\, G(r, \Omega; r_0, \Omega_0) \int d\Omega'\, F^+(r, \Omega'; r')\, f(\Omega' \rightarrow \Omega). \qquad (17)$$

Taking into account (16) and (17), we can rewrite expression (15) in the following manner

$$\int dr\, d\Omega\, F^+(r, \Omega; r')\, LG(r, \Omega; r_0, \Omega_0) =$$
$$= -\int dr\, d\Omega\, G(r, \Omega; r_0, \Omega_0)\,(\Omega\nabla)\,F^+(r, \Omega; r') +$$
$$+\Sigma \int dr\, d\Omega\, G(r, \Omega; r_0, \Omega_0)\, F^+(r, \Omega; r') -$$
$$-\Sigma_s \int dr\, d\Omega\, G(r, \Omega; r_0, \Omega_0) \int d\Omega'\, F^+(r, \Omega'; r')\, f(\Omega' \rightarrow \Omega),$$

According to (7) it is equal to

$$\int dr\, d\Omega\, G(r, \Omega; r_0, \Omega_0)\, L^+F^+(r, \Omega; r').$$

Consequently the conjugate kinetic equation (14) has the form

$$-\Omega \operatorname{grad} F^{+}(\mathbf{r}, \Omega; \mathbf{r}') + \Sigma F^{+}(\mathbf{r}, \Omega; \mathbf{r}') - \\ -\Sigma_s \int d\Omega' F^{+}(\mathbf{r}, \Omega'; \mathbf{r}') f(\Omega' \to \Omega) = \delta(\mathbf{r} - \mathbf{r}'). \tag{18}$$

It is obvious physically that the entire flux $G_0(\mathbf{r}'; \mathbf{r}, \Omega) \equiv F^{+}(\mathbf{r}, \Omega; \mathbf{r}')$ depends only on two variables: on the scattering from an arbitrarily fixed point r' to the source, i.e., $R = |\mathbf{r}-\mathbf{r}'|$ and on the angle between the beam direction Ω and the straight line which connects point r' to the source.

Consequently, in solving the conjugate kinetic equation (18) it is convenient to transform to a spherical system of coordinates letting $R = r-r'$. Equation (18), which is integrated over the azimuth angle φ, will then have the following form

$$-\mu \frac{\partial F^{+}(R, \mu)}{\partial R} - \frac{(1-\mu^2)}{R} \cdot \frac{\partial F^{+}(R, \mu)}{\partial \mu} + \Sigma F^{+}(R, \mu) - \\ -\Sigma_s \int d\Omega' F^{+}(R, \mu') f(\mu' \to \mu) = \frac{\delta(R)}{4\pi R^2},$$

where

$$\mu = \cos(\mathbf{R}; \hat{\Omega}), \text{i.e.}, \mu = \frac{(\mathbf{R}\Omega)}{R}. \tag{19}$$

The mathematical relationship between F^{+} and μ follows from the very form of the conjugate kinetic operator L^{+}, while the relationship between F^{+} and R is due to the isotropic property of the right side of conjugate equation (18).

We note that due to the reciprocal properties of the problem the conjugate operator L^{+} in the considered single velocity approximation differs from L only in the sign before the first term $\Omega\nabla F$. Therefore, the establishment of the entire flux produced by the elementary source, i.e., the solution of conjugate equation (14), is equivalent mathematically to the establishment of /36 the three-dimensional angular distribution of radiation from an isotropic source for the basic kinetic equation.

Solution of the Conjugate Equation by the Method of Moments

The solution of the problem for a point isotropic source may be achieved by various methods. The problem on the distribution of the entire flux from a point isotropic source is solved by the method of Laplace transformation in the case when the scattering indicatrix is represented in a simple form, for example, in the form $f(\mu_0) = \frac{1}{4\pi}$ (ref. 5) or $f(\mu_0) = \frac{1}{4\pi}(1 + 3\bar{\mu}_0\mu_0)$, where

$\bar{\mu}_0$ is the mean cosine of the scattering angle (ref. 6). The angular distribution of the flux in this case remains constant.

The method of spherical harmonics gives the solution of the problem in a general form; however, in the first place, it does not produce a correct behavior of the flux near the source and along all distances in the direction $\mu \sim -1$, and it converges poorly when absorption in the medium is high (ref. 7).

The improvement of the method of spherical harmonics by the introduction of singularities at $R \to 0$ and $\mu \to -1$ (ref. 8) with a subsequent solution of the equations of spherical harmonics gives a satisfactory description of the flux near the source also when $\mu \sim -1$, but apparently at great distances from the source it will hardly yield good convergence when we have a medium with high absorption.

In addition, analytical methods of solving the problem of the type indicated above are hardly expedient for the solution of more complex problems with moderation--in the case of multiple group consideration.

The numerical methods of solving the problem in question, for example the S_n method (ref. 9) and similar methods used by Sh. S. Nikolayshvili (ref. 10), whose application is feasible at small distances, have not been investigated to date from the point of view of their convergence at various (not only small, but large) distances from the source.

Therefore it is expedient to consider this problem by means of the well-known semianalytical method of moments (ref. 11), which is used with equal success both in a single velocity as well as in a multiple velocity problem and which takes into account the nonisotropic scattering, etc. It is known that the methodology which is usually used does not make it possible to obtain distributions at small distances from the source. However, this can be corrected by isolating the singularities in the solution, as done in reference 8. In this case the difference will consist basically of the fact that after isolating the singularities the method of moments rather than the method of spherical harmonics is used.

Let us expand $F^+(R, \mu)$ and $f(\mu' \to \mu)$ in terms of the Legendre polynomials

$$F^+(R, \mu) = \sum_{n=0}^{\infty} \frac{2n+1}{4\pi} F_n^+(R) P_n(\mu); \tag{20}$$

$$f(\mu' \to \mu) = \sum_{l=0}^{\infty} \frac{2l+1}{4\pi} f_l P_l(\mu_0), \tag{21}$$

where $\mu_0 = (\Omega\Omega')$. We substitute expansion (20) and (21) into equation (19), taking into account the properties of the Legendre polynomials

$$P_l(\mu_0) = P_l(\mu)\,P_l(\mu') + 2\sum_{m=1}^{l}\frac{(l-m)!}{(l+m)!}P_l^m(\mu)\,P_l^m(\mu')\cos m(\varphi-\varphi');$$

$$\mu P_n(\mu) = \frac{n+1}{2n+1}P_{n+1}(\mu) + \frac{n}{2n+1}P_{n-1}(\mu);$$

$$(1-\mu^2)\frac{\partial P_n(\mu)}{\partial\mu} = \frac{n(n+1)}{2n+1}[P_{n-1}(\mu) - P_{n+1}(\mu)];$$

$\int d\Omega P_n(\mu)\,P_l(\mu) = \frac{4\pi}{2l+1}\delta_{ln}$ (where δ_{ln} is the Kroenecker symbol) and the fact that the integral over $d\varphi'$ of cos m $(\varphi-\varphi')$ is equal to zero, i.e., $\int_0^{2\pi} d\varphi'$ cos m $(\varphi-\varphi') = 0$. Then in place of (19) we obtain the following equation

/37

$$\sum_{n=0}^{\infty}\left\{P_{n+1}(\mu)\left[-\frac{\partial F_n^+(R)}{\partial R}\cdot\frac{n+1}{4\pi} + \frac{F_n^+(R)}{R}\cdot\frac{n(n+1)}{4\pi}\right] - P_{n-1}(\mu)\times\right.$$
$$\times\left[\frac{\partial F_n^+(R)}{\partial R}\cdot\frac{n}{4\pi} + \frac{F_n^+(R)}{R}\cdot\frac{n(n+1)}{4\pi}\right] + \frac{2n+1}{4\pi}P_n(\mu)\,F_n^+(R)\times$$
$$\left.\times(\Sigma - \Sigma_s f_n)\right\} = \frac{\delta(R)}{4\pi R^2}.$$

Multiplying this equation by $P_l(\mu)$ and integrating over $d\Omega$, we obtain a system of differential equations for $F_l^+(R)$

$$\frac{l(l-1)}{2l+1}\cdot\frac{\partial F_{l-1}^+(R)}{\partial R} + \frac{l}{2l+1}\cdot\frac{\partial F_{l-1}^+(R)}{\partial R} - \frac{l+1}{2l+1}\cdot\frac{\partial F_{l+1}^+(R)}{\partial R} -$$
$$-\frac{(l+1)(l+2)}{2l+1}\cdot\frac{F_{l+1}^+(R)}{R} + \Sigma F_l^+(R) - \Sigma_s F_l^+(R)\,f_l = -\frac{\delta(R)}{R^2}\,\delta_{l,0}. \qquad (22)$$

Multiplying equation (22) by $\Sigma^{n+1}\frac{R^n}{n!}$ and integrating over the entire volume, we obtain a system of algebraic equations for the moments $b_{l,n}$

$$(1-hf_l)b_{l,n} + \frac{(l+1)(n-l)}{2l+1}b_{l+1,\,n-1} + \frac{l(l+n+1)}{2l+1}b_{l-1,\,n-1} = (L-hf_l)\,b_{l,\,n} = \delta_{l,0}\delta_{n,0}, \qquad (23)$$

where $b_{l,n}$ are the three-dimensional angular moments for the neutron flux

$$b_{l,n} = \frac{\Sigma^{n+1}}{n!}\int_0^{\infty} F_l^+(R)\,R^{n+2}\,dR = \frac{\Sigma^{n+1}}{n!}\int_0^{\infty} F^+(R,\mu)\,R^{n+2}P_l(\mu)\,dR\,d\Omega. \qquad (24)$$

Here (L-hf$_t$ is the designation for the operator in the left side of (23); $h = \frac{\Sigma_s}{\Sigma}$. It is easy to see that the system of equations (23) determines only those moments $b_{t,n}$ for which $t \leq n$ and the indices t and n have the same parity.

The neutron flux $F^+(R, \mu)$ may be represented as a sum

$$F^+(R, \mu) = F^{+(0)}(R, \mu) + F^{+(1)}(R, \mu) + \tilde{F}^+(R, \mu), \tag{25}$$

where $F^{+(0)}$, $F^{+(1)}$, $\tilde{F}^+$ are functions which describe the flux of nonscattered neutrons, singly scattered neutrons and multiply scattered neutrons, respectively. It is known that the fluxes of nonscattered neutrons $F^{+(0)}$ and singly scattered neutrons $F^{+(1)}$ have singularities with respect to R near zero and with respect to μ near -1.

The doubly scattered neutrons $F^{+(2)}$ which are contained in the $\tilde{F}^+$ flux also have a singularity, but this singularity is sufficiently weak (logarithmic) (ref. 8), so that $\tilde{F}^+$ may be looked upon as a "smooth" function. The variation in fluxes $F^{+(0)}$ and $F^{+(1)}$ as a function of the coordinate has the form (see, for example, ref. 8)

$$\begin{aligned} F^{+(0)}(R, \mu) &= \frac{e^{-\Sigma R}}{4\pi R^2}\,\delta(1+\mu); \\ F^{+(1)}(R, \mu) &= \frac{\Sigma_s e^{\Sigma R \mu}}{4\pi R\sqrt{1-\mu^2}} \int\limits_{\Pi - \arccos\mu}^{\pi} e^{-\Sigma R\sqrt{1-\mu^2}\,\mathrm{tg}\,\theta_0/2} f(\mu_0)\, d\theta_0, \end{aligned} \tag{26}$$

where $\mu_0 = \cos\theta_0$; θ_0 is the scattering angle.

If we assume that angle θ is small and that $\Sigma R\sqrt{1-\mu^2} \ll 1$, the expression for $F^{+(1)}(R, \mu)$ leads to /38

$$F^{+(1)*}(R, \mu) = \frac{\Sigma_s e^{-\Sigma R} q_t}{16\pi R\sqrt{2(1+\mu)}}, \tag{27}$$

where

$$\begin{aligned} q_t &= \sum_{m=0} \frac{2m+1}{2^m}\left[\frac{(m-1)!!}{(m/2)!}\right]^2 \delta\left[\frac{m}{2} - E\left(\frac{m}{2}\right)\right] f_m = \\ &= 1 + \frac{5}{4} f_2 + 9\frac{9}{64} f_4 + 13\frac{25}{256} f_6 + 17\frac{1225}{16384} f_8 + \ldots \end{aligned}$$

[1]The right part of expression $F^{+(1)}(R,\mu)$ should be multiplied by 4π. Formulas (27), (34), (41) and (70) change correspondingly. Then for $h \leq 0.9$ expression (33) can lead to $b_{2,n} < 0$. In this case we must be satisfied with separation only of $F^{+(0)}(R,\mu)$ or in other words describe the relationship $F^{+(1)*}(R,\mu)$. Making formula (70) precise does not lead to large changes in calculation results, because the moments of function (70) correspond to the actual.

Then the flux of singly scattered neutrons $F^{+(1)}(R, \mu)$ may be represented as a sum of the isolated singularity $F^{+(1)*}(R, \mu)$ of a sufficiently "smooth" residue $\widetilde{F}^{+(1)}(R, \mu)$

$$F^{+(1)}(R, \mu) = \hat{F}^{+(1)*}(R, \mu) + \widetilde{F}^{+(1)}(R, \mu). \tag{28}$$

Thus the total flux may be expressed as a sum

$$F^{+}(R, \mu) = F^{+(0)}(R, \mu) + F^{+(1)*}(R, \mu) + \Phi^{+}(R, \mu), \tag{29}$$

where

$$\Phi^{+}(R, \mu) = \widetilde{F}^{+(1)}(R, \mu) + \widetilde{F}^{+}(R, \mu). \tag{29a}$$

As a result of this the flux is separated into a part $(F^{+(0)} + F^{+(1)*})$, which has a singularity for $R \to 0$, $\mu \to -1$ and a "smooth" part $\Phi^{+}(R, \mu)$ with a relatively weak singularity.

Let us determine the moments of functions $F^{+(0)}$, $F^{+(1)}$, $\widetilde{F}^{+}$ from system (23). It is obvious that $F^{+(0)} \sim h^0$, $F^{+(1)} \sim h^1$, $\widetilde{F}^{+} \sim h^2$ and that the moments of these functions depend on h, i.e., they may be represented in the form

$$\left.\begin{aligned} b^{(0)}_{l,n} &= h^0 B^{(0)}_{l,n}; \\ b^{(1)}_{l,n} &= h^1 B^{(1)}_{l,n}; \\ \widetilde{b}_{l,n} &= h^2 B_{l,n}. \end{aligned}\right\} \tag{30}$$

Then

$$b_{l,n} = b^{(0)}_{l,n} + b^{(1)}_{l,n} + \widetilde{b}_{l,n} = B^{(0)}_{l,n} + hB^{(1)}_{l,n} + h^2 \widetilde{B}_{l,n}. \tag{31}$$

Substituting (31) into equation (23) we obtain a system of equations

$$\left.\begin{aligned} LB^{(0)}_{l,n} &= \delta_{l,0}\,\delta_{n,0}; \\ LB^{(1)}_{l,n} &= f_l B^{(0)}_{l,n}; \\ (L - hf_l)\widetilde{B}_{l,n} &= f_l B^{(1)}_{l,n}. \end{aligned}\right\} \tag{32}$$

By carrying out a successive solution of system (32) we can obtain the three-dimensional angular moments $b^{(0)}_{l,n} = (-1)^l$; $b^{(1)}_{l,n}$; $\widetilde{b}_{l,n}$. Utilizing the values

$b^{(1)}_{l,n}\widetilde{b}_{l,n}$ and the moments $b^{(1)*}_{l,n}$ of the function $F^{+(1)*}(R, \mu)$ and also the additive property of the moments, we can obtain, in accordance with (28) and (29a), the values of the moments $\bar{b}_{l,n}$ of the function $\Phi^{+}(R, \mu)$

$$\bar{b}_{l,n} = \tilde{b}_{l,n} + b^{(1)}_{l,n} - b^{(1)*}_{l,n}, \tag{33}$$

where

$$b^{(1)*}_{l,n} = \frac{(n+1)\,hq_1}{8\sqrt{2}} \int_{-1}^{+1} \frac{P_l(\mu)}{\sqrt{1+\mu}}\, d\mu = (-1)^l \frac{n+1}{4(2l+1)}\, hq_1. \tag{34}$$

To reestablish the angular moments of the function $\Phi^{+}(R, \mu)$ we utilize the following convenient approximation form, analogous to the one described /39 in reference 12

$$\Phi^{+}_l(R) = A_l (\Sigma R)^{\nu_l - 1} e^{-\xi_l \Sigma R}. \tag{35}$$

The parameters A_l, ν_l, ξ_l are selected from the conditions that the first three moments (of the same parity) with $n = l$, $l + 2$, $l + 4$ of approximation (35) coincide with the established values of the corresponding moments $\bar{b}_{l,n}$

$$\nu_l = \frac{9Q - 5 - 2l(1-Q) + \sqrt{1 + 14Q + Q^2}}{2(1-Q)};$$

$$Q = \frac{(l+1)(l+2)}{(l+3)(l+4)} \cdot \frac{\bar{b}^2_{l,l+2}}{b_{l,l}\bar{b}_{l,l+4}};$$

$$\xi_l = \sqrt{\frac{(\nu_l + l + 3)(\nu_l + l + 2)}{(l+1)(l+2)} \cdot \frac{\bar{b}_{l,l}}{\bar{b}_{l,l+2}}};$$

$$A_l = \frac{\bar{b}_{l,l}\xi_l^{\nu_l + l + 2}\Sigma^{2l}\,l!}{\Gamma(\nu_l + l + 2)},$$

where

$$\Gamma(\nu) = \int_0^{\infty} x^{\nu-1} e^{-x}\, dx - \text{γ-function of Euler.}$$

Some difficulties are encountered in the reestablishment of the angular relationship from the known angular moments. The expansion of the flux in terms of spherical harmonics (20) does not converge too well, even after isolating the nonscattered, singly scattered and doubly scattered neutrons, particularly

when the capture is strong. For example, during the isotropic scattering the asymptotic angular distribution is described rather critically (when $h \leqslant 0.5$) by a varying function of the form $(1 + k\mu)^{-1}$, because in this case $k \approx 1\text{-}2e^{-2/h}$. The poor convergence of the series requires that we take into account a large number of its terms, i.e., we must know a large number of angular moments F_l.

In this connection it is not helpful even to know the exact values of the first moments. Apparently we must seek an escape, as in the case when the three-dimensional relationship is reestablished from the three-dimensional moments, specifically by utilizing the approximation equations with parameters which can be expressed in terms of the values $\Phi_l^+(R) = 2\pi \int \Phi^+(R, \mu) P_l(\mu)\, d\mu$.

Let us select the form of the approximation equation which is similar to the asymptotic solution for a single velocity problem (see (53))

$$\Phi^+(R, \mu) = \frac{\alpha(R)}{1 + k(R)\mu} + \sum_{m=0}^{m^*} \beta_m(R) P_m(\mu), \tag{37}$$

where α (R), k (R), β_m (R) are parameters selected from the conditions that the first (m* + 2) angular moments of approximation (37) coincide with the established values of the moments (35).

In the approximation with respect to two angular moments (m* = 0) the function Φ^+ (R, μ) is expressed in the following manner

$$\Phi^+(R, \mu) = \frac{1}{4\pi} \cdot \frac{\Phi_0^+(R) - k(R)\Phi_1^+(R)}{1 + k(R)\mu}, \tag{37a}$$

where k (R) is determined from the transcendental equation

$$\left.\begin{aligned} \varphi_1(k) &= \frac{1 - h_0(k)}{k} = \frac{\Phi_1^+}{\Phi_0^+}(R); \\ h_0(k) &= \frac{2k}{\ln \frac{1+k}{1-k}}. \end{aligned}\right\} \tag{38}$$

The graphs of the function h_0 (k) and φ_1 (k) are shown in figure 1.

In the approximation utilizing the three angular moments (m* = 1) /40

$$\Phi^+(R, \mu) = \frac{\Phi_0^+(R)}{4\pi} + \frac{\Phi_1^+(R)}{4\pi\varphi_1[k(R)]} \left[\frac{h_0[k(R)]}{1 + k(R)\mu} - 1\right], \tag{39}$$

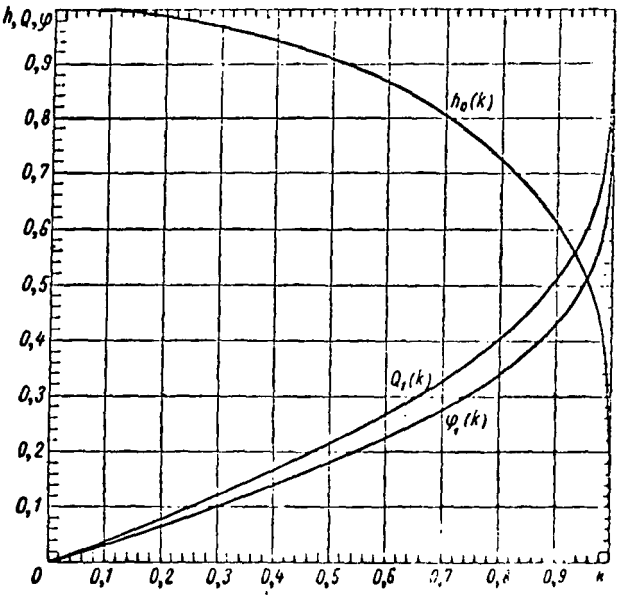

Figure 1. Graph of functions $h_0(k)$, $\varphi_1(k)$ and $Q(k)$ for determining roots of transcendental equations (38) and (40).

where k(R) is determined from the transcendental equation

$$Q_1(k) = \frac{1}{2}\left[\frac{3}{k} - \frac{1}{\varphi_1(k)}\right] = \frac{\Phi_2^+}{\Phi_1^+}(R). \tag{40}$$

The graph of function $Q_1(k)$ is also shown in figure 1. The final expression for the flux of neutrons, when using an approximation in terms of the three angular moments, has the form

$$F^+(R, \mu) = \frac{e^{-\Sigma R}}{4\pi R^2}\delta(1+\mu) + \frac{\Sigma_s q_1 e^{-\Sigma R}}{16\pi R\sqrt{2(1+\mu)}} + \frac{\Phi_0^+(R)}{4\pi} + \frac{\Phi_1^+(R)}{4\pi\varphi_1[k(R)]}\left[\frac{h_0[k(R)]}{1+k(R)\mu} - 1\right]. \tag{41}$$

Asymptotic Behavior of the Entire Flux

At large distances from a point source ($\Sigma R \gg 1$) the angular distribution of the neutron flux must coincide with the case when we have a plane source. Thus, for the problem considered in the present work we can write the asymptotic expression for the entire flux in the form

$$F_{as}^+(R, \mu) = \frac{e^{-k'R}}{R}\Phi(\mu), \tag{42}$$

where k' is some constant, while $\Phi(\mu)$ is determined by the "plane" equation

$$-\mu\frac{\partial F_{as}^+(R, \mu)}{\partial R} + \Sigma F_{as}^+(R, \mu) - \Sigma_s\int d\Omega' F_{as}^+(R, \mu')\, f(\mu' \to \mu) \tag{43}$$

Substituting equation (42) into (43), dividing the resultant equation by Σ and noting that $\Sigma R \gg 1$, we obtain /41

$$\Phi(\mu) = \frac{h}{1+k\mu} \int d\Omega' \Phi(\mu') f(\mu' \to \mu), \tag{44}$$

where $k = k'/\Sigma$. Let us expand $f(\mu' \to \mu)$ in a series of Legendre polynomials (21) and substitute this expansion into equation (44). In this manner we obtain

$$\Phi(\mu) = \frac{h}{4\pi} \cdot \frac{1}{1+k\mu} \sum_{l=0}^{\infty}{}' (2l+1) f_l \Phi_l P_l(\mu), \tag{44a}$$

where $\Phi_l = 2\pi \int_{-1}^{+1} d\mu' \Phi(\mu') P_l(\mu')$. Integrating expression (23) over $d\mu^{-1}$ we obtain

$$\Phi_0 = \sum_{l=0}^{\infty}{}' \frac{h}{2} (2l+1) f_l \Phi_l \int_{-1}^{+1} \frac{P_l(\mu)\, d\mu}{1+k\mu}, \tag{45}$$

We express all Φ_l in terms of Φ_0,

$$\text{i.e., } \Phi_l = C_l \Phi_0. \tag{46}$$

To do this we return to equation (44) and rewrite it in the following form

$$\Sigma(1+k\mu)\Phi(\mu) = \Sigma_s \int d\Omega' \Phi(\mu') f(\mu' \to \mu). \tag{47}$$

We expand $\Phi(\mu)$ in terms of the Legendre polynomials

$$\Phi(\mu) = \sum_{n=0}^{\infty}{}' \frac{2n+1}{4\pi} \Phi_n P_n(\mu). \tag{48}$$

Substituting expansions (21) and (48) into equation (47), we obtain

$$\sum_{n=0}^{\infty} \frac{2n+1}{4\pi} \Phi_n P_n(\mu) \Sigma(1+k\mu) = \Sigma_s \sum_{n=0}^{\infty}{}' \frac{2n+1}{4\pi} \Phi_n f_n P_n(\mu). \tag{49}$$

We multiply expression (49) by $P_l(\mu)$, integrate over $d\mu$ and divide by Φ. In this manner we obtain

$$k\Sigma \frac{l}{2l+1} C_{l-1} + k\Sigma \frac{l+1}{2l+1} C_{l+1} + \Sigma_l C_l = 0, \tag{50}$$

where

$$\Sigma_l = \Sigma - \Sigma_s f_l.$$

From system (50) we successively determine all C_l, beginning with $C_0 = 1$, and further for $l > 0$

$$C_l = -\frac{2l-1}{lk}\cdot\frac{\Sigma_l}{\Sigma}C_{l-1} - \frac{l-1}{l}C_{l-2}. \tag{51}$$

Taking into account (46), substituting the established values of C_l (51) into (45) and breaking off the series at the m-th term, we obtain a transcendental equation which can be used to determine k

$$1 = \frac{h}{2}\sum_{l=0}^{m}(2l+1)f_l C_l(k)\gamma_l(k), \tag{52}$$

where $\gamma_l(k) = \int_{-1}^{+1}\frac{P_l(\mu)}{1+k\mu}d\mu$. It follows from equation (44) that the angular asymptotic property of the function $F^+_{as}(R, \mu)$ is proportional to $(1 + k\mu)^{-1}$, /42

where k is determined by transcendental equation (52) and depends on $h = \Sigma_s/\Sigma$ and on the harmonics of the scattering indicatrix f_l.

Thus the asymptotic behavior of the entire flux is determined by the expression

$$F^+_{as}(R, \mu) = \frac{e^{-k\Sigma R}}{R}\cdots\frac{h\Phi_0}{4\pi}\cdot\frac{1}{1+k\mu}\sum_{l=0}^{\infty}(2l+1)f_l C_l P_l(\mu). \tag{53}$$

To determine k and C_l in expression (53) it is more convenient to utilize the results obtained in the solution of equation (42) in the P_L approximation, i.e., by taking into account all C_l when $l \ll L$ in the system of equations (50). Then the infinite system of homogeneous equations (50) is transformed into a finite system with nonzero solutions under the following condition

$$\Delta_L(k) = \begin{vmatrix} \Sigma_0 & k\Sigma & 0 & 0 & \cdots & 0 & 0 \\ \frac{1}{3}k\Sigma & \Sigma_1 & \frac{2}{3}k\Sigma & 0 & \cdots & 0 & 0 \\ 0 & \frac{2}{5}k\Sigma & \Sigma_2 & \frac{2}{5}k\Sigma & \cdots & 0 & 0 \\ \cdot & \cdot & \cdot & \cdot & \cdots & \cdot & \cdot \\ \cdot & \cdot & \cdot & \cdot & \frac{L-1}{2L-1}k\Sigma & \Sigma_{L-1} & \frac{L}{2L-1}k\Sigma \\ 0 & 0 & 0 & 0 & 0 & \frac{L}{2L+1}k\Sigma & \Sigma_L \end{vmatrix} = 0, \tag{54}$$

where $\Delta_L(k)$ is the determinant of the system.

By expanding $\Delta_L(k)$ in terms of the elements of the last column we obtain a recurrent equation for $\Delta_L(k)$

$$\left.\begin{aligned}
&\Delta_L(k) = \Sigma_L \Delta_{L-1}(k) - \frac{L^2 k^2 \Sigma^2}{4L^2-1}\Delta_{L-2}(k), \text{ when } L \geqslant 2,\\
&\Delta_0(k) = \Sigma_0,\\
&\Delta_1(k) = \Sigma_0\Sigma_1 - \frac{1}{3}k^2\Sigma^2.
\end{aligned}\right\} \qquad (55)$$

The smallest positive root k_{min} of equation (54), which determines the asymptotic behavior of the flux in various approximations P_L, will be equal to

$$\left.\begin{aligned}
&L=1,\ k_{min}=\frac{1}{\Sigma}\sqrt{3\Sigma_0\Sigma_1};\\
&L=2,\ k_{min}=\frac{1}{\Sigma}\sqrt{3\Sigma_0\Sigma_1/1+\frac{4}{5}\frac{\Sigma_0}{\Sigma_2}};\\
&L=3,\ k_{min}=\frac{1}{\Sigma}\sqrt{\frac{35}{18}\Sigma_2\Sigma_3+\frac{14}{9}\Sigma_0\Sigma_3+\frac{3}{2}\Sigma_0\Sigma_1-\sqrt{\left(\frac{35}{18}\Sigma_2\Sigma_3+\right.}}\\
&\sqrt{\sqrt{\left.+\frac{14}{9}\Sigma_0\Sigma_3+\frac{3}{2}\Sigma_0\Sigma_1\right)^2-\frac{35}{3}\Sigma_0\Sigma_1\Sigma_2\Sigma_3}} \quad \text{etc.}
\end{aligned}\right\} \qquad (56)$$

Correspondingly

/43

$$\left.\begin{aligned}
&L=1,\ C_1(k)=-\frac{k\Sigma}{3\Sigma_1},\ C_1(k_{min})=-\sqrt{\frac{\Sigma_0}{3\Sigma_1}};\\
&L=2,\ C_1(k)=-\frac{k\Sigma}{3\Sigma_1\left(1-\frac{4}{15}\frac{k^2\Sigma^2}{\Sigma_1\Sigma_2}\right)},\ C_1(k_{min})=-\sqrt{\frac{\Sigma_0}{3\Sigma_1}\left(1+\frac{4}{5}\frac{\Sigma_0}{\Sigma_2}\right)}\\
&\qquad C_2(k)=-\frac{2}{5}\cdot\frac{k\Sigma}{\Sigma_2}C_1(k),\ C_2(k_{min})=\frac{2}{5}\cdot\frac{\Sigma_0}{\Sigma_2};\\
&L=3,\ C_1(k)=-\frac{k\Sigma}{3\Sigma_1\left[1-\frac{4}{15}\frac{k^2\Sigma^2}{\Sigma_1\Sigma_2\left(1-\frac{9}{35}\frac{k^2\Sigma^2}{\Sigma_2\Sigma_3}\right)}\right]};\\
&\qquad C_2(k)=-\frac{2k\Sigma}{5\Sigma_2\left(1-\frac{9}{35}\frac{k^2\Sigma^2}{\Sigma_2\Sigma_3}\right)}C_1(k);\\
&\qquad C_3(k)=-\frac{3}{7}\cdot\frac{k\Sigma}{\Sigma_3}C_2(k) \quad \text{etc.}
\end{aligned}\right\} \qquad (57)$$

Thus the utilization of equations (54-57) establishes the asymptotic behavior of flux (53) with an accuracy determined by the quantity Φ_0, which is determined by the source term dropped in equation (42) when $\Sigma R \gg 1$. In the case of a point source the solution is rather complicated. Therefore we shall make use of the well-known solution for a plane isotropic source in an infinite homogeneous medium (refs. 13 and 14) and the Marshak theorum (ref. 7), which associates the solution of the problem for a point and plane isotropic neutron source in an infinite medium,

$$F_0^+(R) = -\frac{1}{2\pi R}\left[\frac{d}{dz}F_0^+(Z)\right]\Big|_{Z=R}. \tag{58}$$

Then according to references 13 and 14 and according to equations (43) and (58)

$$\Phi_0 = -\frac{k\Sigma}{2\pi}\cdot\frac{\Delta_L^0(k)}{\Delta'_L(k)}\Big|_{k=k_{min}}, \tag{59}$$

where $\Delta'_L(k)$ is a derivative with respect to $k' = k\Sigma$ of the determinant of system (54), and k_{min} is determined from condition (54), while

$$\Delta_L^0(k) = \begin{vmatrix} 1 & k\Sigma & 0 & 0 & . & . & 0 & 0 \\ 0 & \Sigma_1 & \frac{2}{3}k\Sigma & 0 & . & . & 0 & 0 \\ 0 & \frac{2}{5}k\Sigma & \Sigma_2 & \frac{3}{5}k\Sigma & . & . & 0 & 0 \\ . & . & . & . & . & . & . & . \\ . & . & . & . & . & \frac{L-1}{2L-1}k\Sigma & \Sigma_{L-1} & \frac{L}{2L-1}k\Sigma \\ 0 & 0 & 0 & 0 & . & 0 & \frac{L}{2L+1}k\Sigma & \Sigma_L \end{vmatrix} \tag{60}$$

The determinant $\Delta_L^0(k)$ satisfies relationship (55) when $L \geq 3$, and when $L = 1$ and $L = 2$

$$\begin{aligned} \Delta_1^0(k) &= \Sigma_1, \\ \Delta_2^0(k) &= \Sigma_1\Sigma_2 - \frac{4}{15}k^2\Sigma^2. \end{aligned} \tag{60a}$$

As a result of this, according to equation (59),

$$\left.\begin{aligned} &L = 1,\ \Phi_0 = \frac{3\Sigma_1}{4\pi}; \\ &L = 2,\ \Phi_0 = \frac{3\Sigma_1}{4\pi}\left(1 + \frac{4}{5}\cdot\frac{\Sigma_0}{\Sigma_2}\right)^{-2}; \\ &L = 3,\ \Phi_0 = \frac{1}{4\pi}\cdot\frac{\Sigma_1\Sigma_2\Sigma_3 - \frac{1}{5}k^2\Sigma^2\left(\frac{9}{7}\Sigma_1 + \frac{4}{3}\Sigma_3\right)}{\frac{1}{3}\Sigma_2\Sigma_3 + \frac{4}{15}\Sigma_0\Sigma_3 + \frac{9}{35}\Sigma_0\Sigma_1 - \frac{6}{35}k^2\Sigma^2}\Big|_{k=k_{min}} \end{aligned}\right\} \tag{59a}$$

Distribution of Fast Neutrons in Iron /44

The solution of the single velocity problem presented in the present work may be applied to determine the neutron detector count for a medium consisting of heavy nuclei, in the general case with a variable energy sensitivity of the detector $\sigma_D(E)$.

The kinetic equation for the neutron flux (19) with energy E in the case of a source with a fission spectrum X(E) of power Q_0, and under conditions

where there is good justification for assuming that the inelastic scattering is isotropic, may be written in the form

$$
\begin{aligned}
&-\mu \frac{\partial F^+(R, E, \mu)}{\partial R} - \frac{(1-\mu^2)}{R} \cdot \frac{\partial F^+(R, E, \mu)}{\partial \mu} + \Sigma F^+(R, E, \mu) = \\
&= \int_E^\infty dE' \int d\Omega' \Sigma_{el}(E') f(\mu_0, E', E) F^+(R, E', \mu') + \\
&+ \frac{1}{4\pi} \int_E^\infty dE' \Sigma_{in}(E' \to E) F^+(R, E', \mu') + \frac{\delta(R) Q_0 \chi(E)}{4\pi R^2},
\end{aligned}
\tag{61}
$$

where $f(\mu_0, E', E)$ is the scattering indicatrix which, in the general case, depends on the energy; Σ_{el} and Σ_{in} are the cross section for elastic and inelastic scattering, respectively.

When equation (61) is multiplied by the effectiveness of the detector $\sigma_D(E)$ and subsequently integrated over the energy and expanded in terms of the Legendre polynomial, it is reduced to the following infinite system of equations

$$
\begin{aligned}
&-\frac{l+1}{2l+1} \cdot \frac{1}{R^{l+2}} \cdot \frac{\partial}{\partial R}(R^{l+2} N_{l+1}) - \frac{l}{2l+1} R^{l-1} \cdot \frac{\partial}{\partial R}\left(\frac{N_{l-1}}{R^{l-1}}\right) + \\
&+ \Sigma^D N_l = \int_0^\infty dE\, \sigma_D(E) \int_E^\infty dE' \Sigma_{el}(E') f_l(E', E) F^+{}_l(E') + \\
&+ \delta_{l,0} \int_0^\infty dE\, \sigma_D(E) \int_0^\infty dE' \Sigma_{in}(E' \to E) F^+{}_l(E') + \delta_{l,0} Q_0 S \frac{\delta(R)}{R^2}.
\end{aligned}
\tag{62}
$$

where

$$
N_l(R) = \int_0^\infty \sigma_D(E) F^+{}_l(R, E)\, dE;
$$

$$
S = \int_0^\infty \sigma_D(E) \chi(E)\, dE,
$$

while the subscript D represents the cross section which is averaged out over the neutron spectrum and detector sensitivity. For example,

$$
\Sigma^D = \frac{\int_0^\infty \Sigma(E) \sigma_D(E) F^+(E)\, dE}{\int_0^\infty \sigma_D(E) F^+(E)\, dE}.
$$

By introducing the concept of the cross section for removal from the region of detector sensitivity, we have

$$\Sigma^D_{\text{ув, in, } l} = \frac{\int_0^\infty \sigma_D(E)\,\Sigma_{in}(E)\,F^+_l(E)\,dE - \int_0^\infty dE\,\sigma_D(E)\int_E^\infty \Sigma_{in}(E'\to E)\,F^+_l(E')\,dE'}{\int_0^\infty \sigma_D(E)\,F^+_l(E)\,dE}; \tag{63}$$

$$\Sigma^D_{\text{ув, el, } l} = \frac{\int_0^\infty \sigma_D(E)\,\Sigma_{el}(E)\,F^+_l(E)\,dE - \int_0^\infty dE\,\sigma_D(E)\int_0^\infty \Sigma_{el}(E')\,f_l(E'E)\,F^+_l(E')\,dE'}{\int_0^\infty \sigma_D(E)\,F^+_l(E)\,dE}. \tag{63a}$$

(ув = re (уводд) = removal

The system of equations (62) is reduced to a system of single velocity equations for $N_l(R)$: /45

$$-\frac{l+1}{2l+1}\cdot\frac{1}{R^{l+2}}\cdot\frac{\partial}{\partial R}(R^{l+2}N_{l+1}) - \frac{l}{2l+1}R^{l-1}\frac{\partial}{\partial R}\left(\frac{N_{l-1}}{R^{l-1}}\right) + \Sigma^D_{\text{ув, }l}N_l = \delta_{l,0}\frac{Q_0 S\delta(R)}{R^2}, \tag{64}$$

where

$$\Sigma^D_{\text{ув, }l} = \Sigma^D_{\text{ув, el, }l} + \Sigma^D_{\text{ув, in, }l}\cdot\delta_{l,0} + \Sigma^D_{in}(1-\delta_{l,0}).$$

System (64) is identical to the system of equations (22) for F^+_l, when the source power is Q_0S and when we replace Σ_S by $(\Sigma^D - \Sigma^D_{\text{re, }0})$ and Σ by Σ^D, while replacing f_t with the quantity

$$f^*_l = \frac{\Sigma^D - \Sigma^D_{\text{ув, }l}}{\Sigma^D - \Sigma^D_{\text{ув, }0}}. \tag{65}$$

For the sake of simplicity in determining the cross sections a sufficiently high energy detector Al^{27} (n, α) Na^{24} was considered; the effective threshold for the fission spectrum is near 7 MeV (ref. 15). The energy relationship for the sensitivity of this detector was determined by utilizing data presented in references 16 and 17.

Due to the high threshold of the detector most of the inelastically scattered neutrons are not detected. These neutrons form a composite nucleus, which basically leads to low energy neutrons approximately (5 MeV). Due to the process of a direct interaction of the falling neutron with several nucleons of

the nucleus-target high energy neutrons are generated which fall into the region of detector sensitivity. The cross section of this process (ref. 18) is approximately 10 percent of the cross section for inelastic interaction

σ_{in}^{D} which is approximately equal to 1.4 b for iron in the case of the fission spectrum. (In this region the cross section of inelastic interaction in fact coincides with the cross section of inelastic scattering due to the smallness of the radiation capture effects (n, γ) and due to the reactions (n, α), (n, p) and (n, 2n)). Therefore the cross section for inelastic removal under the threshold of sensitivity for the Al^{27} (n, α) Na^{24} detector may be assumed equal to σ_{re}^{D}, in = 1.26 + 0.14 b for iron. This quantity is in insufficiently good agreement with the experimental measurement of the cross section for inelastic removal under the threshold of sensitivity for the Al^{27} (n, p) Mg^{27} detector (the effective threshold at the fission spectrum is approximately 4.6 MeV (ref. 15)), equal to 1.20 ± 0.09 b (ref. 19). Due to the absence of reliable quantitative data the present work does not take into account the anisotropy in the direction ahead of the neutrons which are inelastically scattered during the process of direct interaction. Qualitative evaluations (refs. 18 and 20) show a slightly smaller degree for this anisotropy compared with the anisotropy for the elastic scattering of neutrons. The effect produced by this error may be considered to be sufficiently small.

For the case of a median composed of heavy nuclei the indicatrix of elastic moderation may be represented in the form (ref. 21)

$$f(\mu_0, E', E) = \varphi(\mu_0, E')\,\delta[E - E'g(\mu_0)], \tag{66}$$

where $g(\mu_0) = 1 - \frac{2}{M}(1 - \mu_0)$ (M is the mass of the scattering nucleus); $\varphi(\mu_0, E')$ is the angular distribution of the elastically scattered neutrons. If we substitute the l-harmonic $f(\mu_0, E', E)$ equal to $f_l(E', E) = \int f(\mu_0, E', E) P_l(\mu_0)\, d\Omega_0$ into equation (63a), we obtain the l-th harmonic for the section of elastic removal

$$\sigma_{\text{ув, el, }l}^{D} = [1 - (1 - \xi)\varphi_l^{D}]\,\sigma_{el}^{D} + \Delta_l^{D}, \tag{67}$$

where σ_{el}^{D} = 1.96 + 0.06 b and φ_l^{D} (the values are presented in table 1) represent the integral cross section and the harmonics of the indicatrix for the elastic scattering, which have been averaged out over the sensitivity of detector and over the neutron spectrum (by utilizing data presented in references 20, 22 and 23); $\xi = \frac{2}{M}(1 - \varphi_1^{D})$ is the mean logarithmic loss of energy during the elastic collision of a neutron with a nucleus of mass M; Δ_l^{D} is a correction for /46

the cross section of elastic removal taking into account the variation in the sensitivity of the detector as a function of neutron energy; in the case when we have a linear law governing the variation of sensitivity (beginning with some threshold energy E_T)

$$\sigma_D(E) = \sigma'_D(E - E_T), \tag{68}$$

This correction is expressed in the form

$$\Delta_l^D = \xi \sigma_{el}^D \varphi_l^D \sigma'_D E_T \frac{\int_{E_T}^{\infty} F^*(E)\,dE}{\int_0^{\infty} \sigma_D(E) F^*(E)\,dE}. \tag{69}$$

The magnitude of this correction is sufficiently small compared with the cross section of elastic removal (approximately 4 percent). Finally, the problem of determining the AI^{27} (n, α) Na^{24} neutron detector count in iron ($E_T \approx 6$ MeV; $\sigma_D \simeq 0.018$ b/MeV) is reduced to the equivalent single velocity problem with parameters $\sigma_{t0t} = 3.39 \pm 0.15$ b (utilizing the data presented in ref. 23); $\sigma_S = 2{,}06 \pm 0.21$ b and using harmonics f_l^*, whose values are presented in table 1.

According to the methodology described in section 2, by utilizing the constants described above we determine the moments $\overline{b_{l,n}}$ by means of equation (33), and from these we determine the characteristics of the angular moments A_l, ν_l, ξ_l (36) (table 2).

According to equations (35) and (41) the reading of a detector in an infinitely homogeneous mass of iron (when utilizing the three moment approximation of equation (39) for the angular relationship), when a point unidirection source of neutrons with unit power is placed into this medium, may be written in the following form in terms of source variables (R, μ)

$$N(R, \mu) = \frac{e^{-\Sigma R}}{4\pi R^2}\delta(1+\mu) + \frac{\Sigma_S q_1 e^{-\Sigma R}}{16\pi R\sqrt{2(1+\mu)}} + \frac{A_0}{4\pi}(\Sigma R)^{\nu_0 - 1} \times$$
$$\times e^{-\xi_0 \Sigma R} + \frac{A_1}{4\pi} \cdot \frac{(\Sigma R)^{\nu_1 - 1}}{\varphi_1[k(\Sigma R)]} e^{-\xi_1 \Sigma R}\left[\frac{h_0[k(\Sigma R)]}{1 + k(\Sigma R)\mu} - 1\right], \tag{70}$$

where the two last terms should be taken into account for those values of ΣR when the last term is positive, i.e., when $\Sigma R \geqslant 2$, while k (ΣR) is determined from (40) and $h_0(k)$ and $\varphi_1(k)$ are determined from (38) or from the graph in figure 1.

TABLE 1. CROSS SECTION OF REMOVAL UNDER THE THRESHOLD OF SENSITIVITY FOR Al^{27} (n, α) Na^{24}.

i	φ_e^D	$\sigma_{re,\,i}^D$, b	f_i^*
0	1.000 ± 0.085	1.330 ± 0.202	1.000 ± 0.224
1	0.828 ± 0.085	1.795 ± 0.273	0.774 ± 0.173
2	0.687 ± 0.014	2.062 ± 0.243	0.645 ± 0.145
3	0.545 ± 0.013	2.330 ± 0.277	0.515 ± 0.117
4	0.396 ± 0.012	2.612 ± 0.316	0.378 ± 0.086
5	0.256 ± 0.004	2.876 ± 0.336	0.250 ± 0.056
6	0.163 ± 0.001	3.053 ± 0.357	0.164 ± 0.037

TABLE 2. CHARACTERISTICS OF THE ANGULAR MOMENTS.

i	A_i, cm^{-2}	ν_i	ξ_i
0	0.03247	0.1198	0.6158
1	0.03863	-0.1327	0.6037
2	0.03945	-0.2727	0.6052

The work of V. P. Mashkovich and S. G. Tsypin (ref. 25) describes an experiment on the measurement of fast fission neutrons by means of the /47

Al^{27} (n, α) Na^{24} detector in an iron prism (γ = 7.86 gm/cm^3) from a unidirectional radiating disk with radius a ≈ 12.5 cm lying in the plane Z = 0. In this case we can neglect the effects produced by the finite dimensions of the prism (approximately 38 × 39 × 54 mean free path lengths) and of the detector (less than 2 percent of the radiating disk area), as well as the angular divergence of the neutron beam (approximately 5°).

Taking into account equation (70) and the weak relationship k(R) when $\Sigma R > 1$, the contribution by the scattered part of the radiation (characterized by expression (70) with the exception of the first term, from each source point with coordinates Z = 0, x, φ (x is the distance of the point from the center of the source; φ is the azimuth angle), and the readings of the detector which is situated in the Z plane at a distance H from the beam axis, when φ = 0 and $|\mu| \geq 0.7$, may be written as

$$N_{\text{pac}}[Z, H'(x, \varphi)] = \frac{\Sigma_s q_1}{16\pi} \cdot \frac{e^{-\Sigma\sqrt{Z^2+H'^2}}}{H'} + \frac{A_0}{4\pi}(\Sigma\sqrt{Z^2+H'^2})^{\nu_0-1} \times$$
$$\times e^{-\xi_0\Sigma\sqrt{Z^2+H'^2}} + \frac{A_1}{4\pi}\frac{(\Sigma\sqrt{Z^2+H'^2})^{\nu_1-1}}{\varphi_1(k)} e^{-\xi_1\Sigma\sqrt{Z^2+H'^2}}\left[\frac{1-\frac{h_0(k)}{k}}{1-\frac{1}{\sqrt{1+H'^2Z^{-2}}}} - 1\right], \qquad (71)$$

(pac = di = distance)

because $R = \sqrt{Z^2 + H'^2}$, where $H'(x, \varphi) = \sqrt{H^2 - 2Hx\cos\varphi + x^2}$.

Finally, the reading of the detector with coordinates (Z, H) per unit area of the radiating disk with radius a may be represented in the form

$$N_a(Z, H) = \frac{e^{-\Sigma Z}}{\pi a^2} + \frac{1}{\pi a^2} \int_0^a dx\, x \int_0^{2\pi} d\varphi N_{\text{рас}}[Z, H'(x, \varphi)]. \tag{72}$$

When Z >> H', by utilizing (35) expression (71) may be transformed in the following manner

$$\begin{aligned} N_{\text{рас}}(Z, H') \simeq \frac{\Sigma_s q_1}{16\pi H'} \exp\left[-\Sigma Z\left(1 + \frac{H'^2}{2Z^2}\right)\right] + \frac{\Phi_0^+(Z)}{4\pi}\left(1 + \right. \\ \left. + \frac{H'^2}{2Z^2} - \frac{H'^4}{8Z^4}\right)^{\nu_0 - 1} \exp\left(-\frac{\xi_0 \Sigma H'^2}{2Z} + \frac{\xi_0 \Sigma H'^4}{8Z^3}\right) + \frac{\Phi_1^+(Z)}{4\pi\varphi_1(k)}\left(1 + \frac{H'^2}{2Z^2} - \right. \\ \left. - \frac{H'^4}{8Z^4}\right)^{\nu_1 - 1} \exp\left(-\frac{\xi_1 \Sigma H'^2}{2Z} + \frac{\xi_1 \Sigma H'^4}{8Z^3}\right)\left[\frac{h_0(k)}{1 - k\left(1 - \frac{H'^2}{2Z^2} + \frac{3}{8}\frac{H'^4}{Z^4}\right)} - 1\right]. \end{aligned} \tag{71a}$$

Along the axis of the radiating disk, i.e., when H = 0 and Z >> a, noting that k ≤ 1, we obtain the following for the detector count (72)

$$\begin{aligned} N_a(Z, H=0) \simeq \frac{e^{-\Sigma Z}}{\pi a^2} + \frac{hq_1}{8\pi} \frac{e^{-\Sigma Z}}{2\pi a^2} \sqrt{\Sigma Z}\Phi_B\left(\frac{\Sigma a}{\sqrt{\Sigma Z}}\right) + \\ + \frac{\Phi_0^+(Z)}{4\pi}\left[1 - \frac{\xi_0 \Sigma a^2}{4Z} + (\nu_0 - 1)\frac{a^2}{4Z^2}\right] + \frac{\Phi_1^+(Z)}{4\pi\varphi_1(k)}\left\{\frac{2Z^2}{a^2} h_0(k) e^{-\xi_1 \Sigma Z(1-k)} \times \right. \\ \times [E_1(\xi_1 \Sigma Z(1-k)) - E_1(\xi_1 \Sigma Z\left(1 - k + \frac{a^2}{2Z^2}\right))] + \\ + \left(1 - \frac{\xi_1 \Sigma a^2}{4Z}\right)\left[h_0(k)(\nu_1 - 1) - \frac{\xi_1 h_0(k)\Sigma Z}{2}(1-k) - 1\right] + \frac{\xi_1 h_0(k)\Sigma a^2}{8Z} - \\ \left. - \frac{\nu_1 - 1}{4Z^2} a^2 + \ldots\right\}, \end{aligned} \tag{73}$$

where $\Phi_B(x)$ is the integral of the probability $\Phi_B(x) = \frac{2}{\sqrt{\pi}} \int_0^x e^{-t^2} dt$, while the function $E_n(x) = \int_1^\infty \frac{e^{-xt}}{t^n} dt$.

At short distances when ΣZ ≤ 2, according to the remark pertaining to /48 equation (70), it is sufficient to consider only the first two terms in expression (73).

The utilization of the asymptotic solution (53) when the neutron flux is represented, similar to equation (29) in the form

$$F^+(R, \mu) \simeq [\text{illegible}](R, \mu) + F_{\text{as}}^+(R, \mu) \tag{74}$$

(subscript as = asymptotic)

leads to the following equation for the detector reading on the beam axis

$$N_a^{as}(Z, H=0) \simeq \frac{e^{-\Sigma Z}}{\pi a^2} + \frac{k\Phi_0}{2\pi k\Sigma a^2}\left[y(Z) - y\left(\sqrt{Z^2+a^2}\right)\right], \tag{75}$$

where y(x) represents a function

$$y(x) = \left(1 - \frac{5}{2} f_2 C_2 + \ldots\right) e^{-k\Sigma x} + \left[k - 3f_1 C_1 + \frac{5}{2} f_2 C_2 \left(\frac{3}{k} - 1\right) - \right.$$
$$\left. - \frac{7}{2} f_3 C_3 \left(\frac{5}{k^2} - 3\right) + \ldots\right] k\Sigma Z\, e^{-k^2\Sigma Z} E_1[k\Sigma(x - kZ)] - \tag{75a}$$
$$- \frac{5}{2}\left(3f_2 C_2 - \frac{7}{k} f_3 C_3 + \ldots\right) E_1(k\Sigma x) + \frac{35}{2} f_3 C_3 \frac{\Sigma Z^2}{x} E_2(k\Sigma x) + \ldots,$$

while the expressions for quantities k, Φ_0, C_1 in various P_1-approximations are presented in the preceding section.

Figure 2 makes a comparison of the experimental data presented in reference 25 with the results calculated by means of equations (73) and (75) for the detector readings on the beam axis, referred to the detector count at the point C = 3.7 cm (H = 0) which is closest to the source. As we can see from this graph the behavior of the flux at large distances is described fairly accurately

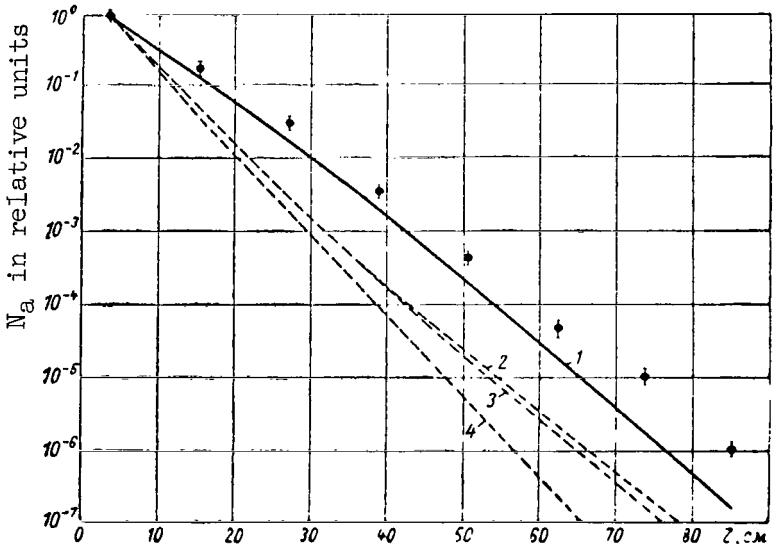

Figure 2. Comparison of experimental and calculated data on readings of detector in iron along axis of beam: 0, experimental values; 1, results of calculations using three moments; 2-4, results of asymptotic solution in the P_1, P_2 and P_3 approximations, respectively.

by an exponential function, i.e., by $F \sim e^{-z/\lambda r}$, where λr is some relaxation length. Let us compare the relaxation lengths of the neutron flux along the central ray of the beam corresponding to various curves in figure 2. The experimental result is $\lambda_r^{ex} = 5.7 \pm 0.3$ cm; the result of calculations using the three moments is $\lambda_r^M = 4.85$ cm, i.e., it differs from λ_r^{ex} by approximately 15 percent; the result of the asymptotic solution is $\lambda_r^{P1} = 3.8$ cm; $\lambda_r^{P2} = 4.9$ cm; $\lambda_r^{P3} = 5.1$ cm, i.e., it is described quite well by the relative variation in the flux with distance. For the purpose of comparison we present the mean free /49 path length of neutrons $\lambda = 3.50 \pm 0.17$ cm.

Let us consider the neutron flux distribution outside the central ray of the beam. Figure 3 shows the distribution of the entire neutron flux in plane Z = 38.8 cm, when a point unidirectional source of unit power with radiation directed along the Z axis is placed at point Z = 0, H = 0, computed by the method of moments in accordance with equation (70), with the utilization of the asymptotic solution for the P_1, P_2 and P_3 approximations (See eq. (53)). The difference in the results obtained by the method of moments and by the asymptotic solution is rather high near the source ray and is smoothed out to some extent as we move away from it. For purposes of comparison figure 3 presents the distribution of neutron flux $N_{is}(R)$ (subscript is = isotropic) from a point isotropic source with unit power at the point Z = 0, H = 0. This distribution may be obtained by integrating expression (70) over $d\Omega$

$$N_{из}(R) = \frac{1}{4\pi} \int N(R, \mu)\, d\Omega = \frac{e^{-\Sigma R}}{4\pi R^2} + \frac{\Sigma_s q_1 e^{-\Sigma R}}{16\pi R} + \frac{A_0}{4\pi} (\Sigma R)^{\nu_0 - 1} e^{-\xi_0 \Sigma R} \qquad (70a)$$

(из = is = isotropic)

We can see that the distribution from a unidirectional source, at sufficiently large distances from the line of radiation direction, approaches the distribution from an isotropic source. This makes it possible to analyze the behavior of the flux using the law $e^{-R/\lambda_r(H)}/R$, where $\lambda_r(H)$ is some relaxation length whose value approaches the asymptotic relaxation length for an isotropic source $\lambda_{r,\,as}$, when H increases. For example, in the considered plane Z = 38.8 cm in the region from H = 60 cm to H = 70 cm, the behavior of the flux from a points unidirectional source may be described by the following relaxation lengths: when using the method of moments $\lambda_r = 5.3$ cm; in the asymptotic solution $\lambda_r^{P1} = 4.1$ cm; $\lambda_r^{P2} = 4.9$ cm; $\lambda_r^{P3} = 5.1$ cm.

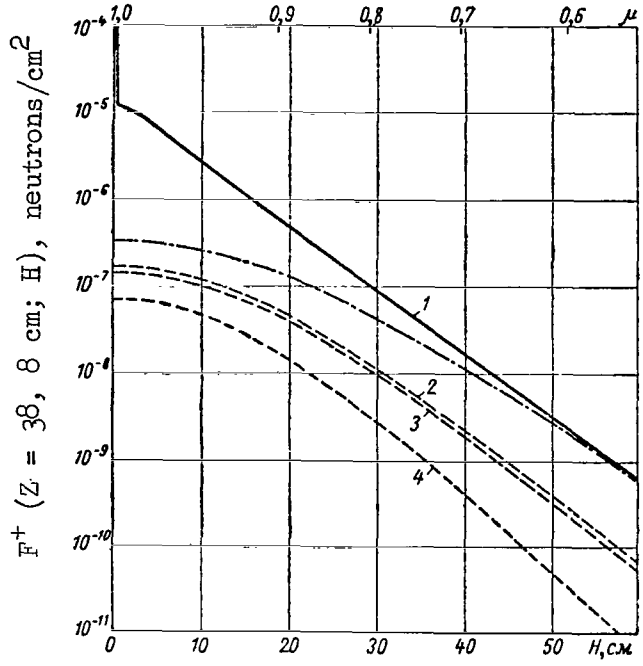

Figure 3. Distribution of neutron flux in iron in plane Z = 38.8 cm from a point unidirectional source of unit power placed at point Z = 0 (H = 0), with radiation directed along Z axis: 1, calculations by method of moments; 2-4, asymptotic solution in P_1, P_2 and P_3 approximations, respectively.

For comparison we present distribution from a point isotropic source of unit power at point Z = 0, H = 0, dot-dash curve.

For comparison we present the asymptotic relaxation lengths for an iso-/50 tropic source: according to the method of moments $\lambda_{r,\ as} = 5.65$; according to the method of spherical harmonics $\lambda_{r,\ as}^{P_1} = 4.4$ cm; $\lambda_{r,\ as}^{P_2} = 5.4$ cm; $\lambda_{r,\ as}^{P_3} = 5.7$ cm; $\lambda_{r,\ as}^{I9} = 6.3$ cm.

For the flux distribution from a unidirectional radiating disk with radius a when Z >> H > a we obtain the following approximate equation from (71a)

$$N_a(Z, H) \simeq \frac{hq_1 Z}{8\pi a H^2} e^{-\Sigma Z - \frac{\Sigma(H^2+a^2)}{2Z}} \left[\left(1 + \frac{a^2}{4H^2}\right) I_1\left(\frac{\Sigma H a}{Z}\right) + \right.$$
$$+ \left(1 + \frac{5}{4}\cdot\frac{a^2}{H^2} - \frac{Z}{\Sigma H^2}\right)\frac{a}{2H} I_2\left(\frac{\Sigma H a}{Z}\right) +$$
$$\left. + \left(11 + \frac{5}{2}\cdot\frac{a^2}{H^2} - 7\,\frac{Z}{\Sigma H^2}\right)\frac{a^2}{4H^2} I_3\left(\frac{\Sigma H a}{Z}\right) + \ldots \right] + \qquad (76)$$

$$+\frac{Z}{2\pi a\Sigma H}\left[\frac{1}{\xi_0}t_0(Z,\ H)-\frac{1}{\xi_1\varphi_1(k)}t_1(Z,\ H)\right]+$$
$$+\frac{\Phi_1^+(Z)\,Zh_0(k)}{2\pi a\Sigma H\xi_1\varphi_1(k)}e^{-\xi_1\Sigma\frac{(H^2+a^2)}{2Z}}\left\{\left[\frac{2Z^2}{H^2}\left(1+\frac{a^2}{H^2}\right)+\nu_1-1\right]I_1\left(\frac{\xi_1\Sigma Ha}{Z}\right)+\right.$$
$$+\left[\frac{2Z^2}{H^2}\left(3+2\frac{a^2}{H^2}\right)-\frac{4Z^3}{\xi_1\Sigma H^4}+\nu_1-\frac{3}{2}\right]\frac{a}{H}I_2\left(\frac{\xi_1\Sigma Ha}{Z}\right)+$$
$$\left.+\left[\frac{2Z^2}{H^2}\left(5+3\frac{a^2}{H^2}\right)-\frac{8Z^3}{\xi_1\Sigma H^4}+\nu_1-2\right]\frac{a^2}{H^2}I_3\left(\frac{\xi_1\Sigma Ha}{Z}\right)+\ldots\right\},$$

where $I_n(x)$ is a Bessel function with an imaginary argument; $h_0(k)$, $\varphi_1(k)$ are functions of $k(\Sigma R)$ which is determined from (40), where $R=\sqrt{Z^2+H^2}$. The function $t_n(Z, H)$ designates the following expression

$$t_n(Z,\ H)=\Phi_n^+(Z)\,e^{-\xi_n\frac{\Sigma(Z^2+a^2)}{2Z}}\left\{\left[1+\frac{\nu_n-1}{2Z^2}(a^2+H^2)\right]I_1\left(\frac{\xi_n\Sigma Ha}{Z}\right)+\right.$$
$$+\left[1+\frac{\nu_n-1}{2Z^2}\left(a^2-H^2-\frac{2Z}{\xi_n\Sigma}\right)\right]\frac{a}{H}I_2\left(\frac{\xi_n\Sigma Ha}{Z}\right)+ \qquad (76a)$$
$$\left.+\left[1+\frac{\nu_n-1}{2Z^2}\left(a^2-H^2-\frac{4Z}{\xi_n\Sigma}\right)\right]\frac{a^2}{H^2}I_3\left(\frac{\xi_n\Sigma Ha}{Z}\right)+\ldots\right\}\quad(n=0;\ 1).$$

When $H \gg Z > a$ we can neglect the dimensions of the disk and utilize equation (70) for a point source. When $Z < a < H$, by utilizing (71) and (72) we arrive at the following approximate equation

$$N_a(Z,\ H)\simeq\frac{ha_1}{8\pi aH}e^{-\Sigma H-\frac{\Sigma}{2H}\left[Z^2+a^2\left(1-\frac{Z^2}{2H^2}\right)\right]}\times$$
$$\times\left\{\left[1+\frac{a^2}{4H^2}-\frac{\Sigma a^2}{4H}\left(1+\frac{5}{2}\frac{a^2}{H^2}\right)\right]I_1(\Sigma a)+\right.$$
$$+\left[5+\frac{25}{4}\cdot\frac{a^2}{H^2}-\frac{\Sigma a^2}{2H}\left(3+5\frac{a^2}{H^2}+3\frac{\Sigma a^2}{2H}\right)\right]\frac{a}{2H}I_2(\Sigma a)+$$
$$+\left[17+\frac{45}{2}\cdot\frac{a^2}{H^2}+\frac{3\Sigma a^2}{2H}+\Sigma H\left(1-\frac{27}{\Sigma^2H^2}\right)\right]\frac{a^2}{4H^2}I_3(\Sigma a)+\ldots\Big\}+$$
$$+\frac{1}{2\pi\Sigma a}\left[\frac{1}{\xi_0}\omega_0(ZH)-\frac{1}{\xi_1\varphi_1(k)}\omega_1(Z,\ H)\right]+ \qquad (77)$$
$$+\frac{\Phi_2^+(H)\,h_0(k)}{2\pi\xi_1\Sigma a\varphi_1(k)}e^{-\frac{\xi_1\Sigma}{2H}\left[Z^2+a^2\left(1-\frac{Z^2}{2H^2}\right)\right]}\times$$
$$\times\left\{\left[\left(1+\frac{Z}{H}\right)\left(1+\frac{\xi_1\Sigma a^2}{4H}\right)-\frac{a^2}{H^2}\left(1-\frac{2Z}{H}\right)\right]I_1(\xi_1\Sigma a)+\right.$$
$$+\left[3+5\frac{Z}{H}+\frac{\xi_1\Sigma a^2}{2H}\left(2+5\frac{Z}{H}+3\frac{a^2}{H^2}-\frac{3}{4}\frac{\xi_1\Sigma a^2}{H}\right)-\right.$$
$$\left.-\frac{a^2}{H^2}\left(\frac{3}{4}+3\nu_1\frac{a}{H}-\frac{Z}{H}\right)\right]\frac{a}{2H}I_2(\xi_1\Sigma a)+$$
$$\left.+\left[3+6\frac{Z}{H}+\frac{\xi_1\Sigma a^2}{2H}\left(5+8\frac{Z}{H}+3\frac{\xi_1\Sigma a^2}{H}\right)+\xi_1\Sigma H-\frac{8}{\xi_1\Sigma H}\right]\frac{a^2}{4H^2}I_3(\xi_1\Sigma a)+\ldots\right\}$$

where the function $\omega_n(Z, H)$ is defined by the following expression /51

$$\omega_n(Z,\ H)=\Phi_n^+(H)\,e^{-\frac{\xi_n\Sigma}{2H}(Z^2+a^2)}\left\{\left[1+\frac{\xi_n\Sigma a^2}{4H}\left(1+\frac{3}{2}\frac{a^2}{H^2}\right)-\frac{4Z^2+a^2}{4H^2}\right]I_1(\xi_n\Sigma a)+\right.$$
$$\left.+\left[3+\frac{9}{4}\cdot\frac{a^2}{H^2}+\frac{1-\nu_n}{\xi_n\Sigma H}+\frac{\xi_n\Sigma(a^2-Z^2)}{H}-\frac{3}{2}\cdot\frac{\xi_n\Sigma a^4}{H^3}\left(1+\frac{\xi_n\Sigma H}{4}\right)\right]I_2(\xi_n\Sigma a)+\ldots\right\}. \qquad (77a)$$

In figure 4 experimental data (ref. 25) on the distribution of neutrons in different planes Z as a function of H are compared with the results of calculations performed by means of equations (70), (76) and (77).

The computed data agree well with experimental results with respect to the variation in the neutron flux distribution as a function of H. Some of the disagreements in the absolute values of the fluxes as Z increases may be explained by the following reasons:

(1) the application of approximation schemes utilizing three rather than more moments;

(2) a rather large error in the cross sections used in the calculation (~15 percent), for example: h = 0.61 ± 0.09; in addition, when formulating the cross sections for this group of neutrons we did not take into account the variation of the spectrum as the distance from the source increased;

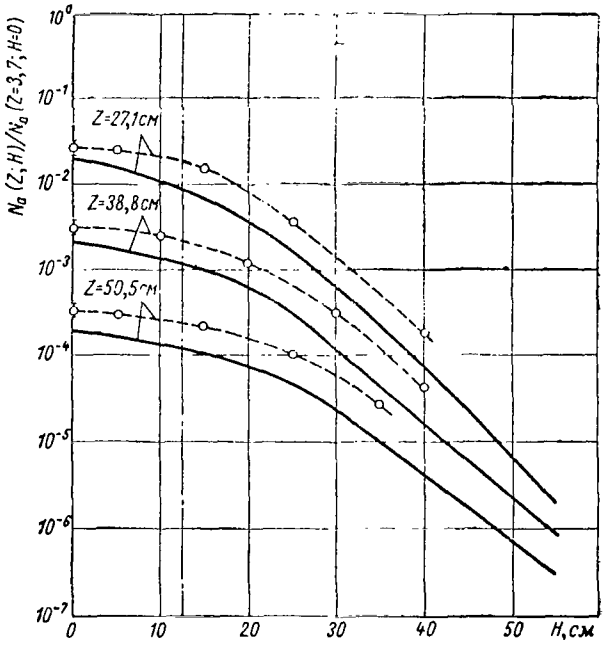

Figure 4. Comparison of experimental and computed data on readings of detector in different planes Z as function of distance to central ray H: ⊥○⊥, experimental values for activity of indicator; solid curves, calculation by method of moments; vertical dot-dash curve shows boundary of beam.

(3) some idealization in the computation scheme of the experiment which we have mentioned above. /52

In conclusion the author expresses his gratitude to O. K. Malyugin for carrying out the numerical calculations.

REFERENCES

1. Marchuk, G. I. and Orlov, V. V. IN: Neutron Physics (Neytronnaya fizika). Gosatomizdat, Moscow, 1961.

2. Usachev, L. N. Equation for the Value of Neutrons, Reactor Kinetics and Theory of Perturbations (Uravneniye dlya tsennosti neytronov, kinetika reaktora i teoriya vozmushcheniy). IN: Reaktorostroyeniye i teoriya reaktorov. Izd-vo AN SSSR, Moscow, 1955.

3. Kadomtsev, B. B. Dokl. AN SSSR, 113, 541, 1957.

4. Breshenkova, Ye. B. and Orlov, V. V. Atomnaya Energiya, 10, 175, 1961.

5. Case, K. M., Hoffman, F. and Placzek, G. Introduction to the Theory of Neutron Diffusion. Vol. 1, Los Alamos, 1953.

6. Devison, B. The Theory of Neutron Transport (Teoriya perenosa neytronov). Atomizdat, p. 284, Moscow, 1960.

7. Marshak, R. E., Brooks, H. and Hurwitz, H. Nucleonics, Vol. 4, No. 6, p. 43, 1949; Vol. 5, No. 1, p. 59, 1949.

8. Petrov, E. Ye. and Usachev, L. N. Spatial and Angular Distribution of Neutrons from a Point Source Taking into Account the Anisotropy of Scattering (Prostranstvennoye i uglovoye raspredeleniye neytronov ot tochechnogo istochnika s uchetom anizotropii rasseyaniya). IN: Teoriya i metody rascheta reaktorov. Gosatomizdat, Moscow, 1962.

9. Karlson, B. and Bell, F. Solution of the Transport Equation by the S_n Method (Resheniye transportnogo uravneniya S_n metodom). IN: Fizika yadernykh reaktorov. Atomizdat, Moscow, 1959.

10. Nikolayshvili, Sh. S. Single Velocity Problem Concerning the Angular Distribution of Neutrons Generated by a Point Isotropic Source at the Center of a Sphere (Odnoskorostnaya zadacha ob uglovom raspredelenii neytronov ispuskayemykh tochechnym izotropnym istochnikom v tsentre sfery). IN: Teoriya i metody rascheta reaktorov. Gosatomizdat, Moscow, 1962.

11. Marshak, R. E. Revs. Mod. Phys., Vol. 19, 185, 1947.

12. Nikolayshvili, Sh. S. Atomnaya Energiya, Vol. 10, 271, 1961.

13. Broder, D. L., Kurkin, S. A., Kutuzov, A. A., Levin, V. V. and Orlov, V. V. Investigation of Three-dimensional Energy Distribution of Neutrons in Various Media (Izucheniye prostranstvenno-energeticheskikh raspredeleniy neytronov v razlichnykh sredakh). IN: Trudy Vtoroy Mezhdunarodnoy konferentsii po mirnomu ispol'zovaniyu atomnoy energii. Dokl. sovetskikh uchenykh, Vol. 2, Atomizdat, 1959.

14. Marchuk, G. I. and Nikolayshvili, Sh. S. Application of the Method of Spherical Harmonics to the Problems of the Transport Theory. I. Some Properties of the P_n Approximation (Primeneniye metoda sfericheskikh garmonik k zadacham teorii, perenosa. I. Nekotoryye svoystva P_n-priblizheniya) IN: Teoriya i metody rascheta reaktorov. Gosatomizdat, Novosibirok, 1962.

15. Grundl, G. and Usner, A. Nucl. Sci. Eng., Vol. 8, 598, 1960.

16. Grundl, J. A., Henkel, R. L. and Perkins, B. L. Phys. Rev., Vol. 109, 425, 1958; Yuasumi, S. J. Phys. So. Japan, Vol. 12, 443, 1957; Forbes, S. G. Phys. Rev., Vol. 88, 1309, 1952.

17. Mani, G. S., McCallum, G. J. and Ferguson, A. T. G. Nucl. Phys., Vol. 19, 535, 1960; Kern, B. D., Thompson, W. E. and Ferguson, J. M. Nucl. Phys., Vol. 10, 226, 1956; Schmitt, H. W. and Halperin, J. Phys. Rev., Vol. 121, 827, 1961.

18. McGregor, M. H. Nuclear Interactions at Low Energies and the Nuclei Structure (Intéractions nucléaires aux basses energies et structure des noyaux). Congrès international de physique nucléaire, p. 609, Paris, 1959.

19. Bethe, H. A., Beyster, J. R. and Carter, R. E. J. Nucl. Energy, Vol. 4, 147, 1957.

20. Coon, J. H., Davis, R. W. et al. Phys. Rev., Vol. 111, 250, 1958.

21. Kochergin, V. P. and Orlov, V. V. Atomnaya Energiya, Vol. 6, 54, 1959.

22. Beyster, J. R. Walt, M. and Salmi, E. W. Phys Rev., Vol. 104, 1319, 1956.

23. Anderson, J. D., Gardner, C. C. et al. Phys. Rev., Vol. 110, 160, 1958.

24. Hughes, D. J. and Schwartz, R. B. Neutron Cross Sections, BNL-325, 1958.

25. Mashkovich, V. P. and Tsypin, S. G. Atomnaya Energiya, Vol. 11, 251, 1961.

APPLICATION OF THE METHOD OF "REMOVAL CROSS SECTIONS" TO ANALYSIS OF SHIELDING WITHOUT HYDROGEN

D. L. Broder, A. A. Kutuzov, V. V. Levin and V. V. Frolov

A rather convenient method for computing the three-dimensional distri- /52
bution of neutron fluxes in shieldings which contain hydrogen is the method of removal cross sections (refs. 1 and 2).

The essence of this method, which is rather simple for the practical calculations of shielding, consists of finding the cross section of an element contained in the shielding which is equivalent to the cross section of neutron absorption in a group with an energy interval $\Delta E = E - E_{th}$. This cross section, called the "removal cross section," is composed from the absorption cross section, from part of the cross section for elastic scattering and from a large part of the section for inelastic scattering.

Elastic scattering by light nuclei affects the absorption of the fast /53
neutron (its removal from the energy interval $E - E_{th}$), both due to the drop in the energy of neutrons during the scattering act as well as due to the elongation of the neutron path from the shielding caused by the change in the flight direction. For a heavy nucleus only the second factor is significant. Inelastic processes lead to a large drop in energy during a smaller nonisotropic scattering property of the neutron and therefore make a large contribution to the removal cross section when the initial energy of the neutron is sufficiently high. The calculation of the fast neutron flux in the case of a source which radiates a spectrum of neutrons, using this methodology, is carried out by means of equation

$$\Phi(z) = \int_{E_{\text{пор}}}^{\infty} S(E)\, D(E, E_{\text{пор}}, 0z)\, G(z)\, e^{-\Sigma_{rem}(E)(1-0)z}\, dE,$$

(Subscript пор = th = threshold)

where S(E) is the spectrum of the source neutrons; Σ_{rem} is the removal cross section; D (E, E_{th}, θ_z) is the three-dimensional distribution of fast neutrons in the energy interval $E - E_{th}$ when the initial energy is E; G(x) is a geometric factor; z is the distance from the source to the point of measurement; θ is the volumetric concentration of the moderating hydrogen-containing medium.

We note that the applicability of this method is assumed when the following definite conditions are satisfied.

1. The distribution of the neutron flux is computed in a medium consisting of a hydrogen-containing moderator, in which the substance which moderates the neutrons according to the removal cross section is distributed in a homogeneous manner or in the form of slugs.

2. The layer of this moderator placed between the slug of the "removing" substance and detector, or (in the case of a homogeneous medium) the distance from the source to the detector, must not be less than a certain quantity r_0 (E, E_{th}). Furthermore, in this case r_0 depends on the properties of the "removing" substance. This method may be used for smaller thicknesses, but the value of the removal cross section must be lowered.

A direct application of the method of removal cross section for computing all groups of moderated neutrons is difficult in some cases, for example, in homogeneous mixtures, because the value of the removal cross section measured by means of a detector sensitive to slow neutrons may vary as a function of the homogeneous mixture composition. At the same time, this effect is substantially less for fast neutrons.

It has been proposed to compute the fluxes of neutrons formed as a result of the moderation of fast neutrons by applying the age approximations (refs. 3 and 4). The sources of moderation consisted of a three-dimensional distribution of a fast group of neutrons computed by the method of removal cross sections.

References 4 and 5 assume that if we neglect the question concerning the buildup of neutrons with small energies, we can attempt to transfer the method of utilizing removal cross section to a medium which contains light moderators in place of hydrogen. In these references a moderator of this type consisted of boron carbide in a mixture of iron and lead. The removal cross sections of iron, lead and water were measured when these were uniformly mixed with boron carbide and also when they were placed into the latter as slugs. It turned out that the removal cross section of these substances in boron carbide, measured by the fission chambers with Th^{232} and U^{235} coincide and are close in magnitude to the removal cross section of these substances measured in water.

The present work presents additional experimental data which prove that it is possible to generalize the method of removal cross sections and apply it to heavier moderating media. In these experiments the moderating media consisted of aluminum. Neutron sources with E = 4 MeV and 14.9 MeV were used. The removal cross sections of iron and lead in boron carbide were also measured with a neutron fission spectrum and a removal cross section of iron with the spectrum of the VVR reactor (ref. 6).

Experimental Setup

The sources of neutrons consisted of the D (d, n) He^3 reaction with /55 initial neutron energy of E = 4 MeV, T (d, n) He^4 (E = 14.9 MeV), and a U^{235} disk placed on the beam of thermal neutrons removed from the reactor of the first atomic electric power station in the world.

The sources had the form of disks with a diameter of 10 mm for sources of single energy neutrons and a diameter of 46 mm for sources of the fission spectrum.

Fast neutrons were detected by means of a Th^{232} fission chamber. A detailed description of the detector is given in references 4 and 5. The geometry of the optics is similar to the one described in reference 5. The aluminum prisms were made up from sheets with dimensions 1000 × 1000 × 10 mm^3. The iron and lead plates had dimensions 710 × 710 × 10 mm^3 and were used to make up slugs with a thickness up to 100 mm. The tanks with water, prisms from polyethylene and plexiglas had transverse dimensions of 1000 mm. Measurements in the VVR reactor were carried out using a barrier geometry. The geometry of this experiment is described in detail in reference 6. In these measurements an analysis was made of the effect of γ-rays and of slow neutrons on the count of the Th^{232} fission chamber. Their effect was eliminated by using filters made of lead and boron carbide.

Measurements and Results

Figures 1 and 2 show the measurements made by means of the Th^{232} fission chamber of the attenuation of fast neutron fluxes in aluminum and in uniform mixtures of aluminum with iron and lead, using neutron sources of E = 4 and 14.9 MeV. Similar measurements were carried out for assemblies from aluminum in which blocks of iron, lead, plexiglas ($C_5H_8O_2$) and polyethylene (CH_2) were placed between the source and the detector and also in uniform mixtures of aluminum with plexiglas. On the basis of these measurements calculations were made of the removal cross sections for iron, lead, polyethylene and /59 plexiglas in aluminum (figs. 3 and 4). The results of measurements using fission neutron spectrum in boron carbide, in uniform mixture of boron carbide with iron and lead and in boron carbide with iron slugs of thickness 100 mm are shown in figure 5, and the removal cross sections for iron and lead computed from these data are shown in the table.

The results of the measurements using the VVR reactor in graphite with a mixture of 7 percent boron by weight, and in boron-treated graphite and in water behind the iron layer are shown in figures 6-8. The broken line shows the attenuation of neutrons obtained from calculations in which the value of the removal cross section was assumed to be equal to 0.168 cm for measurements in water and 0.154 cm for measurements in the graphite treated with boron.

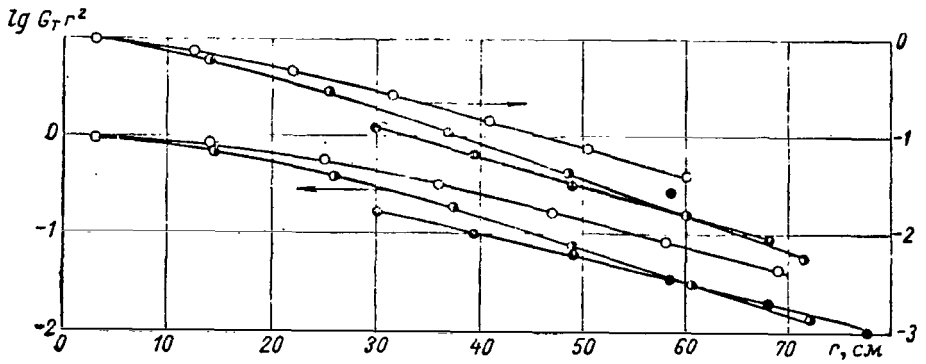

Figure 1. Three-dimensional distribution of fast neutrons measured by means of Th^{232} fission chamber (for left ordinate E = 14.9 MeV, for right E = 4 MeV): O, in aluminum; ◑, in a uniform mixture with iron (the thickness of iron layers was 2 cm and of aluminum layers 9.5 cm); ●, aluminum behind iron slug with thickness of 10 cm.

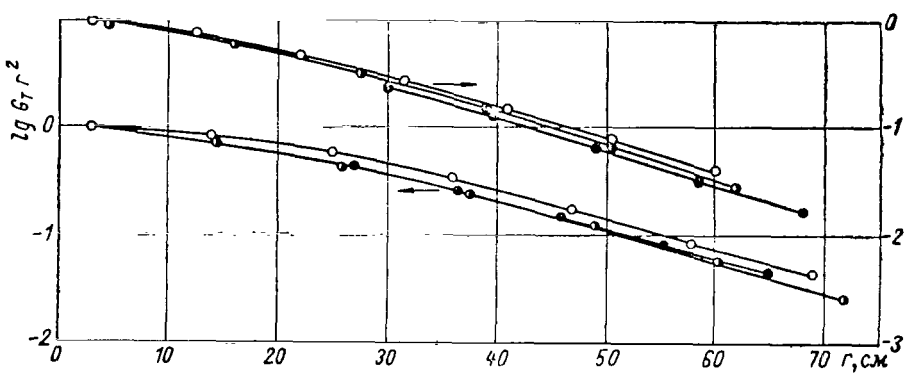

Figure 2. Three-dimensional distribution of fast neutrons measured by means of Th^{232} fission chamber (for left ordinate E = 14.9 MeV, for right E = 4 MeV): O, in aluminum; ◑, in uniform mixture of Pb with Al (thickness of lead layer was 2 cm and of aluminum layer 9.5 cm); ●, in aluminum with lead slug of thickness of 10 cm.

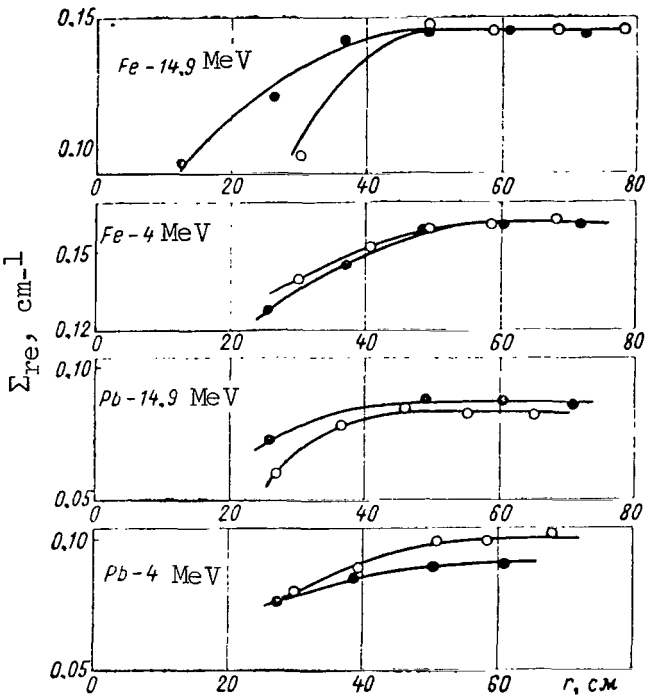

Figure 3. Variation in removal cross section of iron and lead in aluminum for neutrons with energies E = 4 MeV and 14.9 MeV; ● , as function of distance between source and detector in uniform mixtures; O , as function of distance between slug of the removal material and the detector.

Discussion of Results

The table presents removal cross sections for neutrons of the fission spectrum and for single energy neutrons with E = 4 and 14.9 MeV measured in water, boron carbide and aluminum. The removal cross sections measured in the present work as well as those obtained by other authors are presented. From the comparison of quantities presented in the table and from the examination of results shown in the figures we can draw the following conclusions.

1. The method of removal cross sections is applicable to the calculation of shieldings in which other light media such as boron carbide or aluminum are used as moderators in place of water.

2. The magnitude of the removal cross sections for most of the investigated substances depends very little on the selection of the moderator medium. Thus for the spectrum of the VVR reactor the removal cross section of iron in graphite treated with boron is 10 percent lower than during measurements in water. However, this discrepancy does not exceed the measurement errors.

We should note that in principle it is also possible to use the method of removal cross sections when we have a very heavy moderator. However, the

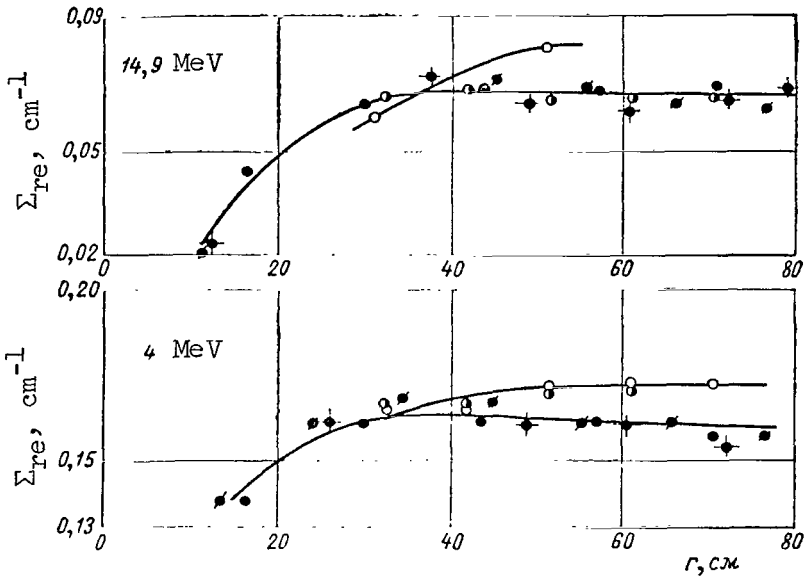

Figure 4. Variation in removal cross section of polyethylene and plexiglas in aluminum for neutrons with energies E = 4 MeV and 14.9 MeV: O , polyethylene, obtained from measurements in slug geometry (thickness of polyethylene slug was 11.1 cm); ◑ , plexiglas, obtained from measurements in slug geometry (thickness of plexiglas layer was 12.4 cm); and in uniform mixtures; ⊘ , thickness of plexiglas layers 1 cm; ⊕ , thickness of plexiglas layers 2 cm; ● , thickness of plexiglas layers 4 cm. (Subscript re = removal.)

variation in the removal cross section as a function of the atomic number of the moderator is weak when the atomic weights of the moderator are relatively small (at least up to A = 27), and this leads to a substantial decrease in the removal cross section when the atomic weights of the moderator are very high. Thus the removal cross section of iron measured in H_2O for neutrons with energy 4 MeV is equal to 0.168 cm, whereas the same cross section measured in a moderator of iron (the quantity inverse of the relaxation length) is equal to 0.132 cm. In addition, the removal cross section in a heavy moderator may depend substantially on the energy threshold of the detector used to measure this cross section.

3. Both in the uniform mixtures and in the slug geometry the removal cross section becomes saturated with relatively small distances r_0.

4. In boron carbide as well as in water measurements made with the detector of the chamber with U^{235} type give a value for the cross section equal

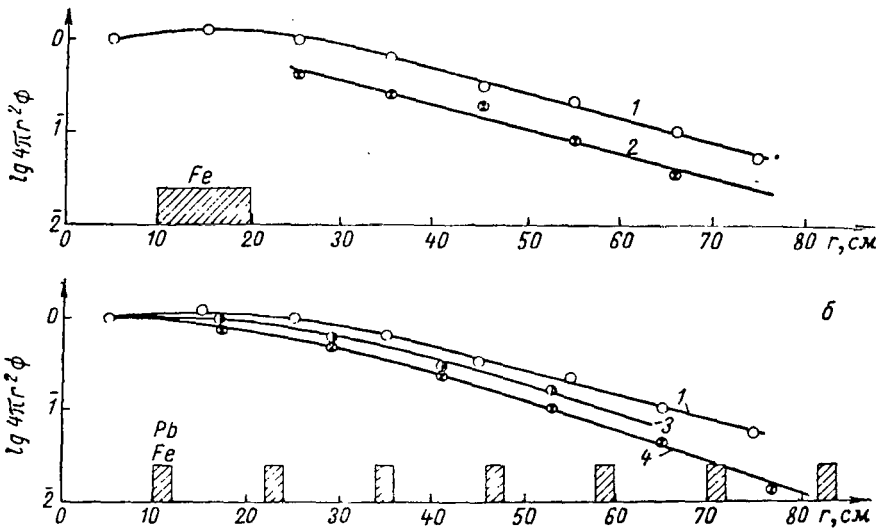

Figure 5. Three-dimensional distribution of gas neutrons from neutron source of fission spectrum in boron carbide behind iron slug (a) and in uniform mixtures of boron carbide with lead and iron (b): 1, in boron carbide; 2, in boron carbide behind iron slug; 3, in uniform mixture of boron carbide with lead; 4, in uniform mixture of boron carbide with iron.

to that measured by means of threshold detectors for fast neutrons--Th^{232} chamber.

5. At a sufficient distance, greater than r_0, the removal cross sections, measured in a uniform mixture and in slug geometry, are close.

6. The quantity, which is the inverse of the relaxation length, at sufficiently large distance from the source is equivalent to the removal cross section of the given material in the material itself and for light media, as we can see from the table. Such a quantity must be close to the removal section of this material in other media. An exception to this is the quantity λ_{rel}^{-1} for graphite with neutron energy 14.9 MeV. Apparently such exceptions are possible in media with large "dips" in the total cross section at energies smaller than the initial energy of the neutron. In the cross section of carbon such a dip is observed at an energy of 6.7 MeV. The removal cross section measured in such media at large distances from the source must correspond to the energy at which we have a dip in the cross section of the moderator. This apparently explains the abnormally large relaxation length in graphite for neutrons with an initial energy of 14.9 MeV. The reciprocal of the relaxation length in graphite for E = 14.9 MeV is equal to 0.0416 cm, and the cross section for the removal of graphite in water is 0.077 cm.

REMOVAL CROSS SECTIONS MEASURED IN WATER, BORON CARBIDE AND ALUMINUM.

Material	Density in g/cm^3	Nuclear density $nuc/cm^3 \times 10^{24}$	E_0 = 4 MeV				E_0 14.9 MeV				Fission spectrum		
			Σ_{re} B H_2O	Σ_{re} B B_4C	Σ_{re} B Al	$\Sigma = 1/\lambda_{rel}$	Σ_{re} B H_2O	Σ_{re} B B_4C	Σ_{re} B Al	$\Sigma = 1/\lambda_{rel}$	Σ_{re} B H_2O	Σ_{re} B B_4C	Σ_{re} B Graphite treated with boron
Polyethylene CH_2	0.92	0.0394*	---- ----	---- ----	0.168 ---	0.182[8] ----	---- ----	---- ----	0.081 ---	0.072[8] ----	0.112[3] ----	--- ---	--- ---
H_2O	1.00	0.0335*	0.159[6,8] ----	0.165[4] ----	--- ---	0.159[6,8] ----	0.076[6,8] 0.066	0.084[4] ----	--- ---	0.076[6,8] ----	---- ----	--- ---	--- ---
Plexiglas $C_5H_8O_2$	1.18	0.00846*	---- ----	---- ----	0.171 0.161	0.160[8] ----	---- ----	---- ----	0.066 **0.067**	0.066[8] ----	---- ----	--- ---	--- ---
Boron carbide B_4C	1.67	0.0182*	---- ----	0.083[5] ----	--- ---	0.083[5] ----	0.076[9] ----	0.058[5] ----	--- ---	0.058[5] ----	0.078 0.085	--- ---	--- ---
Graphite C	1.67	0.0836	---- 0.094**[8]	---- ----	--- ---	0.088[6] ----	0.077[9] 0.057**[8]	---- ----	--- ---	0.042[6] ----	0.068[3] 0.075[2]	--- ---	--- ---
Aluminum Al	2.7	0.0602	0.07 ----	---- ----	0.071 ---	0.071 ----	0.087[9] 0.066 ----	---- ----	0.063 ---	0.063 ----	0.079[1,3] ----	--- ---	--- ---
Iron Fe	7.83	0.0848	---- 0.160[10]	0.169[4] 0.171[5]	0.162 0.162	0.132[6,7] ----	0.134[9] 0.113[10]	0.137[4] 0.136[5]	0.145 0.145	0.121[6,7] ----	0.167[1,2] 0.168[3]	0.161 0.155	0.154 ---
Lead Pb	11.34	0.033	---- ----	0.113[4] 0.113[5]	0.101 0.092	0.067[7] ----	0.112[9] ----	0.097[4] 0.096[5]	0.084 0.088	0.0645[6,7] ----	0.108[2] 0.115[1] 0.117[3] ----	--- 0.112	--- ---

Remark: For each substance the upper horizontal series of values refers to the measurements carried in a slug geometry, and the lower pertains to measurements carried out in uniform mixtures. The square brackets ([ ]) refer to literature sources from which the removal cross sections were taken.

*Nuclear density expressed in molecules per cubic centimeter.

**Obtained by computations from experimental attenuation curves in polyethylene and from computed curves in hydrogen.

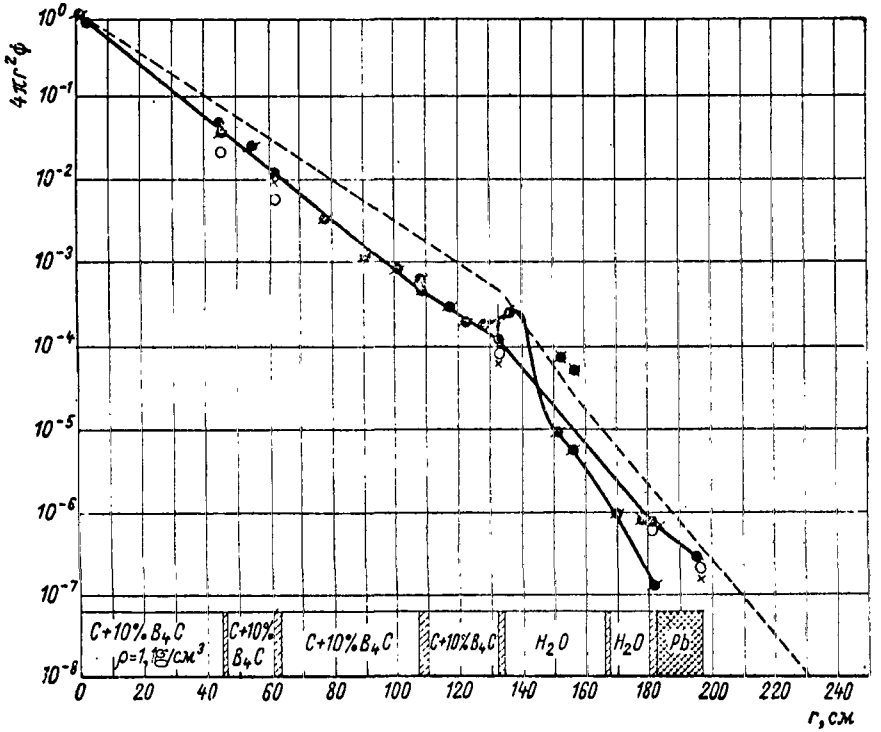

Figure 6. Three-dimensional distribution of neutrons from spectrum of VVR reactor in mixture of graphite with 7 percent boron by weight (infinite geometry): ●, U^{235} in cadmium; ●, U^{235} without cadmium; ×, ZnS (Ag); ●, Th^{232} (fast neutrons); O, all-wave counter (total flux); – – – – – calculated (for carbon with boron carbide Σ_{rem} = 0.049 cm^{-1}); ———, experimental.

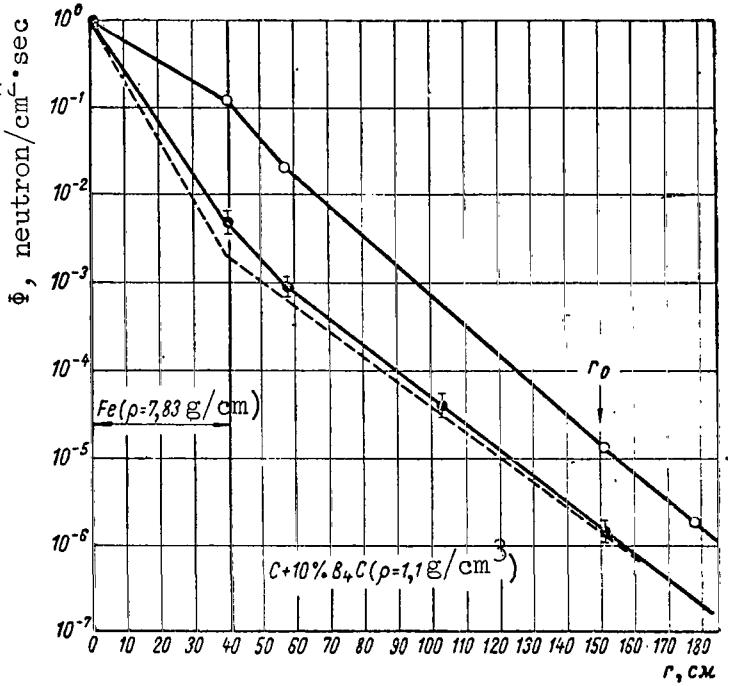

Figure 7. Three-dimensional distribution of neutrons from spectrum of VVR reactor in mixture of graphite with 7 percent boron by weight behind layer of iron with thickness of 40 cm (barrier geometry): – – – – – calculated (for iron Σ_{rem} = 0.154 cm^{-1}); ———, obtained experimentally; O, all-wave counter (total flux); ⊤●⊥, Th^{232} (fast neutrons).

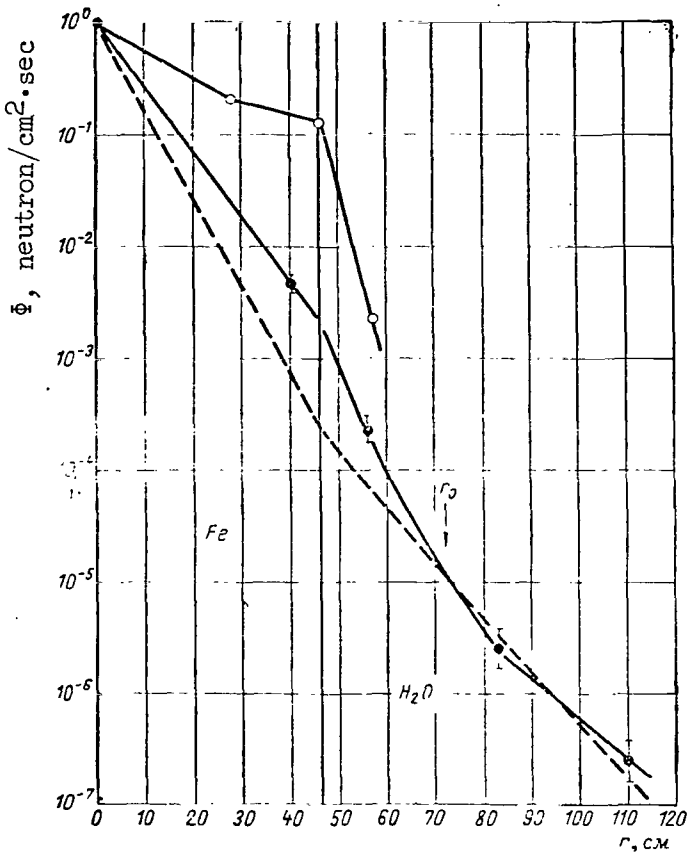

Figure 8. Three-dimensional distribution of neutrons from spectrum of VVR reactor in water behind layer of iron with thickness 46 cm (barrier geometry): – – – – – computed for iron $\Sigma_{re} = 0.168$ cm^{-1}); ———, obtained experimentally; O , all-wave counter (total flux); ⊥●⊥ , Th^{232} (fast neutrons).

7. The practical application of the method of removal cross sections /60 for computing the distribution of a fast neutron group with a low lower boundary of the group, with values of removal cross sections obtained for measurements in water, is possible only when a light moderating medium is present. An example of this is the sufficient discrepancy between the quantities λ_{rel}^{-1} and Σ_{re} for iron and lead.

8. When a light component is absent in the shielding the application of the method is possible, if we know the removal cross section of the material in

the given medium or if the lower boundary of the energy group is sufficiently raised. Apparently it is possible to select a boundary energy such that the removal cross section of a given material will not depend on the composition of the medium situated behind the removing material.

The author expresses his gratitude to V. P. Bogdanov, S. G. Osipov, G. V. Rykov, V. S. Tarasenko and A. I. Chusov, who participated in making the measurements.

REFERENCES

1. Shielding of Nuclear Reactors. Edited by T. Rockwell (Zashchita yadernykh reaktorov. Pod redaktsiyey T. Rokvella). Izd-vo I. L., Moscow, 1958.

2. Burgeois, J., Lafore, P. et al. Methods and Experimental Coefficients Used in the Computation of Reactor Shielding. A/Conf./15/P/1190, 1958.

3. Price, B., Horton, C. and Spinney, K. The Shielding of Nuclear Radiations (Zashchita ot yadernykh izlucheniy). Izd-vo I. L., Moscow, 1959.

4. Broder, D. L., Kutuzov, A. A. and Kondrashov, A. P. Three-dimensional Distribution of Neutrons in Mixtures of Boron Carbide with Fe and Pb. IN: Neutron Physics (Prostranstvennyye raspredeleniya neytronov v smesyakh karbida bora s Fe i Pb. V Sb: Neytronnaya fizika). Gosatomizdat, Moscow, 1961.

5. --- Atomnaya Energiya, Vol. 6, 578, 1959.

6. Broder, D. L., Kurkin, S. A., Kutuzov, A. A., Levin, V. V. and Orlov, V. V. Three-dimensional Energy Distribution of Neutrons in Various Media. IN: Transactions of the Second International Conference on the Peaceful Utilization of Atomic Energy. Reports of Soviet Scientists, Vol. 2, Nuclear Reactors and Nuclear Power Engineering (Prostranstvenno-energeticheskiye raspredeleniya neytronov v razlichnykh sredakh. V kn.: Trudy Vtoroy mezhdunarodnoy konferentsii po mirnomu ispol'zovaniyu atomnoy energii. Dokl. sovetskikh uchenykh. T. 2--Yadernyye reaktory i yadernaya energetika). Atomizdat, Moscow, 1959.

7. Broder, D. L., Kutuzov, A. A., Levin, V. V., Orlov, V. V. and Turusova, A. V. Atomnaya Energiya, Vol. 7, 313, 1959.

8. Broder, D. L., Kutuzov, A. A. and Levin, V. V. Inzh.-fiz.zh., Vol. V, No. 2, 47, 1962.

9. Degtyarev, S. F., Kukhtevich, V. I., Sinitsyn, B. I. and Tsypin, S. G. The Removal Cross Sections of Fast Neutrons with Energies of 3 and 15 MeV. IN: Neutron Physics (Secheniya vyvedeniya bystrykh neytonov s energiyami 3 i 15 Mev. V sb: Neytonnaya fizika). Gosatomizdat, Moscow, 1961.

10. Broder, D. L. Atomnaya Energiya, Vol. III, 55, 1957.

EXPERIMENTAL JUSTIFICATION FOR THE MULTIPLE GROUP METHODS IN THE COMPUTATION OF BIOLOGICAL SHIELDING

D. L. Broder, A. P. Kondrashov, A. A. Kutuzov, V. A. Naumov, Yu. A. Sergeyev and A. V. Turusova

Introduction /60

The calculation of biological shielding is associated with the determination of three-dimensional energy distributions of neutrons in media containing light and heavy nuclei. A series of methods has been developed which in some manner or other are based on the solution of the kinetic equations. We may mention such numerical methods of solving the three-dimensional energy problem as the polynomial method (ref. 1) and the method of solving the single velocity problem in the P_9-approximation which has been developed for heavy media (ref. 2).

However, the first method, which can be applied to any medium in principle, requires cumbersome computation work and therefore is not applicable to the practical calculation of shielding. The second method, presented in reference 2, does not take into account the moderation of neutrons due to elastic collisions with nuclei and for this reason can be applied only to the calculation of heavy media.

References 3 and 4 propose an analytical method for solving the energy /61 problem which utilizes the calculation of a group of fast neutrons by the semi-empirical method of "removal cross sections" with subsequent estimation of moderation in the age approximation. This method is interesting, because it automatically takes into account all of the processes which lead to the moderation of fast neutrons including inelastic scattering and moderation due to elastic processes into the energy region below 1-1.5 MeV, where the inelastic processes for most of the nuclei begin to play a secondary role. The shortcoming of this method is that it can be applied only at large distances from the source in the region of an equilibrium spectrum.

In the present work an effort is made to verify experimentally the method which can be used to calculate the three-dimensional energy distributions of neutrons at any distances from the neutron source. Two methods of solving the problem are considered: the 10-group and 7-group method in a diffusion and age-diffusion approximation, respectively. The applicability of approximations of this type to calculating shielding is not obvious when strong absorption is present. Moderation by hydrogen also complicates the applicability of these

methods to a significant degree. We should note the case when the thickness of the layers is small, which limits the possibility of applying the given calculation methods. When the neutron energies are high, it is also important to bear in mind that the scattering of neutrons by most of the medium and heavy nuclei is nonisotropic. However, there is a series of circumstances which permits us to hope that the prospects of applying these methods are favorable. Factors of this type should include the large contribution of inelastic processes when the neutron energies are greater than 1 MeV.

The scattering of neutrons during inelastic collisions is isotropic, and the nonisotropic nature of elastic scattering may be compensated for by introducing the transport scattering cross section. At lower energies the elastic scattering becomes more isotropic. The absorption processes begin to play a large role only in the lower groups. On the basis of these statements an effort has been made to substantiate the applicability of these methods of calculation experimentally.

The 7-group method was developed for the purpose of introducing certain corrections and improvements in the calculation of fast neutron groups. The basic idea consists of assigning a three-dimensional distribution of a fast neutron group with energy $E > 1.5$ MeV, using the semiempirical method of "removal cross sections" with subsequent calculation utilizing the age-diffusion approximation.

As we know, the age model is insufficiently convincing for a medium containing hydrogen. However, it is shown in reference 5 that the difference between the results obtained by carrying out the calculations by means of the age approximation and the results of the exact solution even for water at distances from the source, where the age consideration is valid, does not exceed 30 percent. This situation makes it possible for us to hope that the results of our calculations will be favorable.

The refinements made here pertain therefore only to groups of neutrons with $E > 1.5$ MeV, which as a rule determine the three-dimensional distribution of neutron fluxes. Both methods of calculation were applied to the calculation of three versions of shielding of relatively small thickness with and without boron. Boron was introduced for the purpose of investigating the questions of the applicability of the diffusion and the age-diffusion approximations to the calculation of shieldings with different absorption of neutrons in the thermal and above thermal regions. These same versions were investigated experimentally.

The simplicity of the calculation method according to the initial scheme should have provided for a small number of energy groups. However, the path from a large number of groups to a small number appears to be more natural. It is for this reason that the 7- and 10-group systems of constants were developed. At the present time we are completing work for the contraction of a 10-group system of constants down to a 3-group system. Work is also being carried out to refine the computation technique by applying the P_2-approximations. This is particularly important in the region where we have groups of fast neutrons

which determine the three-dimensional distributions at large distances in the shielding.

Selection of Groups in the 7- and 10-Group Methods

The breakdown of the energy region into groups is shown in the table. /62 As we can see from the table, the region of fast neutrons, $E > 0.7$ MeV, which is most important from the point of view of a correct determination of the place where neutrons are absorbed in the shielding (and consequently the determination of the three-dimensional distribution of capture radiation sources), is broken down into four intervals. The boundaries of the groups in this region are selected in such a way that the transverse scattering cross section of hydrogen, nickel, iron, chromium and lead change very little within the limits of each group. When the groups are selected in this manner the neutrons generated during fission are distributed rather uniformly over the groups. This makes it possible to take into account the leakage of neutrons from the reactor more accurately. The uppermost group covers a region of energies from 4 MeV to ∞. A more detailed breakdown of this interval is not expedient, because there is a relatively small amount of data on the transverse cross sections of inelastic scattering and on the angular distribution of scattered neutrons for this region of energies. The lower boundary of the region of fast neutrons approximately coincides with the threshold of the inelastic scattering of the elements which have been mentioned.

The next region of intermediate neutrons from 40-700 keV contains two groups and one group from 1-40 keV. This is a transient region from the moderation mechanism which takes place by inelastic scattering to the moderation

10-Group method			7-Group method		
Group No.	Lower level of group in eV	Neutrons	Group No.	Lower level of group in eV	Neutrons
1	$4 \cdot 10^6$		1	$1.5 \cdot 10^6$	Fast
2	$2.5 \cdot 10^6$	Fast	2	$9 \cdot 10^5$	
3	$1.5 \cdot 10^6$		3	$4.5 \cdot 10^5$	Intermediate
4	$7 \cdot 10^5$		4	$3 \cdot 10^3$	
5	$3 \cdot 10^5$	Intermediate	5	3.3	Resonance
6	$4 \cdot 10^4$		6	E_{bound}	
7	$1 \cdot 10^3$		7	0	Thermal
8	6.7	Resonance			
9	E_{bound}				
10	0	Thermal			

mechanism resulting from elastic processes and is also a transient region from the spectrum of fast neutrons to the Fermi spectrum. The lower boundary of the second group in this region (40 keV) is selected as the energy for a definite establishment of the Fermi spectrum. Three groups are isolated below 40 keV up to the arbitrary boundary of the Maxwellian spectrum. Two of these are situated in a region where there is a significant probability for resonance capture. This is an energy region with the Fermi distribution of neutrons. An exception to this is the ninth group where the spectrum may differ from the Fermi spectrum to a large or small degree due to the increase in the probability of the neutron absorption processes. It was assumed that the neutrons which are moderated beyond the lower boundary of the ninth group are in thermal equilibrium with the medium and thus represent the thermal group.

In the 7-group method, the group of fast neutrons with $E > 1.5$ MeV was computed on the basis of the "removal cross sections" method. The remaining groups also differ slightly in the selection of the energy boundaries. However, the basis of this selection is the same as for the case of the 10-group method.

Neutron Spectrum in the 10-Group Method

Fast Neutrons (0.7 MeV $< E < \infty$). It was assumed that the fast neutrons in the active zone of the water reactor and outside it have the spectrum /63

$$\Phi(E) = \frac{\int_E^\infty \Sigma_s(E')\chi(E')\, e^{-\frac{1}{\xi}\int_E^{E'} \frac{\Sigma_c}{\Sigma_c+\Sigma_s}\cdot\frac{dE}{E}}\, dE'}{\xi\Sigma E} + \chi(E), \qquad (1)$$

where $\chi(E')$ is the spectrum of fission neutrons; Σ_c, Σ_s, ξ are constants for H_2O. In the first two upper energy groups this spectrum practically coincides with the fission spectrum. The constants are averaged out over the spectrum (1) for all elements.

Intermediate and Resonance Neutrons ($E_{bound} < E < 0.7$ MeV). It was assumed that the spectrum of moderated neutrons in some medium containing a three-dimensional energy distribution of neutrons is formed by the medium itself. Apparently this assumption is valid if the neutron in a given medium travels several free path lengths. If the medium has small dimensions (less than the free path length), this assumption does not lead to substantial errors due to the small number of interactions with the medium. Since expression (1) assigns a spectrum in hydrogen, the cross sections for hydrogen and for the associated oxygen, carbon(for media CH_2, H_2O, $C_5H_8O_2$) were averaged considering the "weight" of spectrum (1) flux. In the ninth group the form of the flux was computed from the expression

$$\Phi(E) = \frac{1}{\Sigma E \sqrt{1+\Sigma_c/\Sigma_s)^2}}. \qquad (2)$$

For all media when absorption was small ($\Sigma_c/\Sigma_s \ll 1$) the variation in the flux as a function of energy was taken as specified by the equation

$$\Phi(E) = \frac{e^{-\int_E^{\infty} \frac{\Sigma_c}{\xi\Sigma_s}\frac{dE'}{E'}}}{\xi\Sigma E} \qquad (3)$$

and in the case of strong absorption as specified by equation

$$\Phi(E) = \frac{1}{\xi\Sigma E} e^{-\left\{\left(M+\frac{1}{3}\right)\frac{\Sigma_c}{\Sigma_s} - \frac{1}{3}M\left(\frac{\Sigma_c}{\Sigma_s}\right)^2\right\}}. \qquad (4)$$

Spectra (1-4) were borrowed by us from references 6 and 7.

Initial Equations and Group Constants for the 10-Group Method

A system of group constants was constructed as it applies to the diffusion equation, which may be written in the following form for group j

$$D_j\nabla^2\Phi_j - \Sigma_j\Phi_j + S_j^{\text{мод}} + S_{fj} = 0, \qquad (5)$$

where $\Phi_j = \int_{\Delta E_j} \Phi(E)\,dE$ is the integral flux of neutrons in a group with width ΔE_j; $D_j = \frac{1}{3\Sigma_{trj}}$ is the diffusion coefficient; $\Sigma_j = \Sigma_{cj} + \Sigma_{inj} + \Sigma_{sj} + \Sigma_{fj}$ is the total cross section for removal from group j; Σ_{cj}, Σ_{fj}, $\Sigma_{inj} = \sum_{h=j+1}^{10} \Sigma_{injh}$ and $\Sigma_{sj} = \sum_{h=j+1}^{10} \Sigma_{sjh}$ are the cross sections of absorption, fission, inelastic and elastic removal for group j, respectively; Σ_{trj} is the transport cross section; $S_j^{\text{мод}} = \sum_{h=1}^{j-1} \Phi_h(\Sigma_{shj} + \Sigma_{inhj})$ is the source in the group due to the moderation of neutrons; $S_{fj} = \sum_{h=1}^{10} (\nu_f\Sigma_f)_h\Phi_h \int_{\Delta E_j} \chi(E)\,dE$ is a source in the group due to fission. The macroscopic group cross sections are obtained in terms of the respective microscopic cross sections σ_{cj}, σ_{inj}, σ_{fj} and others. The group microscopic cross sections were determined in the following manner

/64

$$\sigma_{cj} = \int_{\Delta E_j} \Phi(E)\,[\sigma_{n\gamma}(E) + \sigma_{n\alpha}(E) + \sigma_{np}(E)]\,dE \Big/ \int_{\Delta E_j} \Phi(E)\,dE; \qquad (6)$$

$$\sigma_{jj} = \int_{\Delta E_j} \Phi(E)\,\sigma_f(E)\,dE \Big/ \int_{\Delta E_j} \Phi(E)\,dE; \tag{7}$$

$$\sigma_{in\,jh} = \int_{\Delta E_h} \int_{\Delta E_j} \sigma_{in}(E, E')\,\Phi(E)\,dE\,dE' \Big/ \int_{\Delta E_j} \Phi(E)\,dE, \tag{8}$$

where ΔE_k is the width of a group into which a neutron passes as a result of inelastic scattering.

The cross section of elastic removal from group to group was computed by means of an equation analogous to (7). If we note that elastic scattering takes out neutrons from the interval whose width $\Delta E_\alpha = E_{min}\ 1\text{-}\alpha/\alpha$ (E_{min} is the lower boundary of the group; $\alpha = (A\text{-}1/A\text{+}1)^2$) for heavy elements is substantially less than the width of the group, we have the following expression in the case of elastic scattering

$$\sigma_{sj\to j+1} = \frac{\xi\sigma_s\overline{\Phi_\alpha(u)}}{\int_{\Delta E_j} \Phi(u)\,du}, \tag{9}$$

where $\overline{\Phi_\alpha(u)}du$ is the average flux over the width ΔE_α, reduced to unit lethargy, while

$$\xi = \xi_0\ (1 - \overline{\cos\theta}), \text{ where } \xi_0 = 1 + \alpha/1\text{-}\alpha\ \ln\alpha.$$

The diffusion coefficient was computed in terms of the quantity $1/\sigma_{tr}$

$$\frac{1}{\sigma_{trj}} = \frac{\int_{\Delta E_j} \Phi(E)\,dE/\sigma_{tr}(E)}{\int_{\Delta E_j} \Phi(E)\,dE}, \tag{10}$$

where $\sigma_{tr}(E) = \sigma_{n\gamma}(E) + \sigma_{np}(E) + \sigma_{n\alpha}(E) + \sigma_f(E) + \sigma_s(E)(1-\mu) + \sigma_{inj}(E)$. The variation in the microscopic cross sections as a function of energy is taken from references 8 and 9. The group equations (1) written in the finite difference form were solved numerically by difference factorization. The calculation procedures have been presented in detail by G. I. Marchuk (ref. 10).

The calculations were carried out using plane geometry, because the experimental assemblies were added on towards the end of the reactor. We should point out that leakage of neutrons from the active zone and from the end screens was taken into account by introducing the term $\varkappa^2 D$ into the total group cross section where $\varkappa^2 = \left(\frac{2{,}405}{R}\right)^2$ for the active zone and $\varkappa^2 = \left(\frac{\pi}{a}\right)^2 + \left(\frac{\pi}{b}\right)^2$ for the screens

(R, a, b are the equivalent radius of the active zone and the transverse dimensions of the screens, respectively).

Results of the 10-Group Calculations

The results of calculations made by the 10-group method are represented in figures 1-3, where a comparison is made of Cu^{63} copper foil activations by thermal neutrons Q_T, above thermal neutrons Q_{TH} and the total activation $Q = Q_T + Q_{TH}$. /66

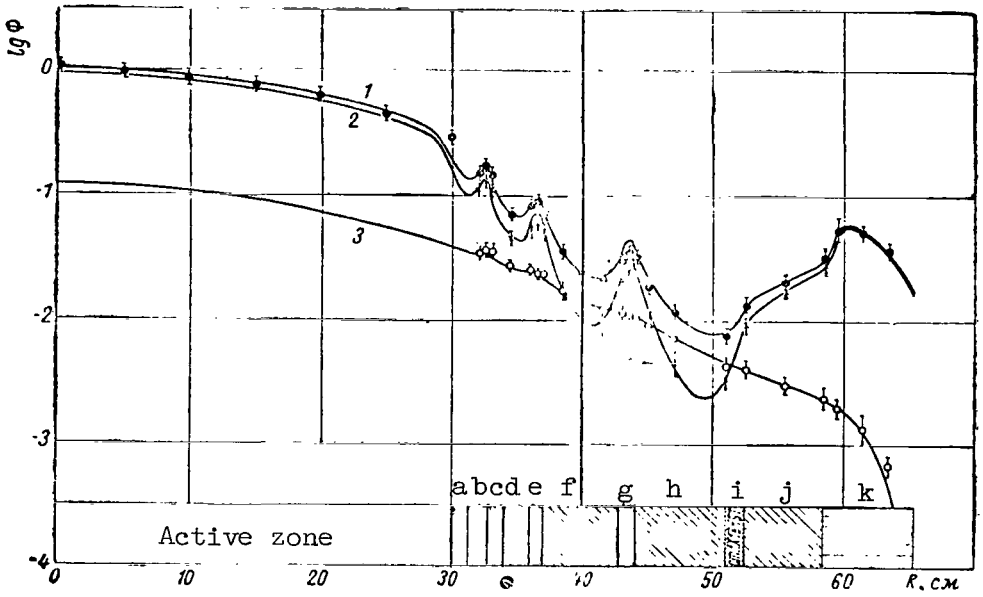

a - 1Kh18N9T steel
b - No. 3 steel
c - Plexiglas
d - 1Kh18N9T steel
e - Plexiglas
f - 1Kh18N9T steel
g - Plexiglas
h - No. 3 steel
i - 1Kh18N9T steel
j - Lead
k - Polyethylene

Figure 1. Spatial distribution of copper foil activations in active zone and in shielding (version No. 1): ⊤●⊥ for total activation (experimental results); ⊤○⊥ for activation foils in cadmium cases (experimental results); ⊤×⊥, for activation by thermal neutrons--cadmium difference (experimental values); 1, total activation computed by 10-group method; 2, cadmium difference according to 10-group method; 3, activation of copper and cadmium computed by 10-group method.

The values of activations were determined from the group cross sections of copper activation $\Sigma_j^{Cu^{63}}$ by means of relationships

$$Q_{th} = \int_{E_{Cd}}^{\infty} \Phi(E)\,\Sigma^{Cu^{63}}(E)\,dE = \sum_{j=1}^{9} \Phi_j \Sigma_j^{Cu^{63}} - Q_R; \tag{11}$$

$$Q_T = \int_{0}^{E_{rp}} \Phi(E)\,\Sigma^{Cu^{63}}(E)\,dE = \Phi_{10}\Sigma_{10}^{Cu^{63}} + Q_R. \tag{12}$$

$$Q = \int_{0}^{\infty} \Phi(E)\,\Sigma^{Cu^{63}}(E)\,dE = \sum_{j=1}^{10} \Phi_j \Sigma_j^{Cu^{63}}. \tag{13}$$

(Subscript rp = bound)

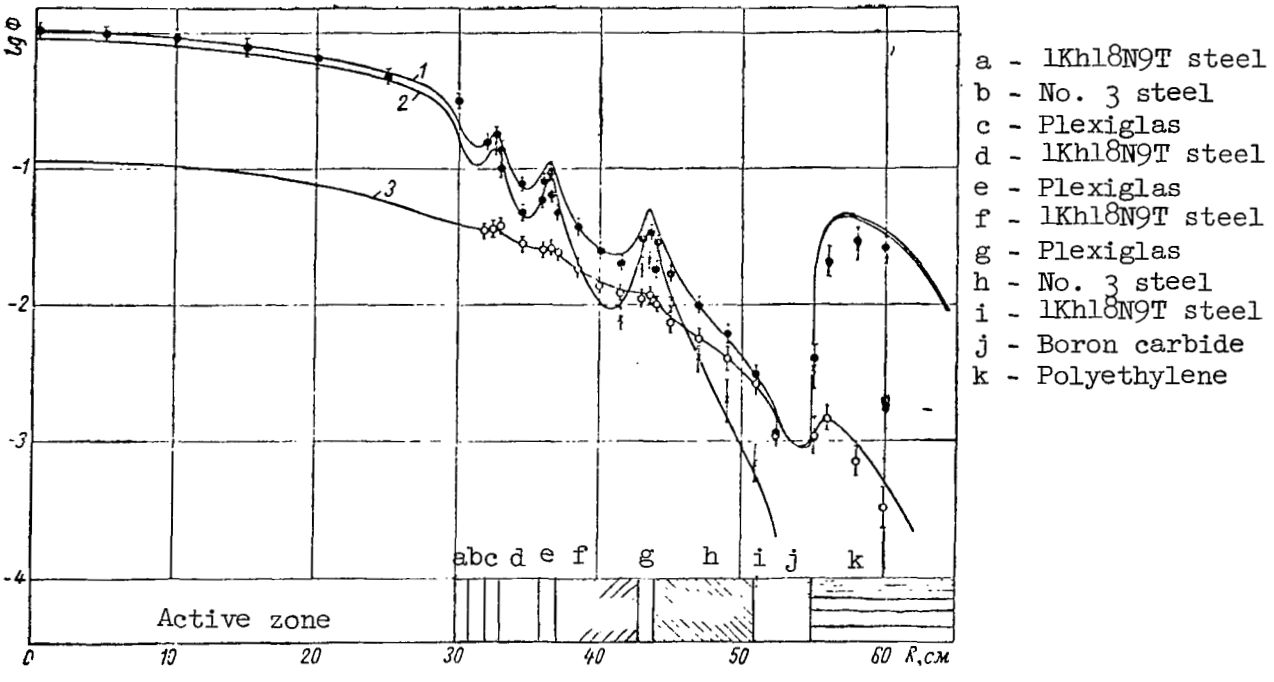

Figure 2. Spatial distribution of copper foil activation in active zone and in shielding (version No. 2): ● for total activation (experimental values); ○ for activation of foils in cadmium cases (experimental values); ✳ for activation by thermal neutrons--cadmium difference (experimental values); 1, total activation computed by 10-group method; 2, cadmium difference according to 10-group method; 3, activation of copper in cadmium computed by 10-group method.

The energy of the cadmium boundary $E_{Cd} \simeq 0.4$ MeV) does not coincide with the boundary energy of the thermal group ($E_{bound} = 0.17$ eV); therefore the activation of the interval 0.7 eV < E < 0.4 eV by neutrons must be added to the quantity $\Phi_{10}\Sigma_{10}^{Cu^{63}}$. The quantity Q_R was computed on the basis of spectra obtained in the 10-group calculation and partially on the basis of expressions (1-4) mentioned previously.

Analogous calculations whose results agree well with experiments were carried out for the activation distributions of indium foil from a point neutron fission source in water and for the Th^{232} fission chamber count from a source of monoenergetic neutrons (E = 4 MeV) in iron. /67

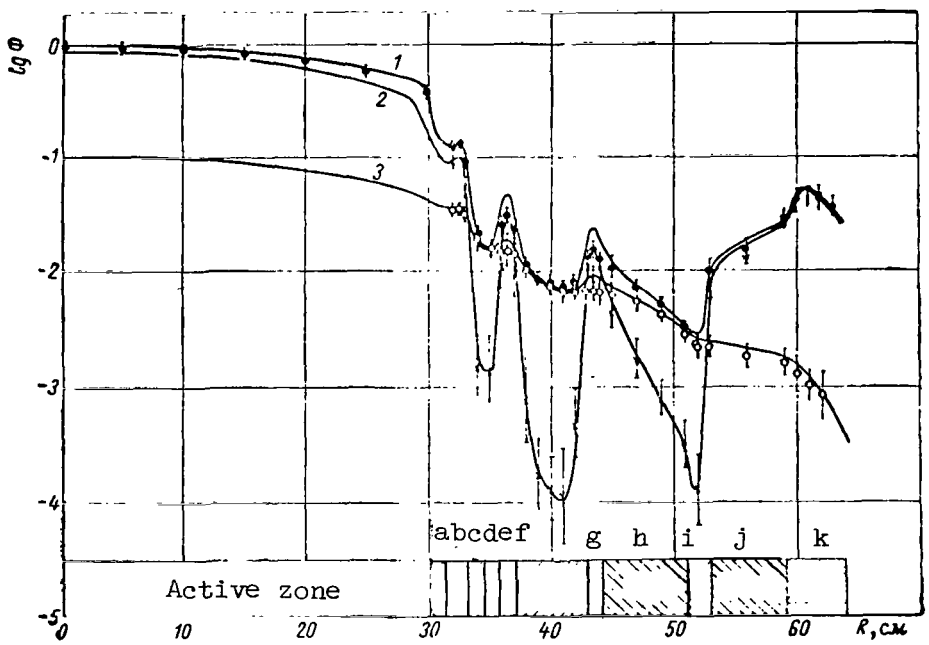

a - 1Kh18N9T steel
b - No. 3 steel
c - Plexiglas
d - Boron steel
e - Plexiglas
f - Boron steel
g - Plexiglas
h - No. 3 steel
i - Boron steel
j - Lead
k - Polyethylene

Figure 3. Spatial distribution of copper foil activation in active zone and in shielding (version No. 3): ⊤●⊥ for total activation (experimental values); ⊤○⊥ for activation of copper foils in cadmium cases (experimental values); ⊤✳⊥ for activation by thermal neutrons (cadmium difference) (experimental values); 1, total activation computed by 10-group methods; 2, cadmium difference according to 10-group method; 3, activation of copper in cadmium computed by 10-group method.

Initial Equations and Group Constants of the 7-Group Method

The three-dimensional energy distribution of neutrons in an age-diffusion approximation is described by the following system of equations:

$$\nabla D_1 \nabla \Phi_1 - \Sigma_{re,1} \Phi_1 = -S \quad (14)\text{--equation for the first group;}$$

$$\frac{\partial q}{\partial u} - \nabla D \nabla \Phi + \Sigma_c \Phi = 0 \quad (15)\text{--equation of moderation for the second, third ... (m-1) groups;}$$

$$\nabla D_T \nabla \Phi_T - \Sigma_{cT} \Phi_T = -q(r, u_T) \quad (16)\text{--equation for the thermal group,}$$

where $q(u) = (\xi\Sigma_s + \gamma\Sigma_c)\,\Phi(u)$; S_j are the fission sources; $D = \frac{1}{3\Sigma_{tr}}$ is the diffusion coefficient; Σ_c is the capture cross section.

By using simple transformations the system of equations (14-16) for any j-th group expanded in the interval of logarithmic energy u_{j-1}-u_j is reduced to the form

$$D_j \nabla^2 \Phi_j - \Sigma_j \Phi_j = -S_j \quad (j = 1, \ldots, m). \tag{17}$$

This equation for the first group of neutrons with $E > 1.5$ MeV was solved only for the active zone. In the shielding the distribution of neutron fluxes with this energy was obtained from experimental data. It was assumed that in the interval u_{j-1}-u_j the function $q(u, r)$ is approximately equal to its value at the end of the interval when the logarithmic energy is u_j.

In this case

$$\Phi_j = \begin{cases} \Phi_1 & \text{when } j = 1; \\ q(u_j, r)\,\frac{1}{\Delta u_j} \int\limits_{u_{j-1}}^{u_j} \frac{du}{\xi\Sigma_s + \gamma\Sigma_c} = q(u_j, r)\,\mu_j & j = 2, \ldots, m-1; \\ \Phi_T & j = m. \end{cases}$$

The diffusion coefficient is equal to

$$D_j = \begin{cases} \frac{1}{3\Sigma_{tr_1}} & \text{when } j = 1; \\ \int\limits_{u_{j-1}}^{u_j} \frac{du}{3\Sigma_{tr}(\xi\Sigma_s + \gamma\Sigma_c)} \Big/ \int\limits_{u_{j-1}}^{u_j} \frac{du}{\xi\Sigma_s + \gamma\Sigma_c} & j = 2, \ldots, m-1. \\ \frac{1}{3\Sigma_{tr_T}} & j = m. \end{cases}$$

The cross section for removal from the group is equal to

$$\Sigma_{yn\,j} = \begin{cases} \Sigma_{yn} & \text{when } j=1; \\ \left[\int\limits_{u_{j-1}}^{u_j} \frac{1}{\xi\Sigma_s+\gamma\Sigma_c}\cdot\frac{P_j(u_j)}{P_j(u)}\,du\right]^{-1} & j=2,\ldots,m-1; \\ \Sigma_{cr} & j=m, \end{cases}$$

where

$$P_j(u) = e^{-\int\limits_{u_{j-1}}^{u}\frac{\Sigma_c}{\xi\Sigma_s+\gamma\Sigma_c}du'}$$

The discharge of neutrons from a given group j includes the transition into the group j + 1 due to elastic scattering and absorption of neutrons in the given group /68

$$S_j = \begin{cases} S_{jj} = \frac{\nu_j Q_-}{K_{\text{eff}}} & \text{for active zone} \quad j=1; \\ S_{jj} = 0 & \text{for shielding screens;} \\ S_j^{\text{mod}} = P_j(u_j)\,\Sigma_j\frac{\mu_j}{\mu_{j-1}}\Phi_{j-1} = \Sigma_j\eta_j\Phi_{j-1} & \text{for } j=2,\ldots,m-1; \\ S_j^{\text{mod}} = \frac{\Phi_{m-1}}{\mu_{m-1}} & \text{for } j=m; \\ \Delta u_j = u_j - u_{j-1}. \end{cases}$$

However, we should point out that calculations utilizing both the diffusion and the age-diffusion approximations have significant shortcomings. Basically these shortcomings are associated with the impossibility of describing the behavior of fast neutrons at large distances from the source. Therefore the solution of equation (14) cannot be utilized for the computation of the distribution of all intermediate neutrons. The fast group can be assigned more accurately either by solving the kinetic equation in the P_2 or P_3 approximation, or by obtaining the "removal cross sections" by means of the semiempirical method or from the experimental relaxation length.

The fast group was assigned in the following manner: the active zone was broken down into a series of elementary volumes, each of which was considered as a point source with the fission spectrum. The attenuation of neutrons in the water of the active zone and in the plexiglas between the steel screens was taken from the attenuation curve for the fluxes of fast fission neutrons in water, as presented in reference 1. Experimental data for relaxation length (ref. 2) was utilized for the attenuation of fast neutron fluxes in steel and in lead.

It was assumed that in the polyethylene, which is placed behind a sufficiently heavy layer of iron, the attenuation of fast neutrons takes place with a relaxation length of 5.2 cm (ref. 11). By adding the fluxes from all of the

elementary volumes of the active zone, the distribution of fast neutrons with energies greater than 1.5 MeV was obtained, which served as the source for the first intermediate group.

Figure 4 shows the three-dimensional energy distribution computed by seven groups for a spherical source.

A comparison of measured and computed copper foil activations by neutrons of all energies is shown in figures 5 and 6.

The copper foil activation cross sections were averaged out inside each group as in the 10-group method (see equations (11-13)). However, it was assumed that inside the group Φ (u) = const.

Experimental Setups and Detectors

The experimental verification of the method employed in these computations was carried out utilizing a critically assembled reactor with water moderator. The active zone was assembled from rods with uranium enriched with the 235 isotope. The rods were placed in a tank with distilled water. The active zone was put together in a hexahedral tank with a 27.4 cm side; the height of the zone was 62.6 cm; this tank was placed into another tank which was also

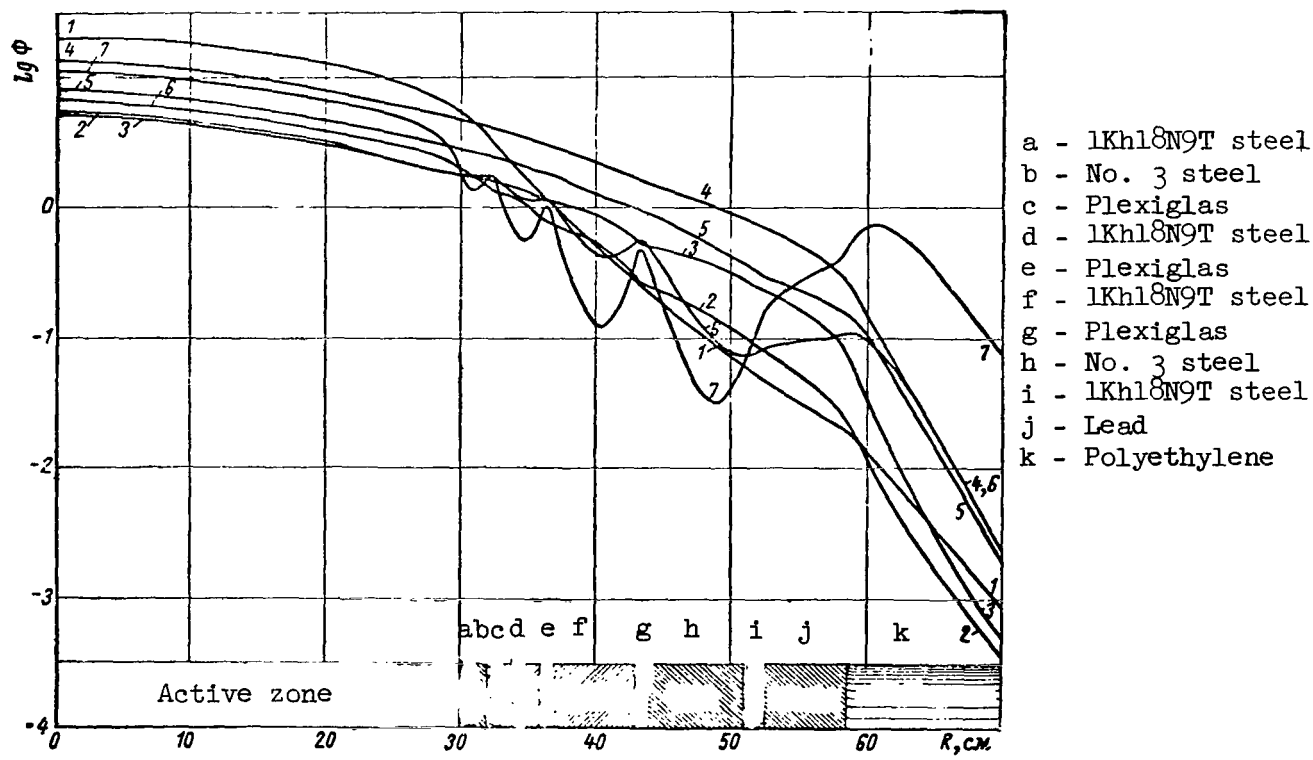

Figure 4. Distribution of various neutron groups computed by 7-group method: 1-7, numbers of neutron groups.

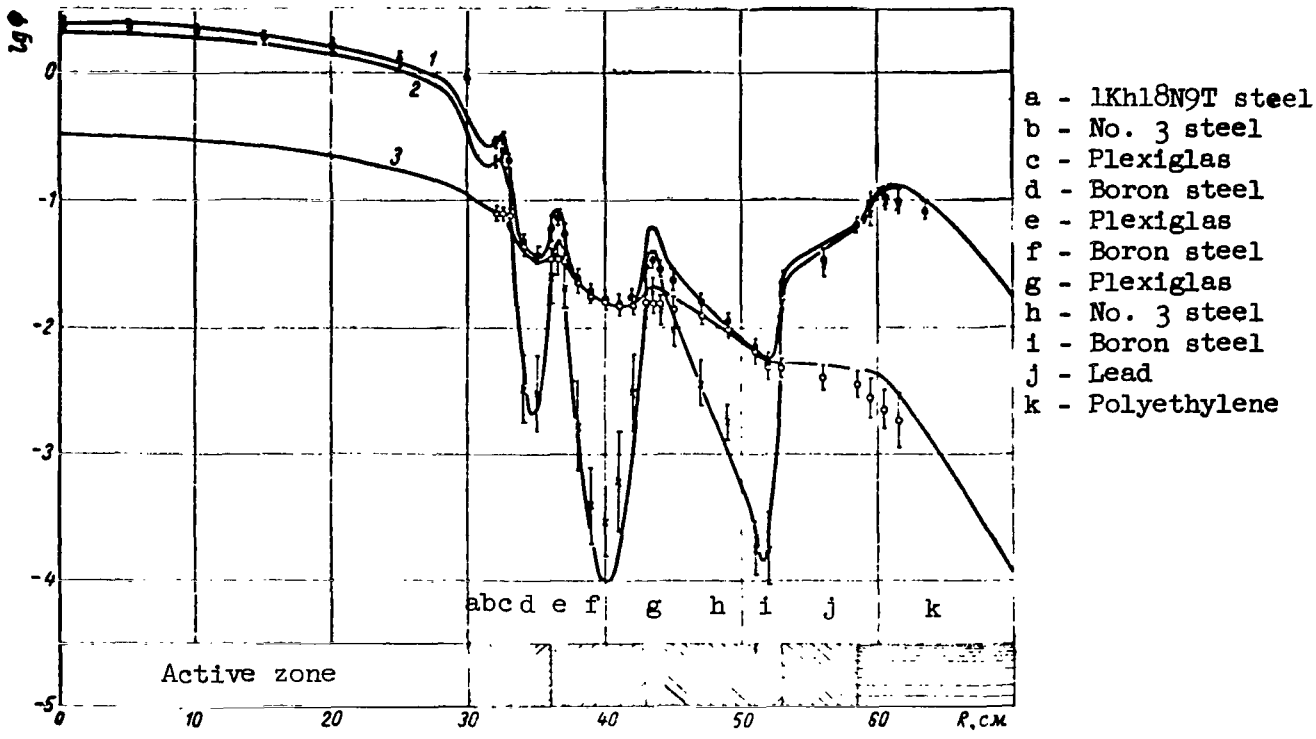

Figure 5. Three-dimensional distribution of copper foil activations in active zone and in shielding (version No. 3): ⊥●⊥ for total activation (experimental values), ⊥○⊥ for activation of foils in cadmium cases (experimental values), ⊥⊼⊥ for activation by thermal neutrons (cadmium difference) (experimental values); 1, total activation computed by the 7-group method; 2, cadmium difference according to 7-group method; 3, activation of copper in cadmium, computed by 7-group method.

hexahedral with a 50 cm side and the internal tank was filled with water. The interval between the external and internal tanks was designed to accommodate the side water reflector. The lower reflector consisted of the test screens. These screens, as well as the assembly simulating the reactor vessel and shielding were placed on a special lifting device and during operation /72 were moved flush against the bottom of the water tank which contained a critical assembly. Figure 7 shows the schematic of the installation.

The distributions of neutrons were measured for three versions of the lower reflector. The assemblies which simulated the screens, the vessel and the shielding were put together from sheets of 1Kh18N9T stainless steel, No. 3 steel,

plexiglas, polyethylene, boron steel and lead. The dimensions of the plates were as follows: plates from boron steel were 550 X 600 mm with a thickness of 10 mm, plates from stainless steel had a hexahedral form with a 460 mm side and a thickness of 15 mm. Plates made of plexiglas also had a hexahedral form with the same dimensions as those made of stainless steel. Polyethylene was assembled from plates of rectangular form with dimensions 930 X 600 mm. Plates of No. 3 steel and of lead were of rectangular form and had dimensions of 660 X 710 mm with a thickness of 10 mm. The composition of the experimental assembly for each version is shown in the figure showing the corresponding experimental results.

The measurements of neutron fluxes in the assemblies were carried out by measuring the activity of copper foils induced by the neutrons. The foils had the shape of circles with a diameter of 20 mm and a thickness of 0.2 mm. The weight of individual indicators was checked by weighing them on an analytical

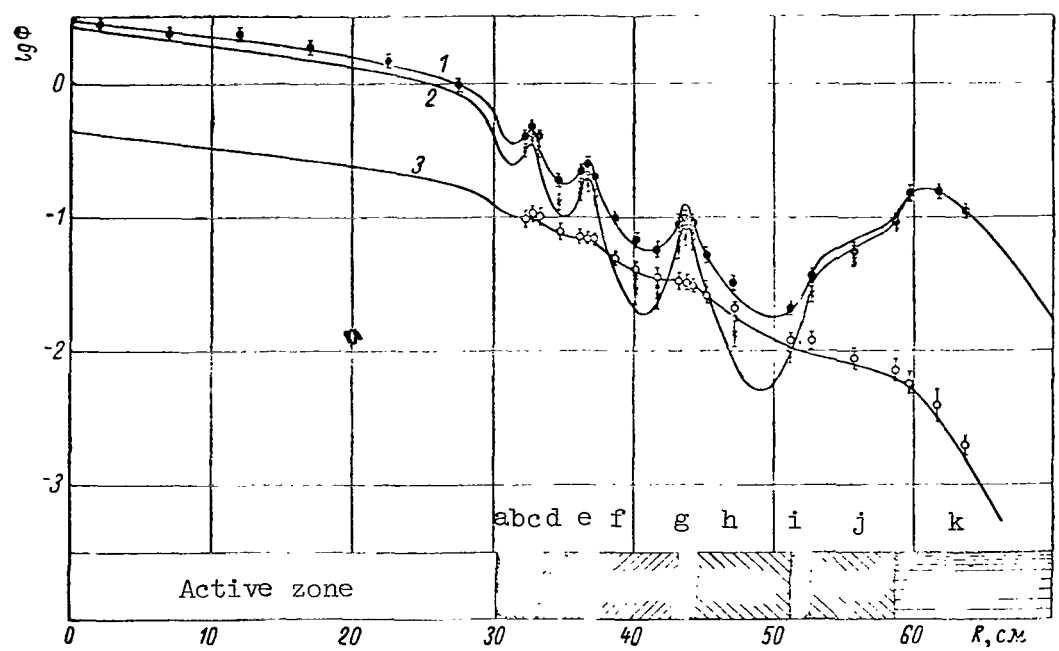

Figure 6. Three-dimensional distribution of copper foil activations in active zone and in shielding (version No. 1): ⊤●⊥ for total activation (experimental values); ⊤○⊥ for activation of foils in cadmium cases (experimental values): ⊤✳⊥ experiment for activation by thermal neutrons (cadmium difference); 1, total activation computed by 7-group method; 2, cadmium difference according to the 7-group method; 3, activation of copper and cadmium, computed by 7-group method.

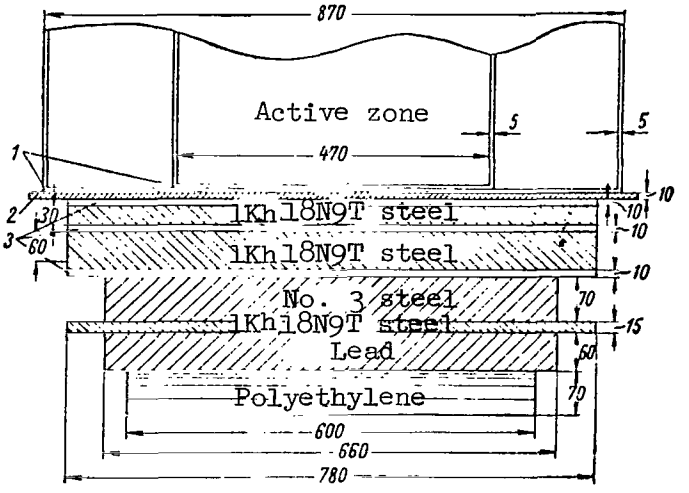

Figure 7. Schematic of experimental setup: 1, walls of internal and external tanks of active zone; 2, plate which held active zone; 3, plexiglas.

balance. The difference in the weight of individual foils did not exceed 1 percent. Measurements were carried out using foils contained in cadmium cases with wall thickness of 0.5 mm and also with foils not contained in cadmium cases. The indicators were placed between the sheets of materials used in the assembly and then into the cavities of special inserts placed into channels at half the thickness of the plexiglas which was situated in the layers between the screens. The indicators were placed along the vertical which passed through the center of the critical assembly. The activity of copper foils was measured by means of an end Geiger-Müller counter with a mica window.

The β-decay of the Cu^{64} isotope resulting from the reaction Cu^{63} (n, γ) Cu^{64} was recorded. The activity of the indicator produced by the isotope ($T_{1/2}$-12.8 hr) was isolated by analyzing the indicator decay curve. The intensity of indicator count was measured for a period of 72 hr. Each time its activity at the instant of reactor stoppage was computed from the measurements of the β-activity decay of the indicator. The reactor power was controlled by means of a boron counter. All measurements were recomputed to correspond to the same reactor power.

Result of the Measurements

Measurements were made of the three-dimensional distributions of thermal and intermediate neutrons in three experimental assemblies of screens and shielding along the axis of the active zone. Thermal neutrons were measured with copper indicators and a U^{235} fission chamber, and in the experimental assemblies they were measured by means of copper indicators. Intermediate /73

neutrons were measured in the assembly by means of copper indicators contained in cadmium cases. In these measurements the indicators had the form of circles with a diameter of 7 mm and a thickness of 0.07 mm.

The three-dimensional distributions of neutron density were measured in three versions. The computations were made for these same versions as indicated above. The results of the experiments are shown in figures 2-5, together with the computed data. The dots in figures 2 and 4 show the measurement data in version No. 1. The entire experimental assembly consists of alternating layers of No. 3 steel, stainless steel (1Kh18N9T), plexiglas, lead and polyethylene. Figure 3 shows the results of measurements and computations for an experimental assembly similar to version No. 1, in which, however, the lead layer is replaced with a layer of boron carbide having a density of 1.1 g/cm^3 and a thickness of 20 mm. Figures 5 and 8 show experimental data and computations for an assembly version utilizing layers of boron steel as screens. For all versions the experimental data coincided with the computed curves and with each other at the point lying on the boundary of the first layer of water (of plexiglas) from the side of the active zone. /74

Discussion of Computational and Experimental Results

A comparison of the computations of three-dimensional neutron flux distributions according to the activation of copper indicators for three assembly versions with experimental results has made it possible to verify the applicability of the utilized multiple group method and has made it possible to confirm the correct selection of the system of constants. The following conclusions can be drawn on the basis of this comparison.

1. Both the 7- as well as the 10-group method and the selected system of group constants are suitable for computing the three-dimensional energy distributions in mixtures of iron with water and lead for the measured thicknesses.

2. These methods produce satisfactory results (within the limits of 20 percent) for media containing boron, for example, in boron steels and in a medium with boron carbide layers. The deviations are computed values from experimentally measured values, for the activation of copper indicators in plexiglas layers may be associated both with the nondiffusion nature of the problem as it applies to the layers of the medium which bounds the strong absorber, as well as with the deviation of the true neutron spectrum in these layers from the neutron spectra which were used to average out the group constants.

3. The 7-group computation was also carried out for the purpose of refining the three-dimensional distribution of fast neutron groups which determine the three-dimensional distribution of moderated neutron fluxes. This distribution of fast neutrons in this case was computed by the method of removal cross sections utilizing the experimentally measured three-dimensional neutron distributions in various media. The present work has not obtained a direct experimental verification supporting the high accuracy of the 7-group

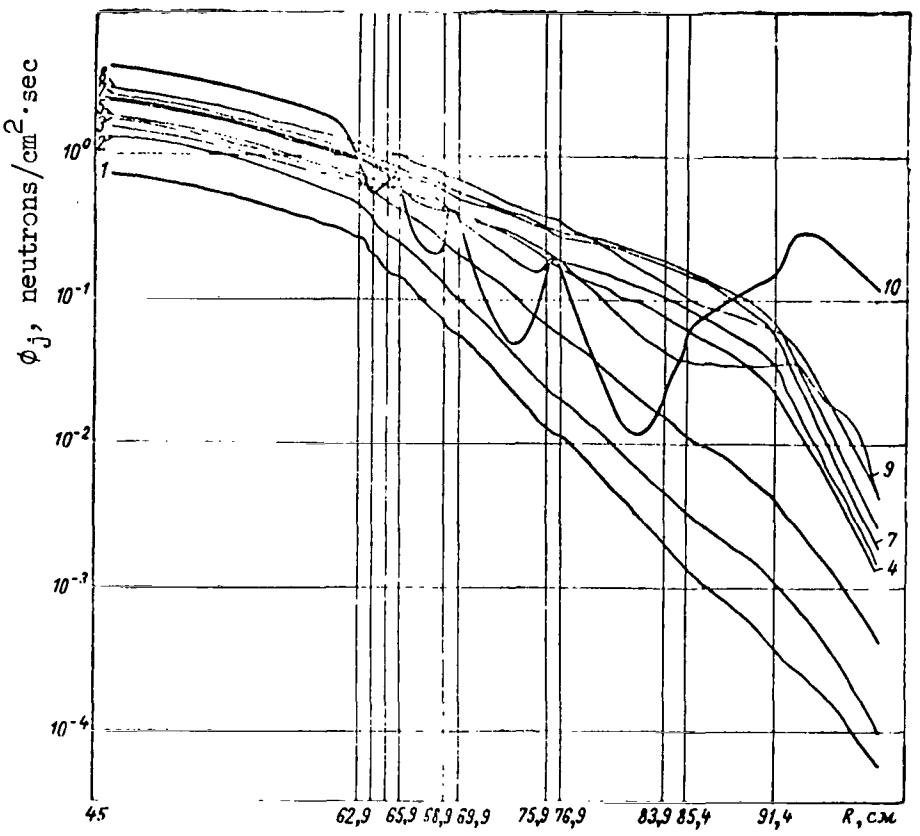

Figure 8. Distribution of various neutrons groups computed by means of 10-group method: 1-10, numbers of neutron groups.

computation compared with the 10-group computation. For the thickness used in the measurements both methods agree sufficiently with the experimental data. We can only assume that when the shielding thickness is great and when hydrogen concentrations are large there must be an inaccuracy in a calculation of fast neutron groups when we use the diffusion approximation as in the case of the 10-group method. Therefore, along with the application of the 7-group calculations or of analogous methods utilizing the experimentally determined distributions of fast neutrons it is necessary to apply more accurate analytical methods of calculation in fast groups; for example, calculations using the P_2-approximation.

REFERENCES

1. Gol'dshteyn, G. Principles of Reactor Shielding (Osnovy zashchity reaktorov). Moscow, Gosatomizdat, 1961.

2. Broder, D. L., Kutuzov, A. A., Levin, V. V., Orlov, V. V. and Turusova, A. V. Atomnaya Energiya, 7, 313, 1959.

3. Price, B., Horton, C. and Spinney, K. Shielding Nuclear Radiations (Zashchita ot yadernykh izlucheniy). Moscow, Izd-vo I. L., 1959.

4. Broder, D. L., Kondrashov, A. P. and Kutuzov, A. A. Three-dimensional Distributions in Mixtures of Boron Carbide with Fe and Pb. IN: Neutron Physics (Prostranstvennyye raspredeleniya v smesyakh karbida bora s Fe i Pb. V sb.: Neytronnaya fizika). Moscow, Gosatomizdat, 1961.

5. Holte, G. Arkiv fys. 8, 15, 1953.

6. Nuclear Reactors. Materials published by the Atomic Energy Commission, USA. 4. 1. Moscow, Izd-vo I. L., 1956.

7. Nuclear Reactors. Vol. I. The Physics of Nuclear Reactors (Yadernyye reaktory. T. I. Fizika yadernykh reaktorov). Moscow, Izd-vo I. L., 1956.

8. Hughes, D. J. and Harvey, L. A. Neutron Cross Sections, BNL-325, New York, 1958.

9. Gordeyev, I. V., Kardashev, D. A. and Malyshev, A. V. Handbook on Nuclear Physical Constants for the Design of Reactors (Spravochnik po yaderno-fizicheskim konstantam dlya rascheta reaktorov). Moscow, Atomizdat, 1960.

10. Marchuk, G. I. Numerical Methods of Designing Nuclear Reactors (Chislennyye metody rascheta yadernykh reaktorov). Moscow, Atomizdat, 1958.

11. Broder, D. L., Kutuzov, A. A., Levin, V. V. and Frolov, V. V. The Application of the Method of "Removal Cross Sections" for the Computation of Shielding Which Does not Contain Hydrogen (Primeneniye metodiki "secheniy vyvedeniya" dlya raschetov zashchity, ne soderzhashchey vodoroda). Page 70 of this volume.

APPLICATION OF EMPIRICAL DATA TO THE CALCULATION OF SHIELDING

B. I. Sinitsyn and S. G. Tsypin

The utilization of the removal cross sections for the computation of /75
shielding against neutrons still remains as the simplest and most productive method. For this reason the method of removal cross sections has undergone further development in recent years. There is rather extensive material in the literature devoted to the investigation both of the experimental as well as of the computational side of the problem (refs. 1-6).

The authors of the present work have made an effort to generalize results of investigations pertaining to the determination and utilization of removal cross sections in order to comprehend them critically and also to extend the scope of application of the empirical constants for computing different forms of neutron shielding.

Basic Determination. Removal Cross Section for Heterogeneous Media

If a plate of some heavy substance (different from hydrogen) is placed in a homogeneous medium containing hydrogen (for example, in water) the law for the attenuation of neutrons beyond this shielding may be written in the form

$$D(R, T) = D_{\text{H}}(R - T)\, e^{-\Sigma T}, \tag{1}$$

(H = hydrogen)

where D (R, T) is the neutron dose at the distance R from the source; D_H (R-T) is the neutron dose in the pure hydrogen-containing material when the plate is absent; Σ is the removal cross section in cm^{-1}; T is the thickness of the plate in cm. When we have a collection of plates of the heavy component with different atomic weights A, expression (1) is given in the form

$$D(R, T) = D_{\text{H}}(R - \Sigma T_i)\, e^{-\sum_{i}^{n} \Sigma_i T_i}, \tag{1a}$$

where Σ_i and T_i are the removal cross section and the thickness of the layer substance of the i-th component, respectively. The quantity Σ_i which is determined experimentally refers to some minimum distance from the investigated medium R_{min} at which point Σ_i remains practically constant within given limits (for example with an accuracy up to 10 percent). The physical meaning of R_{min} consists of the fact that it characterizes the minimum distance from which the effect of plate perturbation on the spectrum becomes small. R_{min} depends on the energy of the incident neutrons and on the material of the plate. Problems associated with variations in R_{min} as a function of the effective detector threshold value will be considered below.

Removal Cross Section for Homogeneous Media

If the medium consists of a uniform mixture of hydrogen and a heavy component, we have

$$D(R, A) = D_H(R)\, e^{-\sum_1^n \sigma_i \frac{N}{A_i} \varrho_i R}, \qquad (2)$$

where D (R, A) is the neutron dose at the distance R from the source in the homogeneous medium; D_H (R) is the neutron dose at the distance R from the source in pure hydrogen with equivalent volumetric density; σ_i is the microscopic removal cross section of the i-th component; A_i and ϱ_i are the atomic weight and volumetric density of the i-th component, respectively. Expression (2) is valid if the hydrogen concentration in the mixture is approximately 0.5-1 percent by weight (ref. 7).

It should be pointed out that in reference 8 the value of the removal /76 cross section in a homogeneous hydrogen-containing medium is determined from expression

$$N(R, A) = N_H(R)\, e^{-\sum_1^n \sigma_i' \frac{N}{A_i} \varrho_i R}, \qquad (2a)$$

where N (R, A) is the density of thermal neutrons at the distance R from the source; N_H (R) = $N_0\, e^{-\Sigma_H(E)R}$ (Σ_H (E) is the total cross section of hydrogen for neutrons with a given initial energy E); σ_i' is the microscopic removal cross section which differs from the value σ_i determined by means of expression (2).

The application of this expression to the determination of removal cross section values for oxygen from measurements of thermal neutrons made by a detector in water gives a value of $\sigma_0' = 0.91$ barn for the fission spectrum. On the other hand the utilization of neutron dosage attenuation in water and in hydrogen (computed by the method of moments) gives us a value $\sigma_0 = 0.74$ barn. Nevertheless, in selecting expression (2) or (2a) we should give preference to (2), because in the first place the values of the removal cross sections obtained from expression (2) can be utilized in any combination of these elements with hydrogen, whereas expression (2a) is not always valid (for example, in the case when we add an element which produces a high absorption of thermal neutrons). In the second place expression (2) is more convenient for computing the shielding, because it can be used to obtain the value of the dose directly, whereas expression (2a) is valid only for the flux of thermal neutrons. In the third place expression (2) makes it possible, as we shall see below, to utilize the values of the removal cross sections in order to assign the upper group of neutrons in the multiple group methods of computing neutron shieldings (by utilizing the effective energy thresholds above 2-3 MeV).

However, the specified preference does not ignore the utilization of a thermal detector to measure the removal cross sections. In particular, when measurements are made in heterogeneous media using the fission spectrum and also when using monoenergetic neutrons the thermal detector is used with success. We must only be sure that the perturbation produced by the plate is small and that for this reason the detector is moved away from the plate by a sufficient distance. This is possible because at some distances R from the source the following relationship will be satisfied

$$\frac{D(R, T)}{D(R, 0)} = \frac{N(R, T)}{N(R, 0)},$$

where D (R, T) and D (R, 0) is the value of the dose at the distance R from the source behind the plate in the hydrogen-containing medium and the value of the dose in the same medium, but without the plate, respectively; N (R, T) and N (R, 0) are the readings of the thermal detector in the hydrogen-containing medium at the distance R from the source behind the plate and the reading of the thermal detector in the same medium, but without a plate, respectively. To obtain the removal cross sections in homogeneous media the thermal detector should be utilized with considerable discretion.

Investigations with Sources of Monoenergetic Neutrons

The method of removal cross sections was developed with application to neutrons having a fission spectrum. In actual cases the initial neutron spectrum may differ from the fission spectrum (particularly in the range of energies below 2-3 MeV). In such cases it is necessary to have assurance that the utilization of removal cross sections will not lead to significant errors. To

achieve this we must know the energy relationship of the removal cross sections for different elements--$\Sigma_{re}(E)$ (re = removal). Then for any neutron spectrum S(E) the dose at the distance R from the source will be proportional to

$$D(R) \approx \int_E S(E)\, D_H(R, E)\, e^{-\Sigma_{re}(E)T}\, dE.$$

References 3-6 contain extensive experimental material devoted to the investigation of the relationship between removal cross sections and the energy of incident neutrons for whole series of various shielding materials. /77 The results of the references cited above make it possible to construct a relationship between the removal cross sections for carbon, iron and lead as a function of energy in the region of 0.5-15 MeV. These relationships are shown in figures 1-3.

Figure 4 shows the removal cross sections for oxygen obtained from the calculation of the fast monoenergetic neutron dose in water (ref. 9). The dose attenuation of neutrons in hydrogen is determined by means of the expression

$$D(R) = D_0 B(R)\, e^{-\Sigma_H R},$$

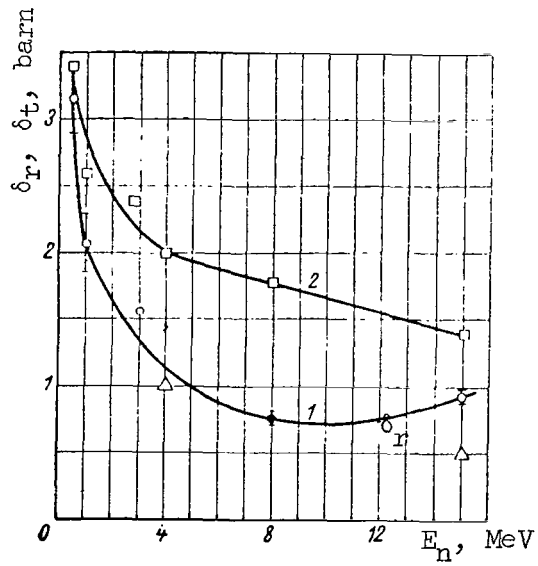

Figure 1. Variation in removal cross sections (1) and in total cross sections (2) as function of energy for carbon: O, results of measurements (ref. 5); ●, removal cross sections for energy of 8 MeV taken from reference 1; Δ, results obtained by measuring reverse relaxation length in carbon (ref. 22); □, total cross sections (ref. 20).

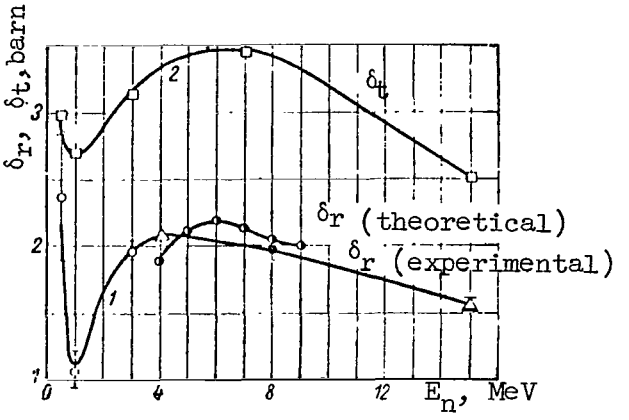

Figure 2. Variation in removal cross sections (1) and in total cross section (2) as function of energy for iron: O, results of measurements (ref. 5); ●, removal cross section at energy of 8 MeV taken from reference 1; Δ, results obtained from measurements in heterogeneous mixture of iron and B_4C (ref. 6); □, total cross sections (ref. 20). Theoretical calculations ◑ taken from reference 3.

where D_0 is the value of the dose when R = 0; $B(R) = 1 + \Sigma_H R$; Σ_H is the total cross section of hydrogen for the given energy; R is the distance from the source. The expression for $B(R) = 1 + \Sigma_H R$ obtained from the neutron penetration problem using the "dead ahead" method agrees sufficiently well with exact calculations carried out by the method of moments.

Thus, for example, when the neutron energy is 8.1 MeV and R = 120 cm, the deviation of the approximate equation from the exact one for the case of water is 25 percent (ref. 10).

The analysis of this reference makes it possible to establish the fact that the magnitude of removal cross sections varies very little for intermediate and heavy nuclei in the energy range 3-15 MeV. At the same time, it is precisely this region which is characteristic for the fission spectrum. For such light elements as beryllium boron and carbon the removal cross sections are substantially increased when the energy is 3 MeV. A substantial variation in the removal cross sections is observed in the region 0.5-1 MeV (basically repeating the variation in the total cross section as a function of energy).

On the basis of these rules we can make several conclusions regarding the utilization of removal cross sections in a series of practical cases. If the

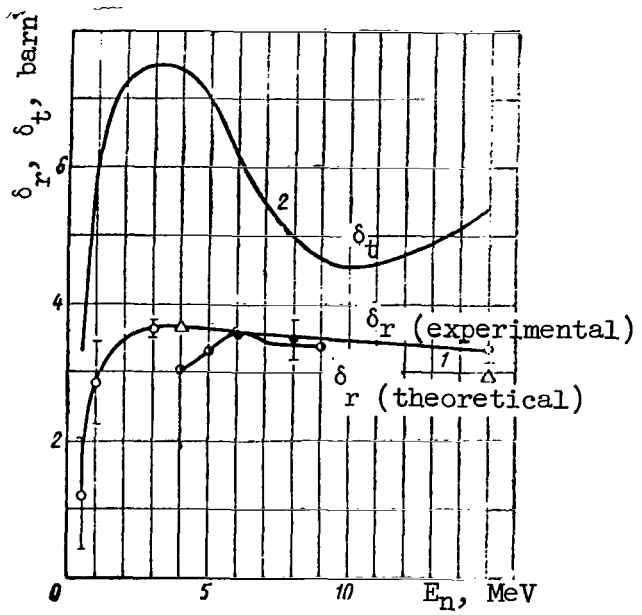

Figure 3. Variation in removal cross sections (1) and in total cross sections (2) as function of energy for lead: O, results of measurements (ref. 5); ⊥●⊥, removal cross section for an energy of 8 MeV taken from reference 1; Δ, results obtained from measurements in heterogeneous mixture of lead and B_4C (ref. 6). Total cross sections taken from reference 20. Theoretical calculations ◑ taken from reference 3.

initial spectrum of neutrons leading the reactor is not too distorted in the region 2-3 MeV, it is possible to utilize the removal cross sections determined for the fission spectrum without introducing substantial corrections. When there are substantial distortions of the spectrum in the region 2-3 MeV, /78 it is necessary to introduce corrections which can be substantial, particularly when light materials such as beryllium, boron or carbon are utilized. The distortion of the spectrum in the region 0.5-2.0 MeV does not usually affect the results due to the strong filtration of these energies by hydrogen and may serve as a source of errors only when the source or the plate are approached.

In the case of a homogeneous medium the removal cross section for a complex spectrum may be determined from the following expression

$$e^{-\Sigma_B R} = \frac{\int_{E_1}^{E_2} S(E)\, D_{II}(R, E)\, e^{-\Sigma(E) R}\, dE}{\int_{E_1}^{E_2} S(E)\, D_{II}(R, E)\, dE}, \qquad (3)$$

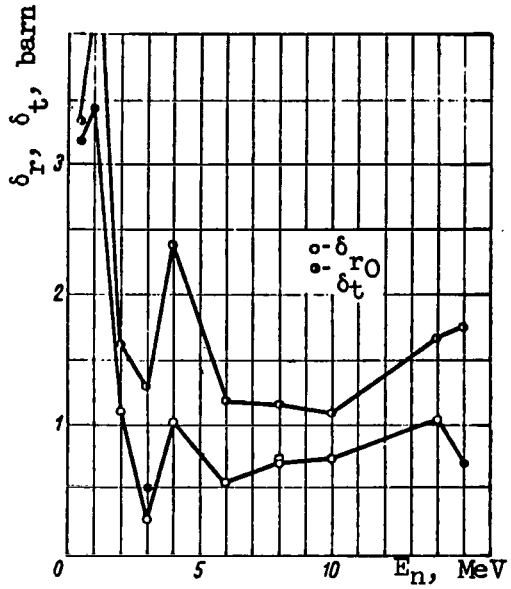

Figure 4. Variation in removal cross sections as a function of energy for oxygen. Results are obtained on basis of expression (2); dose attenuation in hydrogen was computed by using "dead ahead" approximation. Attenuation in water is obtained by the following methods: O , computed by method of moments (ref. 9); ● , obtained from experimental results (ref. 5); □ , obtained from results using fission spectrum (ref. 1); ◑, total cross sections (ref. 20).

where S(E) is the dose spectrum of the source, rem/MeV; D_H (R, E) is the dose attenuation in hydrogen. Similarly for a heterogeneous medium we have

$$e^{-\Sigma_B T} = \frac{\int_{E_1}^{E_2} S(E)\, D_{cp}(R, E)\, e^{-\Sigma(E)T}\, dE}{\int_{E_1}^{E_2} S(E)\, D_{cp}(R, E)\, dE}, \qquad (3a)$$

(B = re; cp = med for medium)

where D_{med} (R, E) is the dose attenuation of neutrons in the given hydrogen-containing medium. The distance R from the source (or from the plate) for which expressions (3) and (3a) are valid, of course cannot be too small; specifically they should not be taken less than R_{min}. In a particular case when

S(E) represents the neutron fission spectrum the validity of expressions (3) and (3a) may be verified, if we utilize the energy relationship of removal cross sections for carbon, oxygen, iron and lead, as shown in figures 1-4. The results of the comparisons are presented in table 1. /79

An investigation was carried out to study the influence of the effective neutron registration threshold for the region where the removal cross sections are applicable. It was carried out for neutrons with an energy of approximately 15 MeV. Three types of detectors were used: thermal detector (proportional counter filled with BF_3), Th^{232} fission chamber (effective threshold 2 MeV) and a Cu^{63} (n, 2n) Cu^{62} indicator (effective threshold 12.8 MeV, ref. 11). The following materials were studied: aluminum, iron, copper and lead. The results of the investigations carried out by S. F. Degtyarev, V. I. Kukhtevich and B. I. Sinitsyn are presented in table 2. As we can see from table 2, the removal cross sections measured by different detectors coincide within the limits of experimental errors.

TABLE 1.

Element	Removal cross section (ref. 13), barn	Removal cross section given by expressions (3) and (3a), barn
Carbon	0.81 ± 0.05	0.84
Oxygen	0.74*	0.67
Iron	1.98 ± 0.08	1.91
Lead	3.53 ± 0.30	3.58

*Results of the computations using the method of moments for the penetration of fission spectrum neutrons through water and hydrogen.

TABLE 2. REMOVAL CROSS SECTION FOR CERTAIN ELEMENTS MEASURED BY DETECTORS WITH VARIOUS THRESHOLDS.

Element	Σ_{re}/ρ, $cm^2/e \cdot 10^2$		
	BF_3	Th^{232}(n, f)	Cu^{63}(n, 2n) Cu^{62}
Aluminum	2.77 ± 0.35	2.85 ± 0.16	2.63 ± 0.22
Iron	1.70 ± 0.04	1.68 ± 0.08	1.81 ± 0.11
Copper	1.74 ± 0.10	1.58 ± 0.08	1.45 ± 0.19
Lead	0.99 ± 0.05	0.86 ± 0 07	0.83 ± 0.08

Table 3 shows the distances R_{min} for various detectors. Measurements were carried out in water behind the aluminum, iron, copper and lead. We can see that as the effective threshold of the detector is increased R_{min} decreases and consequently the limits of application of the method are extended. We should expect R_{min} to be of the order of 25-30 cm when a dosimeter is used to measure fast neutrons.

Investigations Utilizing the Fission Spectrum Neutron Sources

The measurements of removal cross sections for neutrons of the fission /80 spectrum were carried out using the LTSF experimental setup at the Ok-Riga National Laboratory (ref. 13) and also by the authors of reference 3 for certain shielding materials. These measurements pertain to heterogeneous media. The results of the measurements are presented, for example, in references 10, 8 and 12. Reference 10 presents the results of measuring the removal cross sections for neutrons of the fission spectrum utilizing a collimated beam. As a result the values of the cross sections are substantially greater than those presented in reference 13, as is to be expected. The results of reference 10 cannot be used directly by themselves; however, a comparison of these data with data contained in reference 13 make it possible to carry out an auxiliary determination of cross section values for such elements as sodium, sulfur, titanium and cadmium. Measurements in partially homogenized media such as a mixture of iron and lead in water have been carried out in the USSR as well as abroad (refs. 13 and 8). The removal cross sections computed for such mixtures are close or coincide with cross sections obtained from heterogeneous mixtures.

It should be pointed out that most of the experiments on measuring the removal cross sections were carried out for application in heterogeneous media. The investigation of such mixtures as iron and lead in water (refs. 8 and 13) should be referred to some intermediate category between a heterogeneous and a homogeneous medium. Investigations in an ideal homogeneous medium (ref. 10) showed that the removal cross section in a homogeneous medium is somewhat less than the removal cross section measured in a heterogeneous medium. However, this difference lies within the limits of experimental errors.

TABLE 3. VARIATION IN R_{min} AS A FUNCTION OF THE EFFECTIVE ENERGY THRESHOLD OF THE DETECTOR.

R_{min}, cm	Detector
65	BF_3
15-20	$Th^{232}(n, f)$
5	$Cu^{63}(n, 2n)\ Cu^{62}$

The determination of the removal cross section for hydrogen from a mixture of CH and CH_2 (computation by the method of moments, ref. 10) using a fission spectrum gave a value which coincides with the value measured in the heterogeneous medium within 5 percent. The calculations were carried out by utilizing the dose attenuation of neutrons in hydrogen computed by the method of moments (ref. 14). The removal cross section of oxygen in a homogeneous medium for 3 and 14 MeV, computed from the results of calculating the penetration of monoenergetic neutrons through water (ref. 9), may be compared with the heterogeneous removal cross section. The comparison has not made it possible to draw convincing conclusions in view of substantial experimental errors. However, we should assume that the difference in the removal sections for a homogeneous and a heterogeneous medium lies within the limits of 5-10 percent, or we may even assume that the cross sections coincide.

The practical application of removal cross sections is not exhausted merely by the calculations of fast neutron dose. Recently, in connection with the development of the multiple group methods of computing shielding, the removal cross sections are used to assign the neutron distribution of the upper group or of the "leading group" as it is sometimes called (for example, in refs. 2, 8, 15, 16, etc.).

We should note that in these and in other works, as a rule, the sharp energy boundaries of the leading group are not determined. Therefore it is expedient to use the available information and to conduct a more detailed analysis of the interrelation between removal cross sections and the value of the detector energy threshold. Even in the early works of Blizard (ref. 17), Chapman and Storrs (ref. 13) and in others, the removal cross section for fission spectrum neutrons was identical with the portion of the total neutron cross section having an average energy of approximately 8 MeV. This situation can be verified visually by comparing the dose attenuation curves in water for neutrons of the fission spectrum and for monoenergetic neutrons. It was found that the dose of attenuation curve for fission spectrum neutrons is parallel in the interval of 90-120 cm to the dose curve of neutron attenuation for an energy of 8 MeV. However, this does not give us any information for determining the energy interval of the "leading group" of neutrons. To determine this interval more precisely than its lower boundary, another approach can be proposed.

It follows from table 3 that the distance R_{min} decreases as the threshold of the detector is increased. This can be explained by the fact that the /81 maximum distortion of the neutron spectrum takes place in the region of low energies. It is logical to assume that as the effective threshold of the detector is increased, only those neutrons will be recorded whose spectrum is practically undistorted, and the distance R_{min} will tend to zero.

Thus, by using a higher detector threshold we essentially replace the hydrogen-containing medium which serves as a filter of lower energy neutrons, with this threshold. On the other hand, this is equivalent to the measurement of the reciprocal relaxation length $1/\lambda$ in the test medium. Below we shall attempt to find the effective energy threshold of a detector, for which the

cross section, which is obtained by calculations using the reciprocal relaxation length of fast neutrons, established experimentally, will be close in value to the removal cross section measured under standard conditions of the type described in reference 13.

Table 4 shows a series of elements for which the removal cross sections and the cross sections obtained from the reciprocal relaxation lengths of fast neutrons in the investigated media are compared. The effective energy threshold in beryllium and carbon is determined on the basis of known computed spectra N (E, R) (ref. 10) according to the following expression

$$4\pi R^2 \int_0^\infty \Sigma(E)\, N(E, R)\, dE = k e^{-\sigma_{1/\lambda} \frac{N}{\lambda} \rho R}, \qquad (4)$$

where $\Sigma(E)$ represents the cross section of some idealized detector which can be represented in the form

$$\Sigma(E) = \begin{cases} 1, & E \geq E_{\text{пор}}; \\ 0, & E < E_{\text{пор}}; \end{cases}$$

(пор = th = threshold)

k is the normalizing multiplier; $\sigma_{1/\lambda}$ is the cross section computed from the reciprocal relaxation lengths. Expression (4) is valid to substantial distances equal to 65 and 72 cm for beryllium and carbon (the density of beryllium is 1.84 g/cm^3, and the density of carbon is 1.67 g/cm^3). By varying E_{th} we can achieve a situation where $\sigma_{1/\lambda}$ will be close in value to the removal cross section given in reference 13. Computations have shown (table 4) that the value E_{th} in beryllium and in carbon is approximately 3 MeV.

TABLE 4. COMPARISON OF REMOVAL CROSS SECTIONS WITH CROSS SECTIONS OBTAINED FROM RECIPROCAL RELAXATION LENGTHS.

Element	Removal cross section (ref. 13), barn	Cross section from reciprocal relaxation lengths, barn	Detector
Beryllium	1.07 ± 0.06	1.15 (ref. 10)	Ideal detector
Boron	0.97 ± 0.10	1.12	P (n, p)
Carbon	0.81 ± 0.05	0.75 (ref. 10)	Ideal detector
Oxygen	0.99 ± 0.10	0.70 (ref. 18)	P (n, p)
Iron	2.00 ± 0.06	1.81 (ref. 19)	S (n, p)
Nickel	1.89 ± 0.10	1.90	S (n, p)

Remark: The effective threshold for all elements is equal to 3 MeV.

For average and heavy nuclei this threshold will be particularly retained, because the variation in the spectrum of fission neutrons during transmission through such media is small. For the remaining elements in table 4 (beryllium, oxygen, iron, nickel) the cross sections established from the reciprocal relaxation lengths are obtained from measurements of three-dimensional neutron distributions by means of P^{31} (n, p) Si^{31} and S^{32} (n, p) P^{32} threshold detectors.

Generally speaking the magnitude of the effective detector threshold depends on the form of the neutron spectrum. As a rule, for fast neutrons the effective energy threshold is determined under the assumption that the neutrons are distributed according to the fission spectrum and are inside. /82 The basis for this is the situation that above 2-3 MeV the neutron spectrum inside the medium for average and heavy elements does not depend on the distance and is similar to the fission spectrum. If the composition of the medium includes light elements, the spectral distribution may vary substantially as we move away from the source. Consequently the value of the effective detector threshold may also change. For some detectors with practical application the effective energy threshold for the spectrum of neutrons inside light media are determined in the measurements of the three-dimensional neutron distributions. Such light media are hydrogen, beryllium and carbon for which the three-dimensional energy distributions are known (refs. 10 and 14). The effective energy threshold is determined from the expression

$$\int_0^\infty \Sigma(E)\, N(E,\ R)\, dE = k \int_{E_{\text{пор}}}^{\infty} N(E,\ R)\, dE, \tag{5}$$

where $\Sigma(E)$ is the macroscopic cross section of the corresponding reaction taken from reference 20; k is the proportionality factor.

Equality (5) is not strictly satisfied for various distances R; however, by varying k and E_{th} we can achieve the best matching in the right and left sides in a wide range of distances R. In this case the variation of E_{th} affects the slope of the resulting three-dimensional distribution in the right side of equality (5), while the variation of k signifies parallel displacement along the axis of the ordinates, so that a constant k has the meaning of an effective cross section of reaction.

It follows from table 5 that the effective energy threshold of detectors P (n, p) and S (n, p) is equal to 3 MeV and depends very little on the form of the spectrum. This may serve as a basis for the proposition that the effective energy threshold is retained for medium and heavy elements. For oxygen $\sigma_{1/\lambda}$ is determined from the expression

$$\Phi_{H_2O}(R) = e^{-\Sigma R} 4\pi \int_0^\infty \Sigma_p(E)\, N_n(E,\ R)\, R^2\, dE, \tag{6}$$

TABLE 5. EFFECTIVE ENERGY THRESHOLD FOR VARIOUS NEUTRON DETECTORS.

Detector	Effective energy threshold	
	From spectra in H_2, Be, C	From the spectrum of fission neutrons (ref. 11)
U^{238}, Th^{232}	~2	1.7
P(n, p), S(n, p)	~3	2.8
Al(n, p)Mg	~5	4.7
Al(n, α)Na	6-7	7.0

where $\Phi_{H_2O}(R)$ is the experimentally measured neutron attenuation function in water which is measured by the detector P (n, p) with the geometric factor excluded; $\Sigma_p(E)$ is the cross section of reaction P^{31} (n, p)Si^{31}; N_H (E, R) is the differential numerical neutron spectrum in hydrogen at a distance R from a point isotropic source of the fission spectrum.

The data presented in table 4 permit us to draw a conclusion regarding the fact that the removal cross sections are close to cross sections obtained on the basis of the reciprocal relaxation lengths when the effective registration threshold is near 3 MeV.[1]

It also follows from table 4 that the removal cross sections may be /83 applied to compute the penetration of fast fission spectrum neutrons even in media which do not contain hydrogen (if we consider the energy region above 3 MeV).

It is of interest to compare the removal cross sections with cross sections obtained on the basis of group cross sections systems (ref. 21). The asymptotic solution of the single velocity kinetic equation[2] in the transport approximation has the form

[1]The cross sections obtained from the reciprocal relaxation lengths for lower values of the effective energy thresholds coincide much less with the removal cross sections; this is clearly seen from the data in table 6.

[2]It can be shown that the asymptotic solution of the single velocity kinetic equation in the transport approximation coincides with the asymptotic solution of the single velocity kinetic equation for isotropic scattering if in the latter we make the substitutions $\Sigma_{total} \rightarrow \Sigma_{transport}$ and $\Sigma_{decay} \rightarrow \Sigma^s_{transport}$.

$$\Phi(R) \sim Ae^{-R/L}, \tag{7}$$

where L is determined from reference 12 by means of the expression

$$\frac{L\Sigma_{tr}^{s}}{2} \ln \frac{L\Sigma_{tr}+1}{L\Sigma_{tr}-1} = 1, \tag{8}$$

where Σ_{tr} is the total transport cross section;

$\overset{s}{\Sigma}_{tr}$ is the scattering transport cross section.

In the group approximations the transport cross section (total and scattered) is written as $\Sigma_{tr} = \Sigma_{tr}^{s} + \Sigma_{re}$, where Σ_{tr} and Σ_{tr}^{s} are the group transport cross section and the scattered transport cross section; Σ_{re} is the group removal cross section.

We shall interpret the asymptotic cross section as the cross section which is obtained from the quantity L in equation (8) according to the expression

$$\sigma_{ac} = \frac{1}{L} \cdot \frac{A}{N\varrho} . \tag{9}$$

Table 6 presents the removal cross sections σ_{re}, cross sections obtained from the reciprocal relaxation length $\sigma_{1/\lambda}$ and asymptotic cross sections σ_{as} for the energy group 1.4 - ∞ MeV.

Conclusions

On the basis of the results which have been presented we can draw the following conclusions. /84

1. The removal cross sections from reference 13 for media containing hydrogen may be used in practice at all times, if the spectrum of neutrons leaving the reactor is not too distorted in the region 1.5-3.5 MeV. Exceptions to this are light elements like beryllium, boron, carbon, whose removal cross sections increase in this region of energies, which must be taken into account in exact calculations.

2. The removal cross sections measured in heterogeneous media may be used to compute homogeneous media. The difference in cross sections apparently is not greater than 5-10 percent for all elements.

3. The utilization of the removal cross sections for computing homogeneous media is applicable for any distances from the source. The greatest deviation

TABLE 6. COMPARISON OF THE REMOVAL CROSS SECTIONS, ASYMPTOTIC CROSS SECTIONS AND CROSS SECTIONS OBTAINED FROM THE RECIPROCAL RELAXATION LENGTHS FOR VARIOUS ELEMENTS.

Element	Removal cross section	$\sigma_{1/\lambda}$, barn	Effective threshold, energy MeV	Asymptotic cross sections, 1.4 - ∞ MeV	Removal cross sections obtained by other means
Lithium.	1.01 ± 0.04			1.03 (21)	-
Beryllium. . . .	1.07 ± 0.06	1.15 (10)	3	1.20 (21)	-
		0.91 (10)	7		
Boron.	0.97 ± 0.10	1.12*	3	1.08 (21)	-
Carbon	0.81 ± 0.05	0.75 (10)	3	-	-
Nitrogen	-	-	-	1.11 (21)	-
Oxygen	0.99 ± 0.10	0.7 (18)**	-		0.74 (9)***
Sodium	1.33 ± 0.17****	-	-	1.58 (21)	1.47 (1, 10)*****
					1.20 (1, 10)******
Iron	2.00 ± 0.06	1.56 (6, 19)	2	1.87 (21)	-
		1.81 (19)	3	-	-
		1.88 (19)	7	-	-
Nickel	1.89 ± 0.10	1.90	3	1.95 (21)	-
Copper	2.04 ± 0.11	1.78*******	2	2.04 (21)	-
Zirconium. . . .	2.36 ± 0.12	-	-	2.53 (21)	-

*Cross section obtained from measurements in B_4C (ref. 7) by subtracting C cross section.

**Cross section obtained from expressions in reference 6.

***Cross section obtained from expression which is analogous to (6) by replacing Σ_p (E) with f (E) where f (E) is the power of the dose corresponding to a unit neutron flux with energy E.

****Cross section obtained from the analysis of data for the collimated removal cross sections (ref. 8).

*****Cross section obtained on the basis of the relationship $\sigma_{re} = 2/3\sigma_t$ for 8 MeV.

******Cross sections obtained from the interpolation of the curve showing the variation in the removal cross sections as a function of the atomic number.

*******Data presented by V. I. Golubev and M. N. Nikolayev.

[1]All figures within parentheses are references.

from exact computations will be at distances of two to three relaxation lengths from the source, but it will not exceed 25-30 percent.

4. To compute the dose by utilizing the removal cross sections we should use the dose attenuation for hydrogen.

5. For a detector with an effective energy threshold of 3 MeV the cross sections obtained from the reciprocal relaxation lengths in media free of hydrogen practically coincide with removal cross sections taken from reference 13.

6. An increase in the effective energy threshold decreases R_{min}.

7. To assign the upper group in multiple group calculation methods we can utilize the removal cross sections from reference 13 by assigning an effective energy threshold of 3 MeV to them or by using the quantities $\sigma_{1/\lambda}$ corresponding to the effective energy threshold of 3 MeV.

For the case of hydrogen-containing media the values of the cross sections are selected in the same manner, whereas the attenuation of neutrons in hydrogen must correspond to the selected effective energy threshold.

8. The asymptotic cross sections σ_{as} for the group 1.4 - ∞ MeV are close to the removal cross sections obtained in reference 13.

9. For a more detailed description of the three-dimensional energy distributions of fast neutrons (E > 1 MeV) it is desirable to have a large selection of empirical constants corresponding to various energy groups in the region of 1-18 MeV.

The authors express their deep gratitude to A. I. Leypunskiy for valuable remarks expressed when discussing the results of the present work.

The authors are also grateful to I. I. Bondarenko, V. I. Kukhtevich, Yu. A. Kazanskiy, A. A. Abagyan, D. V. Pankratov and A. P. Suvorov for valuable advice in preparing the material for publication.

REFERENCES

1. The Shielding of Mobile Installations with Nuclear Engines. Collected Translations edited by V. V. Orlov and S. G. Tsypin (Zashchit a transportnykh ustanovok s yadernym dvigatelem. Sb. (per). Pod red. V. V. Orlova i S. G. Tsypina). Moscow, Izd-vo I. L., 1960.

2. Cooper, K., Jones, J. and Horton, C. Some Problems of Designing Metal and Hydrogen Reactor Shielding. Transactions of the Second International Conference on the Peaceful Utilization of Atomic Energy. Selected reports of foreign scientists, Vol. 3--The Physics of Nuclear Reactors (Nekotoryye problemy rascheta metallo-vodorodnoy zashchity reaktora. Trudy Vtoroy Mezhdunarodnoy konferentsii po mirnomu ispol'zovaniyu atomnoy energii. Izbr. doklady insotrannykh uchenykh. T. 3. Fizika yadernykh reaktorov). Moscow, Atomizdat, 1959.

3. Bourgeois, J. et al. Methods and Experimental Coefficients Used in the Computation of Reactor Shielding. A/Conf/15/1190 (1958), France, Second United Nations International Conference on the Peaceful Uses of Atomic Energy.

4. Kukhtevich, V. I., Sinitsyn, B. I. and Tsypin, S. G. Atomnaya Energiya, Vol. 5, 565, 1958.

5. Kukhtevich, V. I. and Sinitsyn, B. I. Atomnaya Energiya, Vol. 10, 511, 1961.

6. Broder, D. L., Kutuzov, A. A. and Kondrashov, A. T. Atomnaya Energiya, Vol. 6, 558, 1959.

7. Wood, D. E. Nucl. Sci. Eng., Vol. 5, 45, 1959.

8. The Shielding of Nuclear Reactors. Edited by T. Rockwell. (Zashchita yadernykh reaktorov. Pod red. T. Rokvella). Moscow, Izd-vo I. L., 1958.

9. Aronson, R., Certaine, J. and Goldstein, H. Penetration of Neutrons from a Point Isotropic Monoenergetic Sources in Water. Report NYO-6269, 1954.

10. Gol'dshteyn, G. The Principles of Reactor Shielding (Osnovy zashchity reaktorov). Moscow, Gosatomizdat, 1961.

11. Grundl, J. and Usner, A. Nucl. Sci. Eng., Vol. 8, 598, 1960.

12. Price, B., Horton, C. and Spinney, K. The Shielding of Nuclear Radiation (Zashchita ot yadernykh izlucheniy). Moscow, Izd-vo I. L., 1959.

13. Chapman, G. T. and Storrs, C. L. Effective Neutron Removal Cross Sections for Shielding, AECD-3978, 1955.

14. Aronson, R. Neutron Penetration in Hydrogen. NDA 150-39, June 11, 1954.

15. Clark, M. D. J. Nucl. Energy, Vol. 6, 16, 1961.

16. Spinney, K. T. Nucl. Power, Vol. 5, 13, 1960.

17. Blizard, E. P. Ann. Rev. Nucl. Sci., Vol. 5, 73, 1955.

18. Tsypin, S. G. Atomnaya Energiya, Vol. 12, 300, 1962.

19. Mashkovich, V. P. and Tsypin, S. G. Atomnaya Energiya, Vol. 11, 251, 1961.

20. Hughes, D. J. and Schwartz, R. A. Neutron Cross Sections, BNL-325, 1958.

21. Gordeyev, I. V., Kardashev, D. A. and Malyshev, A. V. Handbook on Nuclear Physical Constants for the Design of Reactors (Spravochnik po yaderno-fizicheskim konstantam dlya rascheta reaktorov). Moscow, Atomizdat, 1960.

22. Broder, D. L., Kutuzov, A. A., Levin, V. V., Orlov, V. V. and Turusova, A. V. Atomnaya Energiya, Vol. 7, 313, 1959.

23. Aronson, A., Certaine, J. et al. Penetration of Neutron from a Point Isotropic Fission Source in Water. Report NYO-6267, 1954.

COMPUTATION OF NEUTRON DIFFUSION IN A TWO-DIMENSIONAL PROBLEM BY MEANS OF THE P_2-APPROXIMATION

G. Ya. Rumyantsev

The Transport Equations in the P_2-Approximation

The P_2-approximation of the method of spherical harmonics compared /85 with the P_1-approximation (the elementary theory of diffusion) is an approximation of a higher order, and it is therefore natural to expect that in general it should be more accurate. Nevertheless, to date the P_2-approximation and other even approximations have not received practical application. The boundary conditions which were customarily assigned in the method of spherical harmonics (the conditions for the continuity of all spherical harmonics individually) are incorrect in even approximations (ref. 1).

It is shown in refs. 2, 3 and 4 that the boundary conditions may be formulated in a correct mathematical form for approximations of any orders, so that there is no basis for ignoring even approximations.

The theory of diffusion based on the P_2-approximation in most cases is more accurate compared with the conventional diffusion theory and not as complicated as the P_3-approximation, whereas in one-dimensional problems it has almost the same order of complexity as the P_1-approximation.

In the present work we shall consider the application of the P_2-approximation to the calculation of neutron diffusion in heterogeneous media in cases when diffusion takes place not only in the direction perpendicular to the boundaries, but also along them. Here the difference between the P_2- and the P_1-approximations is most pronounced.

We shall assume that these sources are isotropic and that their power is described by the function S. By solving both equations of the method of spherical harmonics in the P_2-approximation we can obtain the following relationship between the diffusion flux I and the integral flux Φ, which plays the role of the diffusion law (in place of the Fick law) (refs. 1, 2 and 4)

$$\left(\frac{3}{\Sigma_2}\nabla^2-\Sigma_1\right)\mathbf{I}=\operatorname{grad}\left[\Phi\left(1+\frac{\Sigma_0}{\Sigma_2}\right)-\frac{S}{\Sigma_2}\right] \tag{1}$$

Here and in the future

$$\Sigma_0=\Sigma-\Sigma_s=\Sigma_a;$$
$$\Sigma_1=3(\Sigma-\Sigma_s\bar{\mu}_0)=3\Sigma_{tr};$$
$$\Sigma_2=5(\Sigma-\Sigma_s\overline{P_2(\mu_0)}).$$

The second relationship is the conventional neutron balance equation /86

$$\operatorname{div}\mathbf{I}+\Sigma_0\Phi=S. \tag{2}$$

Eliminating I from these two equations we obtain the following equation for the function Φ

$$\nabla^2\left[\Phi\left(1+\frac{4\Sigma_0}{\Sigma_2}\right)-\frac{4S}{\Sigma_2}\right]-\Sigma_0\Sigma_1\Phi+\Sigma_1S=0. \tag{3}$$

It can be rewritten in a different form

$$\nabla^2\tilde{\Phi}-\varkappa_0^2\tilde{\Phi}+\Sigma_1\tilde{S}=0, \tag{4}$$

where

$$\tilde{\Phi}=\left[\Phi\left(1+\frac{4\Sigma_0}{\Sigma_2}\right)-\frac{4S}{\Sigma_2}\right];$$
$$\varkappa_0^2=\frac{\Sigma_0\Sigma_1}{1+4\Sigma_0/\Sigma_2};\quad \tilde{S}=\frac{S}{1+4\Sigma_0/\Sigma_2}$$

Obviously the equation of form (4) does not differ from the conventional diffusion equation.

The important special feature of equation (1) is that unlike the Fick law it is a differential equation with respect to I. Consequently we can have a component $\mathbf{I}^*$ which represents the solution of the homogeneous equation

$$-\frac{3}{\Sigma_2}\nabla^2\mathbf{I}^*-\Sigma_1\mathbf{I}^*=0. \tag{5}$$

This part of the solution is not associated directly with function Φ. As we can see from equation (5), it damps out when the relaxation length is of the order of $(\Sigma_1\Sigma_2)^{-1/2}$, i.e., it differs from zero only near the boundary. In addition, component $\mathbf{I}^*$ must be subjected to definite conditions to satisfy

equation (2). Solution I^* approximates the nonasymptotic angular distribution due to the first paths of neutrons close to the boundary. It introduces additional coefficients to the general solution, so that it is possible to achieve a continuity of not only the normal component of the diffusion flux but also of the tangential components.

It is true that in the P_2-approximation we have a discontinuity in the integral flux Φ. This is explained by the fact that in the P_2-approximation function Φ describes only the asymptotic part of the neutron flux, which in the exact solution must be discontinuous. The continuity of all components of the diffusion flux is important in determining the average effective macroscopic diffusion coefficient of the medium. By using an example of a plane lattice we shall show a computation scheme for the macroscopic diffusion coefficient in the direction parallel to the layers of the medium. The neutron diffusion in the transverse direction is quite well described even in the P_1-approximation (ref. 5). The consideration of this problem in the P_2-approximation does not present any special interest.

Neutron Diffusion in a Plane Lattice

Let us assume that in a medium composed of plane parallel layers, the z axis is directed across the layers, while the x axis is parallel to the layers. Let us consider a medium which is semi-infinite in the x direction, assuming that the power of sources in any layer depends linearly on x

$$S(x, z) = w(z)(a + bx). \tag{6}$$

Let us find a solution of equation (3) in a similar form

$$\Phi(x, z) = \varphi(z)(a + bx). \tag{7}$$

(Such a distribution of flux Φ must be established far away from the boundary of the medium, i.e., we are seeking an asymptotic solution.)

The vector equation (1) may be written in the form of two scalar equations /87

$$\left(\frac{3}{\Sigma_2}\nabla^2 - \Sigma_1\right) I_x = b\left[\varphi\left(1 + \frac{\Sigma_0}{\Sigma_2}\right) - \frac{1}{\Sigma_2} w\right]; \tag{8}$$

$$\left(\frac{3}{\Sigma_2}\nabla^2 - \Sigma_1\right) I_z = \left[\frac{\partial\varphi}{\partial z}\left(1 + \frac{\Sigma_0}{\Sigma_2}\right) - \frac{1}{\Sigma_2}\cdot\frac{\partial w}{\partial z}\right](a + bx). \tag{9}$$

It is easy to foresee that I_x will not depend on x and that I_z should be sought in the form

$$I_z = q(z)(a + bx). \tag{10}$$

Then equations (8) and (9) will have a more concrete form

$$\left(\frac{3}{\Sigma_2}\cdot\frac{\partial^2}{\partial z^2} - \Sigma_1\right) I_x = b\left[\varphi\left(1 + \frac{\Sigma_0}{\Sigma_2}\right) - \frac{1}{\Sigma_2}w\right], \tag{11}$$

$$\left(\frac{3}{\Sigma_2}\cdot\frac{\partial^2}{\partial z^2} - \Sigma_1\right) q = \frac{\partial\varphi}{\partial z}\left(1 + \frac{\Sigma_0}{\Sigma_2}\right) - \frac{1}{\Sigma_2}\cdot\frac{\partial w}{\partial z}. \tag{12}$$

To these equations we must add equation (2), which in this case assumes the form

$$-\frac{\partial}{\partial z}\cdot I_z + \Sigma_0\Phi = S \tag{13}$$

or by taking into account (6), (7) and (10)

$$\frac{\partial q}{\partial z} + \Sigma_0\varphi = w. \tag{14}$$

It is obvious that equations (12) and (14) form an independent subsystem, while equation (11) may be solved after the subsystem. Let us find the solution of the equations for a single layer.

We differentiate equation (12) with respect to z and then eliminate $\frac{\partial}{\partial z}q$ by means of equation (14). As a result we obtain

$$\frac{\partial^2}{\partial z^2}\left[\varphi\left(1 + \frac{4\Sigma_0}{\Sigma_2}\right) - \frac{4w}{\Sigma_2}\right] - \Sigma_1\Sigma_0\varphi + \Sigma_1 w = 0. \tag{15}$$

For simplicity we shall assume that for each layer the density of sources does not depend on z, i.e., w (z) = const; then

$$\left[\left(1 + \frac{4\Sigma_0}{\Sigma_2}\right)\frac{\partial^2}{\partial z^2} - \Sigma_1\Sigma_0\right]\varphi + \Sigma_1 w = 0. \tag{16}$$

The solution of equation (16) is well known

$$\varphi = A_0 \operatorname{ch}\varkappa_0 z + B_0 \operatorname{sh}\varkappa_0 z + \frac{w}{\Sigma_0},$$

where

$$\varkappa_0^2 = \frac{\Sigma_0\Sigma_1}{1 + 4\Sigma_0/\Sigma_2}. \tag{17}$$

We now turn to equation (12)

$$\left(\frac{3}{\Sigma_2}\cdot\frac{d^2}{dz^2}-\Sigma_1\right)q=\varkappa_0\left[A_0\operatorname{sh}\varkappa_0 z+B_0\operatorname{ch}\varkappa_0 z\right]\left(1+\frac{\Sigma_0}{\Sigma_2}\right). \tag{18}$$

From this we have

$$q(z)=\varkappa_0\left[A_0\operatorname{sh}\varkappa_0 z+B_0\operatorname{ch}\varkappa_0 z\right]\frac{\Sigma_2+\Sigma_0}{3\varkappa_0^2-\Sigma_1\Sigma_2},$$

or by taking into account expression (17)

$$q(z)=-\frac{\varkappa_0}{\Sigma_1}\left[A_0\operatorname{sh}\varkappa_0 z+B_0\operatorname{ch}\varkappa_0 z\right]\left(1+\frac{4\Sigma_0}{\Sigma_2}\right). \tag{19}$$

This solution could also contain the characteristic solution

$$q^*(z)=A_1'\operatorname{sh}\varkappa_1 z+B_1'\operatorname{ch}\varkappa_1 z,$$

where $\varkappa_1$ is the additional characteristic number; /88

$$\varkappa_1^2=\frac{\Sigma_1\Sigma_2}{3}. \tag{20}$$

However, A_1' and B_1' must be assumed to be equal to zero, because otherwise equation (14) cannot be satisfied.

The coefficients A_0 and B_0 are determined by conditions at the external boundaries of the medium or by the properties of symmetry and also by the continuity conditions for the functions (ref. 4)

$$I_z \text{ and } \Phi\left(1+\frac{4\Sigma_0}{\Sigma_2}\right)-\frac{4S}{\Sigma_2}. \tag{21}$$

The continuity of functions (21) is equivalent to the continuity of functions

$$q(z) \text{ and } \varphi(z)\left(1+\frac{4\Sigma_0}{\Sigma_2}\right)-\frac{4w(z)}{\Sigma_2}. \tag{22}$$

As we can see, this first part of the computation depends on the quantity b. Consequently the established solution will be valid also for the one-dimensional problem corresponding to the case b = 0. If, on the other hand, $b \neq 0$, it is necessary to solve equation (11). Its solution will have the form

$$I_x = b\left[(A_0 \operatorname{ch} \varkappa_0 z + B_0 \operatorname{sh} \varkappa_0 z)\frac{\Sigma_2+\Sigma_0}{3\varkappa_0^2-\Sigma_1\Sigma_2} - \frac{w}{\Sigma_1\Sigma_0}\right] + I_x^*. \tag{23}$$

Here I_x^* is the solution of the homogeneous equation

$$\frac{3}{\Sigma_2}\cdot\frac{\partial^2}{\partial z^2} I_x^* - \Sigma_1 I_x^* = 0, \tag{24}$$

which must not be equal to zero, because equation (13) does not place any requirements on it. Let us rewrite solution (23), taking into account expressions (17)

$$\begin{aligned} I_x = -\frac{b}{\Sigma_1}\Big[&(A_0 \operatorname{ch} \varkappa_0 z + B_0 \operatorname{sh} \varkappa_0 z)\left(1+\frac{4\Sigma_0}{\Sigma_2}\right)+ \\ &+\frac{w}{\Sigma_0} + A_1 \operatorname{ch} \varkappa_1 z + B_1 \operatorname{sh} \varkappa_1 z\Big] \equiv bp(z). \end{aligned} \tag{25}$$

Coefficients A_1 and B_1 are determined from the known properties of the solution and from the conditions of continuity for the functions (ref. 4)

$$I_x \text{ and } \frac{1}{\Sigma_2}\left[\frac{\partial I_x}{\partial z} + \frac{\partial I_z}{\partial x}\right] \tag{26}$$

or

$$p(z) \text{ and } \frac{1}{\Sigma_2}\left[\frac{\partial p(z)}{\partial z} + q(z)\right]. \tag{27}$$

If the layer medium is a periodic lattice, we can determine the average macroscopic flux $\langle I_x \rangle$ in the following manner

$$\langle I_x \rangle = \frac{1}{l}\int_z^{z+l} I_x(z)\,dz, \tag{28}$$

where l is the pitch of the lattice.

The average diffusion coefficient may be determined by various means depending on the form used to write down the macroscopic diffusion law. If the macroscopic diffusion law is written in the P_2-approximation

$$\langle I_x \rangle = -\langle D_x \rangle \frac{\partial}{\partial x}\left\langle \Phi\left(1+\frac{4\Sigma_0}{\Sigma_2}\right) - \frac{4w}{\Sigma_2}\right\rangle, \tag{29}$$

then

$$\langle D_x\rangle = -\frac{\langle p(z)\rangle}{\left\langle \varphi(z)\left(1+\frac{4\Sigma_0}{\Sigma_2}\right)-\frac{4w(z)}{\Sigma_2}\right\rangle}. \tag{30}$$

If, on the other hand, the macroscopic behavior of neutrons is described by the P_1-approximation /89

$$\langle I_x\rangle = -\langle D_x\rangle\frac{\partial}{\partial x}\langle\Phi\rangle, \tag{31}$$

then

$$\langle D_x\rangle = -\frac{\langle p(z)\rangle}{\langle\varphi(z)\rangle}. \tag{32}$$

The averaging of functions φ and $\varphi\left(1+\frac{4\Sigma_0}{\Sigma_2}\right)-\frac{4w}{\Sigma_2}$ must be carried out in a manner analogous to (28). For a nonabsorbing medium without sources the difference between the two cases which have been mentioned disappears.

The macroscopic diffusion coefficient for a double layer nonabsorbing lattice without sources, obtained by the method described above, has the form

$$\langle D_x\rangle = \frac{1}{h+h'}\left\{\frac{h}{\Sigma_1}+\frac{h'}{\Sigma_1'}-\frac{(\Sigma_1'-\Sigma_1)^2\operatorname{th}\varkappa_1 h\operatorname{th}\varkappa_1' h'}{(\varkappa_1\Sigma_1'\operatorname{th}\varkappa_1' h'+\varkappa_1'\Sigma_1\operatorname{th}\varkappa_1 h)\Sigma_1\Sigma_1'}\right\}, \tag{33}$$

where h and h' are the thicknesses of the layers. Comparing the results shown by equation (33) with the results of Ya. V. Shevelev (ref. 5), we see that the maximum error of equation (33) is approximately 6 percent (the comparison was carried out for a lead-water lattice, (ref. 4)).

The continuity of I_x in the P_2-approximation and in other even approximations makes it possible for us to maintain that the equations for $\langle D_x\rangle$, similar to equation (33), obtained in some even approximation, for small-layer thickness will give the fusion coefficient of the homogeneous mixture, which is a correct physical result. Equation (33) also has these properties. On the other hand, in approximations of odd order this transition must not exist, due to the discontinuity of the flux I_x which is retained no matter how small the thickness of the layers.

Obviously the methodology which has been described also makes it possible to find the real diffusion coefficient D_x at each point of the medium. However, it will then be a function of z.

REFERENCES

1. Devison, B. The Theory of Neutron Transport (Teoriya perenosa neytronov). Moscow, Atomizdat, 1960.

2. Rumyantsev, G. Ya. Atomnaya Energiya, Vol. 10, 26, 1961.

3. --- Utilization of Even Approximations in the Method of Spherical Harmonics. IN: The Investigation of Critical Parameters in Reactor Systems (Ob ispol'zovanii chetnykh priblizheniy v metode sfericheskikh garmonik. V sb.: Issledovaniya kriticheskikh parametrov reaktornykh sistem). Moscow, Gosatomizdat, 1960.

4. --- The Method of Spherical Harmonics in the Theory of Neutron Transport in the P_2-approximation (Metod sfericheskikh garmonik i teoriya perenosa neytronov v P_2-priblizhenii). Dissertation, MIFI, 1961.

5. Shevelev, Ya. V. Atomnaya Energiya, Vol. 11, 224, 1957.

INVESTIGATION OF THE ACCURACY OF VARIOUS APPROXIMATIONS IN THE PROBLEM OF THREE-DIMENSIONAL ENERGY AND ANGULAR DISTRIBUTION OF NEUTRONS

V. M. Veselov

When investigating the accuracy of various approximate methods for /89
solving the kinetic equation which describes both the three-dimensional transport as well as the retardation of neutrons (from the point of view of applying these methods to analyze shielding), it is particularly important to investigate /90
the degree to which these methods give a satisfactory description of the distribution: (a) of fast neutrons, which make a substantial contribution to the power of the dose, and (b) low energy neutrons, which produce a strong γ-radiation when they are captured by the nuclei of various elements.

In the present article we consider the lower approximation methods of spherical harmonics (P_1, P_2, P_3) and some of their modifications on the basis of the simplest problems of the three-dimensional and angular distribution of neutrons from a two-dimensional isotropic monoenergetic source in an infinite homogeneous medium. In this medium, absorption, the effects of chemical bond and inelastic scattering are absent, the mean free path l is constant, scattering is isotropic in the system of the mass center.

This relatively simple problem is important, because it considers the problem in the "pure" form, avoiding all types of side effects which would be manifested in a problem of greater reality and which would substantially complicate the picture of the convergence of various approximations. Furthermore, this problem has a solution obtained by Wick (refs. 1 and 2) for a moderator with a nuclear mass $M = 1$ for $u \gg 1$ at short distances from the source and with $uz \gg 1$ at large distances (in the case $M > 1$ these conditions, respectively, transform into $u/\xi \gg 1$ and $uz/\xi \gg 1$). The problem is also solved by Bethe, Tonks and Hurwitz (ref. 3) (in the B_2-approximation) for the case $M = 9$ under the condition $u/\xi \gg 1$. These solutions have been utilized as "exact" solutions and all other approximate solutions have been compared to them.

The Wick method, which is also described in the works of Marshak (ref. 4) and Devison (ref. 5), and which is rigorously proved by M. V. Maslennikov (ref. 6), includes the utilization of an expansion in terms of the Legendre polynomials. It is therefore convenient to apply it to the solution of the formulated problem. However, this method, which is somewhat modified when it is

applied to the solution of the problem in the P_N-approximation, although it gives a sufficiently good answer to the second problem formulated above, does not give a satisfactory answer to the first, because it is applicable only for relatively high moderations.

To fill this gap it is useful to study the energy moments from the density of collisions per unit interval of energy, in addition to studying the density of collisions per unit interval of lethargy $\Psi(z, u, \mu)$ when $u/\xi \gg 1$. In other words, it is convenient to investigate the integrals

$$\int_0^{E_0} \Psi(z, \mu, E) E^n dE,$$

which characterize the distribution of neutrons whose energy increases as n increases. In this case the following obvious relationship must be satisfied

$$\Psi(E) dE = \Psi(u) du.$$

We note that as u increases, the convergence of the method of spherical harmonics improves, because the anisotropy of the angular distribution of neutrons which undergo a large number of collisions with the nuclei is substantially less. Therefore, in the investigation of the function $\Psi(z, u, \mu)$ a minimum lethargy was selected for which the Wick conditions were still satisfied.

We expand the density of collisions $\Psi(z, u, \mu)$ and the scattering function $f(\mu_0, u-u')$ in series of Legendre polynomials and substitute them into the kinetic equation for the given problem. After the usual transformations we obtain a system of equations

$$\frac{m}{2m+1} \cdot \frac{\partial \Psi_{m-1}(z, u)}{\partial z} + \frac{m+1}{2m+1} \cdot \frac{\partial \Psi_{m+1}(z, u)}{\partial z} + \Psi_m(z, u) =$$
$$= \int_{u-r}^{u} du' \Psi_m(z, u') f_m(u-u') + \delta(u)\delta(z)\delta_{m_0} \text{ for } m = 0, 1, 2, \ldots. \quad (1)$$

Here the mean free path λ is taken as the unit of length; δ_{m_0} is the Kronecker symbol; /91

$$\Psi_m(z, u) = 2\pi \int_{-1}^{1} d\mu \Psi(z, u, \mu) P_m(\mu);$$
$$f_m(u-u') = 2\pi \int_{-1}^{1} d\mu_0 f(\mu_0, u-u') P_m(\mu_0), \quad (2)$$

are the m-th harmonics of the density of collisions and the scattering function; r is the interval of collisions.

During the solution of the problem in the P_N-approximation we limit ourselves to (N + 1) equations, i.e., N takes on the values 0, 1, 2, ..., (N-1), N.

In the system of equations (1), written in the P_N-approximation, we adopt the Laplace transformation with respect to the lethargy with parameter η and the Fourier transformation with respect to the coordinate with the parameter k. As a result we obtain the following system of equations

$$(2m+1)[1-g_m(\eta)]\Phi_m(\eta, k)-k[m\Phi_{m-1}(\eta, k)+ \\ +(m+1)\Phi_{m+1}(\eta, k)]=\delta_{m0} \text{ for } m=0, 1, \ldots, N \quad [1], \tag{1a}$$

where

$$\left.\begin{aligned}\Phi_m(\eta, k)&=\int_{\ldots}^{\ldots} e^{kz}\,dz\int_0^{\infty} e^{-\eta u}\Psi_m(z, u)\,du;\\ g_m(\eta)&=\int_0^{\infty} e^{-\eta t} f_m(t)\,dt.\end{aligned}\right\} \tag{3}$$

Ψ_m (z, u) is now obtained by means of the inverse Laplace-Fourier transformation

$$\Psi_m(z, u)=\frac{1}{(2\pi i)^2}\int_{-i\infty}^{i\infty} e^{-kz}\,dk\int_{\sigma-i\infty}^{\sigma+i\infty} e^{\eta u}\Phi_m(\eta, k)\,d\eta. \tag{4}$$

It is difficult to express the function Φ_m (η, k) (from equation 1a) in the form convenient for integration. Therefore integrals (4) are approximated. By investigating the system of equations (1a) we can conclude that (refs. 1 and 2) Ψ_m (η, k) has poles at the points $\eta = \eta$ (k) in the complex η-plane; the multivalued function η (k) is determined from the condition that the determinant of system (1a) is equal to zero. Wick showed that for $N = \infty$ one of the poles for $0 \le k \le 1$ lies on the real axis and is greater than zero, while the remaining poles have a real part less than zero and play a minor role when u are large (when $M > 1$ the condition $u/\xi \gg 1$ is required in place of $u \gg 1$). This is also true for a finite N, but in this case k lies in the interval $0 \le k \le k_1 > 1$.

Therefore the integral of the inverse Laplace transform may be taken by means of the theory of residues; the integral of the inverse Fourier transform is taken by the saddle point method. We now obtain an equation which is analogous to the Wick equation (ref. 2)

$$\Psi_m(z, u)=(2\pi\eta_0''u)^{-1/2}R_m(k_0)\exp(-k_0z+\eta u), \tag{5}$$

where

$$\eta_0 = \eta(k_0);\ \eta_0' = \eta'(k_0);\ \eta_0'' = \eta_0''(k_0).$$

The saddle point k_0 in the saddle point method is obtained from the condition

$$-z + \eta'(k_0)\, u = 0. \tag{5a}$$

Equation (5) may be applied to solve the problem in various approximations, and in this case only η (k) and R_m (k) will have a form which depends on the selected approximation. R_m (k) is obtained from the equations /92

$$R_0(k_0) = \frac{\eta'(k_0)\,\Phi_0^2(k_0, \eta_0)}{2\sum_{n=0}^{\infty}(n+1)\,\Phi_n(k_0\eta_0)\,\Phi_{n-1}(k_0\eta_0)}; \quad \text{[см. 2]}$$

$$\frac{R_m(k_0)}{R_0(k_0)} = \frac{M_{m-1}^{m-1}(k_0\eta_0)}{m!\,k_0^m}, \tag{6}$$

where M_{m-1}^{m-1} is the minor of the basic determinant of the system of equations (1a), formed by the first m lines and columns with numbers from 0 to m-1. Φ_0/Φ_n are obtained from equation (1).

By utilizing equation (5) we can find Ψ_0 (z, u)--the integral density of collisions over the angles, and also Ψ_m (z, u), which gives us the angular distribution of neutrons at various distances from the source.

The basic difficulty associated with the solution of the problem in the P_N-approximation consists of finding η (k) and two of its derivatives by the method of the successive approximation and tabulated differentiation. This is complicated by the form of the function g_m (η) (ref. 3) when M > 1, which makes it necessary to apply interpolation up to the fourth degree. The problem of finding η (k) may be simplified, if we expand g_m (η) in Taylor's series of η and limit ourselves to a certain number of terms corresponding to the order of the P_N-approximation

$$g_m(\eta) = g_m(0) + \frac{\partial g_m(0)}{\partial \eta}\eta + \frac{1}{2}\frac{\partial^2 g_m(0)}{\partial \eta^2}\eta^2 + \ldots \tag{7}$$

Let us consider the coefficients of the Taylor series

$$\frac{\partial^n g_m(0)}{\partial \eta^n} = \frac{\partial^n}{\partial \eta^n}\left\{\int_0^\infty e^{-\eta l} f_m(l)\,dl\right\}_{\eta=0} = \\ = (-1)^n \int_0^\infty l^n f_m(l)\,dl = (-1)^n I_m^n, \tag{8}$$

where I_m^n is the n-th moment of the m-th harmonic of the scattering function which is easy to determine for any values of m and n

$$I_0^0 \equiv 1;$$
$$I_0^1 \equiv \xi = a(1-\alpha+\alpha\ln\alpha);$$
$$I_0^2 \equiv \overline{\xi^2} = 2\xi - a\alpha\ln^2\alpha;$$
$$I_1^0 \equiv \overline{\mu_0} = \frac{2}{3M};$$
$$I_1^1 \equiv \overline{\Delta u \mu_0} = -\frac{2M^3-6M+4}{12M}\ln\alpha - \frac{6M^2-10}{9M}; \tag{9}$$
$$I_2^0 \equiv \frac{3}{2}\overline{\mu_0^2} - \frac{1}{2};$$
$$\overline{\mu_0^2} = \frac{3-M^2}{4} - \frac{(M^2-1)^2}{16M}\ln\alpha;$$
$$a = \frac{(M+1)^2}{4M};$$
$$\alpha = \frac{(M-1)^2}{(M+1)^2}.$$

If we solve the problem in the P_1-approximation and limit ourselves to two terms for m = 0 in equality (7) and to one term for m = 1, we obtain the age approximation; if we leave one more term for m = 0 and for m = 1, we obtain an approximation which will be called $P_1\overline{\xi^2}$ in the future. Similarly, when solving the problem in the P_2-approximation, if we leave two terms in equality (7) for /94 the case m = 0, one term for the case m = 1 and no terms for the case m = 2, we obtain a P_2-age approximation; if we leave an extra term everywhere we obtain the approximation $P_2\overline{\xi^2}$.

The integral density of collisions over the angles Ψ_0 (z, u) computed by the above method in the P_1, age, P_2, P_2-age, $P_2\overline{\xi^2}$, P_3-approximations is shown in figure 1 for a moderator with M = 1 for a fixed lethargy u = 10.

Figure 2 shows the calculation results for the angular distribution of neutrons of lethargy u = 10 at various distances from the sources, when M = 1 in the P_1-, P_2-, P_3-approximations. This figure also shows the curves for the angular

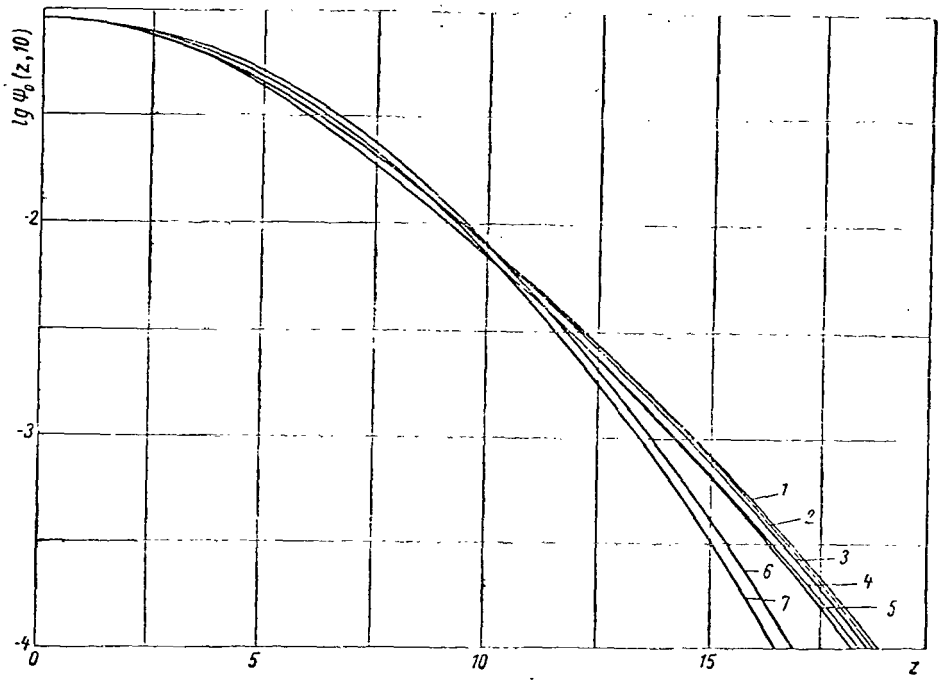

Figure 1. Variation in logarithm of density of collisions as function of distance to source (expressed in terms of mean free path length) with fixed lethargy u = 10 for a moderator with M = 1: 1, Wick solution; 2, P_3-approximation; 3, P_2-approximation; 4, $P_2\overline{\xi^2}$-approximation; 5, P_2-age approximation; 6, P_1-approximation; 7, age approximation.

distribution of neutrons of lethargy u = 10 at various distances from the sources, when M = 1 in the P_1-, P_2-, P_3-approximations. This figure also shows the curves for the angular distribution in the P_4-approximation obtained by an evaluation utilizing the results of calculations in the P_3-approximation, using an approximate equation which is easy to derive

$$\frac{R_{m+1}}{R_0} = \frac{(m+1)k}{(2m+3)(1-g_{m+1})} \cdot \frac{R_m}{R_0}, \qquad (10)$$

where k_0 for a given z is taken from the calculation of the P_m-approximation.

The results of computing Ψ_0 (z, u) in the P_1, age, $P_1\overline{\xi^2}$, P_2, P_2,-age, /96 $P_2\overline{\xi^2}$-approximations for M = 9 and u = 3 are shown in figure 3, while figure 4 shows the angular distribution for the same case in the P_1-, P_2- and P_3-approximations (estimation).

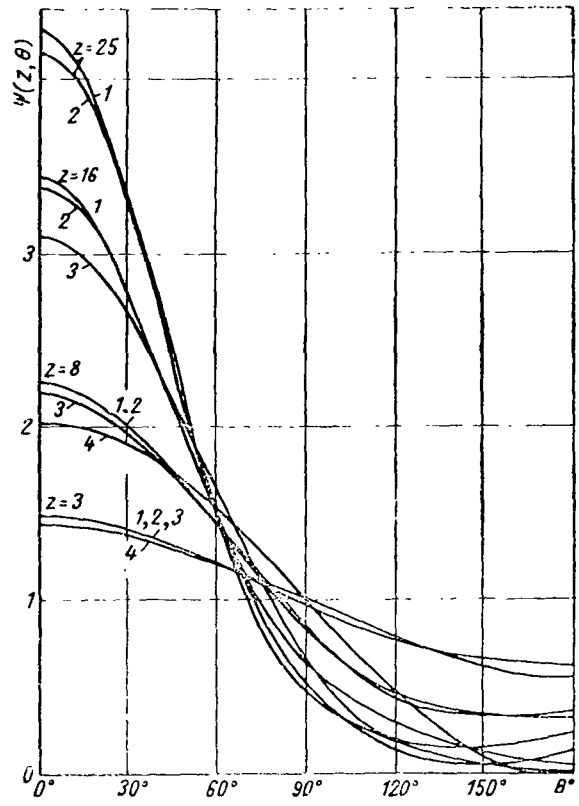

Figure 2. Angular distribution of neutrons in moderator with M = 1 and fixed lethargy u = 10 for various distances z from source: 1, P_4-approximation (evaluation); 2, P_3-approximation; 3, P_2-approximation; 4, P_1-approximation.

A discussion of the results obtained until now, as we have already stated, makes it possible to answer only the second question concerning the accuracy with which the various approximations describe the distribution of low energy neutrons. To clarify their accuracy in describing the distribution of fast neutrons we consider the integrals

$$J_n(z) = \int_0^{E_0} \Psi_0(z, E) E^n dE, \tag{11}$$

when n = 1 this is simply the energy flux of neutrons since $\iota = 1$.

It is easy to show that

$$J_n(z) = E_0^n \int_0^{\infty} \Psi_0(z, u) e^{-nu} du = E_0^n J_n^*(z), \tag{12}$$

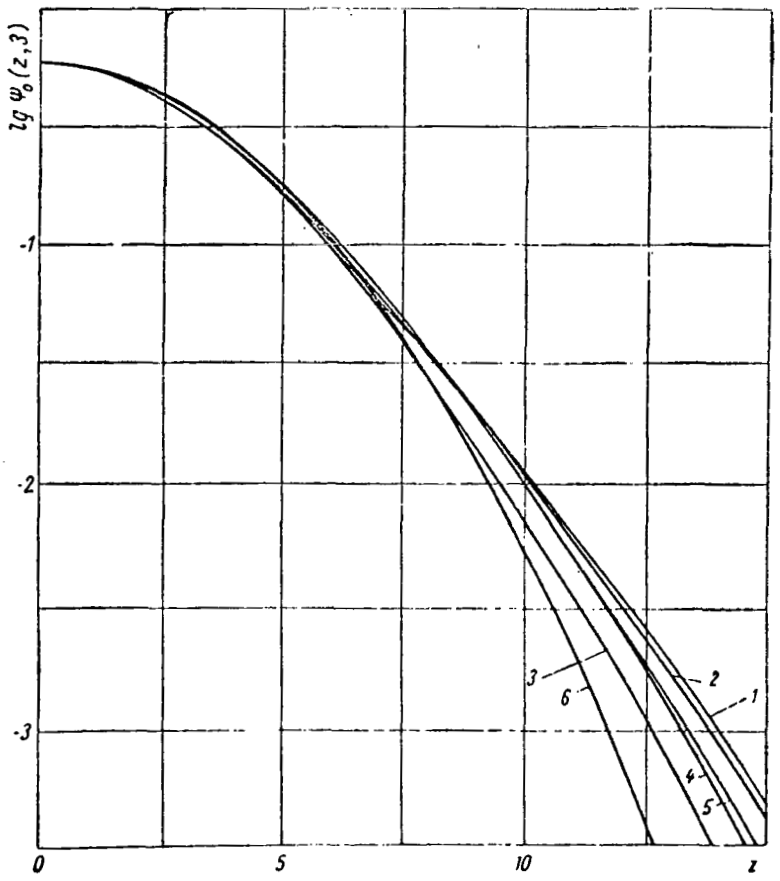

Figure 3. Variation in logarithm of density of neutron collisions with lethargy u = 3 as function of distance to source (in terms of mean free path length) for moderator with M = 9: 1, solution of Bethe, Tonks and Hurwitz; 2, P_2-approximation, 3, P_2-age approximation; 4, P_1-approximation; 5, $P_1\overline{\xi^2}$-approximation; 6, age approximation; ($P_2\overline{\xi^2}$-approximation coincides with Bethe, Tonks and Hurwitz solution to distance of z = 17).

i.e., it is sufficient to investigate $J_n^*(z)$. This is easier than investigating $\Psi(z, u, \mu)$, because in this case it is not necessary to take the inverse Laplace transform. J_n^* may be written in the form

$$J_n^*(z) = \frac{1}{2\pi i}\int_{-i\infty}^{i\infty} e^{-hz}\Phi_0(k,\eta)_{\eta=n}\,dk. \qquad (13)$$

The function $\Phi_0(\eta, k)$ calculated in the P_N-approximation has k poles in the complex plane situated at the points k_{0i}. Their number depends on the number N of the P_N-approximation. Therefore we can write

$$J_n^*(z) = \sum_i e^{-k_{0i}z} \operatorname{res} \Phi_0(k_{0i}, n),$$

where k_{0i} is determined for any $\eta = n$ from the condition that the determinant of the system of equations (1a) is equal to 0; the residues are found easily. The calculation of the quantities J_1^* and J_2^* as a function of z was carried out for a moderator with M = 1 and M = 9 in various approximations and is represented in tables 1 (M = 1) and 2 (M = 9), where all of the approximations are compared with P_4 for different values of z. /97

The expressions $J_1^*(z)$ and $J_2^*(z)$ under the integral sign in terms of u for certain values of z were obtained for the case M = 9 by calculation from the Bethe, Tonks and Hurwitz solution (ref. 3). The graphs of these quantities are shown in

TABLE 1.

z	$J_1^*(z) P_N/J_1^*(z) P_4$			$J_2^*(z) P_N/J_2^*(z) P_4$		
	P_1/P_4	P_2/P_4	P_3/P_4	P_1/P_4	P_2/P_4	P_3/P_4
2	1,279	0,970	0,954	1,048	0,832	0,774
6	0,667	1,019	1,013	0,418	1,014	1,012
12	0,179	0,839	0,985	0,054	0,652	0,951
20	0,030	0,608	0,928	—	0,337	0,815
30		0,406	0,859	—	0,148	0,672

TABLE 2.

z	$J_1^*(z) P_N/J_1^*(z) P_4$			$J_2^*(z) P_N/J_2^*(z) P_4$		
	P_1/P_4	P_2/P_4	P_3/P_4	P_1/P_4	P_2/P_4	P_3/P_4
2	1,107	0,988	0,990	1,151	0,991	0,927
6	0,915	1,012	1,002	0,800	1,018	1,007
12	0,699	0,982	1,000	0,401	0,916	0,993
20	0,465	0,939	0,994	0,158	0,789	0,969
30	0,280	0,889	0,987	0,049	0,654	0,937

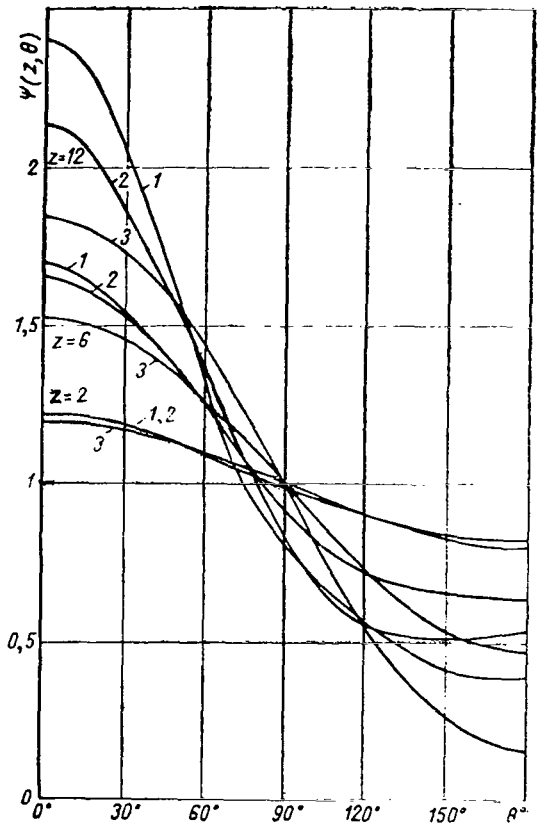

Figure 4. Angular distribution of neutrons of lethargy u = 3 in moderator with M = 9 at various distances z from source: 1, P_3-approximation (estimation); 2, P_2-approximation; 3, P_1-approximation.

figures 5 and 6. They make it possible to evaluate the energy of neutrons which make the maximum contribution to $J_1^*(z)$ and $J_2^*(z)$.

Discussion of Results

We make a qualitative comparison of the solutions of the problem in different approximations with the "exact" solutions of Wisk, Bethe and others.

P_1-approximation. We can see from fig. 1 that the P_1-approximation for M = 1 gives us an increased value of collisions density $\Psi_0(z, u)$ at distances to 10 mean free path lengths. This can be explained in the following manner. Scattering by nuclei with M = 1 is characterized by a large release of energy, so that the energy of the neutron can immediately vary from E_0 to the thermal energy and inverse scattering does not take place. Therefore the angular distribution of

neutrons has a strong maximum at $\theta = 0^\circ$ even at rather small distances from the source (θ is the angle between the direction of the neutron path and the normal to the source plane). The first Legendre polynomial alone cannot describe this strong anisotropic relationship sufficiently well. This inaccuracy which extends to a distance of 10 mean free paths is characterized by the decrease in the number of neutrons which travel at small angles and an increase in the number of neutrons which travel at angles close to 90° (fig. 2).

However, it is known that neutrons which are scattered over small angles possess the highest probability for moving far away from the source. Consequently in the P_1-approximation a smaller number of neutrons has a chance to penetrate a great distance compared to what actually takes place. This produces a buildup of neutrons near the source and a decrease in their number at large distances from the source. Therefore it is not expedient to utilize the P_1-approximation for a moderator with M = 1. The error in Ψ_0 (z, u) reaches a value of 15 percent at a distance of approximately five mean free paths even

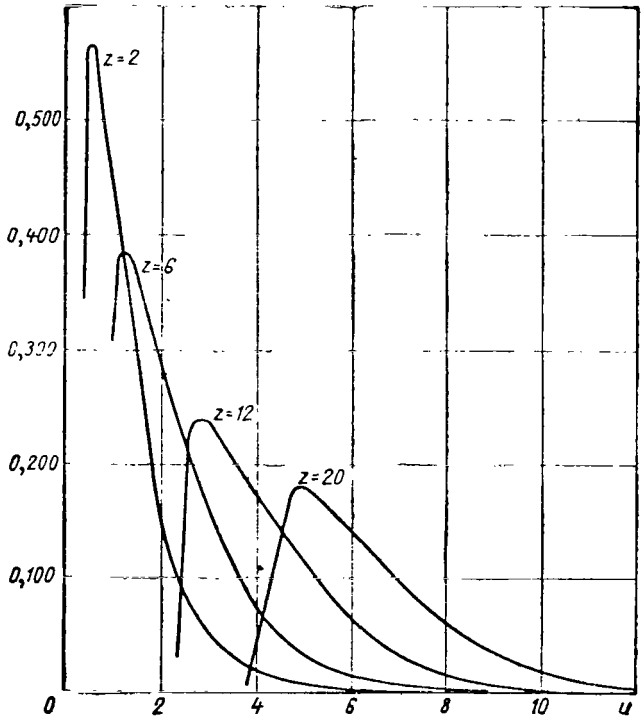

Figure 5. $\Psi_0(z, u)e^{-u}$ at different distances from source in B_2-approximation. Function is normalized so that $\int_0^\infty \Psi_0(z, u)e^{-u}\,du = 1$.

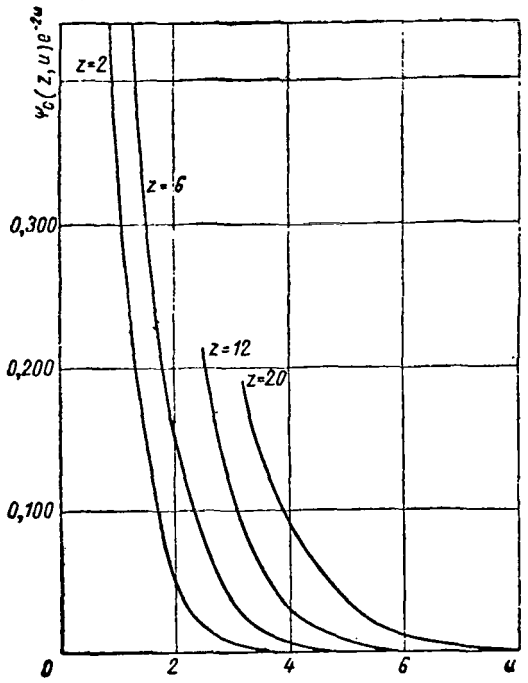

Figure 6. $\Psi_0(z, u)e^{-2u}$ at different distances from source in B_2-approximation. Function is normalized in such a way that $\int_0^\infty \Psi_0(z, u)e^{-2u}\,du = 1$.

for neutrons of relatively small energy (u = 10). For large energies the deviation of the solution in the P_1-approximation from the "exact" solution is even greater, because in this case we take into account neutrons which have undergone a smaller number of collisions with the moderator nuclei and their angular distribution is even more anisotropic.

Everything that has been stated above, but to a lesser degree, may be referred to a moderator with M = 9. However, in this case the anisotrophy of the angular distribution is less so that the effects described above are much weaker. At distances up to nine mean free paths when u = 3, the error does not exceed 5-6 percent (figs. 3 and 4). At large distances the P_1-approximation /98 for M = 9 becomes unsatisfactory; when z = 12, the error is greater than 25 percent.

P_2-approximation. The P_2-approximation both for M = 1 and for M = 9 turns out to be substantially more accurate than P_1 (figs. 1 and 3). This is explained by the fact that when we take into account the second Legendre polynomial, we substantially refine the angular variation of the function $\Psi(z, u, \mu)$

compared with the P_1-approximation (figs. 2 and 4). The difference between the quantity $\Psi_0(z, u)$ computed "exactly" in the P_2-approximation reaches the value of 10 percent only at distances equal to approximately 20 mean free paths in the case M = 1, u = 10 and 12 mean free paths in the case M = 9, u = 3, which is incomparably better than in the P_1-approximation.

P_3-approximation. The angular and spatial distribution in this case is even better than in the P_2-approximation (figs. 1 and 2). At a distance of 25 mean free paths the error does not exceed 3 percent for M = 1.

Let us now consider other approximations which result from P_1 and P_2 after simplified assumptions are made concerning the energy relationship of the scattering function, i.e., the age approximation, $P_1\overline{\xi^2}$ approximation, P_2-age approximation, $P_2\overline{\xi^2}$-approximation.

Age approximation. This approximation is obtained from P_1 if we neglect all moments of the scattering function except ξ and $\overline{\mu_0}$, i.e., this approximation is within the framework of the P_1-approximation.

It then follows that this approximation is applicable only in the case when P_1 produces satisfactory results and the quantities $\overline{\xi^2}$ and $\Delta\overline{u\mu}_0$ are small. When M = 1, both propositions are untrue, but nevertheless, as we can see from figure 1, at small distances from the source the age approximation is substantially better than P_1. However, at large distances it is not as good which, however, is not significant because at this point P_1 is entirely unsatisfactory. Therefore in the case M = 1 at small distances it is advantageous to utilize the age approximation rather than P_1 as being much simpler and more accurate. Therefore there is also no reason for taking into account $\overline{\xi^2}$ and $\Delta\overline{u\mu}_0$, because the approximation $P_1\overline{\xi^2}$ obtained in this manner must be closer to P_1 than the age approximation and consequently is less accurate than the latter.

It can be shown that when we transfer from $P_1\overline{\xi^2}$ to an age approximation, the dropping of $\overline{\xi^2}$ and $\Delta\overline{u\mu_0}$ which are large when M = 1 (equal, respectively, to 2 and 4/9) is equivalent to a change in the scattering function, such that a

large number of neutrons are scattered over small angles, i.e., the angular distribution in this case improves and the spatial distribution also improves.

In the case M = 9, the spatial distribution in P_1, $P_1\overline{\xi^2}$ and in the age approximation coincide at small distances from the source (fig. 2). This is explained by the fact that for M = 9 $\overline{\xi^2}$ and $\overline{\Delta u \mu_0}$ are small (+ 0.059 and -0.058) and their effect is not yet felt. On the other hand, at large distances $\overline{\xi^2}$ and $\overline{\Delta u \mu_0}$ become substantial and must be taken into account.

We should note that the quantities $\overline{\xi^2}$ and $\overline{\Delta u \mu_0}$ affect Ψ_0 (z, u) in one direction and their effect is approximately of the same order so that it is logical to apply the $P_1\overline{\xi^2}$ approximation rather than the Greyling-Hertzel approximation which does not take into account $\overline{\Delta u \mu_0}$. We can also see from fig. 3 that the error incurred in going from approximation P_1 to $P_1\overline{\xi^2}$ is directed in such a way that the approximation $P_1\overline{\xi^2}$ turns out to be more accurate than P_1.

The P_2 age and $P_2\overline{\xi^2}$ approximations. For M = 1 the curves for these approximations coincide completely up to distances of 25 mean free path lengths (fig. 1). It is difficult to investigate the reasons for this in detail. Apparently the effect produced by the quantities $\overline{\xi^2}$, $\overline{\Delta u \mu_0}$, $\frac{3}{2}\overline{\mu_0^2} - \frac{1}{2}$ is mutually compensated in a particular moderator, such as the moderator with a nuclear mass of M = 1.

In the case M = 9, the approximations P_2-age approximation, the $P_2\overline{\xi^2}$ and P_2-approximations coincide at small distances, while at large distances the consideration of $\overline{\xi^2}$, $\overline{\Delta u \mu_0}$ and $\frac{3}{2}\overline{\mu_0^2} - \frac{1}{2}$ corrects the sharp drop of the curve /99 in the P_2-age approximation (fig. 3). In this case it also turns out that $P_2\overline{\xi^2}$ is closer to the "exact" solution than P_2, which is important, because calculations in the $P_2\overline{\xi^2}$ approximation are substantially simpler than the calculations in the P_2-approximation.

These considerations make it clear that in computing the distribution of neutrons with small energies approximations P_2 and $P_2\overline{\xi^2}$ represent a great step forward compared to P_1 and the age approximation.

Let us now discuss the results presented in tables 1 and 2. First of all we note that the approximations which take into account only a finite number of moments for the scattering function cannot describe the integrals J_n^* correctly for M = 1.

Indeed, in this case $g_0(\eta)$ has the form

$$g_0(\eta) = \frac{1}{1-\eta}$$

and when $\eta > 1$, expansion (7) loses its meaning. Therefore when investigating $J_1^*(z)$ and $J_2^*(z)$ these approximations are not considered. If M > 1, the situation is different and expansion (7) may be achieved when $\eta > 1$. However, the convergence of (7) is not as good when η increases, and when η is greater than η_1, it disappears completely. Therefore, in computing $J_1^*(z)$ these approximations can still be used, and they give approximately the same results as obtained in the calculation of $\Psi_0(z, 3)$. However, the computation of $J_2^*(z)$ in these approximations leads to unsatisfactory results.

Therefore the age, $P_1\overline{\xi^2}$, P_2-age, and $P_2\overline{\xi^2}$ approximations cannot be used in computing the distribution of neutrons with high energy. In tables 1 and 2 only the P_1-, P_2-, and P_3-approximations are compared with P_4.

Table 1, which refers to M = 1, shows that in order to compute the distribution of fast neutrons approximation P_1 is unsuitable in practice; P_2 may be used only for short distances from the source (z < 10), while P_3 turns out to be substantially better.

In the case M = 9 the maximum contribution to the integral $J_1^*(z)$ at distances up to 20 mean free path lengths yield neutrons with lethargies up to u = 6 (fig. 5). Therefore the convergence picture for different approximations is approximately the same as for $\Psi_0(z, u)$ when u = 3. Approximations P_2 and P_3 describe $J_1^*(z)$ quite well up to z = 30. The basic contribution to the integral $J_2^*(z)$ is made by neutrons with smaller lethargies (fig. 6). Therefore approximation P_1 becomes entirely unsuitable when z > 10, and P_2 is substantially better

than this, but substantially worse than P_3 (the error for z = 20 is 20 and 6 percent respectively).

In conclusion the author expresses his gratitude to V. V. Orlov and G. Ya. Rumyantsev for formulating the problem and for their constant attention while the work was being performed.

REFERENCES

1. Verde, M. and Wick, G. Phys. Rev., Vol. 71, 852, 1947.

2. Wick, G. Phys. Rev., Vol. 75, 738, 1949.

3. Bethe, H., Tonks, L. and Hurwitz, H. Phys. Rev., Vol. 80, 11, 1950.

4. Marshak, R. Rev. Mod. Phys., Vol. 19, 185, 1947.

5. Devison, B. The Theory of Neutron Transportation (Teoriya perenosa neytronov). Moscow, Atomizdat, 1960.

6. Maslennikov, M. V. Dokl. AN SSSR, Vol. 120, 59, 1958.

APPLICATION OF CONJUGATE EQUATIONS TO THE CALCULATION OF RADIATION SHIELDING

G. I. Marchuk and Zh. N. Bel'skaya

The work of B. B. Kadontsev (ref. 1) formulated a conjugate equation /99 with respect to any linear functional in the problem of radiation transport. Later the results presented in reference 1 were generalized by G. I. Marchuk and V. V. Orlov (ref. 2). Their work proposes a method for the construction of conjugate equations for a wide class of linear nonhomogeneous equations, /100 as well as the construction of the theory of perturbations.

In the present work the authors have made an effort to apply the results of references 1 and 2 to the calculation of radiation shielding. The solution of the problem is obtained in the simple diffusion approximation in order not to mask the principal features of the problem by insignificant calculation steps. The generalization of the results to the case of nondiffusion approximation, which is of practical interest (for example, within the framework of the P_N-approximation), is not difficult and is carried out by the method presented in reference 3.

Let us consider a multiple layer system occupying volume G bounded by surfaces S_1 and S_2. The physical characteristics of the medium which determine the interaction of neutrons with a substance are constant inside each layer. The group values f^j of the neutron flux falling on surface S_1 are assigned. It is required to compute the total flux and the dose of neutrons leaving the shielding.

The problem is solved in the P_1-approximation by a multiple group method with the aid of the basic and conjugate equations of the reactor.

$$\left.\begin{aligned} \nabla\varphi_1^j + \Sigma_{\text{уд}}^j \varphi_0^j &= \sum_{i=1}^{j-1} \Sigma_{in}^{i\to j} \varphi_0^i + \Sigma_a^{j-1} \varphi_0^{j-1}; \\ \frac{1}{3}\nabla\varphi_0^j + \Sigma_{tr}^j \varphi_1^j &= 0 \end{aligned}\right\} \qquad (1)$$

(уд = re = removal)

Let us consider a multiple group system of basic equations (ref. 3) and the multiple group system of equations conjugate with respect to system (1),

$$\left.\begin{aligned} -\nabla\varphi_1^{*j}+\Sigma_{y_B}^j\varphi_0^{*j}&=\sum_{l=j+1}^{m}{}^{j\to l}\Sigma_{in}\varphi_0^{*l}+\Sigma_3^j\varphi_0^{*j+1};\\ -\frac{1}{3}\nabla\varphi_0^{*j}+\Sigma_{lr}^j\varphi_1^{*j}&=0. \end{aligned}\right\} \tag{2}$$

The calculation of the three-dimensional energy distribution of neutrons in the P_1-approximation is reduced to the solution of the multiple group system of equations (1) with boundary conditions

$$I^j=f^j \text{ on } S_1$$

and

$$2\varphi_{1n}^j-\varphi_0^j=0 \text{ on } S_2. \tag{3}$$

We determine the conjugate system of equations with respect to a specific functional for which we select either the total flux of neutrons leaving the shielding or the biological dose of neutron action leaving the shielding. In order that the system of equations (2) be a conjugate system (1), it is necessary that the following relationship be satisfied

$$\sum_{j=1}^{m}\int_G(\nabla\varphi_0^{*j}\varphi_1^j+\nabla\varphi_0^j\varphi_1^{*j})\,dr=0. \tag{4}$$

It is easy to see this if we multiply the first equation (1) by φ_0^{*j} and the second by $3\varphi_1^{*j}$, and if we multiply equations (2), respectively, by φ_0^j and $3\varphi_1^j$. Summating the results over j we integrate over the volume G and subtract one system thus obtained from the other. Utilizing the Gauss-Ostrogradskiy theorem we transform relationship (4) into the form

$$\sum_{j=1}^{m}\int_{S_2}(\varphi_0^{*j}\varphi_{1n}^j+\varphi_0^j\varphi_{1n}^{*j})\,ds-\sum_{j=1}^{m}\int_{S_1}(\varphi_0^{*j}\varphi_{1n}^j+\varphi_0^j\varphi_{1n}^{*j})\,ds=0. \tag{5}$$

We select the positive direction to be that of the external normal to surface S_2 and that of the internal normal to surface S_1. We let I^+, I^- be the density of the neutron flux through surfaces S_1 and S_2, respectively, in the positive and negative directions of the normals to this surfaces /101

$$I^{+} = \frac{1}{2}\varphi_0^j + \frac{1}{2}\varphi_{1n}^j;$$

$$I^{-} = \frac{1}{2}\varphi_0^j - \frac{1}{2}\varphi_{1n}^j.$$

We shall consider the sums contained in relationship (5). Since the flux of neutrons from the vacuum to surface S_2 is absent, we arrive at the condition $\varphi_{1n}^j = \frac{\varphi_0^j}{2}$ on S_2. Consequently,

$$\sum_{j=1}^{m} \int_{S_2} (\varphi_0^{*j}\varphi_{1n}^j + \varphi_0^j \varphi_{1n}^{*j})\, ds = \frac{1}{2}\sum_{j=1}^{m} \int_{S_2} \varphi_0^j (\varphi_0^{*j} + 2\varphi_{1n}^{*j})\, ds. \tag{6}$$

We determine the conjugate system of equations in such a way that relationship (6) supplies a complete dose of outgoing radiation. For this purpose we let

$$\varphi_0^{*j} + 2\varphi_{1n}^{*j} = \gamma^j \text{ at } S_2, \tag{7}$$

where γ^j is a factor of biological action. Then

$$\sum_{j=1}^{m} \int_{S_2} (\varphi_0^{*j}\varphi_{1n}^j + \varphi_0^j \varphi_{1n}^{*j})\, ds = \frac{1}{2}\sum_{j=1}^{m} \int_{S_2} \gamma^j \varphi_0^j\, ds = B(S_2),$$

where $B(S_2)$ is the total dose of the outgoing radiation. On the other hand, from condition (5) we obtain

$$B(S_2) = \sum_{j=1}^{m} \int_{S_1} (\varphi_0^{*j}\varphi_{1n}^j + \varphi_0^j \varphi_{1n}^{*j})\, ds. \tag{8}$$

Let us assume that the following relationship exists on surface S_1

$$\varphi_0^{*j} - 2\varphi_{1n}^{*j} = 0, \tag{9}$$

Then

$$B(S_2) = \sum_{j=1}^{m} \int_{S_1} \frac{\varphi_0^{*j}}{2} (\varphi_0^j + 2\varphi_{1n}^j)\, ds = 2\sum_{j=1}^{m} \int_{S_1} \varphi_0^{*j} I^{+j}\, ds.$$

Thus the dose of the outgoing radiation may be obtained by means of one of the two equations

$$B(S_2)=\begin{cases}\frac{1}{2}\sum\limits_{j=1}^{m}\int\limits_{S_2}\gamma^j\varphi_0^j\,ds;\\ 2\sum\limits_{j=1}^{m}\int\limits_{S_1}\varphi_0^{*j}I^{+j}\,ds.\end{cases}\qquad(10)$$

In systems with spherical symmetry

$$B(S_2)=\begin{cases}\frac{1}{2}S_2\sum\limits_{j=1}^{m}\gamma^j\varphi_0^j;\\ 2S_1\sum\limits_{j=1}^{m}\varphi_0^{*j}I^{+j}.\end{cases}\qquad(11)$$

If we let $\gamma^j=2$ in equations (7) and (10), we arrive at the total flux of the outgoing radiation.

The solution of the system of equations (1) in conjunction with boundary conditions (3) and of system (2) with boundary conditions (7) and (9) is obtained by the method of finite differences with a subsequent application of difference factorization described in reference 3.

To obtain the equations of the theory of perturbations we proceed /102 in the following manner. Together with the unperturbed system (1) we consider a system of perturbed equations

$$\left.\begin{aligned}&\nabla\varphi_1'^j+\Sigma_{\text{ув}}'^j\varphi_0'^j=\sum_{l=1}^{j-1}\Sigma_{1n}'^{l\to j}\varphi_0'^l+\Sigma_3'^{j-1}\varphi_0'^{j-1};\\&\tfrac{1}{3}\nabla\varphi_0'^j+\Sigma_{tr}'^j\varphi_1'^j=0.\end{aligned}\right\}\qquad(12)$$

We assume that the multiple group constants in the system of equations (12) are expressed in terms of the constants for the unperturbed problem by relationship A' = A + δA.

We propose further that the boundary conditions for the perturbed system (12) will be the same as those for the unperturbed system, i.e.,

$$\left.\begin{aligned}&I'^j=f^j\ \text{at}\ S_1;\\&2\varphi_{1n}'^j-\varphi_0'^j=0\ \text{at}\ S_2.\end{aligned}\right\}\qquad(13)$$

Multiplying the equations of system (12), term by term, by φ_0^{*j} and $3\varphi_1^{*j}$, we summate the result over j and integrate over volume G. Then we obtain

$$\sum_{j=1}^{m}\int_{G} dr\left[\varphi_0^{*j}\left(\nabla\varphi_1^{'j}+\Sigma_{y\pi}^{'j}\varphi_0^{'j}-\sum_{l=1}^{j-1}{}^{l\to j}\Sigma_{in}^{'}\varphi_0^{'l}-\Sigma_3^{'j-1}\varphi_0^{'j-1}\right)+\right.$$
$$\left.+\varphi_1^{*j}\left(\nabla\varphi_0^{'j}+3\Sigma_{lr}^{'j}\varphi_1^{'j}\right)\right]=0. \qquad (14)$$

Furthermore, by multiplying equation (2), respectively, by $\varphi_0^{'j}$ and $3\varphi_1^{'j}$ we summate the result over j and integrate over volume G. Then we obtain

$$\sum_{j=1}^{m}\int_{G} dr\left[\varphi_0^{'j}\left(-\nabla\varphi_1^{*j}+\Sigma_{y\pi}^{j}\varphi_0^{*j}-\sum_{l=j+1}^{m}{}^{j\to l}\Sigma_{in}\varphi_0^{*l}-\Sigma_3^{j}\varphi_0^{*j+1}\right)+\right.$$
$$\left.+\varphi_1^{'j}\left(-\nabla\varphi_0^{*j}+3\Sigma_{lr}^{j}\varphi_1^{*j}\right)\right]=0. \qquad (15)$$

We now subtract relationship (15) from relationship (14) and make use of the conjugate nature of the solutions φ_0^{j}, φ_1^{j} with respect to φ_0^{*j}, φ_1^{*j}. Then it is easy to obtain the following equation

$$\delta B(S_2)=-\sum_{j=1}^{m}\int_{G} dr\left(\delta\Sigma_{y\pi}^{j}\varphi_0^{*j}\varphi_0^{'j}-\varphi_0^{*j}\sum_{l=1}^{j-1}\delta\,{}^{l\to j}\Sigma_{in}^{'}\varphi_0^{'l}-\right.$$
$$\left.-\delta\Sigma_{\pi}^{j-1}\varphi_0^{*j}\varphi_0^{'j-1}+3\delta\Sigma_{lr}^{j}\varphi_1^{*j}\varphi_1^{'j}\right). \qquad (16)$$

If the quantities in equation (16) marked with primes are replaced by corresponding quantities without primes, we arrive at the equation of the theory of small perturbations.

Although the theory of small perturbations cannot be applied to the problems of shielding theory to find the absolute value for the variation in the dose of the outgoing radiation when the physical properties of the system vary, it can, nevertheless, show the tendency associated with a variation in the dose.

The large number of important applications for the equation of perturbations (16) may include the calculation of experiments on the transmission of neutrons. In this case the equation of small perturbations may be used, for example, to evaluate many factors, including the various errors of the experiment.

REFERENCES

1. Kadontsev, B. B. Dokl. AN SSSR, Vol. 113, 541, 1957.

2. Marchuk, G. I. and Orlov, V. V. Theory of Conjugate Equations. IN: Neutron Physics (K teorii sopryazhennykh uravneniy. V sb.: Neytronnaya fizika). Moscow, Gosatomizdat, 1961.

3. Marchuk, G. I. Methods of Calculating Nuclear Reactors (Metody rascheta yadernykh reaktorov). Moscow, Gosatomizdat, 1961.

ATTENUATION OF FAST NEUTRONS IN NONHYDROGEN MODERATORS

B. R. Bergel'son

The problem associated with the determination of fast neutron attenuation in materials which do not contain hydrogen atoms occurs in the design of radiation shielding for reactor vessels and also in the design of biological shielding which cannot contain materials with hydrogen. In analyzing radiation shielding we must deal with neutrons whose energy is E ≥ 0.5-1 MeV and whose source consists of fission spectrum neutrons. It is well known that in this case the kinetic equation must be solved to obtain sufficiently reliable results. /103

For plane geometry the kinetic equation for the transport of neutrons is written in the form

$$v\cos\vartheta\frac{\partial n}{\partial x}+\frac{v}{l}n=\int\frac{v'}{l_s}W(\mathrm{p},\mathrm{p}')\,n\,d\mathrm{p}'+Q. \qquad (1)$$

Here $N(x)=\int n(x,\mathrm{p})\,d\mathrm{p}$ is the number of neutrons at point x; p is the neutron impulse; l is the mean free path length in the moderator; l_s is the scattering path in the moderator; ϑ is the angle between neutron velocity vector v and x direction.

The probability for the transition of a neutron from an element of the phase space dp' into the element of the phase space dp during elastic collision with the nucleus of the moderator is obtained from the law of energy E conservation and impulse p conservation. For isotropic scattering in the system of inertia center (ref. 1)

$$W(\mathrm{p},\mathrm{p}')=\frac{1}{8\pi}\left(\frac{M+m}{Mm}\right)^2\left(\frac{2m}{E}\right)^{1/2}\delta\left(E-E'+\frac{(\mathrm{p}-\mathrm{p}')^2}{2M}\right)$$

(M and m are the mass of the scattering nucleus and neutron, respectively). The plane source of neutrons of the fission spectrum is

$$Q=A(p)\sqrt{\frac{2}{\pi e}}\,\mathrm{sh}\sqrt{2E}\,e^{-E}\delta(x)=\chi(E)\,\delta(x).$$

The factor A (p) is obtained from the condition of normalization

$$\int_{p} Q\,dp = I_0\delta(x),$$

where I_0 is the power of the neutron source.

Assuming that the right side of equation (1) is a known function, we solve the differential equation. Then in place of the integral-differential equation (1) we obtain the Payerls equation

$$n(x, \cos\vartheta, E) = \frac{\chi(E)}{\cos\vartheta\, v}\, e^{-\frac{x}{l(E)\cos\vartheta}} + \int_{x_1}^{x} \frac{dx'}{\cos\vartheta}\, e^{-\frac{x-x'}{l(E)\cos\vartheta}} \int \frac{v'}{v}\cdot\frac{1}{l_s(E')} W(p, p')\, n(x', \cos\vartheta', E')\, dp'. \quad (2)$$

The first and second term in the right side of equation (2) determine, respectively, the contribution to n (x, cos ϑ, E) of "direct streaming" neutrons from the source and of the moderated neutrons.

Equation (2) may be simplified somewhat by integrating over φ' in the right side of the equation, which causes the δ-function to disappear in W.

The limits of integration in the integral part of equation (2) are determined twice: according to energy E from the laws of energy conservation or, what is the same, from the condition that the expression under the sign of the δ-function becomes equal to zero, and according to coordinate x_1 from the boundary conditions of the problem.

The problem on the interaction of fast neutrons with the reactor vessel had the following specific conditions. In the semispace filled with a medium which serves the role of the moderator, plane sources of neutrons of the /104 fission spectrum are situated at a distance δ from the boundary with vacuum. The actual conditions of the problem differ from those formulated above in that the medium behind the source (the active zone of the reactor) does not consist of a pure moderator, whereas the medium in front of the source (reflector) does not have a boundary with the vacuum. However, calculations will show that these differences are not substantial for the following reasons.

1. The mean free path of the neutron in moderator l (E) is several times less than the considered thickness of reflector δ; therefore the composition of the medium behind the source has practically no effect on the value of n (x, cos ϑ, E) (near the boundary), which determines the flux of neutrons of interest to us from the medium into the vacuum.

2. The energy of the large part of neutrons which fly out of the reflector into the vacuum with $E \geq E_1$ (E_1 is the threshold energy of the problem) is close or equal to E_1. Therefore the effect of the double reflection of neutrons--first from the steel wall into the moderator and then back from the moderator to the wall (with an energy $E \geq E_1$)--is insignificant.

Utilizing the value of n (x, cos ϑ, E), we can use equation (2) to determine the flux of neutrons from the reflector

$$I = \int_{E_1}^{\infty} dE \int_{\Omega} vn(x, \cos\vartheta, E)\, mp \cos\vartheta\, d\Omega. \tag{3}$$

Integration over the solid angle $d\Omega$ is carried out over the hemisphere ($0 \leq \cos\vartheta \leq 1$).

In order to take into account the difference between the true configuration of uranium blocks in a reactor and the plane geometry of the assigned problem, we consider the influence function of the point source $f(r) = \frac{B}{4\pi r^2} e^{-r/\lambda}$. The values of B and λ are computed from a relationship which can be obtained easily if the infinite plane source of neutrons is considered to be a set of point sources, i.e.,

$$I = B \frac{\delta}{2\lambda} \int_{\delta/\lambda}^{\infty} \frac{e^{-t}}{t^2}\, dt. \tag{4}$$

Calculations show that a function of the relationship (4) type well describes the relationship I = I (δ) obtained from (3) for the values of δ in the interval of 3-6 relaxation lengths.

This method of computing the attenuation of fast neutrons in the layers of the moderator is quite accurate, if we assume that the total cross sections and the scattering cross sections for the nuclei of the moderator in the energy interval 1-10 MeV are known with a sufficient degree of accuracy.

The solution of the considered problem requires a large expenditure of computer time; it is therefore expedient to consider the possibility and the method of solving the problem by means of the age approximation. As we know, the age approximation may be utilized only when definite conditions are satisfied (ref. 2). However, in the considered problem the energy of most of the source neutrons is close to or coincides with threshold energy E_1, and the necessary conditions are not very well satisfied. In this connection we should bear in mind that the unknown flux is determined primarily by the neutrons of the source whose energy E is substantially greater than E_1. Calculations show that for such moderators as graphite and heavy water, $E \approx 7$-8 MeV, because the mean free path of neutrons in the considered moderators increases noticeably as the energy of neutrons increases. If we take this into account, then the conditions for applying the age approximation to the given problem are satisfied in a proper manner.

The flux of neutrons from the reflector with energy $E \geq E_1$ may be expressed in the following manner

$$I = \int_{E_1}^{\infty} \sqrt{\frac{2}{\pi e}} \operatorname{sh} \sqrt{2E}\, e^{-E} [I_1(E) + I_2(E)]\, dE. \tag{5}$$

The flux of "direct streaming" neutrons from the infinite plan source may be obtained from simple geometric considerations /105

$$I_1(E) = I_0 \frac{\delta}{l(E)} \int_{\delta/\lambda(E)}^{\infty} \frac{e^{-t}}{t^2} dt. \tag{6}$$

The flux of moderating neutrons is equal to

$$I_2(E) = I_0 \int_0^{\infty} \frac{dx}{l_s(E)} \int_{\delta - x/l(E)}^{\infty} \frac{e^{-t}}{t} dt \int_0^{\tau_1(E)} \frac{\partial q(x, x', \tau)}{\partial x'}\Big|_{x'=0} d\tau, \tag{7}$$

where x = 0 at the extrapolated boundary of the medium in the vacuum; τ_1 (E) is the age of the neutrons with energy E_1, whereas

$$I_0 \int_{\delta - x/l(E)}^{\infty} \frac{1}{l_s(E)} \frac{e^{-t}}{t} dt = f(x). \tag{8}$$

Equation (8) gives the distribution of neutrons which undergo one collision with the nucleus of the moderator, across the thickness of the reflector, i.e., the distribution of the sources of moderated neutrons (the energy loss of the neutron during the first collision is not taken into account). The density of neutron moderation from the plane infinite source in the semi-infinite layer of the moderator which borders the vacuum, has the form

$$q = \frac{1}{\sqrt{4\pi\tau}} \left[e^{-\frac{(x'-x)^2}{4\tau}} - e^{-\frac{(x'+x)^2}{4\tau}} \right], \tag{9}$$

where x is the coordinate of the source; x' is the running coordinate. After substituting equations (6), (7) and (9) into relationship (5) we obtain

$$\begin{aligned} I = I_0 \int_{E_1}^{\infty} \sqrt{\frac{2}{\pi e}} \operatorname{sh} \sqrt{2E}\, e^{-E} \left\{ \frac{\delta}{l(E)} \int_{\delta/l(E)}^{\infty} \frac{e^{-t}}{t^2} dt + \right. \\ \left. + \int_0^{\delta} \left[\int_{\delta - x/l(E)}^{\infty} \frac{e^{-t}}{t} dt - \frac{2}{\sqrt{\pi}} \int_{x/2\sqrt{\tau_1(E)}}^{\infty} e^{-t^2} dt \right] \frac{dx}{l_s(E)} \right\} dE. \end{aligned} \tag{10}$$

The extension of integration over x into the region δ-∞ in accordance with the considerations presented above does not introduce any substantial correction to quantity I.

Expression (10) represents a double integral over energy E and coordinate x of the tabulated functions--the integral exponents of the first and second order and the integral of errors. The integration of equation (10) may be carried out without a computer.

When the moderator consists of D_2O and of a distributed source for which the conditions of applicability of the age approximation are not too well satisfied, flux I may be computed by both methods, i.e., by means of equation (3) to solve the Payerls equation by the method of iteration using the M-20 computer, and by means of equation (10). The determination of l (E); l_s (E); $\overline{\cos\vartheta}$; ξ is achieved by using data from references 3 and 4. The age of neutrons is calculated by means of equation

$$\tau_1 = \int_{E_1}^{E} \frac{l_s l_{tr}}{3\xi} \cdot \frac{dE}{E}$$

with a correction for the small number of collisions (ref. 2).

From the results obtained it follows that for δ = 30-50 cm flux I, computed by means of equation (10), has a lower value compared with the one obtained from the solution of the kinetic equation, by approximately 30-50 percent. For a problem of the considered type this accuracy may be considered satisfactory.

When calculating the biological shielding of reactors the solution of /106 the kinetic equation for the transport of neutrons also encounters large difficulties due to the necessity of considering a wide interval of neutron energies and a great shielding thickness. When computing a shielding made of material not containing hydrogen atoms, the author believes that is is also possible to use the age approximation in accordance with the methodology presented above. When the shielding thickness is $\delta > 5\lambda$, it is apparently expedient to replace l (E) in equation (8) by the length of the "removal" which is determined as

$$l_r = [\Sigma(E) - \overline{\cos\vartheta}\,\Sigma_s(E)]^{-1},$$

and to replace l_s (E) with the transport length l_{tr} (E).

A wide monoenergetic parallel beam of neutrons $E_0 \geq E_1$, passing through a plane layer of shielding not containing hydrogen atoms into vacuum, may be expressed in the following manner

$$I = I_1\left\{1 + \operatorname{erf}\left(\frac{\delta}{2\sqrt{\tau}}\right) + e^{-\frac{\delta}{l_r(E_0)}+\frac{\tau}{l_r^2(E_0)}}\left[\operatorname{erf}\left(\frac{\delta}{2\sqrt{\tau}} - \frac{\sqrt{\tau}}{l_r(E_0)}\right) - \right.\right.$$
$$\left.\left. - \operatorname{erf}\left(\frac{\sqrt{\tau}}{l_r(E_0)}\right)\right]\right\}\frac{l_r(E_0)}{l_{tr}(E_0)}.$$

Here $\tau = \tau\ (E_0, E_1)$ is the age of neutrons with energy E_1; erf $x = \frac{2}{\sqrt{\pi}} \int_0^x e^{-t^2}\, dt$.

When the shielding represents a mixture of various elements, $\bar{\tau}$, l_r and l_{tr} are computed by means of equations from reference 2.

If one of the elements is iron, the effect of inelastic scattering when $E_0 > 1$ MeV is taken into account by introducing a corresponding correction into τ_{Fe} (ref. 5).

When a strong absorber of neutrons is present in the shielding such as boron, the decrease in I due to the absorption of neutrons with $E \leq 10^3$-10^2 eV is evaluated by introducing the coefficient

$$\alpha = \exp\left(-\int_0^{\tau_1} \frac{d\tau}{L^2}\right).$$

In conclusion the author expresses his gratitude to B. L. Ioffe and I. Ye. Kobzarev for the help rendered in carrying out this work.

REFERENCES

1. Akhiyezer, A. and Pomeranchuk, I. Some Problems Associated with the Theory of the Nucleus (Nekotoryye voprosy teorii yadra). Moscow, Gostekhizdat, 1950.

2. Galanin, A. D. The Theory of Nuclear Reactors with Thermal Neutrons (Teoriya yadernykh reaktorov na teplovykh neytonakh). Moscow, Atomizdat, 1959.

3. Hughes, D. Neutron Cross Sections. BNI-325, 1958.

4. Gordeyev, I. V., Kardashev, D. A. and Malyshev, A. V. Handbook of Nuclear Physical Constants for the Calculation of Reactors (Spravochnik po yaderno-fizicheskim konstantam dlya rascheta reaktorov). Moscow, Atomizdat, 1960.

5. Horton, C. C. A.E.R.E. P/M 115 SWP/40.

ANGULAR DISTRIBUTION OF NEUTRONS AT SMALL DISTANCES FROM THE SOURCE IN AN ISOTROPICALLY SCATTERING MEDIUM

V. A. Kon'shin

References 1-3 present the solution of a single velocity problem for neutrons in an isotropically scattering medium. It is interesting to consider the distribution of neutrons in a homogeneous infinite isotropically scattering medium. /106

When the source is an infinite plane passing through the center of the coordinates, the equation for the transport of neutrons has the form (ref. 4) /107

$$\mu \frac{\partial I(\tau, \mu)}{\partial \tau} + I(\tau, \mu) = \\ = k \int_{-1}^{+1} d\mu' \int_{0}^{2\pi} I(\tau, \mu') F\left(\mu\mu' + \sqrt{1-\mu^2}\sqrt{1-\mu'^2}\cos\varphi'\right) d\varphi' + \frac{S_0 \delta(\tau) f(\mu)}{\Sigma_t} \tag{1}$$

with the boundary condition $I(\tau, \mu)\big|_{\tau \to \infty} = 0$. Here $I(\tau, \mu)$ is the distribution function of neutrons with directional cosine μ at the distance τ (the distance is measured in units of the mean free path); k is the ratio of the scattering cross section Σ_s to the total cross section Σ_t, i.e., $k = \frac{\Sigma_s}{\Sigma_t} \leq 1$. The angular distribution of the source is given by expression $f(\mu)$, where μ is the cosine of the angle between the normal to the plane and the direction of motion of the neutron. In the present problem we consider a plane isotropic source [$f(\mu) = 1$].

The solution of equation (1) may be obtained by the method of Fourier transformation. Multiplying equation (1) by $e^{-ia\tau}$ and integrating over τ within the limits $-\infty$ - $+\infty$, we obtain an integral equation for the Fourier transform in the form

$$(1 + ia\mu)\bar{I}(a, \mu) = k \int_{-1}^{+1} d\mu' \int_{0}^{2\pi} F(\mu_0)\bar{I}(a, \mu')\, d\varphi' + q, \tag{2}$$

where $q = s_0/\Sigma_t$. The scattering indicatrix $F(\mu_0)$ will be represented as an expansion in terms of the Legendre polynomials, limited to three polynomials

$$F(\mu_0)=\sum_{n=0}^{n=2}\frac{2n+1}{4\pi}b_nP_n(\mu_0)=\frac{1}{4\pi}[1+3b_1P_1(\mu_0)+5b_2P_2(\mu_0)], \tag{3}$$

where

$$b_n=2\pi\int_{-1}^{+1}F(\mu_0)P_n(\mu_0)\,d\mu.$$

After integrating (2) over φ' and taking into account (3) we obtain

$$\bar{I}(\alpha,\mu)=\frac{k}{2}\int_{-1}^{+1}\bar{I}(\alpha,\mu')\left[\frac{1}{1+i\alpha\mu}+\frac{3b_1\mu}{1+i\alpha\mu}\mu'+\frac{15}{2}b_2\frac{\mu^2}{1+i\alpha\mu}\mu'^2+\right.$$
$$\left.+\frac{7,5}{2}b_2\frac{(1-\mu^2)}{1+i\alpha\mu}(1-\mu'^2)-\frac{5}{2}b_2\frac{1}{1+i\alpha\mu}\right]d\mu'+\frac{q}{1+i\alpha\mu}.$$

This is the Fredholm integral equation of the second kind with a degenerate nucleus. We write it in the form

$$\bar{I}(\alpha,\mu)=\frac{k}{2}\int_{-1}^{+1}\bar{I}(\alpha,\mu')\left[\left(1-\frac{5}{2}b_2\right)\frac{1}{1+i\alpha\mu}\cdot 1+\frac{3b_1\mu}{1+i\alpha\mu}\mu'+\right.$$
$$\left.+\frac{15}{2}b_2\frac{\mu^2}{1+i\alpha\mu}\mu'^2+\frac{7,5b_2}{2}\frac{(1-\mu^2)}{1+i\alpha\mu}(1-\mu'^2)\right]d\mu'+\frac{q}{1+i\alpha\mu}= \tag{4}$$
$$=\frac{k}{2}\int_{-1}^{+1}\bar{I}(\alpha,\mu')\left[\sum_{k=1}^{k=4}a_k(\mu)g_k(\mu')\right]+\frac{q}{1+i\alpha\mu}.$$

We should like to point out that the same result is obtained by utilizing the theorem for the addition of the Legendre polynomials

$$P_n(\mu_0)=P_n(\mu)P_n(\mu')+2\sum_{m=1}^{m=n}\frac{(n-m)!}{(n+m)!}P_n^m(\mu)P_n^m(\mu')\cos m(\varphi-\varphi'),$$

from which after integration over φ' we obtain: /108

$$\int_0^{2\pi}d\varphi'P_0(\mu_0)=2\pi;\quad\int_0^{2\pi}d\varphi'P_1(\mu_0)=P_1(\mu)P_1(\mu')2\pi=2\pi\mu\mu';$$
$$\int_0^{2\pi}d\varphi'P_2(\mu_0)=P_2(\mu)P_2(\mu')2\pi=2\pi\frac{3\mu^2-1}{2}\cdot\frac{3\mu'^2-1}{2}.$$

Substituting these expressions into equation (2) and taking into account (3), we obtain equation (4).

From the theory of integral equations with degenerate nuclei it is known that the integral equation of the form

$$\varphi(x)-\lambda\int_a^b K(x,s)\,\varphi(s)\,ds=f(x),$$

where

$$K(x,s)=\sum_{i=1}^{i=n} a_i(x)\,g_i(s)$$

has a solution

$$\varphi(x)=f(x)+\lambda\sum_{i=1}^{i=n} c_i a_i(x).$$

In this case c_i is a constant which is determined from the system of equations

$$c_i-\lambda\sum_{k=1}^{k=n} a_{ik}c_k=f_i, \tag{5}$$

where

$$a_{ik}=\int_a^b g_i(s)\,a_k(s)\,ds;\quad f_i=\int_a^b g_i(s)\,f(s)\,ds.$$

For our case the solution of integral equation (4) will be written in the form

$$\overline{I}(\alpha,\mu)=\frac{q}{1+i\alpha\mu}+\frac{k}{2}\left[C_1\frac{\left(1-\frac{5}{2}b_2\right)}{1+i\alpha\mu}+C_2\frac{3b_1\mu}{1+i\alpha\mu}+\right.$$
$$\left.+C_3\frac{\frac{15}{2}b_2\mu^2}{1+i\alpha\mu}+C_4\frac{\frac{7,5}{2}b_2(1-\mu^2)}{1+i\alpha\mu}\right]$$

The constants c_i are determined from system (5), whose determinant is

$$D\left(\frac{k}{2}\right)=\begin{vmatrix}\left(1-\frac{k}{2}a_{11}\right) & -\frac{k}{2}a_{12} & -\frac{k}{2}a_{13} & -\frac{k}{2}a_{14}\\ -\frac{k}{2}a_{21} & \left(1-\frac{k}{2}a_{22}\right) & -\frac{k}{2}a_{23} & -\frac{k}{2}a_{24}\\ -\frac{k}{2}a_{31} & -\frac{k}{2}a_{32} & \left(1-\frac{k}{2}a_{33}\right) & -\frac{k}{2}a_{34}\\ -\frac{k}{2}a_{41} & -\frac{k}{2}a_{42} & -\frac{k}{2}a_{43} & \left(1-\frac{k}{2}a_{44}\right)\end{vmatrix}$$

Here

$$a_{ki} = = \int_{-1}^{+1} g_k(\mu')\, a_i(\mu')\, d\mu';$$

$$a_{11} = \int_{-1}^{+1} 1 \cdot \frac{\left(1 - \frac{5}{2} b_2\right)}{1 + i\alpha\mu'} d\mu' = \left(1 - \frac{5}{2} b_2\right) \frac{2}{\alpha} \operatorname{arctg} \alpha;$$

$$a_{21} = \int_{-1}^{+1} \mu' \frac{\left(1 - \frac{5}{2} b_2\right) d\mu'}{1 + i\alpha\mu'} = \left(1 - \frac{5}{2} b_2\right) \frac{2i}{\alpha^2} (\operatorname{arctg} \alpha - \alpha);$$

$$a_{31} = \left(1 - \frac{5}{2} b_2\right) \frac{2}{\alpha^2} \left(1 - \frac{1}{\alpha} \operatorname{arctg} \alpha\right);$$

$$a_{41} = \left(1 - \frac{5}{2} b_2\right) \left\{\frac{2}{\alpha} \operatorname{arctg} \alpha - \frac{2}{\alpha^2} \left(1 - \frac{1}{\alpha} \operatorname{arctg} \alpha\right)\right\};$$

$$a_{12} = 3b_1 \frac{2i}{\alpha^2} (\operatorname{arctg} \alpha - \alpha);$$

$$a_{22} = 3b_1 \frac{2}{\alpha^2} \left(1 - \frac{1}{\alpha} \operatorname{arctg} \alpha\right);$$

$$a_{32} = 3b_1 \frac{2i}{\alpha^4} \left(\alpha - \frac{\alpha^3}{3} - \operatorname{arctg} \alpha\right);$$

$$a_{42} = 3b_1 \left\{\frac{2i}{\alpha^2} (\operatorname{arctg} \alpha - \alpha) - \frac{2i}{\alpha^4} \left(\alpha - \frac{\alpha^3}{3} - \operatorname{arctg} \alpha\right)\right\};$$

$$a_{13} = \frac{15}{2} b_2 \frac{2}{\alpha^2} \left(1 - \frac{1}{\alpha} \operatorname{arctg} \alpha\right);$$

$$a_{23} = \frac{15}{2} b_2 \frac{2i}{\alpha^4} \left(\alpha - \frac{\alpha^3}{3} - \operatorname{arctg} \alpha\right);$$

$$a_{33} = \frac{15}{2} b_2 \frac{2}{\alpha^2} \left(\frac{1}{\alpha^2} - \frac{1}{3} - \frac{1}{\alpha^3} \operatorname{arctg} \alpha\right);$$

$$a_{43} = \frac{15}{2} b_2 \frac{2}{\alpha^2} \left\{\left(1 - \frac{1}{\alpha} \operatorname{arctg} \alpha\right) - \left(\frac{1}{\alpha^2} - \frac{1}{3} - \frac{1}{\alpha^3} \operatorname{arctg} \alpha\right)\right\};$$

$$a_{14} = \frac{7{,}5}{2} b_2 \left\{\frac{2}{\alpha} \operatorname{arctg} \alpha - \frac{2}{\alpha^2} \left(1 - \frac{1}{\alpha} \operatorname{arctg} \alpha\right)\right\};$$

$$a_{24} = \frac{7{,}5}{2} b_2 \left\{\frac{2i}{\alpha^2} (\operatorname{arctg} \alpha - \alpha) - \frac{2i}{\alpha^4} \left(\alpha - \frac{\alpha^3}{3} - \operatorname{arctg} \alpha\right)\right\};$$

$$a_{34} = \frac{7{,}5}{2} b_2 \left\{\frac{2}{\alpha^2} \left(1 - \frac{1}{\alpha} \operatorname{arctg} \alpha\right) - \frac{2}{\alpha^2} \left(\frac{1}{\alpha^2} - \frac{1}{3} - \frac{1}{\alpha^3} \operatorname{arctg} \alpha\right)\right\};$$

$$a_{44} = \frac{7{,}5 b_2}{2} \left\{\frac{2}{\alpha} \operatorname{arctg} \alpha - \frac{4}{\alpha^2} \left(1 - \frac{1}{\alpha} \operatorname{arctg} \alpha\right) + \frac{2}{\alpha^2} \left(\frac{1}{\alpha^2} - \frac{1}{3} - \frac{1}{\alpha^3} \operatorname{arctg} \alpha\right)\right\}.$$

$$f_1 = \frac{2q}{\alpha} \operatorname{arctg} \alpha;$$

$$f_2 = \frac{2qi}{\alpha^2} (\operatorname{arctg} \alpha - \alpha);$$

$$f_3 = \frac{2q}{\alpha^2} \left(1 - \frac{1}{\alpha} \operatorname{arctg} \alpha\right);$$

$$f_4 = \frac{2q}{\alpha} \operatorname{arctg} \alpha - \frac{2q}{\alpha^2} \left(1 - \frac{1}{\alpha} \operatorname{arctg} \alpha\right).$$

Quantity $k = \frac{\Sigma_s}{\Sigma_t}$ was selected equal to 0.95. The scattering indicatrix /109

$F(\mu_0)$ was taken in the form shown in figure 1. The coefficients b_n of the

expansion F (μ_0) in terms of the Legendre polynomials have the following values: $b_0 = 1$; $b_1 = 0.4104$; $b_2 = 0.2486$. The solution of integral equation (4) is represented in the form

$$\bar{I}(\alpha, \mu) = \frac{q}{1+i\alpha\mu} + \frac{k}{2}\left[C_1(\alpha)\frac{0{,}378}{1+i\alpha\mu} + C_2(\alpha)\frac{1{,}23\mu}{1+i\alpha\mu} + \right.$$
$$\left. + C_3(\alpha)\frac{1{,}87\mu^2}{1+i\alpha\mu} + C_4(\alpha)\frac{0{,}94(1-\mu^2)}{1+i\alpha\mu}\right],$$

where the constants C_i (α) are determined as above.

I (τ, μ) are obtained by means of the inverse Fourier transformation /110

$$I(\tau, \mu) = \frac{q}{2\pi}\int_{-\infty}^{+\infty}\frac{(\cos\alpha\tau + i\sin\alpha\tau)(1-i\alpha\mu)}{1+\alpha^2\mu^2}d\alpha +$$
$$+\frac{0{,}378k}{4\pi}\int_{-\infty}^{+\infty}\frac{(\cos\alpha\tau + i\sin\alpha\tau)(1-i\alpha\mu)}{1+\alpha^2\mu^2}C_1(\alpha)\,d\alpha +$$
$$+\frac{1{,}23\mu k}{4\pi}\int_{-\infty}^{+\infty}\frac{(\cos\alpha\tau + i\sin\alpha\tau)}{1+i\alpha\mu}C_2(\alpha)\,d\alpha + \qquad (6)$$
$$+\frac{1{,}87\mu^2 k}{4\pi}\int_{-\infty}^{+\infty}\frac{(\cos\alpha\tau + i\sin\alpha\tau)(1-i\alpha\mu)}{1+\alpha^2\mu^2}C_3(\alpha)\,d\alpha +$$
$$+\frac{0{,}94(1-\mu^2)k}{4\pi}\int_{-\infty}^{+\infty}\frac{(\cos\alpha\tau + i\sin\alpha\tau)(1-i\alpha\mu)}{1+\alpha^2\mu^2}C_4(\alpha)\,d\alpha.$$

Separation into real and complex parts shows that the complex part is an odd function α and consequently the integral from - ∞ to + ∞ vanishes. It can be shown that the first term in equation (6) represents a nonscattered radiation. Indeed, we have

$$\frac{q}{2\pi}\int_{-\infty}^{+\infty}\frac{\cos\alpha\tau + \alpha\mu\sin\alpha\tau}{1+\alpha^2\mu^2}d\alpha =$$
$$= \frac{q}{\pi}\int_{0}^{\infty}\frac{\cos\alpha\tau + \alpha\mu\sin\alpha\tau}{1+\alpha^2\mu^2}d\alpha =$$
$$= \begin{cases}\frac{q}{|\mu|}e^{-\left|\frac{\tau}{\mu}\right|} & \text{for} \quad \tau/\mu > 0, \ \tau \neq 0; \\ 0 & \text{for} \quad \tau/\mu < 0, \ \tau \neq 0.\end{cases}$$

The nonscattered flux I_0 (τ) is obtained by integrating over μ

$$I_0^{\text{real}}(\tau) = \int_{-1}^{+1}\frac{e^{-\left|\frac{\tau}{\mu}\right|}}{|\mu|}d\mu = E_1(\tau),$$

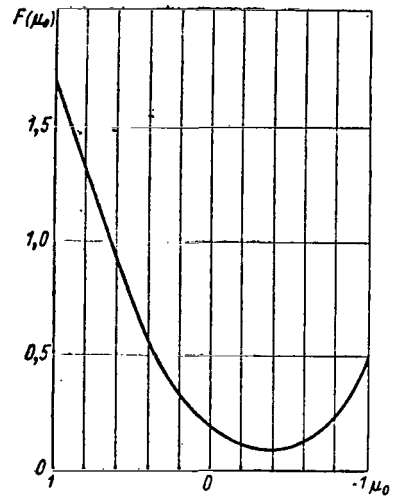

Figure 1. Scattering indicatrix.

where $E_1(\tau)$ is the integral exponent. For a point source (ref. 1) we obtain

$$I_0^{\text{real}}(r) = -\frac{1}{2\pi r^2}\cdot\frac{d}{dr}E_1(r) = -\frac{1}{2\pi r}\left\{-\frac{e^{-r}}{r}\right\} = \frac{e^{-r}}{2\pi r^2}.$$

The angular distribution of the scattered radiation is given by the remaining terms of equation (6)

$$\begin{aligned} I_{\text{scatter}}(\tau, \mu) = {} & \frac{0{,}378kq}{2\pi}\int_0^\infty \frac{(\cos\alpha\tau + \alpha\mu\sin\alpha\tau)}{1+\alpha^2\mu^2} C_1(\alpha)\,d\alpha + \\ & + \frac{1{,}23kq}{2\pi}\int_0^\infty \frac{(\alpha\mu\cos\alpha\tau - \sin\alpha\tau)}{\alpha^2\mu^2}\mu C_2(\alpha)\,d\alpha + \\ & + \frac{1{,}87kq}{2\pi}\int_0^\infty \frac{(\cos\alpha\tau - \alpha\mu\sin\alpha\tau)}{1+\alpha^2\mu^2}\mu^2 C_3(\alpha)\,d\alpha + \\ & + \frac{0{,}94kq}{2\pi}\int_0^\infty \frac{(\cos\alpha\tau + \alpha\mu\sin\alpha\tau)}{1+\alpha^2\mu^2}(1-\mu^2) C_4(\alpha)\,d\alpha. \end{aligned} \tag{7}$$

Let us transform the first term of equation (7)

$$\begin{aligned} & \int_0^\infty \frac{\cos\alpha\tau + \alpha\mu\sin\alpha\tau}{1+\alpha^2\mu^2} C_1(\alpha)\,d\alpha = \int_0^1 \frac{\cos\alpha\tau + \alpha\mu\sin\alpha\tau}{1+\alpha^2\mu^2} C_1(\alpha)\,d\alpha + \\ & + \int_1^\infty \frac{\cos\alpha\tau + \alpha\mu\sin\alpha\tau}{1+\alpha^2\mu^2} C_1(\alpha)\,d\alpha = \int_0^1 \frac{\cos\alpha\tau + \alpha\mu\sin\alpha\tau}{1+\alpha^2\mu^2} C_1(\alpha)\,d\alpha + \end{aligned} \tag{8}$$

$$+\int_0^1 \frac{\cos\frac{\tau}{l}+\frac{\mu}{l}\sin\frac{\tau}{l}}{l^2+\mu^2}\,dl\cdot C_1\left(\frac{1}{l}\right).$$

Analogous transformations may be carried out for the remaining terms of equation (7). To evaluate integrals (8) we must investigate the behavior of functions under the integral sign in the interval from 0 to 1. The transcendental equation, the expression for the denominator $C_1(\alpha)$ /111

$$-1.25\alpha^7\operatorname{arctg}\alpha-1.3\alpha^5\operatorname{arctg}\alpha+2.8\alpha^3\operatorname{arctg}\alpha-4.73\alpha\operatorname{arctg}\alpha-$$
$$-0.64\alpha^2(\operatorname{arctg}\alpha)^2+1.14(\operatorname{arctg}\alpha)^2+1.41\alpha^6-2.16\alpha^4+3.28\alpha^2+\alpha^8=0$$

in the interval from 0-1 has one real root $\alpha_1 = 0.7332$ and double multiple roots at zero. The equation, i.e., the denominator of expression $C_1\left(\frac{1}{t}\right)$,

$$-1.25t\operatorname{arctg}\frac{1}{t}-1.3t^3\operatorname{arctg}\frac{1}{t}+2.8t^5\operatorname{arctg}\frac{1}{t}-4.73t^7\operatorname{arctg}\frac{1}{t}-$$
$$-0.64t^6\left(\operatorname{arctg}\frac{1}{t}\right)^2+1.14t^8\left(\operatorname{arctg}\frac{1}{t}\right)^2+1.41t^2-2.16t^4+3.28t^6+1=0$$

does not have a real root in the interval from 0 to 1. Therefore the second integral of (8) may be evaluated numerically.

The first integral of (8) has a singularity at the point $\alpha_1 = 0.7332$. We represent this integral in the form

$$\int_0^1 \frac{\cos\alpha\tau+\alpha\mu\sin\alpha\tau}{1+\alpha^2\mu^2}C_1(\alpha)\,d\alpha=\int_0^{\alpha_1-\varepsilon}+\int_{\alpha_1-\varepsilon}^{\alpha_1}+\int_{\alpha_1}^{\alpha_1+\varepsilon}+\int_{\alpha_1+\varepsilon}^{1}, \qquad (9)$$

where $\varepsilon \to 0$. In expression (9) the first and fourth integral are computed exactly, whereas the second and third integrals are computed by using the expansion of function $C_1(\alpha)$ in the Loran series in the neighborhood of the singular point $\alpha_1 = 0.7332$. If $C_1(\alpha) = \frac{\varphi(\alpha)}{\psi(\alpha)}$, then

$$C_1(\alpha)=\frac{A_{-1}}{\alpha-0,7332}+\sum_{k=-1}^{k=\infty}A_k(\alpha-0.7332)^k. \qquad (10)$$

Taking only the first term in expression (10), we have

$$\frac{\varphi(\alpha)}{\psi(\alpha)}=\frac{A_{-1}}{\alpha-0,7332}, \text{ where } A_{-1}=\frac{\varphi(0.7332)}{\psi'(0.7332)}=0.3403.$$

The calculation of the remaining integrals in equation (7) were carried out in a similar manner.

The results of the calculations carried out to determine the angular distributions of the scattered radiation $I_{scatter}(\tau, \mu)$ for $\mu = -1; -0.5; 0; 0.5; 1$ and $\tau = 0.1; 0.5; 1$ are presented in figure 2. The quantity $I_{scatter}(\tau, \mu)$ is shown in units of $q = \frac{S_0}{\Sigma_t}$, where S_0 is the source power.

We can see from figure 2 that the angular distribution of the scattered radiation for $\tau = 0$ is symmetric with respect to $\mu = 0$, as was to be expected for a plane isotropic source. As the distance from the source is increased, the peak of the angular distribution is displaced from $\mu = 0$ to $\mu = 1$, i.e., /112 the neutrons fly forward. A comparison with the isotropic scattering of neutrons (ref. 2) shows that in the case of the anisotropically scattering medium the peak of the angular distribution is displaced closer to $\mu = 1$ ($\theta = 0^\circ$), as was to be expected.

Thus when $\tau = 0.5$, the maximum of the peak is displaced from $\mu \approx 0.2$ (isotropic scattering) to $\mu \approx 0.5$ (anisotropic scattering).

It should be noted that when the distance τ from the source is increased, the multiplier $\left\{\frac{\cos\frac{\tau}{l} + \frac{\mu}{l}\sin\frac{\tau}{l}}{l^2+\mu^2}\right\}$, which is under the integral sign, begins to oscillate. Therefore, in computing the angular distributions the value of $I_{scatter}(\tau, \mu)$ for $\mu = 0$ and $\tau = 1$ dropped out from the general behavior of the curve.

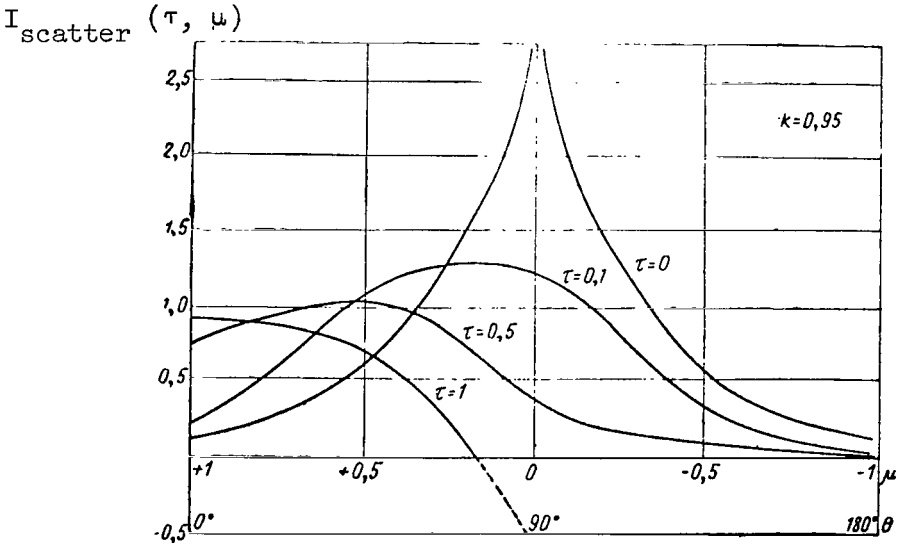

Figure 2. Angular distribution of neutrons at small distances from the source.

Consequently it is necessary to have a more accurate evaluation of the second integral of (8) with the oscillating function under the integral sign.

In conclusion the author expresses his gratitude to E. Ye. Petrov, V. V. Orlov and V. Ya. Pupko for their interest in this work.

REFERENCES

1. Marshak, R. E., Brooks, H. and Hurwitz H. Nucleonics, Vol. 4, No. 6, 43, 1949; Vol. 5, No. 1, 59.

2. Beach, L. A., Shapiro, P. et al. Nucl. Sci. Eng., Vol. 6, 66, 1959.

3. Weinberg, A. and Wigner, E. The Physical Theory of Neutron Chain Reactions. Chicago University Press, Chicago, Illinois, p. 236, 1958.

4. Marshak, R. E. Rev. Mod. Phys., Vol. 19, 185, 1947.

THE QUESTION OF RADIATION SOURCE GEOMETRY

D. L. Broder, Ye. N. Goryanina, G. M. Levis,
K. K. Popkov and S. M. Rubanov

The sources of neutrons and γ quanta in atomic energy installation /112
are the active zone of the reactor, its vessel, the reflector and the elements of shielding, piping system and heat exchanges with radioactive heat carrier. All these sources have different geometric shapes and dimensions. However, in most cases for purposes of computation they can be represented in the form /113
of radiating points, lines, discs, infinite plates, spheres, etc. This approximation of the geometric shapes of radiation sources in practical calculations is necessary, not only because it substantially reduces the volume of calculations, but also because it makes it possible to apply certain calculation methods which are valid only for sources of the simplest geometric form. Thus, for example, the multiple group calculations of three-dimensional energy distributions of neutrons may be carried out only for plane cylindrical or spherical geometry. Calculations of the transmission of fast neutrons and γ quanta through the shielding are carried out by means of constants obtained for radiation sources of the simplest geometric forms. The possibility of applying these constants for sources of a more complex geometry is not obvious.

The simplest radiation source is a point source. The radiation flux $\varphi(r)$ from such a source which is situated in an absorbing medium and which radiates q particles/sec at a distance r may be obtained from the relationship

$$\varphi(r) = \frac{q}{4\pi r^2} f(r), \tag{1}$$

where the function f(r) determines the attenuation of the radiation flux in the substance. The function f(r), both for the γ radiation as well as for the neutrons, may be represented in the form of an exponential series

$$f(r) = \sum_i a_i e^{-\sum_m k_{im} r_m} \tag{2}$$

Here a_i and k_{im} depend on the properties of the shielding, on the nature of radiation and on its energy.

For neutrons at a certain distance from the source we have

$$f(r) = \sum B_i \Delta S_{E_i} e^{-r/\lambda_i}, \tag{3}$$

where ΔS_{E_i} determines the spectrum of the source, and B_i and λ_i determine, respectively, the factors of initial buildup and the relaxation length of neutrons with energy E_i.

For the γ quanta

$$f(r) = \sum_i [A_1^i e^{-(1+\alpha_1^i)\mu_i r} + A_2^i e^{-(1+\alpha_2^i)\mu_i r}] = \\ = \sum_i B_i(\mu_i r) e^{-\mu_i r}. \tag{4}$$

In expression (4) A_1^i, A_2^i, α_1^i and α_2^i are the coefficients of the exponential representation of the buildup factor for the scattered γ radiation, which depends on the material of the shielding and on the energy of the γ quanta, while μ_i is the linear attenuation coefficient for the γ radiation with energy E_i. A similar expression may be written for the attenuation function of the γ radiation intensity; it will differ from expression (4) only in that instead of the dose factor for the buildup of the scattered γ radiation it will contain the energy buildup factor.

When the absorbing medium consists of several layers of different materials expressions (3) and (4) become more complicated. Thus for fast neutrons the utilization of the method of the removal cross sections makes it possible to write equations (2), (3) and (4) in the form

$$f(r) = \sum_i B_i \Delta S_{E_i} e^{-\frac{r}{\lambda_i} 0 - \sum_m 0_m \varrho_m \sigma_{rem}^{mi} r} \tag{5}$$

where θ is the volumetric portion of the light (removing) shielding component; θ_m is the volumetric portion of the heavy shielding component; $\varrho_m \sigma_{rem}^{mi}$ is the macroscopic cross section for the removal of neutrons of the i-th energy group by the layer m which enters into the composition of the shielding. /114

For γ quanta in a heterogeneous medium the buildup factor for the scattered γ radiation may be represented in the following manner (ref. 1)

$$B_i = \sum_{n=1}^{N} B_n^i \left(\sum_{l=1}^{n} \mu_l^i r_l \right) - \sum_{n=2}^{N} B_n^i \left(\sum_{l=1}^{n-1} \mu_l^i r_l \right), \tag{6}$$

where N is the number of shielding layer; $\mu_l^i r_l$ is the thickness of the l-th layer of the shielding in terms of the mean free paths of the γ quanta of the i-th energy group. Similar expressions for the buildup factor of the γ radiation make it possible to retain the representation of the attenuation function $f(r)$ in the form of an exponential series for any combinations of shielding layers.

To compute the functions for the spacial distribution of radiation fluxes from extended sources, the latter are broken down into elementary volumes dV (areas dS or segments dl), each of which is considered as a point source with power q_V dV particles/sec. The total radiation flux in the shielding φ (r) at the point r is determined by the integral over the entire volume (surface or length) of the source

$$\varphi(\mathbf{r}) = \frac{1}{4\pi} \int_{V_s} \frac{q_V(\mathbf{r}_s) f(\delta_s \delta_{l_1} \delta_{l_2} \ldots \delta_{l_m})}{(\mathbf{r}_s - \mathbf{r})^2} dV_s = \frac{1}{4\pi} \sum_i a_i \int_{V_s} \frac{q_V(\mathbf{r}_s) e^{-k_s \delta_s - \sum_n k_{in} \delta_{ln}}}{(\mathbf{r}_s - \mathbf{r})^2} dV_s. \tag{7}$$

Since summation over i is not reflected in the results of integration, it is entirely proper to consider an integral of the form

$$\varphi_i = \int_{V_s} \frac{q_V^i(\mathbf{r}_s) e^{-k_s \delta_s - \sum_n k_{in} \delta_{ln}}}{4\pi (\mathbf{r}_s - \mathbf{r})^2} dV_s. \tag{8}$$

The expressions for various extended sources obtained in this manner may be easily applied to specific versions of shielding calculation by taking into account all of the terms of the sum in equation (7).

In many works (refs. 2 and 3-5) distribution functions for radiation fluxes are computed for sources of different geometric form. These calculations show that the plane isotropic infinite source (as well as the point source) is fundamental, and for most extended sources the functions of three-dimensional flux distribution may be expressed in terms of the function of a plane source. Here are some examples.

1. The radiation flux from an isotropically radiating spherical source of radius R at a distance r, φ_{sp} (R, r) may be computed in the following manner (refs. 3 and 6)

$$\varphi_{сф}(R, r) = \frac{R}{r}[\varphi_{пл}(r-R) - \varphi_{пл}(r+R)], \tag{9}$$

(сф = sp = spherical; пл = pl = plane)

where φ_{pl} (x) is the radiation flux at the distance x from an infinitely radiating plane.

2. For a cylinder of radius R we have the approximate expression (8).

$$\varphi_{цил}(R, r) \approx \sqrt{\frac{R}{r}}\,\varphi_{пл}(r-R), \tag{10}$$

(цил = cy = cylindrical)

where φ_{cy} (R, r) is the radiation flux from an infinite cylindrical surface radiator at a point situated at a distance r from its axis.

3. The radiation flux from a source which has the form of a disk with /115 radius R at a distance r along the normal to its center φ (R, r) may be computed by using the equation

$$\varphi_{диск}(R, r) = \varphi_{пл}(r) - \varphi_{пл}(\sqrt{R^2+r^2}). \tag{11}$$

(диск = disk)

Thus a sufficiently large number of those surface radiation sources most frequently encountered in calculations may be represented by means of a plane isotropic infinite source.

The radiation flux φ_{pl} (r) at the point situated at distance r from the surface of a plane infinite isotropic source is determined by means of expression

$$\varphi_{пл}(r) = q_r E_1(kz). \tag{11a}$$

In expression (11a) kz_1 is the thickness of the shielding in terms of relaxation length; $E_n(x) = x^{n-1}\int_x^\infty \frac{e^{-t}}{t^n}dt$ is the integral exponential function.

Let us analyze the degree of accuracy associated with the widespread current method of computing radiation fluxes behind the shielding, which consists basically of breaking down the entire computation process into two parts: (1) the computation of radiation flux on the surface of the source; (2) the computation of particle transmission from the surface source through the shielding, assuming that the angular distribution of this flux is isotropic.

Let us consider an infinite volumetrically radiating plate with thickness d. We assume that the specific power[1] of the radiation sources $q_V(x)$ is distributed along the thickness of the plate according to the law $q_V(x) = q_0 e^{k_n x}$ where x is the distance of the considered point from the surface of the plate; q_0 is the specific power of radiation sources when $x = 0$[1]. The quantity k_n characterizes the slope of the source distribution curve; when $k_n > 0$ we have an increasing exponent; when $k_n = 0$ $q_V(x) = \text{const} = q_0$ the distribution of sources is constant and does not depend on x and, finally, when $k_n < 0$, the distribution curve represents a descending exponent. Introducing the spherical system of coordinates in such a way that the polar axis coincides with the internal normal to the surface of the plate, while the origin of the coordinates is on its surface, we can compute the radiation flux $\varphi(0)$ on the surface of the plate at the origin of the coordinates.

In this case

$$\varphi(0) = \frac{q_0}{4\pi}\int_0^{2\pi}\int_0^{\pi/2}\int_0^{d/\cos\vartheta} e^{-k_n(r\cos\vartheta - d) - k_s r}\sin\vartheta\, d\varphi\, d\vartheta\, dr, \qquad (12)$$

where k_s is the linear radiation attenuation coefficient in the material of the plate.

---

[1] In practice this type of distribution is universal, because the specific powers of sources for the captured or activated γ radiation in the plane layers of the shielding follow an exponential law. Usually two to three exponents are sufficient to approximate the existing distribution with satisfactory accuracy.

Integrating expression (12), we can show (refs. 3 and 4), that

(1) if $q(x) = q_0 = \text{const}$,

$$\varphi(0) = -\frac{q_0}{2k_s}[1 - E_2(k_s d)] \tag{13}$$

for the semispace $d \to \infty$, therefore

$$\varphi(0) = -\frac{q_0}{2k_s}; \tag{13a}$$

(2) when $q(x) = q_0 e^{k_n x}$,

$$\varphi(0) = -\frac{q_0}{2k_n}\left\{\ln\left|\frac{k_n + k_s}{k_s}\right| - e^{-k_n d}E_1(k_s d) + E_1[(k_n + k_s)d]\right\}. \tag{14}$$

When $k_s = -k_n$, expression (14) becomes indeterminant of the type $\infty-\infty$. /116

To solve it we must use the expansion (ref. 2)

$$E_1(x) = \sum_{n=1}^{\infty}(-1)^{n-1}\frac{x^n}{n\cdot n!} - 0{,}577 - \ln|x|,$$

which is valid for small values of x

$$\ln\left|\frac{k_n + k_s}{k_s}\right| + E_1[(k_n + k_s)d] = \ln[d(k_n + k_s)] - \ln k_s d +$$
$$+ \sum_{n=1}^{\infty}(-1)^n\frac{d^n(k_n + k_s)^n}{n\cdot n!} - 0.577 - \ln[d(k_n + k_s)]\Big|_{k_n \to -k_s} = -\ln k_s d - 0.577.$$

As a result we obtain

$$\varphi(0) = -\frac{q_0}{2k_s}[\ln k_s d + e^{-k_s d}E_1(k_s d) + 0.577]. \tag{14a}$$

Taking the fluxes on the surface of the plate $\varphi(0)$ as the specific power of the surface source q_F, we can compute the three-dimensional distribution of radiation fluxes in the shielding by means of equation (11a).

A direct calculation of the radiation flux behind the shielding, taking into account the self-absorption of radiation in the plate material, is reduced to the calculation of the following integral

$$\varphi = \frac{q_0}{4\pi} \int_0^{2\pi} \int_0^{\pi/2} \int_{\frac{d}{\cos\vartheta}}^{\infty} e^{-k_n(r\cos\vartheta - d) - k_s\left(r - \frac{a}{\cos\vartheta}\right) - \frac{k_t x}{\cos\vartheta}} \sin\vartheta \, d\vartheta \, dr \, d\varphi, \tag{15}$$

where $k_t x$ is the thickness of the shielding layers (in terms of relaxation lengths); a is the distance from the surface of the radiating plate to the point under consideration.

When $q(x) = q_0 = \text{const}$,

$$\varphi = \frac{q_0}{2k_s} \left| E_2(k_t x) - E_2(k_t x + k_s d) \right|. \tag{16}$$

If, on the other hand, $q(x) = q_0 e^{k_n x}$, we have

$$\begin{aligned} \varphi = \frac{q_0}{2k_n} \Big\{ E_1(k_t x) - e^{k_t x \frac{k_n}{k_s}} E_1\left[k_t x \left(\frac{k_n}{k_s} + 1 \right) \right] - e^{-k_n d} E_1(k_t x + k_s d) + \\ + e^{(k_t x + k_s d)\frac{k_n}{k_s} - k_n d} E_1\left[(k_t x + k_s d)\left(\frac{k_n}{k_s} + 1 \right) \right] \Big\} \end{aligned} \tag{17}$$

The numerical results of calculations carried out by means of these equations for different values of k_n and k_s are presented in figure 1.

Figure 1 shows the ratios of the radiation fluxes behind the shielding of thickness $k_t x$, computed in two stages, to the fluxes computed by the direct method. As we can see from the figure, for a shielding thickness from $k_t x = 2$ 20, for most versions calculation in two stages produces deviations which do not exceed 30-50 percent. In order to understand the computation results presented in figure 1 more clearly, we shall examine the angular distribution of radiation fluxes on the surface of the plate[1] for various values of $k_s d$ and $k_n d$ presented in figures 2-4.

---

[1] In this case the radiation flux on the surface of the plate is interpreted as the number of quanta (particles) which intersect the area of 1 cm^2 per unit time when this area is perpendicular to the direction of travel of the particle.

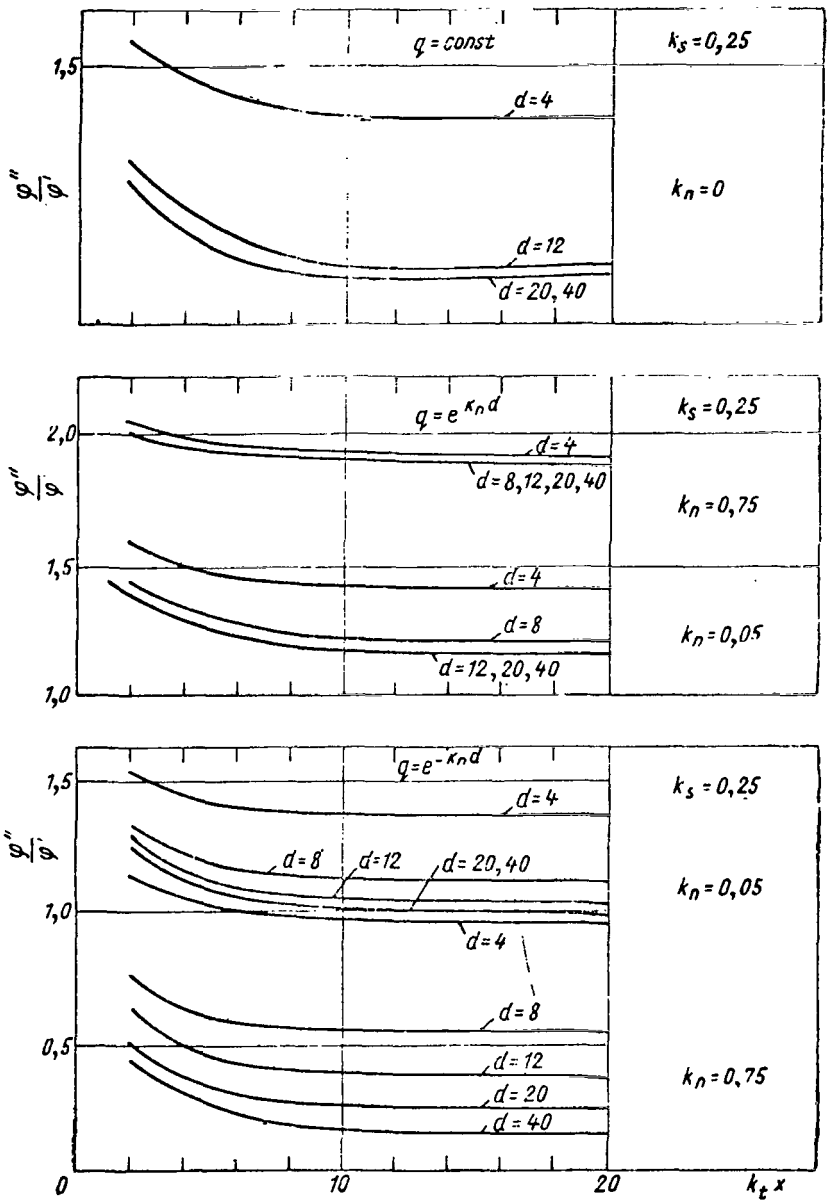

Figure 1. Ratio of fluxes behind shielding computed by approximate and exact methods.

In the case of a sufficiently thin plate the flux on its surface is anisotropic and has a minimum value in the direction of the normal; as the thickness of the plate increases (when we have a constant distribution of radiation sources along its thickness) an isotropy of angular distributions takes place. These considerations clarify the reason for the increase in the fluxes /118 beyond the shielding, computed in two stages. A large increase in the case of thin plates is produced by the incorrect proposition on the isotropic nature of the flux at the surface of the plate. The same explanation can be given for

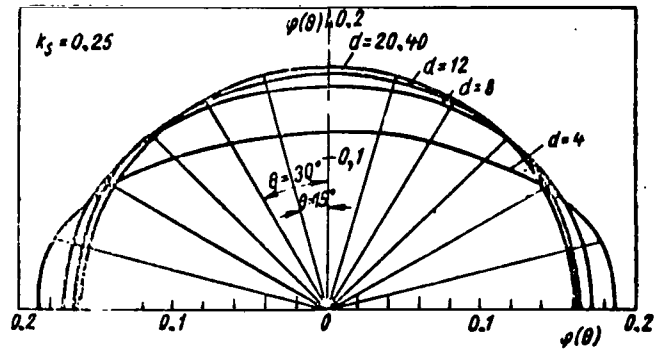

Figure 2. Angular distribution of flux on surface of plate when $q = q_0 = \text{const}$.

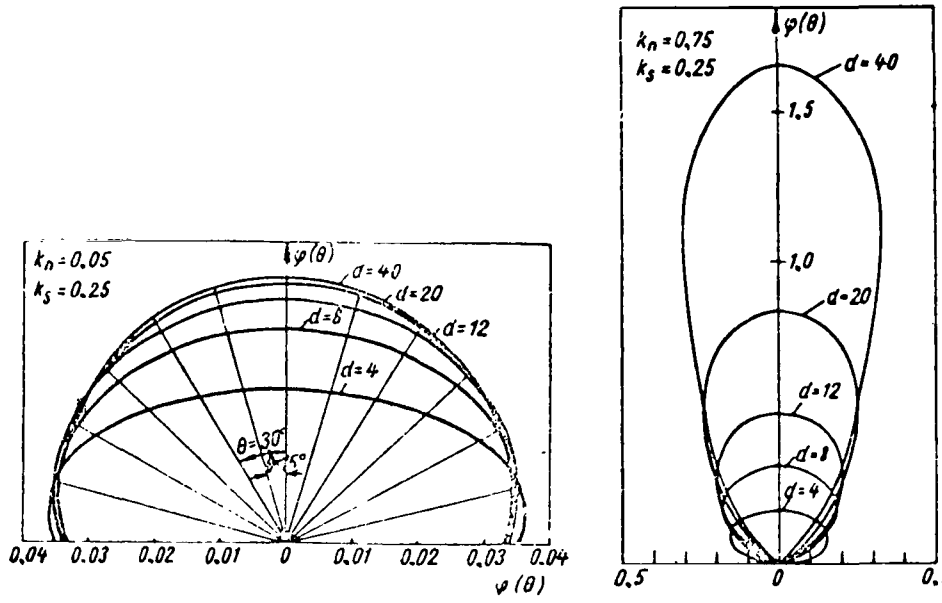

Figure 3. Angular distribution of flux on plate surface when $q(x) = q_0 e^{-k_n x}$.

the increase in the fluxes beyond the shielding, which have been computed in two stages for the case of large positive $k_n d$.

A reverse picture is observed for a descending function of source distribution (negative k_n). In this case the angular distribution on the surface of the plate has a maximum value in the forward direction, so that a calculation performed in two stages produces lower values for the flux behind the shielding.

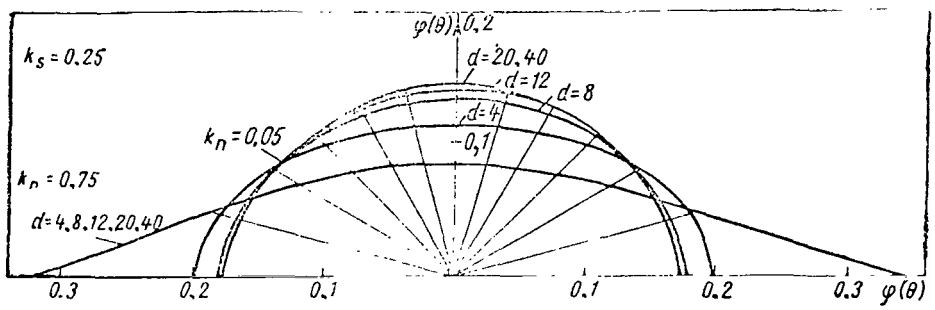

Figure 4. Angular distribution of the flux on surface of plate when $q(x) = q_0 e^{k_n x}$.

Thus, in computing the shielding we may use the method with the intermediate calculation of the flux on the surface of the source only when $k_n \geq 0$. When $k_n < 0$, particularly for large absolute values of k_n, we must carry out the calculations directly, in spite of the fact that this increases the volume of computations substantially.

REFERENCES

1. Broder, D. L., Kayurin, Yu. P. and Kutuzov, A. A. The Transmission of Gamma Radiation Through Heterogeneous Media (Prokhozhdeniye gamma-izlucheniya cherez geterogennyye sredy). P. 287 of this volume.

2. Goldstein, H. Fundamental Aspects of Reactor Shielding. London-Paris, Pergamon Press, 1959.

3. The Shielding of Nuclear Reactors. Edited by T. Rockwell. (Zashchita yadernykh reaktorov). Moscow, Izd-vo I. L., 1959. /119

4. Price, B., Horton, C. and Spinney, K. Shielding Against Nuclear Radiations (Zashchita ot yadernykh izlucheniy). Moscow, Izd-vo I. L., 1959.

5. Gorshkov, G. V. Gamma Radiation of Radioactive Bodies and the Elements of Computing Radiation Shielding (Gamma-izlucheniye radioaktivnykh tel i elementy rascheta zashchity ot izlucheniy). Moscow, Izd-vo AN SSSR, 1959.

6. Nuclear Reactors. Materials of the Atomic Energy Commission, USA (Yadernyye reaktory. Materialy KAE SShA). Moscow, Izd-vo I. L., 1956.

ATTENUATION OF RADIATION IN HETEROGENEOUS SHIELDINGS

N. I. Laletin

Attenuation of Primary Radiation in a Heterogeneous Medium

Radiation shielding is frequently not homogeneous. In this case /119 the attenuation of radiation by the shielding consisting of a sequence of plane layers may be considered, using the same methods as for the case of attenuation by a single layer. On the other hand, the analysis of shieldings pierced with rods and channels and also of shieldings containing hollow spaces of various form requires a special approach.

In this article we shall consider the attenuation of primary radiation (assuming that there are no collisions) in a two-component heterogeneous medium, which consists of a filler medium (the mean free path in this medium is equal to λ_1), containing slugs of arbitrary form (which, however, are bounded by a convex surface) with a different interaction cross section Σ_2 (and $\lambda_2 = 1/\Sigma_2$ accordingly).

We introduce the following designations: $\Sigma(r)$ is the macroscopic cross section of radiation interaction with the substance near point r, $p = v_{sl}/v$, where v_{sl} is the volume of one slug; v is the volume of the filler corresponding to one slug; S is the area of the slug surface; X is the length of a vector segment of assigned direction in the slug; $\Psi(x)\,dX$ is the probability that X will have a definite value. This probability is normalized in such a way that $\int_0^\infty \Psi(X)\,X\,dX = v_{sl}$. Then $\Psi(X)\,dX$ has the following geometric meaning: $\Psi(X)\,dX$ represents the projection of the element of area dS of the slug's surface on vector $r(\vartheta, \varphi)$ in such a way that the length of the vector $r(\vartheta, \varphi)$ segment, which pierces this area in the slug, lies within the limits from X to $X + \delta X$.

Let us consider a large, but finite medium containing N slugs distributed at random; the total volume of the filler is V. Let us determine the following

probabilities for such a medium. Let us assume that a neutron (or γ-quantum) originates at point r_0 in the filler and travels a distance $|r - r_0|$ without collision. Obviously the probability of such an event is equal to $e^{\int_{r_0}^{r} \Sigma(r)\,dr}$, where the integral in the exponent is taken along the ray $|r - r_0|$. In this case there is a definite probability P_0 that the neutron will not intersect any of the slugs or a probability P_n that it will intersect n slugs. In this case point r may lie in the filler or in the slug. In a similar way we can establish a probability that the neutron which originates in the slug will not leave the slug or that if it does leave the slug, it will intersect a certain number of slugs. Point r is again either in the filler or in the slug.

We let ρ be the path traveled by the neutron in the filler and Y be the path traveled in the slugs ($\rho + Y = |r - r_0|$). Let us assume that the generation density of neutrons having a specific direction in the filler is equal to $q_1(\vartheta, \varphi)$, and that in the slugs it is equal to $q_2(\vartheta, \varphi)$. Then the area $\Psi(X)\,dX$ of some slug will be intersected by those neutrons which originate their path inside the cylinder (the base of the cylinder consists of the same area $\Psi(X)\,dX$ and its height is equal to ρ). The proportion of such neutrons in the total mass is equal to $\Psi(X)\,dX\,\rho q_1/V_{q_1} + N v_{sl}\, q_2$. This quantity is a measure of the probability that the neutron, whose path in the filler is equal to ρ and whose direction of flight is given by angles (ϑ, φ), will collide with a given slug in such a way that the maximum possible path in the slug will lie within the limits $X - (X + \delta X)$. The probability of any collision of neutrons of this type with the given slugs will be equal to /120

$$\frac{\rho \int_0^\infty \Psi(X)\,dX q_1}{Vq_1 + N v_{бл} q_2} = \frac{\rho \sigma_0(\vartheta, \varphi)\, q_1}{Vq_1 + N v_{бл} q_2}; \qquad \left[\sigma_0(\vartheta, \varphi) = \int_0^\infty \Psi(X)\,dX\right].$$

(бл = sl = slug)

Since the number of slugs is equal to N, the probability that the neutron which originates in a filler with direction (ϑ, φ) and path length ρ in the filler will intersect at least one slug will be $P_1 = \rho\sigma_0/v$.

We note that in obtaining an expression for P_1 we have not yet made use of the proposition on the random distribution of the slugs. In order to obtain an expression for the probability that n slugs will be intersected, where $n > 1$,

we must use this proposition. The total probability that a neutron which originates in the filler will intersect n slugs will then be represented by the product of the probabilities that it intersects one slug.

$$\prod_{j=1}^{n} \frac{\Psi(X)\,dX}{V} \varrho.$$

The various combinations of N slugs taken n at a time will be

$$C_N^n = \frac{N!}{(N-n)!\,n!}.$$

Therefore the expression $\frac{N!}{(N-n)!\,n!} \prod_{j=1}^{n} \frac{\Psi(X)\,dX}{V}\,\varrho$ will represent the probability that a neutron originating in the filler will intersect not less than any n slugs; in this case its path in the first slug will be X_1, in the second it will be X_2, etc.

By letting N tend to infinity we obtain $\prod_{j=1}^{n} \frac{\Psi(X_j)\,dX_j\varrho}{v\,n!}$ for an infinite medium, and integrating over X_j, we obtain

$$P_n = \frac{(\sigma_0 \varrho)^n}{n!\,v^n}.$$

The probability that none of the slugs will be intersected is obtained from the condition

$$P_0 + P_0P_1 + P_0P_2 + \ldots = P_0\left(1 + \sum_{n=1}^{\infty} P_n\right) = 1.$$

Here the products P_0P_n represent the probability that the neutron intersects exactly n slugs. Substituting the latter equality into the expression for P_n, we obtain

$$P_0 = e^{-\frac{\sigma_0 \varrho}{v}}.$$

If we reason in a similar way, we find that the probability for a neutron originating in the filler and traveling a path ϱ in this filler to intersect (n-1) slugs and to travel a path y after colliding with the n-th slug is given by the expression

$$e^{-\frac{\varrho\sigma_0}{v}} \prod_{j=1}^{n-1} \frac{\varrho\Psi}{v} \cdot \frac{dX_j}{(n-1)!}.$$

The probability that a neutron originating in the slug will intersect (n-1) more slugs and travel a path ρ in the filler is given by the expression /121

$$e^{-\frac{\rho\sigma_0}{v}} \prod_{j=1}^{n-1} \frac{\rho\Psi}{v} \cdot \frac{dX_j}{(n-1)!} \cdot \frac{\Psi\, dy}{v}.$$

If such a neutron collides with one more slug and travels a distance y_1 in this slug, the probability will have the form

$$e^{-\frac{\rho\sigma_0}{v}} \prod_{j=1}^{n-2} \frac{\rho\Psi}{v} \cdot \frac{dX_j}{(n-1)!} \cdot \frac{\Psi\, dy}{v} \cdot \frac{\Psi\, dy_1}{v}.$$

There is still some probability that the neutron travel will be contained entirely within one slug

$$\frac{\Psi(X)(X-r)\,dX}{vP} \quad (\text{r varies from 0-X}).$$

By using these expressions for the probabilities of different events we can solve a series of problems on the propagation of radiation in the considered heterogeneous medium.

For example, let us compute the average mean free path of a particle for the case $q_1 = q_2 = \text{const}$

$$\lambda_{эфф} = \int_{V_{яч}} \frac{dV}{V_{яч}} \int dV' \frac{e^{-\int \Sigma dr} \Sigma(\mathbf{r}')\,|\mathbf{r}-\mathbf{r}'|}{4\pi\,|\mathbf{r}-\mathbf{r}'|^2} =$$

$$= \int_{V_{яч}} \frac{dV}{V_{яч}} \int \frac{d\Omega}{4\pi} \int e^{-\int \Sigma dr} \Sigma r\, dr = \int \frac{dV}{V_{яч}} \int \frac{d\Omega}{4\pi} \left[-e^{-\int \Sigma r} r \Big|_0^{\infty} + \int e^{-\int \Sigma dr} dr \right] = \quad (1)$$

$$= \int_{V_{яч}} \frac{dV}{V_{яч}} \int \frac{d\Omega}{4\pi} \int e^{-\int \Sigma dr} dr = \int \frac{d\Omega}{4\pi} \int dr \int_{V_{яч}} \frac{dV}{V_{яч}} e^{-\int \Sigma dr}.$$

(эфф = eff; яч = cell)

When integrating over the volume of the cell in the last expression we divide the integration region into parts according to the following procedure:

V_1^n is the part of the filler volume such that the radius vector, which has a

value $|r-r'|$ and direction (ϑ, φ) and which originates in this volume, intersects n slugs and terminates in the filler n = 0, 1, ..., ∞); V_2^n is the same radius vector which originates in the same part of the filler volume and intersects n slugs terminating in the (n + 1) slug (n = 0, 1, ..., ∞); V_3^n is a part of the slugs' volume such that the radius vector originating in it intersects n more slugs and is terminated in the filler (n = 0, 1, ..., ∞); V_4^n is the radius vector which originates in this part of the slugs' volume, intersects n slugs and terminates in the slug (n = 0, 1, ..., ∞); V_5 is a part of the slugs' volume such that the radius vector which originates here is contained entirely within one slug.

For the heterogeneous medium under consideration the ratio V_k^n/V_{cell} (k = 1-5) coincides with the probabilities determined above. Taking this into acaount and also transforming from the integration variable r to variable ρ in expression (1) we obtain

$$\lambda_{\vartheta\varphi\Phi} = \int \frac{d\Omega}{4\pi} \left\{ \frac{v}{V_{\text{пч}}} \int_0^\infty e^{-\Sigma_1 \varrho - \varrho \frac{\sigma_0}{v}} d\varrho + \right.$$

$$+ \sum_{n=1}^{\infty} \int_0^\infty \frac{v}{V_{\text{пч}}} e^{-\frac{\varrho\sigma_0}{v} - \Sigma_1 \varrho} d\varrho \int \int_0^\infty \int e^{-\Sigma_2 \sum_{j=1}^{\infty} X_i} \prod_{j=1}^{n} \frac{\varrho\Psi}{v} \frac{dX_j}{n!} +$$

$$+ \sum_{n=0}^{\infty} \int_0^\infty d\varrho e^{-\Sigma_2 \varrho - \frac{\varrho\sigma_0}{v}} \int \int_0^\infty \cdots \int e^{-\Sigma_2 \sum_j X_j} \prod_j^n \frac{\varrho\Psi}{v} \frac{dX_j}{(n-1)!} \int_0^\infty dX \int_0^X \frac{\Psi}{V_{\text{пч}}} e^{-\Sigma_2 y} dy +$$

$$+ \sum_{n=0}^{\infty} \int_0^\infty d\varrho e^{-\frac{\varrho\sigma_0}{v} - \Sigma\varrho} \int \int_0^\infty \int e^{-\Sigma_2 \sum_{j=1}^{n} X_j} \prod_{j=1}^{n} \frac{\varrho\Psi}{v} \frac{dX_j}{n!} \int_0^\infty dX \int_0^X \frac{dX}{v_{\text{пч}}} e^{-\Sigma_2 y} + \quad (2)$$

$$\left. \cdots\cdots\cdots\cdots\cdots\cdots\cdots\cdots\cdots\cdots\cdots\cdots\cdots\cdots\cdots\cdots\cdots\cdots \right\} =$$

$$= \frac{\lambda_1 + \lambda_2 P}{1+P} - \frac{(\lambda_1 - \lambda_2)^2}{\lambda_1 (1+P)} [1 - f(x_1, x_2)];$$

$$f(x_1, x_2) = \int_0^{2\pi} \int_0^{\pi} \frac{\sin\vartheta \, d\vartheta \, d\varphi}{4\pi \left\{ 1 + \frac{4}{x_1} - \frac{1}{S} \int_0^\infty \Psi(X, \vartheta, \varphi) [1 - e^{-\Sigma_2 X}] dX \right\}}.$$

Here f (x_1, x_2) is a function which depends on the dimensions of the slugs /122 $(x_2 = 4v_{sl}/S)$ and on the distance between them $(x_1 = 4v/S)$. The form of the

function is determined by the shape of the slugs. Thus for slugs which have the form of spheres

$$f(x,x_2)=\int_0^1 \frac{v\,dv}{\sqrt{1-v^2}\left[1+\frac{4}{\pi}\cdot\frac{x_2}{x_1}\int_0^1\sqrt{1-u^2}\,e^{-x_2\frac{u}{v}}\,du\right]}. \qquad (3)$$

whereas for infinite circular cylinders (when the axes of all cylinders are parallel)

$$f(x_1,x_2)=\frac{1}{1+\frac{1}{x_1}\left\{1-\frac{8}{9x_2^2}+\frac{8\left(1+\frac{3}{2}x_2\right)}{9x_2^2}e^{-\frac{3}{2}x_2}\right\}}, \qquad (4)^1$$

---

[1]The function f (x_1, x_2) is simply associated with the quantity P_c (x_1, x_2):

$$P_c(x_1,x_2)=\int_{\dot{N}v_{0n}}\frac{\Sigma_2 dv}{\dot{N}v_{0n}}=\int\frac{dv'}{4\pi}=\frac{e^{-\int\Sigma dv}}{|r-r'|^2},$$

which represents the probability that the neutron undergoes its first collision in any slug, assuming that the neutron originates only in the slugs and that the source density there is constant f (x_1, x_2) = 1 + $\frac{x_2}{x_1}$ [P_c (x_1, x_2) -1)]. When $x_1 \to \infty$, the quantity P_c (x_2, ∞) gives us the probability of collisions, determined for an insulated slug. P_c (x_2, ∞) is tabulated in reference 1 for slugs which have the form of an infinite plate, a sphere and an infinite circular cylinder. The quantity P_c (x_1, x_2) is tabulated for a lattice of circular cylindrical slugs with parallel axes in reference 2. For a lattice of spherical slugs and also for slugs of other shapes situated at random not only with respect to the distance between them, but also oriented at random with respect to each other, the quantity P_c (x_1, x_2) is expressed simply in terms of P_c (x_2, ∞):

$$P_c(x_1,x_2)=\frac{1+[1-P_c(x_2,\infty)]\left(\frac{x_2}{x_1}-1\right)}{1+\frac{x_2}{x_1}[1-P_c(x_2,\infty)]}.$$

Let us consider the attenuation of monoenergetic radiation emitted by a plane homogeneous source at an angle ϑ with respect to the normal to the plane of the source. In a homogeneous medium at a distance z from the source the density of particles which have not undergone any collisions will be equal to $Qe^{-\Sigma z/\cos\vartheta}$. In a heterogeneous medium the density of particles at a distance z from the source, generally speaking, will be a function of the coordinates x and y. If distance z is much greater than the linear dimensions of the cell in a heterogeneous medium (in which the slugs are distributed at random), then, by averaging out the density of particles at the distance (z over x and y), /123 we obtain

$$n(z) = \int \frac{dS}{S} e^{-\int \Sigma dr} = e^{-\frac{z}{\lambda_{эфф}\cos\vartheta}}$$

or by replacing the average value over surface S, which intersects an infinitely large number of cells, with the average value over the shell, we have

$$\int_{V_{яч}} \frac{dV}{V_{яч}} e^{-\int \Sigma dr} = e^{-\frac{z}{\lambda_{эфф}\cos\vartheta}}.$$

Integrating the last equality over $r = z/\cos\vartheta$ in the limits 0-∞, we obtain $\lambda_{eff} = \int_{V} \frac{dV}{V_{cell}} \int_{cell} e^{-\int \Sigma dr} dr$, which coincides with the quantity determined by means of expression (2).

This result is naturally generalized for a plane source with an arbitrary distribution of emitted particles and also for a source whose surface is distorted, including the case when its radius of curvature is much larger than the dimensions of the cell in the heterogeneous medium.

Thus, if a layer of homogeneous shielding (characterized by the mean free path λ_{ho}) attenuates the primary radiation by a fixed factor, then in order to attenuate the primary radiation of the same source by the same factor, the thickness of the heterogeneous shielding layer must be equal to

$$x_{гет} = x_{гом}\frac{\lambda_{эфф}}{\lambda_{гом}}; \quad \lambda_{гом} = \frac{1}{\Sigma_{гом}} = \frac{1+P}{\frac{1}{\lambda_1}+\frac{P}{\lambda_2}}. \qquad (5)$$

(гет = he = heterogeneous; гом = ho = homogeneous)

When $\lambda_2 \to \infty$ (medium with cavities)

$$\lambda_{эфф} = \lambda_1 \left(1 + P + \frac{P^2 Q}{1+P} x_1\right) \text{ and } x_{гет} = x_{гом}\left[1 + \frac{P^2}{(1+P)^2} Q x_1\right]; \quad (6)$$

Here Q is a factor which depends only on the shape of the cavity (ref. 3). For spheres Q = 9/16 (approximately 0.5625), for infinite cylinders Q = 2/3.

When $\lambda_1 \to \infty$,

$$\begin{cases} \lambda_{эфф} = \lambda_2 \left\{1 + \frac{1}{1+P} \cdot \frac{P}{P(1+P)[1-P_c(x_2,\infty)]}\right\}; \\ \frac{\lambda_{эфф}}{\lambda_{гом}} = \frac{x_{гет}}{x_{гом}} = 1 + \frac{1}{(1+P)^2} \cdot \frac{P_c(x_2,\infty)}{1-P_c(x_2,\infty)}. \end{cases} \quad (7)$$

When $x_2 \ll 1$,

$$P_c(x_2,\infty) \approx Q x_2 \text{ (ref. 1)}; \quad \frac{\lambda_{эфф}}{\lambda_{гом}} \approx 1 + \frac{1}{(1+P)^2} Q x_2.$$

When $x_2 \gg 1$,

$$P_c(x_2,\infty) \approx 1 - \frac{1}{x_2}; \quad \frac{\lambda_{эфф}}{\lambda_{гом}} \approx 1 + \frac{1}{(1+P)^2} x_2.$$

Let us compare the obtained results with the Smith equation (refs. 4 and 5), obtained for a medium with a random distribution of cavities of arbitrary shape. Smith presents the factor $f = \lambda_{eff}/\lambda_{ho} = 1 + S\Phi^2/2$, where Φ is the ratio of the volume of the cavity to the total volume of the medium (porosity), and S is the average distance between the cavities, measured in units of the mean free path of radiation in a continuous substance. Noting that in terms of the symbols utilized in equation (6), $\Phi = P/1 + P$ and $S = x_1$, we conclude that equation (6) and the Smith equation have the same form, but differ somewhat in the numerical coefficient. In place of the factor 1/2 contained in the Smith equation, equation (6) has the factor Q, which is somewhat greater in value and which differs for cavities of different shapes. Equation (6) is valid for /124 cavities bounded by a convex surface, and therefore, for example, in the case of a medium which represents the layer of shot poured at random we should compare equation (7) with the Smith equation. In this case $\Phi = \frac{1}{1+P}$, $S = x_2$ and equation 7 takes the form $\frac{\lambda_{eff}}{\lambda_{ho}} = 1 + \Phi^2 S \left\{\frac{P_c(S,\infty)}{S[1-P_c(S,\infty)]}\right\}$ i.e., instead of the

factor 1/2 we have the quantity $\frac{P_c(S, \infty)}{S[1-P_c(S, \infty)]}$, which is approximately equal to Q when $S \ll 1$ and equal to $P_c/S\ (1-P_c) \approx 1$ when $S \gg 1$. The difference between the Smith equation and equation (7) is shown in figure 1.

The results are also valid for a heterogeneous medium in which the slugs of arbitrary shape are placed at random. For a medium with slugs having the form of infinite cylinders (with an arbitrary cross section) the results will also be valid when the axes of the cylinders are parallel to the plane of the source, but the cylinders as before are situated at random with respect to each other.

In this case, if we have a medium with an infinite circular cylinder, function $f\ (x_1, x_2)$, which affects λ_{eff}, is determined by equation (4). However, if the axes of the cylinders are parallel to each other and are perpendicular to the plane of the sources, the preceding considerations lose their meaning. In this case radiation attenuation will be described by a function of an entirely different type compared with the one for the case of homogeneous shielding, and the variation can no longer be taken into account by introducing λ_{eff}.

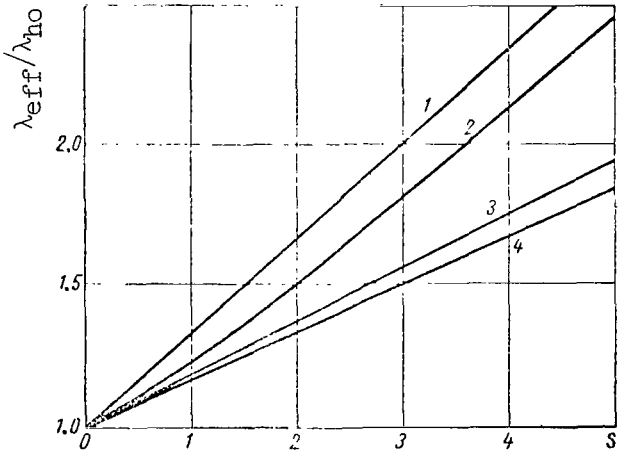

Figure 1. Value of factor obtained by Smith and given by equation (7): 1, relationship $1 + \Phi^2 S$; 2, relationship $1 + \Phi^2 \frac{P_c\ (S, \infty)}{1-P_c\ (S, \infty)}$; 3, relationship $1 + \Phi^2 QS$; 4, relationship $1 + 0.5\Phi^2 S$.

The Diffusion of Monoenergetic Neutrons in a Heterogeneous Medium

Above we considered the propagation of primary radiation from sources in heterogeneous shielding (radiations which do not undergo a single collision). It is also of interest to consider the propagation of scattered radiation in a heterogeneous medium.

In order to understand the qualitative features of the problem we shall consider an idealized case: we shall investigate the propagation of single energy radiation far removed from a source in a heterogeneous scattering non-absorbing medium.

In this case the integral form of the kinetic equation is /125

$$\Phi(\mathbf{r}) = \int \frac{\Sigma(\mathbf{r}')\, e^{-\int_{\mathbf{r}'}^{\mathbf{r}} \Sigma(r)\,dr}}{4\pi |\mathbf{r}-\mathbf{r}'|^2} \Phi(\mathbf{r}')\,dV' + \int \frac{q(\mathbf{r}')\, e^{-\int_{\mathbf{r}'}^{\mathbf{r}} \Sigma dr}}{4\pi |\mathbf{r}-\mathbf{r}'|^2} dV'. \tag{8}$$

Here $\Phi(\mathbf{r})$ is the flux of particles at point r; $q(\mathbf{r})$ is the source density at point r (it is assumed that scattering by all of the nuclei is spherically symmetric).

Let us consider a two-component heterogeneous medium with cylindrical slugs of arbitrary cross section when the directrixes of the cylinders are parallel to each other.

We place an infinite plane source at infinity (i.e., at a distance from the considered region, which is much greater than the mean free path in the components of the medium), and let the source plane be perpendicular to the directrixes of the cylinders.

The second term in equation (8) vanishes and the equation assumes the form

$$\Phi(\mathbf{r}) = \int \frac{\Sigma(\mathbf{r}')\,\Phi(\mathbf{r}')\, e^{-\int_{\mathbf{r}'}^{\mathbf{r}} \Sigma(r)dr}}{4\pi |\mathbf{r}-\mathbf{r}'|^2} dV'. \tag{9}$$

The solution of this equation will be a linear function of z (the z axis is perpendicular to the source plane), which is independent of the coordinates x and y.

Indeed,

$$\int \frac{\Sigma(\mathbf{r}')\, e^{-\int \Sigma dr}}{4\pi |\mathbf{r}-\mathbf{r}'|^2} dV' = \int \frac{d\Omega}{4\pi} \int \Sigma(\mathbf{r}')\, e^{-\int \Sigma dr} dr = \int \frac{d\Omega}{4\pi} \int_0^\infty e^{-\eta_1} = 1$$

and the equation may be written in the form

$$\int \frac{\Sigma(r')\,|\Phi(r')-\Phi(r)|\,e^{-\int \Sigma dr}}{4\pi\,|r-r'|^2}\,dV = 0,$$

i.e., $\Phi(r)$ must be a function of the type that the difference $\Phi(r)-\Phi(r')$ for any point r makes the integral equal to zero. This is possible only if $\Phi(r) = \Phi_0 + (d\Phi/dz)_0\, z$ where Φ_0 and $(d\Phi/dz)_0$ are constants.

Thus the flux of neutrons (and consequently the density of neutrons) is constant along the cross section of the cell in the heterogeneous medium. On the other hand the flux of neutrons through a unit element area, whose normal is parallel to the directing cylinders, will depend on the position of this element in the cell. Indeed,

$$I(r) = \int \frac{\Sigma(r')\,\Phi(r')\cos\vartheta e^{-\int \Sigma dr}}{4\pi\,|r-r'|^2}\,dV' = \left(\frac{d\Phi}{dz}\right)_0 \int \frac{\Sigma(r')\,|r-r'|\cos^2\vartheta e^{-\int \Sigma dr}}{4\pi\,|r-r'|^2}\,dV'.$$

Averaging out the stream I (r) over the transverse cross section of the cell, we obtain

$$\bar{I}(r) = \int \frac{dS}{S_{яч}} \int \frac{\Sigma(r')\,|r-r'|\cos^2\vartheta e^{-\int \Sigma dr}}{4\pi\,|r-r'|^2}\,dV' \left(\frac{d\Phi}{dz}\right)_0 = D_{\parallel}\left(\frac{d\Phi}{dz}\right)_0.$$

It is natural to call the quantity $D_{\parallel}$ the effective coefficient of longitudinal neutron diffusion in a heterogeneous medium. Writing this coefficient in the form

$$D_{\parallel} = \int_{V_{яч}} \frac{dV}{V_{яч}} \int \frac{\cos^2\vartheta e^{-\int \Sigma dr}}{4\pi\,|r-r'|^2}\,dV',$$

we note that it is expressed by an integral of the same type as those which we considered above in determining the attenuation of primary radiation. /126 Consequently this integral may be computed for media with small slugs distributed at random distances from each other

$$D_{\parallel} = \frac{\lambda_1 + P\lambda_2}{3(1+P)} - \frac{(\lambda_1-\lambda_2)^2}{3(1-P)\lambda_1}\,[1 - f_{\parallel}(x_1, x_2)], \qquad (10)$$

where

$$f_{\parallel}(x_1,x_2)=\int_0^{2\pi}\int_0^{\pi}\frac{\cos^2\vartheta\sin\vartheta\,d\vartheta\,d\varphi}{4\pi\left\{1+\frac{4}{x_1 S}\int_0^{\infty}\Psi(X)\left[1-e^{-\Sigma_2 X}\right]dX\right\}}.$$

For slugs which have the form of circular cylinders

$$f_{\parallel}(x_1,x_2)=3\int_0^1\frac{\sqrt{1-v^2}v\,dv}{1+\frac{4}{\pi}\frac{x_2}{x_1}\int_0^1\sqrt{1-u^2}e^{-x_2\frac{u}{v}}du}; \tag{11}$$

when $\lambda_2\to\infty$ $D_{\parallel}=\frac{\lambda_1}{3}\left(1+P+\frac{P^2}{1+P}Q\frac{3}{2}x_1\right)$ (medium with hollow channels);

when $x_1\gg 1$ $f_{\parallel}(x_1,x_2)\approx\int_0^{2\pi}\int_0^{\pi}\cos^2\vartheta\sin\vartheta\left\{\frac{1}{\pi x_1 S}\int_0^{\infty}\Psi(X)\left[1-e^{-\Sigma_2 X}\right]dX\right\}d\vartheta\,d\varphi$ (medium with sparsely distributed rods).

In this limiting case the result also remains valid for media with slugs which form any regular lattice (not limited to those with random distribution). When $x_1 \ll 1$ and $x_2 \ll 1$ $D_{\parallel}\approx D_{ho}=\frac{\lambda_{ho}}{3}$, as was to be expected.

For a heterogeneous medium which has the form of infinite plates (in our proposition concerning the random distribution such plates may intersect each other)

$$f_{\parallel}(x_1,x_2)=\frac{3}{2}\int_0^1\frac{(1-u^2)\,du}{1+\frac{2u}{x_1}\left(1-e^{-\frac{x_2}{2u}}\right)}. \tag{12}$$

For a heterogeneous medium which has the form of infinite plates, the coefficient of longitudinal diffusion is computed simply when the plates are situated parallel to each other at equal distances from each other (ref. 7). In this case

$$D_{\parallel}=\frac{\lambda_1+P\lambda_2}{3(1+P)}-\frac{(\lambda_1-\lambda_2)^2}{\lambda_1(1+P)}\cdot\frac{1}{4x_1}\left[1-4\int_0^1\frac{(1-u^2)u\left(e^{-\frac{x_1}{2u}}+e^{-\frac{x_2}{2u}}-2e^{-\frac{x_1+x_2}{2u}}\right)}{1-e^{-\frac{x_1+x_2}{2u}}}du\right]. \tag{13}$$

Equations (10) and (13) give the same results in the two limiting cases: when $x_1 \gg 1$ and $x_1 \ll 1$; $x_2 \ll 1$. Direct calculation shows that the results

obtained by means of equations (10) and (13) do not differ too much over the entire interval of x_1 and x_2. This situation permits us to maintain that the utilization of equation (10) for media containing slugs which have the form of circular cylinders and are placed in a regular lattice will not lead to a large error for any values of x_1 and x_2.

The situation is the same for distribution of neutrons along the slugs (longitudinal diffusion).

During the distribution of neutrons in the perpendicular direction (transverse diffusion) the solution of equation (9) must be written in the form /127

$$\Phi(\mathbf{r}) = \Phi_0 + \left(\frac{d\Phi}{dx}\right)_0 x + \Delta\Phi(x, y).$$

Here Φ_0 and $(d\Phi/dx)_0$ are constants. The first two terms on the right describe the behavior of the neutron flux averaged out over the cell, and $\Delta\Phi$ (x, y) describes the microstructure of neutron flux. The microstructure $\Delta\Phi$ (x, y) must be proportional to the gradient of the mean flux, and if we have even one axis of symmetry for the shell of the heterogeneous medium, $\Delta\Phi$ (x, y) will be an even function of y and an odd function of x with respect to this axis. We can write $\Delta\Phi$ (x, y) = $(d\Phi/dx)_0$ f (x, y) where f (x, y) depends only on the characteristics of the medium.

The flux through a unit area whose normal is parallel to the x axis will have the form

$$I(\mathbf{r}) = \left(\frac{d\Phi}{dx}\right)_0 \left\{\int \frac{\Sigma(\mathbf{r}')\,|\mathbf{r}-\mathbf{r}'|\sin^2\vartheta\cos^2\varphi}{4\pi\,|\mathbf{r}-\mathbf{r}'|^2} e^{-\int \Sigma dr} dV' + \right.$$
$$\left. + \int \frac{\Sigma(\mathbf{r}')\,f(x', y')\sin\vartheta\cos\varphi\, e^{-\int \Sigma dr}}{4\pi\,|\mathbf{r}-\mathbf{r}'|^2} dV' \right\}.$$

Averaging this flux over the transverse cross section of the cell, we obtain

$$I(\mathbf{r}) = \int_{S_{\text{ш}}} \frac{dS}{S_{\text{ш}}} \left\{\int \frac{\Sigma(\mathbf{r}')\,|\mathbf{r}-\mathbf{r}'|\sin^2\vartheta\cos^2\varphi}{4\pi\,|\mathbf{r}-\mathbf{r}'|^2} e^{-\int \Sigma dr} dV' + \right.$$
$$\left. + \int \frac{\Sigma(\mathbf{r}')\,f(x', y')\sin\vartheta\cos\varphi\, e^{-\int \Sigma dr}}{4\pi\,|\mathbf{r}-\mathbf{r}'|^2} dV' \right\} \left(\frac{d\Phi}{dx}\right)_0 = D_\perp \left(\frac{d\Phi}{dx}\right)_0 \qquad (14)$$

The quantity $D_\perp$ above plays the role of the effective coefficient of transverse diffusion. We can see that the expression for $D_\perp$ may be divided into two parts:

the component $D_\perp'$ which is completely analogous to the coefficient of longitudinal diffusion and a second component $D_\perp''$ which takes into account the presence of microstructure in the distribution of neutron flux. With regard to the calculation of the first component we can repeat everything that has been stated concerning the coefficient of longitudinal diffusion. The second component, however, is more difficult to compute. However, it can be easily obtained in the simplest case: for a heterogeneous medium in the form of plane parallel plates of two types. In this case the solution of equation (9) will have the following form, when the neutron distribution is across the plates.

$$\Phi = \Phi_0 + \left(\frac{d\Phi}{dx}\right)_0 x + \left(\frac{d\Phi}{dx}\right)_0 \left[\frac{\int \Sigma\, dx}{\Sigma_{cp}} - x\right]. \tag{15}$$

(cp = med = medium)

Here the flux microstructure is described by the third term on the right. Using expression (15) to compute the coefficient of transverse diffusion, we obtain $D_\perp = \dfrac{1}{3\Sigma_{med}} = \dfrac{\lambda_{ho}}{3}$, where

$$D_\perp' = \frac{\lambda_1 + P\lambda_2}{3(1+P)} - \frac{(\lambda_1-\lambda_2)^2}{6\lambda_1(1+P)x_1}\left[1 - 4\int_0^1 u^3 \frac{e^{-\frac{x_1}{2u}} + e^{-\frac{x_2}{2u}} - 2e^{-\frac{x_1+x_2}{2u}}}{1-e^{-\frac{x_1+x_2}{2u}}}\,du\right].$$

Thus for a medium consisting of plates without absorption, the coefficient of transverse diffusion for any plate thickness is equal to the diffusion coefficient in the corresponding homogeneous mixture. When the microstructure of the flux is taken into account the magnitude of the transverse diffusion coefficient decreases.

For a heterogeneous medium with circular cylindrical slugs we can maintain that when the diameters of the slugs are much less than the mean free path of neutrons in the filler, the effect of microstructure in the distribution of the flux will be small and the coefficient of transverse diffusion will be represented approximately by the first component /128

$$D_\perp' = \frac{\lambda_1 + P\lambda_2}{3(1+P)} - \frac{(\lambda_1-\lambda_2)^2}{3\lambda_1(1+P)}\,[1 - f_\perp(x_1, x_2)], \tag{16}$$

where

$$f_\perp(x_1, x_2) = \frac{3}{2}\int_0^1 \frac{v^3\,dv}{\sqrt{1-v^2}\left[1 + \frac{4x_2}{\pi x_1}\int_0^1 \sqrt{1-u^2}\,e^{-x_2\frac{u}{v}}\,du\right]}.$$

As the diameters of the slugs increase, the role of the second component becomes more and more pronounced. If, however, we take into account the microstructure, the value of the transverse diffusion coefficient decreases, i.e., $D_\perp \leq D_\perp'$. For slugs with a diameter much greater than the mean free path of neutrons in the filler, the distribution of neutrons between slugs and in the small slugs is described with sufficient accuracy by the elementary diffusion equation. Solving this equation for a cell of a heterogeneous medium, we can find the limiting expression for the effective coefficient of transverse diffusion. This expression will depend on the shape of the slug lattice, and it is not very simple to find its exact value for real lattices (square, triangular, etc.).

The effective coefficients of transverse diffusion may be represented approximately in the form

$$D_\perp^{\text{диф}} = \frac{\lambda_1}{3} \cdot \frac{1 - \frac{\omega}{W} \cdot \frac{\lambda_1 - \lambda_2}{\lambda_1 + \lambda_2}}{1 + \frac{\omega}{W} \cdot \frac{\lambda_1 - \lambda_2}{\lambda_1 + \lambda_2}}. \tag{17}$$

(дифф = diff = diffusion)

Here ω is the area of the transverse cross section of the slug; W is the area of the transverse cross section of the cell. This expression is valid (in the diffusion approximation) for the Wigner-Zeitz cell (when $\omega/W \to 1$, $D_\perp^{\text{diff}} \to \lambda_2/3$ and when $\omega/W \to 0$ $D_\perp^{\text{diff}} \to \lambda_1/3$). It is valid for any lattices when ω/W are small, within the accuracy of terms ω/W inclusive. For a square lattice it is valid with an accuracy to within the terms $(\omega/W)^2$ inclusive, for a triangular lattice (the slugs are placed at the apexes of an equilateral triangle) up to terms $(\omega/W)^3$ inclusive.

Thus, in evaluating the coefficient of transverse diffusion in a heterogeneous medium we can proceed in the following manner. We represent $D_\perp'$ and $D_\perp^{\text{diff}}$ in the form of functions of $x_1 = d/P\lambda_1$ for a fixed parameter $P = \omega/W - \omega$ and let x_1^0 be the point of their intersection, i.e.,

$$D_\perp'(x_1^0) = D_\perp^{\text{diff}}(x_1^0).$$

Then, if we evaluate the effective coefficient of transverse diffusion by means of the expression (16) for $D_\perp^0$ when $x_1 < x_1^0$ and by means of expression (17) for $D_\perp^{diff}$ when $x_1 > x_1^0$, we obtain a sufficiently close approximation for $D_\perp$ /129 over the entire interval for x_1 and x_2 (fig. 2). In this case the true value of $D_\perp$ is, in any case, not greater than the approximate value.

Qualitatively, this picture also takes place when we consider the transmission of neutrons in a heterogeneous medium with bounded slugs (spheres, cubes, etc.). The general solution of equation (9) may again be represented as a superposition of the linear function, which describes the variation in the averaged neutron flux and by means of a function which describes the microstructure of neutron distribution. When the dimensions of the slugs are much less than the mean free path of neutrons in the filler, the microstructure will be small and the effective coefficient of diffusion is described approximately by equation

$$D = \frac{\lambda_1 + P\lambda_2}{3(1+P)} - \frac{(\lambda_1-\lambda_2)^2}{3\lambda_1(1+P)}\left[1 - \frac{1}{1+\frac{4}{x_1}\frac{1}{S}\int_0^{\pi}\int_0^{2\pi}\int_0^{\infty}\Psi(X,\vartheta,\varphi)\left[1-e^{-\Sigma_2 X}\right]d\Omega dX}\right], \tag{18}$$

which is obtained in the same way as equation (16) for a medium with cylinders (it is assumed that the slugs are distributed in a random fashion). If the slugs have the form of spheres with radius R, then $x_2 = \frac{4}{3}\frac{R}{\lambda_2}$ and

$$D = \frac{\lambda_1 + P\lambda_2}{3(1+P)} - \frac{(\lambda_1-\lambda_2)^2}{3\lambda_1(1+P)}\left[1 - \frac{1}{1+\frac{1}{x_1}\left\{1 - \frac{8}{9x_2^2} + \frac{8}{9}\cdot\frac{1+\frac{3}{2}x_2}{x_2^2}e^{-\frac{3}{2}x_2}\right\}}\right]. \tag{19}$$

When the slug dimensions are much larger than the mean free path of neutrons in the filler, we can again use the elementary theory of diffusion. For the effective coefficient of diffusion (in a medium with spheres) we obtain, in this case,

$$D = \frac{\lambda_t}{3}\cdot\frac{1-2\frac{\omega}{W}\cdot\frac{\lambda_1-\lambda_2}{2\lambda_1+\lambda_2}}{1+\frac{\omega}{W}\cdot\frac{\lambda_1-\lambda_2}{2\lambda_1+\lambda_2}}. \tag{20}$$

Here ω is the volume of the slug; W is the volume of the cell of the heterogeneous medium. The equation has been obtained for the Wigner-Zeitz cell, but it is valid for small values of ω/W (for a medium with any distribution of slugs)

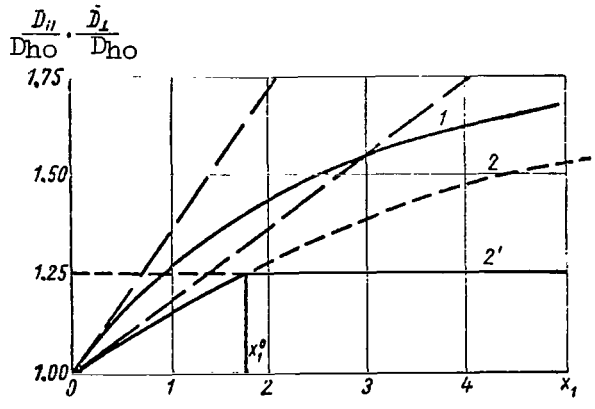

Figure 2. Coefficients of longitudinal and transverse diffusion in heterogeneous medium with circular cylindrical rods (λ_1 = 0.423 cm; λ_2 = 2.75 cm; p = 0.65); 1, $D_{\parallel}/D_{ho}$; 2, $D'_{\perp}/D_{ho}$; 2', $D_{\perp}^{diff}/D_{ho}$.

with a degree of accuracy up to terms ω/W inclusive (ref. 8). For a medium with lattices of high symmetry the equation is valid with a high degree of accuracy.

Equations (10)-(20) are obtained for heterogeneous media without absorption. It can be shown, however, that when conditions $\Sigma_{a1}/\Sigma_1 \ll 1$ and $\Sigma_{a2}/\Sigma_2 \ll 1$ are satisfied, the average flow, as before, will be approximately proportional to the gradient of the average flux and the coefficient of proportionality, i.e., the effective diffusion coefficient will be described by the equations obtained previously. Then the average flux may be expressed by means of the conventional wave equation

$$D\Delta\Psi - \Sigma_a\Psi = 0,$$

where $\Sigma_a = \frac{\Sigma_{a2}\omega + \Sigma_{a1}(W-\omega)}{W}$ is the averaged cross section of absorption.

The quantity $L = \sqrt{D/\Sigma_a}$ plays the role of the effective diffusion length.

By making use of equation (10) for the effective coefficient of longitudinal diffusion in a medium with cylindrical slugs, we obtain the following expression for the quantity $\eta = \frac{L_2}{L_0^2}$ $\left(L_0^2 = \frac{\lambda_1\lambda_{a1}}{3}\right)$

$$\eta = \frac{3D_{\parallel}(1+P)\Sigma_{a1}}{(\Sigma_{a1}+\Sigma_{a2}P)\lambda_1} = \frac{1}{1+P\frac{\Sigma_{a2}}{\Sigma_{a1}}}\left\{1+P\frac{\lambda_2}{\lambda_1}-\frac{(\lambda_1-\lambda_2)^2}{\lambda_1^2}[1-f_{\parallel}(x_1,x_2)]\right\}. \qquad (21)$$

When $\lambda_2 = \infty$ (a medium with the hollow channels), the latter expression /130

takes the form

$$\eta = (1 + P)^2 + \frac{3}{2} Q \frac{x_1 P^2}{2}, \tag{22}$$

i.e., it agrees with the results of Fursov (refs. 6 and 9) and Behrens (ref. 3).

For the transverse diffusion of neutrons in a medium with cylindrical slugs and for diffusion in a medium with spherical slugs we should utilize equations (16) and (18) when the dimensions of the slugs are small, or (17) and (20) when the slugs are large. In this case

$$\frac{L_{\perp}'^2}{L_0^2} = \frac{1}{1 + P \frac{\Sigma_{a2}}{\Sigma_{a1}}} \left\{ 1 + P \frac{\lambda_2}{\lambda_1} - \frac{(\lambda_1 - \lambda_2)^2}{\lambda_1^2} [1 - f_{\perp}(x_1 x_2)] \right\}.$$

When $\lambda_2 = \infty$,

$$\frac{L'^2}{L_0^2} = (1 + P)^2 + \frac{3}{4} Q \frac{x_1 P^2}{2} \text{ for cylinders}$$

and

$$\frac{L_m^2}{L_0^2} = (1 + P)^2 + Q \frac{x_1 P^2}{2} \text{ for spheres.}$$

A Long Hollow Channel in the Shielding

None of the preceding results is applicable to the case of practical interest concerning the propagation of neutrons in a shielding with a long hollow channel. Indeed, let us assume that the medium which fills the semispace $z > 0$ has an infinite cylindrical channel and that an infinite plane source of monoenergetic neutrons is placed in the plane $z = 0$. Near the channel the distribution of neutrons which have not undergone collision will then be different than that in a continuous medium, and the introduction of λ_{eff} is not expedient. Frequently it is also meaningless to introduce the concept of the effective coefficient of diffusion for the scattered neutrons, because in order that the Wick law be valid (i.e., that the flow through some cross section be proportional to the gradient of neutron density at this place) it is necessary that the contribution to the stream is determined by neutrons which have undergone their last collision close to the considered cross section, whereas the contribution from the remote regions is small.

When we have a hollow channel this condition is usually not satisfied. Indeed, neutrons from the very remote regions can reach the section under consideration through the channel without collisions. If we have a plane infinite slit, the concepts "effective coefficient of diffusion" and "effective diffusion length" are meaningless at any distance from the source.

In the case of a hollow circular cylindrical channel the situation is somewhat different. There is a region near the source whose dimensions are of the

order of the free path or of the channel diameter, where it is difficult to make any statement concerning the distribution of neutron density. However, if the neutron absorption is relatively weak and the neutron diffusion length in a continuous medium is much larger than the channel diameter, then behind this region there is another region in which the flow through the transverse cross section of the channel is approximately proportional to the gradient of neutron density. The dimensions of this region are determined by the following conditions (ref. 6)

$$\left(\frac{d}{z_1}\right)^2 \ll 1 \text{ and } \frac{dL^2}{z_2^2} e^{z_2/L} \ll 1,$$

where d is the channel diameter; L is the effective diffusion length; z_1 is the coordinate which characterizes the beginning of the region, and z_2 characterizes the end of the region.

Beyond this point the Wick law is again violated. Qualitatively the picture is explained in the following manner. At any cross section of the channel the value of the stream is determined by neutrons which arrive there directly from the source and by neutrons from the walls of the channel. The stream component due to the first contribution decreases, being inversely proportional to the square of the distance from the source. The second component is proportional to neutron density close to the element of area on the surface of the channel and is inversely proportional to the cube of the distance from this area to the cross section under consideration. /131

In the first region the contribution made by neutrons from the source and that by neutrons scattered by the walls of the channel are comparable. In the second region the contribution by neutrons scattered by channel walls is more prevalent, because the diffusion length is sufficiently large and the basic contribution is made by the close regions. In this region the neutron density increases as z increases in approximately an exponential manner with an "effective diffusion length" given by equation (22). As the distance from the source increases, because the exponential undergoes a greater variation than any other algebraic function, the regions remote from the considered cross section produce an ever-increasing contribution to the stream. Wick's law is violated, the neutron density is not described by the wave equation even approximately and its variation is no longer exponential.

Let us determine the stream of neutrons through the transverse cross section of the channel situated at a sufficiently great distance from the source. We shall assume that the neutron density in the substance along the length of the channel is described by the same exponential which, strictly speaking, furnishes correct values for the density only along the second region. Then we shall have the following stream through a unit cross section

$$I = \int_0^{2\pi} \int_0^{\pi} \int_0^{\infty} \frac{e^{z/L} e^{-r'/\lambda} \cos\vartheta \sin\vartheta \, d\vartheta \, d\varphi \, dr}{4\pi\lambda}$$

(coordinate z is measured from the cross section under consideration).

Carrying out integration over r and evaluating the integral over ϑ, we obtain

$$I \approx \frac{d^2 L}{8z^3} \Phi_0; \tag{23}$$

where Φ_0 is the value of the flux at the beginning of the channel.

We can see from the calculations that the stream through the cross sections of the channel which are remote from the source, due to neutrons from the channel walls, is determined by the region which adjoins the source, and the dimensions of this region are of the order of L. Therefore the error introduced by assuming that the neutron density distribution is exponential along the entire length of the channel is insignificant. Indeed, the deviation from the exponential law in the immediate vicinity of the source will produce an insignificant effect because this region is small. At the same time we neglected the contribution of the third region to the stream.

However, at this point we may have some doubts. Indeed, we can neglect the contribution only if the neutron density varies exponentially. Actually along the third region the density varies at a much slower rate. However, the contribution to the stream from this region does not depend directly on neutron density, but, roughly speaking, depends on the gradient of the density, which actually is much smaller than when we have an exponential variation in neutron density. Consequently we have more reasons for neglecting the contribution of the third region to the stream.

The neutrons flying from the bottom of the channel will also make a contribution to the total stream through the considered cross section. This stream will be equal to

$$I \approx \frac{\pi d^2}{4} \Phi_0 \frac{d^2}{16z^3} \left(1 + \frac{2L}{z}\right). \tag{24}$$

Equation (24) may be used to evaluate the stream (which in this case is approximately equal to the flux) of neutrons at the output of a long channel, starting with the boundary of the active zone and passing through the shielding. The situation that equation (23) is obtained for a channel in a semi-infinite medium is not significant, because the stream is determined by the magnitude of neutron density at the initial region of the channel.

If it is necessary to evaluate the stream at the output of the long channel passing through the shielding and also penetrating the active zone, the component

in equation (24) due to neutrons from the bottom of the channel should be replaced with the stream produced by neutrons flowing out of the channel walls in the active zone. Let us assume that the neutron density along the channel part of length B, which passes through the active zone, is constant. Then by carrying out calculation steps analogous to those used to deduce (23), we obtain /132

$$I_{a.z} \approx \frac{\pi d^2}{4} \Phi_0 \frac{d^2}{16} \left[\frac{1}{z^2} - \frac{1}{(z+B)^2} \right]$$

(a.z = a z = active zone)

and when B << z

$$I_{a.z} \approx \frac{\pi d^2}{4} \Phi_0 \frac{d^2 B}{8z^3}$$

and the total stream

$$I = \frac{\pi d^2}{4} \Phi_0 \frac{d^2 (B+L)}{8z^3}.$$

REFERENCES

1. Case, K. M., Hoffmann, F. and Placzek, G. Introduction to the Theory of Neutron Diffusion. Vol. 1, Los Alamos, 1953.

2. Laletin, N. I. Atomnaya Energiya, Vol. 10, 267, 1961.

3. Behrens, D. J. Proc. Phys. Soc. A., Vol. 62, 607, 1949.

4. Shielding of Nuclear Reactors. Edited by T. Rockwell (Zashchita yadernykh reaktorov. Pod red. T. Rokvella). Moscow, Izd-vo I. L., 1958.

5. Price, B., Horton, C. and Spinney, K. Shielding Nuclear Reactors (Zashchita yadernykh reaktorov). Moscow, Izd-vo I. L., 1959.

6. Laletin, M. I. Atomnaya Energiya, Vol. 7, 18, 1959.

7. Shevelev, Ya. V. Atomnaya Energiya, Vol. 11, 224, 1957.

8. Galanin, A. B. Atomnaya Energiya, Vol. 9, 89, 1960.

9. Zhezherun, I. F. Atomnaya Energiya, Vol. 7, 424, 1959.

SELECTION OF A SYSTEM OF FUNCTIONS FOR THE EXCITATION OF LEVELS DURING ELASTIC SCATTERING OF NEUTRONS BY IRON, NICKEL AND NIOBIUM NUCLEI

D. L. Broder, A. I. Lashuk, I. P. Sadokhin and A. P. Suvorov

A knowledge of the cross section of inelastic scattering of fast /132 neutrons with the excitation of different nuclear levels is extremely important for the calculation of fast reactors and for biological shielding and is of great interest from the standpoint of nuclear theory. This is responsible for the large quantity of experimental works devoted to the study of both the total cross section of neutron inelastic scattering by iron nuclei as well as of the differential cross sections of excitation for different levels. A somewhat smaller number of works is concerned with the study of the excitation cross sections for the nickel and niobium nuclei levels.

Measurements are usually conducted by two methods. The first of these involves the measurement of cross sections by the detection of neutrons. The second consists of studying the spectra of γ-rays which form due to the decay of the excited states produced by the inelastic scattering of neutrons.

Unfortunately to date there has not been a sufficiently exhaustive analysis made of all available data concerning iron and nickel nuclei. The analysis of these data shows that they are far from complete and in many cases do not make it possible to obtain single values for the cross sections of interest. To obtain a clearer picture we carried out experiments to study the cross section of inelastic scattering of neutrons by levels of iron, nickel and niobium nuclei, involving the measurement of the spectra of γ-quanta formed as a result of the decay of the excited states of these nuclei.

In order to obtain monochromatic neutrons in the energy range of 0.8-2.5 MeV we utilized the reaction T^3 (p, n) He^3, which was achieved by means of an electrostatic generator of the Van de Graaf type in the energy range 2.5-4 MeV and the reaction D (d, n) He^3, obtained by means of a cascade accelerator.

The spectrum of the γ-rays was investigated by means of a scintillation γ-spectrometer. The detector consisted of a NaJ (Tl) crystal with dimensions 40 x 40 mm, used with a type FEU-13 photomultiplier. The pulses were analyzed /133 with a 128-channel amplitude analyzer. The neutrons falling on the scattering element were monitored by an all-wave boron counter and a U^{235} fission chamber.

The purpose of the experiment was not to resolve the resonances in the cross section of inelastic scattering produced by the presence of the levels associated with the composite nucleus. Therefore in order to increase the intensity of the neutron source the tritium and deuterium targets had a thickness of 30-50 keV.

The geometry of the experiment was annular (ref. 1).

Iron

In a natural mixture of iron isotopes the most prevalent one of Fe^{56}-91.68 percent; 5.84 percent is represented by Fe^{54}; 2.17 percent by Fe^{57} and 0.31 percent by Fe^{58}. It should be pointed out that the cross sections of inelastic scattering vary rather smoothly from one isotope to another. This simplifies the analysis of experimental results obtained for the natural mixture of isotopes, because the addition of an isotope, which is not too prevalent, to the test sample cannot produce a sudden increase in the output of γ-quanta. In our experiments the effects produced by isotopes with a prevalence of less than 2-3 percent were practically undetected. Therefore, in the case of iron we can expect a detectable contribution to the reading of the detector only because of the inelastic processes associated with the Fe^{54} and Fe^{56} nuclei.

Figure 1 shows the results of measuring the magnitudes of the γ-quanta output cross sections during the inelastic scattering of neutrons as a function of their energy. When the energy of neutrons was 4 MeV, γ-quanta of the following energies were detected: 0.84, 1.02, 1.23, 1.41, 1.81, 2.15 and 2.6 MeV. The analysis of the decay scheme of the excited states of Fe^{56} and Fe^{54} nuclei (ref. 2) has shown that all γ-lines, except 1.41 MeV, are due to the inelastic scattering of neutrons by Fe^{56} nuclei. The γ-quanta with an energy of 1.41 MeV occur as a result of the excitation of the first level of Fe^{54} by the neutrons. In the experiment these quanta are detected only when neutrons with energies greater than 1.41 MeV interact with the iron nuclei and cannot be explained by the cascade transitions in the Fe^{56} nucleus. Thus the cross sections for the output of γ-quanta with energy at 1.41 MeV (fig. 1) correspond to the excitation function for this level of the Fe^{54} nucleus in a natural mixture of isotopes or to cascade transitions from higher levels through the level of 1.41 MeV, when the energy of neutrons is greater than the energy associated with the second level of this nucleus.

Gamma-quanta with an energy of 1.23 MeV are formed during the excitation of the 2.08 MeV level and during the cascade transition through the 0.84 MeV level to the basic state of the nucleus. When the energy of neutrons is greater than 3.26 MeV it is possible to have an addition of γ-quanta with an energy of 1.18

and 1.3 MeV, which corresponds to the excitation of the 3.26 and 3.38 MeV levels. We identify the cross section for the formation of γ-quanta with energy 1.23 MeV with the excitation function for the 2.08 MeV level, because the direct transition into the basic state is apparently improbable because of the large difference in the spins of the excited (4+) state and basic (0+) state.

The γ-quanta with energies of 1.81 MeV can be clearly associated with the excitation of the 2.62 MeV level and with its cascade decay through the 0.84 MeV level. The output cross section of γ-quanta with an energy of 1.81 MeV determines the excitation cross section for the 2.62 MeV level of the Fe^{56} nucleus.

In experiments on β-decay conducted earlier no direct transition from the 2.08 MeV level to the basic state was detected. Therefore γ-quanta with an energy of 2.15 MeV detected by us must correspond to the decay of the excited 3.02 MeV state of the Fe^{56} nucleus through the 0.84 MeV level to the basic state. The experimental data in reference 3 confirm this conclusion, although the earlier work of the same author (ref. 4) contains contradictory indications. Our measurements did not detect the formation of γ-quanta with an energy of 2.15 MeV when the neutron energy was less than 3.5 MeV. Thus the cross sections for the output of γ-quanta with an energy of 2.15 MeV represent excitation cross sections for the 3.02 MeV level of the Fe^{56} nucleus.

Gamma-quanta with an energy of 2.6 MeV are not detected when iron /135 nuclei interact with neutrons whose energy is less than 3.7 MeV. This points to the fact that γ-quanta with an energy of 2.6 MeV are produced by the excitation of the 3.44 MeV level.

These considerations show that the processes of inelastic neutron scattering by the Fe^{56} nuclei are always associated with the radiation of γ-quanta with an energy of 0.84 MeV. The γ-quanta with an energy of 0.84 MeV, when the neutron energy is as high as 2.08 MeV, are due only to the direct transitions of the Fe^{56} nucleus into the basic state from the excited state corresponding to the first 0.845 MeV level. When the neutron energy is greater than 2.08 MeV, the presence of γ-quanta with an energy of 0.84 MeV is due to the direct transition from the first level into the basic state as well as to the cascade transitions through the first level from a higher level of the Fe^{56} nucleus. Other transitions are possible, but apparently have small probabilities and were not detected by us. Thus, direct transition with the radiation of γ-quanta with energies of 3.02 and 3.44 MeV could have been detected by us when the output cross sections of the γ-quanta with this energy were greater than 30 mbarn.

In view of this the output cross section for γ-quanta with energies of 0.84 MeV simultaneously corresponds to the total cross section of inelastic scattering by the Fe^{56} nuclei in the natural mixture of isotopes. The possible decrease in the value of this cross section, caused by neglecting the direct transitions in

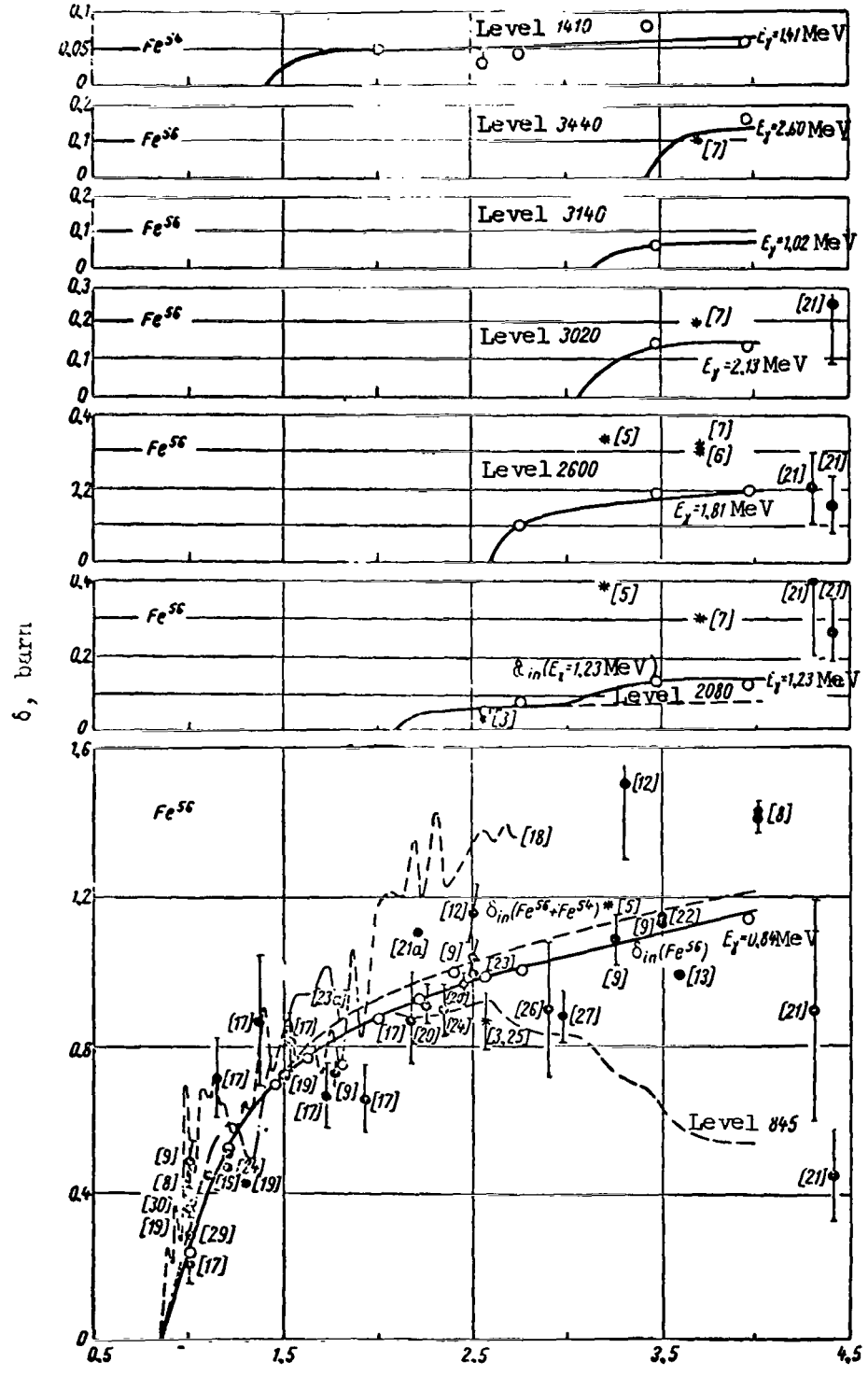

Figure 1. Excitation function for iron isotope levels during inelastic scattering of neutrons.

our evaluation, does not exceed 150 mbarn with a neutron energy of 3.5-4 MeV. The total cross section of inelastic scattering by the natural mixture of isotopes is obviously equal to the sum of output cross sections of γ-quanta with energies of 1.41 and 0.84 MeV.

The excitation function for the 0.84 MeV level is equal to the magnitude of the γ-quanta output with energy of 0.84 MeV after subtracting the excitation functions for levels 2.08, 2.62, 3.02 and 3.44 MeV. The total cross section for inelastic scattering and the excitation function for the 0.84 MeV level is shown in figure 1 by broken lines. This figure also shows the measurement results presented in the published works. The small solid circles in the figure indicate cross sections obtained in measurements involving the detection of secondary neutrons, and the crosses show measurements obtained from the output of γ-quanta. The small light circles indicate the results of our measurements. As we can see from the figure the results of the present work on the total cross section agree relatively well with the results for the total cross sections of inelastic scattering by a mixture of isotopes obtained from the detection of secondary neutrons, and the results on the output of γ-quanta with energies of 0.84 MeV agree with the data from similar investigations. An exception is represented by the data of references 5 and 6. In these reports the output cross sections of γ-quanta with energies 1.23 and 1.81 MeV, measured, respectively, at energies of 3.2 and 3.7 MeV, are greater than those in our data and are close to 0.3-0.4 barn.

Our discussions do not consider reference 7, because the data in this work do not agree with any of the available experimental results. Thus, according to the results of reference 7, the output cross section of γ-quanta with energies of 0.84 MeV for neutrons with energies of 3.4 MeV is equal to 2.26 barn and remains large for large energies.

One of the sources of information on the excitation functions of individual levels of the nucleus target during the inelastic scattering of neutrons is provided by experiments which measure the cross sections for leading threshold detectors (refs. 8-10) below the threshold of sensitivity. Unfortunately there are no ideal threshold detectors whose sensitivity would represent a uniform rectangular step. All existing threshold detectors have a rather indefinite threshold, and the very concept of this threshold must be thoroughly determined in experiments of this type. When the nature of detector sensitivity variation with energy is known, data on the cross sections for leading under the detector sensitivity threshold, which are some integral characteristics of the excitation function, may be used to verify the constructed system of excitation functions for individual levels. Unfortunately most works do not present data on the variation in the sensitivity of threshold detectors with energy, but present data only on the values of the thresholds obtained by extrapolating the sensitivity of detectors to zero. The use of specific thresholds obtained in this manner gives us low values for the excitation functions of low levels. /136

If we use the data on the sensitivity of a detector (ref. 11), the cross section for leading under a threshold of 2.6 MeV, when E_0 = 4 MeV, computed on the basis of the proposed system of excitation functions (fig. 1), coincides with values obtained experimentally by means of a proportional counter (ref. 8) within

the limits of experimental error. The experimental value is 1.30 ± 0.07 barn, and the computed value is 1.24 barn.

A series of reports presents the variation of the cross section for leading under the sensitivity of detector threshold, based on threshold reactions of the (n, p), (n, α), (n, 2n) type. For example in reference 12, a P^{31} (n, p) Si^{31} detector is used for neutron energy of 2.5 MeV, and a Al^{27} (n, p) Mg^{27} detector is used for neutron energies of 3.3 and 4.1 MeV. In reference 13, an S^{32} (n, p) P^{32} detector is used for neutron energy of 3.6 MeV. This is correct only when the given detector is not sensitive to neutrons which are inelastically scattered with the excitation of low levels in the target nucleus. Otherwise, in some cases, the total cross section of inelastic scattering may differ from the cross section for leading under the threshold by a substantial quantity. For example, the measured value of the discharge cross section in reference 13 differs by 25 percent from the value of the total cross section for inelastic scattering.

Nickel

Gamma-quanta of the following energies are detected in the spectra of γ-rays occurring during the inelastic scattering of neutrons with an energy of 3.0 MeV in nickel nuclei: 0.65, 0.82, 1.00, 1.39, 1.96 and 2.17 MeV. In the present work γ-quanta with an energy of 0.86, 1.00, 1.16, 1.33, 1.45, 1.80 and 2.20 MeV have been detected for neutron energy of 3.5 MeV.

We can see from references 2 and 15 that the system of nickel nuclei levels is complex, and the interpretation of the results which have been obtained is rather difficult. The problem of analyzing the results is further complicated by the fact that nickel has two isotopes, Ni^{58}-67.76 percent and Ni^{60}-26.16 percent, which are prevalent to a rather high degree. Based on references 2 and 15 we made an effort to interpret the individual transitions and determine the value of the cross section for the excitation of levels.

Figures 2-4 show the results of our work as well as the data of other authors for cross sections of inelastic neutron scattering by nickel nuclei.

Gamma-quanta with an energy of 1.33 MeV correspond to the decay of the 1.332 MeV level of Ni^{60} nuclei. The output cross section for γ-quanta of this energy is the cross section of excitation for the first level of the Ni^{60} nuclei (1.332 MeV) up to an energy of 2.2 MeV, because when the neutron energy is increased there is also a probability that the 2.159 and 2.285 MeV levels will be excited. The resolution of the spectrometer did not make it possible for us to separate the γ-quanta which occur when each of these levels is excited. Therefore γ-quanta with an energy of 2.2 and 0.86 MeV, which are due to the excitation of

these levels, correspond to the transition into the basic state or to the cascade through the 1.332 MeV level. The fact that the γ-line of 0.86 MeV is due to the excitation of the second and third Ni^{60} levels is also confirmed by the fact that γ-quanta with an energy of 0.86 MeV specifically occur when the neutron energy is increased above 2.2 MeV. The sum of the output cross sections for the γ-quanta with an energy of 0.86 and 2.2 MeV determines the cross section of inelastic scattering with the excitation of the 2.159 and 2.285 MeV levels.

If we subtract the output cross sections of γ-quanta with an energy of 0.86 MeV from the output cross sections of γ-quanta with an energy of 1.33 MeV, it becomes possible to compute the excitation cross sections of the 1.332 MeV level up to an energy of 2.624 MeV. In reference 5 the excitation of energy levels of 2.624 MeV was observed from the output of γ-quanta with an energy of 2.66 MeV. Another possibility for the decay of this state is the cascade transition through the 1.332 MeV level with the emission of 2 quanta with an energy of 1.3 MeV. When the neutron energy is above 2.77 MeV a possibility occurs for the excitation of the 2.772 MeV level in Ni^{58} nuclei and the decay of this state through the first Ni^{58} level of 1.452 MeV. This also leads to the formation of quanta with an energy of 1.3 MeV. Beyond this, up to an energy of 3.1-3.2 MeV there are no versions for the decay of both nickel nuclei levels with /137
the emission of γ-quanta with an energy of 1.33 MeV. Therefore, in determining the excitation cross section of the 1.33 MeV level up to an energy of 3.1 MeV we must establish the portion due to the excitation cross sections of 2.624 and 2.772 MeV levels in the output cross sections of γ-quanta with an energy of 1.33 MeV.

Let us evaluate the excitation cross section for the 2.772 MeV level. In our experiments we did not observe γ-quanta with this energy which points to the absence or low probability of the direct transition. If this is true, the increase in the output cross section of quanta with an energy of 1.45 MeV in the energy range 2.6-3.03 MeV may be due to the excitation of the 2.772 MeV level. This evaluation gives a cross section value of approximately 40 mbarn when the neutron energy is 3.1 MeV. The increment in the output cross section of γ-quanta with an energy of 1.33 MeV when the neutron energy is from 2.62 to 3.1 MeV is 75 mbarn. A cross section of 40 mbarn determines the excitation cross sections for the 2.772 MeV level of Ni^{58} nuclei, and the portion corresponding to the excitation of the 2.624 MeV level of Ni^{60} nuclei is 35 mbarn. In this manner we determine the excitation functions for the 2.624 MeV (Ni^{60}) and 2.772 MeV (Ni^{58}) levels.

After subtracting the output cross sections of γ-quanta with an /138
energy of 1.33 MeV, which were formed due to the decay of the 2.624, 2.772, 2.159 and 2.285 MeV excited states, from the total output cross section of γ-quanta with this energy, we obtain the cross section residue. We broke down this level into the cross section part which refers to the cross section for the excitation of the 1.332 MeV level and into the cross section for the excitation of levels with energies greater than 3 MeV, whose decay may lead to the formation

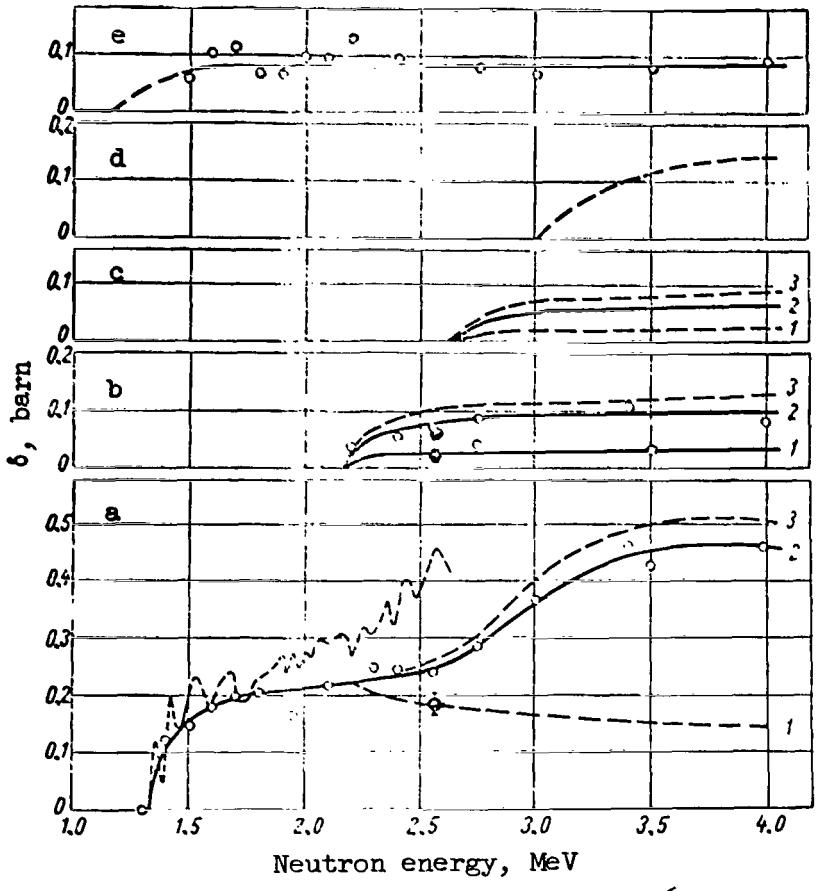

Figure 2. Excitation functions for Ni^{60} energy levels: (●, results of work described in reference 3; – – – – – (left, in fig. 2a) results of work described in reference 18); ○, results of present work); a: 1, excitation cross section for 1.33 MeV level; 2, output cross section of γ-quanta with energy of 1.33 MeV; 3, total excitation cross section for levels of Ni^{60} nuclei; b: 1, output cross section of γ-quanta with energy of 2.2 MeV; 2, output cross section of γ-quanta with energy of 0.86 MeV; 3, excitation cross section for 2.16 and 2.28 MeV levels; c: 1, excitation cross section for 2.624 MeV level; 2, output cross section of γ-quanta with energy of 2.66 MeV; 3, output cross section of γ-quanta with energy of 1.3 MeV due to excitation of 2.624 MeV level; d: excitation cross section of levels with energy greater than 3 MeV; e: output cross section of γ-quanta with energy of 1.16 MeV.

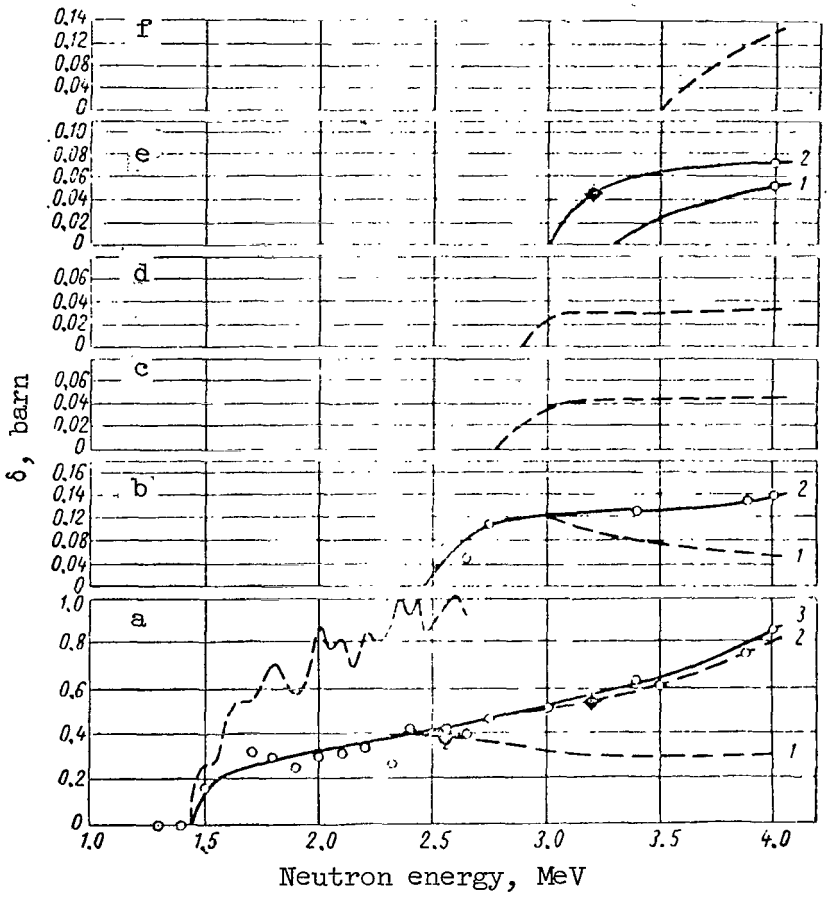

Figure 3. Excitation functions for energy levels of Ni^{58} nuclei: – – – – –, results of work reported in reference 18, left side of; ●, results of work reported in reference 3; -⊕-, results of work reported in reference 5; O, results of present work; a: 1, excitation cross section for 1.452 MeV level; 2, total excitation cross section for levels of Ni^{58} nuclei; 3, output cross section of γ-quanta with energy of 1.45 MeV; b: 1, excitation cross section for the 2.455 MeV level; 2, output cross section of γ-quanta with energy of 1 MeV; c: excitation cross section for 2.772 MeV level; d: excitation cross section for 2.899 and 2.939 MeV levels; e: 1, output cross section of γ-quanta with energy of 1.8 MeV; 2, excitation cross section for 3.035 MeV level; f: excitation cross section for levels with energy greater than 3.5 MeV.

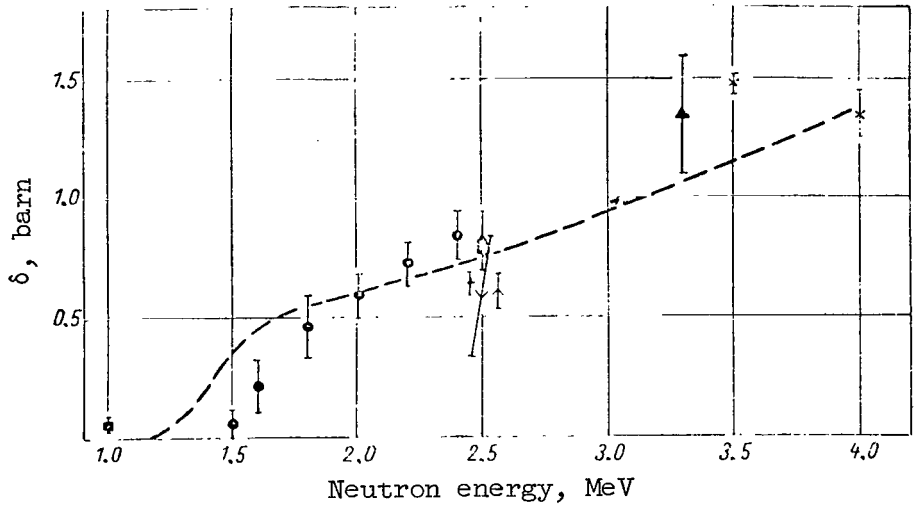

Figure 4. Cross section for inelastic scattering of neutrons by natural mixture of nickel isotopes: – – – – –, results of present work; Λ, reported in reference 3; ■, results of work reported in reference 9; ▲, results of work reported in reference 12; X, results of work reported in reference 19; +, results of work reported in reference 20; ●, results of work reported in reference 17; V, results of work reported in reference 21a.

of quanta with an energy of 1.33 MeV. Figure 2 shows some of the details associated with this analysis.

The total cross section of inelastic scattering by the Ni^{60} nuclei was obtained as the sum of the excitation cross sections for levels 1.332, 2.159, 2.285 and 2.624 MeV and levels above 3 MeV which were not resolved in our measurements.

The analysis for Ni^{58} nuclei was carried out in a similar manner. The excitation of the second 2.458 MeV level leads to the emission of γ-quanta with an energy of 1 and 1.45 MeV. Gamma-quanta with an energy of 1 MeV may also occur during the decay of the 3.035 MeV level as a result of cascade transitions with the radiation of quanta with an energy of 0.6, 1.0 and 1.45 MeV, because γ-quanta with an energy of 3.03 MeV in the spectra of γ-rays were not detected. /139
The output cross section of γ-quanta with an energy of 0.6 MeV (ref. 5) determines the excitation cross section of the 3.035 MeV level, and the difference between the output cross sections of γ-quanta with an energy of 1 MeV and the output cross section of quanta with an energy of 0.6 MeV determines the excitation cross section for the 2.458 MeV level.

The excitation cross section for the 2.772 MeV level is evaluated above.

The 3.260 MeV state after excitation apparently is capable of undergoing a cascade decay with the radiation of quanta with energies of 1.8 and 1.45 MeV. Thus the output cross section of quanta with an energy of 1.8 MeV, which has been measured by us, corresponds to the excitation of the 3.26 MeV level. Here we do not consider the possibility for the cascade decay of the 3.260 MeV state through the 2.458 and 1.452 MeV levels with the radiation of γ-quanta of energy 0.8; 1.0, and 1.45 MeV.

The decay of the 2.899 and 2.939 MeV states is possible with the emission of two quanta with an energy of 1.45 MeV. The analysis and the establishment of excitation cross sections for these levels were carried out in the same manner as for the 2.624 MeV level.

Since the decay of the Ni^{58} excited states takes place through the first excited state--1.452 MeV (we did not detect γ-quanta corresponding to direct transitions from the excited states to the basic state), the subtraction of the sum of excitation cross sections for these levels from the output cross section of γ-quanta with energies of 1.45 MeV makes it possible to compute the excitation function of the 1.452 MeV level up to an energy of 3.418 MeV (the eighth level of Ni^{58} nuclei). If we assume that the excitation function in the energy range of 3.4-4.0 MeV is constant, we obtain the cross section residue which we attribute to the excitation of the Ni^{58} nuclei levels situated above 3.418 MeV.

The excitation functions for the individual Ni^{58} states and the total cross section of inelastic neutron scattering by Ni^{58} nuclei is shown in figure 3.

Due to inelastic scattering of neutrons, the Ni^{61} isotopes (with an abundance of 1.25 percent) and the Ni^{62} isotopes (with an abundance of 3.66 percent) may produce γ-quanta with an energy of 1.16 MeV, which are already detected when the neutron energy is 1.2 MeV.

The total cross section of neutron inelastic scattering by Ni^{58}, Ni^{60}, Ni^{61} and Ni^{62} nuclei is shown in figure 4. The values of the cross sections are given for a natural mixture of isotopes. The circles in the same figure represent the results of measuring the total cross section for inelastic scattering by nickel nuclei obtained from neutron measurements. As we can see from figure 4 our /140 results agree with data presented by other authors.

Niobium-93

Figure 5 shows the curves for the transverse output cross section of γ-quanta generated during the inelastic scattering of neutrons by Nb^{93} nuclei. According to reference 2, the Nb^{93} nuclei contained the following levels: 0.029, 0.765 and 0.986 MeV. Reference 16 presents a schematic for the levels of Nb^{93} nuclei and for the transverse output cross sections of γ-quanta with energies of 0.741, 0.809,

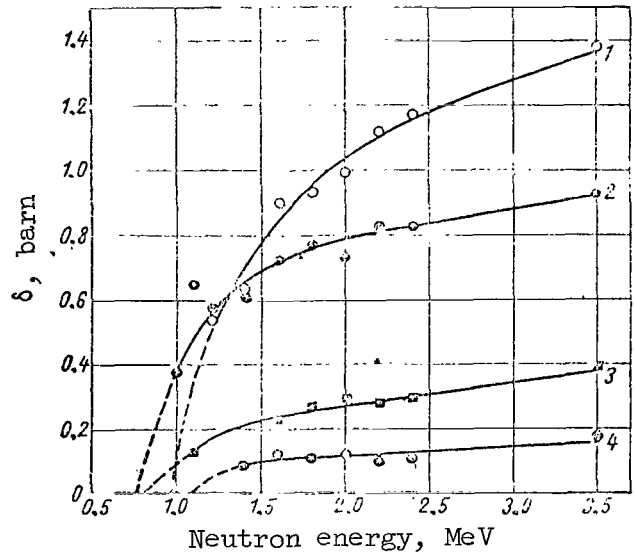

Figure 5. Transverse output cross section of γ-rays during inelastic scattering of neutrons by Nb^{93} nuclei, measured in present work: 1, output cross section for γ-quanta with energy of 0.96 MeV; 2, output cross section of γ-quanta with energy of 0.76 MeV; 3, output cross section of γ-quanta with energy of 0.81 MeV; 4, output cross section of γ-quanta with energy of 1.08 MeV.

0.953 and 1.08 MeV. In our measurements of γ-spectra, occurring during the inelastic scattering of neutrons with energy 3.5 MeV by niobium nuclei, we detected γ-quanta with the following energies: 0.76, 0.81, 0.96 and 1.08 MeV. In studying the output of γ-radiation as a function of energy associated with neutrons which bombard the scattering material, we established that the specified values of γ-quanta energies correspond to the excitation of Nb^{93} nuclei energy levels. Figure 6 presents the values of total cross sections for the inelastic scattering of neutrons by Nb^{93} nuclei obtained in the present work and in other works. The values of the total cross section are obtained by adding the cross sections for levels 0.760, 0.810, 0.960 and 1.08 MeV. As we can see from figure 6, the results of the present work agree sufficiently well with the results presented in references 17 and 16.

The authors express their gratitude to V. S. Stavinskiy for the valuable discussion of the results which have been obtained and to Ye. V. Shestopalov, V. S. Borisov, V. A. Romanov, G. N. Deryagin and A. P. Klimov for their participation in the experiment and for their assistance in the work.

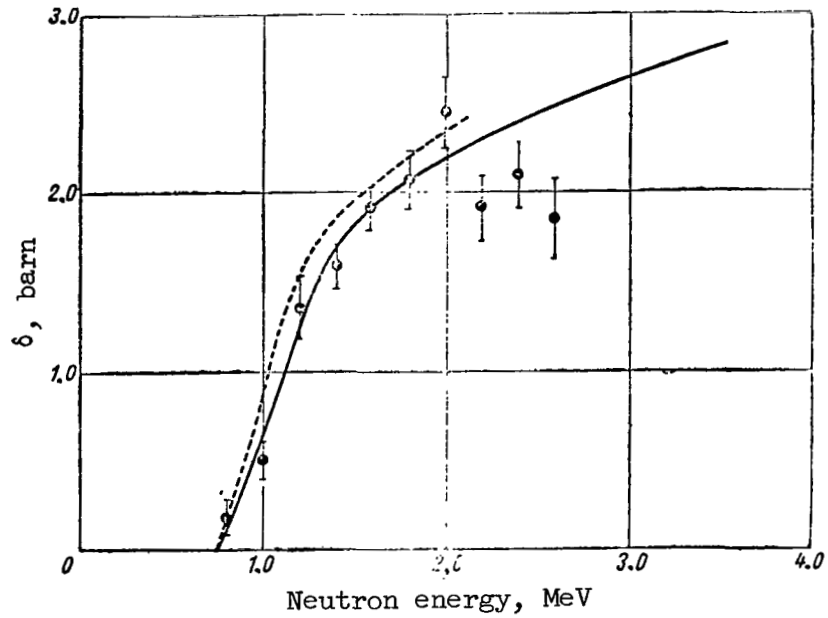

Figure 6. Total transverse cross section of inelastic scattering of neutrons by Nb^{93} nuclei. Solid line, results of present work; ⊥●⊥, results presented in reference 17; broken line, results presented in reference 16.

REFERENCES

1. Androsenko, A. L., Broder, D. L. and Lashuk, A. I. Atomnaya Energiya, Vol. 7, 268, 1959.

2. Dzhelepov, B. S. and Peker, L. K. Diagrams for the Decay of Radioactive Nuclei (Skhemy raspada radioaktivnykh yader). Moscow, Izd-vo AN SSSR, 1958.

3. Day, R. B. Phys. Rev., Vol. 102, 767, 1956.

4. --- Phys. Rev., Vol. 89, 908, 1953.

5. Scherrer, V. E., Allison, B. A. and Faust, W. R. Phys. Rev., Vol. 96, 386, 1954.

6. Rothman, M. A., Hans, H. S. and Mandeville, C. E. Phys. Rev., Vol. 100, 83, 1955.

7. Morgan, I. Phys. Rev., Vol. 103, 1031, 1956.

8. Beyster, J. R., Henkel, R. L. et al. Phys. Rev., Vol. 98, 1216, 1955.

9. Beyster, J. R., Walt, M. and Salmi, E. M. Phys. Rev., Vol. 104, 1319, 1956.

10. Barshall, H. H. et al. Phys. Rev., Vol. 72, 875, 881, 1947.

11. Walt, M. and Beyster, J. R. Phys. Rev., Vol. 98, 677, 1955.

12. Pasechnik, M. V. Inelastic Scattering of Fast Neutrons by Atomic Nuclei. Materials of the International Conference on the Peaceful Utilization of Atomic Energy. Geneva, 1955. Vol. 2, Physics. Experimental Reactors (Neuprugoye rasseyaniye bystrykh neytronov atomnymi yadrami. Materialy mezhdunarodnoy konferentsii po mirnomu ispol'zovaniyu atomnoy energii. Fizika. Eksperimental'nyye reaktory). Moscow, Fizmatgiz, 1958.

13. Batalin, V. O. and Kopytin, S. S. Ukr. fiz. zh., Vol. 3, 158, 1958.

14. Androsenko. A. L., Broder, V. L. and Lashuk, A. I. Atomnaya Energiya, Vol. 9, 403, 1960.

15. Paris, C. H. and Byechner, N. W. Bull. Am. Phys. Soc., Ser. II, Vol. 2, 61, 1957.

16. Nath, N., Rothman, M. A. et al. Nucl. Phys., Vol. 14, 78, 1959.

17. Abramov, A. I. Atomnaya Energiya, Vol. 12, 62, 1962.

18. Kiehn, R. M. and Goodman, C. Phys. Rev., Vol. 95, 389, 1954.

19. Hughes, D. J. and Harvey J. Neutron Cross Sections, BNL-325, 1958.

20. Cranberg, L. and Levin, T. S. Phys. Rev., Vol. 103, 343, 1956.

21. Jennings, B., Weddele, J. B. and Hellens, R. L. Phys. Rev., Vol. 95, 636, 1954; Vol. 99, 621, 1955.

21a. Landon, H. H., Elvin, A. J. et al. Phys. Rev., Vol. 112, 1192, 1958.

22. Taylor, H. L., Lönsjo, O. and Bonner, T. W. Phys. Rev., Vol. 100, 174, 1955.

23. Elliot, E., Hick, D. et al. Phys. Rev., Vol. 94, 144, 1954.

23a. Van Loef, J. J. and Lind, D. A. Phys. Rev., Vol. 101, 103, 1956.

24. Sal'nikov, O. A. Atomnaya Energiya, Vol. III, 106, 1957.

25. Day, R. B. and Walt, M. Phys. Rev., Vol. 117, 1330, 1960.

26. Popov, V. I. Atomnaya Energiya, Vol. III, 498, 1957.

27. Masanao, H. and Shoji, S. J. Phys. Soc. Japan, Vol. 14, 699, 1959.

28. Nath, N., Rothman, M. A. et al. Nucl. Phys., Vol. 13, 74, 1959.

29. Poze, Kh. R. and Glazkov, N. P. Zh. Eksperim. i teor. fiz., Vol. 30, 1017, 1956.

30. Walt, M. and Barshall, H. H. Phys. Rev., Vol. 93, 1062, 1954.

REPRESENTATION OF DECAY CURVES FOR FISSION FRAGMENTS BY FUNCTIONS OF A GIVEN FORM (e^{bt})

V. I. Lebedev, P. Ye. Stepanov

The following problem is solved in order to represent the decay curves of fission fragments obtained experimentally as a sum of functions of given form. /142

Let us assume that we have a function of two variables φ (b, t) determined in a rectangle $[b' \leq b \leq b''] [t_0 \leq t \leq T]$ which is sufficiently smooth and is such that any system of functions φ (b_j, t) for various b_j is linearly independent along the segment $[t_0, T]$. Let us assume that the function f (t) is assigned on the segment $[t_0, T]$ at the points $t = t_i$ (i = 0, 1, ..., N). Let us use $E = E(t_0, T, n, p_i, a_j, b_j)$ to designate the following expression

$$E = \left(\sum_{i=1}^{N} \left[f(t_i) - \sum_{k=1}^{n} a_k \varphi(b_k t_i)\right]^2 p_i\right)^{1/2}, \qquad (1)$$

where $p_i \geq 0$ are weights which are normalized in a specific manner and are selected in such a way as to satisfy the required nature of the approximation.

We formulate the following problem:

(1) it is required to find the minimum n ($n_1 \leq n$) for which min $E < \epsilon_1$, using given values $\epsilon_1 > 0$, n_1, a_k, b_k;

(2) it is required to find min E from a given n;

(3) it is required to find min E from the given values, n, b_k, a_k ($k = 1, 2, \ldots, n$)

The first and second problems are nonlinear, whereas the third is linear. If we use the designations

$$(d,\ g) = \sum_{i=0}^{N} d(t_i)\, g(t_i)\, p_i;$$

$$\|u\| = (u,\ u)^{1/2};\ \overline{b} = (b_1,\ b_2,\ \ldots,\ b_n);$$

$$r_n = f(t) - \sum_{k=1}^{n} a_k \varphi(b_k,\ t);$$

$$\operatorname{grad}_b E = \left(\frac{\partial E}{\partial b_1},\ \ldots,\ \frac{\partial E}{\partial b_n}\right),$$

the following equalities must be satisfied at the point of minimum

$$(r_n,\ \varphi(b_j)) = 0 \tag{2}$$

$$\left(r_n,\ \frac{\partial \varphi(b_j)}{\partial b}\right) = 0, \text{ where } j = 1,\ 2,\ \ldots,\ n. \tag{3}$$

The first and second problems are solved by applying a gradient iteration converging process with an automatic step selection and free of such limitations as: (1) a special selection of the function φ in the interval $[t_0, T]$ of points t_i, and of weight p_i and (2) the necessity of accurately assigning the function $f(t)$ for $t = t_i$ and the computation of second derivatives for the function $\varphi(b, t)$.

Let us assume that we have approximate values for $\overline{a}^q$, $\overline{b}^q$, E^q, $\operatorname{grad}_b E^q$, obtained during the q-th step of the investigated process (b^0 are assigned arbitrarily). We then obtain the following for computing $\overline{a}^{q+1}$, $\overline{b}^{q+1}$, E^{q+1}, $\operatorname{grad}_b E^{q+1}$

$$\overline{\Delta} b^q = -h^q A^q \frac{\operatorname{grad}_b E^q}{\|\operatorname{grad}_b E^q\|};$$

$$\overline{b}^{q+1} = \overline{b}^q + \overline{\Delta} b^q.$$

Using the assigned values of $\overline{b}^{q+1}$, and solving the linear system of equations (2), we find $\overline{a}^{q+1}$ and compute E^{q+1} $\operatorname{grad}_b E^{q+1}$. /143

To solve the second problem we take the required number of successive approximations until one of the following inequalities is satisfied

$$E^q < \varepsilon_1 \tag{4}$$

or

$$\|\operatorname{grad}_b E^q\| < \varepsilon_2. \tag{5}$$

The solution of the first problem is reduced to a successive solution of the second problem for $n = n_1,\ n_1 + 1 \ldots$ until inequality (4) is satisfied. The

transition from n to n + 1 is achieved when inequality (5) with $b_{n+1} = (1 + \frac{1}{n})$ b_n is satisfied. Matrix A is diagonal with positive elements on the principal diagonal. It serves to accelerate the decrease in E, first by providing a more rapid variation in those b_j whose increments do not change their sign and secondly by decreasing the variations of those b_j whose increments Δb_j change their sign. All p_j are determined by means of the equation

$$p_i = \frac{p'_i}{\sum_{i=0}^{N} f^2(t_i)\, p'_i},$$

where $p'_i \geq 0$ and p'_i may be taken as the quantity $p'_i = \min\left(\frac{1}{b^2(t_i)}, \frac{1}{\delta^2}\right)$ where $\delta > 0$ is an assigned number which makes it possible to assign the nature of the approximation. Quantity h^q varies in the following manner

$$h^q = \min\left(h_1^q, \frac{1000E^q}{\|\operatorname{grad}_b E^q\|}\right),$$

where

$$h_1^q = \begin{cases} ah^{q-1} & \text{when } E^q < (1 + 10^{-6})E^{q-1},\ (A^{q-1}\operatorname{grad}_b E^{q-1},\ \operatorname{grad}_b E^q) \geqslant 0; \\ \frac{h^{q-1}}{2} & \text{when } (A^{q-1}\operatorname{grad}_b E^{q-1},\ \operatorname{grad}_b E^q) < 0; \\ \frac{h^{q-1}}{4} & \text{when } (1 + 10^{-6})E^{q-1} \leqslant E^q < \alpha_1 E^{q-1}; \\ \frac{h^{q-1}}{4^p}, & \text{where p is thus selected until condition} \\ & E^{q+1} < a_i E^q \text{ is satisfied.} \end{cases}$$

Here $\alpha \geq 1$, $\alpha_1 \geq 1$ $(\alpha = \frac{9}{8},\ \alpha_1 = \frac{41}{40})$. Such a selection of α provides for an increase in h^q and consequently for the acceleration of the decrease in E, if $\bar{a}^q$, $\bar{b}^q$ are far removed from $\bar{a}$, $\bar{b}$ which give the minimum E; it also takes into account the errors when the values are rounded off; it provides for a decrease in E; it straightens out the trajectory for the variations in vector b and finally it provides for a decrease in h^q when the values of $\bar{a}^q$, $\bar{b}^q$ are close to $\bar{a}$, $\bar{b}$.

This algorithm was programmed on the M-20 electronic digital computer. This program was used to process the decay curves[1] for the U^{235} fission fragments.

[1] The graphs for the decay curves were taken from the journal Nuclear Science Engineering, Vol. 3, 726, 1958.

The curves were represented as the sum $\Sigma a_k e^{-b_k t}$ with an accuracy to 5 percent. The quantities t, n, and b in the computed examples varied within the following limits: $10^2 \leq t \leq 10^9$; $5 \leq n \leq 8$; $10^{-9} \leq b_k \leq 5 \cdot 10^{-3}$.

THE SPECTRUM OF GAMMA-RADIATION PRODUCED BY THE PRODUCTS OF URANIUM FISSION. EFFECTIVE ABSORPTION COEFFICIENTS FOR THE GAMMA-RAY SPECTRUM AND THEIR UTILIZATION FOR THE COMPUTATION OF SHIELDING

V. P. Il'in

Computation of Gamma-Radiation Spectrum Produced by Uranium Fission Products

The γ-radiation spectrum of uranium fission products was computed for /144 wide intervals of time associated with the irradiation of U in a reactor (T = 1-730 days) and its aging after irradiation (t = 1 sec-730 days).

The radiation intensity was normalized by computing it for 1 kW of heat liberation in the uranium irradiated in the reactor.

In this case the β-activity of the i-th isotope (fission product) is equal to

$$A_{\beta_i} = \frac{\omega_{1i} \cdot 3.2 \cdot 10^{13}}{3.7 \cdot 10^{10}} F(T, t) = 8.65 \cdot 10^2 \omega_{1i} F(T, t) \text{ Ci/kW} \quad (1)$$

where for the parent isotope

$$F(T, t) = (1 - e^{-\lambda_{1i} T}) e^{-\lambda_{1i} t}; \quad (2)$$

and for the decay product

$$F(T, t) = \frac{\lambda_{2i}}{\lambda_{2i} - \lambda_{1i}} (1 - e^{-\lambda_{1i} T}) e^{-\lambda_{1i} t} + \left(\frac{\omega_{2i\%}}{\omega_{1i\%}} - \frac{\lambda_{1i}}{\lambda_{2i} - \lambda_{1i}} \right) (1 - e^{-\lambda_{2i} T}) e^{-\lambda_{2i} t}. \quad (3)$$

The gamma-activity of the k-th line for the γ-spectrum of the i-th isotope is determined from its β activity

$$A_{\gamma_{i,k}} = A_{\beta_i} \alpha_k n_k \text{ g·equivalent of radium/kW} \quad (4)$$

where

$$\alpha_k = \frac{3{,}7\cdot 10^{10}\cdot 1{,}6\cdot 10^{-6}\cdot 3600}{4\pi\cdot 0{,}11\cdot 8{,}4\cdot 10^{3}} E_{\gamma_k}\gamma_k = \tag{5}$$

$$= 0.183\cdot 10^{5}\, E_{\gamma_k}\gamma_k \text{ g·equivalent radium/Ci·decay/quantum}$$

Equations (1-5) utilize the following designations and constants: ω_{1i}; ω_{2i} are the yields of the parent isotope and the independent yield of the decay product for each fission of U; $\omega_{1i\%}$ $\omega_{2i\%}$ are the percentage yields of the parent and decay product isotopes for each fission of U; λ_{1i}; λ_{2i} are the decay constants for the parent and the decay product isotopes, respectively; $E_{\gamma k}$ is the quanta energy of the k-th spectrum line, MeV; n_k is the number of quanta with energy $E_{\gamma k}$ for each β-decay; $n_{k\%}$ is the percentage yield of quanta with energy $E_{\gamma k}$ for each β-decay; γ_k is the absorption coefficient of γ-ray energy in air, corresponding to $E_{\gamma k}$, cm^{-1}; 3.2×10^{13} is the number of U fissions per second for 1 kW of heat liberation; 3.7×10^{10} is the number of decays per second for 1 Ci; 1.6×10^{-6} is the energy equivalent of 1 MeV, erg; 8.4×10^{3} is the γ-constant of Ra (the power of the dose produced by 1 g of Ra at a distance of 1 cm behind 0,5 mm of Pt, r/hr). Equations (1-5) were used to compute the γ-activity for each spectrum line associated with the γ-rays of the isotopes.

Details associated with the computations are as follows.

1. When $\lambda_2 > 20\lambda_1$, the calculations of activity for the decay product isotopes were carried out by means of equations (1) and (2), in which the substitution $\lambda_{1i} = \lambda_1$ was made. If $\lambda_1 > 20\lambda_2$, the genealogical association of isotopes was not considered.

2. In computing the accumulation of Xe^{135} it was assumed that it has a large cross section for the absorption of neutrons. For this purpose equation (3) was replaced with equation (3a)

$$F(T,t) = \frac{\lambda_{2i}}{\lambda_{2i}-\lambda_{1i}}(1-e^{-\lambda_{1i}T})e^{-\lambda_{1i}t} + \left(\frac{\omega_{2i\%}}{\omega_{1i\%}} - \frac{\lambda_{1i}}{\lambda'_{2i}-\lambda_{1i}}\right)\frac{\lambda_{2i}}{\lambda'_{2i}}(1-e^{-\lambda'_{2i}T})e^{-\lambda_{2i}t} + \tag{3a}$$

$$+ \frac{\lambda_{2i}\sigma_2\Phi}{(\lambda_{2i}-\lambda_{1i})(\lambda'_{2i}-\lambda_{1i})}e^{-\lambda_{1i}T}e^{-\lambda_{2i}t},$$

where $\lambda'_{21} = \lambda_{21} + \sigma_2\Phi$; $\sigma_2 = 3.5 \cdot 10^6$ barn is the effective absorption cross section of Xe^{135} neutrons; $\Phi = 10^{13}$ neutrons/cm·sec is the flux of neutrons which corresponds approximately to a heat liberation of 3 W/g by natural uranium (assumed arbitrarily). /146

The gamma-spectrum of U fission products is divided into 10 groups, and an effective energy value is selected for each of these groups. The average energy of the groups was selected so that it was equal to the energy of the most intense line, or in the case of competing lines it was close to the highest energy of these lines.

The total γ-activity of the uranium fission products for various values of T as a function of t is shown in figure 1. To make interpolation convenient, figure 2 shows the variation in the total γ-activity as a function of T.

Effective Absorption Coefficients of the Gamma-ray Spectrum and Their Utilization for the Computation of Shielding

In computing the shielding of γ-radiation it is convenient and expedient to utilize the effective absorption coefficients for a wide beam of γ-rays in the shielding material. It is particularly expedient to utilize the effective absorption coefficients of γ-rays in computing shielding against sources of complex geometric form.

The effective absorption coefficient takes into account the buildup of scattered radiation. For a wide monochromatic beam of γ-rays it may be computed by means of the following equation: /147

$$\mu_{eff} = \mu_0 \left(1 - \frac{\ln B}{\mu_0 \Delta}\right), \tag{6}$$

where μ_0 is the linear absorption for a narrow beam of γ-rays of given energy E_γ, cm^{-1}; Δ is the shielding thickness, cm; $B = B(\mu_0\Delta; E_\gamma)$ is the buildup factor for the scattered radiation during the attenuation of the wide γ-ray beam (it can be obtained from the data presented in the work of Fano, ref. 1).

A sufficient accuracy in the computation of shielding is retained when the effective absorption coefficients are utilized. This can be shown by means of an example. Let us assume that the dose power behind the shielding, due to an infinite linear source, is equal to

$$P_{\gamma} = \frac{\Gamma q_L}{R} \cdot 2F(\mu\Delta, B, \vartheta_0), \tag{7}$$

where $\Gamma = 2.3\ 10^6$ μR/sec cm^2/g·equivalent of Ra is a constant; q_L is the activity of 1 running cm of the source, g·equivalent of Ra/cm; R is the distance from the source in cm; $F(\mu_0\Delta, B, \vartheta_0) = \int_0^{\vartheta_0} B(\mu\Delta, \sec\vartheta)\, e^{-\mu\Delta \sec\vartheta}\, d\vartheta$ is the attenuation factor; μ is the linear absorption coefficient; ϑ is the angle of incidence for the rays falling on the shielding.

We can see from equation (7) that in order to evaluate the accuracy of the computations it is sufficient to compare the attenuation factors computed by various methods.

Table 2 presents the attenuation factors computed from data presented by Pibls concerning buildup factors $B_P(\vartheta)$ when the rays falling on the shielding are inclined, using a method which represents the buildup factor as a sum of two exponents (ref. 2) and also using the effective absorption coefficients obtained by means of equation (6). A comparison of the computation results with Pibls' data is carried out with a γ-quanta energy equal to 6 MeV and when the shielding material is iron.

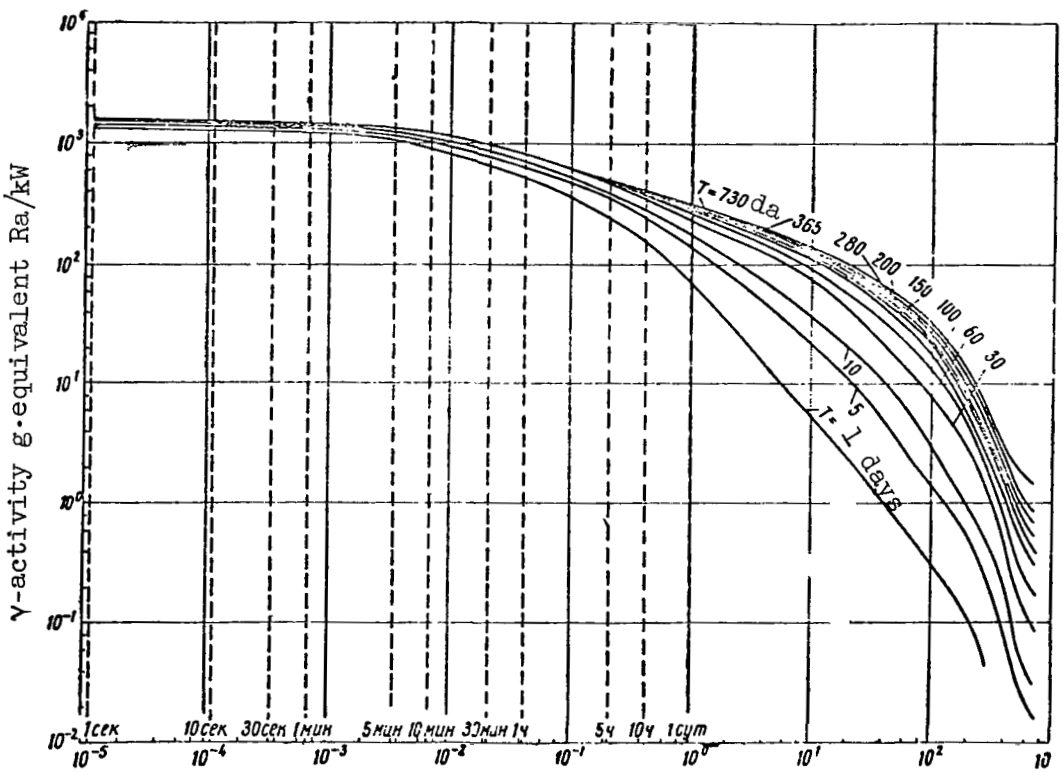

Figure 1. Variation in γ-activity of U^{235} fission products as function of aging time t (in days). Сек = sec; мин = min; ч = hr; сут = days.

TABLE 1

Group	Energy interval, MeV	Average energy, MeV	Group	Energy interval, MeV	Average energy, MeV
1	0-0.38	0.3	6	1.7-2.3	2.19
2	0.38-0.57	0.51	7	2.3-2.7	2.53
3	0.57-0.76	0.72	8	2.7-3.0	2.92
4	0.76-1.2	1.0	9	3.0-4.0	3.5
5	1.2 -1.7	1.6	10	4.0	4.5

We can see from table 2 that the use of the effective absorption coefficient for γ-rays yields results which are sufficiently accurate and makes the computation substantially simpler.

It is expedient to use the advantages associated with the application of the effective absorption coefficients to the computation of shielding when we have a complex spectrum of γ-radiation.

When we have such a complex γ-ray spectrum the effective absorption coefficient in the shielding, which takes into account the buildup of scattered γ-radiation (ref. 1) according to the Fano theory, may be computed by means/166 of the following equation

$$\mu_{eff} = -\frac{1}{\Delta} \ln \frac{\sum_{ik} A_{\gamma_{i,k}} B_k e^{-\mu_k \Delta}}{\sum_{i,k} A_{\gamma_{i,k}}}, \qquad (8)$$

where subscript k represents the number of the energy group; subscript i represents the number of the line in the k-th group; $A_{\gamma i,k}$ represents the intensity of the spectrum line (activity), expressed either in absolute or relative units.

The effective absorption coefficients for γ-ray spectrum of U fission products in water, concrete, iron and lead were computed by using equation (8) and the data of table 3.

The results of this computation are presented in figures 3-11, respectively, for water, concrete (density of 2.3 g/cm^3), iron and lead.

The results of computing the activity of U fission products and the effective absorption coefficients for γ-ray spectrum of fission products (figs. 1-11) may be used conveniently in the practical computation of radiation shielding against sources of various form. In this connection all of the equations presented in the 9th Chapter of Rockwell's book (ref. 2) may be used, if the changes specified in table 3 are taken into account.

TABLE 2

Method of computation	Attenuation factor $F(\mu_0\Delta, B, \vartheta_0)$	$\mu\Delta$		
		2	6	10
According to Pibls	$e^{-\mu_0\Delta}\int_0^{\pi/2} B_P(\vartheta)\,d\vartheta$	0.205	$4.76\cdot10^{-3}$	$1.25\cdot10^{-4}$
$B(\mu_0\Delta) = A_1e^{-\alpha_1\mu_0\Delta} + A_2e^{-\alpha_2\mu_0\Delta}$	$A_1\int_0^{\pi/2} e^{-(1+\alpha_1)\mu_0\Delta\sec\vartheta}\,d\vartheta + A_2\int_0^{\pi/2} e^{-(1+\alpha_2)\mu_0\Delta\sec\vartheta}\,d\vartheta$	0.182	$4.41\cdot10^{-3}$	$1.05\cdot10^{-4}$
$\mu_{eff}(\mu_0\Delta, B)$	$\int_0^{\pi/2} e^{-\mu_{eff}\Delta\sec\vartheta}\,d\vartheta$	0.185	$4.70\cdot10^{-3}$	$1.12\cdot10^{-4}$

The activity of the fission products and μ_{eff} for their spectrum are presented above. They have been computed without taking into account Np^{239}, which is obtained when U^{239} neutrons are absorbed when U is irradiated in the reactor. The Np^{239} yield for each fission of U depends on the conversion ratio (ref. 3).

When the yield of Np^{239} per fission is 100 percent, the gamma-activity due to Np^{239} is equal to

$$A_{\gamma Np} = 57\,(1 - e^{-\lambda_{Np}\tau})\,e^{-\lambda_{Np}t}\ \text{g·equiv of Ra/kW.}$$

The decay constant of Np^{239} can be computed easily from the half life, which is equal to 2.33 days.

The effect of Np^{239} γ-activity is manifested only when the shielding thickness is small (up to 100 cm of water, up to 45 cm of concrete, up to 13 cm of iron or up to 4.5 cm of lead). In these cases the computation of the dose power behind the shielding should be carried out by taking into account the dose produced by neptunium (Np). The effective absorption coefficients for γ-rays of Np μ_{eff} for the shielding thickness specified above are equal to: for water 0.105 cm^2/g; for concrete (γ = 2.3 g/cm^3) 0.071 cm^2/g; for iron 0.102 cm^2/g; for lead 0.32 cm^2/g.

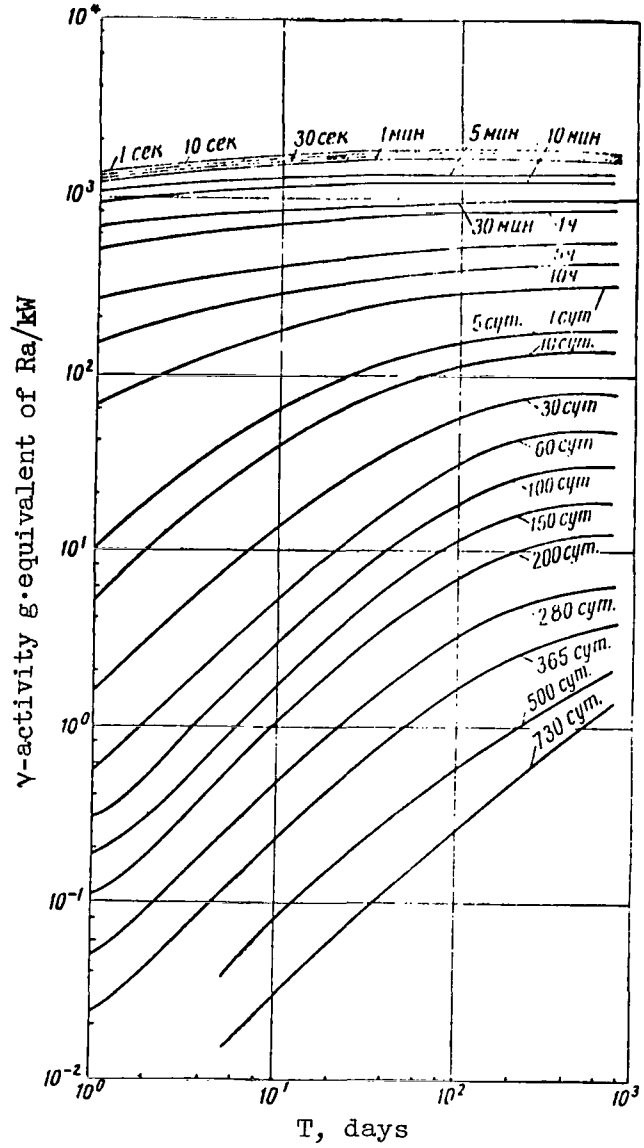

Figure 2. Variation in the γ-activity of U^{235} fission products as function of irradiation time T in reactor. Сек = sec; мин = min; ч = hr; сут = days.

In conclusion the author expresses his gratitude to O. S. Kubasova and N. Ye. Ivanova for their help in preparing the data for the electronic computer and for processing the computation results. /167

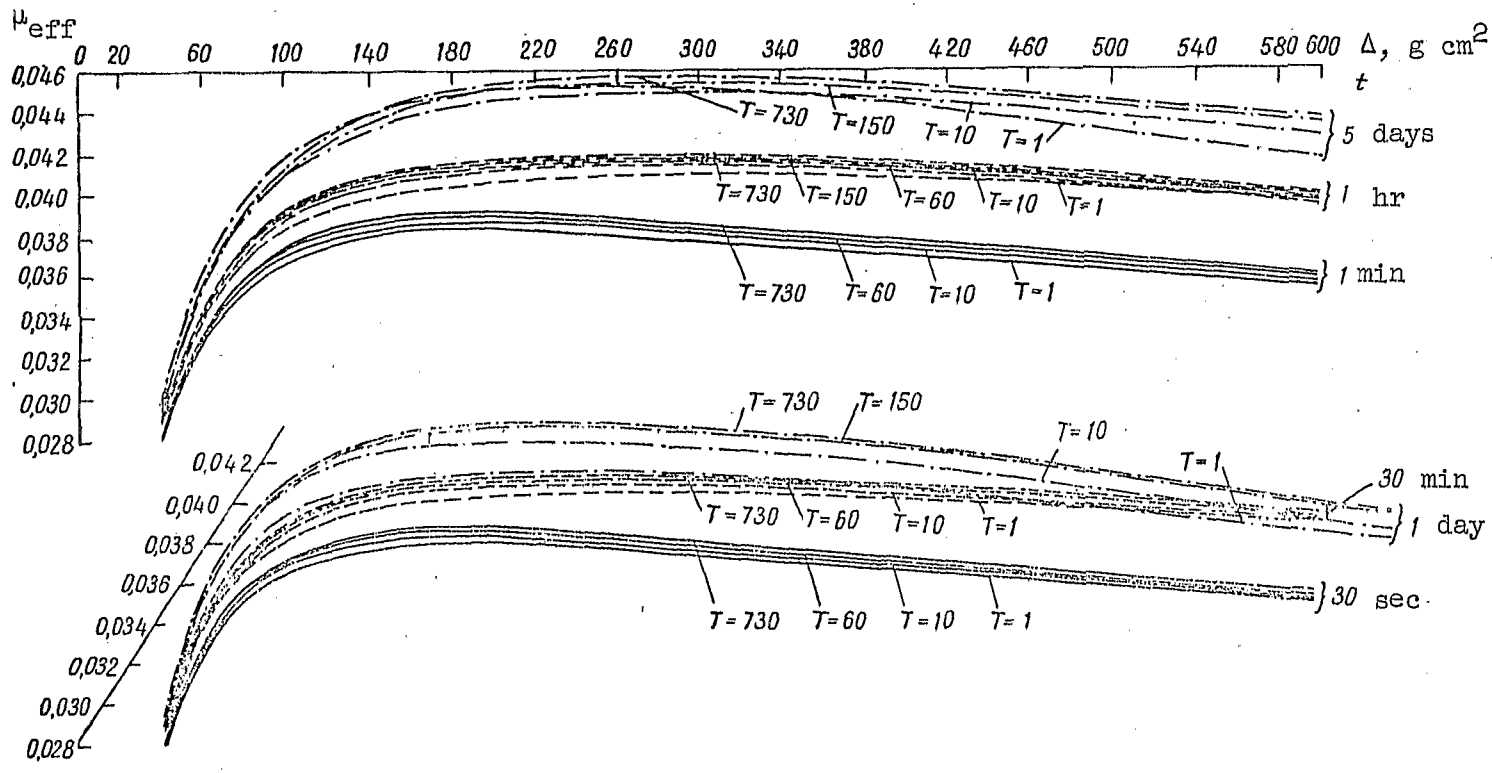
μ_{eff}
0 20 60 100 140 180 220 260 300 340 380 420 460 500 540 580 600 Δ, g cm^2
t
0,046
0,044
0,042
0,040
0,038
0,036
0,034
0,032
0,030
0,028
T=730 T=150 T=10 T=1
5 days
T=730 T=150 T=60 T=10 T=1
1 hr
T=730 T=60 T=10 T=1
1 min
T=730 T=150 T=10 T=1
30 min
T=730 T=60 T=10 T=1
1 day
T=730 T=60 T=10 T=1
30 sec

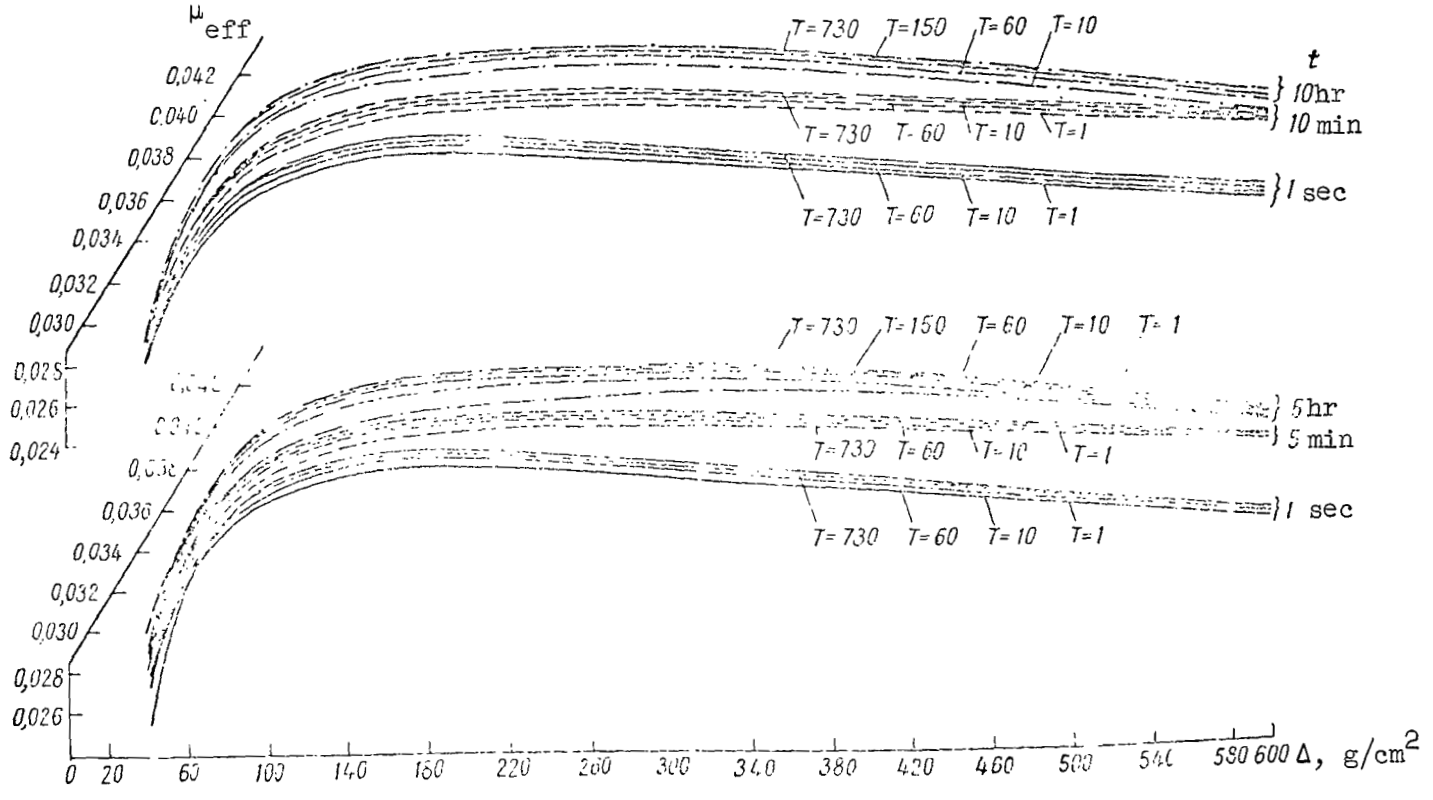

Figure 3. Effective absorption coefficients (μ_{eff}) for spectrum of γ-rays of U fission products in water with aging time t from 1 sec to 5 days.

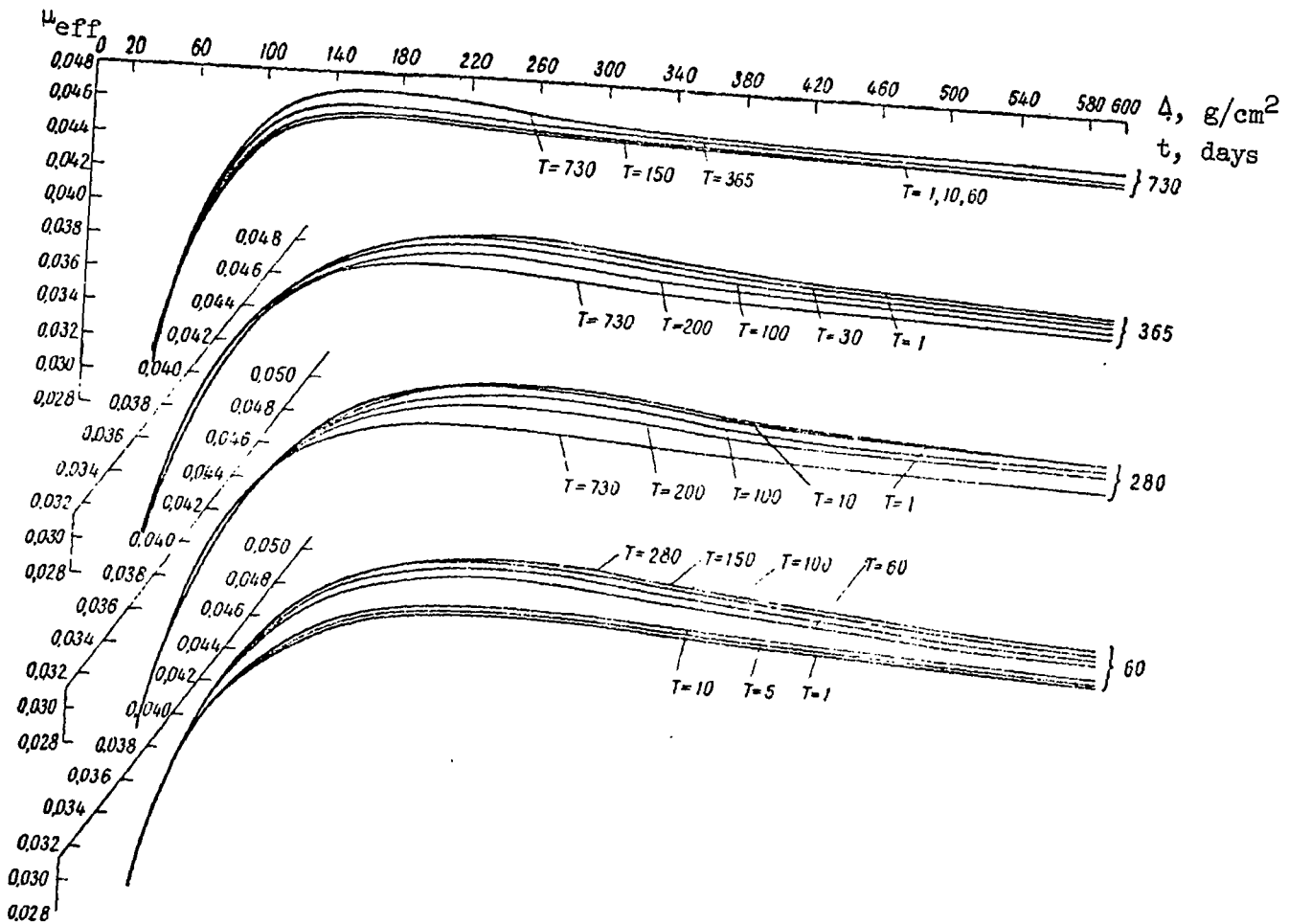
μeff
0 20 60 100 140 180 220 260 300 340 380 420 460 500 540 580 600
Δ, g/cm2
t, days
0,048
0,046
0,044
0,042
0,040
0,038
0,036
0,034
0,032
0,030
0,028
T= 730
T= 150
T= 365
T= 1, 10, 60
730
T= 730
T=200
T= 100
T= 30
T= 1
365
T= 730
T= 200
T= 100
T= 10
T= 1
280
T= 280
T= 150
T= 100
T= 60
T= 10
T= 5
T= 1
60

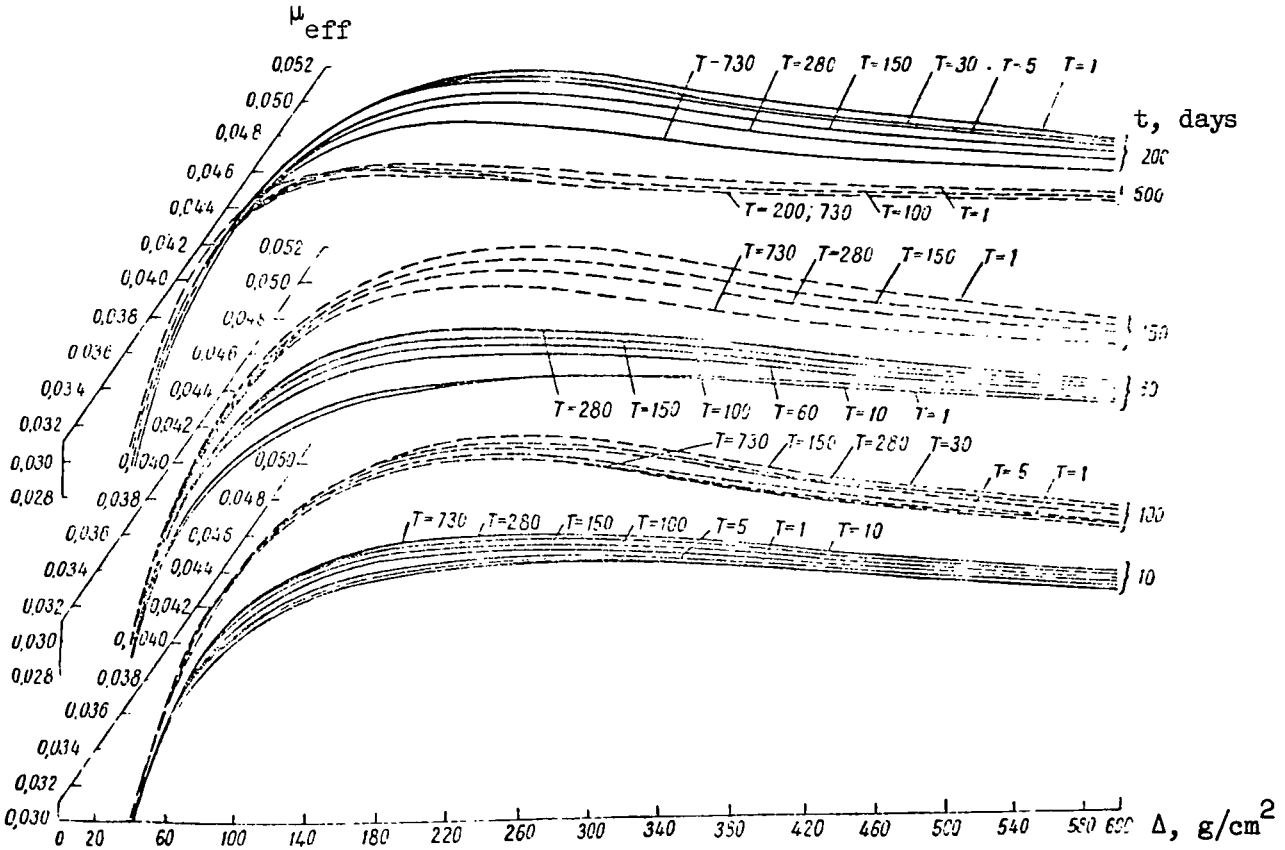

Figure 4. Effective absorption coefficients (μ_{eff}) for γ-ray spectrum of U fission products in water with aging time t from 10 to 730 days.

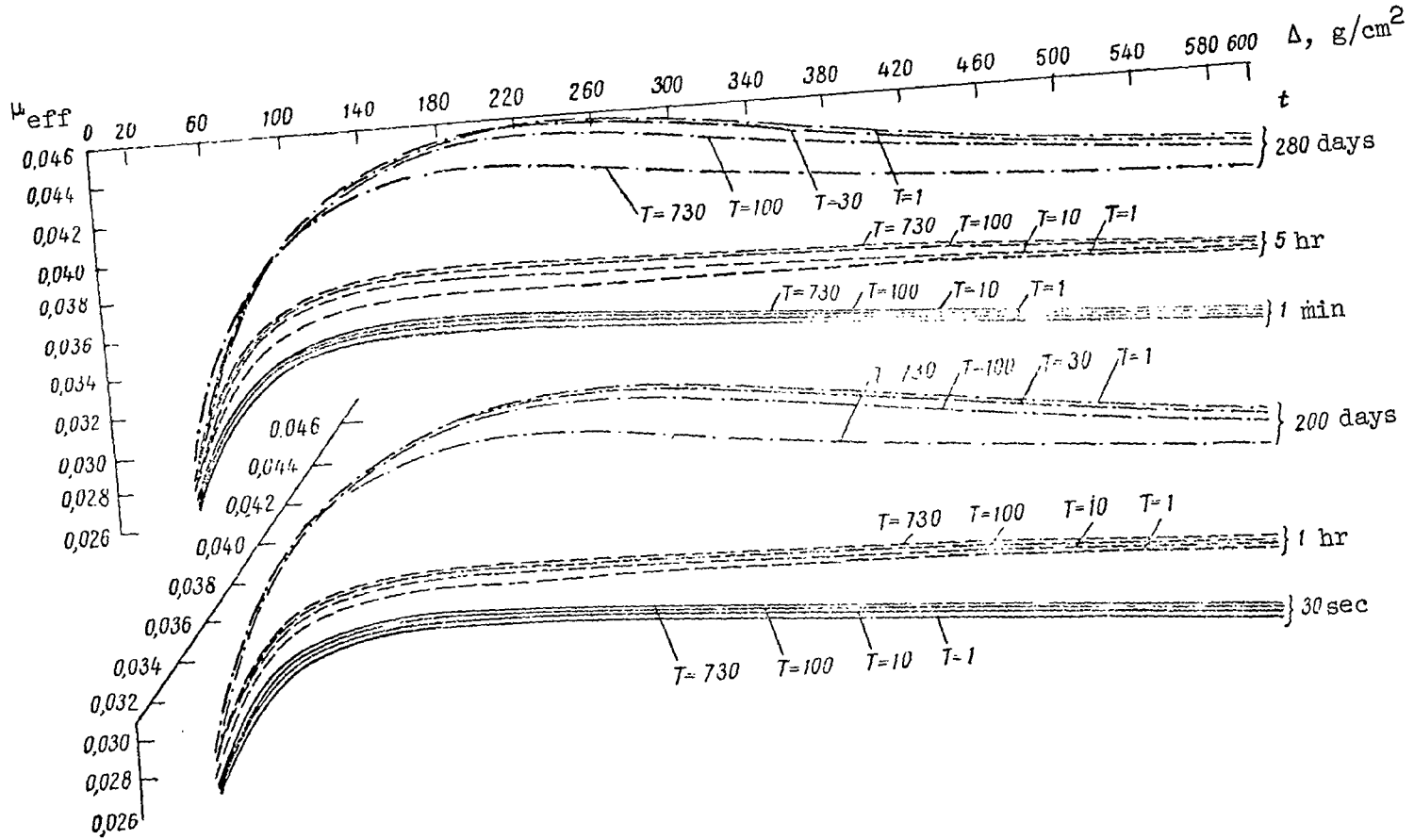
μeff
Δ, g/cm²
t
0 20 60 100 140 180 220 260 300 340 380 420 460 500 540 580 600
0,046
0,044
0,042
0,040
0,038
0,036
0,034
0,032
0,030
0,028
0,026
T=730 T=100 T=30 T=1
280 days
T=730 T=100 T=10 T=1
5 hr
T=730 T=100 T=10 T=1
1 min
T=730 T=100 T=30 T=1
200 days
T=730 T=100 T=10 T=1
1 hr
T=730 T=100 T=10 T=1
30 sec

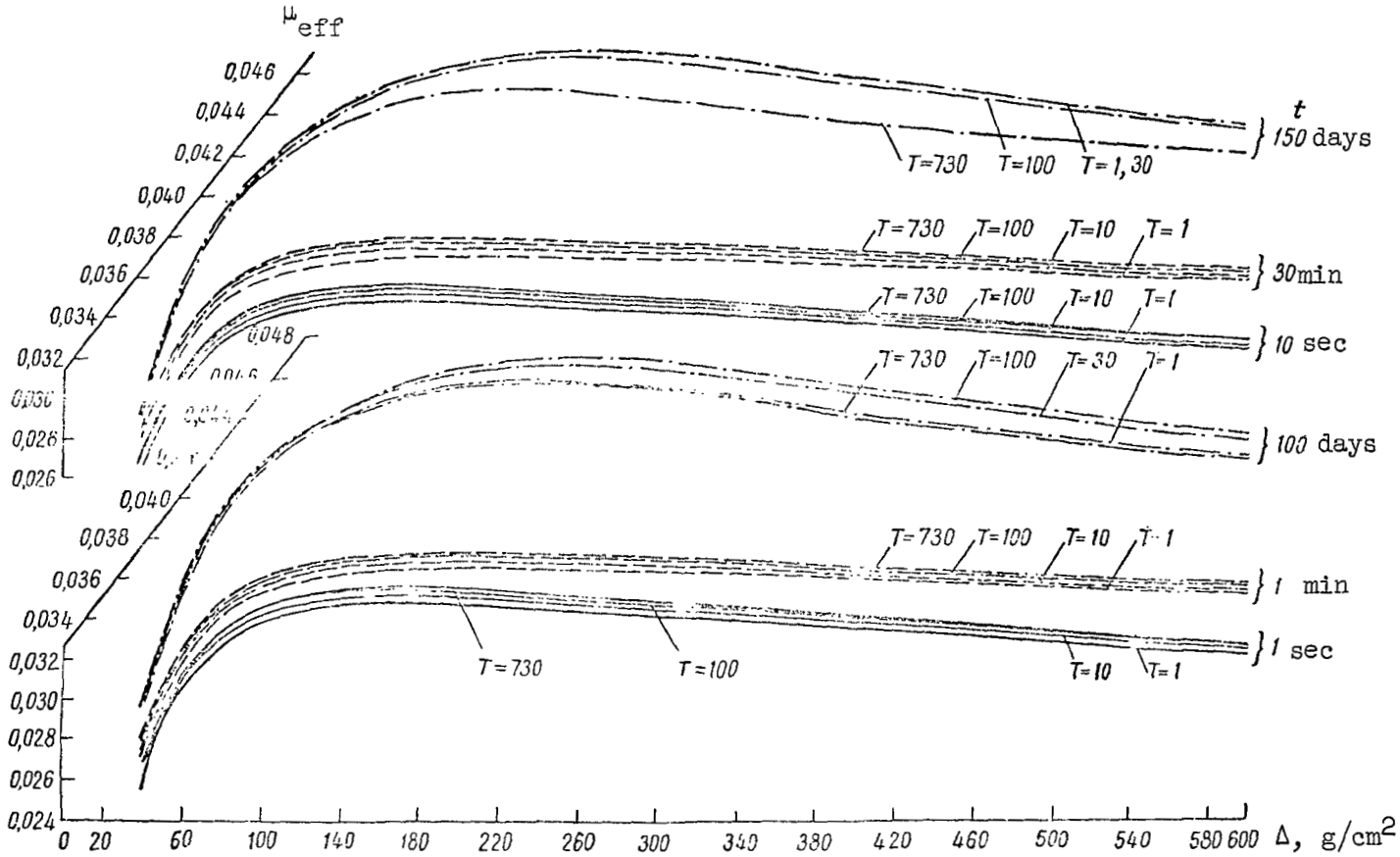

Figure 5. Effective absorption coefficients (μ_{eff}) for γ-ray spectrum of U fission products in concrete with aging time t from 1 sec to 280 days (γ = 2.3 g/cm^3).

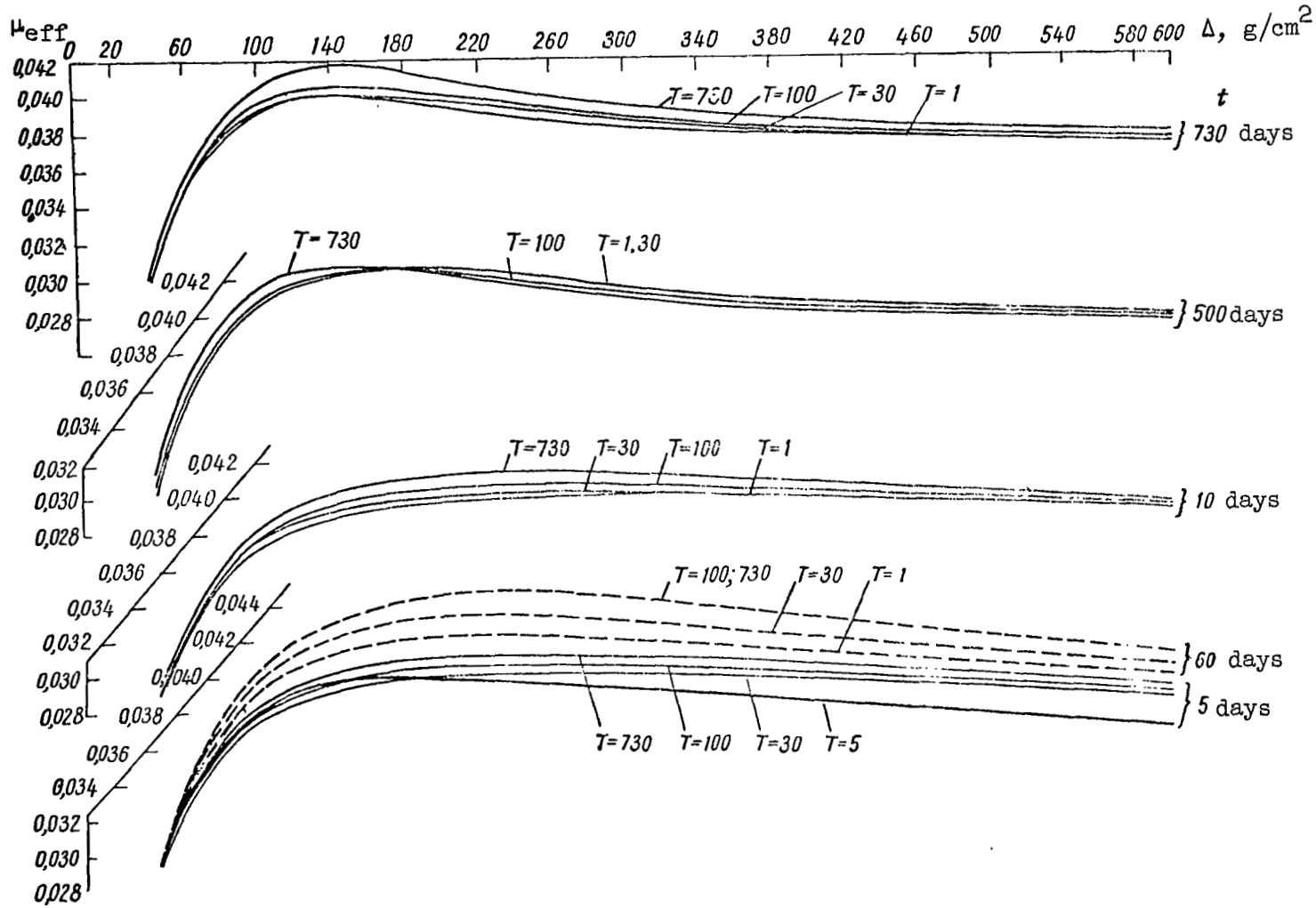
μeff
0 20 60 100 140 180 220 260 300 340 380 420 460 500 540 580 600 Δ, g/cm²
0,042
0,040
0,038
0,036
0,034
0,032
0,030
0,028
T=730 T=100 T=30 T=1
t
730 days
T=730 T=100 T=1,30
500 days
T=730 T=30 T=100 T=1
10 days
T=100; 730 T=30 T=1
60 days
5 days
T=730 T=100 T=30 T=5

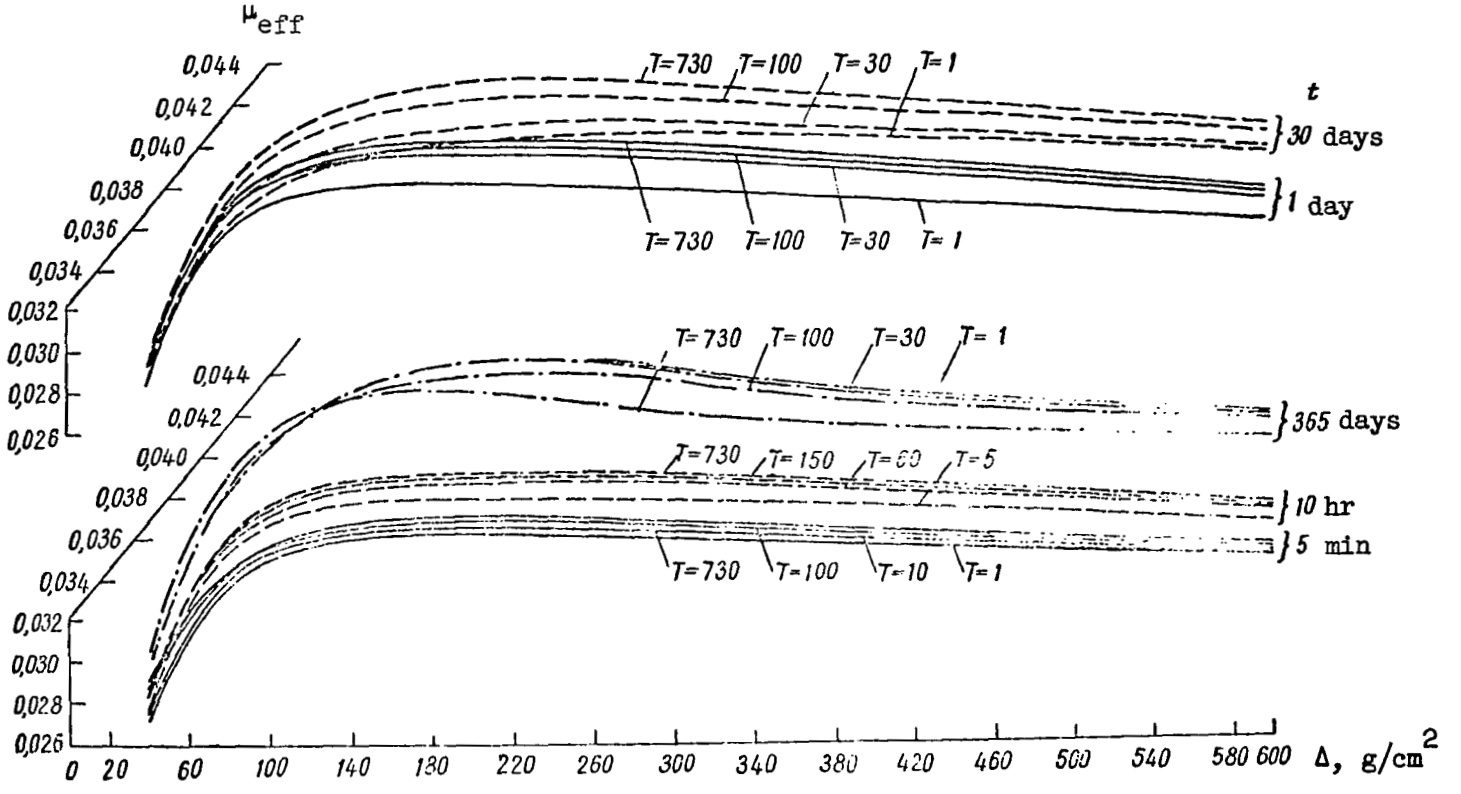

Figure 6. Effective absorption coefficients (μ_{eff}) for γ-ray spectrum of U fission products in concrete with aging time t from 5 min to 730 days (γ = 2.3 g/cm^3).

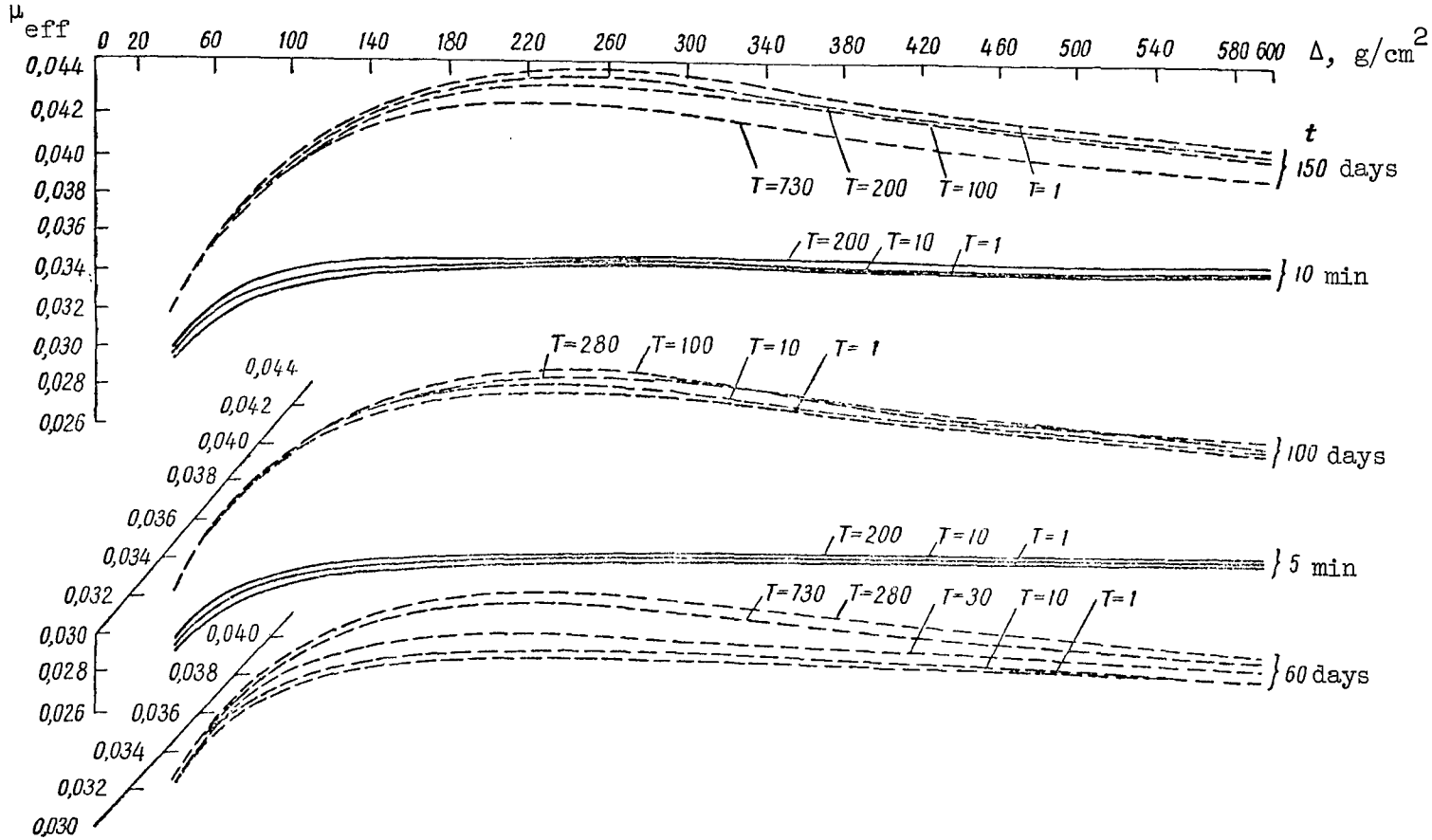
μ eff
0 20 60 100 140 180 220 260 300 340 380 420 460 500 540 580 600 Δ, g/cm²
0,044
0,042
0,040
0,038
0,036
0,034
0,032
0,030
0,028
0,026
t
T=730 T=200 T=100 T=1
150 days
T=200 T=10 T=1
10 min
T=280 T=100 T=10 T=1
100 days
T=200 T=10 T=1
5 min
T=730 T=280 T=30 T=10 T=1
60 days

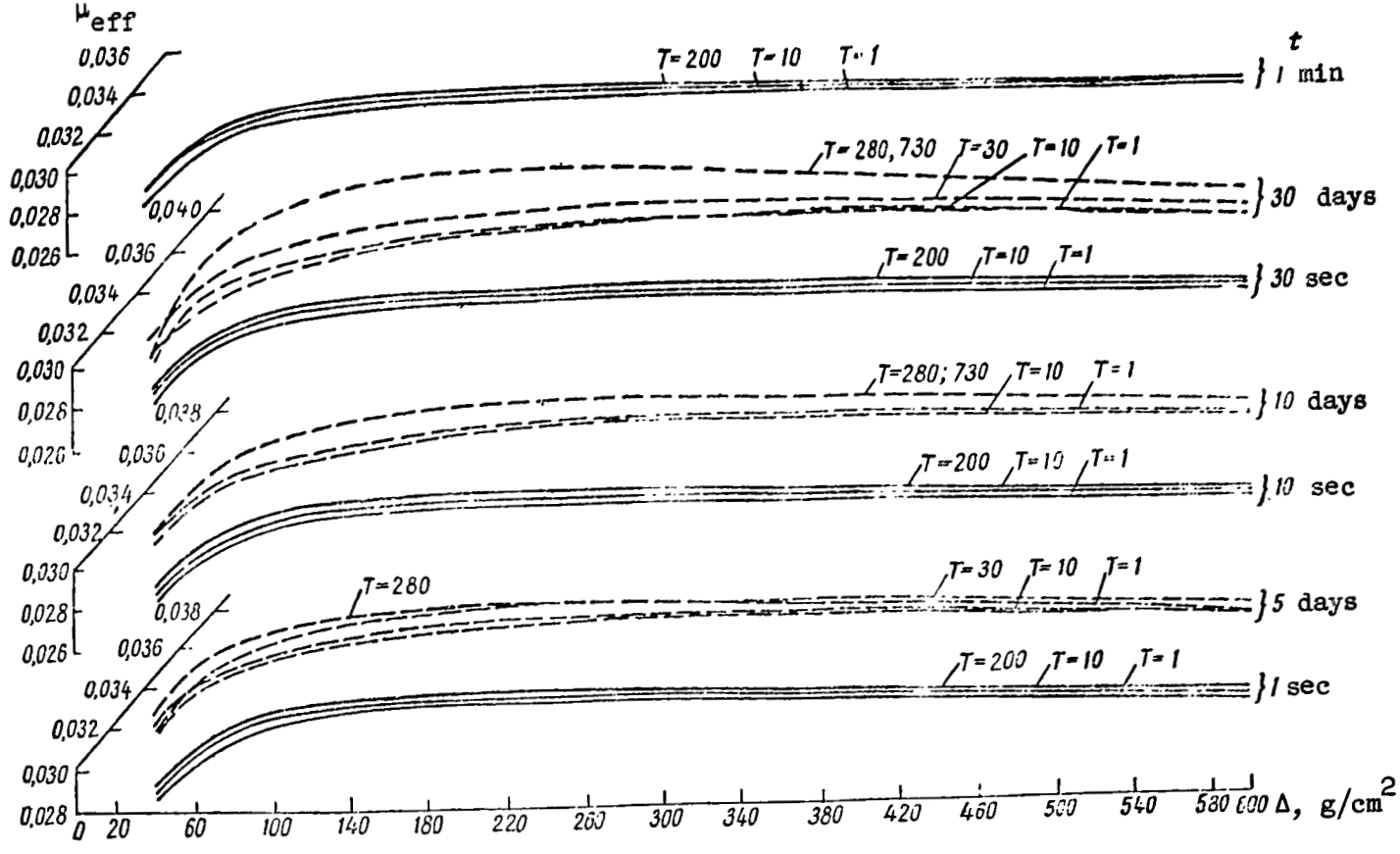

Figure 7. Effective absorption coefficients (μ_{eff}) for γ-ray spectrum of U fission products in iron with aging time t from 1 sec to 150 days.

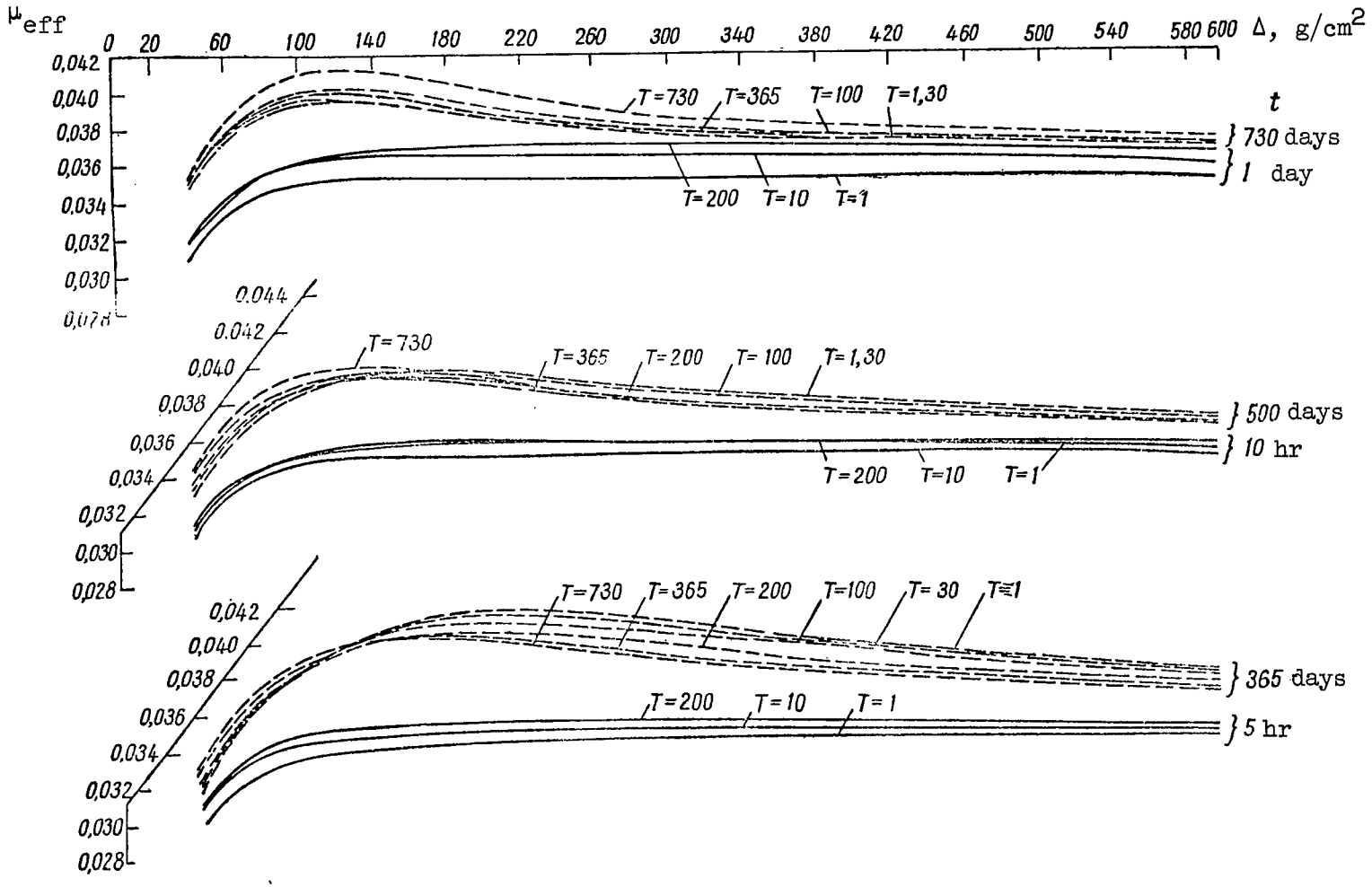
μeff
0 20 60 100 140 180 220 260 300 340 380 420 460 500 540 580 600 Δ, g/cm2
0,042
0,040
0,038
0,036
0,034
0,032
0,030
T=730 T=365 T=100 T=1,30
t
730 days
1 day
T=200 T=10 T=1
0,044
0,042
0,040
0,038
0,036
0,034
0,032
0,030
0,028
T=730 T=365 T=200 T=100 T=1,30
500 days
10 hr
T=200 T=10 T=1
0,042
0,040
0,038
0,036
0,034
0,032
0,030
0,028
T=730 T=365 T=200 T=100 T=30 T=1
365 days
T=200 T=10 T=1
5 hr

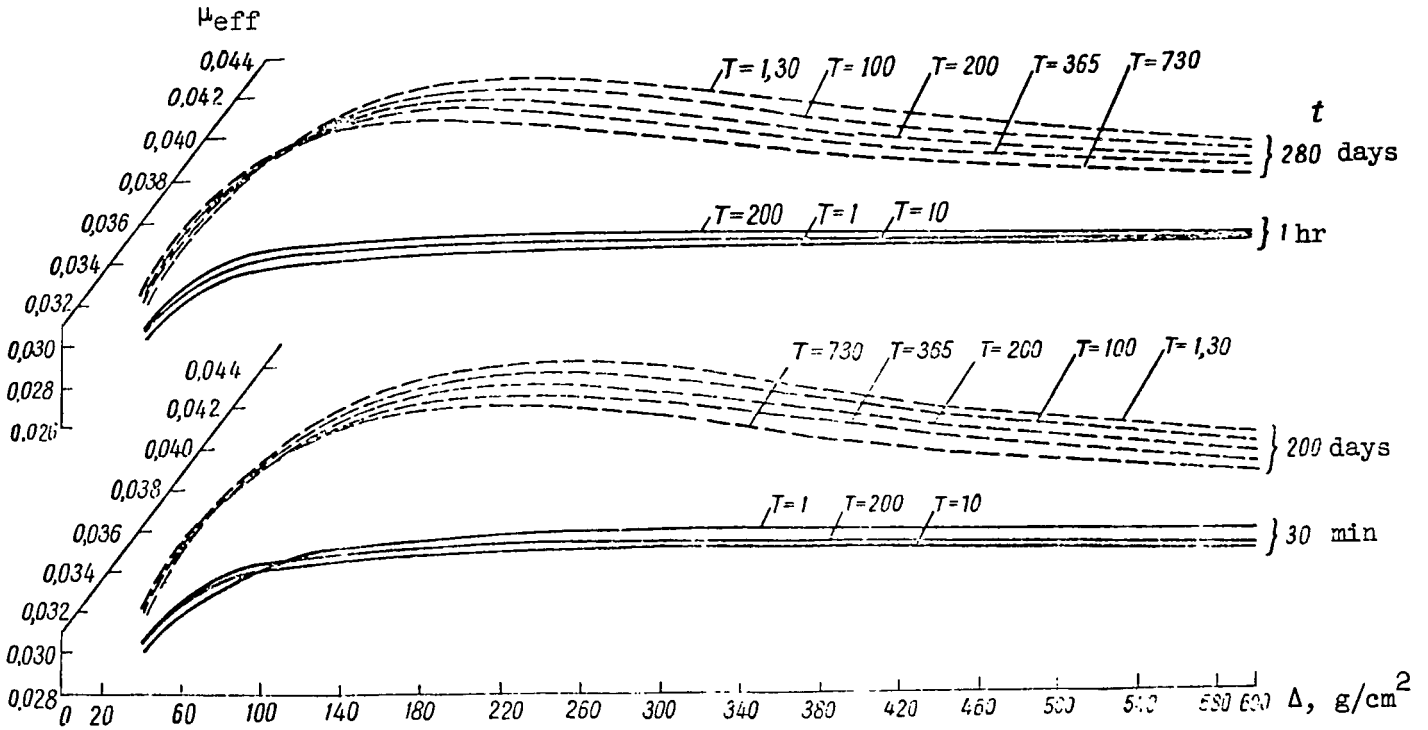

Figure 8. Effective absorption coefficients (μ_{eff}) for γ-ray spectrum of U fission products in iron with aging time t from 30 min to 730 days.

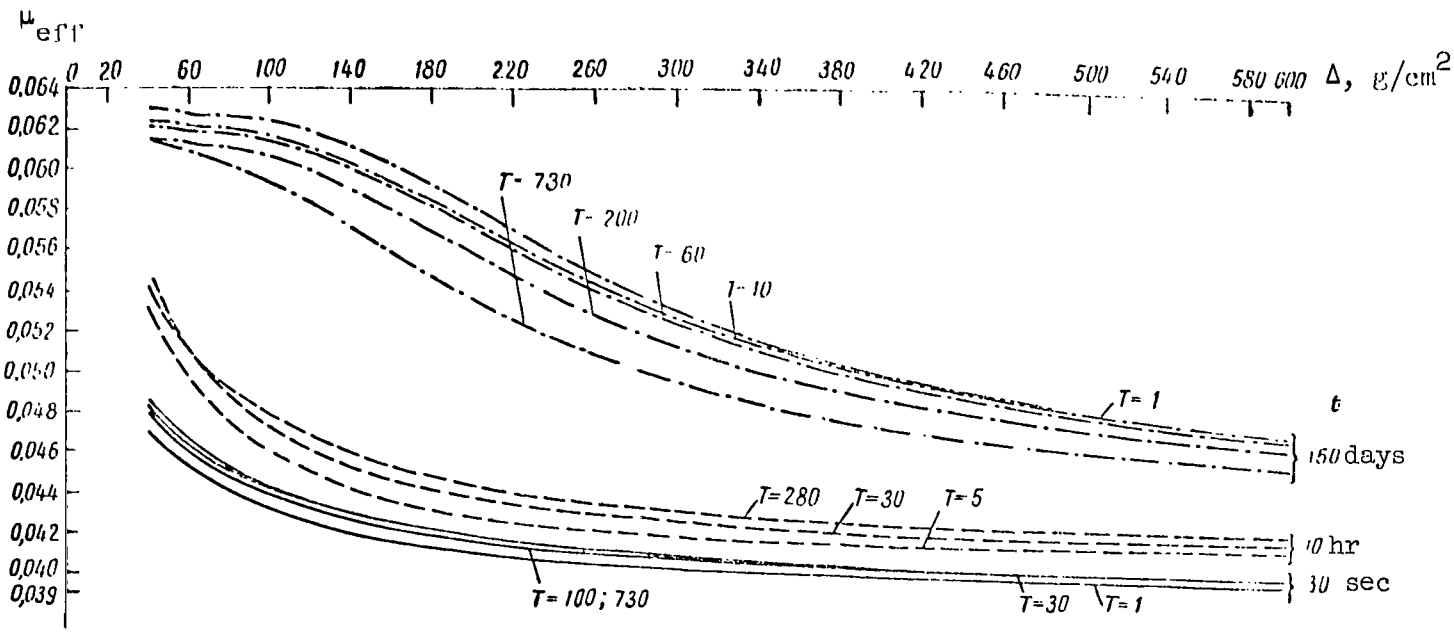
μeff
0,064
0,062
0,060
0,058
0,056
0,054
0,052
0,050
0,048
0,046
0,044
0,042
0,040
0,039
0 20 60 100 140 180 220 260 300 340 380 420 460 500 540 580 600 Δ, g/cm2
T- 730
T- 200
T- 60
T- 10
T= 1
t
150 days
T=280
T=30
T= 5
10 hr
30 sec
T= 100; 730
T=30
T= 1

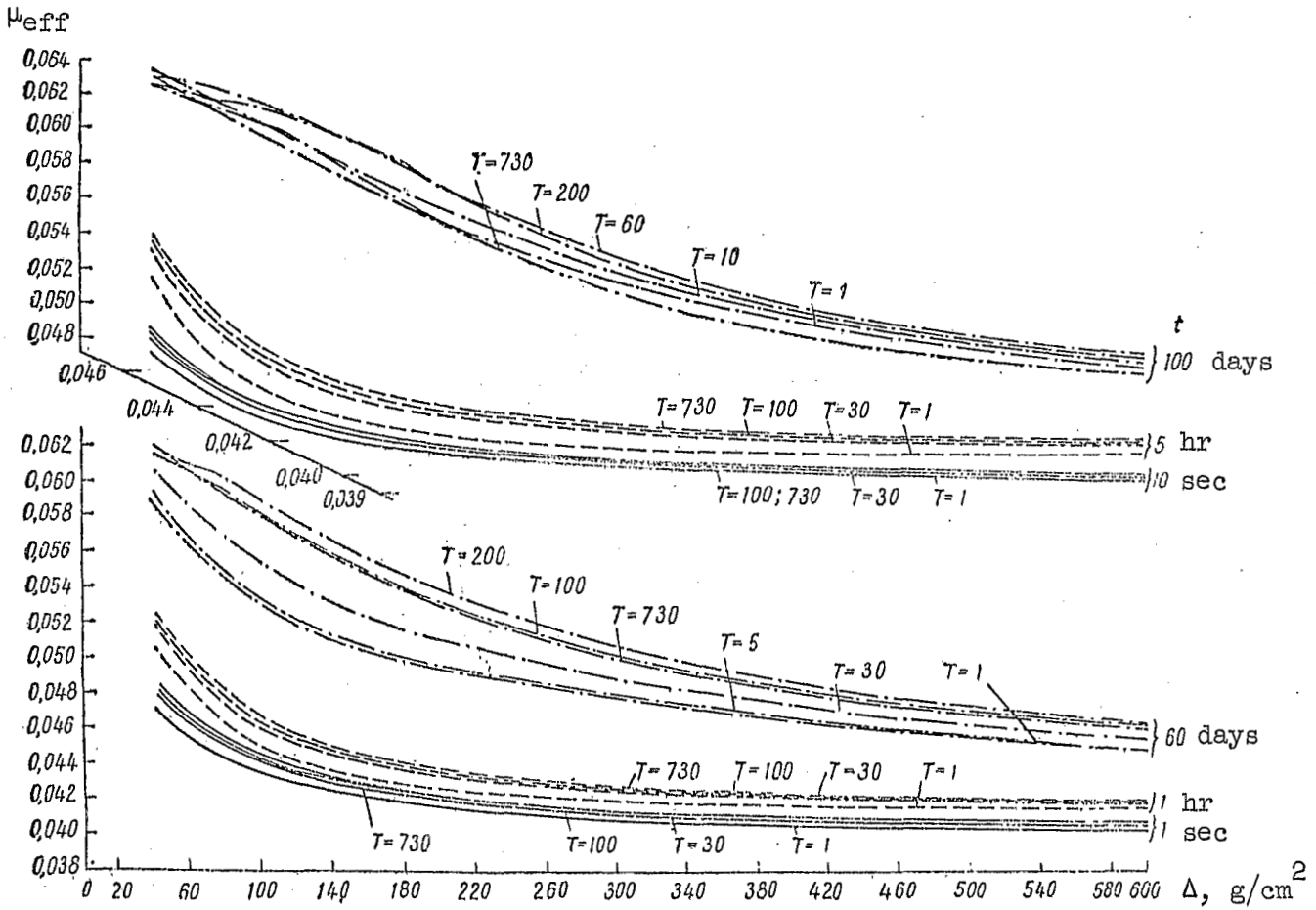

Figure 9. Effective absorption coefficients (μ_{eff}) for γ-ray spectrum of U fission products in lead with aging time t from 1 sec to 150 days.

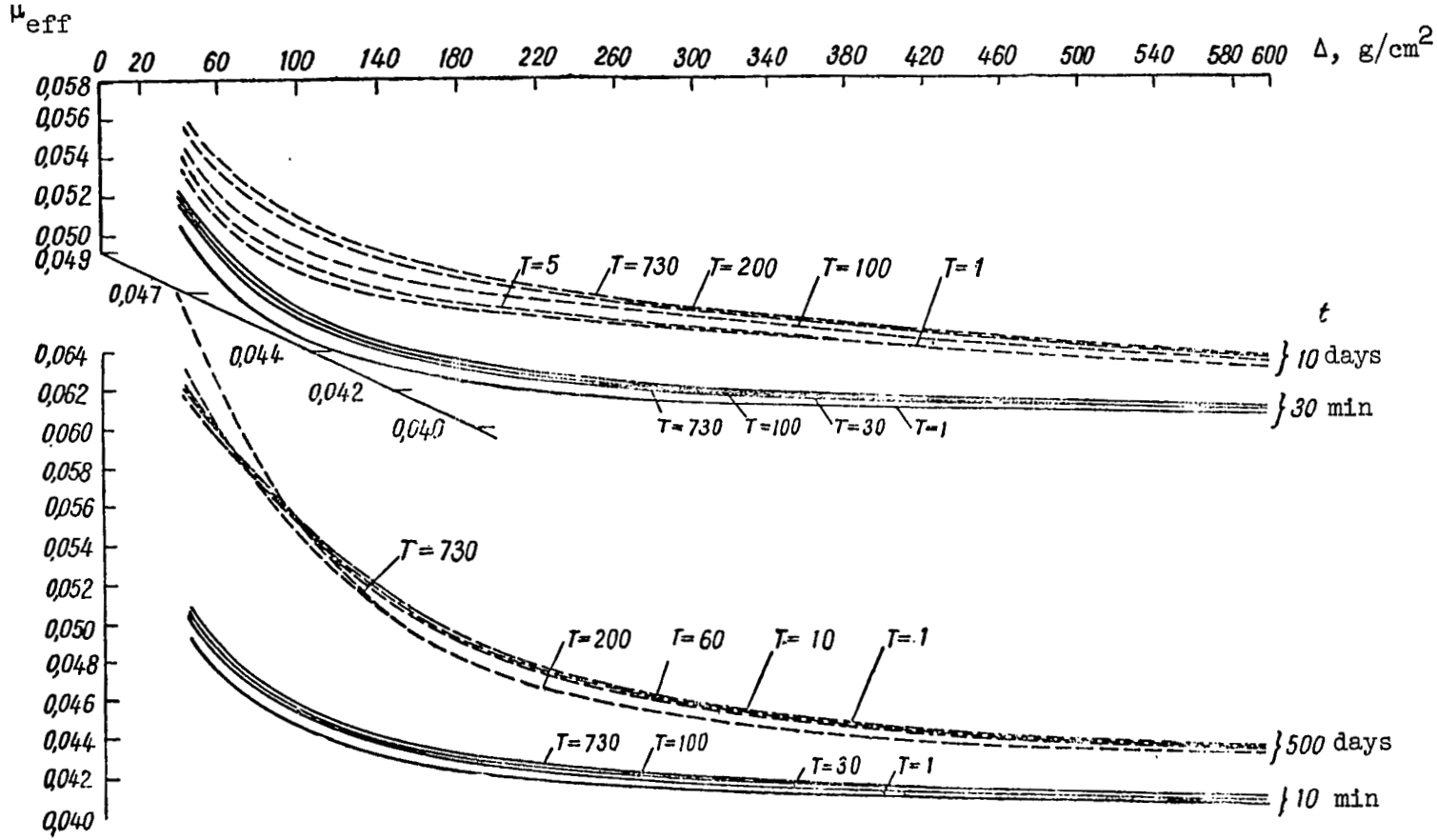
μeff
0 20 60 100 140 180 220 260 300 340 380 420 460 500 540 580 600 Δ, g/cm2
0,058
0,056
0,054
0,052
0,050
0,049
0,047
0,044
0,042
0,040
T=5
T=730
T=200
T=100
T=1
t
10 days
30 min
T=730
T=100
T=30
T=1
0,064
0,062
0,060
0,058
0,056
0,054
0,052
0,050
0,048
0,046
0,044
0,042
0,040
T=730
T=200
T=60
T=10
T=1
500 days
T=730
T=100
T=30
T=1
10 min

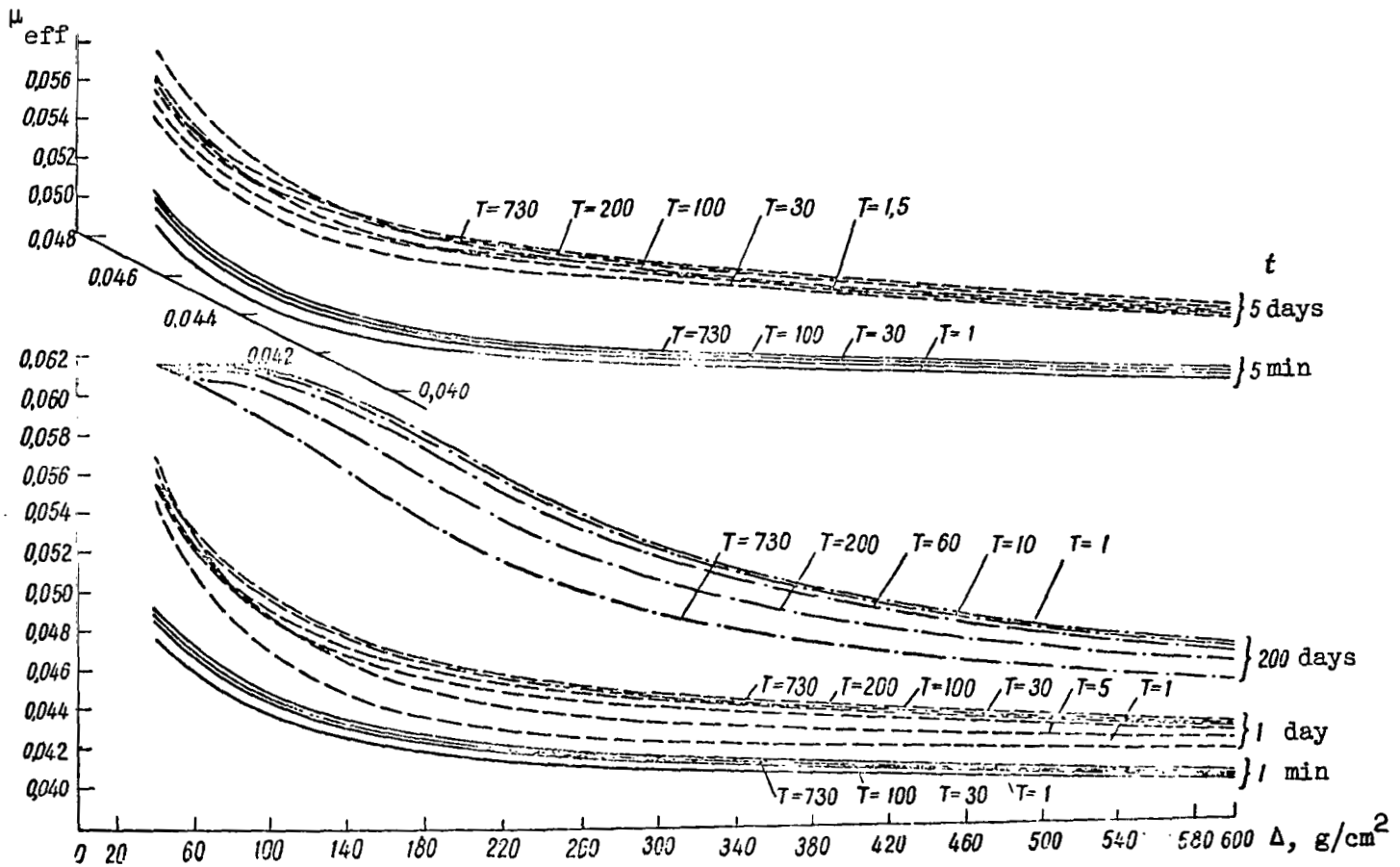

Figure 10. Effective absorption coefficients (μ_{eff}) for γ-ray spectrum of U fission products in lead with aging time t from 1 min to 10 days.

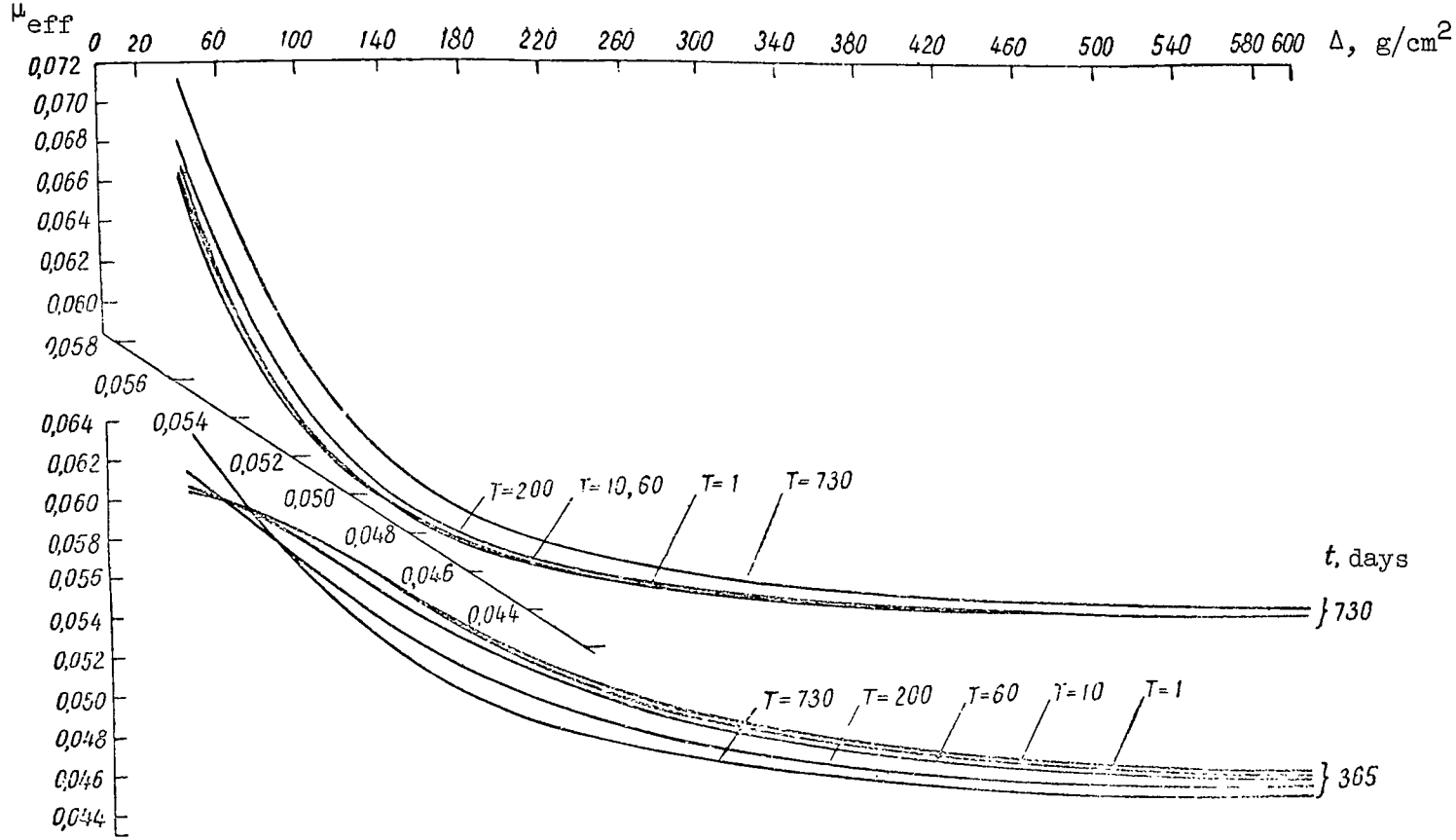
μ_{eff}
0 20 60 100 140 180 220 260 300 340 380 420 460 500 540 580 600 Δ, g/cm²
0,072
0,070
0,068
0,066
0,064
0,062
0,060
0,058
0,056
0,054
0,052
0,050
0,048
0,046
0,044
T=200
T=10, 60
T=1
T=730
t, days
730
T=730
T=200
T=60
T=10
T=1
365

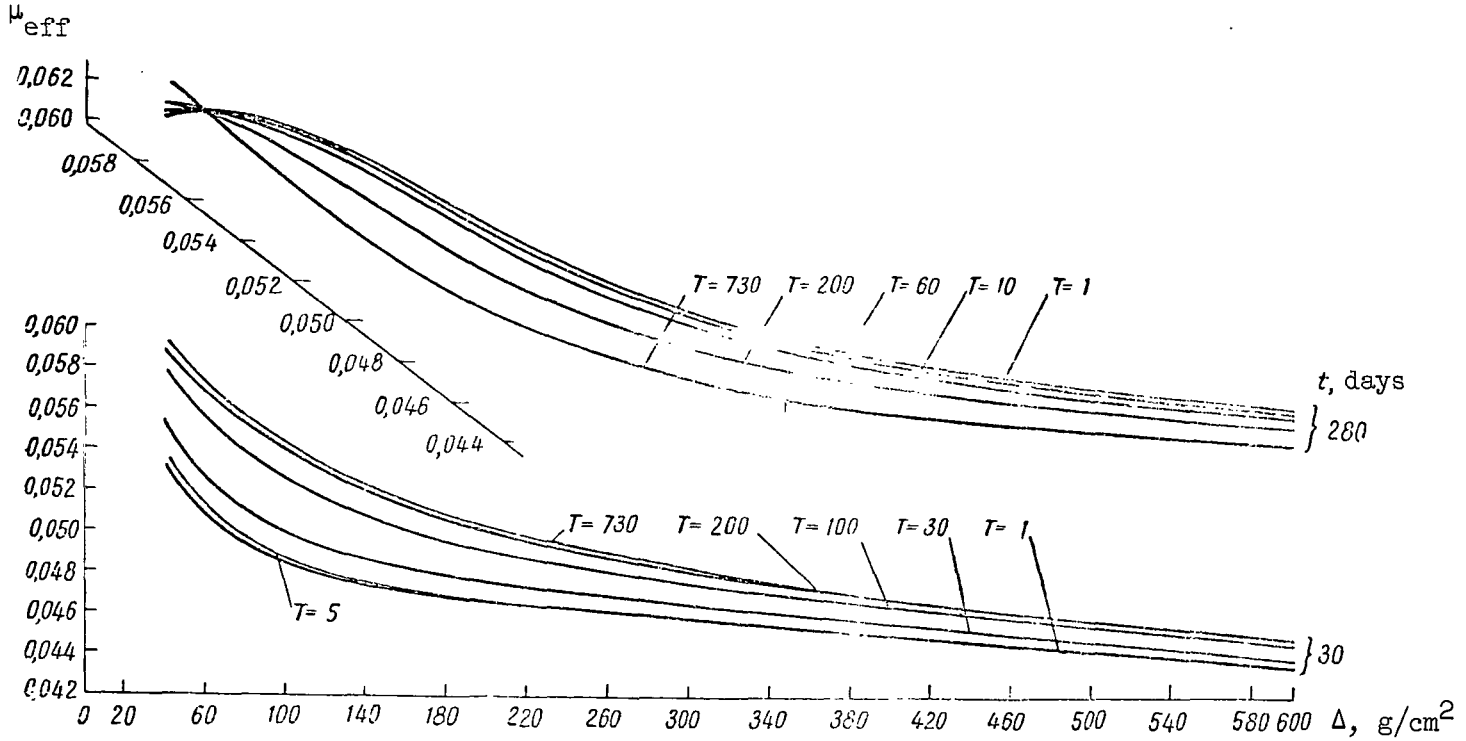

Figure 11. Effective absorption coefficients (μ_{eff}) for γ-ray spectrum of U fission products in lead with aging time t from 30 to 730 days.

TABLE 3. QUANTITIES CONTAINED IN THE EQUATIONS FOR COMPUTING THE DOSE POWER FROM VARIOUS SOURCES AND THEIR EQUIVALENTS PRESENTED IN (REF. 2).

Quantity	Dimension	Equivalent value	
According to Rockwell (ref. 2)		Quantity	Dimension
φ - Flux of γ-quanta	$\frac{1}{cm \cdot sec}$	P_γ - Dose power	$\mu R/sec$
S_0 - Point source power	$\frac{1}{sec}$	Q_0 - Point source activity	g·equivalent of Ra
S_L - Linear source power	$\frac{1}{cm \cdot sec}$	q_L - Linear source activity	g·equivalent of Ra/cm
S_A - Plane source power	$\frac{1}{cm^2 \cdot sec}$	q_S - Plane source activity	g·equivalent of Ra/cm^2
S_i - Volumetric source power	$\frac{1}{cm^3 \cdot sec}$	q_i - Volumetric source activity g·equivalent of Ra	g·equivalent of Ra/cm^3
$b = \mu\Delta$	-	$b = \mu_{eff}\Delta$	-
B - Buildup factor	-	$4\pi\Gamma = 4\pi \cdot 2.3 \cdot 10^6$ - constant	$\mu R/sec \cdot cm^2/g$·equivalent of Ra

REFERENCES

1. Nuclear Reactors. Materials of the Atomic Energy Commission, USA. Part I (Yadernyye reaktory. Materialy KAE SShA). Moscow, Izd-vo I. L., p. 296, 1956.

2. Shielding of Nuclear Reactors. Edited by T. Rockwell (Zashchita yadernykh reaktorov. Pod red. T. Rokvella). Moscow, Izd-vo I. L., 1958.

3. Galanin, A. D. The Theory of Nuclear Reactors Operating with Thermal Neutrons (Teoriya yadernykh reaktorov na teplovykh neytronakh). Moscow, Atomizdat, p. 11, 192, 1957.

AVERAGE CROSS SECTIONS OF THE REACTION FOR THE GAMMA-SPECTRUM OF FISSION FRAGMENTS

V. Kh. Tokhtarov

In the monograph of reference 1 mention is made concerning the possibility of obtaining photoneutrons by using the γ-radiation of U fission products. The same work presents the photoneutron formation cross sections for the same products. Our goal has been to compute the average cross sections of the Be_4^9 (γ, n) Be_4^8 reaction for γ-quanta spectrum of fission products considering different irradiation and aging time. The cross section of this reaction as a function of γ-quanta energy is presented in references 1-3. /167

To simplify the calculations, we break down all of the γ-quanta in a series of intervals according to energy. The cross section of the Be_4^9 (γ, n) Be_4^8 reaction for each such interval is assumed to be constant and equal to the average cross section over this interval. Intervals with the same average cross sections are collected into one group. All of the considered groups are presented in table 1.

The intensity of the γ-quanta sources of i-th energy are computed by means of equation (1) and (2), assuming that U is irradiated for a period T such that the power of heat liberation in it is 1 kW.

1. For the parent isotope

$$Q_i = 3.2 \cdot 10^{13} y \eta_i (1 - e^{-\lambda T}) e^{-\lambda \tau}. \quad (1)$$

2. For the decay product isotope

$$Q_i = 3.2 \cdot 10^{13} y_1 \eta_i \left[\frac{\lambda_2}{\lambda_2 - \lambda_1} (1 - e^{-\lambda_1 T}) e^{-\lambda_1 \tau} + \left(\frac{y_2}{y_2 - y_1} - \frac{\lambda_1}{\lambda_2 - \lambda_1} \right) (1 - e^{-\lambda_2 T}) e^{-\lambda_2 \tau} \right]. \quad (2)$$

Here y is the total yield of the i-th isotope per fission expressed as a fraction; T is the irradiation time; τ is the aging time after irradiation; λ is the decay constant; η_i is the yield of i-th energy γ-quanta per decay.

Subscripts 1 and 2 refer to the parent isotope and to the decay product isotope, respectively.

TABLE 1. AVERAGE CROSS SECTION OF Be_4^9 (γ, n) Be_4^8 REACTION AS A FUNCTION OF γ-QUANTA ENERGY.

Group	Energy interval, MeV	Average cross section of group, $cm^2 \cdot 10^{28}$
1	1.667-1.75	10
2	1.75 -1.8	8
3	2.7 -2.8	7
4	1.8 -1.85 2.65 -2.7	6
5	2.6 -2.65	5.5
6	1.85 -1.95 2.5 -2.6 2.8 -4	5
7	1.95 -2.05	4.5
8	2.05 -2.5	4

The initial data on the isotope fragments are presented in table 2. Isotopes with a half-life of less than 3 min and with a fission yield of less than $3 \cdot 10^{-3}$ percent do not make a noticeable contribution to the total activity and are therefore not considered.

The distribution of γ-quanta sources is assumed to be uniform over the volume. Consequently the flux of j-th group γ-quanta is proportional to the intensity of γ-quanta in the same group, and the averaging out of the reaction cross section over the flux may be replaced by its averaging out over the intensity

$$\bar{\sigma} = \frac{\sum_j Q_j \sigma_j}{\sum_j Q_j}. \qquad (3)$$

Here $\bar{\sigma}$ is the average cross section; σ_j is the cross section of the j-th group; Q_j is the intensity of the j-th group γ-quanta. The results of the computations giving the number of γ-quanta per 1 kW in 1 sec, the average energy of γ-quanta in MeV and the average cross sections of the Be_4^9 (γ, n) Be_4^8 reaction in cm^2 10^{28} are presented in table 3.

TABLE 2. FISSION PRODUCTS.

Isotope and half-life	Total isotope yield per fission, %	Parent isotope and half-life	Total yield for fission of parent isotope, %	Energy of γ-quanta, MeV; decay yield	Literature
Ge^{77} 12 hr	$3.7 \cdot 10^{-3}$	-	-	2.32; 1.06 2; 4.13; 1.74; 0.709	 (4) (5)
As^{78} 91 min	$2 \cdot 10^{-2}$	Ge^{78} 86 min	$1.82 \cdot 10^{-2}$	2.65 0.88	(4)-(6)
Br^{84} 31.8 min	0.9	Se^{84} 3.3 min	0.9	3.93; 9.62 3.28; 2.31 3.03; 3.08 2.82; 1.54 2.47; 0.62 2.17; 1.54 2.05; 1.54 1.9; 13.9 1.74; 1.54	 (4) (5) (6)
Kr^{87} 78 min	2.7	-	-	2.57; 35.3 2.05; 5.04	(6) (7, 8)
Kr^{88} 2.8 hr	3.5	-	-	2.4; 33.4 2.19; 16.7	(5) (6, 7)
Pb^{88} 17.7 min	3.57	Kr^{88} 2.8 hr	3.5	4.87; 0.294 3.68; 0.084 3.52; 0.231 3.24; 0.294 3.01; 0.294 2.68; 2.25 2.11; 0.945 1.85; 21	(5) (6) (7)
Rb^{89} 14.9 min	4.8	Kr^{89} 3.2 min	4.4	3.52; 2.18 2.75; 2.78	(5-8)

TABLE 2. (CONTINUED)

Isotope and half-life	Total isotope yield per fission, %	Parent isotope and half-life	Total yield for fission of parent isotope, %	Energy of γ-quanta, MeV; decay yield	Literature
				2.59; 2.18 2.2; 14.3	
Y^{90} 64.8 hr	5.77	Sr^{90} 28.4 yr	5.77	1.77; $6 \cdot 10^{-4}$	(5-7)
Y^{92} 3.4 hr	5.9	Sr^{92} 2.6 hr	5.3	2.4; 0.179 1.9; 0.895	(5-7)
Y^{93} 11 hr	6.45	-	-	2.14; 0.824; 1.88; 2.23	(4-7)
Zr^{97} 17 hr	5.9	-	-	2.58; 1; 2.2; 2	(4-7)
Mo^{101} 14.61 min	5	-	-	2.08; 16 (conditional spectrum)	(4), (6-8)
Rh^{106} 366.6 days	0.38	-	-	3.45; 0.00945 3.05; 0.00945 2.93; 0.00945 2.66; 0.0189 2.42; 0.0945 2.27; 0.0945 2.1; 0.047 1.96; 0.0567 1.85; 0.00945 1.77; 0.0945 (conditional spectrum)	(5, 7)
Ag^{112} 3.2 hr	10^{-2}	Pd^{112} 21 hr	10^{-2}	2.79; 1.19 2.51; 2.38 2.11; 5.36 1.83; 3.57	(4, 5) (7)

TABLE 2. (CONTINUED)

Isotope and half-life	Total isotope yield per fission, %	Parent isotope and half-life	Total yield for fission of parent isotope, %	Energy of γ-quanta, MeV; decay yield	Literature
Sn^{125} 9.7 days	$1.3 \cdot 10^{-2}$	-	-	1.97; 2.4	(5, 7)
J^{132} 2.3 hr	4.38	Te^{132} 77.7 hr	4.28	2.2; 2.13 1.96; 5.32	(4-7)
J^{134} 52.4 min	8	Te^{134} 44 min	6.7	1.78; 1 (conditional spectrum)	(4, 6)
J^{135} 6.8 hr	6.2	-	-	1.8; 11; 1.72; 19	(4, 6)
Xe^{138} 17 min	4.5	-	-	2.01; 5; 1.78; 5 (conditional spectrum)	(4, 6)
Cs^{138} 32.1 min	5.7	Xe^{138} 17 min	4.5	3.34; 0.5 2.63; 9 2.21; 18	(4, 6) (7, 8)
La^{140} 40.3 hr	6.44	Ba^{140} 13 days	6.24	3.0; 2 2.54; 5.5 1.91; 0.5 (conditional spectrum)	(5, 6)
La^{142} 81 min	5.95	Ba^{142} 6 min	5.65	3.4; 3.13; 2.9; 9.38; 2.4; 34.4; 2.1 18.75; 1.8 9.38	(4, 5) (6)
Pr^{144} 2.85 min	6	-	-	2.2; 0.8	(4, 5)

TABLE 2. (CONCLUDED)

Isotope and half-life	Total isotope yield per fission, %	Parent isotope and half-life	Total yield for fission of parent isotope, %	Energy of γ-quanta, MeV; decay yield	Literature
Eu^{156} 14 days	$1.4 \cdot 10^{-2}$	Sm^{156} 9 hr	$1.4 \cdot 10^{-2}$	2.18; 10 2.14; 6 2.09; 10 2.03; 5 1.97; 1 1.95; 5 1.78; 1 1.74; 1 (conditional spectrum)	(4, 5) (7)

TABLE 3. RESULTS FOR CALCULATION OF AVERAGED OUT CROSS SECTIONS.

τ \ T	1 hr	10 hr	1 day	100 hr	240 hr	1000 hr
1 hr	$7.4\cdot10^{11}$ 2.3 5.3	$2.3\cdot10^{12}$ 2.2 5.3	$2.5\cdot10^{12}$ 2.2 5.5	$2.6\cdot10^{12}$ 2.2 5.5	$2.7\cdot10^{12}$ 2.2 5.5	$2.75\cdot10^{12}$ 2.2 5.5
10 hr	$3.9\cdot10^{10}$ 2.8 6.4	$2.1\cdot10^{11}$ 2 7	$2.9\cdot10^{11}$ 2 7	$3.7\cdot10^{11}$ 2.1 6.65	$4.2\cdot10^{11}$ 2.1 6.4	$5.1\cdot10^{11}$ 2.2 6.2
1 day	$1.2\cdot10^{10}$ 2 6	$4.7\cdot10^{10}$ 2 7.05	$7.75\cdot10^{10}$ 2 6.7	$1.4\cdot10^{11}$ 2.1 5.8	$1.9\cdot10^{11}$ 2.2 5.6	$2.7\cdot10^{11}$ 2.3 5.4
10 days	$3\cdot10^{8}$ 2.4 4.75	$2.9\cdot10^{9}$ 2.4 4.75	$6.8\cdot10^{9}$ 2.4 4.75	$2.4\cdot10^{10}$ 2.4 4.8	$4.6\cdot10^{10}$ 2.5 4.8	$8.9\cdot10^{10}$ 2.5 4.9
30 days	$6.8\cdot10^{7}$ 2.5 2.95	$6.7\cdot10^{8}$ 2.6 4.95	$1.6\cdot10^{9}$ 2.6 4.95	$1.1\cdot10^{10}$ 2.6 5.95	$1.3\cdot10^{10}$ 2.6 4.95	$2.8\cdot10^{10}$ 2.6 4.9
100 days	$2.8\cdot10^{6}$ 2.5 4.6	$2.8\cdot10^{7}$ 2.5 4.6	$6.6\cdot10^{7}$ 2.5 4.55	$2.6\cdot10^{8}$ 2.5 4.5	$5.9\cdot10^{8}$ 2.4 4.5	$1.8\cdot10^{9}$ 2.4 4.4
1 yr	$6.6\cdot10^{5}$ 2.3 4	$6.6\cdot10^{6}$ 2.3 4	$1.6\cdot10^{7}$ 2.3 4	$6.6\cdot10^{7}$ 2.3 4	$1.6\cdot10^{8}$ 2.3 4	6.3^{8} 2.3 4
2 yr	$2.75\cdot10^{5}$ 2.3 4.05	$2.75\cdot10^{6}$ 2.3 4.05	$6.6\cdot10^{6}$ 2.3 4.05	$2.7\cdot10^{7}$ 2.3 4.05	$6.5\cdot10^{7}$ 2.3 4.05	$2.6\cdot10^{8}$ 2.3 4.05

TABLE 3. (CONTINUED)

τ \ T	100 days	0.5 yr	1 yr	2 yr
1 hr	$2.8\cdot10^{12}$ 2.2 5.5	$2.8\cdot10^{12}$ 2.2 5.5	$2.8\cdot10^{12}$ 2.2 5.45	$2.8\cdot10^{12}$ 2.2 5.45

TABLE 3. (CONCLUDED)

T \ τ	100 days	0.5 yr	1 yr	2 yr
10 hr	$5.25 \cdot 10^{11}$ 2.2 6.1	$5.3 \cdot 10^{11}$ 2.2 6.1	$5.3 \cdot 10^{11}$ 2.2 6.1	$5.35 \cdot 10^{11}$ 2.2 6.1
1 day	$2.8 \cdot 10^{11}$ 2.3 5.3	$2.9 \cdot 10^{11}$ 2.3 5.3	$2.9 \cdot 10^{11}$ 2.3 5.3	$2.9 \cdot 10^{11}$ 2.3 5.3
10 days	10^{11} 2.5 4.9	10^{11} 2.5 4.9	$1.1 \cdot 10^{11}$ 2.5 4.8	$1.1 \cdot 10^{11}$ 2.5 4.8
30 days	$3.2 \cdot 10^{10}$ 2.6 4.9	$3.5 \cdot 10^{10}$ 2.6 4.8	$3.8 \cdot 10^{10}$ 2.5 4.8	$4.2 \cdot 10^{10}$ 2.5 4.7
100 days	$3.4 \cdot 10^{9}$ 2.3 4.2	$5.1 \cdot 10^{9}$ 2.3 4.2	$8 \cdot 10^{9}$ 2.3 4.1	$1.1 \cdot 10^{10}$ 2.3 4.1
1 yr	$1.4 \cdot 10^{9}$ 2.3 4	$2.3 \cdot 10^{9}$ 2.3 4	$3.85 \cdot 10^{9}$ 2.3 4	$5.5 \cdot 10^{9}$ 2.3 4
2 yr	$5.85 \cdot 10^{8}$ 2.3 4.05	$9.7 \cdot 10^{8}$ 2.3 4.05	$1.6 \cdot 10^{9}$ 2.3 4.05	$2.3 \cdot 10^{9}$ 2.3 4.05

Remark. The first line gives the number of γ-quanta for 1 kW in 1 sec; the second line gives the average energy of γ-quanta in MeV; the third line gives the averaged out cross section in $cm^2 \cdot 10^{28}$.

In conclusion the author expresses his gratitude to N. P. Vergachev for discussing the results.

REFERENCES

1. White, D. and Berk, J. Beryllium (Berilliy). Moscow, Izd-vo I. L., 1960.

2. Hamermesh, G. and Kimball, C. Phys. Rev., Vol. 90, 1063, 1953.

3. Nathans, R. and Halpern, J. Phys. Rev., Vol. 90, 940, 1953.

4. Strominger, D., Hollander, G. and Seaborg, G. Rev. Mod. Phys., Vol. 30, 585, 1958.

5. Katcoff, S. Nucleonics, Vol. 16, No. 4, 78, 1948.

6. Pappas. The Nuclear Charge Distribution During Fission by Low Energy Neutrons. Materials of the International Conference on the Peaceful Application of Atomic Energy. Vol. 7 (Raspredeleniye yadernogo zaryada pri delenii neytronami maloy energii. Materialy Mezhdunarodnoy konferentsii po mirnomu ispol'zovaniyu atomnoy energii). Moscow, Gostekhizdat, p. 30, 1958.

7. Dzhelepov, B. S. and Peker, L. K. Decay Diagrams for Radioactive Nuclei (Skhemy raspada radioaktivnykh yader). Moscow, Izd-vo I. L., 1958

8. Steynberg and Glendenin. A Survey of Radiochemical Investigations of the Fission Process. Materials of the International Conference on the Peaceful utilization of Atomic Energy. Vol. 7 (Obzor radiokhimicheskikh issledovaniy protsessa deleniya. Materialy Mezhdunarodnoy konferentsii po mirnomu ispol'zovaniyu atomnoy energii). Moscow, Gostekhizdat, p. 11, 1958.

APPLICATION OF THE MONTE CARLO METHOD FOR COMPUTING NUCLEAR RADIATION SHIELDING

V. G. Zolotukhin and S. M. Yermakov

Introduction

Solutions of the kinetic equation which consider the energy relationship of cross sections, the nonisotropic nature of scattering processes and the finite geometry are associated with substantial mathematical difficulties. Therefore in many cases the Monte Carlo method is the only means of solving the problem. /171

As we know, the application of the Monte Carlo method to problems associated with the penetration of neutrons and γ-quanta into a substance is possible, because there is an absence of interaction between particles in real beams. This feature, which makes the fates of individual particles independent, makes it possible to predict the behavior of an aggregate of particles by analyzing a sufficiently large number of observed fates ("histories"). /172

Substantial difficulties are frequently encountered in this direct approach to the solution of problems by the Monte Carlo method. These difficulties, first of all, are associated with the determination of small probabilities. When the unknown probability p is determined by the Monte Carlo method utilizing the ratios $\hat{p} = \frac{M}{N}$ (M is the number of realizations in which the event of interest to us has taken place; N is the total number of realizations), the dispersion of this evaluation is equal to N_p (1-p), while the relative error for determining p is equal to

$$\varepsilon(p) = \frac{(D\hat{p})^{1/2}}{p} = \frac{1}{\sqrt{N}} \sqrt{\frac{1}{p} - 1}, \qquad (1)$$

from which it follows that for small probabilities p we must have a rather large number of realizations N to achieve the desired accuracy.

In problems associated with the transmission of radiation through matter, the low value of probability p may be due to the absorption of particles, leakage from the medium, energy loss due to moderation, etc. However, in cases where the probability p of interest to us is not small the application of the method is always accompanied by a more or less cumbersome procedure. This

basic disadvantage of the method is associated with its slow convergence, which according to expression (1) is of the order of $N^{-1/2}$. This slow convergence is due to the probability nature of the method and does not depend on the special features associated with the problem.

It is known that the Neumann series for the solution of the kinetic equation reduces the radiation transport problem to the computation of multiple integrals, whereas the Monte Carlo method itself, in essence, consists of computing the terms of the Neumann series, which are multiple integrals. In some works of Soviet mathematicians it has been proposed to utilize the sequence of nonrandom points for computing multiple integrals (refs. 1-3). Under definite conditions, when the functions under the integral sign are regular, this provides a higher order of convergence. At the same time the utilization of nonrandom points means that we reject the probabilities scheme associated with the Monte Carlo method. This makes it impossible to make a practical evaluation of the accuracy associated with the results.

On the other hand, practical methods have been developed for decreasing the sampling dispersion, while retaining the normal order of convergence. The present article is a short survey of the basic approaches for increasing the statistical effectiveness of the Monte Carlo method in problems of radiation transport. The most important of these have been tried out on a large number of specific problems.

Practical Methods for Decreasing the Sampling Dispersion

If we are interested in some functional of the kinetic equation solution, the methods described below usually provide an accuracy which is satisfactory for practical purposes when the number of histories is 10^3-10^4.

The Method of Arbitrary Probabilities.[1] In the phase space T we introduce the coordinate r of the scattering point, the direction Ω and energy E of the particle after scattering. The point (r, Ω, E) of space T will be designated by x. We also introduce the transient probability $K(x' \to x)\,dx$, that the particle which has left x' undergoes its next scattering at the element dx near x. In other words, $K(r', \Omega', E' \to r, \Omega, E)\,dr\,d\Omega\,dE$ is the probability that the particle leaving point r' in direction Ω' with energy E' experiences its next scattering in the volume element dr near r at which time it changes its direction and energy in the intervals $d\Omega$ and dE near Ω and E, respectively. The following integral equation is valid for the differential scattering density $\psi(x)dx$,[2] which represents the average number of particles /173

[1] In the American literature it is known as the method of analytical averaging (ref. 4).

[2] The density of scattering is associated with the differential flux $nv = \Phi(r, \Omega, E)$ by the relationship $\Phi(r,\Omega,E) = \int_0^\infty [\psi(r-s\Omega,\Omega,E) + Q(r-s\Omega,\Omega,E)]\, e^{-\tau(r,r-s\Omega,E)}\, ds$, where $\tau(r, r' E)$ is the optical scattering between the points r and r'.

scattered per unit time in a volume element dr and which fly to the cone dΩ near Ω with an energy in the interval dE near E

$$\int_T K(x' \to x)\,[\psi(x') + Q(x')]\,dx' = \psi(x), \tag{2}$$

where Q (x') characterizes the distribution of sources. The solution of equation (2) is given by the Neumann series

$$\left.\begin{aligned} \psi(x) &= \sum_{i=0}^{\infty} \psi_i(x); \\ \psi_i(x) &= \int_T K(x' \to x)\,\psi_{i-1}(x')\,dx'; \\ \psi_0(x) &= \int_T K(x' \to x)\,Q(x')\,dx'. \end{aligned}\right\} \tag{3}$$

Let us consider the determination of some functional $I = (\psi, \varphi) = \int_T \psi(x) \times \varphi(x)\,dx$ by the Monte Carlo method. Utilizing expressions (3) we find

$$(\psi, \varphi) = \sum_{i=0}^{\infty} (\psi_i, \varphi) = \sum_{i=0}^{\infty} I_i, \tag{4}$$

where

$$I_i = \int_T \dots \int_T dx_0\,dx_1 \dots dx_i\,dx Q(x_0)\,K(x_0 \to x_1) \times \\ \times K(x_1 \to x_2) \dots K(x_i \to x)\,\varphi(x).$$

We shall call the Monte Carlo method conventional if we use the true transient probability K (x' → x) of the Markov chain of successive particle scattering for the realization of particle "history." The corresponding process for the random movement of a particle in space T begins with the point x_0, which has a distribution Q (x_0) (it is assumed that $\int_T Q(x_0)\,dx_0 = 1$). Next we establish successively the scattering points $x_0, x_1, \dots, x_n, \dots$ In connection with this it is established each time whether the particle has disappeared due to absorption or leakage or whether the particle undergoes a subsequent scattering. The probability that the particle which has left the point x has disappeared is equal to $g(x) = 1 - \int_T K(x \to x')dx'$, while the scattering probability is $1-g(x)$. Sooner or later this process is disrupted and ends with particle destruction.

We obtain a statistical evaluation $\hat{I}$ of the functional I, if we remember that

$$M\sum_{j=1}^{l}\varphi(x_j)=\int_T\int_T Q(x_0)K(x_0\to x_1)\varphi(x_1)\,dx_0\,dx_1+$$
$$+\int_T\int_T\int_T dx_0\,dx_1\,dx_2 Q(x_0)K(x_0\to x_1)K(x_1\to x_2)\varphi(x_2)+\ldots=\sum_{i=0}^{\infty}(\psi_i,\varphi)=I, \tag{5}$$

where M is the symbol for the mathematical expectation; $x_1, x_2, \ldots, x_l$ are the selected values of the scattering point; l is their total quantity (in this case the exit point for the source particle is assumed to be the zero scattering point). To prove expression (5) we note that the following outcomes for the realization of "histories" are possible; /174

$$\text{SD, SSD, SSSD, ...,}$$

where, for example, SSD signifies a double scattering and a subsequent destruction of the particle. The probability density of chains $\underbrace{SSS\ldots SD}_{i}$ is equal to $Q(x_0)$ $K(x_0\to x_1)\ldots K(x_{i-1}\to x_i)\,g(x_i)$, so that

$$M\sum_{j=1}^{l}\varphi(x_j)=\int_T\int_T K(x_0\to x_1)Q(x_0)\varphi(x_1)g(x_1)\,dx_0\,dx_1+$$
$$+\int_T\int_T\int_T Q(x_0)K(x_0\to x_1)K(x_1\to x_2)[\varphi(x_1)+\varphi(x_2)]g(x_2)\,dx_0\,dx_1\,dx_2+\ldots \tag{6}$$

Noting that $g(x)=1-\int_T K(x\to x')\,dx'$, we find

$$M\sum_{j=1}^{l}\varphi(x_j)=\lim_{n\to\infty}\Big[\sum_{i=0}^{n}(\psi_i,\varphi)-\int\ldots\int Q(x_0)K(x_0\to x_1)\ldots\times$$
$$\times K(x_{n+1}\to x)\sum_{\mu=1}^{n+1}\varphi(x_\mu)\,dx_0\,dx_1\ldots dx_{n+1}\,dx\Big]. \tag{7}$$

It is easy to show that when we limit $\varphi(x)$ the last integral in expression (7) disappears when $n\to\infty$.

It follows from this that the evaluation $\hat{I}$ of the functional $I=(\psi,\varphi)$ may be obtained as the arithmetical mean of the results obtained by individual tests

$$I\cong\hat{I}=\frac{1}{N}\sum_{\mu=1}^{N}\sum_{j=1}^{l_\mu}\varphi(x_j^{(\mu)}); \tag{8}$$

l_μ is the total number of scatterings in the μ-th test; $x_j^{(\mu)}$ is the point of the j-th scattering in the μ-th test.

In the same manner we can determine the dispersion $D\hat{I}$ of the $\hat{I}$. We leave out the calculation steps and present the final result

$$D\hat{I} = \frac{1}{N}[(\psi, \varphi^2) + 2(\psi\,\psi^*, \varphi) - (\psi, \varphi)^2], \tag{9}$$

where $\psi^*(x)$ is the solution of the conjugate equation

$$\int [\varphi(x') + \psi^*(x')]\, K(x \to x')\, dx' = \psi^*(x)$$

with source $\varphi(x)$.

It should be pointed out that if the functional I is small this Monte Carlo procedure will lead to large relative errors in the determination of this functional. Let us assume, for example, that it is necessary to determine the radiation spectrum passing through a thin layer of moderator with high absorption. Since a substantial part of the "histories" will end with the destruction of particles due to absorption, and since most of the particles which have passed through the layer will have an energy close to the source energy, we can conclude that the information on the soft part of the transmitted radiation spectrum will be entirely inadequate.

As we shall show below, the application of the following modification to the Monte Carlo method always decreases the dispersion of estimation $\hat{I}$ (ref. 6).

We introduce the distribution function $K_s(x' \to x)$ for point x /175

where a fictitious particle which has left x' is scattered,

$$K_s(x' \to x) = \frac{K(x' \to x')}{\int K(x' \to x')\, dx'} = \frac{K(x \to x')}{1 - g(x)}$$

and organize the random motion of the particle starting at point x_0 with distribution $Q(x_0)$. Since $\int_T K_s(x \to x')\, dx' = 1$, the random motion of this particle lasts for an infinite period of time. We introduce the random quantity ξ associated with the random motion $x_0 \to x_1 \to x \to \ldots \to x_n \to \ldots$,

$$\xi = \sum_{j=1}^{\infty} W_j \varphi(x_j),$$

where

$$W_j = \prod_{\mu=0}^{j-1} [1 - g(x_\mu)]. \tag{10}$$

The average value of this quantity is equal to

$$M\xi = \sum_{j=1}^{\infty} \underbrace{\int \ldots \int}_{j+1} dx_0 Q(x_0) K_s(x_0 \to x_1)\, dx_1 K_s(x_1 \to x_2)\, dx_2 \ldots$$

$$\ldots K_s(x_{j-1} \to x_j)\, dx_j \varphi(x_j) \prod_{\mu=0}^{j-1} [1 - g(x_\mu)] \int dx_{j+1} K_s(x_j \to x_{j+1}) =$$

$$= \sum_{j=1}^{\infty} \int \ldots \int Q(x_0)\, dx_0 K(x_0 \to x_1)\, dx_1 K(x_1 \to x_2)\, dx_2 \ldots$$

$$\ldots K(x_{j-1} \to x_j) \varphi(x_j)\, dx_j = \sum_{j=1}^{\infty} (\psi_{j-1}, \varphi) = I,$$

from which we obtain the statistical evaluation of the functional I

$$I \approx \hat{I}^* = \frac{1}{N} \sum_{j=1}^{N} \sum_{\mu=1}^{n} W_\mu^{(j)} \varphi(x_\mu^{(j)}), \tag{11}$$

when n is a predetermined number of fictitious particle scatterings such that we can neglect the effect of all subsequent scatterings compared with the statistical error associated with the determination of I. This "threshold for cutting off" the history must be determined on the basis of physical considerations.

The quantity $W_\mu = \prod_{j=1}^{\mu-1} [1 - g(x_j)]$ is frequently called the "weight" of the μ-th scattering. It represents an arbitrary probability for the "survival" of particles which have undergone scattering at points $x_0, x_1, x_2, \ldots, x_{\mu-1}$. This is responsible for the name given to the method.

The dispersion of evaluation $\hat{I}^*$ may be obtained by simple steps

$$D\hat{I}^* = \frac{1}{N} [(\Theta, \varphi^2) + 2(\Theta\psi^*, \varphi) - (\varphi, \psi)^2], \tag{12}$$

where $\Theta(x)$ is the solution of the integral equation

$$\int_T [Q(x') + \Theta(x')] [1 - g(x')] K(x' \to x)\, dx' = \Theta(x).$$

A comparison of expressions (12) and (9) shows that $D\hat{I}^* < DI$.

Various modifications of this method are possible. They are all based on the introduction of the transient probability $\tilde{K}(x \to x')$, associated with $K(x \to x')$ by expression /176

$$\tilde{K}(x \to x') = \frac{K(x \to x')}{\int_{(D)} K(x \to x')\, dx'},$$

where (D) is the region of space T in which the function $\varphi(x)$ assumes the maximum values. A transition of this type must of course be accompanied by the introduction of corresponding weights.

The Semianalytical Monte Carlo Method. This method combines an extremely wide group of approaches, so that at this time we can describe it only in a very general way. The method is based on the utilization of analytical solutions (if such are feasible) to create certain branching in the basic random motion process. If, for example, the main role in Neumann series (ref. 3) is played by the first scattering, while the contribution made by the second, third, etc., represents a correction, it is expedient to find this correction by the Monte Carlo method, and to establish the contribution made by the first scattering analytically. In this case even relatively large errors in the determination of multiple scattering effects does not lead to large errors in the quantity of interest to us. This method of isolating the principal part of the solution serves as an extremely effective means for solving many problems.

In general, if it is possible to integrate the Neumann series over several variables, this always leads to a decrease in dispersion (ref. 7). Thus, in a case of a homogenous semi-infinite layer of finite thickness, the Neumann series may be integrated over the variables $z_1, z_2, \ldots, z_n, \ldots$, where z_i is the coordinate of the i-th dispersion (ref. 8). Integration over the energy variables and the variable angles is carried out by the Monte Carlo method.

The Method of Control Variables (ref. 5). The basic idea behind the method of control variables consists of the following. Let us assume that ξ_0 is some random quantity, which is formed in a random experiment σ. The mathematical expectation ξ_0 is obtained by the Monte Carlo method. Let us assume that $\xi_1, \xi_2, \ldots, \xi_n$ is a series of other random quantities corresponding to experiment σ, the mathematical expectation $M\xi_i$, $(i = 1, 2, \ldots, n)$, however, is known exactly. We form the following random quantity

$$\xi = \xi_0 - \sum_{j=1}^{n} a_j (\xi_j - M\xi_j), \tag{13}$$

where a_j for a while, remain as indeterminant constants. From expression (13) we have $M\xi = M\xi_0$; consequently, the sampled values of ξ may be used to evaluate $M\xi_0$ for any selection of weights a_j. The latter should naturally be selected in such a way that the dispersion $D\xi$ is a minimum. This gives us

$$\frac{\partial}{\partial a_k} M\left[\xi_0 - \sum_{j=1}^{n} a_j (\xi_0 - M\xi_j)\right]^2 = 0,$$

from which we obtain

$$M[\xi_0(\xi_h - M\xi_h)] = \sum_{j=1}^{n} a_j M[(\xi_j - M\xi_j)(\xi_h - M\xi_h)]. \tag{14}$$

Noting that $\rho_{i,\,k} = \frac{M[(\xi_i - M\xi_i)(\xi_k - M\xi_k)]}{\sqrt{D_i D_k}}$ is the correlation coefficient between ξ_i and ξ_k (D_i is the dispersion of ξ_i), we obtain

$$\sqrt{D_i}\rho_{0i}\sqrt{D_0} = \sum_{j=1}^{n} \rho_{i,j} a_j \sqrt{D_i D_j}$$

or, in matrix form $x = (x_1, x_2, \ldots, x_n)$,

$$x_i = a_i\sqrt{D_i};\ \rho_0 = (\rho_{0,1}, \rho_{0,2}, \ldots, \rho_{0,n});$$
$$\sqrt{D_0}\,\rho_0 = Rx,$$

where R is the symmetric matrix

$$R = \begin{pmatrix} \rho_{1,1}\ \rho_{1,2} & \ldots & \rho_{1,n} \\ \rho_{2,1}\ \rho_{2,2} & \ldots & \rho_{2,n} \\ \cdots\cdots\cdots\cdots & & \\ \rho_{n,1}\ \rho_{n,2} & \ldots & \rho_{n,n} \end{pmatrix}.$$

After substitution in $D\xi$ the solution $x = R^{-1}\sqrt{D_0\rho_0}$ gives us /177

$$D\xi = D_0 - 2\sqrt{D_0}(\rho_0, x) + (x, Rx) = D_0[1 - (\rho_0, R^{-1}\rho_0)],$$

from which we conclude that the dispersion ξ decreases compared with the dispersion ξ_0 according to the expression

$$\varepsilon = 1 - (\rho_0, R^{-1}\rho_0).$$

In the particular case of a single control variable n = 1 we have

$$\varepsilon = 1 - \rho_{0,1}^2, \quad a_1 = \rho_{0,1}\sqrt{\frac{D_0}{D_1}}.$$

If $\rho_{0,1} = 0$, dispersion ξ_0 cannot be decreased. If $\rho_{0,1} = 1$, there is a linear relationship between ξ_0 and ξ_1

$$\xi_0 - M\xi_0 = a_1(\xi_1 - M\xi_1).$$

In the case of two control variables n = 2

$$R^{-1}=\begin{pmatrix} \frac{1}{1-\varrho_{1,2}^2}, & -\frac{\varrho_{1,2}}{1-\varrho_{1,2}^2} \\ -\frac{\varrho_{1,2}}{1-\varrho_{1,2}^2}, & \frac{1}{1-\varrho_{1,2}^2} \end{pmatrix};$$

$$\varepsilon=\left(1-\frac{\varrho_{0,1}^2+\varrho_{0,2}^2-2\varrho_{0,1}\varrho_{0,2}\varrho_{1,2}}{1-\varrho_{1,2}^2}\right);$$

$$a_1=\sqrt{\frac{D_0}{D_1}}\cdot\frac{\varrho_{0,1}-\varrho_{0,2}\varrho_{1,2}}{1-\varrho_{1,2}^2};$$

$$a_2=\sqrt{\frac{D_0}{D_2}}\cdot\frac{\varrho_{0,2}-\varrho_{0,1}\varrho_{1,2}}{1-\varrho_{1,2}^2}.$$

The quantity $\varrho = \left(\frac{\varrho_{0,1}^2+\varrho_{0,2}^2-2\varrho_{0,1}\varrho_{0,2}\varrho_{1,2}}{1-\varrho_{1,2}^2}\right)^{1/2}$ is the correlation relationship between ξ_0 and ξ_1, ξ_2, which is well known in mathematical statistics. If $\varrho = 1$, the following linear relationship exists between ξ_0, ξ_1, ξ_2

$$\xi_0-M\xi_0=a_1(\xi_1-M\xi_1)+a_2(\xi_2-M\xi_2).$$

The equations which have been obtained are of a theoretical nature and the weights a_j are not known to us exactly. However, they can be computed approximately by making use of results obtained from the simultaneous observation of values ξ_0, ξ_1, ..., ξ_n used to evaluate those quantities which determine a_j.

The basic difficulty associated with the application of the method of control variables, or as it is frequently called, the method of correlation sampling, involves the establishment of random quantities ξ_1, ..., ξ_n, which are strongly correlated with ξ_0 and whose mathematical expectation must be known. Sometimes the problem can be solved by some numerical method with certain simplifying assumptions. This solution can be used as the mathematical expectation of the corresponding control variable. This approach to the solution of problems of the theory of radiation transport is important, because it associates the method of statistical tests with achievements in the development of conventional numerical methods.

Berger and Doggett (ref. 8) used this method successfully to determine the dose B (t, t) produced by radiation passing through a layer of finite thickness t. The control variable was taken as the dose B (t, ∞) at the depth t in a semiinfinite medium, which can be established with sufficient accuracy by the method of moments. /178

Correlation selection is useful when it is necessary to determine the difference of two close quantities. Positive correlation between these may

make it possible to utilize the same collection of random quantities or histories (ref. 11). Finally, the application of correlation sampling gives a smoother variation in the values of the multiple integral as a function of the parameter than its independent computation for the collection of parameter values (ref. 11).

Substantial sampling. The multiple integral

$$I = \int f(x)\, dx$$

may be computed by the Monte Carlo method utilizing the sampled values x_1, $x_2 \ldots$, x_N of the random quantity ξ, which has a certain arbitrary probability density $g(x)$. Indeed, the mathematical expectation of the random quantity $\frac{f(\xi)}{g(\xi)}$ $M\frac{f(\xi)}{g(\xi)} = \int f(x)\, dx = I$ does not depend on $g(x)$ and is equal to I. However, the dispersion $D\frac{f(\xi)}{g(\xi)} = \int \frac{f(x)}{g(x)}\, dx - I^2$ depends on the selection of $g(x)$. If $g(x) = \frac{|f(x)|}{\int |f(x)|\, dx}$ then $D\frac{f(\xi)}{g(\xi)} = 0$.

Since the integral $\int |f(x)|\, dx$ is unknown, it is not possible to reduce the dispersion to zero, but it is possible to reduce it substantially if we select $g(x)$ in such a way that the ratio $\left|\frac{f(x)}{g(x)}\right|$ varies little in the region of integration.

Local Computation of the Flux

It is obvious that the methods described above are not suitable for the case $\varphi(x) = \delta(x-x^*)$, i.e., when it is necessary to determine the phase density $\psi(x^*)$ of scattering at one fixed point x^*. Indeed, since the phase volume is equal to zero, none of the selected trajectories will pass through point x^*. This case will appear as the limiting case when radiation is recorded with a detector having a rather low effectiveness for counting individual particles emitted by the source. Such a detector produces practically no perturbation of the radiation field, and it may be assumed with good approximation that the number of detector counts is directly proportional to the phase density $\psi(x^*)$.

The following method makes it possible to avoid this difficulty. Let us return to the conventional Monte Carlo method, i.e., let us consider the random motion of a particle with a transient probability $K(x \to x')$. We introduce the random quantity

$$\xi_2 = \sum_{j=1}^{l} K(x_j \to x^*), \tag{15}$$

where x_j, as before, are points of scattering; l is their total number. According

to relationship (5) the mathematical expectation ξ_2 is equal to (we should set $\varphi(x) = K(x \to x^*)$)

$$M\xi_2 = |\psi, K(x \to x^*)| = \int_T K(x \to x^*)\psi(x)\,dx.$$

From the basic equation (2) it follows that

$$\psi(x^*) = M\xi_2 + \int_T Q(x_0)\,K(x_0 \to x^*)\,dx_0, \tag{16}$$

i.e., $M\xi_2$ is the contribution of the scattered radiation to the phase density. $\psi(x^*)$. The contribution of the unscattered radiation is not difficult to compute.

This method can be easily combined with the method of conditional probabilities. As an example let us consider the problem of finding the angular and energy distribution of γ-quanta flux (ref. 9) at point r^* of space in the presence of sources $Q(x_0)$. Let r_j be the radius vector of the j-th /179 scattering point; Ω_j, E_j the direction and energy of γ-quanta after the j-th scattering where the random motion is organized with a transient probability $K_s(x \to x')$. Then the application of the method of conditional probabilities and of relationship (16) gives us the following expression for the scattered part of the flux $\Phi_s(r^*, \Omega, E)$

$$\Delta\dot{\Omega}\Delta E\Phi_s(r^*, \Omega, E) = M\sum_{j=1}^{n} W_j \frac{e^{-\Sigma_t(r_j, E_j)|r_j - r^*|}}{|r_j - r^*|^2} \times \\ \times f(E_j, \Omega_j, \omega_j)\,\gamma(\Omega, \omega_j)\,\Delta(E, \tilde{E}_j), \tag{17}$$

where W_j is the "weight" of the j-th scattering; $\Sigma_t(r, E)$ is the total macroscopic cross section; $(E, \Omega, \Omega')\,d\Omega'$ is the probability that the γ-quantum with energy E will change its direction Ω in the interval $d\Omega'$ near Ω' due to scattering by a free electron; $\omega_j = \dfrac{r_j - r^*}{|r_j - r^*|}$;

$$\Delta(\Omega, \Omega') = \begin{cases} 1, & \text{if } \Omega' \text{ belongs to the interval } \Delta\Omega \text{ near } \Omega; \\ 0, & \text{in the opposite case;} \end{cases}$$

$$\Delta(E, E') = \begin{cases} 1, & \text{if } E' \text{ belongs to the interval } \Delta E \text{ near } E; \\ 0, & \text{in the opposite case;} \end{cases}$$

$\tilde{E}_j = E\,[E_{j-1},\ (\omega_j \Omega_{j-1})]$ is the energy after scattering by an angle $\theta = \arccos (\Omega_{j-1}\omega_j)$ of the γ-quantum which had an energy E_{j-1} before scattering.

The presence of the term $|r_j - r^*|^2$ in the denominator leads to the divergence of dispersion of the random quantity ξ_2. However, this does not present an obstacle for the utilization of the Monte Carlo method. Indeed, the existence of the mathematical expectation $M\xi_2$ establishes the validity of the law of large numbers, i.e., the probability convergence of the mean arithmetical value of results from N experiments to the value of the flux $\Phi_s\ (r^*, E, \Omega)$ (ref. 10). It is, of course, obvious that the absence of dispersion of evaluation, based on relationship (17) leads to the fact that the distribution of the mean arithmetical value of N tests is not asymptotically normal. As a result we cannot evaluate the errors by computing a sampled dispersion, and we must use other methods to evaluate the errors.

This shortcoming of the method for the local computation of the flux involving the absence of dispersion may be removed if we compute the Fourier coefficients of the flux in terms of three-dimensional variables. In this case the concepts presented in reference 11 are valid, and the results of work presented in references 12 and 13 may be used to decrease the dispersion of the Fourier coefficients. In these references interpolation quadratic equations and interpolation equations with random nodes were constructed. In computing the Fourier-Legendre coefficients it is convenient to construct the interpolation polynomials of low order by breaking down the integration region into smaller parts. From the difference of the values for the interpolation polynomials at the boundary of the regions it is easy to obtain an idea of the accuracy associated with the approximation of the unknown function by the interpolation polynomial.

Application of Quadrature Equations with Random Nodes

A further development of the general methods of decreasing a dispersion, based on the construction of interpolation quadrature equations (ref. 12) makes it possible to construct quadrature equations with random nodes of increased accuracy, which are extremely useful for practical applications.

Let us consider the quadrature sum $\sum_{i=0}^{n} A_i f\ (Q_i)$ for the approximate computation of the integral $\int_D f(Q)\, dQ$. Let us assume that $f(Q)$ has been determined and that its squares have been added in the region D of Euclid space k of measurements $Q_i \in D$. If we require that the quadrature equation /180

$$\int_D f(Q)\, dQ \approx \sum_{i=0}^{n} A_i f(Q_i)$$

be exact for assigned linearly independent functions $\varphi_0, \varphi_1, \ldots, \varphi_n$, then if Q_i is fixed the coefficients A_i may be determined uniquely from the conditions

$$\sum_{i=0}^{n} A_i \varphi_j(Q_i) = \int_D \varphi_j(Q)\, dQ. \tag{18}$$

In this case it is necessary to assume that the determinant of the system of linear algebraic equations (18) is different from zero.

Such quadrature equations were considered in reference 12, proceeding from the proposition that the nodes Q_i are selected at random. A function for the probability density of nodes Q_i was constructed and for this function the following equality was valid

$$M \sum_{i=0}^{n} A_i f(Q_i) = \int_D f(Q)\, dQ.$$

The utilization of quadrature sums with random nodes may lead to a substantial gain in the computational work when the function $\varphi_i(Q)$ is successfully selected.

We may require that the quadrature equation (18) be exact for a large number of linearly independent functions $\varphi_0, \varphi_1, \ldots, \varphi_{n+r}$ $(r < n)$. In this case in addition to equality (18) the following equalities must also be satisfied

$$\sum_{i=0}^{n} A_i \varphi_{n+m}(Q_i) = \int_D \varphi_{m,n}(Q)\, dQ \quad (m = 1, 2, \ldots, r).$$

These equalities obviously place additional limitations on the distribution of nodes Q_i in the region D. The quadrature equation with n+1 random nodes, which are exact for more than (n+1)-th linearly independent function, will be called the correlation quadrature equations. The simplest correlation quadrature equations were constructed on the basis of other considerations in references 14 and 15.

In the present work, as an example, we present a sufficiently simple correlation quadrature equation which is successfully used in solving a series of problems associated with the transmission of radiation through a substance.

Let D be a unit hypercube. The quadrature equation

$$\int_0^1 dx^{(1)} \ldots \int_0^1 f(x^1, x^2 \ldots, x^k)\, dx^{(k)} \approx \frac{1}{6} [f(x_0^{(1)}, \ldots, x_0^{(k)}) + f(x_1^{(1)}, \ldots, x_1^{(k)}) + f(x^{(1)}, x^{(2)} \ldots, x^{(k)}) + f(1 - x_0^{(1)}, \ldots, 1 - x_0^{(k)}) + f(1 - x^{(1)}, \ldots, 1 - x_1^{(k)}) + f(1 + x_2^{(1)}, \ldots, 1 - x_2^{(k)})] \quad (19)$$

is exact for unity, $x^{(m)}$ and $(x^{(m)})^2$ (m = 1, 2, ..., k) and the corresponding quadratic sum is the undisplaced evaluation of the integral, if the coordinates of the nodes are equally distributed on the surface,

$$(x_0^{(m)})^2 + (x_1^{(m)})^2 + (x_2^{(m)})^2 = 1,$$
$$x_0^{(m)} \geqslant 0, \quad x_1^{(m)} \geqslant 0, \quad x_2^{(m)} \geqslant 0$$
$$(m = 1, 2, \ldots, k).$$

In computing the transmission of radiation through an infinite plate the number of computational works decreases, when quadrature equation (19) is used, by a factor of 10 if the plate thickness is equal to 1-3 mean free paths, and by a factor of 15 if the thickness is 7-10 mean free paths computed from /181 the initial particle energy.

In the present work we shall not present correlation quadrature equations of more complex form, because at the present time they have been tried in a very small number of examples. However, we should note that their application to increase the effectiveness of the Monte Carlo method is apparently quite promising.

Solving Problems by Means of High-Speed Computers

The qualitative aspects of programming are of great significance when the Monte Carlo method computations are carried out by means of high-speed computers. This problem should be given special consideration. It is clear that the relatively small reduction in the number of operating steps for the computer, when a single particle history is computed, leads to a substantial saving of time necessary to solve the problem as a whole. This places very stiff requirements on the programming of problem solution, analogous to those requirements levied on standard subprograms. The individual units of the program for solving problems associated with the transmission of radiation through a substance by the Monte Carlo method are common for various problems.

If we have a large library of such units, it is possible to provide for rapid and high-quality composition of programs and the wide application of methods for increasing the effectiveness of the Monte Carlo method. It is also necessary to have a special compiling system which takes into account the special features associated with problems of this type and provides for a convenient assignment of information for compilation.

Work on the construction of such a system has been carried out by S. M. Yermakov, I. Ye. Bocharova, B. A. Yefiemenko and others. The availability of such a system makes it possible to carry out the exchange of programming units between interested parties, which is of great significance for the application

of effective computation methods. We note that the adoption of automatic programming language in practice does not in any way decrease the significance of unit programming in this case.

REFERENCES

1. Sobol', I. M. Journal of Computational Mathematics and Mathematical Physics (Zhurnal vychislitel'noy matematiki i matematicheskoy fiziki). Vol. 1, 917, 1961.

2. Korobov, N. M. Dokl. AN SSSR, Vol. 115, 6, 1957; Vol. 124, 6, 1951.

3. Bakhvalov, N. S. Journal of Computational Mathematics and Mathematical Physics (Zhurnal vychislitel'noy matematiki i matematicheskoy fiziki). Vol. 1, 64, 1961.

4. Fanov, U., Spencer, L. and Berger, M. The Transport of Gamma Radiation (Perenos gamma-izlucheniya). Moscow, Gosatomizdat, 1963.

5. Kramer, G. The Mathematical Methods of Statistics (Matematicheskiye metody statistiki). Moscow, Izd-vo I. L., 1948.

6. Vladimirov, V. S. The Theory of Probabilities and its Application (Teoriya veroyatnostey i yeye primeneniye). Vol. 1, 113, 1956.

7. Buslenko, N. P. et al. The Method of Statistical Experiments (The Monte Carlo Method) (Metod statisticheskikh ispytaniy (Metod Monte Karlo)). Moscow, Fizmatgiz, 1962.

8. Berger, M. J. and Doggett, J. J. J. Res. Nat. Bur. Standards, Vol. 56, 89, 1956.

9. Lynch, R. E. J. et al. A Monte Carlo Calculation of Air-Scattered Gamma Rays. ORNL-2292, Vol. I.

10. Gnedenko, B. V. and Kolmogorov, A. N. The Limiting Distributions of Independent Random Quantity Sums (Predel'nyye raspredeleniya summ nezavisimykh sluchaynykh velichin). Moscow, Gostekhizdat, 1948.

11. Frolov, A. S. and Chentsov, N. N. Journal of Computational Mathematics and Mathematical Physics (Zhurnal vychislitel'noy matematiki i matematicheskoy fiziki). Vol. 2, 715, 1962.

12. Yermakov, S. M. and Zolotukhin, V. G. The Theory of Probabilities and its Application, (Teoriya veroyatnostey i yeye primeneniya). Vol. 5, 473, 1960.

13. Yermakov, S. M. Journal of Computational Mathematics and Mathematical Physics (Zhurnal vycheslitel'noy matematiki i matematicheskoy fiziki). Vol. 3, 186, 1963.

14. Hammersley, J. M and Morton, K. W. Proc. Cambridge Philos. Soc., Vol. 52, 449, 1956.

15. Morton, K. W. J. Math. & Phys., Vol. 36, 289, 1957.

PART II. THE EXPERIMENTAL INVESTIGATIONS OF SHIELDING

THREE-DIMENSIONAL ENERGY DISTRIBUTION OF NEUTRONS IN THICK IRON LAYERS

V. P. Mashkovich, V. K. Sakharov and S. G. Tsypin

Iron is a shielding material which is widely used in practice. /182
It is used as a convenient structural material for reactor vessels, in iron and hydrogen-containing mixtures, in thermal and biological shieldings, etc.

In spite of the wide application of iron, information published to date on the three-dimensional distribution of neutrons in iron (refs. 1-4) is still rather limited. Table 1 shows a summary of the basic experimental data on the penetration of neutrons through iron, published in the literature.

The present work is concerned with the investigation of the three-dimensional distribution of fast and intermediate neutrons in iron (ref. 5).

A description of the B-2 experimental setup is presented in reference 5 (see also the article on p. 357 of this volume). The BR-5 reactor (refs. 6, 7 and 8) serves as the neutron source. The spectrum of neutrons incident on the iron prism is presented in figure 1 (refs. 5 and 9). For neutron energy greater than 1 MeV the spectrum is determined by means of a photographic plate /183
with a K-type emulsion having a thickness of 200 μ and manufactured by the engineering photographic plate plant.

The photographic plates are installed in the neutron beam as it leaves the channel of the biological shielding. The spectrum was constructed according to results obtained from more than 2500 recoil proton track measurements with protons escaping forward at an angle of ± 15°. The spectrum which has been obtained takes into account the variation in the cross section of neutron scattering by hydrogen, the background radiation and the finite thickness of the emulsion layer. A comparison of the obtained spectrum with the fission spectrum shows that when the energy is less than 3 MeV there is a slight softening of the obtained spectrum (ref. 5).

The neutrons passed through a channel with a diameter of approximated 250 mm in the shielding and entered a tank which contained a steel prism with dimensions of 1320 x 1360 x 1880 mm (fig. 2a). The neutron beam entered the tank through the middle of the wall whose dimensions are 1320 x 1360 mm. The total angular divergence of the beam was approximately 5°.

TABLE 1. DATA ON THE PENETRATION OF NEUTRONS THROUGH IRON.

Neutron energy	Source characteristics	Measured thickness of iron, cm	Detector	Relaxation length, cm	Literature
4 Mev	Point isotropic	50	Th^{232} (n, f)	7.5	(1)
			P^{31} (n, p) Si^{31}	-	
			S^{32} (n, p) P^{32}	-	
14.9 Mev	the same	50	Th^{232} (n, f)	8.3	(1)
			S^{32} (n, p) P^{32}	-	
Spectrum of reactor neutrons	VVR reactor	45	Th^{232} (n, f)	7.6	(1)
			U^{235} (n, f)	36	(4)
the same	-	-	Np^{237} (n, f)	9.9	(2)
			U^{238} (n, f)	5.55	
			"All-wave" Cd counter	20	
			In Cd	4.26	
			Thermal neutron detector	1.51	
Fast neutrons	-	-		6.0	(3)
Intermediate neutrons	-	-		30	(3)

Thus a unidirectional disk source with angular divergence specified above was used in the experiment. The prism was assembled from nine packs with dimensions of 1320 × 1360 × 117 mm, followed by seven packs with dimensions of 1390 × 1360 × 117 mm. The iron packs differed in thickness by not more than 1 percent. Each iron pack consisted of six sheets with dimensions[1] of 1320 × 1360 × 19.5 mm and had a vertical hole for an iron plug with a diameter of 90 mm and a depth of 830 mm.

The plug which was used to take the measurements contained a groove for the detector holder, which consisted of an iron strip with a device for installing the detectors. The shape of the detector holder corresponded to that of the groove. The iron density was 7.86 g/cm^3; the brand of iron was C_T-0 (with additions of C, Mn, S and P constituting a total of up to 0.6 percent).

During the measurements the iron prism was introduced into the biological shielding to a depth of 1400 mm. Fast neutron detectors consisted of threshold indicators operating according to the reactions S^{32} (n, p)P^{32}, Mg^{24}, (n, p) Na^{24}, Al^{27} (n, α) Na^{24}, whose effective energy thresholds for the incident spectrum were equal to approximately 3, 5 and 7 MeV, respectively. The tracers consisted of disks with a diameter of 35 mm and heights of 6, 2 and 5 mm, respectively. The sulfur tracers were made of chemically pure fused sulfur, the magnesium tracers were made of chemically pure magnesium, and the aluminum tracers were made of chemically pure AV-000 aluminum.

A Th^{232} fission chamber with a height of 4 cm and a diameter of 8 mm (the effective threshold for the incident spectrum is approximately equal to 2 MeV) was used as a detector of fast neutrons.

A SNM-3[2] type proportional counter filled with BF_3 was used to detect intermediate neutrons together with copper tracers with a diameter of 35 mm and a thickness of 1.1 mm, operating according to the reaction Cu^{63} (n, γ) Cu^{64}, and gold tracers with a diameter of 6 mm and a thickness of 4 mg/cm^2 operating according to the reaction Au^{197} (n, γ) Au^{198}.

The above tracers were placed into detector holders of two types. The detector holder for threshold tracers as well as for the copper and gold tracers (fig. 2b) had holes for installing detectors along its entire length, spaced at a distance of 50 mm from each other. In order to fill the air holes, iron disks with a diameter of 35 mm and a thickness of 1 mm were installed into the same holes together with the tracers. These disks were designed in such a way as to eliminate the air gap completely. Small iron cylinders of corresponding

[1] Beginning with the ninth pack the 1320 mm dimension was increased to 1390 mm.
[2] In the future we shall refer to it simply as the boron counter.

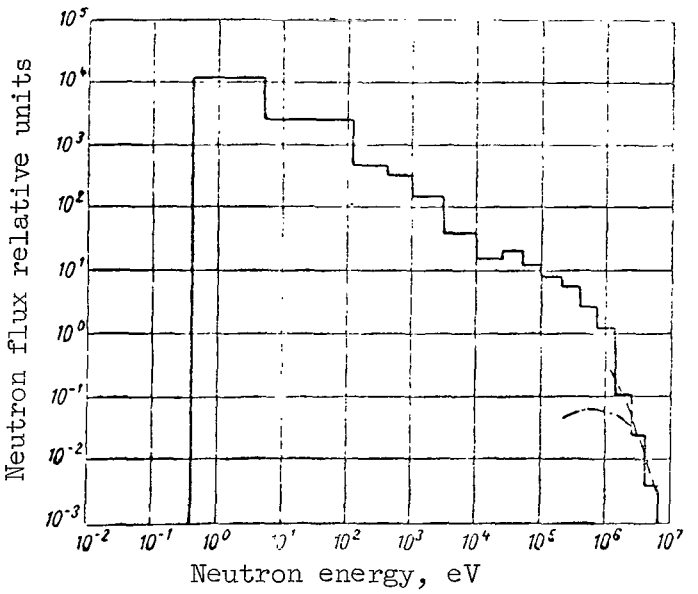

Figure 1. Spectrum of neutrons incident on iron prism; ———— data presented in reference 9; – – – – – data presented in ref. 5; –·–·–· spectrum of fission neutrons.

dimensions were placed into holes which were not occupied by the indicators.

The detector holder for the boron counter and for the Th^{232} fission chamber (fig. 2c) had a hole in the lower part for the counter or for the end chamber and grooves for running a cable to the detector. The displacement of the detector in the vertical direction was achieved by lifting the detector holder and filling the resulting air gap with iron.

The holes in the packs made it possible to place detectors at different points in the iron prism under the plugs and the detector holders. The position of a sensor was fixed with an accuracy of at least 1 mm in the horizontal and vertical directions.

The detectors were placed at various distances r from the source and at a different height h from the central beam in a direction perpendicular to the neutron beam (fig. 3).

The activity induced in the copper, gold and sulfur tracers was determined by constructing the decay curves. Measurements were made using a type B installation with an end SI-2B type counter. The stability of counter installation operation was controlled periodically by means of a uranium standard, and the background radiation was also measured periodically.

The induced activity of aluminum and magnesium tracers could not be /185 determined with this method because of difficulty of distinguishing the basic activity from the activity of the additives. The activity of the added copper

Figure 2. General view of iron prism (a) of detector holder for copper and gold tracers (b) and of detector holder for boron counter (c).

becomes particularly pronounced as the distance from the source increases due to the large difference in the penetration capability of fast and intermediate neutron fluxes. Therefore the activity of aluminum tracers, for example, was determined from the peak of photoelectrons produced in the crystal by Na^{24} γ-rays with energies of 2.76 MeV. Measurements were carried out by means of a scintillation γ-spectrometer with a NaJ (Tl) crystal having dimensions of 80 X 80 mm (ref. 10).

The aluminum tracers were installed in a fixed position close to the scintillating crystal. The energy scale was controlled according to the γ-radiation of the Co^{60} isotope. A correction was introduced for the activity of the Na^{23} $(2 \pm 1)\ 10^{-4}$ percent additive by using a neutron flux of intermediate energy (ref. 11).

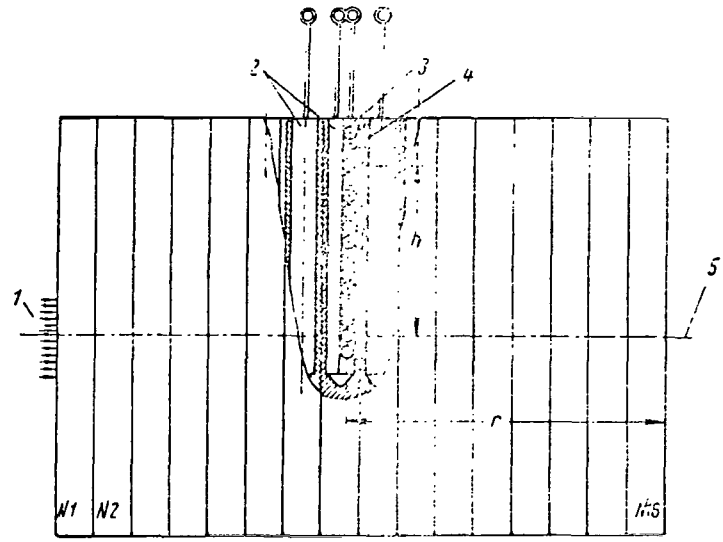

Figure 3. Schematic of experimental setup: 1, source; 2, plug; 3, detector holder; 4, holes for detector; 5, central beam; Nos. 1-16, iron assemblies.

Measurements made with magnesium tracers and with the thorium chamber were corrected for the count due to the addition of U^{235} in the Th^{232} chamber and due to the additional activity of impurities in the metallic magnesium, utilizing the method described in reference 11.

Figures 4, 5 and 6 show, respectively, the activity of sulfur and aluminum tracers and the readings of the thorium chamber as a function of height h for various distances r from the source. The three-dimensional distributions of neutrons measured with the boron counter and with copper and gold tracers agreed within 10 percent.

Figure 7 shows these three-dimensional distributions as a function of h for fixed values of r.

The measured distributions shown in figures 4, 5, 6 and 7 represent the three-dimensional distribution of neutrons from the unidirectional disk source used in the experiment.

Figures 8, 9 and 10 show the neutron attenuation functions for the infinite plane unidirectional source $G_{\infty,p}(r)$, which were determined from measurements made with various tracers according to equations in references 5 and 12,

$$G_{\infty,\ D}(r)\,C = \int_0^{\infty} G_{M}(r, h)\,h\,dh,$$

where $G_{D\ M}(r, h)$ are the distributions shown in figures 4, 5, 6 and 7; C is a constant.

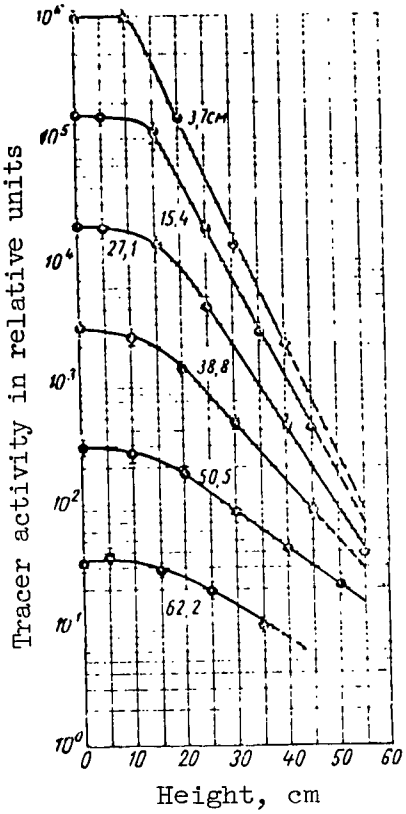

Figure 4. Activity of sulfur threshold tracers as function of height h for various distances r.

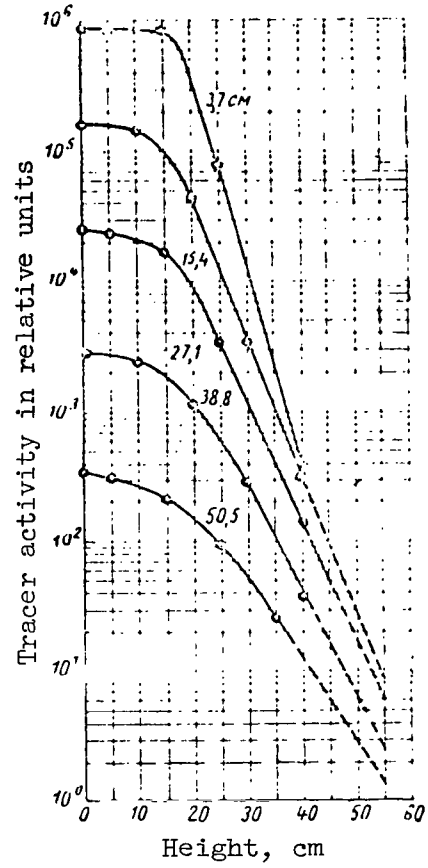

Figure 5. Activity of aluminum threshold tracers as function of height h for various distances r.

Figures 8 and 9 also show the attenuation curves for neutrons in /186 the direction of central beam $G_{D\,M}(r,0)$.

For the case of aluminum tracers figure 9 also shows the neutron attenuation curve in the direction of the central beam measured by the end counter, i.e., without eliminating the effect produced by foreign impurities. These measurements were carried out after aging for a period of 15-20 hr, so that the foreign activities which remained were due only to Cu^{64}, which has a half-life close to the half-life of Na^{24} formed according to the reaction Al^{27} (n, α) Na^{24} and Na^{24} formed according to the reaction Na^{23} (n, γ) Na^{24}.

The results of the measurements carried out with all of the tracers are shown in table 2.

Figure 11 shows the measured cadmium ratios R_{Cd} for copper tracers, i. e., the ratios of readings made with a tracer without a cadmium filter to the readings made by a tracer with a cadmium filter under identical conditions of irradiation.

The filters were built in the form of small cadmium cases with a thickness of 0.6 mm. The curves in figure 11 show that the cadmium ratio is equal to unity within the limits of a 10 percent error.

Analogous results were obtained by measurements taken with gold tracers and boron counters.

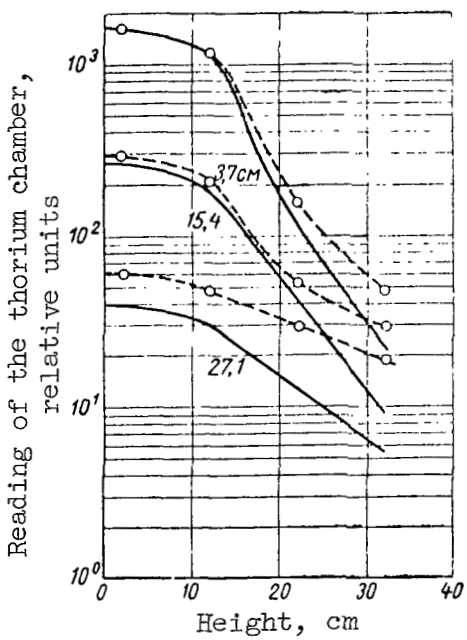

Figure 6. Readings of Th^{232} fission chamber as function of height h for various distances r (– – – – data from direct measurements without corrections for counts due to U^{235} additive).

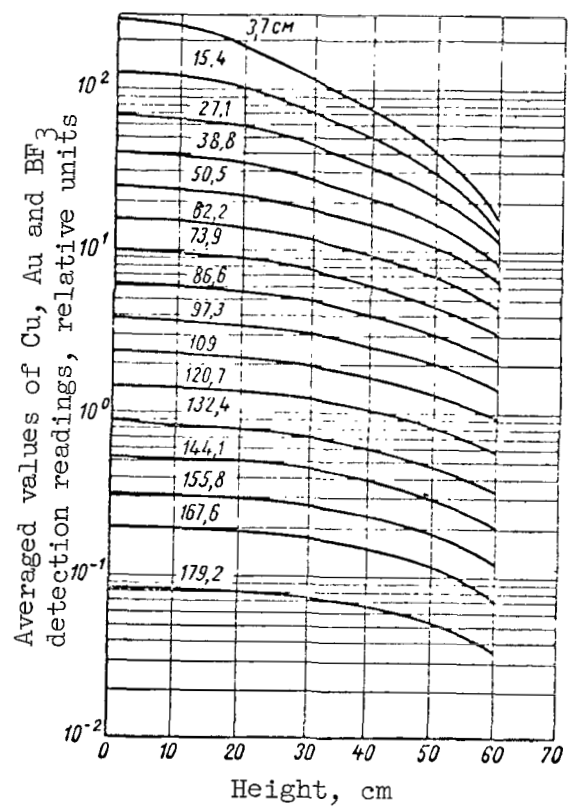

Figure 7. Measured neutron distribution for various values of distance r.

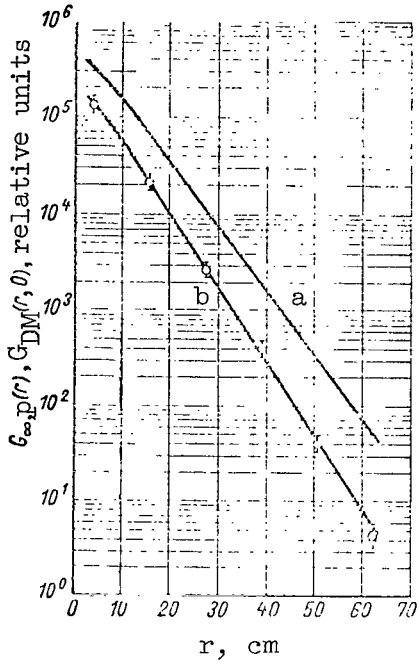

Figure 8. Neutron attenuation function for infinite plane unidirectional source (a) and attenuation curve in direction of central beam (b) measured with sulfur tracers.

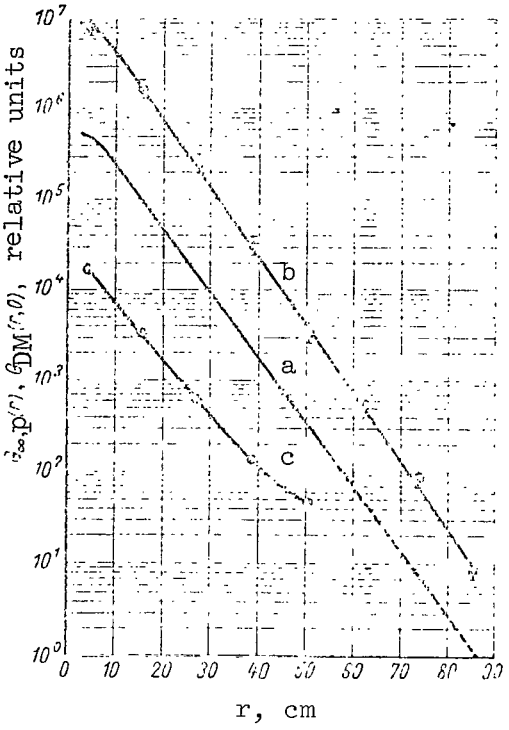

Figure 9. Neutron attenuation function for infinite plane unidirectional source (a) and attenuation curves in direction of central beam corresponding to measurements made with gamma spectrometer (b) and with end counter (c) (measurements made with aluminum tracers).

In the present work measurements were also made of the gold ratio for /187 gold tracers. This ratio is defined as the ratio of tracer readings without a gold filter to tracer readings with a gold filter. The thickness of gold filters was 107 mg/cm^2. The gold ratio was constant and was equal to 4.8 (during measurements with an accuracy of approximately 13 percent).

Let us compare the results which we obtained with known cross sections and with certain computed data.

The relaxation length obtained for measurements with the Th^{232} fission chamber agrees well with data presented in reference 1.

The discrepancy in the relaxation length measured by means of threshold tracers according to reactions S^{32} (n, p) P^{32}, Mg^{24} (n, p) Na^{24} and Al^{27} (n, α) Na^{24} and measured by means of the Th^{232} fission chamber may be explained by the decrease in the cross section when the energy is 1-2 MeV.

The values of relaxation lengths obtained experimentally from measurements with sulfur, magnesium and aluminum tracers agree well with the corresponding value computed according to the removal cross section (ref. 13), differing from the latter by 10 percent. /188

Table 3 shows the computed values of asymptotic cross sections in the transport approximation for several energy groups (p. 99 of this volume).

The computation of these cross sections is based on the adopted group cross sections and on equations for determining the asymptotic diffusion length (ref. 14). /190

The data which have been obtained agree well with cross sections computed from relaxation lengths: $\sigma_{S^{32}\,(n,\,p)\,P^{32}} = 1.81$ barn; $\sigma_{Mg^{24}(n,\,p)\,Na^{24}} = 1.87$ barn; $\sigma_{Al^{27}(n,\,\alpha)\,Na^{24}} = 1.87$ barn.

In order to compare the experimental and theoretical data on the penetration of intermediate energy neutrons, the spectrum of intermediate energy neutrons was computed using the age theory.

We note that the form of the spectrum remains constant over the entire range of iron thicknesses which have been investigated. This agrees well with the constant relaxation length associated with the intermediate neutron flux attenuation over the entire shielding thickness obtained from measurements made by all of the detectors.

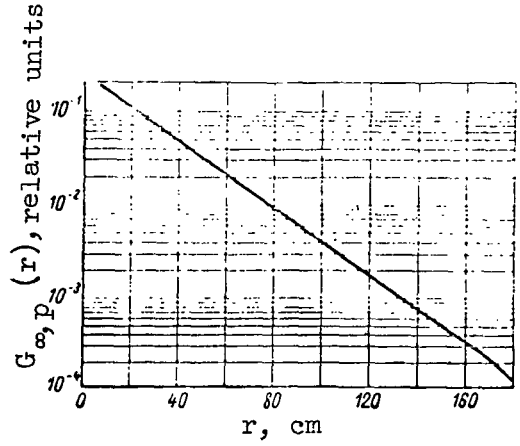

Figure 10. Neutron attenuation function for infinite plan unidirectional source measured with Cu, Au and BF_3.

TABLE 2. RESULTS OF MEASUREMENTS MADE WITH DIFFERENT TRACERS.

Detector	Effective threshold according to incident spectrum MeV	Measured range of thicknesses, cm	Relaxation length, cm
BF_3 counter	-	180	24.4
Cu^{63} (n, γ) Cu^{64}	-	180	24.4
Au^{197} (n, γ) Au^{198}	-	180	24.4
Th^{232} (n, f)	~2	50	7.5
S^{32} (n, p) P^{32}	~3	65	6.5
Mg^{24} (n, p) Na^{24}	~5	40	6.3
Al^{27} (n, α) Na^{24}	~7	85	6.3

TABLE 3. ASYMPTOTIC CROSS SECTIONS IN THE TRANSPORT APPROXIMATION, BARN.

Energy group, MeV	σ_{tr}	σ_{yB}	σ_{tr}^{scat}	σ_{as}
1.4-∞	2.2	0.7	1.5	1.9
1.4-2.5	2.2	0.8	1.4	1.9
2.5-4	2.3	1.0	1.3	2.1
4-6	2.2	1.2	1.0	2.1
6-∞	2.0	1.33	0.7	2.0

Proceeding from the obtained spectrum, a cadmium ratio equal to unity and a gold ratio equal to 5.9 were established. This agrees well with experimental data within the accuracy of experimental and computational error.

The authors express their deep gratitude to O. I. Leypunskiy and V. V. Orlov for useful remarks during the discussion of the work.

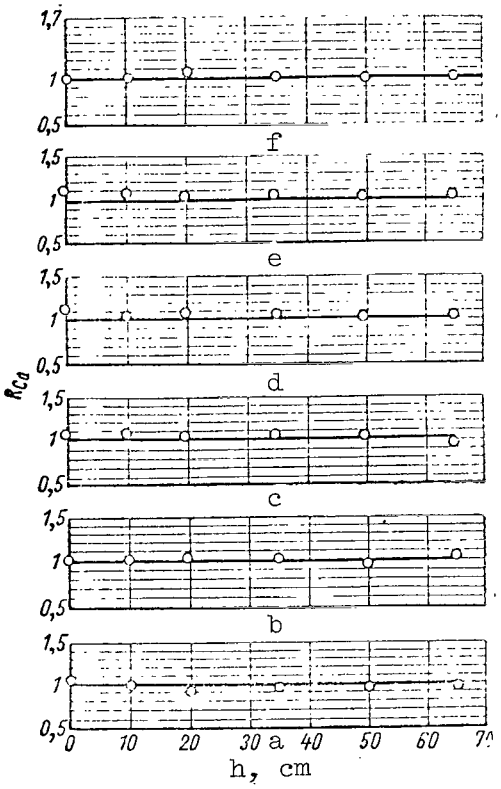

Figure 11. Cadmium ratio for copper tracers as function of height h and distance r, cm: a, r = 3.7; b, r = 50.5; c, r = 73.9; d, r = 97.3; e, r = 120.7; f, r = 144.1.

REFERENCES

1. Broder, D. L., Kurkin, S. A. et al. Investigation of Three-Dimensional Neutron Distributions in Various Media. In Transactions of the Second International Conference on the Peaceful Utilization of Atomic Energy. Reports of Soviet Scientist, Vol. 2. Nuclear Reactors and Nuclear Power Engineering (Izucheniye prostranstvenno-energeticheskikh raspredeleniy neytronov v razlichnykh sredakh. V kn.: Trudy Vtoroy mezhdunarodnoy konferentsii po mirnomu ispol'zovaniyu atomnoy energii. Doklady sovetskikh uchenykh. T. 2 - Yadernyye reaktory i yadernaya energetika). Moscow, Atomizdat, p. 674, 1959.

2. Wood, D. E. Nucl. Sci. Eng. Vol. 5, 45, 1959.

3. Blizard, E. P. Ann. Rev. Nucl. Sci., Vol. 5, 91, 1955.

4. Broder, D. L. Atomnaya Energiya, Vol. 7, 55, 1957.

5. Mashkovich, V. P. and Tsypin, S. G. Atomnaya Energiya, Vol. 11, 251, 1961.

6. Leypunskiy, A. I. et al. Experimental Fast Reactors in the USSR. In Transactions of the Second International Conference on the Peaceful Utilization of Atomic Energy. Reports of Soviet Scientists. Vol. 2, Nuclear Reactors and Nuclear Power Engineering (Eksperimental'nyye bystryye reaktory v SSSR. V kn.: Trudy Vtoroy mezhdunarodnoy konferentsii po mirnomu ispol'zovaniyu atomnoy energii. Doklady sovetskikh uchenykh. T. 2. Yadernyye reaktory i yadernaya energetika). Moscow, Atomizdat, p. 215, 1959.

7. --- Atomnaya Energiya, Vol. 5, 277, 1958.

8. --- Atomnaya Energiya, Vol. 7, 192, 1959.

9. --- Atomnaya Energiya, Vol. 11, 498, 1961.

10. Larichev, A. V. and Cherevatenko, G. A. Investigation of the Sensitivity of a Single Crystal Scintillation γ-spectrometer with a NaJ (Tl) 80 x 80 mm Crystal. In Instruments and Methods of Analyzing Radiations. No. 3 (Issledovaniye chustvitel'n osti odnokristal'nogo stsintillyatsionnogo-spektrometra s kristallom NaJ (Tl) 80 x 80 mm. V sb.: Pribory i metody analiza izlucheniy). Moscow, Gosatomizdat, 1962.

11. Mashkovich, V. P. P. 409 of this volume.

12. Dulin, V. A. et al. Atomnaya Energiya, Vol. 9, 315, 1960.

13. The Shielding of Mobile Installations with a Nuclear Engine. Collection of Translations Edited by V. V. Orlov and S. G. Tsypin (Zashchita transportnykh ustanovok s yadernym dvigatelem. Sb per. pod. red. V. V. Orlova i S. G. Tsypina). Moscow, Izd-vo I. L., 1961.

14. Price, B., Horton, C. and Spinney, K. Shielding of Nuclear Radiations (Zaschita ot yadernykh izlucheniy). Moscow, Izd-vo I. L., 1959.

DEFORMATION OF FAST NEUTRON SPECTRUM IN CONCRETE AND WATER[1]

Yu. A. Yegorov

Measurements of spectrum deformation of fast nuclear reactor /190
neutrons passing through thin concrete layers and water layers were carried out on the nuclear reactor of the Academy of Sciences USSR (ref. 1). The spectra were measured by means of a fast neutron scintillation spectrometer with two sensors (ref. 2). The reactor neutrons were introduced through the side experimental reactor channel, and before entering the spectrometer they passed through a graphite reflector with a thickness of 1 m and a steel plate with a thickness of 16 mm. The spectra were measured in the energy range of 2.1-3.6 MeV.

The neutrons from the experimental reactor channel passed through a collimator (paraffin with borax and lead) and entered the crystal analyzer of /191
the spectrometer--stilbene; neutrons which were scattered by the crystal analyzer at an angle of 70° entered the starting sensor, which consisted of five scintillation counters with a liquid scintillator (a solution of diphenylbutadiene in xylene). The electronic circuits of the spectrometer were connected in such a way that the pulses which entered the pulse amplitude analyzer were proportional to the energy of recoil protons formed in the sensor-analyzers of the spectrometer only when neutrons were scattered at an angle of 70°. The neutron energy was determined from the relationship $E_n = E_p/\sin^2 70^\circ$ (E_n is the neutron energy, MeV).

The spectrometer was calibrated by measuring the α- and β-spectra of several radioactive radiation sources. The transition of the α- and β-particle energy into proton energy was carried out on the basis of data presented in reference 3.

During the investigation of transmission spectra, the concrete plates and little baths with water were placed in front of the spectrometer collimator in the path of neutrons from the experimental channel. The concrete utilized in the experiment has a volumetric weight of 2.2 metric tons/m^3, and was prepared from conventional Portland cement whose chemical composition is given in reference 4.

---

[1] This work was carried out in 1955.

To study the transmission spectra of fast neutrons through water, the latter was poured into thin-walled flat baths made of brass.

The fast neutron spectrum behind the reactor reflector has a maximum at an energy of 2.35 MeV (fig. 1, curve 1); the number of neutrons with this energy is greater than the number of neutrons with the maximum energy by a factor of approximately 40. The form of the spectrum behind the reflector is substantially different from the form of U^{235} fission neutron spectrum. While the nondescending region of fission neutron spectrum is well approximated by a function of the form $N(E_n) \simeq e^{-E_n/1.55}$, according to data presented by Hill (ref. 5), the nondescending region of the measured neutron spectrum behind the reflector may be described by the function $N(E_n) = 1.7 \cdot 10^5 e^{-2.7 E_n}$ (E_n is the energy of neutrons in MeV). Thus the fast neutron spectrum behind the reflector has a form which is different from the fission neutron spectrum. When

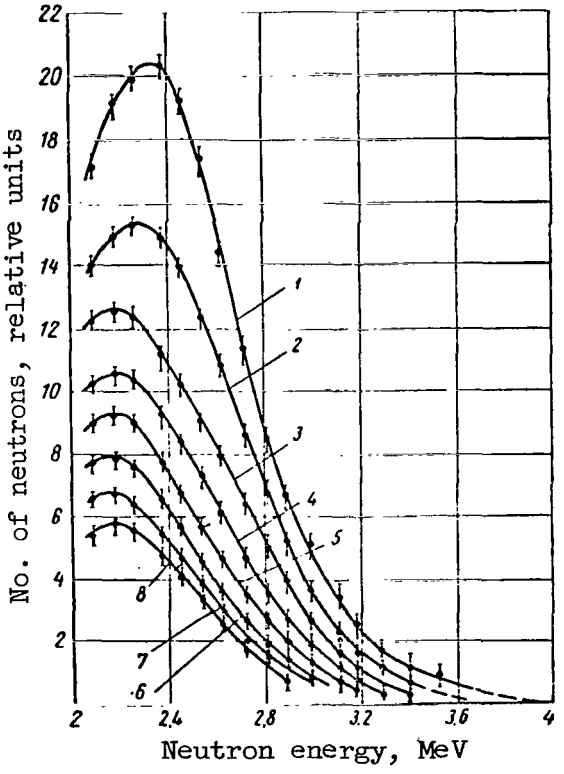

Figure 1. Transmission spectra of fast neutrons through concrete layer of various thickness: 1, spectrum behind reactor reflector; 2, 5 cm; 3, 7.5 cm; 4, 10 cm; 5, 12.5 cm; 6, 15 cm; 7, 17.5 cm; 8, 20 cm.

$E_n < 2.3$ MeV, the number of neutrons is sharply reduced; the relative number of neutrons with $E_n > 3$ MeV is also reduced. The neutron spectrum behind the reflector appears to become monochromatic near the energy of 2.35 MeV. This result coincides with propositions which have been stated, for example, in reference 6.

The results of measuring transmission spectra of fast neutrons through a thin concrete layer are shown in figure 1. Curve 2 is obtained for a concrete thickness of 5 cm, and the remaining curves are obtained when the layer thickness is increased by 2.5 cm each time. As we can see, the form of the /192 spectrum does not differ too much from the spectrum of fast neutrons behind the reactor reflector.

As the thickness of the concrete layer is increased the absolute number of neutrons in the maximum decreases; however, it changes very little with respect to the number of neutrons with the maximum measured energy for given concrete thickness. As the thickness of the concrete layer is increased, the spectrum maximum is gradually displaced in the direction of lower energies: thus when the thickness is 10 cm the spectrum maximum is displaced by approximately 150 keV. In this case the maximum in the spectrum also decreases.

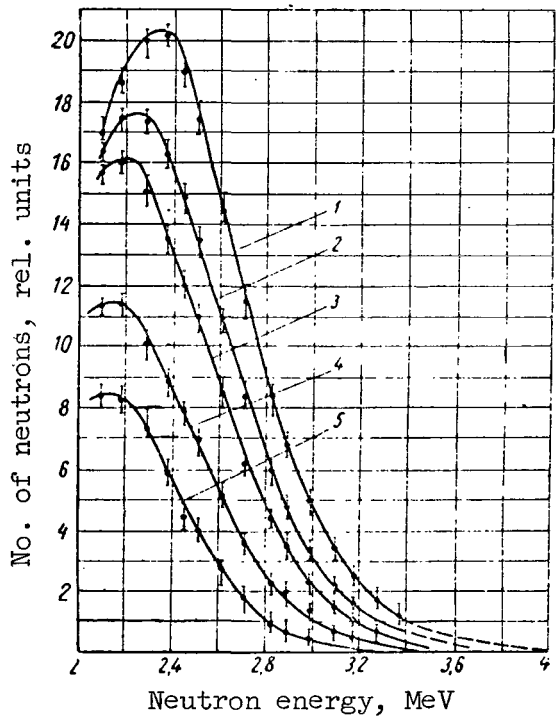

Figure 2. Transmission spectra of fast neutrons through water layers of different thickness: 1, spectrum behind reactor reflector; 2, 2.5 cm, 3, 5 cm; 4, 10 cm; 5, 20 cm.

The spectra of fast neutrons passing through water layers of small thickness vary in approximately the same manner (fig. 2). However, in this case the variation in the form of the spectrum takes place a little more rapidly than when neutrons pass through the concrete. When the water layer thickness is 20 cm, the maximum of neutron spectrum corresponds to an energy of 2.15 MeV. As the water layer thickness is increased, the boundary neutron spectrum energy decreases.

REFERENCES

1. Alikhanov, A. I. et al. Experimental Physical Reactor with Heavy Water. Materials of the Internation Conference on the Peaceful Utilization of Atomic Energy (Opytnyy fizicheskiy reaktor s tyazheloy vodoy. Materialy mezhdunarodnoy konferentsii po mirnomu ispol'zovaniyu atomnoy energii). Geneva, 1955. Vol. 2, Moscow, Fizmatgiz, 1958.

2. Yegorov, Yu. A. Pribory i Tekhnika Eksperimenta, No. 3, 28, 1958.

3. Taylor, G. et al. Phys. Rev., Vol. 84, 1034, 1951.

4. Gusev, N. G. Handbook on Radioactive Radiations in Shielding (Spravochnik po radioaktivnym izlucheniyam i zashchite). Moscow, Medgiz, 1956.

5. Hill, D. L. Phys. Rev., Vol. 87, 1034, 1952.

6. Price, B., Horton, C. and Spinney, K. Shielding of Nuclear Radiations (Zashchita ot yadernykh izlucheniy). Moscow, Izd-vo I. L., 1959.

SHIELDING PROPERTIES OF CERTAIN TYPES OF CONCRETES

V. N. Avayev, G. A. Vasil'yev, A. P. Veselkin,
Yu. A. Yegorov, A. D. Zhirnov,
V. A. Kucheryayev, Yu. V. Orlov, Ye. A. Panov
and Yu. V. Pankrat'yev

The biological shielding of nuclear reactors must attenuate the /193
neutron and γ-radiation fluxes from the active zone in such a way that the total dose power on its surface does not exceed the permissible level. Special concrete with an increased content of hydrogen nuclei and with introduced fillers containing heavy elements and boron compounds is very effective for this purpose.

The increased hydrogen content in concrete is achieved basically by introducing special materials which increase the quantity of water entering into a chemical bond with its composition. The attenuation of fast neutron fluxes by concrete is due primarily to the process of elastic neutron scattering by hydrogen nuclei and the inelastic scattering by iron nuclei or other heavy element nuclei which make up the concrete composition. Neutrons which have lost their energy as a result of these processes, and which have become thermal neutrons, are effectively absorbed by boron nuclei. Boron is introduced into the concrete composition in the form of various compounds, for example, calcium borate.

The introduction of heavy elements into concrete is also necessary for the effective attenuation of γ-ray fluxes, because the absorption of γ-radiation by a substance increases with the specific weight of the substance. The application of reinforcement sections and of cast iron scrap for the coarse filler increases the volumetric weight of concrete to 4-6 metric tons/m^3, which substantially improves its shielding properties (ref. 1).

The investigated concretes had light and heavy elements in their compositions, in the form of fine and coarse fillers and boron containing additions (ref. 2). Test samples were constructed in the form of rectangular plates with dimensions of 600 x 600 x 80 mm^3. The volumetric weight of concretes varied from 2.0 to 4.65 metric tons/m^3, depending on the form of the coarse filler. The compositions of the concretes which were investigated are shown in table 1.

The investigation of the shielding properties of concretes was carried out using sources of radioactive radiations. The attenuation of fast neutron

TABLE 1. COMPOSITION OF SPECIAL CONCRETES.

Concrete No.	Composition No.	Cement type	Filler types		Form of additive	Consumption of materials, kg/m³					Additive in % of entire concrete weight		Water-cement ratio and additive, relative units	Volumetric weight metric ton/m³
			Fine	Coarse		Cement	Sand	Gravel	Water	Additive	B	$CaCl_2$		
1	101	Portland	Magnetite	Serpentine	Calcium borate	210	991	811	262	105	0.5	-	0.8	2.4
2	84	"	---	Reinforcement sections	" "	294	--	3550	260	191	0.5	-	0.9	4.55
3	85	"	---	" "	" "	264	--	3510	285	248	0.75	-	1.08	4.55
4	144	Magnesian	Magnetite	Serpentine	" "	213	1058	865	288	107	0.5	-	0.9	2.53
5	145	Portland	"	"	" "	216	1071	890	256	108	0.5	2	0.8	2.53
6	PD	"	Datolite	Datolite	Datolite	207	421	1584	177	207	3.4	-	0.43	2.6
7	146	Magnesian	---	Reinforcement sections	Calcium borate	323	--	3880	254	208	0.5	-	0.8	4.65
8	147	Portland	Ordinary refractory clay	Ordinary refractory clay	Ordinary refractory clay	374	374	579	300	374	-	-	0.4	2.0
9	148	Portland No. 28 containing boron	Refractory clay No. 31 containing boron	Refractory clay No. 31 containing boron	Refractory clay No. 31 containing boron	382	382	591	260	382	3.44	-	0.34	2.0
10	149	Portland	Datolite	Datolite	Datolite	507	507	784	248	507	2.84	-	0.24	2.55
11	156	Portland No. 20 containing boron	Refractory clay No. 31 containing boron	Ordinary refractory clay	Refractory clay No. 31 containing boron	390	390	603	278	390	2.0	-	0.35	2.05
12	159	Magnesian	---	Reinforcement sections	Calcium borate	325	--	3325	358	325	0.9	-	1.1	4.40

fluxes by the concretes covering the entire spectrum of the Po + Be source in a wide beam was investigated by means of an "all-wave" counter (ref. 3). Measurements were carried out using barrier geometry and a wide beam, keeping a constant distance between the source and the sensor. The attenuating layer was built up from the source to the sensor.

The results of the investigations were used to determine the attenuation of fast neutrons for the entire spectrum of the Po + Be source for the individual concretes. Figure 1 shows the attenuation graphs for concretes Nos. 6, 8 and 12. The error associated with measurements conducted by means of the "all-wave" counter had an average value of 2.5 percent and varied in the limits from 1.6-5.4 percent.

The total attenuation cross sections Σ were computed from the attenuation curves. The calculation was carried out with the rectilinear portion of the attenuation law. The values obtained for Σ are represented in table 2.

The attenuation curves have inflection points for almost all of the concrete samples. When the thicknesses of the attenuating layer are greater than 35-59 cm, the total attenuation cross section Σ decreases. This inflection is explained by the contribution made by neutrons which fall into the counter after multiple scattering by surrounding objects (floor, ceiling) and by the test samples. This contribution increases as the thickness of the attenuating layer is increased. Consequently, a decrease in the value of Σ for large concrete thicknesses, independent of their composition, should be looked upon as an unavoidable experimental error. However, by increasing the thickness of the attenuating layer to 60-80 cm it is possible to determine the slope of the linear attenuation law region more exactly.

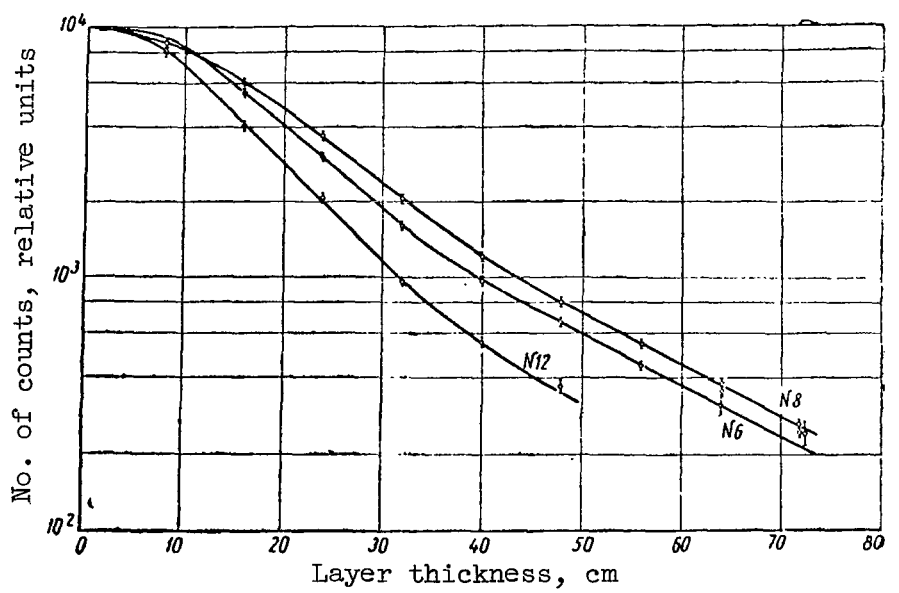

Figure 1. Attenuation of fast neutron fluxes of entire Po + Be source spectrum by concretes Nos. 6, 8 and 12.

TABLE 2. ATTENUATION CROSS SECTIONS FOR NEUTRON FLUXES OF THE ENTIRE Po + Be SOURCE SPECTRUM.

Concrete number	Σ, cm^{-1}	Error, %	Thickness of attenuating layer, cm	Concrete number	Σ, cm^{-1}	Error, %	Thickness of attenuating layer, cm
1	0.0626	4.5	> 15	7	0.0961	2.0	> 15
2	0.0754	3.8	> 15	8	0.0680	3.0	> 15
3	0.0827	3.8	> 15	9	0.0606	2.0	> 15
4	0.0846	4.0	> 15	10	0.0725	5.4	> 15
5	0.06442	2.4	> 15	11	0.0626	2.5	> 15
6	0.0768	2.1	> 15	12	0.0758	3.0	> 10

From the results obtained we can see that the flux of fast neutrons is best attenuated by heavy concretes Nos. 7, 3 and 12, whose composition /195 includes a large quantity of iron. Furthermore, these concretes have a sufficiently high hydrogen content compared to other samples, while concretes Nos. 7 and 12 also contain magnesium, whose total cross section in the region of approximately 1 MeV neutron energies is close to the total cross section of iron in this same region.

It is necessary to point out that many concretes (Nos. 6, 8, 10 and 11) produce the same attenuation of neutrons from the Po + Be source. However, the accumulation of neutrons in the first layers of these concretes is not the same. Therefore the attenuation curves obtained for these are almost parallel when the layer thickness is greater than 15-20 cm. The same is true of concretes Nos. 3 and 4.

The attenuation of thermal neutrons by concretes was also measured with a thermal neutron scintillation counter under conditions of a wide beam. Lithium glass (ref. 4) in conjunction with a FEU-29 photomultiplier was used as the sensor. The initial flux of thermal neutrons in these experiments resulted from the moderation of fast neutrons from the Po + Be source in graphite blocks. Measurements were carried out with and without a cadmium filter. The attenuation curves for thermal neutrons (more precisely for neutrons with energy 0-1.4 eV) were obtained by subtracting the measurement results obtained with the cadmium filter from the respective results obtained without a cadmium filter. Figure 2 shows the curves for the attenuation of thermal neutron flux by concretes Nos. 5, 6 and 8.

All of the test concretes except concrete No. 8 contain boron and /196 therefore produce a sharp attenuation of thermal neutron fluxes even when the concrete layer thickness is relatively small (5-10 cm). As the boron concentration is increased, the slope of the attenuation curves increases. A further increase in the layer thickness (10-40 cm) decreases the slope of the curves and in this region the flux of neutrons moderated in the concrete is weakened. When the concrete thickness is greater than 45 cm, the attenuation curves again undergo a sharp drop. It is obvious that from this boundary only the flux of neutrons which have been previously moderated is weakened. At this point there are no fast source neutrons.

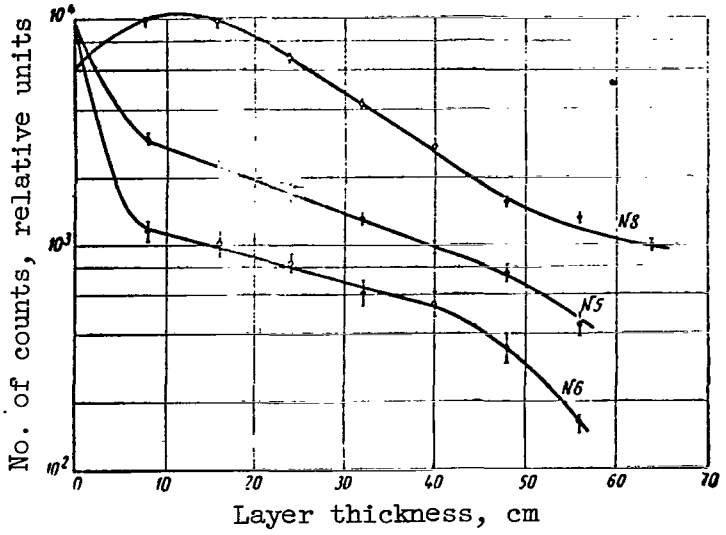

Figure 2. Attenuation of thermal neutron fluxes by concretes Nos. 5, 6 and 8.

TABLE 3. ATTENUATION CROSS SECTIONS FOR THERMAL NEUTRONS (TN).

Concrete number	Percentage of boron in concrete weight	Σ_{TN}, cm^{-1}	Error, %	Thickness of attenuating layer, cm	Concrete number	Percentage of boron in concrete weight	Σ_{TN}, cm^{-1}	Error, %	Thickness of attenuating layer, cm
3	0.75	0.277	10	< 5	8	--	0.0525	4	> 20
	0.0380	0.0380	21	> 10	9	3.44	0.354	15	< 5
4	0.5	0.180	11	< 5			0.0277	35	> 10
		0.0425	10	> 10	10	2.84	0.343	10	< 5
5	0.5	0.183	9	< 5			0.0327	22	> 20
		0.0346	14	> 10	11	2.0	0.198	21	< 5
6	3.4	0.354	11	< 5			0.034	35	> 20
		0.0258	30	> 10					

Concrete No. 8 does not contain boron, and for this reason the curve has a maximum when the concrete layer is approximately 10 cm and then decreases uniformly.

From the attenuation curves for fast neutrons we have determined the attenuation cross sections Σ_{TN}, shown in table 3.

The attenuation of the γ-radiation dose power by the concretes was measured with a scintillation γ-dosimeter without "hard operating" (ref. 5). The attenuation curves of γ-radiation dose power by concretes Nos.3, 4, 9, 10, 11 and 12 are shown in figure 3. The source of γ-radiation consisted of Co^{60} with an activity of approximately 70 milligrams equivalent of Ra. Measurements were carried out using barrier geometry and a wide beam.

The total attenuation cross section of the γ-radiation dose power Σ_γ for various concretes was determined from the attenuation curves. The values of Σ are shown in table 4. Calculation was carried out using the straight section of the curves with an accuracy of the order of 2 percent.

As was expected, the attenuation cross section for the γ-radiation dose power increases with the volumetric weight of the concrete. Since measurements were carried out using "wide" geometry, the initial region of the attenuation curves for the dose is flat, due to the accumulation of the scattered γ-radiation. This is followed by a linear steeper drop, and for concretes with approximately the same volumetric weight (2 metric tons/m^3 for concretes Nos. 8, 9 and 11; approximately 2.5 metric tons/m^3 for concretes Nos. 14, 15, 16 and 20 and 4.5 metric tons/m^3 for concretes No. 7 and 12) the behavior attenuation curves are the same, i.e., the γ-radiation dose power decreases according to

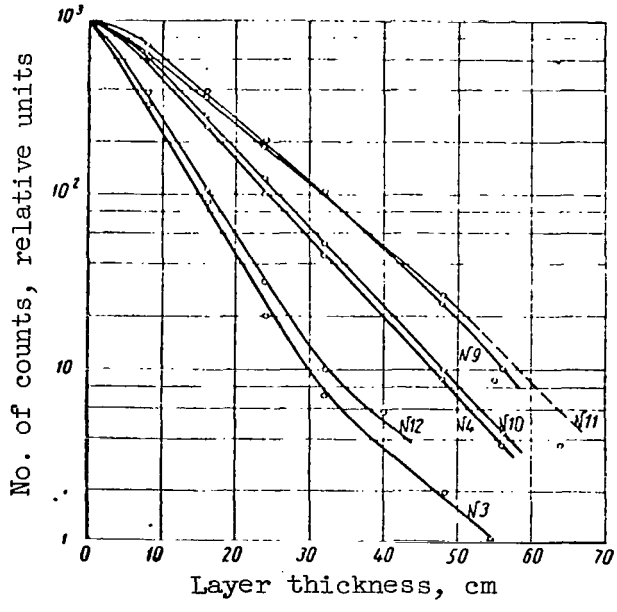

Figure 3. Attenuation of γ-radiation dose power by concretes Nos. 3, 4, 9, 10, 11 and 12.

TABLE 4. ATTENUATION CROSS SECTIONS FOR THE DOSE POWER OF γ-RADIATION.

Concrete number	Volumetric weight, metric tons/m^3	Σ_γ, cm^{-1}	Concrete number	Volumetric weight, metric tons/m^3	Σ_γ, cm^{-1}
3	4.55	0.157	8	2.0	0.0887
4	2.53	0.103	9	2.0	0.081
5	2.53	0.097	10	2.55	0.103
6	2.6	0.103	11	2.05	0.078
7	4.65	0.164	12	4.40	0.146

the same law. Light concretes attenuate γ-radiation, primarily due to Compton scattering, because for energies of the Co^{60} source γ-quanta this process /198 has a higher probability than the photoeffect or the formation of pairs. Therefore for these the slope of the attenuation curves increases for large thicknesses (50-60 cm), because an ever-increasing quantity of γ-quanta leave the flux due to scattering, and the basic contribution to the dose is given by hard nonscattered γ-quanta.

For concretes of average volumetric weight, the attenuation curves are rectilinear up to large thicknesses, whereas the curves for heavy concretes have an inflection at large thicknesses, which may be explained by the accumulation of "soft" γ-quanta.

These investigations show that heavy concretes serve as a more effective shielding from neutrons and γ-radiation. Concretes with a magnesium additive have slightly increased shielding properties compared with concretes utilizing the Portland cement, when the density is the same. The introduction of boron compounds into the concretes produces a strong attenuation of thermal flux.

REFERENCES

1. Price, B. T., Horton, C. C. and Spinney, K. T. Radiations Shielding (Zashchita ot yadernykh izlucheniy). Moscow, Izd-vo I. L., 1959.

2. Arshinov, I. A. P. 500 of this volume.

3. Avayev, V. M. et al. P. 385 of this volume.

4. Voytovetskiy, V. K. and Tolmacheva, N. S. Atomnaya Energiya, Vol. 6, 472, 1959.

5. Yegorov, Yu. A. and Panov, Ye. A. Pribory i Tekhnika Eksperimenta, No. 4, 57, 1961.

THE TRANSMISSION OF GAMMA-RADIATION THROUGH HETEROGENEOUS MEDIA

D. L. Broder, Yu. P. Kayurin, A. A. Kutuzov

Introduction

The calculation of shielding from γ-radiation requires the knowledge /198 of one of the significant characteristics of a material--the buildup factor of γ-radiation. For homogeneous media the buildup factor $B(E_0, x, z, g)$ is a function of the initial γ-radiation energy E_0, the thickness of the material x, the atomic number of the substance z, as well as the form of the source g. By the present time, methods have been developed for computing buildup factors, and such buildup factors have been computed with sufficient accuracy for the majority of shielding materials over a wide range of material thicknesses and energies and for several forms of sources (ref. 1). However, the shielding which is used is usually heterogeneous, i. e., it consists of alternating layers of various materials. The buildup factor of such a medium also depends on the order in which the materials are placed, whereas its variation with E_0, and with the thickness of materials comprising the heterogeneous mixture as well as their atomic numbers are more complex. It is practically impossible to use the method of moments and compute the buildup factors for the entire diversity of such heterogeneous shieldings.

References 1-3 contain certain recommendations based on general physical considerations resulting from the computation of buildup factors for heterogeneous shieldings consisting of two meterials. For example, when the energy of γ-radiation does not reach the energy corresponding to the minimum of the γ-radiation attenuation coefficient curve for any of the materials, it is recommended to take either the buildup factor for only the heavy material over the entire thickness (measured in terms of the mean free path), when the γ-quanta pass through the layer of the heavy material after passing the layer of light material, or to take the derivative of the buildup factors when the order of layer position is reversed. Individual experiments (refs. 4 and 5) confirm these recommendations qualitatively. Reference 1 presents empirical equations for computing the buildup factor for a heterogeneous medium consisting of water and lead (for three mean free paths of each substance). In this case the lead plate was placed behind or in front of a water layer of the same thickness. For heterogeneous media consisting of three or more layers there are generally no recommendations for computing the buildup factors.

In the present work we made an experimental determination of the /199
dose buildup factor for heterogeneous media consisting of various combinations of materials (polyethylene, aluminum, iron, lead), and for γ-quanta energies of 1.25, 2.76 and approximately 6.4 MeV. The source of γ-quanta with an energy of 1.25 MeV was Co^{60} and the source with energy 2.76 MeV was Na^{24}. The reaction F^{19} (p, α) O^{16} was used to obtain γ-quanta of high energy (approximately 6.4 MeV). On the basis of experiments with Co^{60} and on the basis of general physical considerations an empirical equation was obtained for computing buildup factors in a heterogeneous medium consisting of any number of layers of various materials. Experiments with Na^{24} and with a γ-ray source of energy of 6.4 MeV showed that this equation may be used even when the energies of the γ-quanta exceed the critical energy. Basically the experimental buildup factors differ by not more than 15 percent from values computed by means of the given equation.

Buildup Factors for Gamma-rays with an Energy of 1.25 MeV

The experimental buildup factor for a shielding consisting of n layers of various materials and a point monoenergetic source with energy E_0 are determined from the equation

$$B = \frac{D_x^{E_0}}{D_0^{E_0}} \exp\left(\sum_{i=1}^{n} \mu_i^{E_0} x_i\right), \qquad (1)$$

where $D_x^{E_0}$ is the dose behind the test shielding at a distance R; $D_0^{E_0}$ is the dose without the shielding at the same distance R; $\mu_i^{E_0}$ is the total linear attenuation coefficient for γ-rays with energy E_0 for the material of the i-th layer in the "narrow beam" geometry; x_i is the thickness of the i-th layer material.

The experimental setup is shown in figure 1.

The Co^{60} source with an activity of approximately 1 g·equivalent Ra (average energy E_0 = 1.25 MeV) consists of a cylinder with a diameter of 6 mm and a height of 12 mm.

The following shielding materials were investigated: polyethylene, aluminum, iron, lead and various combinations of these materials. All shielding blocks were assembled from plates with a thickness of approximately 10 mm. The dimensions of the iron and lead plates were 700 x 700 mm, and those of polyethylene and aluminum plates were 1000 x 1000 mm. A plastic scintillator (tetraphenylbutadiene and polyvinyltoluene) with a diameter of 103 mm and a height of 180 mm served as the detector. The dosimetery of such a detector is shown in reference 6. The scintillator was connected to the FEU-24 photomultiplier by means of an optical

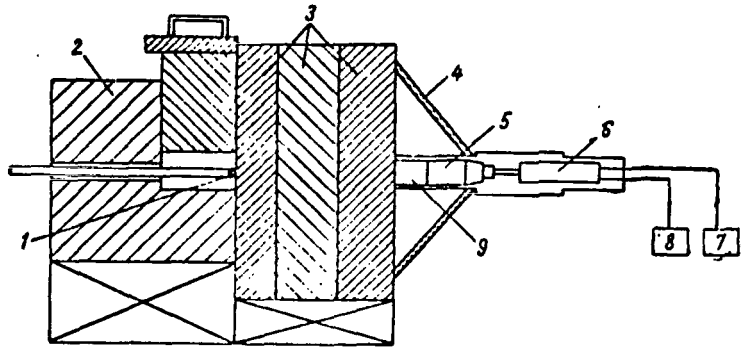

Figure 1. Experimental setup: 1, source; 2, contained; 3, test materials; 4, lead screen; 5, optical waveguide and photomultiplier; 6, preamplifier; 7, photomultiplier power source; 8, amplifier; 9, scintillator detector.

waveguide. The preamplifier and dc amplifier were based on the "Kaktus" type installation, which made it possible to operate in the current mode. The photomultiplier was powered by a high voltage stabilized VS-9 type rectifier. The source container was made of lead and had the form of a cylinder (with a /200 diameter of 500 mm and a height of 500 mm) with a special slide plate and a moveable tube with the source. The lead screen around the detector was used to shield the detector from radiation scattered by the walls and the floor of the room. This radiation would introduce a large and undesirable contribution when taking measurements on shieldings of large thickness. The thickness of the screen was determined experimentally, and its dimensions were selected in such a way as not to disrupt the conditions of a "wide" beam.

The magnitude of the dose without shielding $D_0^{E_0}$ was measured as a function of distance under special conditions which eliminated the effect of scattered radiation. The linear attenuation coefficients for γ-radiation in the test materials were taken from reference 7.

To check the experimental methodology, dose buildup factors for various media were measured in the "infinite" geometry: polyethylene, aluminum, iron. For the case of aluminum and iron the discrepancy between measured and theoretical data did not exceed 7 percent. The experimental buildup factors for polyethylene were compared with the theoretical accumulation factors for water. The values of the polyethylene buildup factor are greater by 10-12 percent than the buildup factors for water.

Since the range of the measured doses was rather wide ($1\text{-}10^5$ relative units), several different degrees of instrument sensitivity were set and measurements were taken using different scales. To compute the buildup factor, the measured doses were reduced to a single scale and to a single sensitivity. Special measurements were made to "match" the scales. The error due to the matching of the scales and the normalization of sensitivity did not exceed $\pm$ 4 percent. The total

experimental error was ± 10 percent (taking into account the inaccuracy associated with the measurement of test plate thicknesses).

The following heterogeneous media were investigated. These consisted of two layers of materials of various thickness

$$\text{Pol}^{1} + \text{Pb};\ \text{Pol} + \text{Fe};\ \text{Fe} + \text{Pb}$$

(the heavy material follows the light material) and Pb + Pol; Fe + Pol; Pb + Fe (light material follows the heavy material).

Of the materials used--polyethylene, aluminum, iron and lead--various heterogeneous mixtures were composed, including 3, 4, 5 and more layers. In mixtures consisting of the same material different material thicknesses were utilized.

A comparison of experimental data with data computed, as recommended in references 1-3, showed that for the specified energy (approximately 1.25 MeV) and with thicknesses of 0.7-15 mean free paths the test materials have a place where the computed and measured doses differ by a factor of 2-4. For mixtures consisting of three or more layers of different materials there are generally no recommendations. The data of the experiments have shown that for such cases the buildup factor does not lie above the maximum or below the minimum buildup factors of homogeneous materials, comprising the heterogeneous mixture, which are taken to have the total thickness of the mixture in terms of the mean free path. For a more exact calculation of the buildup factors for a heterogeneous mixture B_{mix}, an empirical formula of the following form was obtained on the basis of experimental work and on the basis of general physical considerations carried out in the present work:

$$B_{\text{см}} = \sum_{n=1}^{N} B_n \left(\sum_{i=1}^{n} \mu_i x_i\right) - \sum_{n=2}^{N} B_n \left(\sum_{i=1}^{n-1} \mu_i x_i\right), \qquad (2)$$

(см = mixture)

where N is the total number of layers (the layers accounted from the source); $B_n \left(\sum_i^n \mu_i x_i\right)$ is the buildup factor for the homogeneous material of the n-th layer taken for the corresponding thickness expressed in terms of the mean free path.

In a particular case when the heterogeneous medium consists of three /201 materials, for example, Fe + Pb + H_2O with the corresponding thicknesses $\mu_1 x_1$, $\mu_2 x_2$ and $\mu_3 x_3$, expressed in terms of the mean free path, equation (2) gives us

$$B_{\text{см}} = B_{\text{Fe}}(\mu_1 x_1) + B_{\text{Pb}}(\mu_1 x_1 + \mu_2 x_2) - B_{\text{Pb}}(\mu_1 x_1) + \\ + B_{\text{H}_2\text{O}}(\mu_1 x_1 + \mu_2 x_2 + \mu_3 x_3) - B_{\text{H}_2\text{O}}(\mu_1 x_1 + \mu_2 x_2).$$

[1] Pol = polyethylene.

where $B_{Fe}(\mu_1 x_1)$ is the buildup factor for iron over the adopted thickness of the iron layer; $B_{Pb}(\mu_1 x_1)$ is the buildup factor for lead over the adopted thickness of the iron layer; $B_{Pb}(\mu_1 x_1 + \mu_2 x_2)$ is the buildup factor for lead taken over the total thickness of the iron layer and the lead layer; $B_{H_2O}(\mu_1 x_1 + \mu_2 x_2)$ is the buildup factor for water over the thickness of the layer where it is absent, i.e., over the thickness of the iron and lead layers; $B_{H_2O}(\mu_1 x_1 + \mu_2 x_2 + \mu_3 x_3)$ is the buildup factor for water over the thickness of the entire mixture.

In the same way, equation (2) may be written for other heterogeneous mixtures consisting of any number of layers.

The experimental values of the buildup factors for all investigated layers basically agree with values computed by means of the given equation, within the limits of experimental error. Some of the experimental results are shown as a graph for the variation of $B(\mu x)$ in figures 2-5. The buildup factors computed by means of equation (2) are shown by a solid line; the experimental values are shown by the corresponding points.

Figure 2 shows the Pol + Pb case. Here the lead was gradually built up behind each of the polyethylene layers. As we can see from the graph B_{mix} comes closer to the buildup factor of lead as we increase the lead content and decrease the polyethylene content of the given mixture. Analogous results were obtained for Pol + Fe; Fe + Pol and Fe + Pb; Pb + Fe. Figure 3 shows the behavior of the buildup factor for one of the heterogeneous mixtures consisting of six layers.

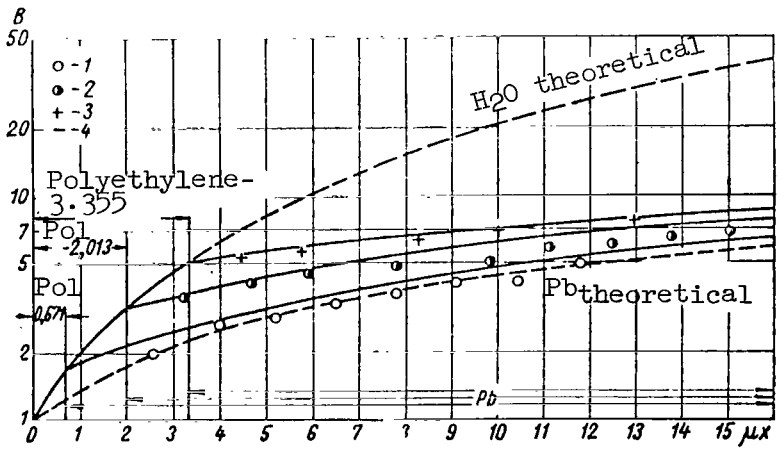

Figure 2. Dose buildup factors for mixtures of polyethylene and lead (E_0 = 1.25 MeV): 1, experimental data for polyethylene thickness of μx = 0.671; 2, μx = 2.013; 3, μx = 3.355; 4, computed by equation (2).

Figures 4 and 5 show the case of a heterogeneous mixture consisting of a large number of thin recurring layers. As we can see from figure 4, for cases of this type the discrepancy between the experimental values and values obtained from equation (2) may exceed 30 percent, which apparently is explained by the small thickness of the layer. The empirical formula was not verified for layers less than $\mu x = 0.7$.

It should be pointed out that when we use the method of Berger and Doggett to take into account the finite dimensions of the medium (ref. 8) (corrections are also presented in reference 3), we obtain results which are much closer to the experimental ones (figs. 3, 4 and 5).

Further experiments were run to verify the applicability of equation (2) to higher energies of the γ-radiation.

Buildup Factors for Gamma-rays with an Energy of 2.76 MeV

The setup, detector, and materials were the same as in the preceding experiment. The Na^{24} source consisted of a sphere with a diameter of 24 mm and a shell made of nickel with a thickness of 0.3 mm filled with compressed NaF powder. Only two basic lines were taken into account during the computations: 2.76 and 1.38 MeV (intensity in the ratio 1:1). The absorption in the nickel shell and self-absorption of the source were not taken into account. The attenuation coefficients for γ-radiation with energies of 2.76 and 1.38 MeV were also taken from reference 7.

The dose produced by a source of this type D_0^{Na} will be expressed in the following manner (when shielding is absent)

$$D_0^{Na} = D_0^{2.76} + D_0^{1.38},$$

where $D_0^{2.76}$ is the dose produced by the 2.76 MeV line; $D_0^{1.38}$ is the dose produced by the 1.38 MeV line.

The gamma constants for these lines are 11.9 and 7.15 R/hr, respectively, i.e.,

$$\frac{D_0^{2.76}}{D_0^{1.38}} = \frac{11.9}{7.15}.$$

Proceeding from these relationships, we obtain /204

$$D_0^{2.76} = 0.625 D_0^{Na},$$
$$D_0^{1.38} = 0.375 D_0^{Na}.$$

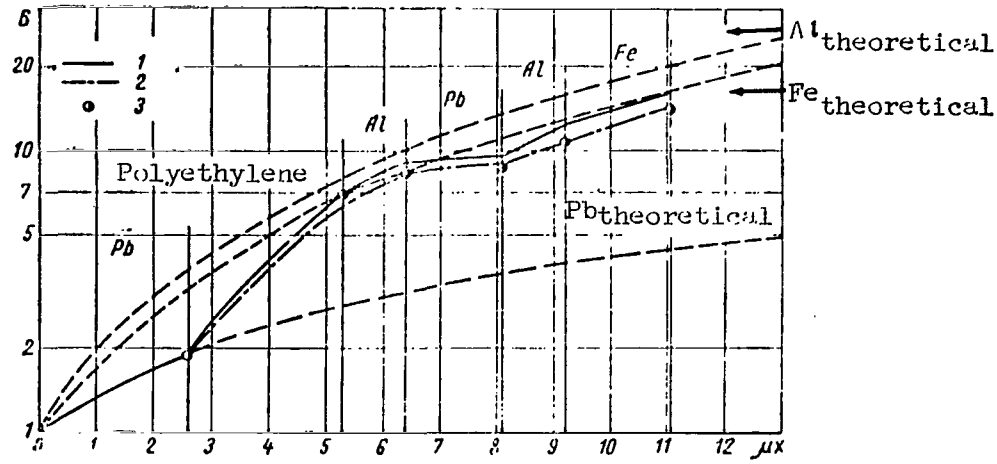

Figure 3. Dose buildup factor for heterogeneous mixture consisting of six layers (E_0 = 1.25 MeV): 1, B_{mix}; 2, compensated for finite dimensions of medium; 3, experimental data.

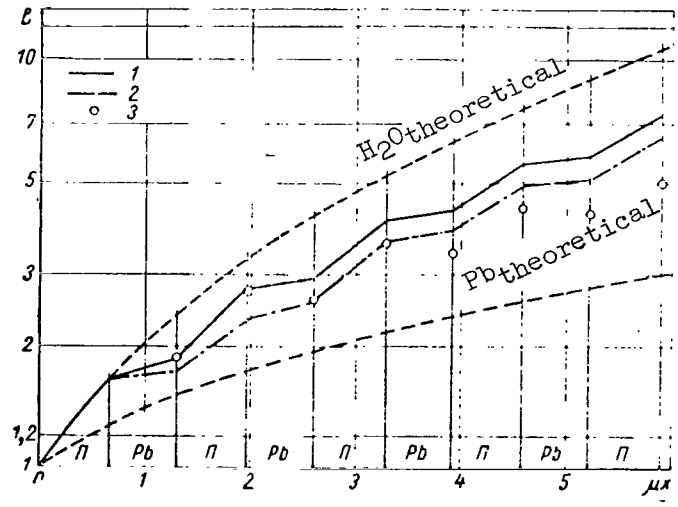

Figure 4. Buildup factor for heterogeneous medium consisting of large number of layers (E_0 = 1.25 MeV): 1, B_{mix}; 2, B_{mix} with corrections; 3, experimental data.

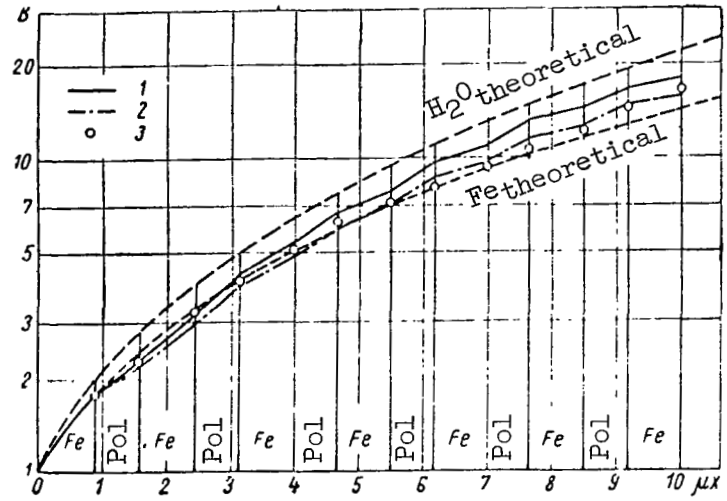

Figure 5. Buildup factor for heterogeneous mixture consisting of large number of layers (E_0 = 1.25 MeV):

1, B_{mix}; 2, B_{mix} with corrections; 3, experimental data.

When a shielding is equal to

$$D_x^{Na} = B_x^{1,38} D_0^{1,38} \exp\left(-\sum_{i=1}^{n} \mu_i^{1,38} x_i\right) + B_x^{2,76} D_0^{2,76} \exp\left(-\sum_{i=1}^{n} \mu_i^{2,76} x_i\right).$$

Consequently,

$$B_x^{2,76} = \frac{D_x^{Na}/D_0^{Na} - 0.375 B_x^{1,38} \exp\left(\sum_{i=1}^{n} \mu_i^{1,38} x_i\right)}{0.625 \exp\left(-\sum_{i=1}^{n} \mu_i^{2,76} x_i\right)}. \quad (3)$$

Here $B_x^{2.76}$ and $B_x^{1.38}$ are the buildup factors of the given heterogeneous mixture for energies of 2.76 and 1.38 MeV, respectively. The values of $B^{1.38}$ for homogeneous media were taken from reference 1. For the heterogeneous media $B_x^{1.38}$ were obtained by two methods:

(1) $B^{1.38}$ was assumed to be identical to $B^{Co^{60}}$ and the results of the preceding experiments were used to determine it, because $B^{1.38}$ is close in value to $B^{Co^{60}}$ (the average energy Co^{60} = 1.25 MeV);

(2) according to equation (2), verified for the Co^{60} source, which must also be valid for the γ-radiation of energy 1.38 MeV due to the monotonic variation of the buildup factor with energy.

For control purposes, buildup factors for homogeneous media Pb, Fe and Al were measured under conditions close to "infinite" geometry. The discrepancy between experiment and theory does not exceed 10 percent. Table 1 shows the results obtained from the investigation of the heterogeneous mixtures. The table lists the materials contained in the heterogeneous mixture (beginning with the source); the thickness of the μx layers in terms of the mean free path; B_{ex}, experimental buildup factors averaged out over three readings; the values of B_{mix} computed by means of equation (2) utilizing data presented in reference 1; and quantity δ showing the discrepancy between experimental and computed data.

As we can see from the data, equation (2) may also be used for an energy of approximately 3 MeV; however, this energy is still not the critical one for any of the test materials, i.e., for the given materials none of the attenuation coefficients for γ-radiation reaches a minimum value. The experiment was run to verify the applicability of equation (2) to heterogeneous mixtures in the region of quanta energies above 3 MeV. /205

Buildup Factors of Gamma-rays with Energies of 6.4 MeV

The F^{19} (p, α) O^{16} reaction was used to obtain γ-radiation of this type. The protons were accelerated by a linear accelerator up to the resonant energy (0.88 MeV) and were directed to the CaF_2 crystal, which had a form close to a sphere with a diameter of approximately 10 mm.

TABLE 1. EXPERIMENTAL AND COMPUTED BUILDUP FACTORS FOR E_0 = 2.76 MEV.

Mixture	$\mu_1 x_1$	$\mu_2 x_2$	$\mu_3 x_3$	B_{ex}	B_{mix}	δ
Pb + Al	2.266	6.750	—	7.32	7.45	1.745
the same	4.493	3.000	—	4.69	5.15	8.94
» »	4.493	4.500	—	5.67	6.42	11.68
» »	4.493	6.750	—	8.21	8.45	2.84
» »	7.271	1.500	—	5.18	5.13	—0.975
» »	7.271	2.250	—	5.36	5.78	7.27
» »	7.271	3.000	—	5.95	6.39	6.88
Pb + Al + Fe	4.493	3.00	1.382	6.11	6.26	2.39
Al + Pb	1.500	7.271	—	4.93	5.03	1.98
the same	3.000	2.294	—	3.71	4.03	7.94
» »	3.000	4.503	—	4.64	5.02	7.57
» »	3.000	7.271	—	5.89	6.43	8.40
» »	4.500	4.047	—	6.34	6.25	—1.44
» »	4.800	3.157	—	5.98	6.05	1.154
» »	4.800	2.266	—	5.85	5.68	—3.00
» »	8.25	0.862	—	8.06	7.88	—2.28
Al + Pb + Al	3.00	2.266	3.00	6.32	6.44	1.86
Fe + Al	2.899	1.500	—	4.00	4.05	1.235
Fe + Al + Pb	2.899	1.500	2.222	4.67	4.67	0

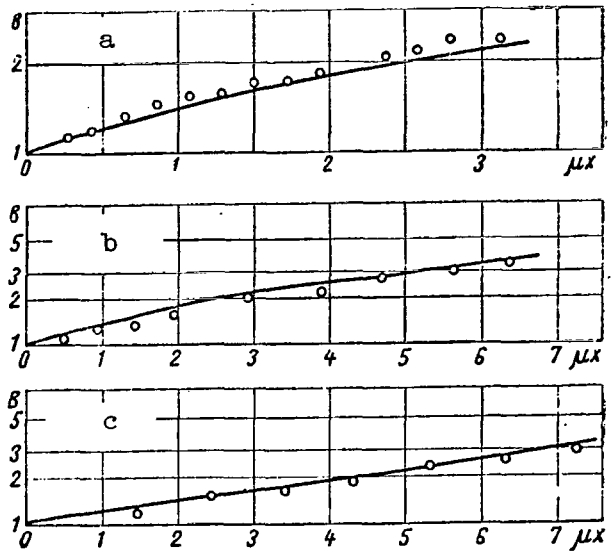

Figure 6. Dose buildup factors for homogeneous media (E_0 = 6.4 MeV) Al (α), Fe (b) and Pb (c): ————, computed data; O, experimental data.

The computation took into account γ-quanta of three basic energies, emitted in the process of the reaction: 6.13, 6.9 and 7.1 MeV with relative intensities of 0.76, 0.025 and 0.21, respectively. In this range of energies the buildup factor varies very little, and proceeding from the relative intensities we can utilize the average effective energy of 6.4 MeV. In the experiment the materials and detector of the preceding experiment were used. The experimental setups did not differ in principle; however, the dimensions and thickness of the protective screen were substantially increased in accordance with the utilized γ-radiation energy and the conditions of the experiment.

The experimental buildup factors were computed by means of equation (1). Since the number of protons falling on the target changes somewhat during the period of measurements, the integral of count during the period of time t was taken, referred to the integral count of the monitor placed at a definite distance from the target. Nevertheless, the instability of the source power reduced the accuracy of this experiment compared to that of the preceding experiment. The total experimental error was ± 17 percent. Evaluations of formation intensity and the effectiveness of photoneutron detection showed that their contribution to the count should not exceed 0.01 percent.

Since there are too few experimental results for the high energy region (even for homogeneous media), the measurement of buildup factors for γ-quanta with energy 6.4 MeV was carried out in the present work for polyethylene, aluminum, iron and lead within the "barrier geometry." The theoretical values of buildup factors are taken from reference 1, corrected for the finite dimensions of the medium according to the method of Berger and Doggett (ref. 8).

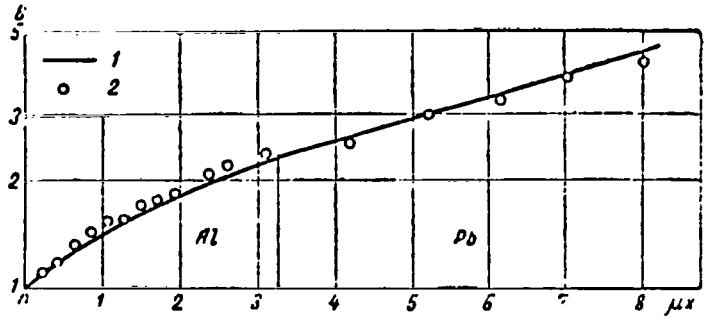

Figure 7. Dose buildup factors for mixture of two materials (E_0 = 6.4 MeV): 1, computed by means of equation (2); 2, experimental data.

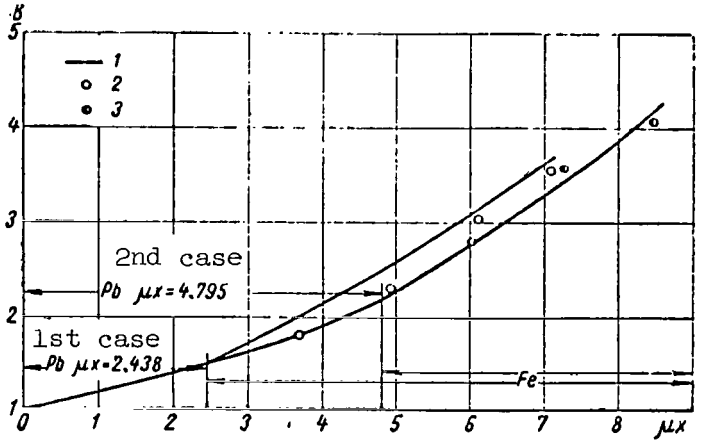

Figure 8. Dose buildup factors for heterogeneous mixture of lead and iron (E_0 = 6.4 MeV): 1, computed by means of equation (2); 2, experimental data for first case; 3, experimental data for second case.

The graphs in figure 6 show some of the measurement results for homogeneous media.

Some of the measurement results for heterogeneous media are shown in the graphs of figures 7, 8 and 9. These figures give the values of measured and computed (by means of equation (2)) buildup factors for γ-quanta of energy of 6.4 MeV in heterogeneous mixtures of Al, Fe and Pb.

Conclusions

The conducted experiments showed that the empirical equations (2) /207 may be used successfully in computing the buildup factors of γ-radiation with

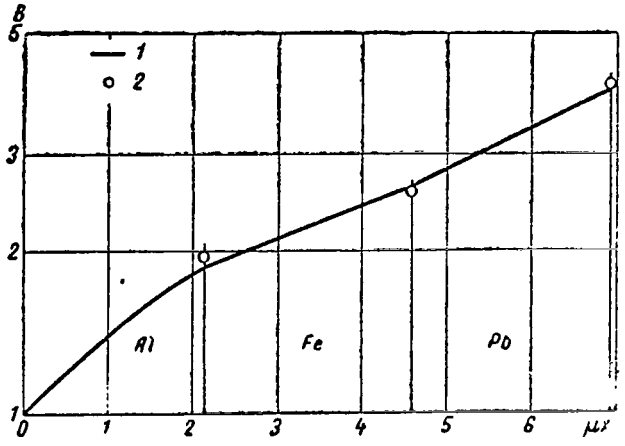

Figure 9. Dose buildup factor for mixture of three materials (E_0 = 6.4 MeV): 1, computed by means of equation (2); 2, experimental data.

energies in the range of 1-6.5 MeV. There is no basis to assume that this equation will not be valid for higher radiation energies. For example, computation by means of this equation and computation by means of a special empirical equation for the case Pb + H_2O (ref. 1) differ by not more than 3 percent for energies of 3 and 10 MeV (in each case, computations were carried out for nine combinations, i.e., the thickness of Pb and H_2O were taken equal to 1, 2 and 3 mean free paths). Within the specified range of energies, computations by means of equation (2) agree with the experimental data obtained by other authors (refs. 4 and 5). The given equation was not verified for lower energies of γ-radiation or for thicknesses greater than 15 mean free paths.

REFERENCES

1. Gol'dshteyn, G. Principles of Reactor Shielding (Osnovy zashchity reaktorov). Moscow, Gosatomizdat, 1961.

2. The Shielding of Nuclear Reactors. Edited by T. Rockwell (Zashchita yadernykh reaktorov). Moscow, Izd-vo I. L., 1958.

3. Price, B. T., Horton, C. C. and Spinney, K. T. Radiation Shielding (Zashchita ot yadernykh izlucheniy). Moscow, Izd-vo I. L., 1959.

4. Tsypin, S. G. et al. Atomnaya Energiya, No. 2, 71, 1956.

5. Kimel', L. R. Atomnaya Energiya, Vol. 2, 173, 1961.

6. Kukhtevich, V. I. et al. Inzh.-fiz. zh., Vol. 3, 4, 125, 1960.

7. Fano, V. Nucleonics, Vol. 11, No. 8, 8, 1953.

8. Berger, M. and Boggett, J. J. Res. Nat. Bur. Standards, 56, 89, 1956.

THE GAMMA-SPECTRUM OF THE EXPERIMENTAL REACTOR

V. N. Avayev, Yu. A. Yegorov, I. Ya. Yemel'yanov, A. D. Zhirnov,
Yu. V. Orlov and V. A. Remizov

A scintillation spectrometer of the electron-positron pair (ref. 1) /207 was used to measure the γ-spectrum of an experimental water-moderated pool-type reactor. The gamma-quanta from the active zone of the reactor were directed to the spectrometer along the lateral experimental channel with a diameter of 100 mm and a length of 2.5 m. To exclude the effect of γ-quanta scattered in the channel, a lead collimator with a length of 180 mm and with a collimating opening diameter of 10 mm was placed in the channel. The spectrometer sensor was installed behind the concrete reactor shielding while the flux of γ-quanta passed through a collimator of 260 mm in length made of paraffin with boron carbide and lead.

The results of the measurements (the detailed γ-spectrum) are shown in figure 1. Since the spectrometer is sensitive to neutrons, although to a rather insignificant degree, measurements were carried out under the same conditions with a bismuth filter with a thickness of 100 mm (fig. 1, curve 2) and a corresponding correction was introduced (ref. 2).

To identify the reactor spectrum, the spectrometer was calibrated by measuring the γ-spectra of Na^{24} and Po + Be sources. The correction for the effectiveness of the spectrometer depending on the energy of the γ-quanta was introduced in accordance with data presented in reference 1. The results of measuring the γ-spectra of TVR (ref. 3) and IRT (ref. 4) reactors as well as data in reference 5 were used to interpret the spectrum.

The processed γ-spectrum of the reactor is shown in figure 2 and in table 1. The basic γ-lines of the reactor's structural materials are isolated in the spectrum; of aluminum (the uranium elements are placed in aluminum shells and assembled in aluminum cartridges), of iron (tube of the slide plate) of chrome and of nickel (tube of the slide plate). The γ-line with an energy of 2.2 MeV is clearly isolated (in our results the energy was 2.18 MeV). This line is due to the radiation capture of neutrons by hydrogen--$H_{(n, \gamma)}D$. Apparently the γ-line with energy of 4.05 MeV may be attributed to U^{239} and represents the unresolved lines with energies of 4.065 and 3.987 MeV (refs. 3 and 5). A γ-line with an energy of 4.63 MeV from U^{239} was detected in reference 3. We were /208 unable to detect this line, possibly due to its small intensity (approximately 1 percent). The γ-lines with energies of 2.53, 6.58 and 7.05 MeV were clearly

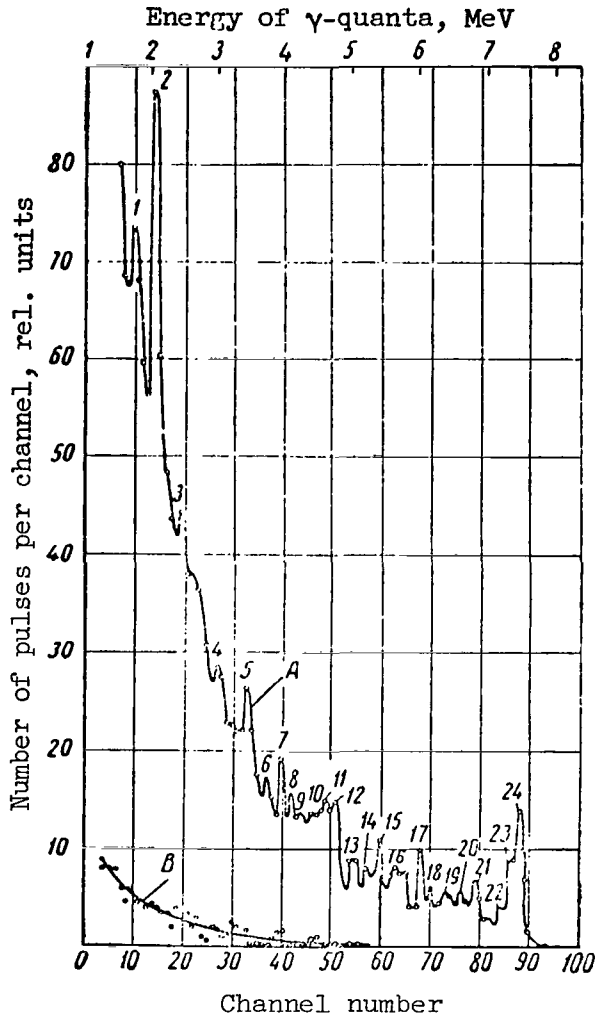

Figure 1. Instrument γ-spectrum of experimental water-moderated reactor (A) and neutron background (B).

isolated in the spectrum. These lines were not detected in references 3 and 4. It is possible that they are due to false coincidences during leakage of only a single annihilation γ-quanta from the central crystal.

Lines of 4.21 MeV (Fe, Ni, Al), of 4.75 MeV (Al, Cr, Fe) and of 6.8 MeV (Al, Ni) apparently represent adjoining unresolved γ-lines with the following energies

4.2 (Fe, Ni) and 4.25 MeV (Al);
4.71 (Al) and 4.78 MeV (Fe, Cr);
6.76 (Al) and 6.83 MeV (Ni).

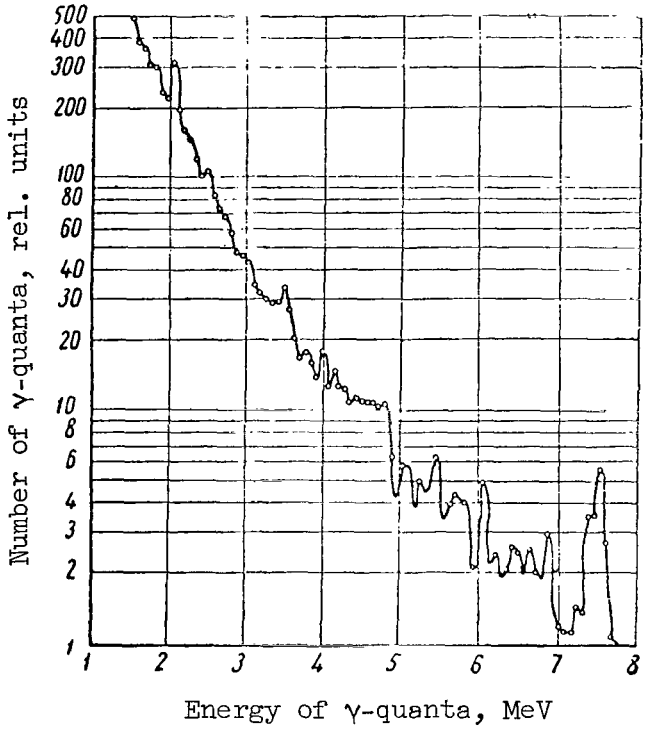

Figure 2. Gamma-spectrum of reactor.

TABLE 1. GAMMA-SPECTRUM OF EXPERIMENTAL REACTOR.[1]

Number	Energy of γ-quanta, in MeV	Source element of γ-radiation	Number	Energy of γ-quanta, in MeV	Source element of γ-radiation
1	1.65	$Al^{28} \rightarrow Si^{28}$; Fe?	13	5.14	Al
2	2.18	H (n, γ) D	14	5.38	Al; Cr
			15	5.59	Cr; Fe
3	2.53	--	16	5.86	Fe; Al
4	3.16	Al; Cr?; Ni	17	6.2	D (n, γ) T; Al
5	3.54	Al; Fe			
6	3.83	Fe; Al	18	6.35	Al
			19	6.58	--
7	4.05	U^{238}; Fe; Ni	20	6.8	Al; Ni
8	4.21	Fe; Ni; Al	21	7.05	--
9	4.37	Fe	22	7.4	Fe
10	4.52	Al?	23	7.6	Fe
11	4.75	Al; Cr; Fe	24	7.73	Al
12	4.9	Al; Cr			

[1] See figure 1.

However, the basic contribution to the unresolved lines is made by the captured γ-radiation from aluminum.

We can see from figure 2 that the spectrum is accompanied by a substantial continuous distribution, which is due to the γ-radiation accompanying the U^{235} fission process and also due to the scattering of γ-radiation in the active zone of the reactor and in water.

The integral yield of γ-radiation N per unit energy interval (1 MeV) /209 is shown in figure 2.

Comparing our results with data presented in references 3 and 4 we should note that the spectrum of the experimental water-moderated reactor is substantially softened, which apparently is explained by the multiple scattering of γ-quanta in water. The reactor spectrum was measured approximately to 7.8 MeV (fig. 2). Gamma-lines with high energy were not detected; this is /210 explained by the fact that in the region of high energies the γ-radiation is basically due to the absorption of neutrons by iron, nickel and chromium. These elements are not present in the active zone of the reactor, and the output of γ-radiation from the tube of the slide plate is small so that only an insignificant part of the captured γ-quanta from the tube could fall into the sensor of the spectrometer.

TABLE 2. INTEGRAL YIELD OF γ-RADIATION N.

E_γ, MeV	2—3	3—4	4—5	5—6	6—7	7—8
N, %	75	15	5	2,2	1,25	1

REFERENCES

1. Avayev, B. N., Yegorov, Yu. A. and Orlov, Yu. V. P. 464 of this volume.

2. Yegorov, Yu. A. and Orlov, Yu V. P. 474 of this volume.

3. Burgov, N. A., Danilyan, G. V. et al. Atomnaya Energiya, Vol. 9, 214, 1960.

4. Groshev, L. V. and Demidov, A. M. Atomnaya Energiya, Vol. 7, 257, 1959.

5. Groshev, L. V., Demidov, A. M. et al. An Atlas of γ-ray Spectra for the Radiation Capture of Thermal Neutrons (Atlas spektrov γ-luchey radiatsionnogo zakhvata teplovykh neytronov). Moscow, Atomizdat, 1958.

6. Harvey, J. Phys. Rev., Vol. 81, 353, 1951.

THE INCLINED INCIDENCE OF GAMMA-RAYS

V. I. Kukhtevich and L. A. Trykov

Introduction

In the practice of designing biological shielding it is sometimes /210 necessary to know the buildup dose factor when we have an inclined incidence of γ-radiation. This problem has not been studied in detail to the present time. Only a few works have been published in the literature containing computed data and only one published work contains experimental data.

Reference 1 uses the method of random tests to compute the attenuation of γ-radiation with energy $E_0 = 4$ MeV in a lead barrier as a function of its thickness $\mu_0 r$ and the radiation incidence angle at the front boundary of the barrier α. Reference 2 presents the energy buildup factors obtained by the method of successive collisions for iron and lead barriers and which are subject to a unidirectional radiation falling at an angle α. Reference 3 presents experimental data on the inclined penetration of γ-rays from Au^{198}, Cs^{137}, Co^{60} through a barrier of concrete, lead and polyethylene. The authors of reference 3 have made a detailed study of barrier thickness (along the normal) of the order of 1 or more mean free paths for $0^\circ \leq \alpha \leq 70^\circ$. However, it is also of interest to consider the penetration of γ-radiation with inclined incidence through shielding barriers of small thickness of the order of 1 mean free path (along the normal) and less.

In the present work we measured the dose D of γ-rays from an infinite unidirectional Co^{60} source behind the barrier shielding.

The angle α between the barrier plane and the direction of incidence of the γ-quanta was varied from 0 to 80°. The following materials and their compositions were used in the measurements: lead (r = 0.7, 0.8, 1.4, 2.75 cm), plexiglas (r = 3, 8, 11, 14 cm) and composite barriers of lead (r = 0.8 cm) and plexiglas (r = 8 cm), where r is the thickness of the shielding along the normal.

In determining the dose buildup factor it was necessary to measure the dose D_0 from the direct beam of γ-quanta in addition to the attenuation value. By substituting D and D_0 into the equation $B_D = D/D_0\, e^{\mu_0 r}$, it is possible /211

to compute the buildup dose factor B_D as a function of $\mu_0 r$ and of the angle α.

The penetration of γ-quanta which were incident at an angle to the composite barriers from heavy and light components were also measured. In this case the light and heavy components were interchanged.

The results were compared with published computed and experimental data (refs. 1-4).

Experimental Setup

The experimental setup is shown schematically in figure 1.

Co^{60} γ-ray source with an activity of approximately 1 Ci was used in the experiment. The diameter of the source was 5 mm, the length of the lead collimator was 300 mm and the diameter of the collimator could be varied from 6 to 30 mm. It was established during the operation that collimators with a diameter of 6 and 8 mm were sufficient, which corresponded to angles β of 30' and 50', respectively. The values of β were obtained experimentally.

The conditions for the infinitely wide unidirectional beam of Co^{60} γ-rays was established experimentally. It was found that the minimum dimension of the light component plate for $0^\circ \leq \alpha \leq 80^\circ$ is sufficient when its length is 2 m and its height is 1 m (when $\alpha = 0^\circ$ the total collection of scattered γ-quanta was achieved when the beam diameter, designed for the shielding, was equal to 80 cm). Although it was possible to utilize shielding plates of smaller height for lead, the plates used in the experiment were of the same value.

To control the value of the γ-quanta angle of incidence a special rotating device was constructed for the shielding. With this device the test shielding on it could be secured, together with the detector and to change the γ-quanta beam incidence angle α from 0 to 90°. This device made it possible to set the angle α with an accuracy of $\pm 1^\circ$. The detector consisted of anisotropic scintillation dose counter of γ-quanta consisting of a stilbene crystal (with a diameter of 30 mm and a height of 15 mm) and the FEU-12B photomultiplier.

The pulses from the cathode follower of the scintillation counter were fed to the "Siren'" type amplifier by means of an RK cable, and from the amplifier

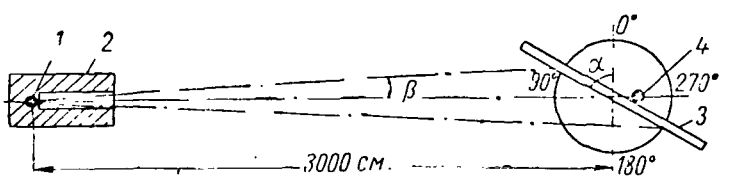

Figure 1. Experimental setup: 1, source; 2, lead collimator; 3, rotating device for barrier shielding; 4, detector.

they were fed to the pulse dose integrator. During the period of measurements the stilbene crystal was placed flush against the plane of the shielding, so that the detector measured the radiation flux. The stability and linearity of this detector was checked before the basic measurements and proved to be quite satisfactory (± 5 percent). Measurements in the interval from 0.22 to 1 MeV were carried out to check the sensitivity of the detector as a function of energy using the method described in reference 5. The deviation from hard operation does not exceed 6 percent, which is within the root-mean-square measurement error.

The Results and Measurement Errors

The results of measuring the penetration of γ-rays which fall at an angle on the test barrier shielding are shown on figures 2-4.

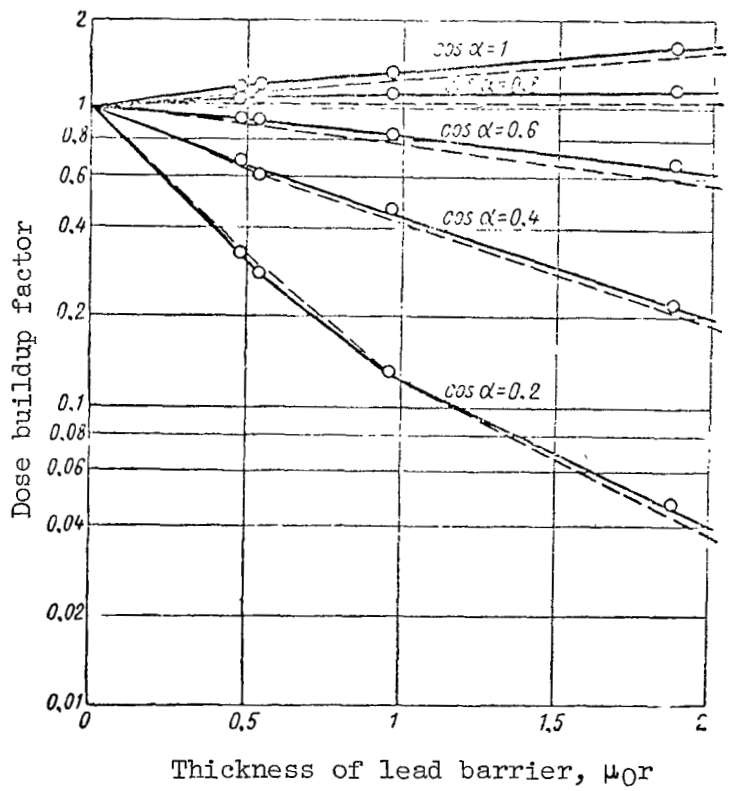

Figure 2. Variation in dose buildup factor as function of lead barrier thickness along normal, in terms of mean free path

for inclined incidence of Co^{60} γ-ray beam: ———, experimental data; – – – – –, computed data.

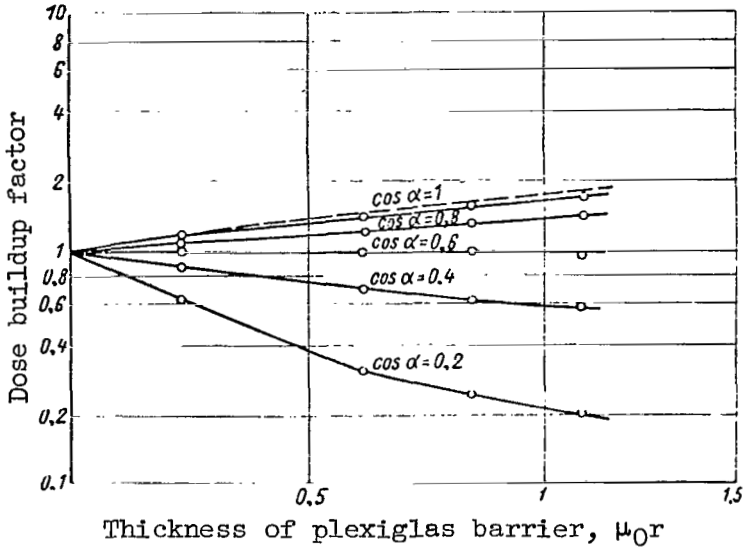

Figure 3. Variation in dose buildup factor as function of plexiglas barrier thickness along normal in terms of mean free path for inclined incidence of Co^{60} γ-ray beam: ———, experimental data; – – – – –, computed data.

Figures 2 and 3 present the results of measuring the dose buildup factor for γ-rays with inclined incidence on a barrier shielding of lead and plexiglas, respectively. /213

The dose buildup factor is determined from the equation $B_D = e^{\mu_0 r} D/D_0$, where μ_0 is the total absorption coefficient of Co^{60} γ-rays in lead, cm^{-1}; r is the thickness of the barrier shielding (along the normal), in cm; D_0 is the dose of γ-rays falling on the barrier, p; D is the dose of γ-rays transmitted through the barrier, p.

Figure 4 shows the results of measuring the composite barriers made up from heavy (lead) and light (plexiglas) components.

The measurement errors computed as the root-mean-square errors are made up of the following components:

(1) error in measuring the shielding thickness (this does not include the error in measuring the thickness due to the nonparallel nature of the incident beam of γ-quanta; this error constitutes approximately 5 percent even when the angle β has a maximum value);

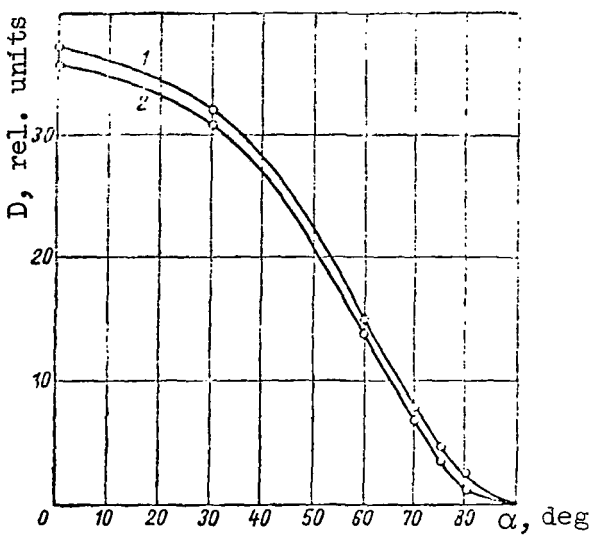

Figure 4. Dose behind composite barrier (D) as function of angle α: 1, plexiglas behind lead; 2, plexiglas in front of lead.

(2) fluctuation in the sensitivity of the dosimeter;

(3) the statistical measurement error.

The total errors constitute approximately 5-10 percent (we neglected the scattering of γ-quanta at the source). We evaluated the back scattering of γ-quanta from the preamplifier structures in the stilbene crystal. The maximum contribution to the measured dose (when $\alpha \geq 60^{\circ}$) did not exceed 2 percent. This error was not introduced into the results.

Discussion of Measurements

The results obtained were compared with published computed and experimental data. Figure 5 compares the buildup factor during the normal incidence of the radiation flux on lead barriers, obtained in the present work, with the results reported in reference 4. In reference 4 the energy buildup factors were computed by the method of moments with a normal incidence of radiation on the shielding barriers.

The broken line in figure 3 represents the energy buildup factor during the transmission of γ-rays through a barrier of water with normal incidence (ref. 4). The solid lines are drawn through experimental points for the dose buildup factor when γ-rays are transmitted through a plexiglas barrier. The computed data for Co^{60} are obtained by interpolation. The computed and experimental results agree well with each other.

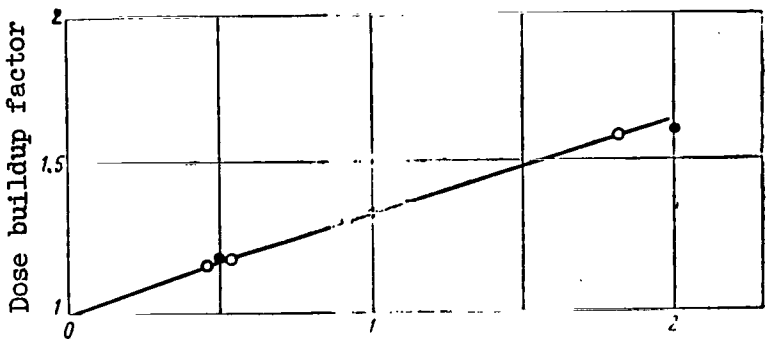

Figure 5. Variation in dose buildup factor as function of lead barrier thickness (normal incidence of Co^{60} γ-rays): ●, experimental points; O, computed points.

The results of measuring the inclined γ-rays incidence on lead barriers are compared with the data of computational work (ref. 2) (see fig. 2). Although the discrepancy is of a systematic nature, it nevertheless falls within the range of experimental and computational errors. A comparison with the results of experimental work reported in reference 3 showed that the data obtained by the authors of the present work agree with these results within 10 percent.

In comparing the obtained experimental data with results reported /214 in reference 3, we observe that the results agree for the light and heavy component during the normal incidence of the γ-quanta beam; the agreement is not quite as good for the inclined incidence of Co^{60} γ-rays on a lead barrier with $\alpha \geq 50^\circ$. The maximum discrepancy is observed for small thicknesses of lead barriers. Reference 3 does not have any data on the inclined incidence of γ-radiation on polyethylene for Co^{60}.

We can see from the data obtained that in order to compute the dose buildup factor during the transmission of Co^{60} γ-rays through a barrier at angles $\alpha \leq 60^\circ$ and mean free paths ≤ 1 it is entirely feasible to use the equation $D = D_0 B_D' e^{-\mu_0 r'}$, where μ_0 is the total absorption coefficient, in cm^{-1}; $r' = r/\cos \alpha$; r is the shielding thickness along the normal; B_D' is the buildup dose factor taken for barrier thickness r' when the incident radiation is normal.

For a light component of low energy when the mean free paths are approximately equal to 1 and when $\alpha > 60^{\circ}$ the buildup factor B', taken for barrier geometry during the normal incidence of γ-quanta beam on it, will have a slightly high value. From the results of measuring the composite barriers we can conclude (fig. 4) that when the light and heavy components are interchanged (with mean free paths approximately equal to 1) no substantial variations are observed.

REFERENCES

1. Berger, M. and Doggett, J. J. Res. Nat. Bur. Standards, Vol. 56, 89, 1956.

2. Peebles, G. H. Report R-240. The Rand Corporation, Santa Monica, California, 1952.

3. Kennedy, R. J. and Wyckoff, H. O. Radiology, Vol. 63, 94, 1954.

4. Goldstein, H. and Wilkins, J. Calculation of the Penetration of Gamma-rays NDA, NYO-3075, 1954.

5. Ricci, R. A. Physica, Vol. 24, 289, 1958.

INVESTIGATION OF THE SPECTRAL AND ANGULAR DISTRIBUTION OF GAMMA-RAYS AFTER TRANSMISSION THROUGH SHIELDING BARRIERS

A. V. Larichev

References 1-6 are devoted to the investigation of spectral and /214 angular distribution of scattered γ-rays. The basic geometries in these references were a point isotropic source (refs. 1 and 2) or a plane unidirectional source with a homogeneous shielding medium (refs. 3-6).

The investigations described in the present work were carried out for /215 the purpose of obtaining additional data, i.e., for other energies of the primary γ-rays. In addition, homogeneous shielding barriers consisting of two layers of materials with different atomic numbers were investigated. The layer thicknesses, expressed in terms of the mean free path, were selected so that they were equal ($\mu_1 x_1 = \mu_2 x_2$).

The experiments were conducted using a setup described in reference 7. The experimental technique was analogous to the one considered in references 4 and 6. The experimental results were processed by means of an inverse matrix for the spectrometer sensitivity function (ref. 8). Sources of γ-rays consisted of Au^{198}, Co^{60} and Na^{24}. Shielding barriers made of lead, iron, aluminum and a combination of two materials were used. The experiments were conducted using sources of two geometries: a point isotropic source and a plane unidirectional source. For the case of a point source (Co^{60}) and homogeneous barriers, the angular and energy distributions of scattered γ-rays obtained by us were in qualitative agreement with the results reported in references 1 and 2.

In cases of plane unidirectional Au^{198} and Na^{24} sources results with qualitative similarity were obtained for the angular variation of scattered radiation intensity per unit solid angle as in the case of the Co^{60} source reported in references 4-6. Figure 1 shows the variation in the logarithm of the scattered radiation intensity per unit solid angle (with corresponding normalization) as a function of the scattering angle Θ for Au^{198} and Co^{60} γ-rays when the source is plane and unidirectional (material Pb, $\mu_0 x = 6$). The experimental points fall quite well on straight lines (in this case the lines are parallel to each other), i.e., the angular variation of the scattered radiation intensity may be expressed by means of the following relationship

$$I(\Theta) = Ae^{-\Theta/\Theta_0}, \tag{1}$$

where A and Θ_0 are constants.

We can see from the results of reference 5 that the slope of straight lines, analogous to the straight lines in figure 1, is practically the same for various thicknesses of the same material. This shows that the constant Θ_0 does not depend on the barrier thickness. The energy relationship of Θ_0 values for various materials is shown in figure 2. We can see that within the limits of experimental error the constant Θ_0 for lead does not depend on the energy of primary γ-rays (fig. 1). It is obvious that in this case the constant A is proportional to the energy buildup factor.

It can be shown that for a plane unidirectional source /216

$$B_E - 1 = kA \left[1 - \frac{1}{\Theta_0} e^{-\pi/2\Theta_0} \right], \tag{2}$$

where B_E is the energy buildup factor; k is the normalizing constant. Expression (2) makes it possible to determine any of the following three quantities from known quantities: A, Θ_0 or B_E.

Investigations with double layer barriers have shown that there is a difference in the intensity of scattered radiation when the order of layer position in the barrier is changed. The variation of the scattered radiation intensity logarithm I (Θ) in a double layer barrier for two source geometries with an initial energy of 0.411 MeV is shown in figure 3. We can see from the figure that for a plane unidirectional source (curves 3, 4) the law expressed by (1) is retained in the case of a double layer shielding, but the slope of the logarithmic lines changes when the order of layer position is changed (the thickness of each investigated material layer was taken equal to 3 mean free paths). For a point source (curves 1, 2) relationship obtained in reference 2 is satisfied rather than the law given by (1),

$$I_\Theta = 2\pi \sin\Theta d\Theta\, I(\Theta) = ae^{-\Theta/\Theta_0}. \tag{3}$$

Figure 4 shows the angular variation in the relative difference $\Delta I(\Theta)/I_0^0$ (I_0^0 is the intensity of the nonscattered radiation), when the grouping order of the layers is changed. Although for a plane unidirectional source the difference in intensity is almost independent of the angle Θ, it has a maximum value at small angles for the point source.

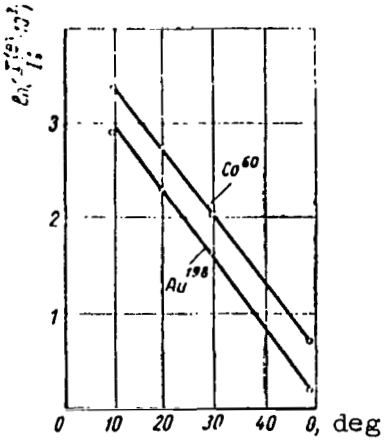

Figure 1. Exponential drop in intensity of scattered radiation per unit solid angle for various γ-quanta energies.

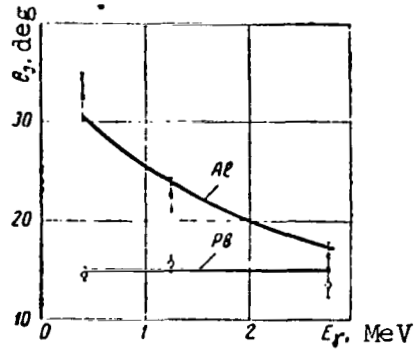

Figure 2. Variation in exponent Θ_0^0 as function of γ-quanta energy E_γ for different materials.

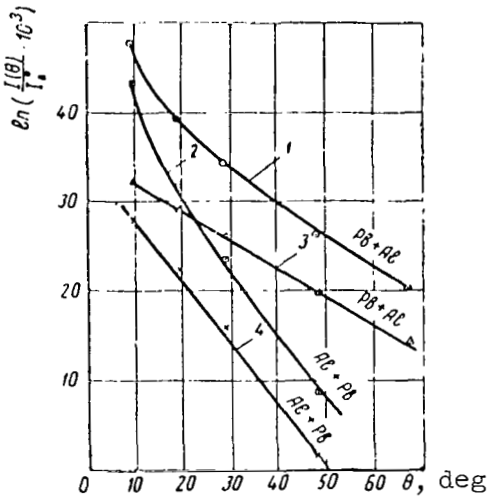

Figure 3. Intensity of radiation scattered in double layer barrier for point (1, 2) and plane (3, 4) source.

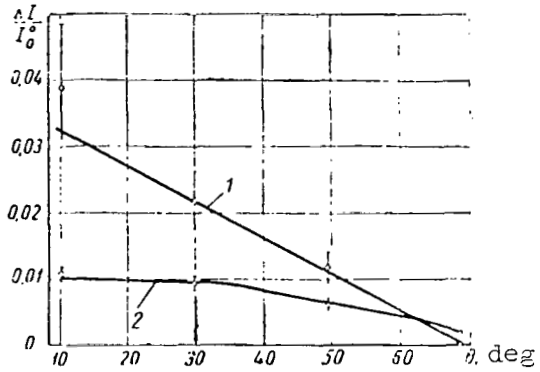

Figure 4. Angular variation of relative difference in intensity of scattered radiation when order of layer grouping is changed in double layer barrier, for two Au^{198} source geometries: 1, point isotropic source; 2, plane unidirectional source.

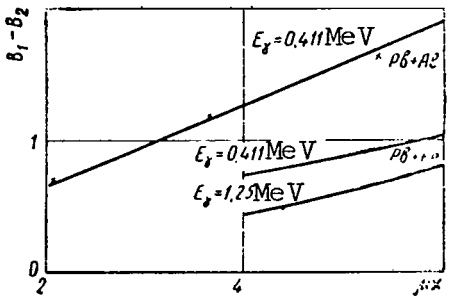

Figure 5. Variation in difference of buildup factors (B_1-B_2) as function of total

double layer barrier thickness μx for initial γ-ray energies, with different barrier composition.

The variation in the difference of the energy buildup factors as a function of the total barrier thickness for two initial γ-rays energies is shown in figure 5. We can see that the difference in the buildup factors decreases as /217 the average atomic number of the composite barrier increases and as the energy of γ-rays increases. For γ-rays with an energy of 2.76 MeV (Na^{24}) we obtained a difference whose value does not depart from the limits of experimental error (± 10 percent). Qualitatively the same result is obtained in approximate calculations.

REFERENCES

1. Whyte, G. N., Canad. J. Phys., Vol. 33, 96, 1955.

2. Kazanskiy, Yu. A. Atomnaya Energiya, Vol. 5, 432, 1960.

3. Hubbell, J., Hayward, E. and Titus, W. Phys. Rev., Vol. 108, 1361, 1957.

4. Stolyarova, Ye. L., Chukhin, S. G. et al. Investigation of Spectral and Angular Distributions of Scattered γ-Radiation in Shielding Barriers for the Case of a Plane Unidirectional Radiation. IN: Instruments and Methods of Radiation Analysis (Issledovaniye spektral'no-uglovykh raspredeleniy rasseyannogo γ-izlucheniya v zashchitnykh bar'yerakh dlya sluchaya ploskogo mononapravlennogo izlucheniya. V sb.: Pribory i metody analiza izlucheniy). No. 3. Moscow, Gosatomizdat, 1962.

5. Larichev, A. V. Atomnaya Energiya, Vol. 11, 443, 1961.

6. Larichev, A. V. and Klimanova, L. F. Angular and Energy Distributions of Co^{60} γ-Rays Scattered in the Al + Bd Heterogeneous Medium. IN: Instruments and Methods of Radiation Analysis (Uglovyye i energeticheskiye raspredeleniya

γ-luchey Co^{60}, rasseyannykh v geterogennoy srede Al + Pb. V sb.: Pribory i metody analiza izlucheniy). No. 3. Moscow, Gosatomizdat, 1962.

7. Stolyarova, Ye. L., Chukhin, S. G. and Larichev, A. V. Setup for Measuring Complex γ-Spectra of Low Intensity. IN: Instruments and Methods of Radiation Analysis (Ustanovka dlya izmereniya slozhnykh γ-spektrov maloy intensivnosti. V sb.: Pribory i metody analiza izlucheniy). No. 3. Moscow, Gosatizdat, 1962.

8. Larichev, A. V. and Laricheva, V. V. The Inverse Matrix for the Sensitivity of a Scintillation Spectrometer. IN: Problems of Dosimetry and Radiation Shielding (Inversnaya matritsa chuvstvitel'nosti stsintillyatsionnogo spektrometra. V. Sb.: Voprosy dozimetrii i zashchity ot izlucheniy). No. 1. Moscow, Gosatomizdat, 1962.

FIELD DOSES AND THE ANGULAR DISTRIBUTION OF GAMMA-RADIATION FROM THE SURFACE OF ISOTROPIC SOURCES AT THE BOUNDARY SEPARATING TWO MEDIA

L. P. Kimel'

In computing the field doses from the surface isotropic sources at /217
points lying in the source plane at some distance from its edge, it is necessary to take into account the presence of the boundary separating two media (for example, earth-air). The presence of the separation boundary does not make it possible to apply directly the known buildup factors computed for homogeneous infinite media, but it requires corrections in the computational equations which take into account the special features associated with the propagation of scattered γ-radiation in nonhomogeneous media.

In the general case, when the media differ radically in their atomic number and density, the determination of such a correction is rather difficult: it is only possible to make an experimental determination or to carry out computations using the method of random tests. The correction factor K for various conditions has been determined in references 1-3. However, none of these works presents an analytical expression for K. Meanwhile, in order to develop a computational equation for the boundary between two media produced by an extended surface source it is necessary to have an analytical expression for the correction factor pertaining to a point source. In the case when the heterogeneous media are close in their atomic number, but differ in density, some simplification of the derivation is possible. As a result of this simplification it is possible to obtain an analytical expression for the correction factor, and the value of K computed by means of this expression agrees satisfactorily with data presented in references 1-3.

Let us consider a point isotropic source lying on the surface of the earth and let us determine the dose at the boundaries separating the earth and the air. The earth (medium 2) and air (medium 1) may be looked upon as media with close atomic number,[1] but with a different density ($\rho_2 \gg \rho_1$).

Since the atomic numbers are close and since the basic process of /218
γ-quanta interaction with material in the energy range of 0.3-3.0 MeV is a Compton scattering process, it follows that

$$B_1(\mu_1 x_1) \approx B_2(\mu_2 x_2),$$

[1] The media water-earth and water-air may also be considered to be close in atomic numbers.

if

$$\mu_1 x_1 = \mu_2 x_2,$$

where B is the buildup factor for infinite homogeneous media; x_1, x_2 is the distance from the source to the test point in media 1 and 2, respectively; μ_1 and μ_2 are the linear attenuation coefficients in media 1 and 2, respectively.

Let us assume that medium 2 is absent and that the source is in an infinite medium 1. Then the dose at some point A, which is at a distance x from the source, may be determined from the expression

$$D_{1,A} = D_{1,0} e^{-\mu_1 x} B_1(\mu_1 x) \quad D_{1,0} e^{-\mu_1 x} + D_{1,p},$$

where $D_{1,A}$ is the dose at the same point A from a point isotropic source situated in the infinite medium 1; $D_{1,0}$ is the dose at the point A due to the primary radiation without taking into account attenuation; $D_{1,p}$ is the dose at point, A from the secondary scattered radiation. It is easy to obtain the following expression

$$D_{1,p} = D_{1,0} e^{-\mu_1 x} [B_1(\mu_1 x) - 1].$$

If we now assume that the lower semispace is a vacuum or an absolute blackbody, the dose from radiation which has been scattered only in the upper semispace will be one half of the total dose produced by the scattered radiation. Consequently,

$$D_{1,p}^{(A)} = \frac{1}{2} D_{1,0} e^{-\mu_1 x} [B_1(\mu_1 x) - 1].$$

In this consideration we do not take into account the variation in the dose due to radiation which moves back and forth between the upper and the lower semispace. However, the variation in the dose due to this effect is small.

By carrying out the same reasoning we obtain the dose from radiation which is scattered only in the lower semispace,

$$D_{2,p}^{(A)} = \frac{1}{2} D_{2,0} e^{-\mu_2 x} [B_2(\mu_1 x) - 1].$$

The total dose at the considered point A from a point source lying at the boundary between the earth and air consists of the sum of doses due to direct nonscattered radiation, attenuated in medium 1, and the scattered radiation from media 1 and 2.

The correction factor K is determined as the ratio of the dose when two media are present to the dose at the same point in a homogeneous infinite media 1:

$$K=\frac{D_{1,0}e^{-\mu_1 x}+\frac{1}{2}D_{1,0}e^{-\mu_1 x}[B_1(\mu_1 x)-1]+\frac{1}{2}D_{2,0}e^{-\mu_2 x}[B_2(\mu_2 x)-1]}{D_{1,0}e^{-\mu_1 x}B_1(\mu_1 x)}.$$

If $D_{1,0} = D_{2,0}$, then

$$K=\frac{1+\frac{1}{2}[B_1(\mu_1 x)-1]}{B_1(\mu_1 x)}+\frac{e^{-\mu_2 x}[B_2(\mu_2 x)-1]}{2e^{-\mu_1 x}B_1(\mu_1 x)}.$$

Let us consider a specific case:

(1) x is small, i.e., $\mu_1 x \cong 0$, $e^{-\mu_1 x}=1$, $B_1(\mu_1 x)=1$.

$$K=1+\frac{1}{2}e^{-\mu_2 x}[B_2(\mu_2 x)-1]. \qquad (1)$$

As we can see, at very close distances from source, K > 1, i.e., the dose increases due to the entry of radiation scattered in medium 2 into the detector.

(2) x is large, i.e., $e^{-\mu_2 x} = 0$

$$K=\frac{1+\frac{1}{2}[B_1(\mu_1 x)-1]}{B_1(\mu_1 x)}. \qquad (2)$$

We note that expression (2) is applicable when the distances between /219 the source and the detector are greater than 0.5 m. When

$$\mu_1 x \to \infty \quad B_1(\mu_1 x) \gg 1 \text{ and}$$
$$K = 1/2,$$

i.e., at large distances the dose at the boundary of separation is two times less than the dose at the same point in a homogeneous infinite medium.

The values of correction factors computed by means of expressions (1) and (2) agree well with data presented in references 1-3.

By taking into account the correction factor, the dose power from a point isotropic source lying on the boundary separating the two media at points which are also situated on the separation boundary, but are at a distance of approximately 0.5 meters from the source, may be described by the expression

$$P_A=\frac{m_0 8.4}{2x^2}e^{-\mu_1 x}[B(\mu_1 x)-1],$$

where m_0 is the activity in gamma-equivalents of radium. If we know the analytical expression for the dose power from a point source, taking into account the boundary condition, we can integrate over the surface of the source and obtain the dose power value for extended isotropic sources at the boundary separating the two media.

In addition to knowing the total dose, it is also important to know the angular energy distribution at the detection point. It is shown in reference 4 that the experimental data presented in reference 5 on the angular distribution may be expressed by empirical equations (for a given distance between the source and detector)

$$\delta(\vartheta) = \frac{0.04}{1.035 - \cos\vartheta} 100 \text{ sr}^{-1}$$

(смер = sr = steradians)

for ϑ from 7.5 to 90° and

$$\delta(\vartheta) = 0.032 \cdot 100 \text{ sr}^{-1}$$

for ϑ from 90 to 180°,

where $\delta(\vartheta)$ is the contribution to the dose (in percent of radiation passing within the limits of one solid angle in the direction ϑ); ϑ is the angle between the lines which join the source and the detector and a selected direction.

We have established that the expression of the form

$$\delta(\vartheta) = \frac{a}{1.035 - \cos\vartheta}, \qquad (3)$$

when the coefficient a is properly selected, gives a good description of the angular radiation dose distribution for arbitrary distances and energies. Within an accuracy which is sufficient for practical computations, it may be assumed that the angular distribution of the dose in the limits from 90 to 180° (rear semispace) does not depend on the angle and is given by equation (3) when $\vartheta = 90°$. It follows from this that if the contribution to the dose from the rear semispace is known, we can determine the coefficient a

$$a = 1.035\,\delta_{\vartheta=90°}. \qquad (4)$$

The contribution to the dose by the energy scattered behind the semispace will be determined as a quantity proportional to the difference of the buildup factors associated with infinite geometry and with barrier geometry (without taking into account the multiple transmission of γ-radiation between the rear space and the front space). Consequently,

$$\delta_{\vartheta=90^\circ} = \frac{(1-C)[B(x,\infty)-1]}{2\pi B(x,\infty)} . \quad (5)$$

Here C is a correction factor for determining the buildup factor in barrier geometry (ref. 6) /220

$$C = \frac{B(x,x)-1}{B(x,\infty)-1},$$

where B (x, x) is the buildup factor for a barrier of thickness x at depth x; B (x, ∞) is the buildup factor for an infinite medium at depth x. Substituting (4) into expression (5), we obtain

$$a = \frac{1.035(1-C)[B(x,\infty)-1]}{2\pi B(x,\infty)}$$

Consequently the angular distribution may be written in the following final form

$$\delta(\vartheta) = \frac{1.035(1-C)[B(x,\infty)-1]}{2\pi B(x,\infty)(1.035-\cos\vartheta)} . \quad (6)$$

The angular distributions computed by means of equation (6) agreed well with experimental values for Co^{60} (ref. 5) and Au^{198} (ref. 7) and with data obtained by the method of random tests for $h\nu_0$ = 1 MeV (ref. 8). If we know the expression for the angular distribution of the dose from a point isotropic source, we can use numerical integration to obtain the angular distribution from extended surface sources.

This work was carried out under the direction of Professor O. I. Leypunskiy, to whom the author expresses his sincere gratitude.

REFERENCES

1. Berger, M. J. Appl. Phys., Vol. 28, 12, 1957.

2. Tibus, G. Nucl. Sci. Eng., Vol. 3, 609, 1958.

3. Kukhtevich, B. I., Shemetenko, B. P. and Sinitsyn, B. I. Atomnaya Energiya, Vol. 8, 66, 1960.

4. Leypunskiy, O. I. The Gamma-Radiation of an Atomic Explosion. (Gamma-izlucheniye atomnogo vzryva). Moscow, Atomizdat, 1959.

5. Sool, B. W. Proc. Roy. Soc., A230, 342, 1955.

6. Berger, M. and Doggett, J. J. Res. Nat. Bur. Standards, Vol. 56, 2, 1956.

7. Leypunskiy, O. I. and Sakharov, V. N. Atomnaya Energiya, Vol. 6, 585, 1959.

8. Leypunskiy, O. I., Strelkov, A. S. et al. Atomnaya Energiya, Vol. 10, 493, 1961.

THE THREE-DIMENSIONAL DISTRIBUTION OF SCATTERED ENERGY FROM A POINT UNIDIRECTIONAL SOURCE

L. P. Kimel' and O. I. Leypunskiy

A point unidirectional source is of interest, because its geometry /220 provides the initial basis for investigating the scattering of γ-radiation from sources with any angular distribution. Such sources of γ-radiation as a point isotropic source, a plane unidirectional source, sources with angular distribution according to the law $\cos^n\Theta$ and others may be considered to be made up of point unidirectional sources. Data on the scattering and absorption of γ-radiation in media from sources with arbitrary angular distribution may be obtained by superposing data on scattering and absorption for point unidirectional sources.

The problem of the three-dimensional distribution of scattered γ-radiation from a point unidirectional source is considered theoretically in only one work (ref. 1), which presents a method of solving the kinetic equation for a point unidirectional source. The numerical solution of the equations obtained requires a great deal of computations on high-speed electronic computers and has not been carried out to date. We investigated experimentally the three-dimensional distribution of scattered γ-radiation from a point unidirectional source.

In the future (for the sake of brevity) the three-dimensional distribution of γ-radiation from a point unidirectional source will be called "the expansion of a narrow beam."

Experimental Setup and Measurement Methods

"The expansion of a narrow beam" was investigated in a water phantom /221 with dimensions of 90 X 90 X 90 cm. A strongly collimated beam of γ-quanta was directed perpendicular to the front wall of the phantom and entered the water at a point 45 cm from the edges of the phantom. The radiation source consisted of Cs^{137} with an activity of 0.43 g·equiv of Ra. In water $\mu_0 = 0.083$ cm^{-1}, when $h\nu_0 = 0.7$ MeV, and consequently the beam of γ-quanta was surrounded by water with a thickness of approximately 4 mean paths of the primary γ-radiation.

The thickness of the water layer in the direction of the beam was greater than seven mean free paths.

When the scattered energy at points 45 cm away from the axis of the beam is measured (measurements at the boundary of the phantom), the error due to the finite size of the phantom may be quite substantial. On the other hand, at points which are situated closer to the axis and are approximately 10 cm from the edge of the phantom, the error due to the finite dimensions of the volume will apparently be negligibly small. This is clear from the following. The scattered radiation which arrives at the detection point from layer 3 (fig. 1) may be looked upon as the back-scattered γ-radiation with respect to the radiation incident on layer 3 from layer 2. The back scattering is characterized by the value of the albedo. It is known that the value of the albedo for a specific energy, reflection material and angle of incidence for the γ-quanta is a function only of the reflector thickness.

Table 1 shows the values of $B(0, x)-1/B(0, \infty)-1$, characterizing the amount of radiation reflected from a barrier of finite thickness $B(0, x)$, normalized with respect to the radiation reflected from a barrier of infinite thickness $B(0, \infty)$ (ref. 2).

We can see from table 1 that for an initial energy of 0.66 MeV and with a normal incidence of the γ-quanta, the albedo for a mean free path of unity is less than the albedo from an infinite layer by only 12 percent. In our case the energy of the scattered radiation is substantially less than 0.66 MeV, and the scattered radiation falls on layer 3 at various angles from 0 to $\pi/2$. Consequently, when measurements are made at points which are not less than 10 cm from the edge of the phantom, the phantom may be looked upon as an infinite volume.

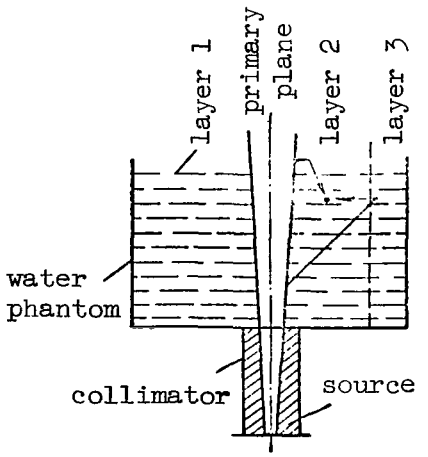

Figure 1. Geometry of experiment.

TABLE 1. THE QUANTITY B(0, x)-1/B(0, ∞)-1 FOR WATER AND γ-QUANTA WITH AN ENERGY OF 0.66 MeV AS A FUNCTION OF ANGLE Θ.

Θ°	Barrier thickness in terms of the mean free paths, $\mu_0 x$		
	0.5	1	2
0	0.65	0.88	0.99
60	0.81	0.96	1.0

The radiation detector consisted of a STS-5 halogen counter with filters (ref. 3). A scintillation detector incorporating an organic crystal of spherical form and with a diameter of 10 mm was used for measurements in the direct beam together with a miniature SI-2BG counter. The readings of these detectors were normalized according to the readings of the halogen counter. /222 The detector was fixed in a holder and could be displaced to any point in the volume of the phantom. The direction of the beam axis was determined in advance. Measurements were made at points lying in a plane normal to the beam axis at distances of 6, 12, 18, 24, 30 and 36 cm from the source along the beam and at distances of 5, 7, 10, 15, 20 and 30 cm from the axis of the beam.

When curves were read for the distribution of scattered energy it was noted that the form of the curve depends appreciably on the diameter of the collimator and on the geometric angle of beam expansion. Figures 2 and 3 show the ratio of detector readings in beams at distances of 0.5 $\mu_0 x$ and 2 $\mu_0 x$ from

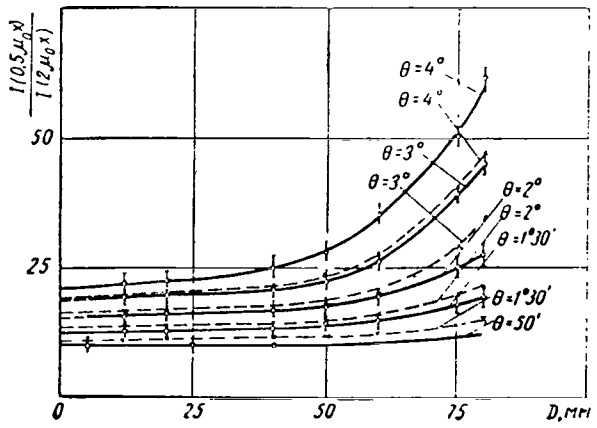

Figure 2. Ratio of detector readings as function of collimator diameter for various angles Θ (Cs^{137} source): ————, h = 12 cm; – – – – –, h = 18 cm.

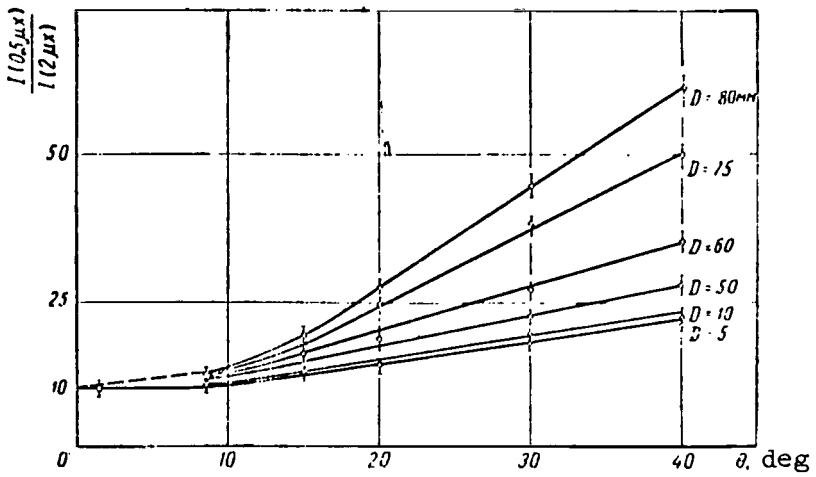

Figure 3. Ratio of detector readings as function of angle Θ for different collimator diameters (h = 12 cm).

the beam axis as a function collimator diameter D and the geometric angle Θ. This ratio increases with the collimator diameter and with the expansion angle. The nature of this increase becomes clear if we note that for large collimator diameters the points lying close to the axis are subject to radiation scattered in the collimator as well as to radiation scattered in water. The portion of energy which is scattered in the collimator and arrives at the detection point increases with the diameter of the collimating hole and the geometric beam expansion angle. At a detection point which is far removed from the beam axis (more than 2 $\mu_0 x$), the radiation which is scattered in the collimator does not fall on the detector. As a result of this the ratio of detector reading at points close to the beam axis increases with the diameter of the collimating opening. From the graphs presented it is clear that the effect of radiation scattered in the collimator will be small when the diameter of the collimator opening is less than 1 cm and when the beam expansion angle is less than 1°. Therefore, all of the measurements on the "expansion of a narrow beam" /223 were carried out with a collimator having an opening diameter of 5 mm and a geometric expansion of 50' (the collimator cut out a beam with a solid angle of 2.4×10^{-5} sr).

Measurement Results

Figure 4 shows the results of measuring the distribution of γ-radiation scattered in water from a point unidirectional source. The experiment was carried out using an entry window diameter of 5 mm and a collimation angle of Θ = 50'. The curves were recomputed for 1 cm^2. Two regions are clearly defined in the graph showing the distribution of scattered radiation: the initial region,

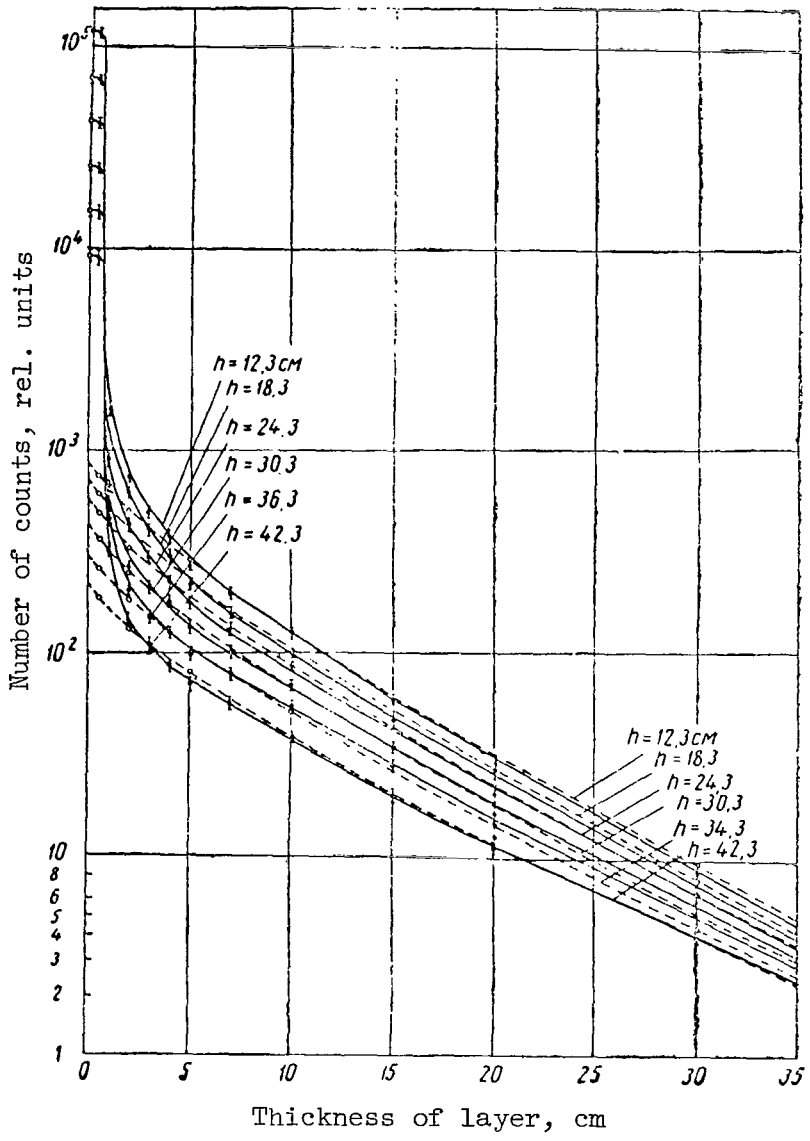

Figure 4. Distribution of γ-radiation scattered in water from point unidirectional Cs^{137} source: ————, experimental value; – – – – – –, computed values.

characterized by a sharp drop in the γ-radiation flux, and a region of relatively smooth variation in flux with distance. The sharp drop in the flux /224 along the first region is explained by the fact that as we move away from the axis of the beam the detector leaves the beam and records only the scattered radiation. The attenuation of the primary radiation along the beam axis takes place according to an exponential law.

It is interesting to obtain an analytic expression for the distribution of energy scattered from a point unidirectional source. We can propose the following method for deriving such an expression.

In reference 4 an infinite extended unidirectional source of γ-quanta and a point detector are represented by an equivalent point unidirectional beam and an infinite detector. For a plane unidirectional beam we can write

$$E = E_0 e^{-\mu_0 h} + E_{pac} = E_0 e^{-\mu_0 h} B, \tag{1}$$

(pac = scat = scattered)

where E is the energy at the considered point in MeV/cm^2; B is a buildup factor (of energy) for a plane unidirectional source; h is the distance along the beam axis in cm; E_{scat} is the scattered energy at the considered point in MeV/cm^2.

Proceeding from the equivalence noted above, the value of the energy E_{scat} may be obtained by integration over an infinite plane of scattered energy distribution from a point unidirectional source

$$E_{pac} = \int_S CL(\alpha, \mu x)\, ds, \tag{2}$$

where L (α, μx) is the distribution function for the scattered energy over a plane situated at a depth h perpendicular to the incident flux of γ-quanta for a point unidirectional source; C, α are constants which must be determined; ds is an element of the surface.

From experimental curves for the distribution of scattered radiation we can see that L(α, μx) must be an exponential function or a similar function. A more detailed analysis of the distribution curves shows that the function L(α, μx) is the King function.

We write the constant C in the form $C = TE_0 e^{-\mu h}$, where T is a new constant which is independent of x and whose dimensions are MeV/cm^2.

In a polar system of coordinates ds = 2πxdx, where x is the distance from the beam axis to the considered point. We rewrite expression (1) in the following form

$$E_0 e^{-\mu_0 h} + 2\pi \int_0^\infty TE_0 e^{-\mu h} \Phi(\alpha, \mu x)\, x\, dx = E_0 e^{-\mu_0 h} B, \tag{3}$$

where $\Phi(\alpha, \mu x)$ is the King function.

Solving equation (3) with respect to α, we obtain

$$\alpha = \sqrt{\frac{2\pi T}{3(B-1)\mu^2}}.$$

The constant T is selected so that it is equal to (from experimental curves)

$$T = \mu h \mu^2.$$

Then α assumes the form

$$\alpha = \sqrt{\frac{2\pi\mu h}{3(B-1)}}.$$

Finally, if the energy of the point unidirectional source is equal to E MeV/sec, the distribution of the scattered radiation from a point unidirectional source is described by the expression

$$E_{\text{pac}}(\mu h, \mu x) = Ee^{-\mu h}\mu^2 \mu h \Phi\left(\sqrt{\frac{3\pi\mu h}{3(B-1)}}; \mu x\right). \quad (4)$$

Figure 4 shows the values of E_{scat} computed by means of equation (4). /225

The discrepancy between computed and experimental values does not exceed 10 percent. The distribution of scattered energy computed by means of equation (4) coincides with the distribution obtained experimentally for Co^{60} (ref. 5), if in the latter we take into account the radiation scattered in the collimator.

The analytical expression for the three-dimensional distribution of scattered radiation from a point unidirectional source makes it possible to determine the buildup factor for a point isotropic source. In this case the point isotropic source is considered as consisting of individual "narrow beams."

A calculation is carried out according to the following scheme. The contribution of the scattered radiation at point A (fig. 5) from γ-radiation is determined over the solid angle $d\Omega$ under the angle Θ. This contribution is determined from the expression

$$dE_{\text{pac}}(\Theta) = \frac{E_0}{4\pi}\mu^2 \mu h(\Theta)\Phi[\alpha, \mu x(\Theta)]e^{-\mu h(\Theta)}d\Omega. \quad (5)$$

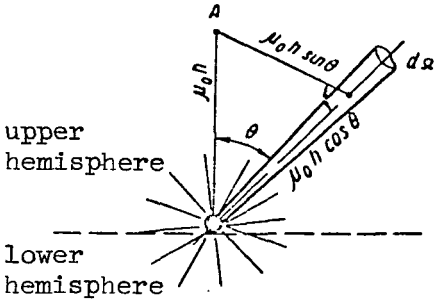

Figure 5. Computation diagram.

The total quantity of scattered energy arriving at point A from the upper semispace is obtained by integrating expression (5) over the solid angle 2π.

The total energy recorded at point A by a spherical isotropic detector of unit cross section, is equal to

$$E_{\text{п}} = \frac{E_0}{4\pi n^2} + \int\limits_{\Omega=2\pi} dE_{\text{рас}}(\Theta)\, d\Omega + f \int\limits_{\Omega=2\pi} dE_{\text{рас}}(\Theta)\, d\Omega,$$

(Π = t = total)

where f is a coefficient which takes into account the portion of scattered energy arriving at the point from the lower semispace; for small values of μh, coefficient f is numerically equal to the albedo of the γ-radiation from a point isotropic source lying on the surface of the reflector; for $\mu h = 2$, $f = 0$.

The buildup factor is the ratio of the total energy recorded at point A to the energy of primary radiation, $B = E_{\text{п}} \Big/ \frac{E_0 e^{-\mu h}}{4\pi h^2}$. Noting that h ($\Theta$) = h cos Θ and x (Θ) = h sin Θ, we obtain a final computational equation for the buildup factor from a point isotropic source

$$B_{\text{t}} = 1 + (1+f)\, 2\pi e^{\mu h} (\mu h)^3 \int\limits_0^{\pi/2} e^{-\mu h \cos\Theta} \Phi(\alpha, \mu x \sin\Theta) \sin\Theta \cos\Theta\, d\Theta. \qquad (6)$$

Table 2 presents the energy buildup factors for water and for point isotropic sources with γ-quanta energies of 0.7 and 1.25 MeV, computed by means of equation (6) and obtained by extrapolating and interpolating the buildup factors taken from reference 6. /226

TABLE 2. ENERGY BUILDUP FACTORS IN WATER FOR A POINT ISOTROPIC SOURCE.

μh	$h\nu_0$ = 0.7 MeV		$h\nu_0$ = 1.25 MeV	
	Computations with equation 6	Data from reference 6	Computations with equation 6	Data from reference 6
0.5	1.45	1.66	1.35	1.45
1	2.22	2.34	2.06	2.0
2	4.5	4.22	3.44	3.26
4	11	10.2	6.76	6.5
7	24	25	12.4	14

As we can see, the discrepancy in the results computed by means of equation (6) and the interpolated data from reference 6 does not exceed 10 percent, which is within the accuracy associated with the determination of buildup factors in reference 6.

The coincidence of buildup factors computed by means of equation (6) with buildup factors determined in reference 6 makes it possible for us to assume that the derived expression (4) gives a corrected description of the three-dimensional distribution of scattered energy from a point unidirectional source.

REFERENCES

1. Breshenkova, Ye. B. and Orlov, V. V. Atomnaya Energiya, Vol. 8, 1, 1961.

2. Price, B. T., Horton, C. C. and Spinney, K. T. Radiation Shielding (Zashchita ot yadernykh izlucheniy). Moscow, Izd-vo I. L., 1959.

3. Sakharov, V. N. Atomnaya Energiya, Vol. III, 61, 1957.

4. Kirn, F. S., Kennedy, R. L. and Wyckoff, H. D. Radiology, Vol. 63, 18, 1954.

5. The Shielding of Nuclear Reactors. Materials of the Atomic Energy Commission, USA (Zashchita yadernykh reaktorov. Materialy KAE SShA). Moscow, Izd-vo I. L., 1958.

6. Goldstein, H. and Wilkins, J. Calculation of the Penetration of Gamma Rays. NDA, NYO-375, 1954.

THE DIFFERENCE IN THE SPECTRA OF GAMMA-RAYS DURING RADIATION CAPTURE OF THERMAL NEUTRONS AND OF NEUTRONS WITH THE REACTOR SPECTRUM

A. T. Bakov, S. P. Belov, Yu. A. Kazanskiy and V. I. Popov

References 1-3 present the results of investigating the spectra of /226 γ-rays during the radiation capture of resonance neutrons. It is pointed out in these works that the spectrum obtained differs from spectra observed during the radiation capture of thermal neutrons. From the standpoint of computing shielding, when taking into account the captured γ-radiation, it is of interest to establish the variation in the spectrum of γ-rays during radiation capture as a function of neutron energy.

The present work presents the results of investigating the spectra of γ-rays associated with the radiation capture of neutrons having the uranium-water reactor spectrum of zero power and filtered by boron carbide with a thickness of 4 cm (a density of 1.2 g/cm^3). The γ-ray detector consisted of a single crystal scintillation spectrometer with a NaJ (Tl) crystal having a diameter of 40 mm and a height of 40 mm. The pulses were analyzed by a 128-channel amplitude analyzer (ref. 4). Evaluations showed that the spectrum of outgoing neutrons has a sharp drop below neutron energy of 100 eV. Above an energy of 2-3 MeV it is practically identical to the fission spectrum. For this neutron spectrum the capture in test materials (iron and nickel) takes place primarily in the region of energies above 100 keV (iron 60 percent, nickel 70 percent).

The basic difficulty associated with measuring the γ-ray spectrum of radiation capture by neutrons with the reactor spectrum is due to the background γ-rays which leave the reactor and the background formed when neutrons are captured in the iodine of the detector itself. In order to reduce the background a layer of bismuth with a thickness of 9 cm was placed over the carbide-boron filter, followed by a layer of lead with a thickness of 8 cm and another layer of bismuth with a thickness of 8.5 cm. Iron and nickel samples (40 x 40 x 2 cm^3) were placed on the bismuth and a neutron shield consisting of a mixture of plexiglas and boron carbide was placed over them (fig. 1). The γ-ray detector shielded with boron carbide was surrounded by a bismuth shield with a thickness of 4 cm. When the background radiation was measured, the iron and nickel samples were replaced with a lead sample whose area was equal to the area of the test samples, while its thickness was selected to provide for an equivalent attenuation of γ-rays with an energy of approximately 5 MeV.

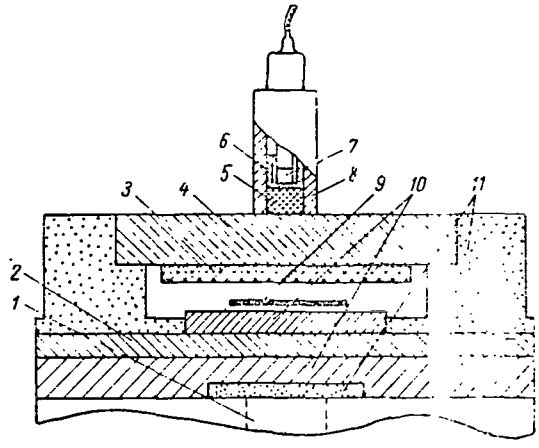

Figure 1. Schematic representation of experimental set for measuring the γ-rays during radiation capture of neutrons with reactor spectrum: 1, active zone of reactor; 2, lead shielding; 3, 4, 5 and 6, neutron shielding consisting of paraffin, plexiglas and boron carbide; 7, sodium iodide crystal; 8, bismuth shielding for detector; 9, test sample; 10, bismuth shielding for reactor; 11, boron carbide shielding.

Figure 2 shows the equipment spectra of amplitudes measured with /227
iron and nickel samples and the background radiation measured with the lead sample. The measurements made with the lead sample and without the sample showed that in the region of γ-ray energies above 5 MeV there is a small number of pulses (approximately 5 percent of the background radiation), which are due to the capture of neutrons in lead, whereas for energies below 5 MeV the amplitude spectra measured without the sample have a larger number of pulses compared with measurements made with the lead samples; this is due to the attenuation effect of the lead screen on γ-rays leaving the reactor and on γ-rays from the radiation capture of neutrons in bismuth.

The equipment spectrum of γ-rays for the radiation capture of neutrons with the reactor spectrum were compared with analogous distributions during the radiation capture of thermal neutrons. The geometric conditions of experiments with thermal neutrons were analogous to the experimental conditions with neutrons having the reactor spectrum. In this case part of the neutron shielding (fig. 1) was replaced by paraffin blocks of equivalent dimensions with the sample inside. In this case the cadmium ratio at the point where the samples were situated turned out to be equal to 30 for the reaction Cu^{65} (n, γ) Cu^{66}. The energy scale of the spectrometer was controlled by means of γ-rays from a Po-α-Be (E_γ = 4.47 MeV) before and after each measurement.

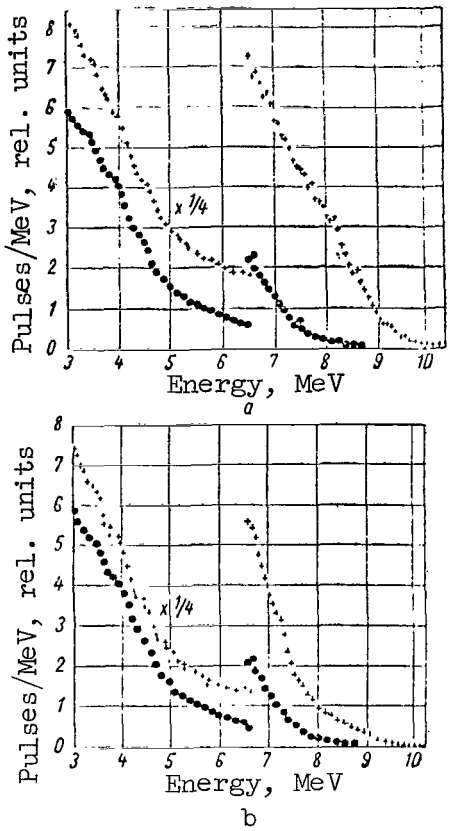

Figure 2. Equipment spectra of amplitudes (+ +), measured with nickel (a), iron (b) samples and equipment spectrum of background radiation (● ● ●), measured with lead sample. (Data normalized with respect to one reactor power and with respect to same measurement time.)

Figure 3 presents the equipment spectra (normalized for E = 6.5 MeV) of γ-rays associated with the radiation capture of thermal neutrons and of neutrons with the reactor spectrum in nickel. The equipment spectrum of pulses due to the γ-ray associated with the radiation capture of thermal neutrons in nickel clearly shows maxima at energies of 9.0, 8.5, approximately 7.5, and 6.8 MeV, which correspond to the most intense lines established from investigations with a magnetic spectrometer (ref. 5). In the equipment spectrum of amplitudes, obtained during the capture of neutrons with the reactor spectrum, a /228 relative increase in the number of γ-quanta with an energy of $E_\gamma < 5$ MeV is observed.

Figure 4 presents the equipment amplitude spectra due to the γ-rays associated with the radiation capture of thermal neutrons and of neutrons with the reactor spectrum in iron. The distributions are normalized for amplitudes corresponding to the γ-ray energy of 7 MeV. During the capture of thermal neutrons

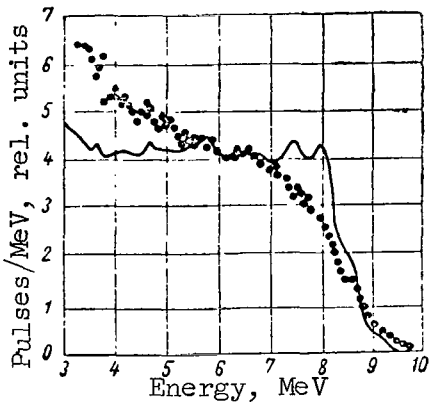

Figure 3. Equipment amplitude spectra due to γ-radiation of thermal neutron capture in nickel (——) and of neutrons with reactor spectrum in nickel (● ● ●). (Distributions normalized for energy of 6.5 MeV.)

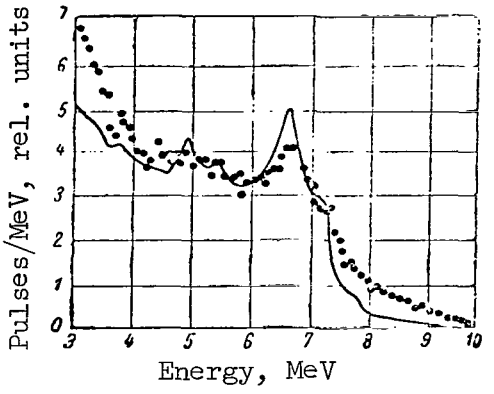

Figure 4. Equipment amplitude spectra due to γ-radiation associated with capture of thermal neutrons (——) and of neutrons with reactor spectrum in iron (● ● ●). (Distributions normalized for energy of 7 MeV.)

there are clearly defined peaks which correspond to the γ-transitions with energies of 7.6, 5.9 and 4.5 MeV in Fe^{57} as well as an unresolved distribution above γ-ray energy of 7.5 MeV, which is associated with radiation transitions in Fe^{55} and Fe^{58} (ref. 5). The equipment amplitude spectrum obtained during the capture of neutrons with the reactor spectrum is shown as substantially deformed: there is a relative increase in the number of γ-quanta with energies greater than 7.5 MeV. The equipment amplitude spectra measured during the capture of thermal neutrons have small statistical errors, because the background distribution of pulses is an insignificant part of the effect. When neutrons with the reactor spectrum are captured, the equipment spectrum of γ-rays, particularly in the energy range below 5 MeV, may contain substantial errors (15-30 percent) due to the fact that the subtraction of the background pulse distribution is not entirely accurate.

The established variations in the spectra of γ-rays associated with the radiation capture of resonant and fast neutrons can be explained as being:

(1) due to the variation in the cross sections of radiation capture of individual isotopes in a natural mixture when the neutron energy increases. A particularly pronounced variation in cross sections may occur when even-odd isotopes are present in noticeable quantities, whose radiation capture cross sections for fast neutrons may be 5-15 times greater than the cross sections of even-even cross sections (ref. 6);

(2) due to the variation in form of the γ-ray spectrum associated with radiation capture as a function of the orbital moment introduced into the nucleus by the neutron. As the neutron energy increases, the probability of neutron radiation capture with moment l_n, which differs from 0, will increase. This may in turn affect the nature of probability redistribution for γ-transitions;

(3) due to the change in the ratio between the capture cross sections associated with direct process and with processes involving the formation of a compound nucleus as a function of neutron energy. This may also lead to a change in the spectrum of γ-rays associated with radiation capture.

At the time our work was completed, an article was published (ref. 7) reporting the results of investigating the spectrum of γ-rays during the capture of neutrons with an energy of 100 keV in nickel. The general nature of spectrum variation compared with the capture of thermal neutrons is analogous to the data we have presented.

The measurements carried out in the present work, in spite of their /229 qualitative nature, show conclusively that the number of captured γ-quanta with energy greater than 6-7 MeV per neutron capture in the thermal and fast region is different. If we assume that the variation of spectra is associated with the redistribution of ratios for the isotropic captured cross sections, then in the case of iron the intensity of γ-quanta with energy greater than 7.5 MeV increases by a factor of 3-4 compared with the case of thermal neutron capture, whereas for nickel it decreases approximately by a factor of 1.3.

In conclusion the author takes this occasion to express his deep gratitude to I. I. Bondarenko for valuable remarks made in the course of the measurements.

REFERENCES

1. Landon, H. H. and Rae, E. R. Phys. Rev., Vol. 107, 1333, 1957.

2. Kennet, T., Bollinger, L. M. and Carpenter, R. T. Phys. Rev. Let., Vol. 1, 76, 1958.

3. Fenstermacher, C. A., Draper, J. E. and Blockelman, C. K. Nucl. Phys., Vol. 10, 386, 1959.

4. Matalin, L. A., Shimanskiy, A. M. and Chubarov, S. I. Pribory i tekhnika eksperimenta, No. 1, 64, 1957.

5. Groshev, L. V., Demidov, A. M. et al. Atlas of γ-Ray Spectra Associated with the Radiation Capture of Thermal Neutrons (Atlas spektrov γ-luchey radiatsionnogo zakhvata teplovykh neytronov). Moscow, Atomizdat, 1958.

6. Belanova, T. S. and Kazachkovskiy, O. D. Atomnaya Energiya, Vol. 14, 185, 1963.

7. Bergquist, J. and Starfelt, N. Nucl. Phys., Vol. 22, 513, 1961.

TRANSMISSION OF GAMMA-RADIATION THROUGH A FLAT SLIT IN SHIELDING

A. P. Veselkin, Yu. A. Yegorov and Ye. A. Panov

Recently a great deal of attention has been devoted to the problem of /229 radiation penetration through slits and heterogeneities in the shielding, because both slits and heterogeneities may be sources of strong radiation leakage and may impair shielding. The weakening of shielding by slits and heterogeneities lends itself to computation only in a limited number of cases. The existing equations and approaches for computing the penetration of radiation through slits and hollows are applicable only when adopted limitations are satisfied (refs. 1 and 2) and do not, in any case, cover the entire diversity of slit shapes (ref. 3) and hollow forms. From this it is clear that the experimental investigation of a decrease in shielding due to slits and heterogeneities is of great significance.

The source of γ-radiation consisted of a linear isotropic Co^{60} source, which was simulated by the forward motion of a point isotropic source (figs. 1 and 2). The dose power was measured by means of a scintillation γ-dosimeter "without hard operation" (ref. 4). The external view of the dosimeter sen-/231 sor is shown in figure 3. The shielding was placed between the source and the dosimeter (fig. 4). The dosimeter reading was automatically recorded on chart paper by means of the EPP-09 device; the motion of the chart paper was synchronized with the displacement of the source. A special circuit was used to turn on the motor. Figure 5 shows an example of a recording obtained when the dosimeter sensor was placed opposite the slit. With this distribution the area is proportional to the dose power at the point where the sensor is placed. The dose power over a length of 160 mm along the shielding in the direction perpendicular to the slit was measured in the course of the experiment.

In the experiment the variation in the dose power behind the shielding with the slit was measured as a function of the properties of material filling the slit and as a function of the shielding material. The shielding material consisted of lead and iron, whereas steel, titanium, aluminum, carbon (graphite with a density of 1.65 g/cm^3 and plexiglas were used to fill the slit. The shielding thickness in all of the measurements was 120 mm, and the height of the slit was 20 mm. The lead shielding was assembled from bricks interlaid with thin lead sheets to eliminate the assembly gaps. The steel shielding was assembled from two steel prisms.

Figure 6 shows the distribution of the γ-dose behind the lead, obtained in the experiments, for all of the materials used to fill the slit. The distributions

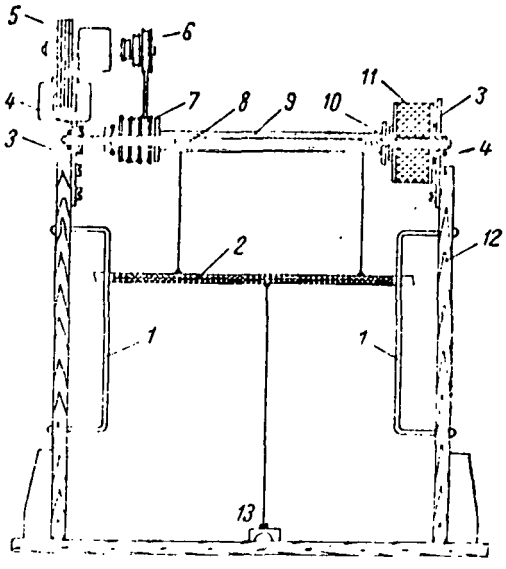

Figure 1. Schematic drawing showing arrangement for displacing source: 1, guideposts; 2, rack & source; 3, bracket; 4, bearing; 5, SD-2 motor; 6 and 7, pulleys; 8, shaft; 9, spool; 10, armature of electromagnetic clutch; 11, electromagnet; 12, stand; 13, end switch.

were obtained in the form of bell-shaped curves whose maximum appears opposite the middle of the slit. As was to be expected, the dose power behind the shielding increases sharply as the specific weight of the material filling the slit decreases. Thus, when steel is replaced with aluminum, the dose power opposite the center of the slit increases by a factor of 6.5. In addition to the increase in the dose power, directly in front of the slit we observed a widening of the distribution curves for the γ-dose with a decrease in the specific weight of the material filling the slit. Apparently this phenomenon is associated with an increase in oblique leakage paths, i.e., a decrease in the specific weight of the slit material weakens the shielding not only for the/232 γ-quanta of the source, which fall perpendicular to the shielding, but also for γ-quanta which fall on the shielding at some angle. This is confirmed to some extent by the fact that the increase in the dose power behind the shielding occurs not only directly in front of the slit, but also in front of shielding parts near the slit. In this case the slit boundary passes approximately opposite the half-height of the distribution curve.

To clarify certain laws we introduce the concept of specific dose, i.e., the dose per unit length behind the shielding,

$$D_1 = \frac{D_s}{l},$$

where D_s is the integral value of the γ-radiation dose behind the shielding with the slit; l is the distance along the shielding where the dose is measured.

The quantity D_s is determined by the area under the dose distribution curve behind the shielding (fig. 5). The decrease in the shielding may be determined from the ratio D_1/D, where D is the specific dose behind the continuous shielding. It is natural that as the specific weight of the material filling the slit decreases, the reduction of shielding due to the presence of the slit increases. To compare the extent of decrease for various materials filling the slit, a graph shown in figure 7 has been constructed. The ratio D_1/D is plotted along the axis of the ordinates, and the density of the material filling the slit ρ in g/cm^3 is plotted along the axis of the abscissas. Some spread in the points

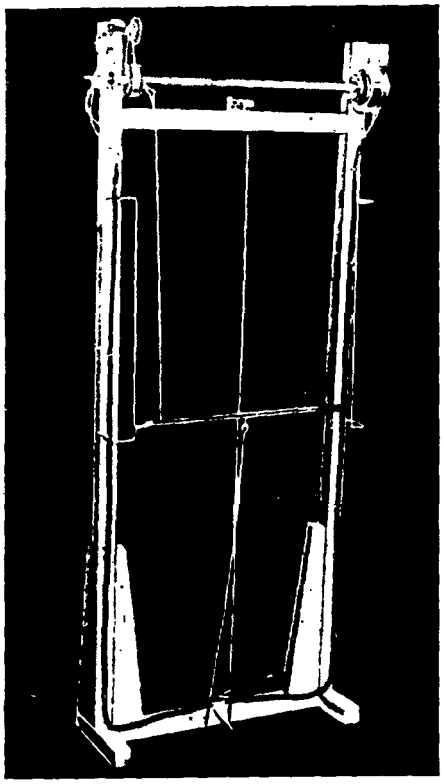

Figure 2. External view of setup for displacing source.

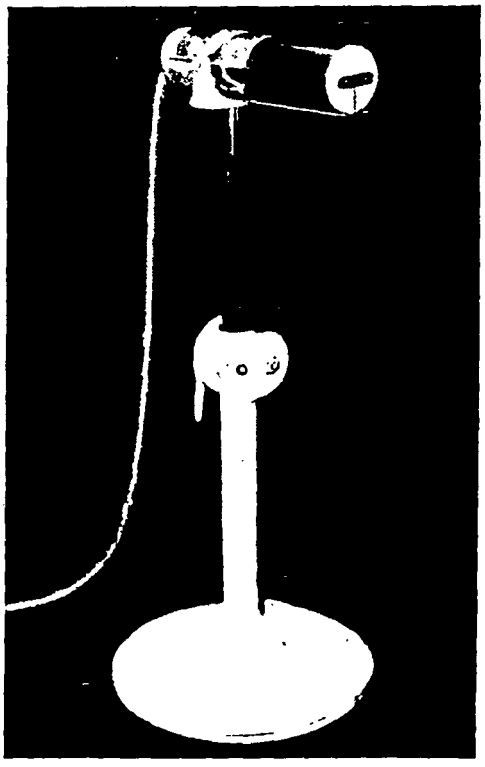

Figure 3. External view of spectrometer sensor on vertically adjustable stand.

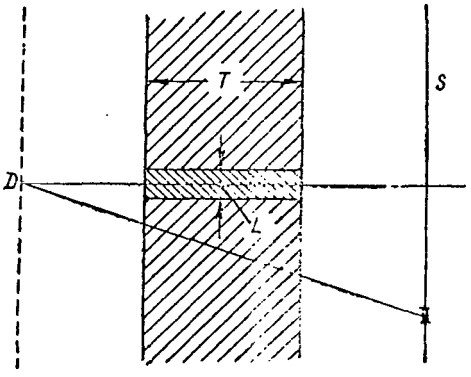

Figure 4. Mutual arrangement of source, sensor and shielding: S, source; D, detector; T, shielding thickness; L, slit height.

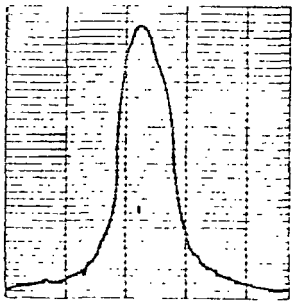

Figure 5. Recording on chart paper of EPP-09 device.

near the straight line is explained by the fact that when the slit material is replaced it is not possible to reproduce exactly the position of the lead bricks.

The result obtained makes it possible to determine the extent of /233 shielding decrease by a slit when it is filled with any material, if we know the dose behind the solid shielding and behind the shielding with a slit for some one slit material. A straight line for steel shielding (fig. 7, curve 2) was constructed in precisely this manner. The specific dose behind the solid shielding and the specific dose behind the shielding with a slit filled with titanium was measured experimentally. For this relationship the distribution D_1/D was also normalized to unity for a solid steel shielding. If distribution 2 is normalized at the point Fe to distributions 1, we can see that the distribution of shielding decrease for the case of steel will intersect the axis of the ordinates above distribution 1. This was to be expected.

Comparing the slopes of straight lines 1 and 2 (fig. 7), we can conclude that as the shielding material becomes lighter, there is a more pronounced variation in the degree of shielding decrease produced by a slit as the specific weight of the material filling the slit decreases.

It is interesting to note that if the ρ axis is replaced with the ρ/ρ_1 axis, where ρ is the specific weight of the shielding material, the point, obtained for the slit in a steel shielding (the material filling the slit is titanium), falls on the same straight line which contains the points obtained for other materials filling the slit in a lead shield (fig. 8). Consequently, we may assume that in terms of the D_1/D and ρ/ρ_1 coordinates the straight lines merge into one. However, this assumption must be verified by additional experiments.

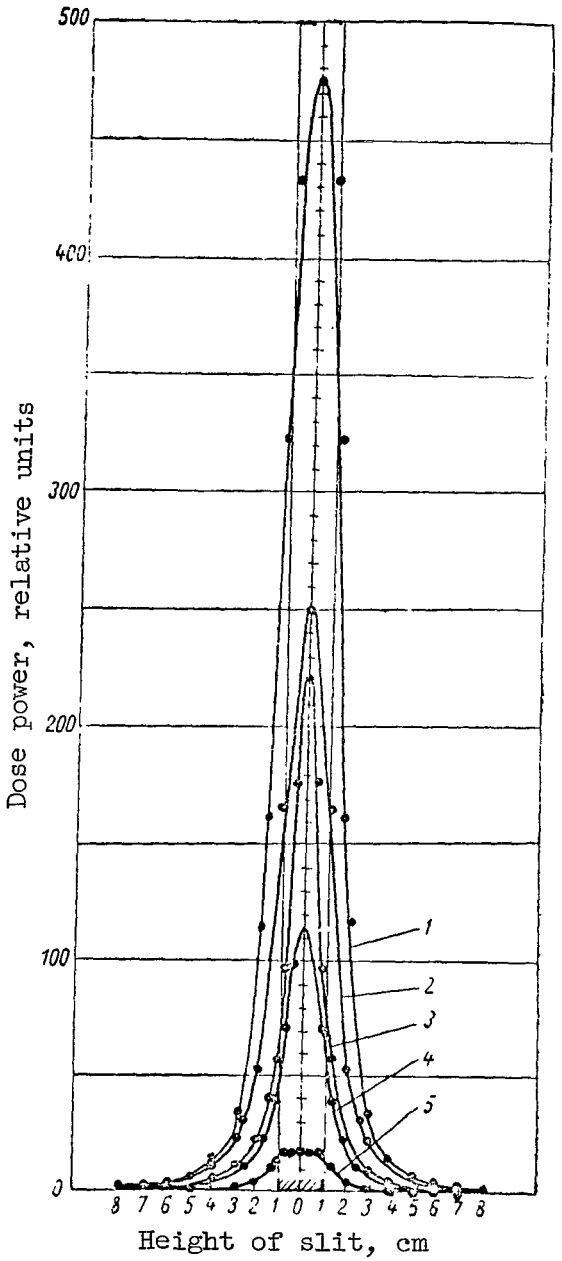

Figure 6. Distribution of γ-dose behind lead shielding with slit made of steel (5); of titanium (4); of aluminum (3); of carbon (2); of plexiglas (1).

The results of the experiment were compared with the calculations of the extent to which the shielding is weakened by the slit, using the methodology proposed in reference 1. The calculations were carried out in the following manner. The dose power due to the γ-radiation of a linear isotropic source,

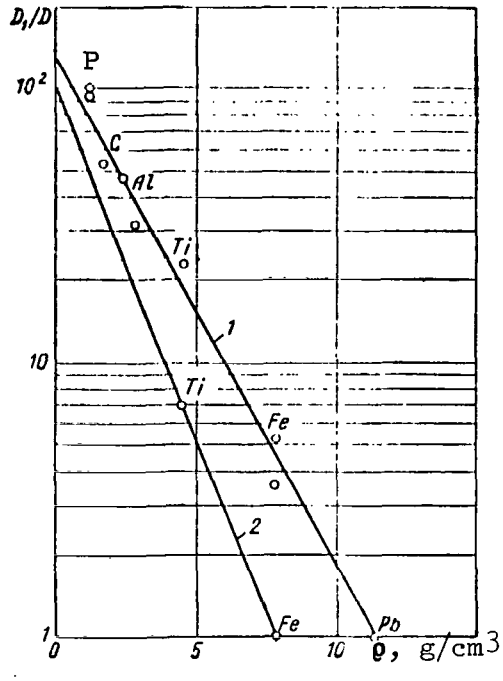

Figure 7. Extent of decrease D_1/D in shielding produced by slit as function of slit material specific weight: 1, lead shielding; 2, steel shielding; O, computed values for steel, concrete and water ; P, plexiglas; C, graphite (ϱ = 1.6 g/cm^3).

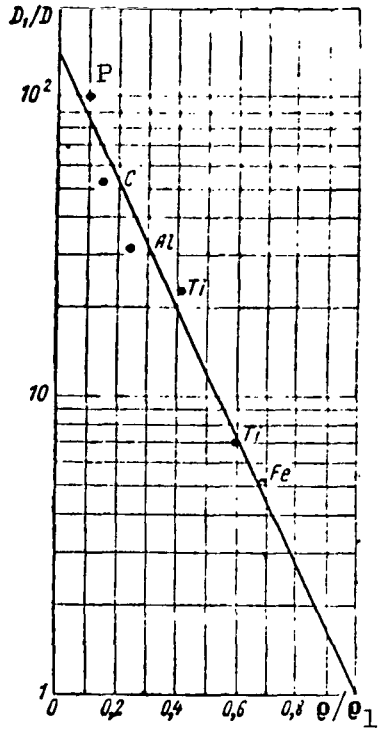

Figure 8. Extent of decrease D_1/D in shielding produced by slit as function of ratio ϱ/ϱ_1: P, plexiglas; C, graphite.

which has passed through a continuous lead shielding, was determined at the point where the detector is situated by means of the following equation

$$P_A(\mathrm{Pb}) = \int_{-\infty}^{\infty} \frac{qK_\gamma}{4\pi(a\sec\Theta)^2} e^{-\mu L\sec\Theta} B(\mu L\sec\Theta, E_\gamma)\, dl,$$

where q is the specific activity of the source; K_γ is the γ-constant; L is the shielding thickness; a is the distance from the detector to the source along the straight line; μ is the coefficient of the linear attenuation of γ-radiation by the shielding; Θ is the angle between the normal and the straight line drawn

from the detector to the element Δl of the source; E_γ is the energy of the source γ-quanta; $B(\mu L \sec\Theta, E_\gamma)$ is the buildup factor written in the form of two exponential terms:

$$B(\mu L \sec\Theta, E_\gamma) = A_1 e^{-\alpha_1 \mu L \sec\Theta} + A_2 e^{-\alpha_2 \mu L \sec\Theta}.$$

Here α_1, α_2, A_1, A_2 are coefficients obtained from tables presented in reference 1.

The dose power for a solid shielding of steel, concrete (ρ = 2.3 metric tons/m^3 and water was computed in exactly the same manner. The dose power behind the solid shielding was greater than the dose power behind the lead shielding by a factor of 42 (for steel), by a factor of 580 (for concrete) and by a factor of 1150 (for water).

Assuming that these materials are used to fill the slit in lead shielding and introducing a correction for the decrease in the shielding due to the slit, expressed in the form

$$\frac{\Phi}{\Phi_0} = \frac{1}{2} \cdot \frac{T}{L}, \qquad (1)$$

and equal to 1/12 in our case (Φ is the flux of γ-quanta at the output from the slit; Φ_0 is the flux of γ-quanta at the entrance to the slit), we can establish the extent of weakening in the shielding produced by a slit filled with each of the enumerated materials. Taking this correction into account, the relative excess of dose power behind the shielding with a slit over the dose power behind a solid lead shielding was equal to 3.5 (for steel), 48 (for concrete) and 96 (for water).

If we plot the values obtained for (D_1/D) calculated in figure 7, we can see that they also fall on the straight line 1. A comparison of experimental data with computed data has shown that the correction for the decrease in shielding produced by the slit, as proposed in reference 1, produces results which coincide with the results of our experiment within the limit of error. Consequently the computation of shielding weakening produced by a flat slit composed of various materials and for various shielding materials may be carried out with this method. /234

REFERENCES

1. Shielding of Nuclear Reactors. Edited by T. Rockwell (Zashchita yadernykh reaktorov). Moscow, Izd-vo I. L., 1958.

2. Price, B. T., Horton, C. C. and Spinney, K. T. Radiation Shielding (Zashchita ot yadernykh izlucheniy). Moscow, Izd-vo I. L., 1958

3. Harrison, J. A. Nuclear Reactor Shielding. London, 1958.

4. Yegorov, Yu. A. and Panov, Ye. A. Pribory i Tekhnika Eksperimenta, No. 4, 57, 1961.

HEAT LIBERATION IN REACTOR SCREENS AND VESSELS

D. L. Broder, A. P. Kondrashov, V. A. Naumov,
K. K. Popkov and A. V. Turusova

Introduction

As we know, a substantial amount of energy (approximately 30 MeV for each act of fission) is liberated inside and outside the active zone due to long mean free path radiations (γ-quanta and neutrons). The energy of neutrons and of γ-radiation which is lost due to interaction with material surrounding the active zone produces an increase in temperature. /234

Of particular concern to designers is the radiation heat liberation in vessels of water-moderated reactors which, in addition to these thermal loads, also experience a static loading due to pressure. The following long chain of physical processes must be taken into account when computing heat liberation: the origin of neutrons and γ-rays, the moderation absorption of neutrons with the formation of capture γ-radiation, the scattering and absorption of γ-rays, the formation of secondary electrons, etc. Therefore, even if we have a correct physical description of these processes, the accuracy associated with the calculation of heat liberation will depend on a large number of factors. In particular, such factors include the yield of γ-rays during the fission act as well as their spectra, the interaction cross sections for neutrons and others; some of these factors are not known with a sufficient degree of accuracy. Under these conditions the experimental verification of the method used to compute heat liberation becomes particularly important. The present work is an effort to substantiate the validity of the applied computation methods.

Methods of Computation

The following processes are taken into account during the computation of heat liberation:

(1) the γ-radiation of the active reactor zone;

(2) the capture γ-radiation occurring in the adjacent structural and shielding materials (thermal screens, reactor vessel, water between the screens);

(3) α particles of the B^{10} (n, α)Li^{7} reactions (for screens made of boron steel).

Other processes, such as the γ-radiation due to the inelastic scattering of fast neutrons, were not taken into account in the calculations, because they introduce an insignificant contribution to the value of the total heat liberation. Thus the value of specific heat liberation Q was determined as the sum

$$Q = Q_\gamma + \delta Q_\alpha, \tag{1}$$

where Q_γ and Q_α are the γ- and α-components of heat liberation, respectively;

$\delta = \begin{cases} 1, & \text{if the computation point is in a boron-containing screen;} \\ 0, & \text{if the computation point is in a screen made of conventional steel.} \end{cases}$

The calculation of the γ-component of heat liberation Q_γ is reduced to the determination of scalar γ-radiation fluxes of various energies φ_γ.

In this case the quantity $Q_\gamma(r)$ at the point r is given by the expression /235

$$Q_\gamma(r) = k \int_E \varphi_\gamma(E, r) E \mu_{en}(E, r) dE, \tag{2}$$

where $\varphi_\gamma(E, r)dE$ is the scalar energy flux of γ-radiation in the interval E to E + dE at point r; $\mu_{en}(E, r)$ is the linear absorption coefficient for the energy of γ-quanta with energy E at point r; k is a coefficient which is determined by the dimensions of quantities contained in expression (2),

$$k = 1.6 \cdot 10^{-3} \text{ W·sec/MeV} = 3.82 \cdot 10^{-14} \text{ cal/MeV}.$$

In the present calculation, integration was replaced by summation over several energy groups of γ-quanta. The following eight energy groups were taken for the calculation: 0-0.5; 0.5-1; 1-2; 2-3; 3-4; 4-5; 5-7; > 7 MeV.

In this case

$$Q_\gamma(r) = k \sum_{j=1}^{8} \varphi_{\gamma j}(r) E_j \mu_{en}(E_j) \tag{3}$$

where E_j is the average energy of the energy group j; $\varphi_{\gamma_j}(r)$ is the scalar flux of γ-radiation pertaining to energy group j from all types of sources at point r.

Quantity $\varphi_{\gamma_j}(r)$ was determined as the sum

$$\varphi_{\gamma j}(r) = \varphi^{a}_{\gamma j}(r) + \varphi^{b}_{\gamma j}(r) + \varphi^{c}_{\gamma j}(r) + \varphi^{d}_{\gamma j}(r) + \varphi^{e}_{\gamma j}(r), \qquad (4)$$

where $\varphi^{a}_{\gamma j}(r)$[1] is the flux of γ-radiation arriving at point r from the active zone; φ^{b}_{γ} is the flux of γ-radiation due to neutron capture in screens and in the reactor vessel excluding the screen which contains the computation point; φ^{c}_{γ} is the flux of γ-radiation associated with the radiation capture of neutrons in the volume of the screen containing the computation point; φ^{d}_{γ} is the flux of γ-radiation due to the capture of neutrons in the water filling the space between the screens; φ^{e}_{γ} is the flux of γ-radiation capture from water outside the reactor vessel.

Since the dimensions of the active zone are greater than the thickness of the screens, the calculations of fluxes were carried out using plane geometry. The quantity φ^{a}_{γ} was computed by taking into account the radial nonuniformity in the specific power of γ-radiation sources contained in the volume of the active zone. The active zone was approximated as an infinite radiating layer assuming that the distribution function of sources q_{γ} is constant over the thickness of the layer $1/\mu_{az}$,

$$\overline{q^{a}_{\gamma}} = \mu_{a.3} \int_{H-\frac{1}{\mu_{a.3}}}^{H} q_{\gamma}(x)\, dx,$$

(a.3 = az = active zone)

where H is the height of the active zone.

According to this it follows from reference 1 that

$$\varphi^{a}_{\gamma} = \frac{\overline{q^{a}_{\gamma}}}{2\mu_{a.3}} \sum_{j=1} A^{Fe}_{j} \left\{ E_2 \left[(1+\alpha^{Fe}_{j}) \sum_{i} \mu_i x_i \right] - E_2 \left[(1+\alpha^{Fe}_{j}) \left(\sum_{i} \mu_i x_i + \mu_S d \right) \right] \right\}, \qquad (5)$$

where μ_{az} is the linear attenuation coefficient of γ-radiation for the material of the active zone; $\sum_{i} \mu_i x_i$ is the thickness of the shielding layers in terms of

---

[1] In the future for the sake of simplicity we shall drop subscript j and shall not indicate coordinate r.

relaxation lengths within the space between the surface of the source and the point where heat liberation is calculated.

Equation (5) utilized the energy buildup factor for the scattered γ-radiation in its exponential approximation (ref. 2)

$$B(\mu x) = \sum_{j=1}^{2} A_j(E)\, e^{-\mu x \alpha_j(E)}.$$

The quantity φ_γ^b is made up of γ-quanta fluxes originating in various /236 screens. Therefore

$$\varphi_\gamma^b = \sum_k \varphi_{\gamma k}^b, \tag{6}$$

where $\varphi_{\gamma k}^b$ is the flux of γ-quanta due to neutron capture in the k-th screen.

The distribution functions for the capture γ-radiation sources across the thickness of the k-th screen $q_{\gamma k}^b(x)$ were approximated as follows:

(a) by a constant (for thin steel screens)

$$\bar{q}_{\gamma k}^b = \frac{1}{d}\int_0^d q_\gamma^b(x')\,dx',$$

where d is the thickness of the source layer; in this case the following equation was used (ref. 1)

$$\varphi_{\gamma k}^b = \frac{q_{\gamma k}^b}{2\mu^{Fe}} \sum_{j=1}^{2} \frac{A_j^{Fe}}{1+\alpha_j^{Fe}} \left\{ E_2\left[(1+\alpha_j^{Fe}) \sum_i \mu_i x_i\right] - E_2\left[(1+\alpha_j^{Fe})\left(\sum \mu_i x_i + \mu_S d\right)\right]\right\}, \tag{7}$$

where μ^{Fe} is the linear attenuation coefficient of γ-radiation for iron;

(b) by two exponents (boron-containing screens and reactor vessel)

$$q_{\gamma k}^b(x) = q_{\gamma k}^b(1)\, e^{-\Sigma_1 x} + q_{\gamma k}^b(2)\, e^{-\Sigma_2 x};$$

In this case we have

$$\left.\begin{aligned}
&\varphi^b_{\gamma k} = \varphi^b_{\gamma k}(1) + \varphi^b_{\gamma k}(2)\\
&\varphi^b_{\gamma k}(1) = \frac{q^b_{\gamma k}(1)}{2\Sigma_1}\sum_{j=1}^{2} A_j^{\mathrm{Fe}}\left\{e^{-\Sigma_1\left(d+\frac{\sum\mu_i x_i}{\mu_S}\right)}E_1\left\langle\left[(1+\alpha_j^{\mathrm{Fe}})-\frac{\Sigma_1}{\mu_S}\right]\sum_i \mu_i x_i\right\rangle -\right.\\
&-e^{-\Sigma_1 d}E_1\left[(1+\alpha_j^{\mathrm{Fe}})\sum_i \mu_i x_i\right] - e^{-\Sigma_1\left(d+\frac{\sum\mu_i x_i}{\mu_S}\right)}E_1\left\langle\left[(1+\alpha_j^{\mathrm{Fe}})-\frac{\Sigma_1}{\mu_S}\right]\times\right.\\
&\left.\left.\times\left(\mu_S d+\sum_i \mu_i x_i\right)\right\rangle + E_1\left[(1+\alpha_j^{\mathrm{Fe}})\mu_S d+\sum_i \mu_i x_i\right]\right\};\\
&\varphi^b_{\gamma k}(2) = -\frac{q^b_{\gamma k}(2)}{2\Sigma_2}\sum_{j=1}^{2} A_j^{\mathrm{Fe}}\left\{e^{\Sigma_2\left(d+\frac{\sum\mu_i x_i}{\mu_S}\right)}E_1\left\langle\left[(1+\alpha_j^{\mathrm{Fe}})+\frac{\Sigma_2}{\mu_S}\right]\sum_j \mu_i x_i\right\rangle -\right.\\
&-e^{\Sigma_2 d}E_2\left[(1+\alpha_j^{\mathrm{Fe}})\sum_i \mu_i x_i\right] - e^{\Sigma_2\left(d+\frac{\sum\mu_i x_i}{\mu_S}\right)}E_1\left\langle\left[(1+\alpha_j^{\mathrm{Fe}})+\frac{\Sigma_2}{\mu_S}\right]\times\right.\\
&\left.\left.\times\left(\mu_S d+\sum_i \mu_i x_i\right)\right\rangle + E_1\left[(1+\alpha_j^{\mathrm{Fe}})\left(\mu_S d+\sum_i \mu_i x_i\right)\right]\right\},
\end{aligned}\right\} \qquad (7')$$

where μ_S is the linear coefficient of γ-ray absorption in the source screen material.

The value of the flux φ^c_γ for the screens with constant source distribution $q^c_\gamma(x) = \overline{q^c_\gamma}$ was computed by means of equation /237

$$\varphi^c_\gamma = \frac{q^c_\gamma}{2\mu_S}\sum_{j=1}^{2}\frac{A_j}{1+\alpha_j}\{2 - E_2[(1+\alpha_j)\mu_S x] - E_2[(1+\alpha_j)\mu_S(d-x)]\}, \qquad (8)$$

where x is the distance of the point where heat liberation was computed from the layer surface.

For a screen with an exponential distribution of source power

$$\left.\begin{aligned}
&q^c_\gamma(x) = q^c_\gamma(1)e^{-\Sigma x};\\
&\varphi^c_\gamma = \frac{q^c_\gamma(1)}{2\Sigma}\sum_{j=1}^{2} A_j\left\langle e^{-\Sigma x}\left\{\ln\left|\frac{\mu_j-\Sigma}{\mu_j}\right| - e^{-\Sigma x}E_1(\mu_j x) + E_1[(\mu_j-\Sigma)x]\right\} + \right.\\
&\left.+e^{\Sigma x}\left\{\ln\left|\frac{\mu_j+\Sigma}{\mu_j}\right|e^{-\Sigma(d-x)}E_1[\mu_j(d-x)] + E_1[(\mu_j+\Sigma)(d-x)]\right\}\right\rangle,
\end{aligned}\right\} \qquad (9)$$

where

$$\mu_j = \mu\ (1 + \alpha_j).$$

The quantity φ_γ^d is the sum of γ-quanta fluxes originating in various layers of interscreen water,

$$\varphi_\gamma^d = \sum_k \varphi_{\gamma k}^d. \tag{10}$$

The computation of $\varphi_{\gamma k}^d$ was carried out without taking into account the absorption of γ-radiation inside the layer (this assumption may be made for thin layers when $\mu_S\ d < 2$), therefore

$$\varphi_{\gamma k}^d = \frac{\overline{q_\gamma^k} d}{2} \sum_{j=1}^{2} A_j^{Fe} E_1 \left[(1 + \alpha_j^{Fe}) \sum_i \mu_i x_i \right]. \tag{11}$$

The flux φ_γ^e of capture γ-radiation from water contained outside the reactor vessel was computed by assuming an exponential approximation for the γ-ray sources

$$q(x) = q_0 e^{-\Sigma x}.$$

In connection with this

$$\begin{aligned}\varphi_\gamma^e = -\frac{q_0}{2\Sigma} \sum_{j=1}^{2} A_j^{Fe} \Bigg\{ & e^{-\Sigma d} E_1 \left[(1 + \alpha_j^{Fe}) \sum_i \mu_i x_i \right] - \\ & - e^{-\left[\frac{(1+\alpha_j^{Fe}) \sum_i \mu_i x_i}{\mu_S} + d \right] \Sigma} E_1 \left[(1 + \alpha_j^{Fe}) \sum_i \mu_i x_i \left(1 - \frac{\Sigma}{\mu_S} \right) \right] - \\ & - E_1 \left[(1 + \alpha_j^{Fe}) \sum_i \mu_i x_i + \mu_S d \right] + \\ & + e^{-\left[\frac{(1+\alpha_j^{Fe}) \sum_i \mu_i x_i}{\mu_S} + d \right] \Sigma} E_1 \left\langle \left[(1 + \alpha_j^{Fe}) \sum_i \mu_i x_i + \mu_S d \right] \left(1 - \frac{\Sigma}{\mu_S} \right) \right\rangle \Bigg\}.\end{aligned} \tag{12}$$

The computation of the α-component of heat liberation Q_α was carried out with the equation

$$Q_\alpha(r) = k E_\alpha \sum_{j=1}^{7} n v_j(r)\, \Sigma_j^\alpha, \tag{13}$$

where $nv_j(r)$ is the flux of neutrons of energy group j at point r; Σ_j^{α} is the macroscopic cross section of the reaction $B^{10}(n, \alpha) Li^7$ for neutrons of energy group j; $E_{\alpha} = 2.31$ MeV is the effective energy of the α-particle.

The three-dimensional energy distribution of neutron fluxes necessary /238 for the computation of radiation sources for distribution functions may be obtained by means of the multiple group methods described in reference 3. The experimental basis for the multiple group methods in reference 3 is a definite guarantee that the computation of γ-ray sources is correct, as well as the computation of heat liberation sources due to the reaction $B^{10}(n, \alpha) Li^7$. In the present work an effort is made to show that the calculation of the γ-component of heat liberation Q_{γ} may be carried out with an accuracy sufficient for engineering purposes when the sources are correctly determined.

The Method of Measurements

Two methods for the experimental determination of heat liberation produced by radiation are known. The first method is calorimetric and consists of a direct measurement to determine the heating of the medium. However, this method is useful only for measuring large heat liberation in intense radiation fluxes. The other method which was used by us is the ionization method, which has high sensitivity and which makes it possible to measure small values of heat liberation. The selection of this method was dictated by the fact that measurements were made using critical reactor assemblies of zero power, where the calorimetric measurements are practically impossible. It was shown in reference 4 that measurements made by both methods agreed to within 5 percent. We utilized an ionization chamber of the capacity type for the detectors.

The ionization of the gas cavity of the chamber under definite conditions (the Gray conditions, reference 5) may be associated with heat liberation in the medium surrounding this cavity. The Gray conditions are concerned with the spectrum of secondary electrons and consist of the following.

If the dimensions of a solid medium exceed the maximum path of electrons formed during the interaction of γ-rays with matter, and if the dimensions of the gas cavity are less than the minimum electron path, then the gas in the cavity will not perturb the velocity distribution of secondary electrons. Then the loss of energy in the solid medium (heat liberation) q and the energy loss in the gas cavity are associated by the Gray relationship

$$\frac{(-dE/dx)_{solid}}{(-dE/dx)_{gas}} = \frac{q}{j_v W}, \qquad (14)$$

where $\left(\frac{dE}{dx}\right)_{solid}$ is the electron energy loss per unit path length in a solid medium or the retardation capacity; j_v is the number of ion pairs formed in a

unit volume of gas during 1 sec; W is the average quantity of energy which is consumed to form ion pairs in the gas.

If we note that the retardation capacities are proportional to the number of electrons, we obtain the following equation for heat liberation

$$q = j_v W \frac{N_{solid}}{N_{gas}} f, \tag{15}$$

where N_{solid}, N_{gas} is the number of electrons in 1 cm^3 of the solid medium and of the gas, respectively; f is the ratio of retardation capacities for solid and gaseous media (per electron), given by the Gaytler expression (ref. 6) and which, in addition to electron energy, depends only on the potential of the ionized atom.

The ionization potential depends very weakly on Z. For example, for Fe, Al and Be the values of f are equal, respectively, to 0.84, 0.94 and 1.04 when f = 1 for air. As we can see from expression (15), the accuracy of the method is determined by the accuracy in determining the quantities W and f and also on the effectiveness of ion collection. The number of ions formed in 1 cm^3 of the gas cavity during 1 sec may be computed from the obvious relationship

$$\Delta U (C_c + C_d) = j_v e t V_c, \tag{16}$$

where ΔU is the variation of the chamber potential during the irradiation time t (sec); C_c, C_d, are the capacities of the chamber and of the measuring devices in pF; e is the electron charge in Coulombs; V_c is the chamber volume in cm^3. /239

Thus we have the final expression for heat liberation in 1 cm^3 of the medium

$$q = Wf \frac{N_{solid}}{N_{gas}} \cdot \frac{1}{e} \Delta U \frac{(C_c + C_d)}{t V_c}. \tag{17}$$

Measurements of heat liberation were carried out in assemblies which simulated typical thermal shielding of a water—moderated reactor with zero power as the radiation source. These assemblies are described in reference 3. In order to measure heat liberation in steel plates, channels were made which were closed with plugs of the same material after the placement of the chamber. Most of the chambers were made of the 1X18N9T steel, while some were made from St. 3 steel. The dimensions of the chambers and their design are shown in figure 1.

The walls of the chamber case were made sufficiently thin; however, the Gray condition concerning the dimensions of the medium surrounding the gas cavity was satisfied, because the chamber was placed into a prism made of the

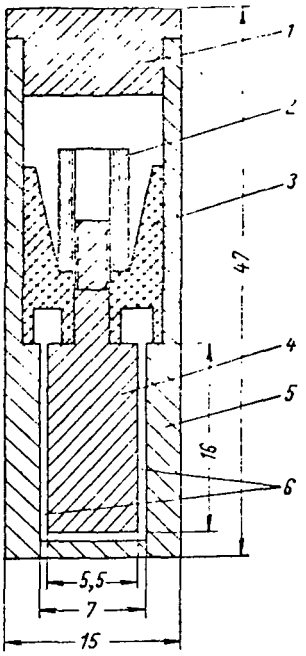

Figure 1. Steel gray chamber: 1, chamber cover; 2, brass nut; 3, teflon insulator; 4, central electrode; 5, chamber shell; 6, operating cavity.

same material as the wall. On the other hand, the chambers, insofar as possible, had small dimensions in order to fix the point accurately where the heat liberation was measured. In order to recompute the ionization and heat liberation it is necessary to know the volume and capacity of the chambers. The capacities were measured with a standard industrial type IIYeF device and were of the order of 4-6 pF when the capacity of the electrometer was 10 pF. The operating volumes were established by successive weighings on analytical balances. For this purpose they were either filled or unfilled with water. For different chambers these volumes were of the order of 0.4-0.7 cm^3.

The gaseous medium in the chamber consisted of air. The variation in chamber potential under the action of secondary β-radiation was measured by means of a standard electrometer. Before the measurements were started, the chamber was tested for the presence of breeding in the gas. Gas breeding was not observed for the operating voltages (up to 60 V). Experiments were carried out with the reactor power levels from a fraction of a watt to several tens watts for different measurement series. The irradiation time of 15 min was selected for the first assembly (fig. 2) and of 20 min for the second assembly (fig. 3).

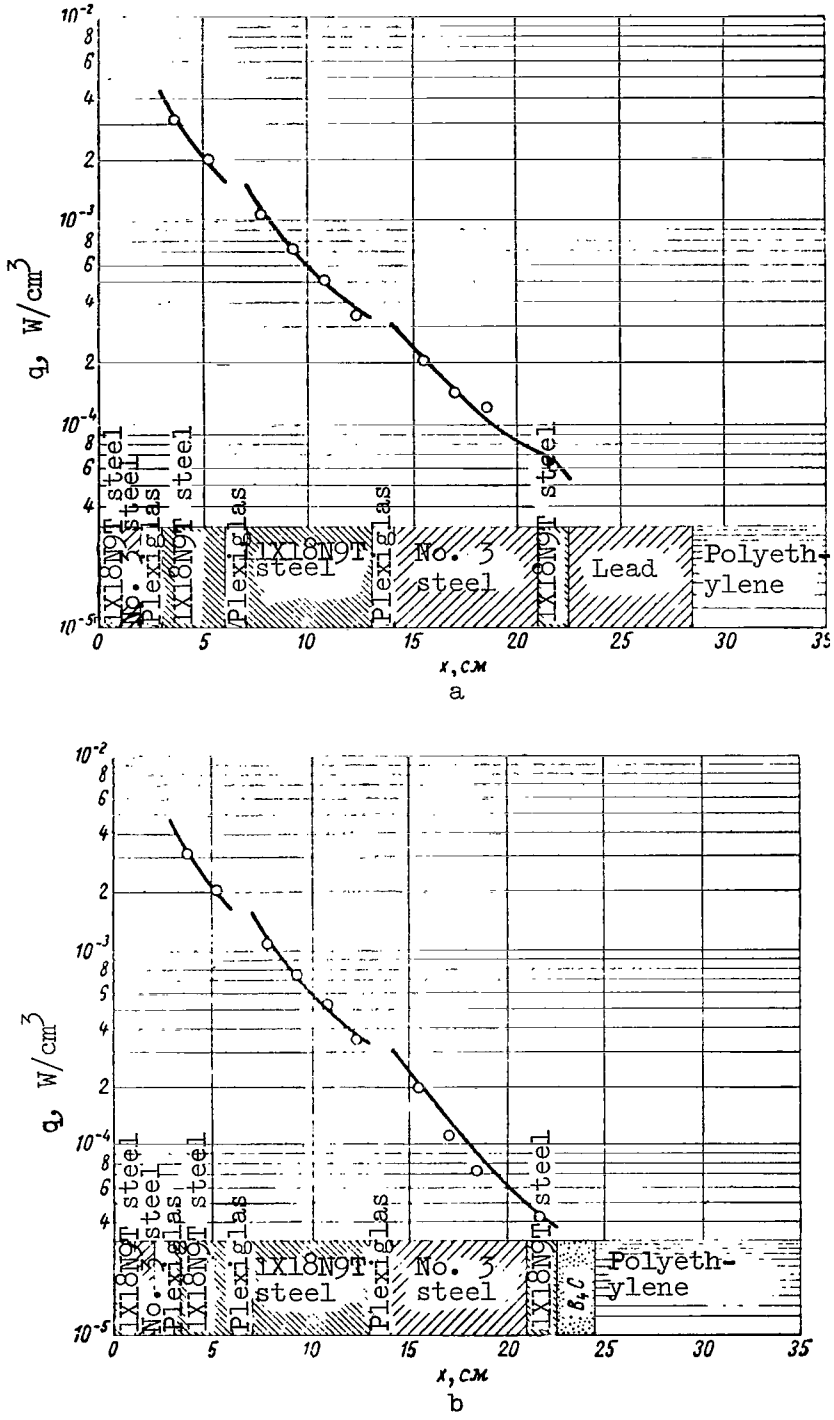

Figure 2. Heat liberation in screens and reactor vessel for first (a) and second (b) versions: ———, computed data; ○, experimental data.

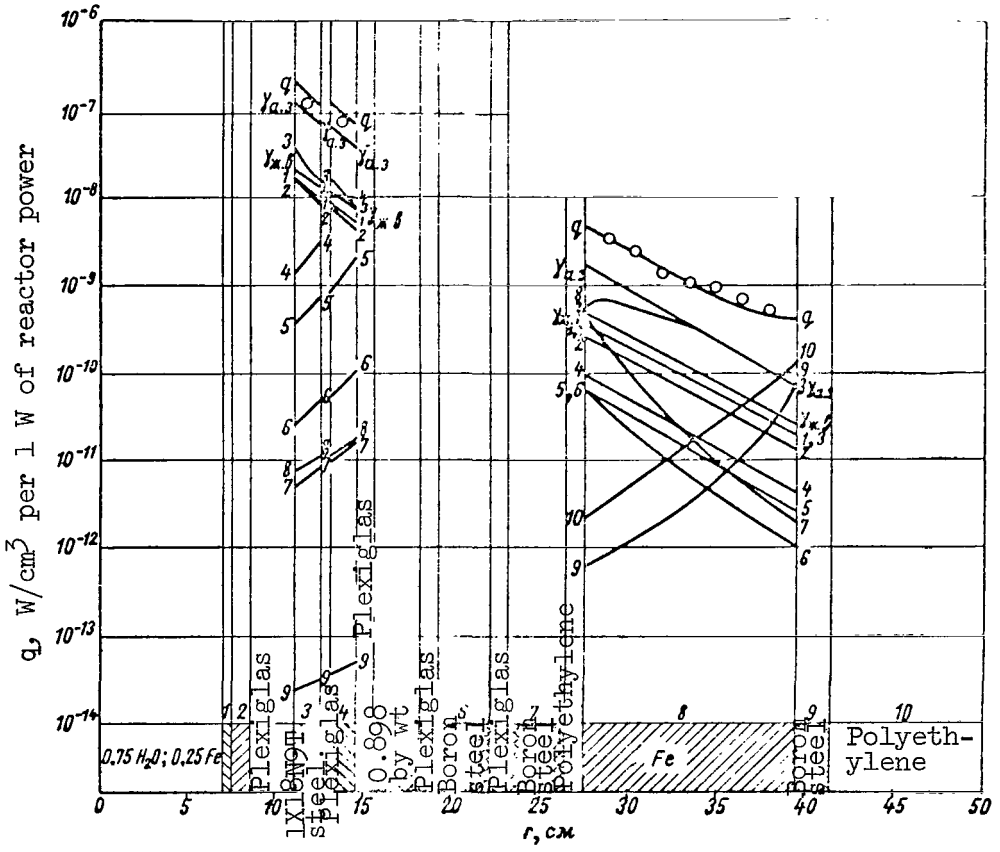

Figure 3. Heat liberation in screens and reactor vessel for third version, due to following: γ-radiation from active zone (γ_{az}); neutron capture in iron-water mixture (γ_{iw}); neutron capture in nine screens (1-9); neutron capture in polyethylene behind vessel (10); q, total heat liberation in absolute units; ———, computed data; ○, experimental data.

Discussion of Results and Conclusions

Figure 2 presents the results of computations and the experimental values of heat liberation for two versions of the vessel and screens of the thermal shielding. The computed specific heat liberation in steel screens and in the vessel q are plotted along the axis of the ordinates in relative units.

During these experiments the power level of the reactor was not controlled during measurements. Therefore, figure 2 presents only a comparison of the relative values of computed data and of results obtained experimentally. The experimental points and the calculated curves were superposed at a distance of

3.7 cm from the active zone. The calculations of heat liberation for the /241 above versions were carried out by using the ten group method to find the three-dimensional energy distribution of neutrons (ref. 3). We can see in figure 2 that the agreement of computed values with experimental values is very good for both versions.

For the third version of the experimental assembly (fig. 3) the calculation of heat liberation was carried out by using the 7 group method to determine the neutron distribution. During the period of experiments with this assembly the reactor power was controlled by means of copper and indium foils, placed at definite points in the active zone. The flux of neutrons was determined in one of the experiments. For this purpose, in addition to the copper and indium foils, the active zone contained gold foils which were then subjected to a count utilizing the β-γ-coincidence method. The reactor power was determined from the known neutron flux. In the remaining experiments we took the ratio of copper and indium foil activity to the activity of the same foils in the experiment for determining the absolute neutron flux. With this ratio we determined the neutron flux as well as the reactor power for each experiment.

Thus figure 3 presents a comparison of the absolute values of heat liberation obtained by computations (curves) and experimentally (points) for the third version. We can see that computed data and experimental data agree well.

The authors evaluated the experimental error which was ± 30 percent /242 and which was composed of the following errors:

error in measuring the voltage in the chamber.....± 2 percent

error in measuring the chamber capacity.....± 6 percent

error in measuring the operating volume of the chamber.....± 14 percent

error in measuring the reactor power (during absolute measurements).± 20 percent

The indefiniteness associated with the evaluation of quantities W and f comprises approximately 3 percent for W and approximately 7 percent for f. These values are taken from reference 4.

The discrepancy between experimental results and computed results does not exceed 15 percent, i.e., it is below the limits of experimental error. This shows that the applied calculation method is quite accurate, and we recommend it for calculating heat liberation in vessels and screens of water-moderated reactors for practical purposes.

REFERENCES

1. Nuclear Reactor Shielding. Edited by T. Rockwell (Zashchita yadernykh reaktorov). Moscow, Izd-vo I. L., 1958.

2. Goldstein, H. and Wilkins, J. Calculation of the Penetration of Gamma-rays. NDA, NTO-3075, 1954.

3. Broder, D. L. et al. P. 81 of this volume.

4. The Physics of Intermediate Reactors. Translated from English Under the Editorship of I. A. Stenbok (Fizika promezhutochnykh reaktorov). Moscow, Gosatomizdat, 1961.

5. Gray, L. H. Proc. Roy. Soc., A156, 578, 1936.

6. Gaytler, V. Quantum Theory of Radiation (Kvantovaya teoriya izlucheniy). Moscow, Izd-vo I. L., 1956.

PART III. EXPERIMENTAL METHODS OF INVESTIGATING SHIELDING AND SHIELDING MATERIALS

INVESTIGATION OF NEUTRON TRANSMISSION THROUGH SHIELDING BY MEANS OF UNIDIRECTIONAL SOURCES (THE B-2 INSTALLATION)

S. G. Tsypin

Introduction

Two typical cases are encountered in the design of nuclear reactor shielding of small dimensions: in the first case the shielding is very close to the reactor, whereas in the second case it is substantially removed from the reactor. In the first case the radiation incident on the shielding may be considered isotropic in the first approximation, in the second case it may be considered unidirectional. These two classes of angular distributions for radiations from the sources may be attenuated in a different manner by the shielding. If this difference is small,[1] we can utilize any of the attenuation functions and in this case, any of the functions would be universal. /243

Furthermore, if we utilize collimated (point unidirectional or limited unidirectional) radiation sources, we can obtain more detailed information on the transmission of radiation through the shielding than when we apply non-collimated sources (refs. 1-9).

Indeed, the most elementary source is a point unidirectional source and also, generally speaking, a monoenergetic source of radiation. By using the attenuation function of such a source it is possible to develop an attenuation function for a source with any angular distribution. In addition, such a source can be used to obtain information on the angular distribution of radiation in the shielding in addition to information on its three-dimensional energy distribution. The B-2 installation was constructed in order to obtain this information and to simulate an infinitely plane unidirectional source utilizing the BR-5 fast neutron reactor (ref. 10).

---

[1] In comparing these attenuation functions it is assumed that the geometric attenuation cannot take place for an isotropic source; in particular, for a point isotropic source if we multiply by the square of the distance between the source and the considered point in the shielding (detector).

B-2 Installation for the Investigation of Shielding

The B-2 installation was built on the north side of the BR-5 fast neutron nuclear reactor (ref. 10). This installation was used to investigate the penetration of neutrons through various shielding media which can be either in a solid or liquid state (fig. 1). The schematic diagram of the B-2 installation is shown in figure 2. The installation consists of the following parts: a channel with slide plates, a movable cart, a tank and a concrete shielding recess surrounding the cart with the tank. The beam of neutrons which passes through 16 cm of nickel reflector enters a channel in the shielding which has a diameter of 25 cm.

The beam geometry (fig. 2) provides for a well collimated source with a collimation half-angle of approximately 2.5°. The radiation exit from the channel is covered with two remotely controlled slide gates: a water gate /244 with a thickness of 150 cm and a cast iron gate with a thickness of 50 cm. The test shielding materials are installed (or poured in the case of a liquid) into a steel tank, with dimensions of 137 X 139 X 217 cm, which in turn is placed on the movable cart.

To facilitate the loading and unloading of shielding materials, the B-2 installation has a special arrangement to move the cart with the tank out of the concrete recess. The construction of the cart and of the tank make it possible to investigate shielding weighing up to 50 metric tons (when iron shielding is investigated, for example, its weight reaches a value of 30 tons, ref. 7). In all experiments to investigate the transmission of neutrons through the shielding the cart with the tank is moved flush against the location of the radiation beam, so that the beam enters the center of the vertical tank wall surface and its cross section has the form of a disk with a diameter of 30 cm.

A concrete recess with a thickness of approximately 1 m is built flush against the reactor. A heavy grade of concrete with a density of 4.3-4.5 g/cm^3 was used. Above the recess there is a cut with a width of 12 cm /245 for introducing radiation detectors into the test shielding. The flux of fast neutrons with energies $E > 2\text{-}3$ MeV at the output of the beam, when the BR-5 nuclear reactor power is 5000 kW, represents approximately 10^{10} neutrons/ $cm^2 \cdot sec$.

In the B-2 installation the neutrons pass through a layer of nickel (16 cm) before they enter the test shielding material from the BR-5 reactor.

Special measurements of the neutron spectrum leaving the channel have shown that above the energy $E > 3$ MeV it agrees well with the neutron fission spectrum (ref. 7). In addition, it also follows from reference 9 that if a nickel layer of thickness 15 cm is placed between the source of fission neutrons and the water, the attenuation function, starting with a water thickness of 40-50 cm from the source, coincides well with the attenuation function

Figure 1. General view of B-2 installation on BR-5 reactor for investigating shielding.

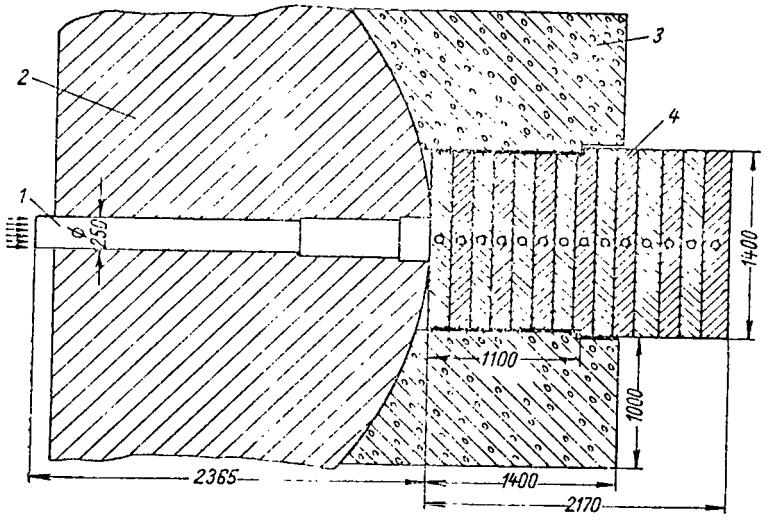

Figure 2. Schematic of B-2 installation on BR-5 reactor for investigating shielding: 1, channel; 2, reactor shielding; 3, concrete shielding; 4, shielding under test.

for neutrons having a fission spectrum (the measurements were carried out by means of the BF_3 thermal neutron counter).

From this description of the B-2 installation it follows that a limited unidirectional source--a unidirectional disk--is used to study the penetration of neutrons in the shielding materials.

Geometric Transformations of Unidirectional Sources

In order to understand the procedure for carrying out measurements with such an unusual disk unidirectional source, it is necessary to consider several remarks.

Let us consider the two classes of surface sources mentioned above: the isotropic and the unidirectional sources. In the first class the elementary source is a point isotropic source, whereas in the second class it is a point unidirectional source. We shall define the direct geometric transformation as the transformation from elementary sources to sources of other geometric form, for example, the transformation of a point isotropic source into a plane isotropic source or into a spherical isotropic source. We shall define the inverse geometric transformations as those involving the transformation from more complex geometric sources to elementary sources.

In the class of isotropic sources, the direct and inverse geometric transformations are always possible,[1] because the attenuation function of a point isotropic source $G_{pi}(R)$ is characterized by a single geometric parameter--by the distance between the source and the observation point (detector) in the shielding.

In the class of unidirectional sources, the inverse transformations are possible only under definite simplifying assumptions. Indeed, even under the simplest conditions: isotropic detector, homogeneous and infinite medium, the attenuation function of a point unidirectional source $G_{pu}(R, \Theta)$ or $G_{pu}(R, h)$ is characterized by two spatial coordinates (fig. 3).

The equivalence of moving the source or the detector makes it possible for us to assume that the schemes shown in figure 3a and b are the same. This situation is usually utilized in carrying out the measurements. In particular, the detector of the B-2 installation was displaced along the central ray /246 of the unidirectional disk source R, as well as in the perpendicular direction h, for different values of R, or there was an angular displacement Θ with respect to the center of the disk for different values of R. These attenuation functions ($G_{pu}(R, h)$ or $G_{pu}(R, \Theta)$ make it possible to obtain substantially more information compared with the attenuation function $G_{pu}(R)$, which yields nothing more than information about the isotropic sources.

---

[1] It is assumed that the medium containing the source is infinite and homogeneous, and that the radiation detector is isotropic.

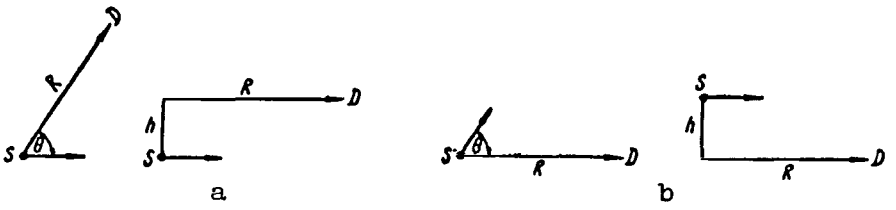

Figure 3. Geometry of experiments in which source is fixed, while detector is fixed (b). S, source; D, detector; Θ, angular rotation of source or of detector; h, height to which source or detector is raised; R, distance between source and detector.

Direct Transformations. It is easy to see that if we know the attenuation functions G_{pu} (R, Θ) or G_{pu} (R, h), we can find the attenuation function for a source with any angular distribution. We shall present several simple examples.

(a) The attenuation function for a point anisotropic source is equal to

$$G_{pa}(R) = C \int_0^{2\pi} d\varphi \int_0^{\pi} f(\Theta)\, G_{pu}(R, \Theta) \sin\Theta\, d\Theta, \qquad (1)$$

where f (Θ) is the function for the anisotropy of the source radiation. In particular when f (Θ) = 1 expression (1) is transformed into G_{ps} (R).

(b) The attenuation function for an infinite plane unidirectional source $G_{\infty p}$ (R) is equal to

$$G_{\infty,p}(R) = C \int_0^{2\pi} d\varphi \int_0^{\infty} G_{pu}(R, h)\, h\, dh \qquad (2)$$

etc.

(p = plane)

Unfortunately it is very difficult to work with point unidirectional neutron sources due to their small intensity. In this connection it is more expedient in practice to use bounded unidirectional sources.

The attenuation functions of bounded unidirectional sources will vary with the dimensions of the source. Thus, for example, in measuring the attenuation function for a unidirectional disk source along the central beam G_{du} (R, 0) in any medium as a function of source diameter, the attenuation functions G_{du}

(R, 0) will differ from each other more and more as the diameter increases and as the slope of the attenuation curve decreases. However, it is possible to find a unidirectional source whose attenuation function will not vary with an increase in the dimensions of the source. A plane infinite unidirectional source is of this type.

From an analogy with expression (2) we can write

$$G'_{\infty p}(R) = C \int_0^{2\pi} d\varphi \int_0^{\infty} G_{pu}(R, h)\, h\, dh. \tag{3}$$

We shall show that expression (3), within the accuracy of the constant, coincides with expression (2).

Indeed, let us represent G_{du} (R, h) as a superposition of G_{pu} (R, h), in which case, expression (3) may be written in the form

$$\begin{aligned} G'_{\infty p}(R) &= C \int_0^{2\pi} d\varphi \int_0^{\infty} G_{du}(R, h)\, h\, dh = C \int_s dS G_{du}(R, h) = \\ &= C \int_s dS \sum_{i=0}^{n} G_{pu}(R, h_i)\, \Delta\sigma_i = C \sum_{i=0}^{n} \Delta\sigma_i \int_s G_{pu}(R, h_i)\, dS = \\ &= C \int_0^{2\pi} d\varphi \int_0^{\infty} G_{pu}(R, h)\, h\, dh \sum_{i=0}^{n} \Delta\sigma_i *, \end{aligned} \tag{4}$$

where dS is the elementary area of the integration surface; $\Delta\sigma_i$ is the element of source area.

It follows from the comparison of expressions (4) and (2) that $G'_{\infty p}$ (R) and $G_{\infty p}$ (R), indeed, differ only in the value of the constant multiplier. /247

We should also note that the radiation attenuation function depends on the angular distribution of the source radiation. Comparing the results of theoretical works (ref. 9) on the penetration of γ-rays, we see that there is a slight difference in the attenuation functions G_{ps} (R) R^2 (R is the distance between the source and the considered point in the shielding) and $G_{\infty p}$ (R).

Table 1 uses the data of reference 9 to present the energy ratios G_{ps} (R) $R^2/G_{\infty p}$ (R) for γ-quanta with energies of 0.5, 1, 3 and 8 MeV in water,

*It is possible to replace h_i with h in the integral since integration over h from zero to ∞ always produces the same result regardless of the source position in space.

TABLE 1. COMPARISON OF THE ENERGY ATTENUATION FUNCTIONS G_{ps} (R) R^2 AND $G_{\infty p}$ (R) γ-RAYS WITH ENERGIES 0.5, 1, 3 AND 8 MeV IN WATER, IRON AND URANIUM G_{ps} (R) $R^2/G_{\infty p}$ (R).

Medium	Energy, MeV	σ_s/σ	Shielding thickness in terms of γ-ray mean free path lengths					
			1	2	4	7	10	15
Water	0.5	0.66	0.93	1.26	1.48	1.73	1.97	2.17
	3	0.41	1.00	1.04	1.08	1.12	1.14	1.16
	8	0.29	1.01	1.02	0.99	1.04	1.05	1.03
Iron	0.5	0.65	0.97	1.09	1.20	1.44	1.59	1.76
	3	0.38	0.99	1.03	1.08	1.13	1.17	1.21
	8	0.19	0.99	1.00	1.03	1.07	1.11	1.17
Uranium	1	0.36	1.01	1.02	1.04	1.07	1.10	1.02
	3	0.26	0.99	1.01	1.03	1.07	1.12	1.16
	8	0.10	0.99	1.00	1.02	1.07	1.16	1.47

iron and uranium. In addition, the table presents data corresponding to the ratio of scattering cross sections to the total γ-quanta attenuation cross section in the substance σ_s/σ. We can see from table 1 that the maximum discrepancy between these functions, which is approximately equal to two, takes place when the shielding thickness is 15 mean free paths of γ-rays and the ratio $\sigma_s\sigma \sim 0.7$. When the ratio $\sigma_s/\sigma \leq 0.4$, this discrepancy seldom exceeds 10-20 percent, i.e., the attenuation functions G_{ps} (R) R^2 and $G_{\infty p}$ (R) practically coincide.

We can expect, from an analogy with γ-ray sources, that the attenuation functions G_{ps} (R) R^2 and $G_{\infty p}$ (R) will also coincide for the neutron sources. To investigate this problem the B-2 installation was used to measure the attenuation functions $G_{\infty p}$ (R) of fast and thermal neutrons in water by means of a threshold P^{31} (n, p) Si^{31*} detector and by means of a thermal neutron detector BF_3 (ref. 6), respectively.

*Data obtained by V. A. Dulin, Yu. A. Kazanskiy, V. P. Mashkovich, B. I. Sinitsyn, L. K. Fometskiy and S. G. Tsypin.

Figure 4 represents these attenuation functions. This figure also shows the attenuation function $G_{ps}(R)\,R^2$ for neutrons of the fission spectrum for the case of the $P^{31}(n, p)\,Si^{31}$ threshold detector, computed by means of data presented in reference 9. In addition, figure 4 shows the attenuation function $G_{ps}(R)\,R^2$ for neutrons of the fission spectrum in water, which is measured by means of a thermal neutron detector containing the BF_3 counter. This attenuation function is obtained from the attenuation function of a disk isotropic neutron source with a fission spectrum, in water (ref. 6).

As we can see from figure 4, there is good agreement between the attenuation function for the neutron spectrum of the B-2 and $G_{pi}(R)\,R^2$ installations and the attenuation function $G_{\infty p}(R)$ for neutrons of the fission spectrum both for fast neutrons and for thermal neutrons in water. /246

Inverse Transformations. From the material presented above it follows that the attenuation function $G_{du}(R, h)$ contains less information than the $G_{pu}(R, h)$ function; however, if certain simplifying assumptions are made,

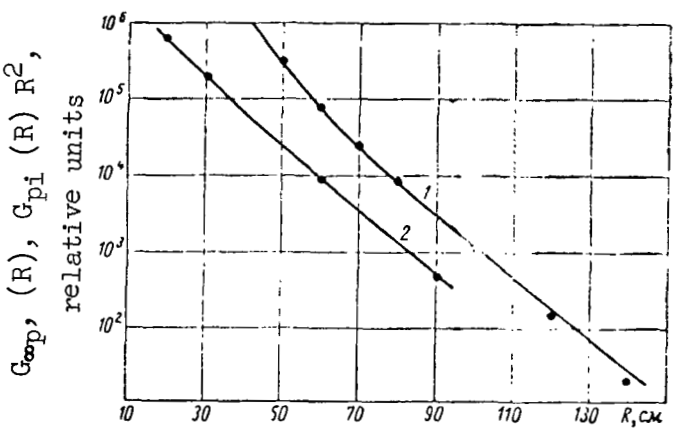

Figure 4. Comparison of attenuation functions $G_{ps}(R)\,R^2$ (●) for point isotropic neutron sources of fission spectrum multiplied by square of distance between source and detector with attenuation functions of plane infinite unidirectional sources with neutron spectrum of B-2 installation, $G_{\infty p}(R)$ for various layers of water R, measured by detectors of: 1, thermal neutrons (counter with BF_3); 2, fast neutrons ($P^{31}(n, p)\,Si^{31}$).

we can obtain additional information from the unidirectional disk sources and the accuracy of such information will, of course, be limited by these assumptions. Figure 5 shows the attenuation functions G_{du} (R, h) measured by the threshold detector Al^{27} (n, α) Na^{24} of fast neutrons in iron on the B-2 installation (ref. 7). An examination of these curves shows that within the limits of the beam radius the curves are almost constant or vary little, and then vary almost exponentially with h in such a way that as R increases, the slope of the curves becomes more shallow (a similar picture takes place for water, reference 6).

Assuming that the slope of the exponential part of the curves in the attenuation functions G_{pu} (R, h) and G_{du} (R, h) is retained and knowing G_{du} (R, h), we can find the approximate value of G_{pu} (R, h). This assumption concerning the coincidence of the slope of these functions is confirmed, for example, in the case of a unidirectional disk (ref. 1) and a unidirectional point (ref. 2) source of γ-rays from Co^{60} in water. This situation is also confirmed by the close slopes of the exponential part of the attenuation curve for neutrons measured in water by means of BF_3 thermal neutron counters for various diameters of neutron beams--30 (ref. 6) and 3.8 cm (ref. 11).

The proposition stated above makes it possible for us to seek the attenuation function G_{pu} (R, h) in the form

$$G_{pu}(R, h) = A(R)e^{-h/\lambda(R)}, \tag{5}$$

where A(R) is the term in front of the exponent, which depends only on the distance between the source and the detector R in the medium; λ (R) is the relaxation length for the attenuation function G_{pu} (R, h) as a function of h, corresponding to the slope of the exponential part of attenuation function G_{du} (R, h) for a given distance between the source and the detector R. Then, by substituting G_{du} (R, h), which has been measured along the central beam of the disk source with radius a G^{a}_{du} (R, 0), as a superposition G_{pu} (R, h), we find A(R). After simple transformations we obtain

/249

$$A(R) = \frac{CG^{a}_{du}(R, 0)}{2\pi\{\lambda^2(R) - \lambda(R)e^{-a/\lambda(R)}[a + \lambda(R)]\}}, \tag{6}$$

where C is a constant.

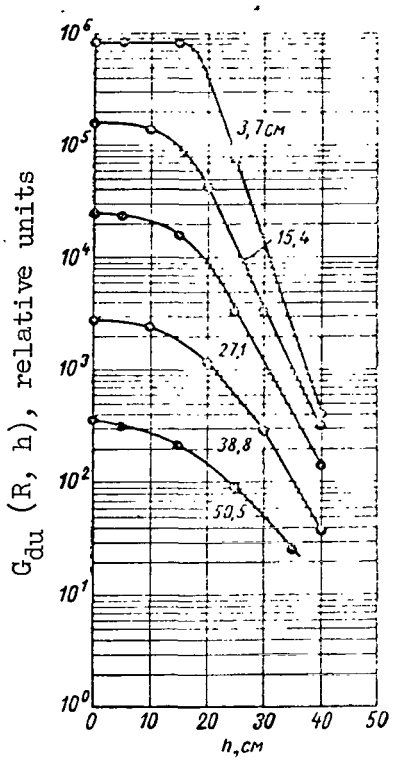

Figure 5. Attenuation functions for unidirectional disk source with neutron spectrum of B-2 installation G_{du} (R, h) for various thicknesses of iron measured by means of Al^{27} (n, α) Na^{24} threshold detector.

Finally, we may write

$$G_{pu}(R, h) = \frac{CG^{a}_{du}(R, 0)\, e^{-h/\lambda(R)}}{2\pi\{\lambda^2(R) - \lambda(R)\, e^{-a/\lambda(R)}[a + \lambda(R)]\}}. \qquad (7)$$

Let us attempt to analyze expressions (5) and (7) which we have obtained. First of all we should note that when h = 0 the attenuation function G_{pu} (R, h) for a point isotropic detector must correspond to the attenuation function under conditions of good geometry. In practice this is easily achieved, for example, for a well collimated source of γ-rays and for a detector with small dimensions (ref. 2).

During the measurement of the neutron attenuation function G_{du} (R, h) on the B-2 installation in various media, detectors of small dimensions were also

used. Therefore, the function G_{pu} (R), which is equal to A (R) when h = 0, agrees with the attenuation function measured under conditions of good geometry, i.e.,

$$A(R) = C_1 e^{-\Sigma_T R}, \tag{8}$$

where Σ_T is the total macroscopic cross section of neutron interaction with the material; C_1 is a constant.

Expression (5) also makes it possible for us to compute the buildup factors for the scattered neutron radiation B (R). They can be obtained most simply for a plane infinite unidirectional source of neutrons. Substituting expression (5) into (2) and making use of expression (8), we find

$$B\ R) = C\lambda^2(R). \tag{9}$$

Finally, by using expression (2) we can construct the attenuation function G_{du} (R, h) for a source of radius a as a function of h. It is easy to show that /250

$$G''_{du}(R, h) = CA(R) \int_0^a \varrho\, d\varrho \int_0^{2\pi} e^{-\frac{\sqrt{\varrho^2+h^2+2h\varrho\cos\varphi}}{\lambda(R)}} d\varphi. \tag{10}$$

Let us illustrate this presentation by means of an example involving the attenuation functions G_{du} (R, h) measured on the B-2 installation in water using P^{31} (n, p) Si^{31} fast neutron detectors. Figure 6 shows the attenuation functions $G_{\infty p}$ (R), G_{du} (R, 0), of a narrow beam at the point computed by means of equation (6) in water for neutrons of the B-2[1] installation spectrum and for the P^{31} (n, p) Si^{31} detector.

As we can see from figure 6, the function A (R) (triangles), computed by means of equation (6) agrees relatively well with the true attenuation function for a narrow beam.

Table 2 presents the buildup factors (the buildup factor for a thickness of 16.5 cm is assumed to have a unit value), computed by means of equation (9) and by exact integration of distributions G_{du} (R, h) for an infinite plane unidirectional source according to equation (3).

---

[1] For the P^{31} (n, p) Si^{31} detector, these functions coincide with the attenuation functions for neutrons of the fission spectrum (see above).

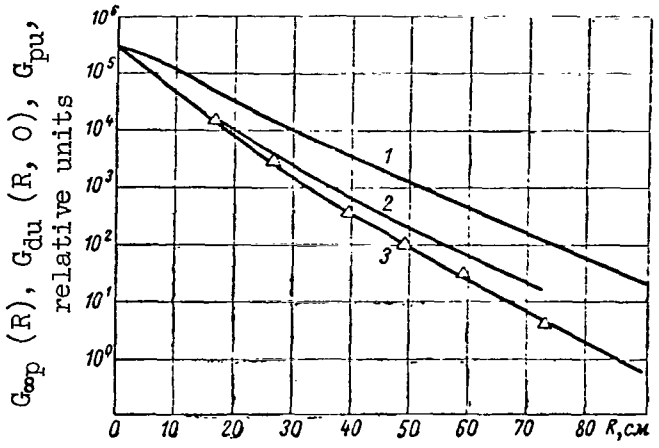

Figure 6. Attenuation function for neutrons of B-2 installation in water using P^{31} (n, p) Si^{31} detector: 1, $G_{\infty p}$ (R); 2, G_{du} (R, 0); 3, narrow beam geometry; Δ, points computed by equation (6).

TABLE 2. RELATIVE BUILDUP FACTORS OF NEUTRONS SCATTERED IN WATER B (R) FOR AN INFINITE UNIDIRECTIONAL SOURCE OF NEUTRONS WITH A FISSION SPECTRUM MEASURED BY MEANS OF P^{31} (n, p) Si^{31}.

Thickness of water in cm	B (R)		Thickness of water in cm	B (R)	
	According to equation (9)	Exact integration by means of equation (3)		According to equation (9)	Exact integration by means of equation (3)
16.5	1	1	49.5	2.8	3.8
26.5	1.4	1.7	59.5	4.4	5.0
39.5	1.9	2.9	72.5	6.1	6.9

As we can see from the table there is a more or less satisfactory agreement between results computed by means of equation (9) and those obtained from exact integration by means of equation (3).

Finally, figure 7 presents the attenuation functions G_{du} (R, h) as a function of h, measured experimentally and computed by means of expression (10). It follows from figure 7 that there is reasonable agreement between experimental and computed data.

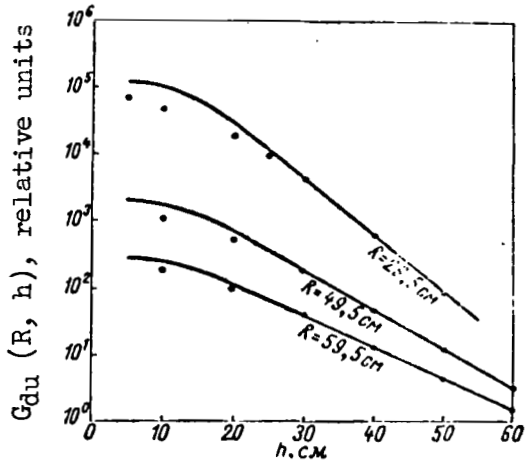

Figure 7. Attenuation functions for unidirectional disk neutron source of B-2 installation in water for P^{31} (n, p) Si^{31} detector: ———, experimental data; ●, computed data obtained by means of equation (10).

Conclusions

1. The attenuation functions G_{du} (R, h) for the disk unidirectional source of neutrons with the B-2 installation spectrum in different shielding materials makes it possible for us to obtain information on the three-dimensional energy distribution of neutrons as well as on the angular distribution of neutrons in these media.

2. Under some assumptions (see above) the attenuation functions for /251 unidirectional disk neutron sources in shielding materials may be used to obtain information on the attenuation functions for unidirectional point neutron sources. As a result it is possible to construct a source with any angular distribution of radiation emitted by it.

3. The attenuation functions G_{du} (R, h) make it possible to construct the attenuation functions $G_{\infty p}$ (R) for a plane infinite unidirectional source of neutrons with the B-2 installation spectrum in different shielding media. These functions in turn coincide with the following attenuation functions:

(a) for a source of neutrons with the fission spectrum when the neutron energy is E > 2-3 MeV;

(b) for a source of neutrons of the fission spectrum for all energy groups beginning with some thickness of the hydrogen-containing shielding;

(c) for $G_{ps}(R)\,R^2$, when the effective absorption cross section is greater than or equal to half of the total cross section for the interaction of fast neutrons with matter (for example, for neutrons having an energy of $E > 3$ MeV).

4. The merit of the B-2 installation neutron source is its high intensity which makes it possible to study the spectral distribution of fast neutrons in various shielding media (ref. 12). The use of B-2 neutron sources is not associated with difficulties produced by the indefiniteness of source geometry which exists for other sources.

In conclusion the author wishes to express his deep gratitude to A. I. Leypunskiy for valuable advise in the formulation of the problem associated with the investigation of neutron penetration of various media from unidirectional sources. The author also expresses his deep gratitude to I. I. Bondarenko, V. V. Orlov, V. I. Kukhtevich, Yu. A. Kazanskiy, B. I. Sinitsyn, Ye. S. Matusovich, B. P. Shemetenko, Sh. S. Nikolayshvili, V. P. Mashkovich and A. A. Abagyan for valuable remarks during the discussion of results obtained in the present work.

The author also expresses his indebtedness to D. S. Pinkhasik and N. N. Aristarkhov for their great assistance in constructing the B-2 installation.

REFERENCES

1. The Shielding of Nuclear Reactors. Edited by T. Rockwell (Zashchita yadernykh rektorov). Moscow, Izd-vo I. L., 1958.

2. Kukhtevich, V. I. and Shemetenko, B. P. Atomnaya Energiya, Vol. 12, 204, 1962.

3. Kukhtevich, V. I., Tsypin, S. G. and Shemetenko, B. P. Atomnaya Energiya, Vol. 5, 636, 1958.

4. Kukhtevich, V. I. et al. Atomnaya Energiya, Vol. 4, 138, 1958.

5. Kimel', L. P. and Leypunskiy, O. I. P. 322 of this volume.

6. Dulin, V. A. et al. Atomnaya Energiya, Vol. 9, 315, 1960.

7. Mashkovich, V. P. and Tsypin, S. G. Atomnaya Energiya, Vol. 11, 251, 1961.

8. Breshenkova, Ye. B. and Orlov, V. V. Atomnaya Energiya, Vol. 10, 175, 1961.

9. Protection of Mobile Installations with a Nuclear Engine. Collected Translations, Edited by V. V. Orlov and S. G. Tsypin (Zashchita transportnykh ustanovok s yadernym dvigatelem. Sb. pod red. V. V. Orlova i S. G. Tsypina). Moscow, Izd-vo I. L., 1961.

10. Leypinskiy, A. I., Grabin, V. G. et al. Experimental High-speed Reactors in the USSR. IN: Transactions of the Second International Conference on the Peaceful Uses of Atomic Energy. Reports of Soviet Scientists. Vol. 2, Nuclear Reactors and Nuclear Power Engineering (Eksperimental'nyye bystryye reakory v SSSR. V kn.: Tr. Vtoroy mezhdunarodnoy konferentsii po mirnomu ispol'zovaniyu atomnoy energii. Dokl. sovetskikh uchenykh. T. 2--Yadernyye reaktory i yadernaya energetika). Moscow, Atomizdat, p. 215, 1959.

11. Stinson, W. P. Nucleonics, Vol. 12, No. 9, 50, 1954.

12. Dulin, V. A. et al. Atomnaya Energiya, Vol. 9, 318, 1960.

EXPERIMENTAL METHODS OF INVESTIGATING SHIELDING (RADIATION DETECTORS)

V. A. Dulin, Yu. A. Kazanskiy and Ye. S. Matusevich

Introduction

The development of nuclear power engineering places ever-increasing /251 requirements on the accuracy of computing the biological shielding of nuclear reactors. For this reason it has become necessary to analyze not only the total dose beyond the shielding, but also the detailed characteristics (for example, the three-dimensional and energy distribution of neutrons and γ-rays in the shielding, the angular and energy distribution of neutrons and γ-rays /252 on the surface of the shielding, etc.). At the present time, all modern methods of recording radiation are used in the investigation of three-dimensional, angular and energy distributions of radiation which has penetrated the shielding.

The following general requirements must be satisfied by sensors of radiation ionization when they are used in the investigation of shielding: (1) a wide sensitivity range, because the study of three-dimensional distributions usually requires high radiation attenuations (of the order of 10^5-10^7); (2) high detector "selectivity," i.e., the low sensitivity of γ-detectors to neutrons, and vice versa. Indeed, in such materials as iron, when it is necessary to investigate, for example, the transmission of fast neutrons, the sensor of fast neutrons must be insensitive to γ-rays and to soft neutrons with a very large coefficient, because γ-rays and soft neutrons are attenuated with the relaxation length of $\lambda \sim 25$ cm, whereas fast neutrons are attenuated with a relaxation length $\lambda \sim 7$ cm; (3) small detector dimensions for measurements taken inside the medium; (4) the spectral distributions of neutrons and γ-rays, which leave the shielding and which are in the shielding itself, are continuous and, as a rule, drop off as the radiation energy is increased. This last situation lowers the requirements for the resolving energy capacity of selected spectral instruments and makes it possible to use the matrix method with success for the transformation of measured amplitude distributions into energy spectra.

Exhaustive information on the transmission of radiation in shielding is contained in the angular energy distribution at each point of space for different geometries, in functions of anisotropy and in the energies of radiation sources. The ability to obtain such information is outside the limits of possibility associated with experiment and theory and, in most cases, is not necessary. Thus, in developing computational methods, information which is

relatively incomplete is quite useful, for example, for three-dimensional distribution of γ-ray and neutron dose in shielding, the behavior of neutron fluxes with energies above a certain threshold, the angular distribution of γ-ray and neutron fluxes on the surface of the shielding, etc. This makes it possible to apply rather simple and effective methods for the investigation of shielding--methods associated with the utilization of dose chambers, threshold tracers, fission chambers and others.

The Measurement of Integral Characteristics

The Dose of γ-Rays. Very early investigations on the attenuating properties of shielding pertain to the measurement of radiation dose. This approach is associated with the fact that the dose has a very definite practical meaning, whereas the measurement of the dose is simpler and sometimes the only possible approach. The measurements of γ-ray doses in homogeneous media have agreed excellently with the numerical computations carried out by the method of moments and have made the further experimental investigation of buildup factors in simple geometries quite superfluous. An extensive and exhaustive survey of dose measurements is given by G. Gol'dshteyn (ref. 1).

A rather widespread and reliable method of measuring the dose of γ-rays, which is not new, involves measurements by means of small ionization chambers which satisfy the Gray conditions. The theory of miniature chambers, their construction and characteristics are presented in detail in the monograph of K. K. Aglintsev (ref. 2). In addition to measuring the dose (which requires a chamber with air-equivalent walls), small chambers are used to study problems associated with heat liberation in the shielding. In this case the walls of the chamber are made of the same material as the medium (ref. 3).

The most valuable properties of such chambers are their small size (which accounts for their wide application in the measurement of γ-ray doses inside the medium) and their capacity to operate in fields of high power (up to 1000 R/hr). The chambers have low sensitivity to neutrons. Chambers which are carefully constructed do not lose their charge over a period of hundreds of hours, and therefore they can be used in fields of γ-rays with power to /253
0.01 R/hr. The latter situation makes it possible to measure the dose distribution in large shielding thicknesses when the power of radiation sources is constant. The characteristic features of the chamber include the time discontinuity between irradiation and the measurement of residual charge and the inverse proportionality between exposure and power of the measured radiation field.

The sensitivity of ionization chambers is proportional to their volume; therefore, in order to measure doses outside the shielding it is necessary to utilize large chambers (up to 100 liters) which operate in conjunction with a standard electrometer amplifier, for example, of the "Kaktus" type. A detector of this type makes it possible to measure γ-ray doses of the same order as the natural background. It is shown in reference 4 that ionization chambers with air-equivalent walls whose volume is 1 to 100 liters do not exhibit any noticeable degree of "hard operation." When large ionization chambers are

used to measure γ-ray doses in the presence of neutrons, particularly thermal neutrons, there is a danger of ionization contribution by the N^{14} (n, p) C^{14} reaction because the cross section of this reaction is 1.75 barn for thermal neutrons and is comparable with the scattering cross section of γ-quanta by the atom.

Recently there has been a wide application of dosimetry devices based on the application of scintillation counters. The scintillation γ-dosimeter, which consists of an organic scintillator (anthracene, toluylene or plastic scintillators), joined by means of optical wave guides (or directly) to the cathode of a photomultiplier whose current is fed to an electrometer, has a high sensitivity and a satisfactory dose characteristic. The dose characteristic may depend on the dimensions of the selected crystals (ref. 5). However, for every crystal with a diameter of 100 mm and a height of 220 mm (terphenyl in polystyrene) the dose characteristic is practically the same as the characteristic of the anthracene crystal with a diameter and height of 6 mm (ref. 4).

A typical problem characterizing the application of a scintillation current dosimeter is the measurement of angular and spatial distributions of scattered γ-radiation from sources of different geometry (ref. 6). In these measurements anthracene crystals with a diameter from 6 to 12 mm and a thickness of 6 mm have been used. The light is transmitted to the cathode of the FEU-12 photomultiplier by means of a long optical fiber made of plexiglas and used to decrease the perturbation of the medium by the case of the device. The current from the plate of the FEU is amplified by a standard electrometer amplifier of the "Kaktus" type which has several versions of the output unit. When an anthracite crystal with a diameter of 12 mm and a height of 6 mm is used, the sensitivity of the entire device is $3 \cdot 10^{-4}$ R/hr per fission. The upper sensitivity limit may be varied over a wide range of photomultiplier voltages.

The utilization of the scintillation current dosimeter with a large crystal makes it possible to carry out measurements of rather low intensity doses and at high γ-ray energies. An example of this is the measurement of buildup factors for γ-rays with energies of approximately 6 MeV in a heterogeneous shielding (ref. 7).

The basic shortcoming of such devices is the impossibility of measuring γ-ray doses in the presence of neutrons. When utilizing current dosimeters, we should take into account their high sensitivity to temperature fluctuations, associated with the strong temperature dependence of photomultiplier dark currents.

A rather successful method for improving the characteristics of a scintillation dosimeter is the method of summating the pulse amplitudes, first applied to measure the dose due to fast neutrons (ref. 8). Such an amplitude summator was used in the work of V. I. Kukhtevich and L. A. Trykov (ref. 9) for measuring the γ-ray dose. The number of counts made by the amplitude summator is proportional to the sum of output pulse amplitudes.

Since the dark currents in the photomultiplier are produced by a large number of small pulses, the application of a summator with initial discrimination makes it possible to eliminate the noise background with practically no change in the dose characteristics and in the sensitivity of the device, which is equivalent to an increase in the sensitivity of the dosimeter. In this operating version the lower sensitivity limit is determined exclusively by the /254

cosmic background radiation, and the measured effect may be of the order of 10^{-6} R/hr. The upper limit which naturally depends on the dimensions of the scintillator, is approximately 0.1 R/hr for a standard toluylene crystal.

We should note that the operating threshold of the amplitude summator (approximately 3 with a linearity up to 130 V) may introduce a substantial error (up to 20-50 percent) in the measured dose when there is a noticeable variation in the radiation spectrum in the region of small energies at test points, for example, in the study of angular dose distributions. This conclusion may be reached on the basis of a sharp, almost exponential rise in the region of small amplitudes which suppresses most of the amplitude equipment distributions when measurements are made by means of organic scintillators. To eliminate the error associated with the presence of a threshold, it is sufficient in most cases to count the number of recorded pulses, to multiply this number by the magnitude of the threshold and add it to the measured effect.

In principle it is possible to use the scintillation pulse dosimeter of γ-rays to measure the dose of γ-rays in neutron fields. In this case we must make use of the difference in the shape of proton and electron pulse amplitudes (ref. 10). The use of discrimination according to the form of amplitudes opens up the possibility of designing a universal dosimeter which would record the γ-ray dose and the neutron dose simultaneously.

The Neutron Dose. At the present time it is impossible to determine accurately the relative biological effectiveness of neutrons (RBE) as a function of the energy, because it depends on assumptions which have been adopted a priori on the type of damage to an organism, which serves as the basis. It also depends on the ratio of deep and surface doses, on the angular distribution of neutrons in a phantom, etc. By combining the adopted propositions, variations of 5 to 30 in the ratio of RBE for thermal neutrons and neutrons with an energy of 1 MeV have been obtained (ref. 11). This situation regarding the values of RBE substantially complicates the construction of a neutron dosimeter.

From the engineering point of view it is particularly difficult to build a detector which measures the dose in the region of slow and intermediate neutrons. It is precisely these neutrons which are of paramount importance in many cases. Although a rather large number of fast neutron dosimeters is known, (see, for example, the survey in reference 12), only the tissue-equivalent (polyethylene) proportional counter is used for measuring the dose in shielding (refs. 8 and 13). The use of such a counter with an amplitude summator has produced good results.

Typical parameters of a polyethylene proportional counter[1] are as follows: for a threshold corresponding to neutron energy of 0.5 MeV, the ratio of neutron registration effectiveness to the γ-ray registration effectiveness is more than 10^6, the sensitivity of the counter (diameter of 15 mm and length of 60 mm) is approximately 0.005 pulses/neutrons·cm^{-2}, the amplification factor of the electronic circuit is approximately 10^4; when it is filled with ethylene the operating voltage is approximately 2000-3000 V. The gas amplification mode places higher requirements on the stability of the high voltage.

An isodose dosimeter is used for measuring the neutron dose beyond the shielding and for studying neutron scattering. This dosimeter is based on selecting the thickness of the moderator, which contains a boron counter. The effectiveness of such a device was thoroughly investigated in the range of neutron energies from thermal to 10 MeV (ref. 14). The results for neutron energies from 1 eV to 1 keV were particularly valuable.

The characteristic of detector effectiveness almost corresponds to the/255 dose curve.[2] Two versions of a dosimeter have been proposed: a cylindrical version (with a moderator thickness of 15 cm) and a spherical version (with a moderator thickness of 20 cm), which make it possible to measure the dose independently of neutron energy with a maximum deviation of 40-50 percent. For the real neutron spectrum the error is substantially less. The advantage of the device is its high sensitivity to neutrons with almost zero sensitivity to γ-rays, and the possibility of utilizing standard electronic equipment (the "Siren," "Chernik" and "Tyul'pan" type devices, and others).

We should like to point out that the nature of neutron RBE, when neutron energy is greater than 1 MeV, makes it possible to utilize threshold neutron detectors when measuring the dose inside a medium. Such detectors, for example, may consist of the Th^{232} fission chamber, type P^{31} (n, p) Si^{31} threshold tracers, etc., and such detectors are sufficiently accurate.[3]

The Measurement of Neutron Fluxes. The technique of measuring spatial distributions of neutron fluxes in shielding does not differ in principle from the measurement of fluxes during the solution of other problems. We should only note certain special features associated with measurements in shielding, which place higher requirements on detectors: the necessity of measuring large changes in flux intensities; very large changes in the intensity ratio of γ-rays and neutrons (from 10^{-3} in heavy shieldings to 10^5-10^7 in light

[1] Data presented by V. K. Daruga and B. I. Sinitsyn.
[2] The dose curve was selected by the authors from the analysis of existing data published in the literature, taking into account the approved permissible doses.
[3] Data obtained by B. I. Sinitsyn and S. G. Tsypin.

shieldings) and in the ratios between the intensities of various neutron energy groups.

Thus, in studying the transmission of fast neutrons in iron by means of fission chambers it is necessary to have a high order of separation of fissionable materials from impurities which break down into thermal neutrons. However, even if complete refinement is achieved, the results of the measurements may be incorrect due to the (γ, f) reaction; the source of high energy γ-rays may be the capture of neutrons (ref. 15).

The same high requirements with regard to elimination of impurities which produce γ-activity pertain to threshold tracers. We mention an interesting method of determining the relative activity of tracers by means of a scintillation γ-spectrometer (ref. 15). This method increases the sensitivity of detectors substantially as a result of an increase in their thickness and lowers the background of the interfering radiation by selecting a suitable energy interval for the spectrometer.

In general the value of the effective detector threshold depends on the form of the neutron spectrum. As a rule, for fast neutrons, the effective energy threshold is determined under the assumption that the neutrons inside the test medium are distributed according to the fission spectrum. Analysis carried out in reference 16 has shown that the value of the effective threshold depends very little on the form of the neutron spectrum. Thus, for a P^{31} (n, p) Si^{31} detector (energy threshold of 0.9 MeV) the effective energy threshold over the fission spectrum is equal to 2.8 MeV, whereas the computed threshold for the spectrum in large thicknesses of light materials (hydrogen, beryllium, carbon) is equal to approximately 3 MeV.

The Spectra of Gamma-rays

At the present time the investigations on the spectral distribution of γ-rays are carried on in two basic directions:

(1) the procurement of data on the spectra of γ-radiation sources (for example, reactors, volumetric γ-ray sources, etc.);

(2) the measurement of angular and spectral distributions at the boundary of the medium, which also describe the radiation sources and, on the other hand, are entirely necessary for computing shadow shielding, the penetration of γ-rays in heterogeneous media, i.e., in those problems which do not yet lend themselves to the analytical approach.

The spectral distributions of γ-rays inside homogeneous media, computed by the method of moments, for a large number of cases (refs. 17 and 18) /256 agree well with experimental data (refs. 19 and 20) for γ-ray source energies of 0.5-1.5 MeV. It is expedient to carry out the measurement of spectral distributions inside media by using a γ-ray source with an energy of 4-10 MeV,

i.e., in that region of energies where the calculations in reference 17 do not take into account the formation of retarding and annihilation γ-radiations, and with γ-ray sources of a wide energy range in some special cases, for example, in air (ref. 18).

The most widespread detector for investigating the spectra of γ-rays is the single crystal scintillation γ-spectrometer with a NaJ (Tl) crystal. Indeed, such spectrometers are of relatively simple design, have a satisfactory energy resolution and, what is most important, a high effectiveness. Many works are devoted to the problem of investigating the characteristics of a single crystal scintillation γ-spectrometer. Of these we shall only mention references 21-25.

The disadvantage of the single crystal scintillation spectrometer consists of the fact that the γ-quanta with a single energy correspond to a continuous spectrum of pulse amplitudes. This requires a mandatory transformation of measured amplitude distributions into energy spectra, particularly when measurements are made in shielding media, where the energy distributions are of a continuous nature. On the other hand, the continuity of investigated γ-ray spectra makes it possible to neglect corrections for energy resolution.

In the general case the problem of transforming amplitude distributions into energy spectra is reduced to the solution of an integral equation by means of a direct or inverse matrix (ref. 22). In order to construct the matrix we must have information on the forms of pulse amplitude distributions, which depend on the energy of γ-radiation, forms and dimensions of the crystal, source geometry, collimation conditions, etc.

In a series of works (refs. 22, 25 and 26) the forms of the pulse amplitude distributions were established experimentally, i.e., the equipment spectra of pulse amplitudes were measured during the registration of monoenergetic γ-quanta. Many works (refs. 21, 23 and 27) are also devoted to computational methods for determining the form of pulse amplitude distributions.

The computations carried out by the method of "random" Monte Carlo tests cover a wide range of γ-ray energies and crystal dimensions. Basically they can be divided into two groups: calculations for the case of the unidirectional γ-ray beam which falls on the center of a cylindrical crystal (ref. 23) and for the case of normal γ-ray incidence on the end of the crystal (ref. 27).

The advantages of the experimental method for determining the form of pulse amplitude distributions is associated with the fact that in this case the multiple secondary effects are taken into account automatically. Such effects, for example, are scattering in the collimator, absorption and scattering in the packing of the crystal, reverse scattering, geometry of the experiment, etc. The limitations of this method are associated with the fact that there are few convenient monoenergetic sources in the region of energies above 2.5 MeV without the accompanying radiation (retardation, scattered neutron, etc.). Below the energy of 2.5 MeV, the experimental determination of pulse amplitude distribution forms is substantially simpler than the analytical determination, particularly when we are investigating the spectra of γ-rays from nonpoint sources (for example, ring geometry, and the absence of collimation).

At the present time the literature contains a sufficient number of computed and experimental data which may be used to select the form of amplitude distributions for the particular crystal. The problem of selection is substantially simplified, because the forms of amplitude distributions are relatively unaffected by the form and dimensions of the crystals.

In regard to effectiveness, the situation is somewhat more complex. In the range of energies below 2.5 MeV the effectiveness is usually determined from the photo peak. Although the effectiveness determined from the photo peak depends critically on the dimensions of the crystal and on the energy of the γ-radiation, there are many methods (ref. 25) for a reliable determination of ef- /257
fectiveness. We should like to point out a rather simple and reliable method presented in reference 28, which utilizes the scattering of γ-quanta by a free electron at various angles where the energy and intensity of the γ-quanta are easily computed.

In the region of γ-ray energies above 3 MeV the very concept of effectiveness is not determined in the same manner by various authors. Thus, in reference 22 the effectiveness is determined as the total probability of γ-quantum interaction in a crystal, which is meaningful when we process the equipment spectra by means of the inverse matrix. In reference 27 effectiveness according to the photo peak was determined up to an energy of 8 MeV; this method of determining effectiveness for high energies is difficult in practice, because the photo peak merges with the Compton distribution and with pair peaks. For large crystals (with a diameter of 70-100 mm and a height of 100 mm) and for poor energy resolution (the pair triad is not clearly resolved), it is meaningful to determine the effectiveness from the number of pulses recorded as a result of total absorption with the emission of one or both annihilation γ-quanta.

When the spectra of γ-rays are measured by means of spectrometers with NaJ (Tl) crystals in mixed fields, a question arises concerning the background pulses due to neutrons which have entered the crystal (capture γ-radiation, of the recoil nucleus). In the measurement of γ-rays having energies above 1 MeV, the basic role in this background is played by γ-rays of neutron capture in iodine, whose capture cross section even for neutron energies of approximately 1 MeV is 0.1 barn. Depending on the conditions of the experiment and on the formulated problem, this background may be of paramount importance even when the ratio of γ-rays to neutrons is 1:1. We can propose the measurement of capture γ-ray background radiation from the residual J^{128} β-activity which has a convenient period for measurements. When measuring γ-rays with an energy below 0.5 MeV, we should take into account the possibility that pulses due to the recoil nuclei of sodium will appear.

The Spectra of Neutrons

Data on the energy distribution of neutrons in shieldings are of interest from the standpoint of the biological dose due to neutrons, the origin of capture γ-radiation, activation, heat liberation, etc. If the computation of capture γ-radiation requires such information on the neutron spectrum in the region of low

energies, then it is important to know the spectrum of fast neutrons to compute the penetration of neutrons through the medium.

A device that could measure the spectra of neutrons over the entire energy region does not exist. The methods which are widely used to measure the neutron spectrum in shielding utilize thermal, resonance and threshold tracers, He^3 chambers and integral methods of recoil nuclei with the utilization of ionization chambers and scintillation counters.

The main advantages of tracers for taking measurements in the shielding consist of their total insensitivity to γ-rays and the possibility of utilizing them in large numbers to obtain the three-dimensional distribution of neutrons. When selecting a tracer for measuring neutrons in a definite energy region, we should take into account the half-life of the reaction product, the value of the cross section and also the presence of possible impurities involving other elements as well as of other reactions involving the element of interest to us or its isotopes (if these exist).

The basic activity of the tracer is separated from activities due to other reactions and impurities according to the half-life period. In some cases it is not possible to do this, if the periods for the half-life of activities are close or if they coincide. Thus when measuring high energy neutrons in hydrogen-containing media it is not possible to separate the 5-min activity of the Cu^{65} (n, γ) Cu^{66} reaction from the 10-min activity of the Cu^{63} (n, 2n) Cu^{62}.

From the standpoint of separating extraneous activities, the tracers /258 β^+-decay occurring during reactions (n, 2n) are most convenient. The γ-radiation with energy of 511 keV, which occurs during the annihilation of the positron, is measured by means of a scintillation γ-spectrometer. At this time it is also relatively easy to determine the absolute number of captures in the tracer.

In evaluating the energy distribution of fast neutrons in shielding, a collection of tracers with different thresholds is used. It is convenient to know the relative number of reactions in the collection of tracers for a stream of monoenergetic neutrons or for neutrons with a known spectrum (refs. 29 and 30). Thus the collection of threshold tracers Cu^{63} (n, 2n) Cu^{62}; Sb^{121} (n, 2n) Sb^{120}; Fe^{56} (n, p) Mn^{56}; Al^{27} (n, p) Mg^{27}; P^{31} (n, p) Si^{31}, which were utilized in reference 29, was activated in a stream of neutrons with an energy of 15 MeV.

Usually the resonance tracers can be "associated" with the thermal region which eliminates many difficulties associated with information on the absolute output of β-particles from the tracer, with the effectiveness and geometry of the β-counter and others. By activating the same collection in an unknown spectrum and knowing the relationship between the cross section of each tracer and energy, the matrix method of processing the tracers or the method of successive approximations may be used to find the spectral distribution of neutrons (refs. 29 and 30).

The disadvantage of threshold tracers is their low sensitivity to neutrons and the large difficulties associated with processing the results. Inexact information on the variation of the tracer cross sections as a function of energy introduces a large error in the determination of the neutron spectra. Furthermore, the repeated utilization of tracers with a large half-life is frequently impossible (the S^{32} (n, p) P^{32} reaction with $T_{1/2}$ = 14 days).

In the region of neutron energies from 0.2 to 2 MeV the spectrometer may consist of a small ionization chamber filled with He^3 and Ar (ref. 31). The reaction He^3 (n, p) T takes place with a liberation of energy Q = 760 keV. Its cross section is well known. For neutrons with energies less than 1 MeV the form of the equipment spectrum has a simple interpretation, for large energies it is necessary to use the matrix method. The fabrication of a chamber and its filling with helium at a pressure of several atmospheres is a rather difficult problem. In addition, the practical application of the chamber for measurements in the shielding is difficult due to its high sensitivity to thermal and resonance neutrons. For the energy resolution of the thermal peak which can be obtained in practice (approximately 10 percent) this leads to its distribution over a region covering several hundred keV.

Hydrogen-containing ionization chambers which make it possible to measure neutron spectra in the region from 0.3-0.4 to 3-4 MeV are more common. To obtain the neutron spectrum from the equipment spectrum a differentiation technique is used. When efforts are made to measure large neutron energies, a substantial role is played by the wall effect, which impairs the energy resolution and does not make it possible to use the differentiation technique. The sensitivity of hydrogen-containing ionization chambers to neutrons is a quantity of the order of 1 percent and is very small with respect to γ-rays. The construction of large ionization chambers with pressures measured in tens of atmospheres, for the purpose of decreasing the role of the wall effect encounters technical difficulties; the presence of the background γ-radiation is more pronounced for large chambers and for large gas pressures.

From the standpoint of the wall effect, energy resolution, dimensions and effectiveness, hydrogen-containing organic scintillators are rather convenient. Their utilization as neutron detectors and as spectrometers has been rather limited to date due to their high sensitivity to γ-rays. Thus a toluylene crystal has approximately the same effectiveness with respect to neutrons with energies of 2 MeV and γ-rays of the same energy.

The development of methods for discriminating against γ-rays (refs. 10 and 32) has made it possible to utilize a toluylene crystal as a spectrometer for fast neutrons ($\geq$ 1 MeV). One method of measuring the spectrum of fast /259 neutrons consists of utilizing a single crystal scintillation spectrometer with discrimination against γ-rays during the scintillation time (ref. 33). The energy distribution of such a spectrometer with the mass-produced FEU-11 photomultiplier and a toluylene crystal with dimensions of 20 X 30 mm is equal to $15/\sqrt{E}$ percent, which constitutes 15 percent and 4 percent for neutrons with

energies of 1 and 15 MeV, respectively. The effectiveness of such a crystal as a neutron counter for energies of several MeV is 10 percent, and its effectiveness as a spectrometer is one order less (due to the necessity of using the differentiation technique when processing the equipment spectra).

The known linearity of the light output from the toluylene crystal V (E) as a function of proton recoil energy constitutes an additional difficulty in adjusting the spectrometer and processing the equipment spectrum. In processing the spectrum it is also necessary to know the variation in the derivative of the crystal light output as a function of recoil proton energy. According to the Birks theory (ref. 34), this relationship is expressed in terms of the ionization density dE/dx and the parameter KB, which characterizes the probability of scintillation quenching in the crystal. This parameter KB may vary by 50 percent for various crystals.

In determining the KB for a specific crystal it is not necessary to plot the relationship V (E) for many neutron energies. Having recorded the equipment spectrum of the monoenergetic neutron beam, for example, with an energy of 14-15 MeV (the T (D, n) reaction), it is sufficient to select a value for KB so that the corresponding derivative of the light output provides for the transformation of the equipment spectrum of recoil protons into an ideal "step."

The utilization of large crystals is difficult due to the presence of multiple scattering and the impossibility of utilizing a simple technique for processing equipment spectra in this case. For a toluylene crystal with dimensions of 20 X 30 mm the effect of multiple scattering begins to take place at energies of less than 2 MeV.

Due to the statistical nature of crystal scintillation and the fluctuation in the number of photoelectrons from the photocathode, the leading edges of voltage pulses from recoil protons and electrons are spread. Therefore, the minimum energy which is measured in the spectrum (the spectroscopic threshold of the spectrometer) depends on the degree of γ-ray suppression. We may assume that all of the discrimination schemes described in the literature (refs. 10 and 32) provide approximately the same relationship between the spectroscopic threshold and the degree of γ-ray suppression. Thus, when the γ-ray count decreases by a factor of 10^2 and 10^4, the spectroscopic threshold is equal to 0.8 and 1.5 MeV, respectively. It should be pointed out that charges should not exceed several kHz (kcps). For large charges the variation in the spectroscopic threshold as a function of γ-ray suppression deteriorates due to the superposition of pulses from the γ-rays.

In conclusion we make the following remarks. The utilization of spectrometers (both neutron and γ-ray) is particularly expedient in the study of angular energy radiation distributions leaving the shielding. However, in this case we have a nontrivial problem of detector collimation. Although the question of γ-ray collimation has been studied more or less (ref. 21) from the standpoint of distortions introduced by the collimator into the measured spectral distribution, the method of determining the absolute effectiveness of a collimator in the case of an inexact source has not been worked out in general. The problem is further

complicated during the collimation of neutrons due to large values of the albedo from any substance and due to small interaction cross sections compared with those of γ-rays.

The author takes this opportunity to express his deep gratitude to A. I. Abramov, V. I. Kukhtevich, V. P. Mashkovich, V. I. Popov, B. I. Sinitsyn and S. G. Tsypin for valuable communications which were utilized in the present work.

REFERENCES

1. Gol'dshteyn, G. Principles of Reactor Shielding (Osnovy zashchity reaktorov). Moscow, Gosatomizdat, 1961.

2. Aglintsev, K. K. The Dosimetry of Ionizing Radiations (Dozimetriya ioniziruyushchikh izlucheniy). Moscow, Gostekhizdat, 1957.

3. Broder, D. L., Kondrashov, A. P. et al. P. 81 of this volume.

4. Kukhtevich, V. I., Matusevich, Ye. S. et al. Inzh.-fiz. zh., Vol. 3, 125, 1960. /260

5. Radiation Dosimetry. Edited by J. Cain and G. Bratsnell (Radiatsionnaya dozimetriya). Moscow, Izd-vo I. L., 1958.

6. Kukhtevich, V. I. and Shemetenko, B. P. Atomnaya Energiya, Vol. 12, 236, 1962.

7. Broder, D. L., Kayurin, Yu. P. and Kutuzov, A. A. See p. 287 of this volume.

8. Hurst, J. S. et al. The Dosimetry of Fast Neutrons. Materials of the International Conference on the Peaceful Uses of Atomic Energy. Geneva, 1955 (Dozimetriya bystrykh neytronov. Materialy mezhdunarodnoy konferentsii po mirnomy ispol'zovaniyu atomnoy energii. Zheneva, 1955). Moscow, Gostekhizdat, 1956.

9. Kukhtevich, V. I. and Trykov, L. A. P. 304 of this volume.

10. Owen, R. B. Proc. Internat. Symp. on Nuclear Electronics. Paris, 1959.

11. Shal'nov, M. I. The Tissue Neutron Dose (Tkanevaya doza neytronov). Moscow, Atomizdat, 1960.

12. Price, B. The Recording of Nuclear Radiation (Registratsiya yadernogo izlucheniya). Moscow, Izd-vo I. L., 1960.

13. Caswell, R. S. et al. Nucl. Sci. and Eng., Vol. 2, 143, 1957.

14. Androsenko, Kh. D. and Smirenkin, G. N. Pribory i Tekhnika Eksperimenta, No. 5, 64, 1962.

15. Mashkovich, V. P. and Tsypin, S. G. Atomnaya Energiya, Vol. 12, 251, 1961.

16. Sinitsyn, B. I. and Tsypin, S. G. P. 99 of this volume.

17. The Shielding of Mobile Installations with a Nuclear Engine. Collected translations, edited by V. V. Orlov and S. G. Tsypin (Zashchita transportnykh ustanovok s yadernym dvigatelem. Sbornik per. pod red. V. V. Orlova i S. G. Tsypina). Moscow, Izdo-vo I. L., 1961.

18. Leypunskiy, O. I. et al. The Penetration of γ-Radiation into Matter (Prokhozhdeniya γ-izlucheniya v veshchestve). Moscow, Fizmatgiz, 1960.

19. Hayward, E. Phys. Rev., Vol. 86, 493, 1952.

20. Kazanskiy, Yu. A., Belov, S. P. and Matusevich, Ye. S. Atomnaya Energiya, Vol. 5, 457, 1958.

21. Maeder, D. et al. Helv. Phys. Acta, Vol. 27, 1, 1956.

22. Hubbell, J. H. Rev. Scient. Instrum., Vol. 29, 65, 1958.

23. Berger, M. and Doggett, J. J. Res. Nat. Bur. Standards, Vol. 56, 535, 1956.

24. Dixon, W. R. and Aitken, J. H. Canad. J. Phys., Vol. 36, 1624, 1958.

25. Kazanskiy, Yu. A. Pribory i Tekhnika Eksperimenta, No. 4, 32, 1959.

26. Motz, J. W. Phys. Rev., Vol. 100, 1560, 1955.

27. Müller, W. F. and Snow, W. Rev. Scient. Instrum., Vol. 31, 49, 1960.

28. Ricci, R. A. Physica, Vol. 24, 289, 1958.

29. Belov, S. P., Dulin V. A. et al. Atomnaya Energiya, Vol. 6, 663, 1959.

30. Dulin, V. A., Mashkovich, V. P. et al. Atomnaya Energiya, Vol. 9, 318, 1960.

31. Abramov, A. I. Pribory i Tekhnika Eksperimenta, No. 4, 56, 1959.

32. Brooks, F. D. Nucl. Instrum. and Methods, Vol. 4, 151, 1959.

33. Dulin, V. A., Kazanskiy, Yu. A. et al. Pribory i Tekhnika Eksperimenta, No. 2, 35, 1961.

34. Birks, D. Scintillation Counters (Stsintillyatsionnyye schetchiki). Moscow, Izd-vo I. L., 1955.

COUNTERS AND DOSIMETERS FOR INVESTIGATING SHIELDING AND THE SHIELDING PROPERTIES OF MATERIALS

V. N. Avayev, G. A. Vasil'yev, Yu. A. Yegorov,
V. A. Kucheryayev, Yu. V. Orlov, Yu. V. Pankrat'yev and
Ye. A. Panov

At the present time the most diverse materials and their combinations /260 are used for reactor shielding; the shielding properties of materials as well of their combinations do not always lend themselves to computation. At the same time, when part of the reactor equipment is used for its shielding it is not possible accurately to compute the attenuation of radiation in the reactor. For this reason the shielding properties of materials and their combinations have to be studied experimentally, and the design of shielding must be checked by using a prototype or an existing installation.

When the shielding properties of materials and their combinations are studied, the following quantities are usually determined: the attenuation coefficients for fluxes of γ-quanta and neutrons of various energies; power attenuation coefficient for the dose of γ-radiation and fast neutrons; the output and spectrum of the capture γ-radiation; the activation of materials in the flux of neutrons and the deformation of the γ-radiation spectra of neutrons during penetration through the material.

As a rule these same quantities are measured when investigating a completed shielding or its prototype. Measurements of these quantities are carried both under conditions of barrier geometry as well as under conditions which are close to "semi-infinite" geometry. Devices manufactured by plants such as type SP γ-radiation dosimeter, KPN-1 radiometer and others cannot always be used for /261 measurements of this type. Therefore we fabricated several devices which we describe below.

Scintillation spectrometers are used to investigate the spectral composition of γ-radiation and neutron fluxes. The descriptions of spectrometers are presented in references 1-4.

The problem of radiation penetration through slits and hollows in shielding becomes particularly significant in designing complex shielding. Special equipment, described in reference 5, has been developed to study this problem.

Scintillation counters are used to study the attenuation of fluxes due to γ-quanta as well as those due to fast and slow neutrons and in most cases are fabricated in two versions: with large and small dimensions. Small counters are designed to take measurements under conditions of "semi-infinite" geometry.

The scintillation counter for γ-quanta is used to study the attenuation of γ-quanta flux of given energy and in essence consists of a single crystal scintillation γ-spectrometer. An FEU-11B photomultiplier with an NaJ (Tl) spectrometer crystal with diameter and height of 40 mm is mounted in the counter sensor. The crystal and the photomultiplier are placed in a lightproof case with thin aluminum walls. The cathode follower is also placed in the case. During the measurements the sensor is placed in a lead collimator. The signal from the counter is transmitted to linear pulse amplifiers through the cathode follower and after amplification is fed to a single channel differential pulse amplitude analyzer, whose channel width can be controlled over a wide range. The number of pulses is recorded by the counting circuit.

Before the counter is used to take the measurements, the γ-spectrum of the radiation source is taken and the position of the pertinent γ-line is determined in the analyzer channels. Then the respective threshold and width of the analyzer channel are set and measurements are carried out without changing them.

A method of this type makes it possible to create conditions which are close to "good geometry" without special collimation, and to study the attenuation of a narrow energy group of γ-quanta.

The scintillation counter for measuring fast neutron fluxes consists of a FEU-11B photomultiplier, whose photocathode contains a plastic ZnS (Ag) + plexiglas scintillator (with a diameter of 30 mm and a height of 10 mm). The miniature version of the fast neutron counter is assembled with a FEU-31 photomultiplier and a plastic scintillator of the same composition (with a diameter of 16 mm and a height of 10 mm). The signals from the counters are transmitted to the recording equipment through cathode followers, and in the miniature version of the counter the cathode follower uses a 6Zh1B tube. The application of a miniature photomultiplier and tube has made it possible to achieve small dimensions for the sensor: a diameter of 27 mm and a length of 275 mm (fig. 1). This makes it possible to utilize it in the "semi-infinite" geometry. /262

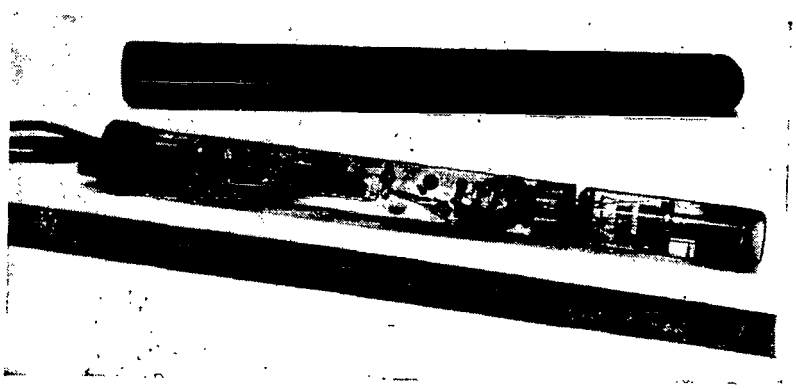

Figure 1. External view of small scintillation counter (case removed).

The sensor with the plastic scintillator is designed to study the attenuation of neutron flux with energy of $\geqslant$ 2 MeV,[1] and when recording the neutron flux with a γ-radiation background the pulses from the latter are chopped off by selecting a corresponding threshold of the integral analyzer connected to the recording circuit of the counter. In order to select the necessary threshold of the analyzer, the sensor is placed in a γ-field with a dose power of 200 μR/sec, and a threshold is selected in such a way that the pulses from the γ-quanta are not recorded. Usually the γ-field is produced by means of a Co^{60} source.

A relatively large scintillation counter of fast neutrons can be placed in a collimator made of paraffin and boron carbide during the measurements. When measurements are made in a barrier geometry, a minature sensor with a collimator is used. On the other hand, when measurements are made in a "semi-infinite" geometry, the sensor is placed in special openings in the shielding and up to 10 sensors are used simultaneously, depending on the dimensions of the shielding.

The fast neutron scintillation counter (fig. 2), which is analogous to the one described, is used as a "monitor" during reactor measurements. The scintillator is attached to the FEU-29 photomultiplier which is installed in a standard case for the type VSF high voltage rectifier. The sensor is mounted on a tripod whose height can be regulated. During the measurements sensors without a collimator are used.

In the case where the dimensions of the test shielding, or some other reasons do not permit the placement of even miniature counters inside the shielding, a sensor is used which contains a plastic optical fiber between /263 the scintillator and the photomultiplier (fig. 3). The length of the optical fiber may reach 60 cm. A further increase in the length of the optical fiber makes the measurements very difficult, because the light flux at the photocathode is substantially decreased (ref. 6). The optical fiber has a diameter of 10 mm and has a light collector at the end facing the scintillator (ref. 7). The diameter of the plastic scintillator is the same as the diameter of the optical fiber. The optical fiber with the scintillator is placed in a thin-walled aluminum tube. The sensor with the optical fiber has been used, for example, to measure the distribution of fast neutrons in water behind a steel plate.

A scintillation counter with a toluylene crystal (diameter of 30 mm, height 20 mm) is used to measure the flux of fast neutrons in the energy range from 1 to 10 MeV. Discrimination against the background γ-radiation is achieved by adopting a scheme proposed in reference 8, which uses the difference in the scintillation time of the toluylene crystal during irradiation by protons and electrons (ref. 9).

---

[1] A large number of experiments on the reactor have shown that the effective threshold of the sensor with the ZnS(Ag) + plexiglas scintillator coincides with the effective threshold of the P^{31} (n, p) Si^{31} reaction.

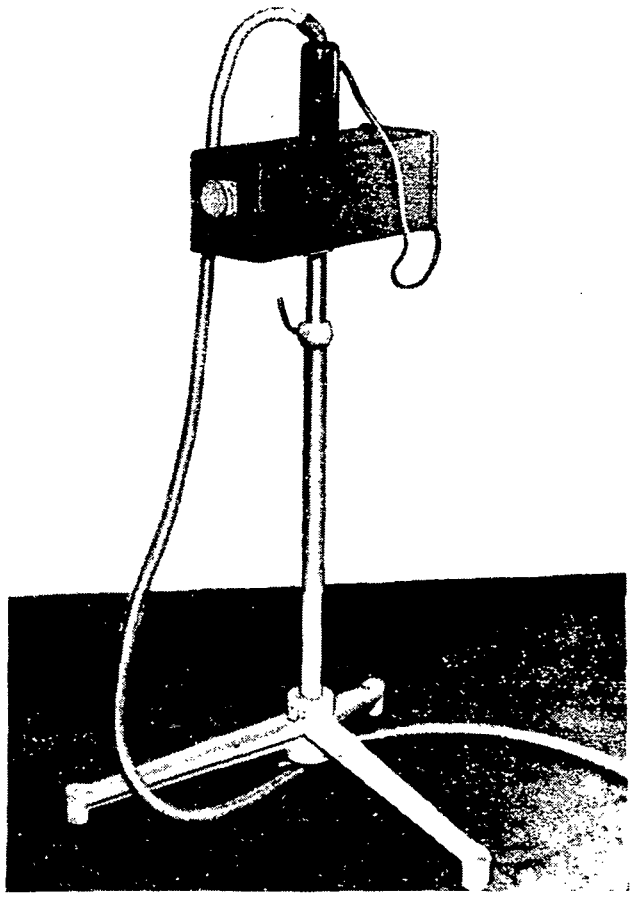

Figure 2. External view of fast neutron counter monitor.

The block diagram of the fast neutron counter is shown in figure 4. The effectiveness of recording neutrons in the energy range of 1-10 MeV is equal to 10-2 percent, respectively, whereas the effectiveness of recording γ-quanta is approximately 10^4 times less. The total maximum loading of the counter must not exceed 10^5 pulses/sec. The fast neutron counter with a toluylene crystal is utilized in measurements on the nuclear reactor.

The slow neutrons scintillation counter also consists of two versions: a sensor of relatively large dimensions and a small sensor. In the first version, the type FEU-29 photomultiplier is used, whereas in the second version the type FEU-31 photomultiplier is used. The scintillator in the slow neutron counters consists of glass whose composition is $Li_2O \cdot 3SiO_2$ (ref. 10), and the recording of slow neutrons is achieved by means of the $Li^6 + n \rightarrow \alpha + H^3$ reaction. In our sensors we utilized glass enriched 100 percent with Li^6. The dimensions of the

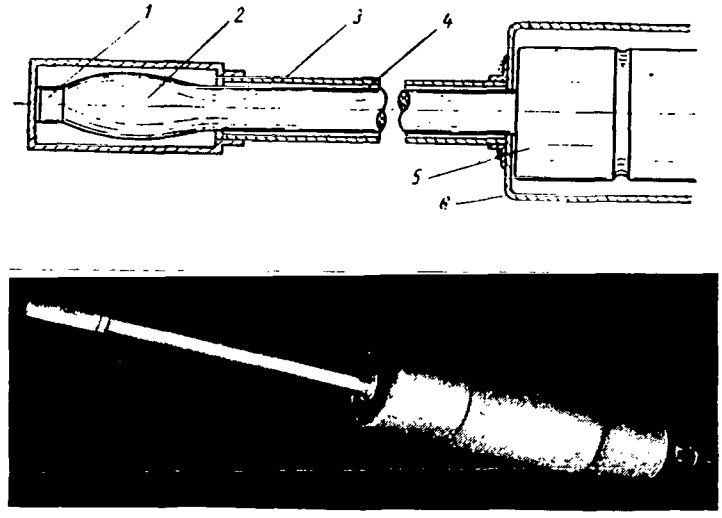

Figure 3. Schematic cross section (upper drawing) and the external view (lower picture) of fast neutron counter with optical waveguide: 1, scintillator; 2, optical waveguide; 3, optical waveguide tube; 4, reflector; 5, photomultiplier; 6, photomultipler case.

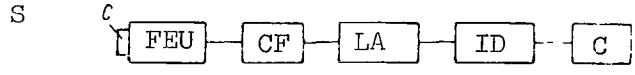

Figure 4. Block diagram of fast neutron counter with toluylene crystal: S, radiation source; C, crystal; FEU, photomultiplier with circuit for discriminating against the γ-background radiation; CF, cathode follower; LA, linear amplifier; ID, integral discriminator; C, counter.

scintillation glasses were as follows: thickness (in both cases) 3 mm, diameter of 25 and 20 mm, respectively. The dimensions of the small sensor are the same as the dimension of the sensor for the fast neutron counter with the FEU-31 photomultiplier (fig. 1).

A slow neutron counter utilizing the FEU-35 photomultiplier was constructed for taking measurements under conditions of "semi'infinite" geometry. The external diameter of this counter's case is 40 mm, and its length is 140 mm. /264 A sensor of this type, for example, was used to measure the distribution of thermal neutrons in polyethylene (ref. 11).

During measurements the slow neutron counter is connected to a circuit with a single channel analyzer whose channel width can be controlled over a wide range.

In this scheme we utilized a standard single channel AADO-1 analyzer. Before measurements are made, the amplitude distribution of counter pulses is read and the threshold and analyzer channel width are selected in such a way that only those pulses are recorded whose amplitude corresponds to the peak in the distribution.

For measurements in the barrier geometry the slow neutron counter is placed in a collimator made of cadmium and boron carbide. The case of the collimator is made of cadmium with a thickness of 1.5-2 mm, and the boron carbide is poured inside between the cadmium walls. The thickness of the boron carbide layer is approximately 5 cm. The use of a collimator whose composition contains an effective moderator is not permissible, because this leads to the distortion of true results. A cadmium shutter which can be lowered to cover the opening in the collimator by means of a cord is attached above the collimating opening. By taking measurements with a lowered and lifted shutter the cadmium ratio in the flux of neutrons behind the shielding may be measured.

The collimator with the sensor is attached to a portable lifting device with a rack (fig. 5) so that the sensor can be moved in the vertical direction. This is necessary when measuring the distribution of slow neutron flux behind the shielding of a plane source, which is nonhomogeneous along the vertical direction. The height of the sensor is measured by means of a scale installed on the rack.

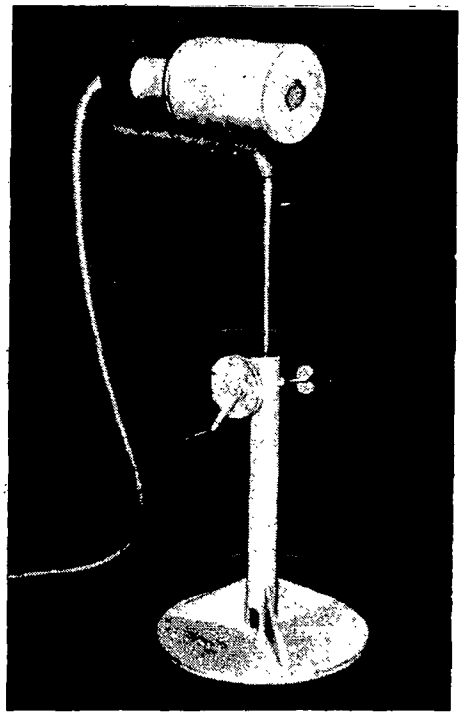

Figure 5. External view of thermal neutron counter in collimator on vertically adjustable device.

The sensitivity of the slow neutron counter to γ-rays is usually controlled by taking the amplitude distribution of pulses from the γ-radiation of Zn^{65} of Co^{60}, i.e., from γ-quanta with energies of 1-1.25 MeV. In spite of the fact that during measurements, for example, with a Po + Be source or on a reactor, there are γ-quanta with energies of 4.46 MeV present in the first case, and γ-quanta with energies up to 7-10 MeV in the second case, a control of this type is sufficient.

This is confirmed by the following considerations. The specific weight of the scintillation glass is approximately 2.5 g/cm^3, i.e., in its γ-radiation absorption properties glass is close to aluminum whose specific weight is /265 2.7 g/cm^3. The value of γ-radiation attenuation coefficients of aluminum for these energies is less (see table below) than for γ-radiation with an energy of 1-1.25 MeV (ref. 12), i.e., with all other conditions equal (which can thus be maintained by control), the number of recorded γ-quanta with energies of 4.5-10 MeV will be at least two times less than the number of recorded γ-quanta with energies of 1-1.25 MeV.

In addition, the mean free path length of electrons with energies of 4.5-10 MeV in aluminum is 8.5-19.2 mm (ref. 12), whereas for electrons with energies of 1.25 MeV the mean free path length is equal to 2.02 mm. Consequently, the light flashes produced by the absorption of γ-quanta of higher energies are, on the average, smaller in amplitude than the light flashes during the absorption of γ-quanta with energies of 1.25 MeV, because the greatest part of secondary electrons in the scintillator is not completely retarded. An effect of this type can be observed even when measurements are made with the γ-radiation of Na^{24}(E_γ = 2.76 MeV), even though the attenuation coefficient for the μ-radiation of Na^{24}(μ = 0.1 cm^{-1}) and the mean free path length of secondary electrons with corresponding energies (R = 4.75 mm) are closer to the analogous values for the γ-quanta of Zn^{65} and Co^{60}.

However, in a series of cases when the flux of γ-quanta substantially exceeds the flux of slow neutrons, the number of γ-quanta counts becomes comparable with the number of slow neutron counts. When measurements are made under these conditions, in order to eliminate the background γ-radiation a bismuth screen with a thickness of approximately 100 mm is installed in the counter along the

ABSORPTION COEFFICIENT μ AND FREE PATHS R OF ELECTRONS IN ALUMINUM FOR DIFFERENT ENERGIES.

E_e, MeV	μ, cm^{-1}	R, mm	E_e, MeV	μ, cm^{-1}	R, mm
1.25	0.149	2.02	7.5	0.069	14.3
4.5	0.079	8.44	10	0.062	19.2

path of the flux. When the results of measurements are processed, a correction is introduced for the attenuation of the neutron flux by the bismuth (ref. 1).

The all-wave neutron counter is used to establish the attenuation law for the flux of neutrons with energies from zero to the maximum value in the spectrum of the source. The all-wave neutron counter utilizes a SNM-5 gas discharge counter filled with the BF_3 gas. The SNM-5 counter is placed in a paraffin cylinder whose wall thickness is 80 mm. The end of the counter is covered with a cadmium cap whose thickness is 1.2 mm. The end of the paraffin cylinder facing the source contains eight depressions (with a diameter of 20 mm and a depth of 80 mm) for smoothing out the variation in the effectiveness of the counter as a function of neutron energy in the region of small energies. We note that the variation in the effectiveness of an all-wave counter as a function of neutron energy was not investigated by us; however, since the construction of our counter is close to the construction of the counter described in reference 13, we may assume that the variation in effectiveness as a function of energy is the same.

The paraffin cylinder is wrapped with a cadmium layer 2.5 mm thick on the outside and is placed in a shielding cylindrical screen made of paraffin with boron carbide. The signal from the SNM-5 counter is preamplified in a preamplifier located right at the counter and is transmitted by means of a coaxial cable to the amplifier and the integral discriminator. The γ-background radiation is eliminated by selecting the corresponding threshold for the operation of the discriminator, which is achieved by placing a source of γ-radiation (usually Co^{60}) close to the all-wave counter to produce a dose power of 200 μR/sec at the SNM-5 counter.

The all-wave counter together with the preamplifier is placed on a light cart. The height of the counter with respect to the floor may be varied in discrete steps by means of a rod.

A fast neutron dosimeter is used to measure the attenuation of /266
fast neutron dose power in test materials and for measuring the dose power of fast neutrons behind the shielding. Based on the results presented in references 14 and 15 which showed that liquid and plastic organic scintillators may be used for the dosimetry of fast neutrons, we fabricated a scintillation dosimeter with a plastic scintillator (polystyrene + terphenyl + Roror), installed on the FEU-25 photomultiplier. The scintillator consists of a sphere with a diameter of 38 mm which has a cut section along the diameter of the FEU-25 photocathode. The optical contact between the scintillator, and the photocathode is achieved by means of mineral oil. The photomultiplier and the scintillator are placed into a thin-walled aluminum case.

The photomultiplier current is integrated at the input of the scheme and is amplified by a dc current amplifier. The sensitivity of the dc current amplifier is controlled by varying the resistance in its input circuit. The amplified current of the photomultiplier which is proportional to the dose power of fast neutrons, is measured with an M-24 microammeter connected to the plate

circuit of the dc current amplifier. When the supply voltage to the photomultiplier is 1350 V, the maximum sensitivity of the dosimeter is 0.5 millionth of the physical equivalent of R/sec per division of the device. The photomultiplier is powered by a cascade voltage multiplier which uses the ABC-5-1a selenium stacks; the voltage is stabilized by means of a voltage-stabilizing tube. Before measuring the dosimeter is calibrated in a flux of fast neutrons from the Po + Be source.

The fast neutron scintillation dosimeter of this type has one substantial shortcoming, specifically that the dosimeter is equally sensitive to fast neutrons and to γ-quanta. For this reason measurements in the presence of background γ-radiation must be carried on with two dosimeters simultaneously-- with a fast neutron scintillation dosimeter and with a γ-dosimeter insensitive to fast neutrons. Furthermore, the γ-dosimeter must have a "hard operation," which is the same as the "hard operation" of the neutron dosimeter. The type SP γ-dosimeter with a 1 liter ionization chamber and with thin aluminum walls (ref. 15) satisfies the necessary requirements. The result of the measurements, i.e., the dose power of fast neutrons, is obtained in the form of the difference between the readings of the scintillation neutron dosimeter and of the γ-dosimeter reduced to the same current.

The effect of background γ-radiation on the dosimeter reading may also be eliminated by carrying out additional measurements using a bismuth screen (ref. 1).

A scintillation γ-dosimeter without "hard operation" is used to measure the dose powers of γ-radiation in place of ionization γ-dosimeters, since, in the first place, the dosimeter has no "hard operation" and, in the second place, it has a rather high sensitivity with a substantially smaller sensitive volume. As shown in reference 16, in order to eliminate the effect of γ-quanta energy on the sensitivity of a scintillation dosimeter, the latter uses a combined scintillator composed of an organic and an inorganic scintillator. For this purpose an organic plastic scintillator based on polystyrene with an addition of terphenyl and Roror and an inorganic CsJ(Tl) crystal scintillator is used.

The plastic scintillator is fabricated in the form of a cylinder with a diameter and height of 50 mm. A hole with a diameter of 10 mm is drilled along the axis of the cylinder to its center, and a CsJ(Tl) crystal with a volume of

1.5 cm^3 is placed into this hole. At the top the hole is covered with a plug made of the plastic scintillator. To improve the optical contact, all of the touching surfaces of the scintillators are lubricated with mineral oil. On the outside the scintillator is covered with a reflector. A scintillator of this type is mounted on the FEU-29 photomultiplier, whose current is fed to a dc current amplifier when carrying out measurements. The dc current amplifier has seven sensitivity ranges (ref. 17): 0.3, 1.5, 9.5, 30, 150, 750 and $3 \cdot 10^3$ μR/sec for a midscale reading of the M-24 device connected to the plate circuit of the dc current amplifier. The minimum measurable power of γ-radiation dose

is equal to $2 \cdot 10^{-3}$ μR/sec, i.e., the sensitivity of the dosimeter varies /267
by a factor of more than 10^6 by merely switching the ranges.

To eliminate zero drift the power supply for the dc current amplifier is stabilized. It has been observed during the operation of the dosimeter that the zero drift during two hours does not exceed 1 scale division when operation is carried out in the first range. The external view of the γ-dosimeter is shown in figure 6.

The FEU-29 photomultiplier is powered from a cascade multiplier stabilized by means of the SG-5B voltage-stabilizing tube. The sensor of the dosimeter is isotropic with respect to sensitivity, and therefore the dosimeter is usually used without a collimator during measurements. If, on the other hand, collimation is necessary in the course of the experiment, the sensor is placed in a lead collimator whose output opening has a diameter of 50 mm; this dimension cannot be decreased, because the dosimeter operates without the hard mode only in the case when the flux of γ-quanta streams over the scintillator.

The dose power of γ-radiation inside a hollow cylindrical source of γ-radiation is measured by means of the second version of the scintillation γ-dosimeter without "hard operation." The second variation of the dosimeter differs from the first in the dimensions of the scintillator and is placed in a special collimator during measurements. The diameter of the plastic scintillator is 30 mm and its height is 25 mm. The volume of the CsJ(Tl) crystal is 0.85 cm^3. The collimator consists of a steel cylinder (fig. 7) with the dosimeter sensor situated inside it, such that the lower edge of the collimator coincides with the surface of the photomultiplier photocathode. A cast iron plate is attached to the bottom of the cylinder by means of steel rods. The distance between the plate and the cylinder is equal to the height of the scintillator. This collimator construction measures the dose power from a narrow annular layer of the cylindrical source.

During the measurements the collimator with the sensor is suspended by steel cables and is lowered along the axis of the γ-radiation source. The scintillation γ-dosimeter is sensitive to fast neutrons and, as shown in reference 15,

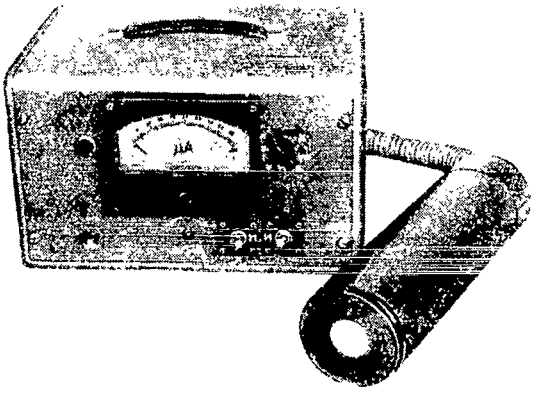

Figure 6. External view of the γ-dosimeter without "hard operation."

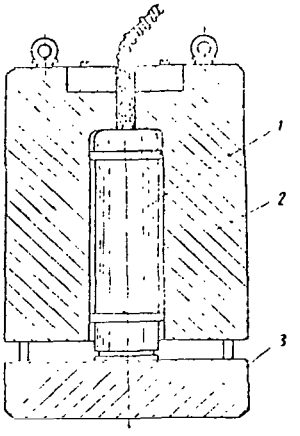

Figure 7. Schematic cross section of device for measuring dose power of γ-radiation inside hollow cylindrical source: 1, dosimeter sensor; 2, side shielding; 3, bottom shielding.

may be used to measure the dose power of γ-radiation in the presence of fast neutrons only when the flux of γ-quanta is approximately 8-10 times greater than the flux of fast neutrons.

The universal rack is designed for operation with some of the described devices (for example, with the scintillation γ-quanta counters of fast and thermal neutrons), as well as for the determination of the induced activity in the radioactive tracers. By using switches the devices assembled on the universal stand may be hooked up in several different combinations to make /268 specific measurements.

Figure 8 shows the block diagram of the universal rack. Signals from the sensors are fed to terminals A and A' or B, and the signals from the sensors which are fed to the terminals A and A' go to the mixer M. The signals from the mixer for the input B are fed to the linear pulse amplifier LPA. The amplifier has two outputs, one of which is connected to the integral pulse discriminator PD, while the other is connected to a single channel pulse analyzer PA. The outputs of the discriminator and the analyzer may be connected either to the counter C, or to the logarithmic count rate meter LCRM. In addition to these circuits the universal rack contains stabilized rectifiers for powering of these circuits and of cathode followers in the sensors and in the high voltage stabilized rectifiers for powering the photomultipliers.

The individual circuits of the universal rack have the following characteristics.

The linear pulse amplifier LPA consists of a preamplifier with a gain of 3 and of a basic amplifier. The variable resistance in the feedback loop of the amplifier makes it possible to control its gain from 75 to 250. A cathode follower utilizing the 6N6P double triode is connected to the output of the amplifier.

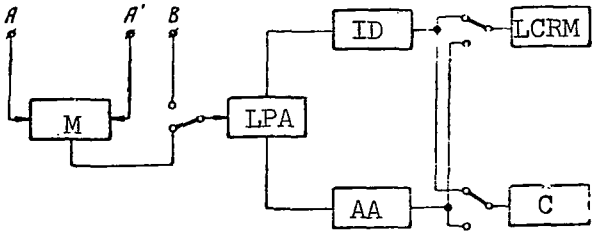

Figure 8. Block diagram of universal rack: M, mixer; LPA, linear pulse amplifier; ID, integral discriminator; AA, single-channel amplitude analyzer; C, counter; LCRM, logarithmic count rate meter.

Two identical and independent signals are obtained at the cathodes of 6N6P. The upper boundary of the amplifier pass band is equal to approximately 5MC; the amplifier is linear up to signal output voltages of 100 V.

The mixer stage M uses the 6N15P double triode with a common cathode load. The amplitude characteristics of the mixer stage are linear up to 5.5 V at the output.

The integral discriminator ID uses a circuit of successive limiting with the D2Zh diode. A signal which has passed through the limiter triggers the single flip-flop oscillator. The cutoff voltage of the limiter is measured by means of a voltmeter. A signal with standard amplitude (approximately 25 V) and duration (approximately 1.2 μsec) may be fed to the counter or to the logarithmic count rate meter from the output of the integral discriminator.

The signal from the second output of the amplifier is fed to the single-channel pulse amplitude analyzer. The analyzer circuit consists of two successive diode limiters with different cutoff voltages. The width of the analyzer channel is controlled and may be set equal to 1, 2, 3, 5, 7, 10 and 24 V. The cutoff voltage (analyzer threshold) is fed to the limiter from a variable voltage divider. All of the resistors in the divider are wire-wound and are selected with an accuracy up to 0.2 percent.

The amplitude characteristics of the single channel analyzer is linear up to 100 V at the output. The magnitude of the pulse at the output of the analyzer is approximately 30 V. The resolving time of the analyzer is approximately equal to $3 \cdot 10^{-6}$ sec. The counter circuit is similar to the circuit of the PS-10,000 device. The conversion factor is 10^4.

The logarithmic count rate meter LCRM uses a circuit with diode measuring networks (ref. 18). The output voltage from the count rate meter which is proportional to the logarithm of the input signal frequency, is measured by means of an M-24 microammeter or is recorded on chart paper by means of an electronic

PSRI automatic potentiometer. The statistical error associated with the recording of potentiometer readings does not exceed 10 percent.

The zero reading of the logarithmic count rate meter corresponds to /269 an input of 6 pulses/sec.; to set the zero reading of the count rate meter, a voltage controlled by a potentiometer is fed to the input of the dc current amplifier. The range of pulse repetition rates, fed to the input of the logarithmic count rate meter which can be measured without any switching, is equal to approximately 10-80,000 pulses/sec.

The logarithmic count rate meter has 2 auxillary devices: a level indicator and a differentiator. The differentiator makes it possible to vary the rate of signal frequency variation at the input of the count rate meter. The level indicator makes it possible to obtain a signal when the frequency of the input signals to the count rate meter reaches a definite value.

All of the devices in the universal rack, except the counter, are fed from stabilized rectifiers. The photomultiplier is fed from a standard VSF stabilized rectifier.

All circuits and units which have been described are assembled on one rack, whose external view is shown in figure 9. The dimensions of the rack are 185 X 50 X 60 cm. The basic units of the universal rack are mounted in such a way that there is free access to all of the circuits during operation.

From the description given for the universal rack it is clear that it can be used to determine the following quantities:

(1) the activity of tracers by measuring the number of γ-quanta with energies exceeding assigned values;

(2) the activity of tracers by measuring the number of γ-quanta of given energy (i.e., according to one γ-line);

(3) the activities of tracers by measuring the number of β-particles with energies greater than the specified value;

(4) the half-life of the induced tracer activity by means of the same measurements as used to determine activity, which also permits the simultaneous measurement of tracer activity and its half-life;

(5) the nature of the induced activity, i.e., to identify the induced activity according to the γ- and β-spectrum and according to the half-life;

(6) the attenuation of γ-quanta flux of specified energy by means of a scintillation counter;

(7) the attenuation of neutron fluxes by means of corresponding counters.

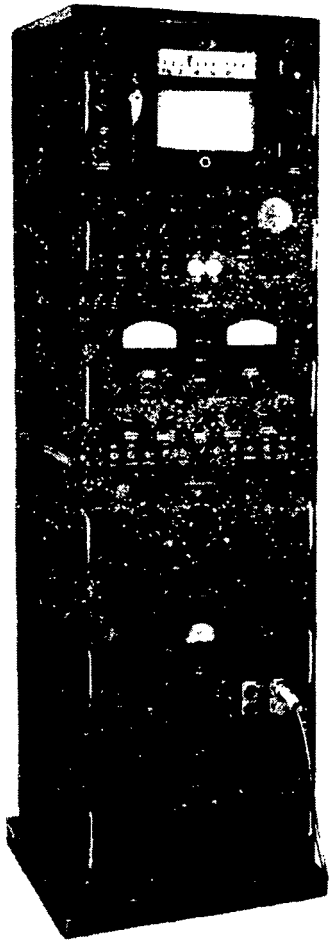

Figure 9. External view of universal rack.

The device just described is called the universal rack because of the relatively large number of problems solved with it. However, the universal rack is basically designed to operate with radioactive tracers (ref. 19).

By using the devices described above it is possible to determine /270 most of the quantities which characterize the shielding properties of materials and to clarify the qualities of specific shielding.

V. M. Isakov, D. I. Chupyrin, A. I. Vasil'yev, V. N. Kozyrev and Yu. G. Anisimov participated in the mounting and adjustment of the devices. The authors take this occasion to express their gratitude to them.

REFERENCES

1. Yegorov, Yu. A. and Orlov, Yu. V. P. 474 of this volume.

2. Avayev, V. N., Yegorov, Yu. A. and Orlov, Yu. V. P. 464 of this volume.

3. Yegorov, Yu. A. and Pankrat'yev, Yu. V. P. 451 of this volume.

4. Chesnokov, A. D. Pribory i Tekhnika Eksperimenta, No. 5, 69, 1957.

5. Veselkin, A. P., Yegorov, Yu. A. and Panov, Ye. A. P. 336 of this volume.

6. Yegorov, Yu. A. and Khukorev, D. S. Pribory i Tekhnika Eksperimenta, No. 4, 136, 1960.

7. Tove, P. A. Rev. Scient. Instrum., Vol. 27, 143, 1956.

8. Broek, H. W. Rev. Scient. Instrum., Vol. 31, 1063, 1960.

9. Owen, R. B. Trans. I.R.E. P.G. NS, Vol. 5, 198, 1958.

10. Voytovetskiy, V. K. and Tolmacheva, N. S. Atomnaya Energiya, Vol. 6, 472, 1959.

11. Avayev, V. N., Veselkin, A. P. et al. Atomnaya Energiya, Vol. 15, 17, 1963.

12. Gusev, N. G. Handbook on Radioactive Radiations and Shielding (Spravochnik po radioaktivnym izlucheniyam i zashchite). Moscow, Medgiz, 1957.

13. Rossi, B. and Shtaub, G. Ionization Chambers and Counters (Ionizatsionnyye kamery i schetchiki). Moscow, Izd-vo I. L., 1951.

14. Yegorov, Yu. A. and Khvostionok, R. Ye. Dosimeter for Fast Neutrons. IN: Devices and Methods of Analyzing Radiation (Dozimetr bystrykh neytronov. V sb.: Pribory i metody analiza isluchenij). Moscow, Atomizdat, 1957.

15. Yegorov, Yu. A. and Kucheryayev, V. A. Inzh.-fiz. zh., Vol. IV, 117, 1961.

16. Yegorov, Yu. A. and Panov, Ye. A. Inzh.-fiz. zh., Vol. IV, 130, 1961.

17. --- Pribory i tekhnika eksperimenta, No. 4, 57, 1961.

18. Chesnokov, A. D. Logarithmic Count Rate Meter (Logarifmicheskiy intensimetr). Moscow, Izd-vo VINITI, 1957.

19. Avayev, V. N., Voskresenskiy, Ye. V. et al. P. 400 of this volume.

APPLICATION OF RADIOACTIVE TRACERS IN THE INVESTIGATION OF SHIELDING

V. N. Avayev, Ye. V. Voskresenskiy, Yu. A. Yegorov and Yu. V. Orlov

Radioactive tracers are widely used to record neutrons during the in- /270
vestigation of nuclear reactor shielding and the shielding properties of materials. This is not accidental: radioactive tracers have advantages over other types of neutron detectors. Such advantages first of all include the possibility of recording neutrons with energies greater than a certain definite value (threshold tracers) or with energies in a rather narrow interval of values (resonance tracers). Radioactive tracers are also convenient because they have small dimensions and can be placed inside the shielding in places not readily accessible to other types of detectors. At the same time, they do not form the undesirable cavities and do not perturb the neutron flux. By utilizing radioactive tracers of various dimensions it is possible to measure neutron fluxes of various intensity. The undisputed advantage of radioactive tracers is their absolute insensitivity to γ-radiation.

Radioactive tracers may be used to measure neutron spectra. However, when fast neutron spectra are measured by means of threshold tracers the accuracy is very small (ref. 1), because the activation cross sections are not known with sufficient accuracy. Nevertheless, the spectrum can be evaluated by means of tracers (refs. 2 and 3).

A significant disadvantage of radioactive tracers is their small effectiveness, particularly in the case of threshold tracers whose activation cross section does not exceed several tens of millibarns (ref. 4). The low effectiveness of tracers is explained to some degree by the fact that the induced activity of tracers is usually measured by means of gas discharge counters /271
which have an effectiveness of the order of 1 percent for γ-radiation, and if the geometry of the measurements is taken into account, it is substantially less. A certain increase in the effectiveness is possible when tracer activity is measured by means of β counters (AS-1, STS-5, S1-3V and others, ref. 5). However, this is not always convenient, because when tracers of large dimensions are used the self-absorption of β particles is very large.

To increase the effectiveness of recording the induced activity by means of tracers we utilize scintillation counters: 4π-counter for measuring the activity of cylindrical tracers and 2π-counters for measuring the activity of plane tracers.

Measurements showed that the effectiveness of recording the γ-radiation of tracers by means of a 4π-counter is close to 100 percent. This situation has made it possible to use tracers of relatively small dimensions for measuring neutron fluxes. The tracers had the form of cylinders with a diameter of 8 mm and a height of 5-50 mm (Al, P, J and others) and in the form of hollow cylinders with the same dimensions and a wall thickness of 0.1-0.3 mm (Au, In and others). The introduction of tracers of these dimensions into the test shielding does not disrupt the distribution of the neutron flux in the shielding.

The 4π-counter consists of two FEU-43 photomultipliers with a CsJ (Tl) crystal of 60 mm diameter and of 30 mm in height connected to each one (fig. 1). Both crystals are packed into a single common container and are separated from each other by a thin aluminum partition. A hole with a diameter of 10 mm is drilled in the center along the diameter of the crystals, and an aluminum tube with a wall thickness of 0.5 mm is inserted into this hole. To make mounting convenient, the unit with the crystals is installed on two washers of plexiglas, 10 mm thick, which serve as optical waveguides. The unit with the crystals and the photomultipliers is placed into a steel shielded booth. The booth has the form of a cylinder, with the photomultipliers and crystals placed along its axis. Each of the photomultipliers is inserted into a tube which can be moved into or removed from the booth. The free ends of the tube contain dividers of the voltage supply for the photomultipliers and the cathode followers. The sleeve nuts at the ends of the cylinder press the crystal unit against the /272

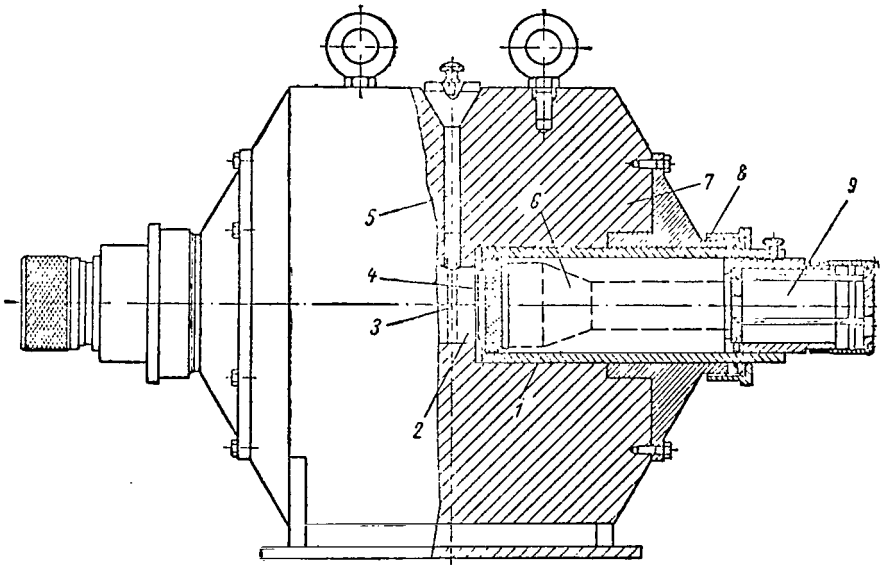

Figure 1. Cross section of 4π-counter for measuring activity of cylindrical tracers: 1, photomultiplier tube; 2, unit with crystals; 3, tracer in holder; 4, washer serving as optical waveguide; 5, irregularly shaped plug; 6, photomultiplier; 7, shielding; 8, sleeve nut; 9, space for divider and for cathode follower.

photomultipliers, thus achieving good optical contact. The thickness of the shielding at the point where the crystal units are situated is 200 mm.

There is an opening at the top of the shielding which is covered with an irregularly shaped plug holding the tracer. The tracer in the plug and the plug in the shielding are always installed identically, so that the conditions of activity measurements are always the same during the experiments.

Cylindrical tracers are installed in tubes made of plexiglas with a diameter of 9 mm and a wall thickness of 0.5 mm. The total height of the plexiglas holder is 90 mm. During irradiation the tracer may be placed into an opening in the shielding with a diameter of 10 mm, if it is irradiated without a cadmium or a boron cadmium filter; when tracers with filters are irradiated, the opening in the shielding must have a diameter of 15 and 32 mm, respectively.

The external view of the 4π-counter is shown in figure 2.

The number of pulses is recorded by means of the universal rack with the single channel pulse analyzer connected into the measurement channel (ref. 6). Since the amplification factors of the photomultiplier may differ, the pulses from both photomultipliers pass through a mixer before being fed to the amplifier; this mixer smoothens out those pulse amplitudes due to the same absorption of γ-quanta energy in both crystals.

The same electronic arrangement but without the mixer, is also used to measure the activity of plane radioactive tracers. A counter containing an NaJ (Tl) crystal with a diameter and height of 40 mm and the FEU-41 multiplier are placed vertically in a shielding booth made of lead. The lower part of the booth contains two small removable platforms, which are placed one over the other and which are used to hold the tracers during the measurements. The upper platform is designed for taking measurements without a collimator, and when a tracer is placed on the lower platform the flux of γ-quanta from the tracer is collimated.

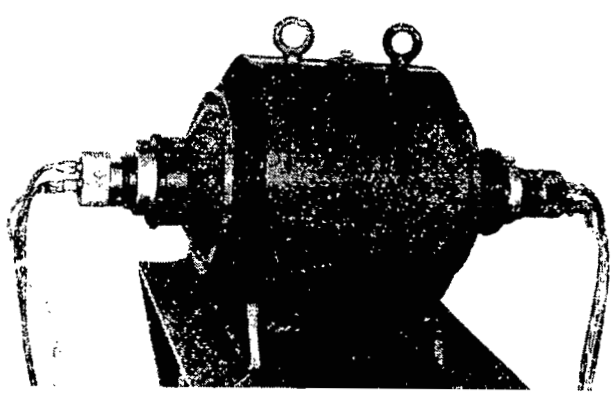

Figure 2. External view of 4π-counter.

The activating material of the plane tracer is applied on a plexiglas base with a thickness of 1 mm; the dimensions of the tracer vary from 5 × 5 to 40 × 40 mm with a layer thickness of 0.1-4 mm.

Scintillation counters have a high efficiency and with good shielding record a substantial amount of background radiation. Therefore, when measuring the activity of a tracer the counters are connected to the spectrometers circuit, so that instead of recording the total number of pulses from the counter, only those pulses are recorded which correspond to the more intense γ-line or a group of γ-lines most characteristic of a given tracer. With this type of recording it becomes possible to reduce the background radiation recording substantially, while the number of useful recordings is insignificantly reduced compared with the integral count. Consequently the isolation of the γ-line substantially improves the ratio of the useful count to the background radiation, and also makes it possible to reduce the requirements for the chemical purity of the tracer material.

The table presents the basic characteristics of radioactive tracers which are used, as well as the energies of the most intense γ-lines, the characteristics of pertinent reactions and the energy interval isolated during recording. As we can see from the table the gold tracer has the simplest decay scheme. /275

Figure 3 shows the amplitude distribution obtained by measuring the induced activity of gold by the 4π-counter. The broken line in this figure shows the amplitude distribution of background radiation pulses. By recording pulses in the amplitude interval Δu it is possible to achieve a decrease in the background radiation by more than a factor of 5, while the useful count remains practically the same.

In the iodine spectrum (see table) in addition to the basic γ-line with energy of 0.455 MeV, other γ-lines are present. However, in selecting the interval Δu = 0.28-0.78 MeV for the recording, these lines, are not recorded; however, a maximum ratio of the useful count to the background radiation is obtained. The interval Δu for the Mn^{55} tracer is selected on the basis of the same considerations.

There is no characteristic γ-line in the decay scheme of In^{116}, and a wide interval Δu (fig. 4) is selected in order not to reduce the "useful" count. Nevertheless, the peak in the soft region of the spectrum is not recorded, because the background radiation is very high in this region of amplitudes.

The method described for the isolation of the energy interval during /276 the determination of induced tracer activity is particularly useful when measurements are made with such tracers as aluminum, i.e., when the γ-lines due to the basic reaction are accompanied by γ-lines of elements formed as a result of associated reactions. The following two reactions are used to record fast neutrons by means of aluminum tracers Al^{27} (n, p) Mg^{27} and Al^{27} (n, α) Na^{24}. In addition to these reactions, the Al^{27} (n, γ) Al^{28} reaction also takes place

TABLE 1. BASIC CHARACTERISTICS OF RADIOACTIVE TRACTERS.

Basic reaction					Associated reactions				Energy interval isolated during recording, MeV
Reaction	Effective threshold, resonance energy	Half-life	Energy of γ-quanta, MeV	Quanta output per decay, %	Reaction	Effective threshold, resonance energy	Half-life	Energy of γ-quanta (MeV) and output per decay, %	
Al^{27} (n, p) Mg^{28}	5.3 MeV	9.51 min	0.84 1.015 0.175	70 30 0.66	Al^{27} (n, γ) Al^{28} Al^{27} (n, α) Na^{24}	Thermal 8.6 MeV	2.31 min 14.9 hr	1.78 (100) 1.38 (100) 2.76 (100)	0.41-0.95
Al^{27} (n, α) Na^{24}	8.6 MeV	14.9 hr	1.38 2.76	100 100	Al^{27} (n, γ) Al^{28} Al^{27} (n, p) Mg^{27}	Thermal 5.3 MeV	2.31 min 9.51 min	1.78 (100) 0.84 (70) 1.01 (30) 0.175 (0.66)	1.1 -2.85
Mn^{55} (n, γ) Mn^{56}	330 eV	2.6 hr	0.845 1.8 2.1 2.56	100 29 15 1	Mn^{55} (n, α) V^{52}	-	3.8 min 16 hr	0.096 (100) 1.44 (100) 0.59 -	0.51-2.2
In^{115} (n, γ) In^{116}	1.45 eV and thermal neutrons	54 min	1.274 0.87 0.406 2.09 1.48 0.137	75 28 25 25 21 3	-	-	-	-	0.38-4
J^{127} (n, γ) J^{128}	~30 eV	25 min	0.455 0.540 0.75 0.99	17.2 1.8 0.91 0.29	J^{127} (n, 2n) J^{126}	-	13 days	0.386 (66)	0.28-0.78
Au^{197} (n, γ) Au^{198}	4.9 eV	2.69 days	0.412 1.087 0.677	99.9 0.5 0.5	-	-	-	-	0.21-0.6

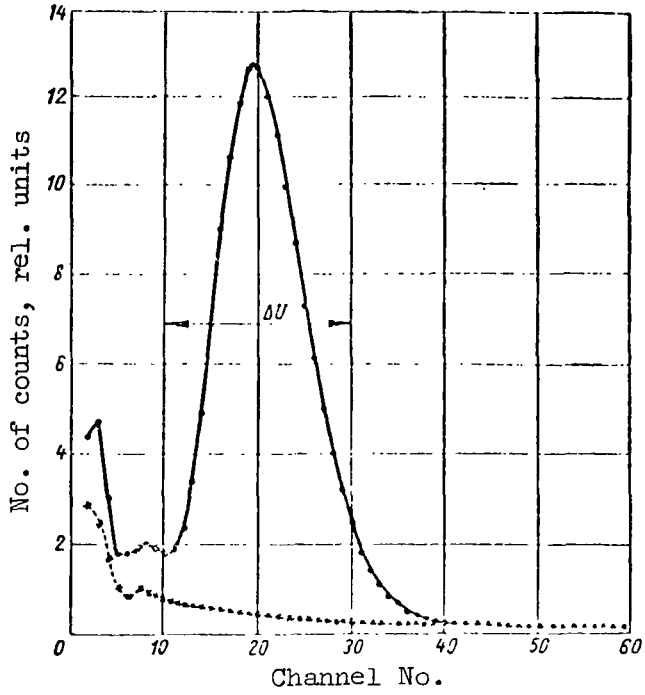

Figure 3. Amplitude distribution for Au^{198} γ-radiation measured by 4π-counter (broken line shows amplitude distribution of background radiation).

in aluminum. When very pure aluminum is used for the tracer the Al^{27} (n, γ) Na^{24} reaction may be separated rather easily from two others, because the half-life of Na^{24} is equal to 14.9 hr, whereas for Mg^{27} and Al^{28} it is 9.51 and 2.3 min, respectively. However, it is rather difficult to divide the (n, p) and (n, γ) reactions by periods, particularly if the measured neutron spectrum contains a large number of thermal and above-thermal neutrons. This irradiation condition may be encountered when measuring the distribution of fast neutrons with energies ≥ 5 MeV, for example, in iron-water shielding. In this case, even when a boron-cadmium filter is used, it is impossible to avoid the activation of aluminum as a result of the (n, γ) reaction; when γ-radiation is recorded without isolating the energy interval, the count is basically due to Al^{28}, and it is difficult to determine the activity of Mg^{27}.

Figure 5 shows the γ-spectra from a plane aluminum tracer, measured by means of a single crystal scintillation counter. The first curve was obtained 10 min, the second 17 min and the third 34 min after the end of irradiation. The peak with an energy of 0.84 MeV, corresponding to the basic Mg^{27} γ-line, is clearly seen, as well as the peak with E_γ = 1.78 MeV, corresponding to the

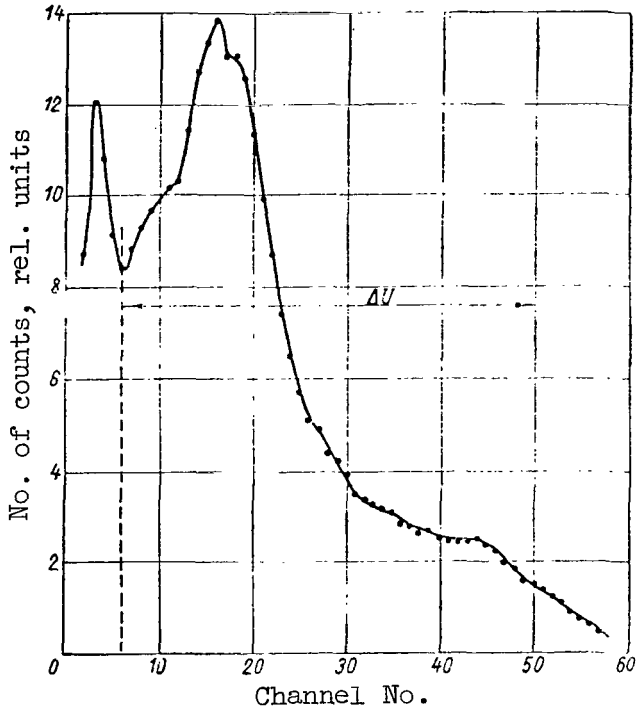

Figure 4. Amplitude distribution for In^{116} γ-radiation measured by 4π-counter.

only Al^{28} γ-line. On the third curve these peaks are substantially decreased and a peak appears for E_γ = 1.38 MeV, corresponding to the Na^{24} γ-line. If we select Δu = 0.41-0.95 MeV for the recording, it is easy to isolate the Mg^{27} γ-line without a substantial loss in the useful count. However, in this case the contribution made by the Na^{24} and Al^{28} γ-lines is substantially reduced. This method of measuring induced activity of threshold tracers after irradiation in the presence of a thermal and above-thermal neutron flux is most reliable. As an example figure 6 shows the distribution of the fast neutron flux ($E_n \geq 5.3$ MeV) in water, measured by means of the Al^{27} (n, p) Mg^{27} reaction. An aluminum tracer weighing 6 g was used to measure the distribution of the fast neutron flux for a length up to 120 cm. The experimental reactors served as the neutron source. The results of investigating the relaxation length λ agree well with existing data.

The experience of this work has shown that the method of determining the induced activity of radioactive tracers by isolating the most intense γ-line or group of γ-lines has justified itself; the electronic equipment operated in a stable manner during the course of measurements and did not introduce noticeable errors.

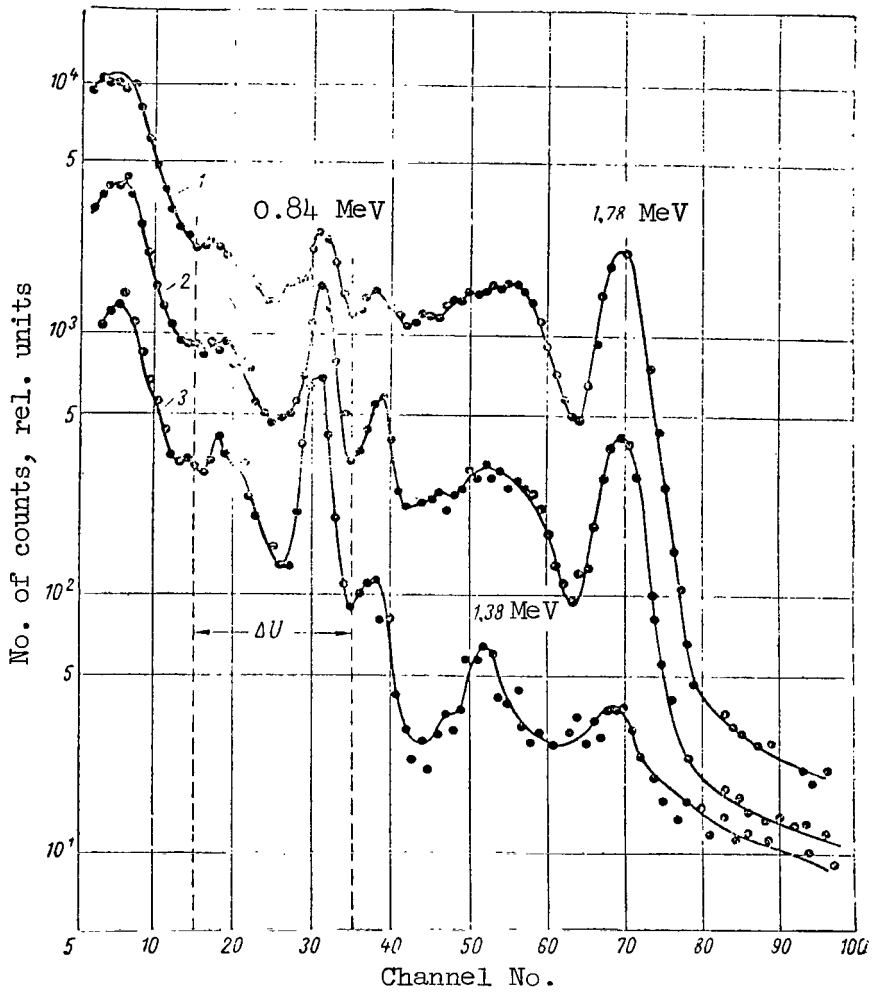

Figure 5. Amplitude distribution for γ-radiation of irradiated Al^{27}. Measured with 2π-counter after end of irradiations: 1, after 10 min; 2, after 17 min; 3, after 34 min.

The authors express their gratitude to D. I. Chupyrin for installing and adjusting the electronic equipment and thank N. Ye. Vasin for developing the design of the 4π-counter.

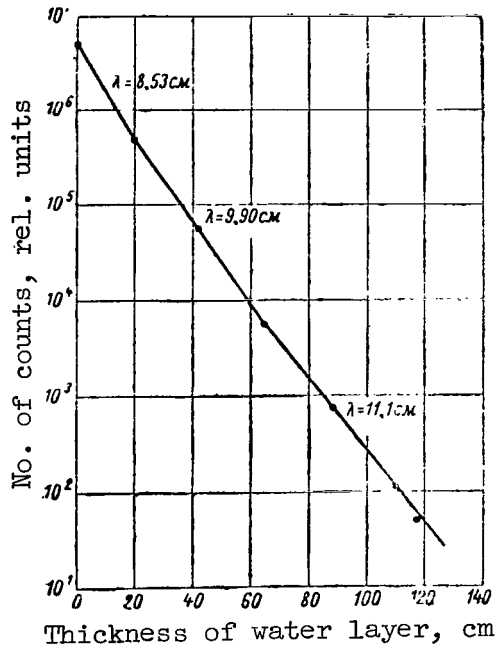

Figure 6. Distribution of fast neutron flux ($E_n \geq 5.3$ MeV) with fission spectrum in water, measured by aluminum tracer (Al^{27} (n, p) Mg^{27} reaction): λ, relaxation length.

REFERENCES

1. Price, B. Recording of Nuclear Radiation (Registratsiya yadernogo izlucheniya). Moscow, Izd-vo I. L., 1960. /277

2. Experimental Nuclear Reactors (Yadernyye reaktory dlya issledovatel'skikh tseley). Materials of the Atomic Energy Commission USA. Moscow, Izd-vo I. L., p. 29, 1956.

3. Dulin, V. A. et al. Atomnaya Energiya, Vol. 9, 318, 1960.

4. Vlasov, N. A. Neutrons (Neytrony). Moscow, Gostekhizdat, 1955.

5. Handbook On Dosimetric, Radiometric and Electron-Physical Devices, Counters, Scintillators and Photomultipliers (Spravochnik po dozimetricheskim radiometricheskim i elektronno-fizicheskim priboram, schetchikam, stsintillyatoram i fotoumnozhitelyam). Moscow, Atomizdat, 1959.

6. Avayev, V. N. et al. P. 385 of this volume.

MEASUREMENT OF FAST NEUTRON FLUXES IN SHIELDING WHEN THERE IS A BACKGROUND OF INTENSE INTERMEDIATE NEUTRON FLUXES

V. P. Mashkovich

It has been reported in references 1-3 that in experiments with /277
threshold tracers the induced activity is usually determined by constructing the decay curves.

Based on the analysis of decay curves we can exclude the effect of extraneous impurities. This method of determining activity is used only when the half-life of the basic activity is different from the half-life of activities associated with impurities or with the basic element as a result of other reactions. In most cases, during the practical utilization of threshold detectors this requirement is satisfied. However, detectors are encountered for which the half-lives of the associated activities are close or equal to the half-life of the basic activity.

In determining the basic activity of such threshold detectors we encounter two cases when the resulting associated activity consists of (1) an isotope which is different from the isotope of the basic activity, but which has a close half-life; and (2) an isotope which is also formed as a result of the basic reaction.

Usually both cases are encountered when a tracer is irradiated with fast neutrons with a background of large thermal and intermediate neutron fluxes.

The associated activity produced by the thermal neutrons can be easily eliminated by placing the detector in a cadmium filter. Therefore in practice the problem is reduced to the measurement of activity caused by fast neutron fluxes on the background of intense intermediate neutron fluxes.

For these cases we propose the following method of determining the activity.

In the first case, when the basic reaction produces an isotope different from the isotope of the associated activity, the isolation of the basic activity can best be carried out by the spectrometric method: it is necessary to isolate that radiation energy of the basic activity isotope which does not exist in the spectrum of the associated activities. The activity under investigation may be evaluated from the intensity of the isolated line.

In the second case the application of the spectrometric method is impossible due to the same composition of the isotopes' radiation. The isolation of

the basic activity may be carried out only when the basic and associated reactions take place with neutrons of different energy ranges. The basic reaction usually takes place with fast neutrons and the associated reaction usually takes place with intermediate neutrons. The specified energy groups must be attenuated in a different manner within the shielding material (the fast neutrons are attenuated considerably more than the intermediate neutrons), which takes place for many shielding materials with medium and large atomic weights. In this case the attenuation curve for the neutron flux, measured with the specified detectors, has two clearly defined regions, characterized by a high attenuation of fast neutrons (first region) and a weak attenuation of intermediate neutrons (second region). Beginning with some shielding thickness the entire activity of the threshold detector is almost totally due to activation in the flux of intermediate neutrons (this is controlled by the course/278 of the attenuation curve which is measured with a detector of only intermediate neutrons).

In this case the region of the attenuation curve where all of the activity is practically due to activation with intermediate neutrons is extrapolated into the region of smaller thicknesses in accordance with the attenuation curve measured by a detector of intermediate neutrons only. If we subtract from the corresponding values of threshold detector activity due to activation by fast and intermediate the corresponding activity due to intermediate neutrons, we obtain an attenuation curve of the flux for fast neutrons only.

We note that this method is also applicable in the first case.

In particular, both of these methods were used in the experimental determination of three-dimensional fast neutron distribution in iron with the aid of the threshold Al^{27} (n, α) Na^{24} tracer (ref. 4). As we know, the fluxes of fast neutrons in iron are attenuated considerably more than the fluxes of neutrons with intermediate energy. As a result, even after penetrating relatively small thicknesses of iron, the neutron fluxes of intermediate energy exceed substantially the fast neutron fluxes, and the added tracer activity is thus substantial during the side reactions associated with neutrons of intermediate energy.

The measurements of neutron fluxes in iron were carried out with the experimental arrangement described in reference 4. As pointed out in reference 4, it is impossible to determine the activity of aluminum tracers by constructing decay curves, because the half-life (12.8 hr) of the associated activity formed in the copper additive as a result of the Cu^{63} (n, γ) Cu^{64} reaction is difficult to separate, in practice, from the half-life of Na^{21}, which is equal to 15 hr.

In this case a spectrometric method of determining activity was used. A scintillation γ-spectrometer containing a NaJ (Tl) crystal (80 x 80 mm) was used with a 100-channel amplitude analyzer (ref. 5). The aluminum detectors were placed in a fixed position near the scintillator. The energy scale was controlled according to the Co^{60} γ-radiation. The γ-spectra of one of the

threshold detectors as a function of time lapsed after the end of irradiation. This is shown in figure 1, where we can clearly see the peaks of photoelectrons produced in the crystal by γ-quanta with energies of 1.38 and 2.76 MeV, due to the basic Na^{24} isotope, and peaks of Cu^{64} γ-radiation with energies of 1.38 and 0.51 MeV. The activity of aluminum tracers (due to the basic reaction) was determined from the area under the photoelectron peaks produced in the crystal by the Na^{24} γ-radiation with energy of 2.76 MeV.

The relative saturation activity of the tracer was determined from the equation

$$N(r, h) = \frac{CPe^{\lambda t}}{(1 - e^{-\lambda T})(1 - e^{-\lambda t_0})},$$

where N (r, h) is the saturation activity of the tracer placed at the point with coordinates r, h of the iron prism; P is the area bounded by the photopeak of Na^{24} γ-quanta with an energy of 2.76 MeV; T is the irradiation time of the tracer; t_0 is the time during which the tracer was subjected to counts;

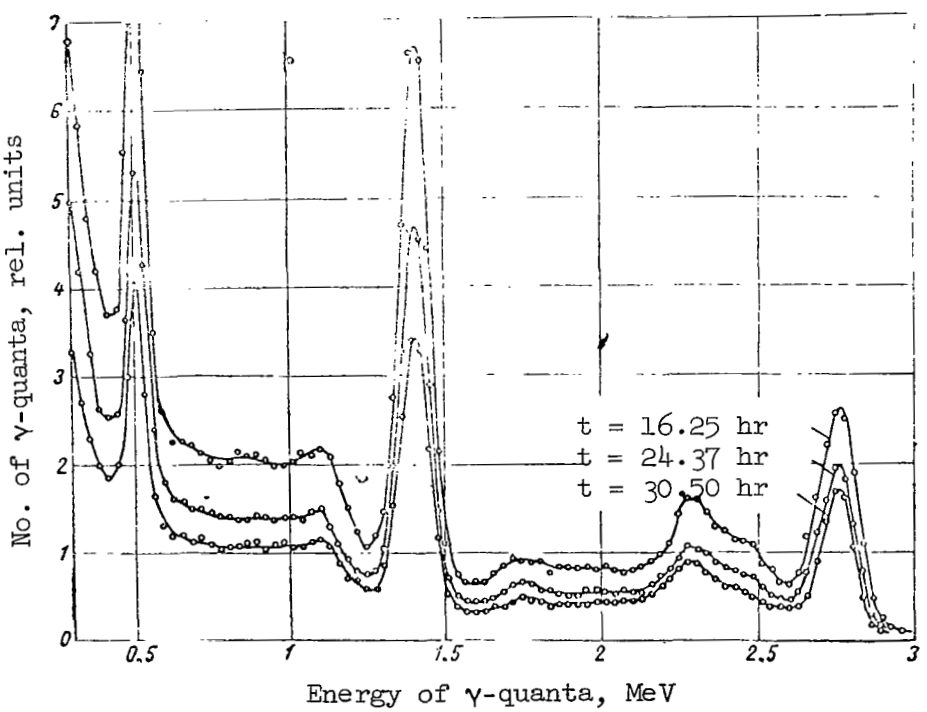

Figure 1. Gamma-spectra of activated aluminum tracer at different instants of time after termination of irradiation.

t is the time between the end of irradiation and the beginning of tracer counting.

Figure 2 shows the γ-spectra of detectors which are placed in the direction of the central beam. These data are used to construct an attenuation curve in the direction of the central beam (fig. 3, curve 1), from which we can see that beginning with an iron thickness of approximately 50 cm, measurements in the direction of the central beam begin to reveal the activity of the additive Na^{23} $[(2 \pm 1)\cdot 10^{-4}\%]$ in the aluminum tracer. Due to the Na^{23} (n, γ) Na^{24} reaction with intermediate neutrons, radioactive Na^{24} is also formed as a result of the basic reaction. In this case the use of only a single spectrometric method makes it impossible to determine that portion of activity due to the basic /279 reaction, and it becomes necessary to utilize the second method.

Figure 3 (curve 1) shows the activity due to fast neutrons according to the reaction Al^{27} (n, α) Na^{24} and due to intermediate neutrons according to the reaction Na^{23} (n, γ) Na^{24}. Curve 1 has two regions: (1) [r = (0 to 30-40 cm], which characterizes a strong attenuation of fast neutrons and is due almost entirely to activation by fast neutrons; (2) (r > 90 cm), which characterizes the insignificant attenuation of intermediate neutrons due almost entirely to activation by neutrons of intermediate energy according to the reaction Na^{23} (n, γ) Na^{24} (in this region the behavior of the curve corresponds to that of the attenuation curve which is measured by a detector of only thermal and intermediate neutrons).

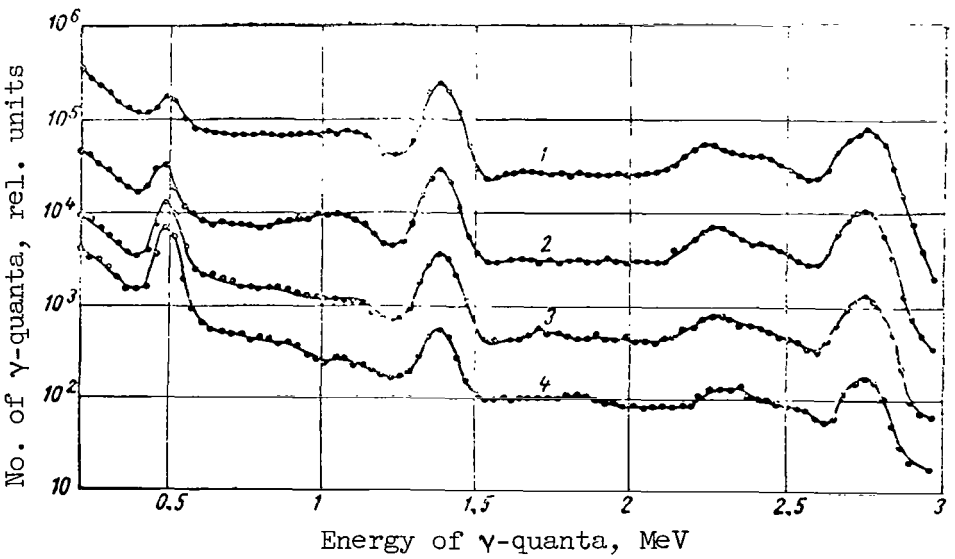

Figure 2. Gamma-spectra of activated aluminum tracers as function of iron shielding thickness r.

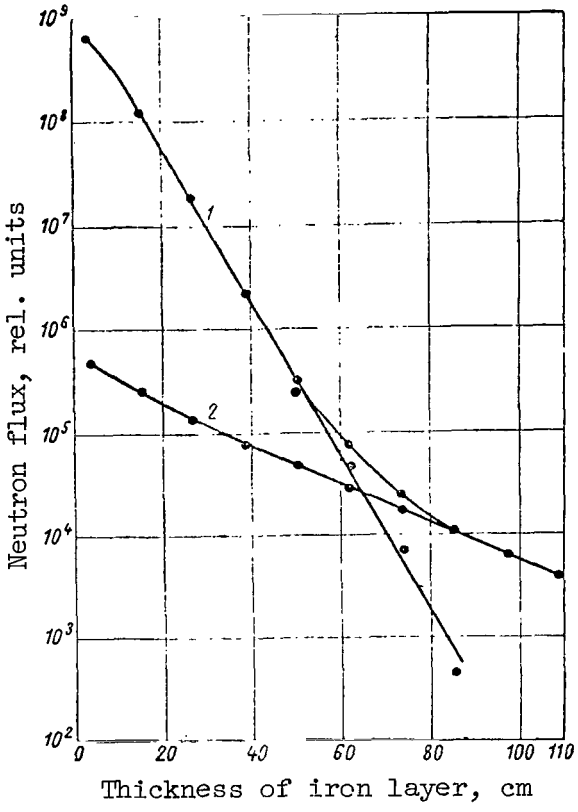

Figure 3. Attenuation of neutron fluxes in direction of central beam in iron prism from experimental data: 1, with aluminum threshold tracers; 2, with thermal and intermediate neutron detector.

Continuing the region due to the activation by intermediate neutrons, in the direction $r < 90$ cm (fig. 3, curve 2) in accordance with data from the measurement of intermediate neutron fluxes, and subtracting the values on curve 2 from the corresponding experimental points on curve 1, we obtain a curve for the attenuation of fast neutron fluxes.

The measurement of fast neutron flux attenuation for $r > 85$ cm requires aluminum tracers with a smaller addition of Na^{23}. The same method was used in reference 4 to introduce a correction for the activation of the detector according to the associated reactions and during measurements in directions perpendicular to the central beam.

This example illustrates how the difficulties which are encountered can be bypassed by using threshold tracers for the measurement of fast neutron fluxes in the presence of a strong background of intermediate energy neutrons.

In spite of a certain complexity associated with our method it must be used frequently, because the threshold tracers have definite advantages, /281 the basic ones being insensitivity to γ-rays and simplicity of operation.

The author expresses his deepest gratitude to O. I. Leypunskiy and S. G. Tsypin for valuable advice during the discussion of the present work and to Yu. K. Yermakov who participated in taking the measurements.

REFERENCES

1. Dulin, V. A. et al. Atomnaya Energiya, Vol. 9, 318, 1960.

2. Broder, D. L. et al. Atomnaya Energiya, Vol. 7, 313, 1959.

3. Price, B. Recording of Nuclear Radiations (Registratsiya yadernogo izlucheniya). Moscow, Izd-vo I. L., 1960.

4. Mashkovich, V. P. and Tsypin, S. G. Atomnaya Energiya, Vol. 11, 251, 1961.

5. Larichev, A. V. and Cherevatenko, G. A. The Investigation of the Sensitivity of a Single Crystal Scintillation Spectrometer with NaJ (Tl) 80 x 80 mm Crystal. IN: Instruments and Methods of Analyzing Radiations (Issledovaniye chustvitel'nosti odnokristal'nogo stsintillyatsionnogo spektrometra s krystallom NaJ (Tl) 80 x 80 mm. V sb.: Pribory i metody analiza izlucheniy, No. 3). Moscow, Gosatomizdat, 1962.

APPLICATION OF RANDOM SAMPLING TO THE COMPUTATION OF SPECTROMETER CHARACTERISTICS FOR GAMMA-RADIATION AND FAST NEUTRONS

V. N. Avayev, Yu. A. Yegorov and Yu. V. Orlov

The study of continuous γ-radiation and neutron spectra can be carried out most conveniently by using scintillation γ-radiation spectrometers with total absorption of γ-quanta energy, i.e., spectrometers with a scintillator of large dimensions (ref. 1) and spectrometers of fast neutrons with a single sensor (ref. 2). Spectrometers of γ-radiation with crystals of large dimensions have a series of definite advantages compared to scintillation spectrometers of other types; however, their basic advantage is that with the high effectiveness of recording γ-quanta the magnitude of photocontribution is rather large. In spite of the small effectiveness of the fast neutron spectrometer described in reference 2, it is convenient for taking measurements, because it has only one sensor and does not require the collimation of the neutron flux. The processing of measurement results obtained by spectrometers is possible, if we know the form of the instrument lines of the monochromatic radiations for a series of energy values and the variation in the effectiveness as a function of γ-radiation and neutron energy. In the case of the scintillation γ-spectrometer in the range of γ-quanta energies from approximately 100 KeV to 3 MeV, the form of the instrument line and the effectiveness may be determined experimentally (ref. 3) by measuring the γ-spectra of the radioactive sources of γ-radiation (Ce^{141}, Hg^{203}, Cs^{137}, Zr^{95}, Zn^{65}, Na^{24} and others). On the other hand, for large γ-radiation and fast neutron energies the experimental determination of effectiveness and of the form of the line is associated with great difficulties. The calculation of these quantities for both spectrometers may be carried out by the method of random sampling (Monte Carlo method). Below we consider this method of computing the characteristics of spectrometers (refs. 4 and 5). /281

To make the analysis simple we shall solve the plane problem in both cases, i.e., we shall assume that all of the scattering and absorption processes take place in the xy plane. The solution of the three-dimensional problem does not differ in principle from the solution of the plane problem.

Computation of the γ-spectrometer Characteristics

Let us assume that a collimated flux of γ-quanta with energy E_0 falls on the axis of a cylindrical scintillator with diameter D and height H. Let us

consider the "fate" of one γ-quantum which has entered the scintillator. We determine the coordinate of the first interaction of γ-quantum with the material of the scintillator, l_0, from the equation

$$l_0 = \frac{1}{\mu(E_0)} \ln \frac{1}{1-y_1}, \tag{1}$$

where $\mu(E_0)$ is the total linear attenuation coefficient of γ-radiation /282

by the scintillator material; y_1 is the first random number (ref. 6) and $0 \leq y_1 \leq 1$.

If $l_0 \leq H$, the γ-quantum has interacted with the scintillator; if, on the other hand, $l_0 > H$, the γ-quantum has gone beyond the limits of the scintillator. Let us assume that $l_0 \leq H$, i.e., that the γ-quantum has interacted with the scintillator. Sine the γ-quantum may interact with this scintillator by one of three processes (photoeffect, Compton effect and the effect associated with the formation of pairs), we now determine the interaction process which has taken place. For this purpose we compare the random number y_2 with the probability that a particular process of interaction has taken place

$$0 \leq y_2 \leq \frac{\tau(E_0)}{\mu(E_0)}; \tag{2}$$

$$\frac{\tau(E_0)}{\mu(E_0)} < y_2 \leq \frac{\tau(E_0)+\sigma(E_0)}{\mu(E_0)}; \tag{3}$$

$$\frac{\tau(E_0)+\sigma(E_0)}{\mu(E_0)} < y_2 \leq 1, \tag{4}$$

where $\tau(E_0)$ and $\sigma(E_0)$ are the linear attenuation coefficients of γ-radiation due to the photoeffect and to Compton scattering, respectively.

If inequality (2) is satisfied we have absorption of the γ-quantum as a result of the photoeffect; if inequality (3) is satisfied we have Compton scattering of the γ-quantum, and finally, if (4) is satisfied the γ-quantum has formed a pair.

Let us assume that inequality (3) is satisfied, i.e., that scattering has occured. Let us determine energy E_1 of the scattered γ-quantum

$$y_3 = \int_{E_1}^{E_0} \frac{d\sigma}{dE_1} \frac{dE_1}{\sigma(E_0)}, \tag{5}$$

where y_3 is the third random number; $d\sigma/dE^1$ is the differential Klein-Nishin-Tam cross section for the electrons.

From the known relationships we now determine the angles ϑ and φ for the scattering of the electron and of the γ-quantum, respectively. The γ-quantum scattered in the direction φ is again considered as the γ-quantum of the source, but this time with an energy E_1. We determine the energy for the recoil electron $\acute{E}_e = E_0 = E_1$. Since during the retardation process within the scintillator the electron loses its energy to retardation radiation and ionization, we determine energy E_T, which is lost by the electron for the retardation radiation. For simplicity we assume that this energy E_T is imparted to a single γ-quantum

$$y_4 = \frac{\int_0^{E_T} E'_T \Phi(E_e, E'_T)\, dE'_T}{\left(\frac{dE}{dx}\right)_{\text{ион}} + \left(\frac{dE}{dx}\right)_{\text{рад}}}, \qquad (6)$$

(ион = ion = ionization; рад = rad = radiation)

where $\Phi(E_e, E'_T)$ is the probability for the formation of a γ-quantum of retardation radiation by an electron with energy E_e; $\left(\frac{dE}{dx}\right)_{ion}$ and $\left(\frac{dE}{dx}\right)_{rad}$ are the average ionization and radiation energies lost by the electron during its motion in the scintillator, respectively; y_4 is the fourth random number.

We assume that the quantum with energy E_T moves in the direction of electron motion, i.e., in the direction of angle ϑ, and we consider it as the γ-quantum of the source. On the other hand, the energy of the electron expended by it for ionization is determined as $E_{e_1} = E_e - E_T$. If equation (6) is not satisfied for any values of E_T, we assume that the entire energy of the electron E_e is expended for ionization. Since the path of the electron in the scintillator is complex, in determining the path length we use the assumption proposed in reference 5. According to this the path of the electron is divided into 2 parts: a rectilinear part and a part where the electron may be scattered in any direction. If the length of the rectilinear path is contained within the scintillator, we assume that the electron has not left the limits of the scintillator and that its entire energy is absorbed by the scintillator. If, on the other /283 hand, the rectilinear path is not contained entirely within the scintillator, only part of the energy, proportional to the path in the scintillator, is absorbed.

Let us assume that inequality (2) is satisfied, i.e., the γ-quantum of the source is absorbed by the scintillator as a result of the photoeffect. The electron energy E_e is determined as the difference of energies $E_0 - E_x$, where

E_x is the energy of the characteristic radiation of the scintillator material.

The "fate" of the electron is considered in the same way as the "fate" of the Compton electron, and in this case the direction of electron motion is assumed to coincide with the direction of γ-quantum motion. The direction of characteristic γ-quantum escape is determined from the relationships

$$\vartheta_1 = 360^\circ\ y_5 \text{ and } \varphi = 360^\circ\ y_6. \tag{7}$$

The point at which the photoeffect has taken place is considered to be the point where the quantum of characteristic radiation has formed. We consider the characteristic γ-quantum as a source γ-quantum.

If the γ-quantum has formed a pair, we determine the positron energy E_n using the random number y_7

$$y_7 = \frac{\int_{m_0c^2}^{E_n+m_0c^2} \Phi(E_n')\,dE_n'}{\varkappa(E_0)}, \tag{8}$$

where $\Phi(E_n')$ is the probability that a positron with energy E_n' has been formed.

The electron energy is determined from the expression

$$E_e = E_0 - E_n - 1.02 \text{ MeV}. \tag{9}$$

The direction of electron and positron motion is assumed to coincide with the direction of γ-quantum motion. The "fate" of the electron and of the positron until the latter is annihilated is considered in the same way as the "fate" of the Compton electron. The point at which the positron is annihilated is considered to be the end of its rectilinear path, and the emerging annihilation γ-quanta are considered as the source γ-quanta. The escape direction of a single annihilation γ-quantum is determined from expression (7), whereas the other γ-quantum is considered to move in the opposite direction.

Thus the motion of the source γ-quanta in the scintillator and the motion of its scattering products are considered successively until they are either absorbed in the crystal or leave its limits. For each source γ-quantum the portion of energy used up for ionization as a result of the secondary processes is determined. A calculation of this type is repeated for a large number of source γ-quanta.

The results obtained in this manner are used to construct the computed spectra--histograms, which characterize the resolution of the spectrometer (without taking into account the physical resolution due to the resolution of the scintillator and the photomultiplier). A comparison of the number of "absorbed" γ-quanta with the number of considered γ-quanta determines the effectiveness of the spectrometer.

In order to obtain histograms which accurately reflect the true picture of resolution and effectiveness of the γ-spectrometer it is necessary to consider large number of source γ-quanta. Such computations are usually carried out by electronic computers. The method described above is used for programming. However, it is not always possible to carry out the computations on the computer for scintillators of different dimensions and compositions as well as for γ-quanta of different energies. Having carried out the computation for a scintillator of one composition and of certain dimensions, the results may be extended to scintillators of other dimensions and compositions. However, for a more accurate extrapolation it is necessary to make a trial calculation (even if this has to be done manually). In order to simplify this problem we consider the case of a two-dimensional scintillator. Manual calculation is also carried out by means of the methodology which has been described. Graphs and nomograms may be constructed to accelerate and simplify calculations by /286 means of the above equations.

Let us consider the successive steps of computing the characteristics of a γ-spectrometer with a NaJ(Tl) crystal by means of graphs. The point of first γ-quantum interaction with the scintillator material may be determined from nomogram No. 1 (fig. 1). The numbers on the curves correspond to the initial energy of the γ-quantum. The three-zone nomogram (fig. 2) is used to determine the form of interaction for a given γ-quantum energy. If a photoeffect has taken place the absorbed energy is determined as $E_e = E_\gamma - 30$ keV, where 30 keV is the energy of the characteristic iodine radiation (we neglect the characteristic radiation of sodium). If Compton scattering has occured, nomogram No. 3 (fig. 3) is used to determine the energy of the scattered γ-quantum. The angle of scattering is computed. If there has been a pair formation, then nomogram No. 4 (fig. 4) is used to determine the positron energy, and expression (9) is used to determine the electron energy. If the electron and positron energy is greater than 1 MeV, the energy of the retardation radiation quantum is determined (fig. 5). The motion of secondary γ-radiation and of multiple scattered radiation is considered by means of these nomograms.

The same type of nomogram can be constructed for the CsJ(Tl) crystal, while nomograms Nos. 3 and 4 (figs. 3 and 4) remain unchanged.

Figure 6, for example, shows the histogram for the CsJ(Tl) crystal with a diameter and height of 80 mm, computed manually with the aid of nomograms for γ-quanta with an energy of 7.6 MeV. The histogram obtained in the same manner for γ-quanta with energies of $E_\gamma = 1$ MeV and for a NaJ(Tl) crystal with a diameter and height of 80 mm is shown in figure 7. The additional maxima are clearly traced on the histograms.

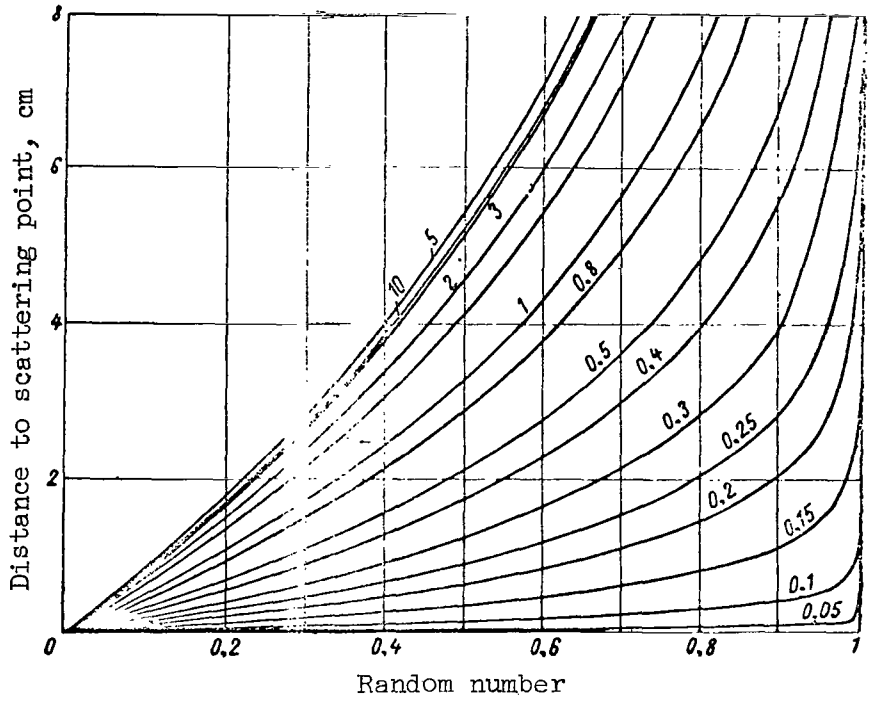

Figure 1. Nomogram No. 1, determination of point of first γ-quantum interaction with scintillator material.

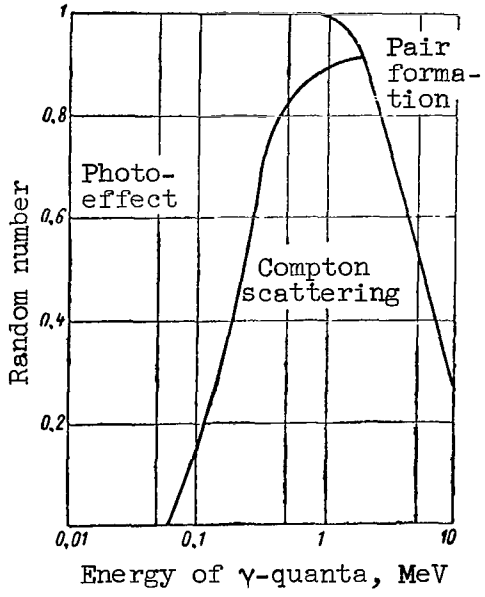

Figure 2. Nomogram No. 2, determination of γ-quanta interaction with scintillator material.

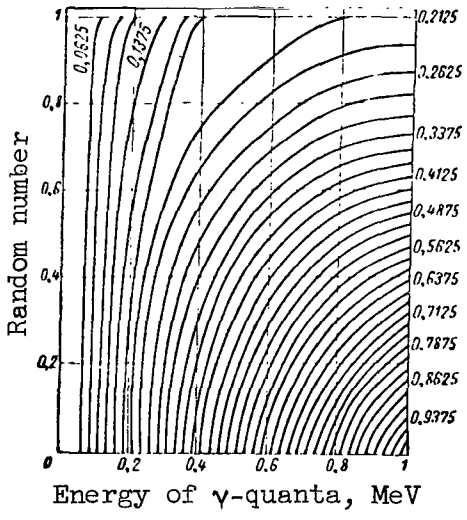

Figure 3. Nomogram No. 3, determination of scattered γ-quantum energy.

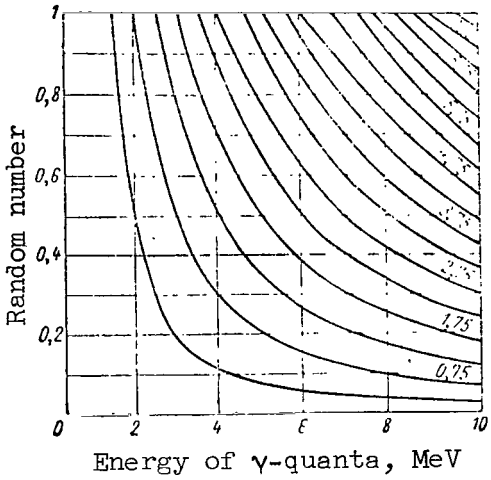

Figure 4. Nomogram No. 4, determination of positron energy.

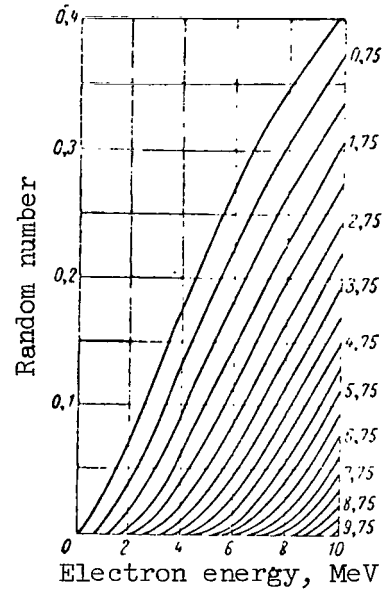

Figure 5. Nomogram No. 5, determination of retardation radiation quantum energy.

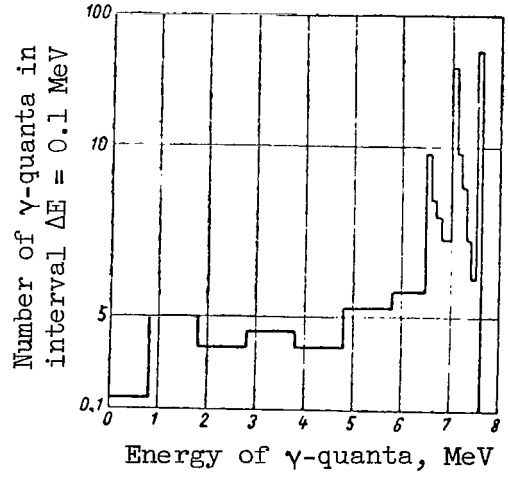

Figure 6. Histogram for γ-quanta with energies of 7.6 MeV computed by nomograms for CsJ(Tl) crystal (crystal diameter and height, 80 mm).

Obviously manual calculations do not give the necessary accuracy; however, the accuracy is quite sufficient, for example, for determining the magnitude of the photocontribution. Indeed a comparison of results obtained manually with the results presented in reference 7 shows fairly good agreement (fig. 8).

Calculation of Neutron Spectrometer Characteristics

The scintillator of the fast neutron spectrometer with a single sensor always contains materials with hydrogen and boron. The source neutrons, which undergo multiple scattering by hydrogen nuclei, produce a light pulse which is proportional to the neutron energy in magnitude. If the neutron energy is rather small after scattering, the neutron is captured by boronwhich results in a second light pulse due to the absorption of α-particles produced in the reaction B (n, α) Li. A certain amount of time elapses between the formation of the proton pulse and of the pulse from the α-particle. If both of these pulses are fed to a circuit with delayed coincidence, we can select from all of the pulses produced by the counter only those produced by neutrons which have lost almost all of their energy in the scintillator. By measuring their amplitude we can determine the energy of the source neutrons. Obviously the delay time plays an important role in the operation of such a spectrometer, because it determines the resolution and effectiveness of the spectrometer.

To determine the effectiveness and resolution of a fast neutron scintillation spectrometer, and also to achieve a rational selection of the delay time, it is necessary to solve a problem which is formulated in the /287

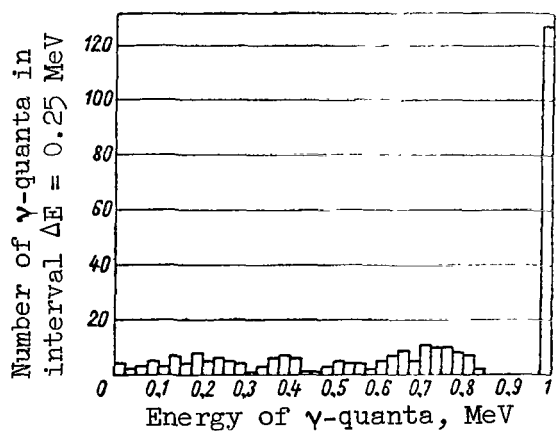

Figure 7. Histogram for γ-quanta with energies of 1 MeV computed by nomograms for NaJ(Tl) crystal (diameter and height, 80 mm).

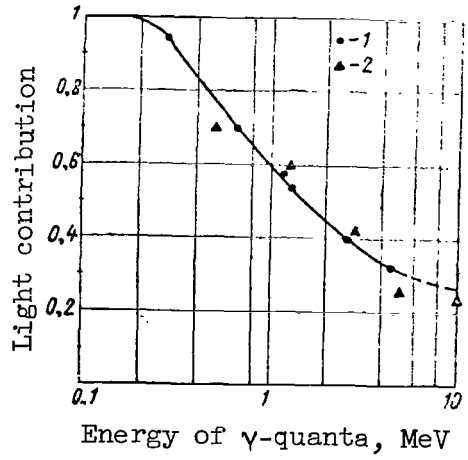

Figure 8. Variation and photocontribution as function of γ-quanta energy for NaJ(Tl) crystal (diameter and height, 80 mm): 1, data presented in reference 7; 2, result of calculations by nomograms.

following manner: a flux of neutrons with energies E_0 falls along the axis of a cylindrical scintillator whose composition includes nuclei of hydrogen, carbon, oxygen and boron; it is required to determine the time t_0 from the instant of the first scattering by hydrogen to the instant when the boron nucleus captures a neutron and to determine the portion of energy lost by the neutron as a result of scattering by hydrogen nuclei, and further to determine the ratio n_b/n_0 where n_0 is the flux of source neutrons, and n_b is the number of neutrons captured by boron after scattering by hydrogen. Since the neutron scattering cross sections by nuclei of hydrogen and carbon are large compared with capture cross sections, and the capture cross section by boron nuclei is large compared with the scattering cross section, we may assume that the hydrogen and carbon nuclei only scatter the neutrons (in view of the fact that $E_0 \leq 10$ MeV the inelastic scattering of neutrons by carbon nuclei need not be considered), whereas the boron nucleus only absorbs them. At the same time the scattering and absorption of oxygen by the nuclei need not be considered, because the total cross section of oxygen is small compared with the cross sections of hydrogen, carbon and boron.

The first operation in obtaining the solution is accomplished according to equation (1), except that we must use $\Sigma(E_0)$ in place of $\mu(E_0)$, i.e., we must use the total cross section of neutron interaction with the scintillator material. Having determined t_0 from the number y_2 (ref. 6), we determine the nucleus with which the neutron interacts the first time. When

$$0 \leq y_2 \leq \frac{\Sigma_H(E_0)}{\Sigma_H(E_0) + \Sigma_c(E_0) + \Sigma_B(E_0)}, \tag{10}$$

(H = hydrogen; B = boron)

the neutron is scattered by hydrogen; when

$$\frac{\Sigma_H(E_0)}{\Sigma_H(E_0) + \Sigma_c(E_0) + \Sigma_B(E_0)} < y_2 \leq \frac{\Sigma_H(E_0) + \Sigma_c(E_0)}{\Sigma_H(E_0) + \Sigma_c(E_0) + \Sigma_B(E_0)}, \tag{11}$$

the neutron is scattered by carbon and when

$$\frac{\Sigma_H(E_0) + \Sigma_c(E_0)}{\Sigma_H(E_0) + \Sigma_c(E_0) + \Sigma_B(E_0)} < y_2 \leq 1 \tag{12}$$

the neutron is absorbed by the boron nucleus.

We use the random number y_3 to determine the scattering angle ϑ when a neutron is scattered by hydrogen

$$\vartheta = \frac{\arccos(1 - 2y_3)}{2} \tag{13}$$

and by carbon

$$\vartheta = \arccos(1 - 2y_3). \tag{14}$$

Knowing the scattering angle ϑ, we determine the neutron energy after scattering. For scattering by hydrogen

$$E_1 = E_0 \cos^2\vartheta \tag{15}$$

and by carbon

$$E_1 = 1/12 E_0 (1.72 + 0.23 \cos\vartheta). \tag{16}$$

If we assume that scattering is symmetric, we can determine the azimuthal angle of direction for the scattered neutron from the random number y_4

$$\varphi = 360^\circ \; y_4 \tag{17}$$

This consideration is continued until the neutron leaves the cell or is absorbed by boron. For the scattering of neutron by hydrogen we assume that the proton recoil energy is completely absorbed by the scintillator. For those source neutrons which were absorbed by boron after scattering by hydrogen we find $\sum_i E_{pi}$, which is the total energy of recoil protons, i.e., the portion of neutron energy which is expended to form the proton pulse, and $\sum_i t_i$--the time spent by the neutron during scattering (t = 0 during the first scattering by the hydrogen nucleus), until the time when the nucleus is captured by boron. After computing the number of "useful" cases and knowing n_0--the number of considered cases, we determine the effectiveness of registration $\epsilon = n_b/n_0$. Indeed, the effectiveness of the spectrometer may be determined by the graphic integration of the distribution curve interval for the number of neutrons captured by boron as a function of time within the limits of resolving time associated with the

/288

coincidence circuit. An interval of width 2τ is selected at the point corresponding to the delay time (τ is the resolving time of the coincidence circuit). The portion of neutron energy expended on the formation of the proton pulse determines the energy resolution of the spectrometer.

The characteristics of the fast neutron scintillation spectrometer must be computed in the same fashion as for the γ-spectrometer utilizing an electronic computer. Manual calculations give us only a general idea concerning the nature of such a spectrometer, but still makes it possible for us to obtain several useful conclusions.

With this purpose in mind a graphic computation was made of spectrometer characteristics manually for a liquid scintillator placed into a cylindrical cell with a diameter and height of 80 mm for neutrons with an energy of $E_0 = 4$ MeV. This scintillator consisted of trimethyl borate mixed with an equal quantity of xylene. The solution of the problem, like the solution of the problem for the γ-spectrometer, utilized graphs constructed from the presented equations. To simplify the calculations it was assumed that the neutron does not change its direction of motion after second scattering.

The "fate" of 1900 source neutrons was investigated; the number of "useful" cases was 46. The table shows the amplitude distributions of neutron pulses which characterize the resolution of the spectrometer. ΔE_1 is the neutron energy at which the neutron is absorbed by boron, and ΔE_2 is the energy lost by the neutron as a result of scattering by carbon nuclei. It was assumed that in view of the small light output of the scintillator, when it is excited by carbon recoil nuclei, the amplitude of the light signal is determined only by the absorption of recoil neutron energy, i.e., the loss of neutron energy as a result of scattering by carbon nuclei takes place in a "useless" fashion.

From the table we can see that $\Delta E_1 + \Delta E_2$ is small compared with the neutron energy E_0 of the source, i.e., the natural resolution of the spectrometer due to its principle of operation is small. Consequently the spectrometer resolution is basically determined by the resolution of the scintillator and the resolution of the photomultiplier. This conclusion, in particular, points to the definite advantages of a fast neutron spectrometer with a single sensor: the processing of measurement results is simplified, because the operation for transforming from recoil proton energy distribution into neutron energy distribution is dropped. The variation in the number of neutrons absorbed by

$(\Delta E_1 + \Delta E_2)$, eV	0—100	100—10^3	10^3—10^4	10^4—$5\cdot10^4$	$5\cdot10^4$—10^5	10^5—$1{,}5\cdot10^5$	$1{,}5\cdot10^5$	$3\cdot10^5$
n	21	7	7	2	4	2	2	1

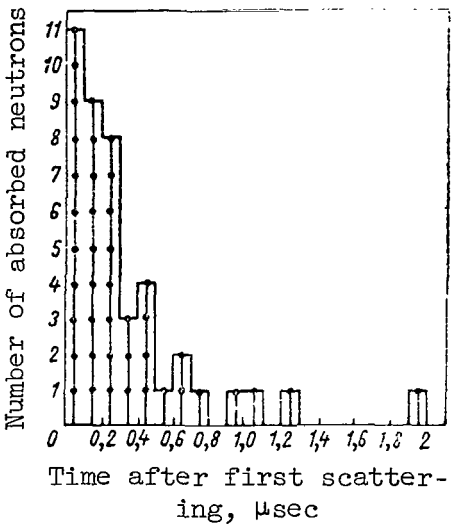

Figure 9. Variation in number of neutrons absorbed by boron in time interval Δt as function of time t_0.

boron in the time interval Δt as a function of the time t_0 (fig. 9) shows that a large part of neutrons is absorbed by boron in a small interval of time after the first scattering by hydrogen. It follows that under the adopted assumptions the magnitude of delay in the spectrometer control channel must not be large.

The results which we obtained were compared with results obtained by computations carried out by means of an electronic computer. Comparisons showed that the results of manual calculations, even when the number of considered cases is small, make it possible to select rational parameters for the spectrometer and agree well with results obtained by means of an electronic computer when a substantially larger number of cases is considered (ref. 8).

The authors express their gratitude to V. N. Ignatenko for carrying out the calculations.

REFERENCES

1. Foot, P. S. and Koch, H. W. Rev. Scient. Instrum., Vol. 25, 746, 1954.

2. Marshall, R. S. Phys. Rev., Vol. 89, 896, 1953.

3. Kazanskiy, Yu. A. Priobory i Tekhnika Eksperimenta, No. 4, 32, 1959.

4. Kahn, H. Nucleonics, Vol. 6, No. 3, 27, 1950.

5. Buslenko, N. P. and Shreyder, Yu. A. The Method of Statistical Tests (Metod statisticheskikh ispytaniy). Moscow, Fizmatgiz, 1961.

6. Kendall, M. C. and Smith, B. B. Tracts for Computers, p. 24, 1939.

7. Berger, M. J. and Doggett, J. J. Res. Nat. Bur. Standards, Vol. 56, 355, 1956.

8. Avayev, V. N. et al. P. 428 of this volume.

CALCULATION AND ANALYSIS OF THE CHARACTERISTICS OF A SPECTROMETER WITH BORON-HYDROGEN SCINTILLATOR

V. N. Avayev, Yu. A. Yegorov, Yu. V. Orlov, A. S. Frolov and N. N. Chentsov

The measurement of neutron energy is one of the most difficult problems of nuclear spectrometry. Neutrons produce almost no ionization and therefore can be detected only by recording the secondary particles formed as a result of neutron interaction with matter. As a rule, neutron energy is determined from the measurement of secondary particle energy. The measurement of neutron energy is further complicated, if the flux of investigated neutrons is accompanied by γ-radiation. /289

There are several methods for determining the energy of fast neutrons. The method of recoil nuclei is most common, apparently because it has the smallest number of disadvantages compared with other methods. Indeed, the method of radioactive tracers, for example, makes it possible to determine the spectrum only qualitatively; the method of nuclear reactions is difficult, while the method of flight time has been used only with pulse neutron sources (ref. 1) to date.

Scintillation spectrometers occupy a special place in the method of recoil nuclei, because they have sufficiently high effectiveness and good energy resolution. Furthermore, the results of measurements are processed rather easily and complex electronic circuits are not required.

Fast neutron scintillation spectrometers with two sensors are most common. One of these sensors produces a pulse whose amplitude is proportional to the recoil proton energy, and the other sensor records the neutron scattering angle (refs. 2-6). The source neutron energy is determined from the relationship $E_n = kU_p/\sin^2 \vartheta$, where U_p is the pulse amplitude proportional to the recoil proton energy when such protons are formed by the scattering of neutrons over an angle ϑ; k is the factor of proportionality.

The elimination of background γ-radiation, when measurements are taken with such spectrometers, is achieved by utilizing "delayed" coincidences. Fast neutron spectrometers with two sensors are used to measure the spectra of various sources and also to measure the spectra of nuclear reactors (ref. 7). /290 However, according to their principle of action spectrometers with two sensors

can operate only when the flux of neutrons is collimated. Obviously this situation limits the number of problems which can be solved by means of a spectrometer with two sensors or requires multiple measurements over different angles. This approach must be used, for example, when measuring fast neutron spectra behind the shielding.

In recent times wide use has been made of spectrometers with a single hydrogen-containing sensor; the discrimination against background γ-radiation in such spectrometers is achieved as a result of time difference in the de-excitation of the scintillator, when it is excited by protons and by electrons (refs. 8-12). Spectrometers with a single hydrogen-containing sensor may operate without a collimator. The lower boundary of the measurable proton energy is usually less than 0.7 MeV. Spectrometers with a hydrogen-containing sensor are also used for various measurements. However, it is not possible to use such spectrometers for taking measurements in the presence of background γ-radiation (ref. 13).

Spectrometer with a Boron-Hydrogen Scintillator

Reference 14 proposes a scintillation spectrometer with a single sensor whose scintillator contains hydrogen and boron. Results have been communicated for the case of a cylindrical vessel (with a height and diameter of 50 mm), filled with a mixture consisting of equal volumes of phenylcyclohexane and methyl borate, activated with 3 g/liter of terphenyl and 10 mg of diphenyl hexatriene per 1 kg of mixture. For neutron energy of 14 MeV the effectiveness of the spectrometer with such a sensor was 0.15 percent, and the energy resolution was 10 percent.

On the basis of the short description presented in reference 14, we envision the following block diagram (fig. 1) and operating principle of the spectrometer with the boron-hydrogen scintillator. The fast source neutrons which enter scintillator S as a result of single scattering by an angle close to 90°, or as a result of several scatterings by hydrogen nuclei, become slow neutrons and are captured by the boron nuclei. The recoil protons formed as a result of these processes produce a pulse whose amplitude is proportional to the energy of source neutrons, while the α-particles from the reaction $B^{10} + n \rightarrow Li^{7} + \alpha$ create a second pulse, i.e., each neutron recorded by the spectrometer produces 2 pulses such that there is a certain delay between the appearance of the first (proton) pulse and the second pulse (due to α-particle).

The signal from the sensor of the photoelectron multiplier is transmitted along two channels, the principal channel and the control channel. In the control channel the signal travels along two circuits to a coincidence circuit CC, with a delay line DL connected to one of the circuits. The delay time is selected in such a way that the proton pulse and the pulse from the α-particle arrive at the coincidence circuit at the same time. If coincidence occurs, the control single flip-flop oscillator CSFFO is triggered. The signal in the principal channel passes through delay line DL, amplifier A and the electronic gage EG and then is fed to the pulse amplitude analyzer PAA. As we can see the circuit must be constructed in such a way that only those source neutrons which have transmitted all or almost all of their energy to the scintillator are recorded.

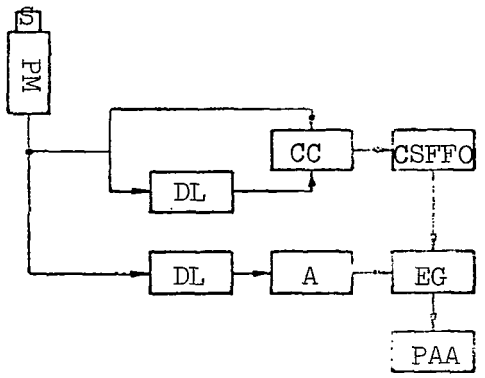

Figure 1. Block diagram of scintillation spectrometer with boron-hydrogen scintillator. A, amplifier; CC, coincidence circuit; PM, photomultiplier; CSFFO, control single flip-flop oscillator; DL, delay line; S, scintillator; EG, electronic gate; PAA, pulse amplitude analyzer.

The basic quantity which determines the operation of the spectrometer /291 is the delay in the circuit of the spectrometer control channel.

According to data presented in reference 14 (E_{n0} = 14 MeV), the average interval between the instant of proton pulse appearance and the appearance of the pulse from the α-particle is equal to two μsec when the scintillator utilizes natural boron (18.8 percent B^{10}) and is approximately 0.25 μsec when the scintillator utilizes boron enriched to 94 percent with the B^{10} isotope.

By considering the principle of operation of the spectrometer with boron-hydrogen scintillator we can see that the spectrometer may operate without a collimated neutron beam; the processing of measurement results with such a spectrometer is very simple; in essence it is only necessary to introduce a correction for the effectiveness. The lower limit of measured neutron energies may be small, at any rate lower than the limit for a spectrometer with a single hydrogen-containing sensor or for a spectrometer with the LiJ (Eu) crystal (ref. 15).

These advantages of the spectrometer make it a useful device for the study of spectra associated with the penetration of fast neutrons through various shielding materials under conditions of barrier and "infinite" geometry. However, the existing literature does not present the necessary data to construct such a spectrometer. The following quantities remain unknown:

(1) the variation in the effectiveness of the spectrometer as a function of neutron energy;

(2) the variation in the effectiveness as a function of scintillator volume and the relationships for hydrogen and boron concentration;

(3) the time distribution of pulses from α-particles (when time is measured from the instant of the first neutron scattering);

(4) the variation in the energy resolution of the spectrometer as a function of neutron energy.

For this reason an effort has been made to compute these quantities manually by the Monte Carlo method (ref. 16). The results of this calculation have made it possible to draw several useful conclusions and to begin the design of the spectrometer.

However, the results of manual calculations did not include the total spectrometer characteristics and did not make it possible to select the necessary parameters for the electronic circuits of the spectrometer (delay time, resolution time of the coincidence circuit). The use of the manual approach to obtain more detailed information is associated with large time expenditures, and for this reason the detailed calculations for the characteristics of the spectrometer were carried out by means of an electronic computer.

Formulation of the Problem for the Calculation

The scintillator consists of a sphere with a diameter D or a cylinder with a diameter and height D. The scintillator contains materials consisting of hydrogen, carbon and boron. The presence of oxygen nuclei is neglected (ref. 16). A neutron flux with energy E is directed along the diameter of the sphere (or along the axis of the cylinder). To simplify the problem it is assumed that: (1) the scattering of neutrons by hydrogen and carbon nuclei in the system of the inertia center is isotropic; (2) a neutron which is moderated to an energy of 0.025 eV does not change its energy in the future; (3) the cross section of neutron absorption by boron nuclei in the energy range from 0.025 eV to 10 MeV varies according to the law $1/\sqrt{E}$.

The problem consisted of determining the following quantities:

the probability of neutron absorption by boron nucleus after scattering by hydrogen and carbon nuclei;

the time from the instant of the first neutron scattering by hydrogen to the time when the neutron is absorbed by the boron nucleus;

the neutron energy at the instant of its absorption by the boron nucleus (for neutrons which have first interacted with hydrogen or carbon nuclei);

the portion of neutron energy lost during scattering by hydrogen nuclei (for neutrons absorbed after such scattering by boron nuclei).

The problem was solved for two scintillator dimensions (diameters of 40 and 80 mm). Three scintillator compositions were considered. These consisted of equal mixtures of the following: /292

(1) xylene (C_8H_{10}) and trimethyl borate [$B(OCH_3)_3$] (unenriched boron);

(2) phenylcyclohexane ($C_{10}H_{16}$) and tri-isobutyl borate [$B(OC_4H_9)_3$];

(3) xylene (C_8H_{10}) and trimethyl borate [$B(OCH_3)_3$] (boron enriched to 80 percent with B^{10}.

For convenience of calculations it was assumed that the third composition differs from the first in the boron concentration. The concentration of element nuclei in the three scintillator compositions is shown in table 1.

TABLE 1. CONCENTRATION OF ELEMENT NUCLEI (cm^{-3}) IN THE THREE SCINTILLATOR COMPOSITIONS.

Element	Composition		
	First	Second	Third
Hydrogen.....	$5.7 \cdot 10^{22}$	$5.7 \cdot 10^{22}$	$6.8 \cdot 10^{22}$
Boron.....	$3 \cdot 10^{21}$	$1.2 \cdot 10^{22}$	$1.26 \cdot 10^{21}$
Carbon.....	$3.3 \cdot 10^{22}$	$3.3 \cdot 10^{22}$	$2.4 \cdot 10^{22}$
Oxygen.....	$2.4 \cdot 10^{22}$	$2.4 \cdot 10^{22}$	$3.78 \cdot 10^{21}$

The problem was solved for several initial neutron energies: 0.5, 1, 2, 4, 6, 8 and 10 MeV.

Computation of Spectrometer Characteristics

As we have already pointed out, the calculation of spectrometer characteristics was carried out by the method of statistical sampling (the Monte Carlo method).

Since the considered process is one without aftereffects, the trajectory of neutrons in the scintillator (fig. 2) was constructed successively as a "chain" of interactions with the nuclei of the scintillator material in a 6th dimensional space (x, y, z, ω, E), where x, y, z are the Cartesian coordinates of the neutron; ω is the direction of neutron motion between interactions and E is the neutron energy.

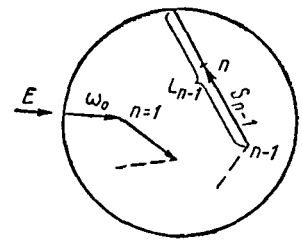

Figure 2. Neutron motion in scintillator.

The effectiveness of the spectrometer u was computed as the mathematical expectation of a certain functional of the neutron trajectory ξ (T)

$$u = M\varphi[\xi(T)]. \tag{1}$$

The other quantities were computed in the same manner. For example, the distribution of neutrons captured by boron nuclei after scattering by hydrogen or carbon nuclei were determined from the following equation according to energy groups R_n (E)

$$R_n(E) = \{r_n^{(i)}(E)\}_{(i=1, 2, \ldots, i_{fin})}, \tag{2}$$

where $r_n^{(i)} = M\psi^{(i)}[\xi(T)]$; i is the number of the energy interval, the number of intervals being equal to i_{fin}.

In selecting the mathematical model of the process in the scintillator it was noted that the overwhelming portion of the incident neutron flux leaves the volume of the scintillator without interacting with its substance at all, or without being captured by boron nuclei after scattering (ref. 17). Therefore, in order to "read" the maximum information from each trajectory and not to play up the "parasitic" histories, the motion of the neutron "packet" was modeled according to the "arbitrary escape" scheme, i.e., particles with a certain mass were considered. During each collision with the nucleus of the scintillator substance, such a particle is scattered in accordance with the usual law of neutron scattering, while its motion is always strictly within the volume of the scintillator (fig. 2). /293

Let us follow the transition of a particle in our model from the (n-1)-th position to the n-th position along the played direction ω_{n-1}. As we know, the mean free path of a neutron is distributed according to the law

$$F(S) = e^{-\Sigma_{n-1}S} \tag{3}$$

(Σ_{n-1} is the macrascopic cross section of the scintillator substance when the neutron energy is E_{n-1}; S is the path length of the neutron between collisions).

The probability that the particles will escape beyond the volume of the scintillator without interacting with the nuclei of the scintillator material, while moving along the beam ω_{n-1}, is equal to

$$\Omega_{n-1} = e^{-\Sigma_{n-1} L_{n-1}}, \tag{4}$$

where L_{n-1} is the distance to the boundary of the scintillator from the point of the (n-1)-th scattering (x_{n-1}, y_{n-1}, z_{n-1}) in the direction ω_{n-1}. The free path of a fictitious particle, under conditions when it does not escape beyond the limits of the scintillator, has a distribution given by the arbitrary law

$$P(S) = \frac{e^{-\Sigma_{n-1} S}}{1 - e^{-\Sigma_{n-1} L_{n-1}}}. \tag{5}$$

From collision to collision the fictitious particle losses part of its mass

$$m_n = m_{n-1} \gamma_n (1-\Omega_{n-1}), \tag{6}$$

where γ_n is the probability of scattering during the (n-1)-th collision.

On the basis of these statements we can conclude that the functional φ has the following form

$$\varphi = \sum_{n=1}^{\infty} (1 - \gamma_n) m_{n-1} (1 - \Omega_{n-1}). \tag{7}$$

Here the summation is extended over all of the collisions, while $m_0 = 1$.

Although the trajectory of such an "eternal" particle is infinite, we can "cut if off" at a mass which is less than some assigned value ϵ. The value ϵ is selected in such a way that the dropped mass is within the limits of statistical accuracy of the solution.

The trajectory of a particle is constructed in the following manner.

The Origin of a Particle (n = 0). The initial coordinates of the trajectory are taken as the coordinates of the source (x_{sou}, y_{sou}, z_{sou}), and a direction and initial energy E_0 are assigned to the "packet."

The Motion of the Particle from Collision to Collision. Between collisions n and n-1 the particle with energy E_n moves uniformly and in a rectilinear fashion

along the selected direction ω_n. The probability of particle escape from the system Ω_n is computed and the mean free path length S_n is obtained from the distribution P (S);

The Collision of a Particle. The coordinates of the (n + 1)-th scattering are computed from the coordinates of the n-th scattering (x_n, y_n, z_n) from the vector ω_n and the quantity S_n. After this the quantity γ_{n+1} is computed, and finally the value of particle mass m_{n+1} after the (n + 1)-th collision is computed;

Selection of New Direction and Energy After Collision. The type of nucleus involved in the collision is played out. A new direction of motion is isotropically played out in the system of particle mass center and of this nucleus. This is then recomputed in the direction ω_{n+1}, using the laboratory system of coordinates. The energy losses due to the occurring elastic scattering are determined;

Termination of Trajectory. If $m_{n+1} < \epsilon$, the trajectory ends, i.e., simulation along an assigned trajectory is continued until the mass of the "packet" becomes less than ϵ.

The group of evaluating functionals is recomputed at each collision. The values of these functionals averaged out over the respective number of constructed trajectories make it possible to obtain the following information.

The basic statistic quantities are as follows: /294

u--the true effectiveness of the spectrometer (the effectiveness for neutrons captured by boron nuclei after scattering by hydrogen nuclei);

$\tilde{u}$--evaluation of the second moment of the random quantity u; u is used to compute the guaranteed absolute accuracy of the quantity u (following the law of three root mean square errors);

p--the total portion of neutrons absorbed by the scintillator material, i.e., the total effectiveness of the spectrometer;

ω--the average number of neutrons which have escaped beyond the limits of scintillator volume;

Δ--the schematic error, i.e., the portion of dropped trajectories of low probability; we note that $p + \omega + \Delta = 1$; $n^{(1)}$, $n^{(2)}$, ..., $n^{(29)}$ is the time distribution for the quantities u, i.e., the portion of "effective" (captured

by the boron nucleus even after a single collision with the hydrogen nucleus) neutrons in each interval of time. The time is measured from the moment when a neutron is scattered by the hydrogen nucleus. A standard linear time scale is adopted: each of the intervals from 0 to $t' = 2^{-3}$ μsec and further from $t = 2^k$ to $t = 2^{k+1}$ μsec ($k = -3, -2, \ldots, 2$) is divided into 4 equal intervals. The last interval is 2^3 μsec $\leq t < \infty$. Altogether 29 intervals were considered; $\theta^{(1)}, \theta^{(2)}, \ldots, \theta^{(29)}$ is the energy distribution of "effective" neutrons. The boundaries of the energy intervals are selected according to lethargy. A group of thermal neutrons with lethargy of 20.5 was also isolated.

Additional statistical quantities are as follows:

M--the average number of neutron collisions with the scintillator material nuclei before absorption or escape;

P--the average number of neutron collisions with hydrogen nuclei before absorption or escape;

Q--the average number of neutron collisions with carbon nuclei before absorption or escape ($P + Q = M$);

$w^{(1)}, \ldots, w^{(n)}$--the portion of neutrons which have escaped beyond the limits of the scintillator immediately after the n-th scattering ($n = 1, 2, 3, \ldots$);

n--the average trajectory length of the fictitious particle in the assumed model.

Other quantities were also computed, including the three-dimensional distributions of "effective" neutrons.

As we shall show below, the information which has been obtained made it possible to make a complete judgment on the structure of the investigated physical process and to evaluate the quality of the adopted mathematical model.

We note that the selection of the model and the construction of the specialized program were based on numerical experiments carried out by means of a simple program and also on the results of computations carried out manually (ref. 16).

The accuracy of the calculations was evaluated by the direct method (i.e., by the deviation of the basic quantity u) and by an indirect method (by comparison of successive outputs of numerical information achieved by comparing computations carried out by means of different sensors). The analysis of results shows that the error in the quantity u does not exceed 10-15 percent.

In order to grasp the analytical relationships between the characteristics of the spectrometer, the series of measurements were made dependent (ref. 18). The utilization of dependent tests has made it possible to reduce the vol- /295 ume of the work substantially. Although the random errors in this case are high, the qualitative picture which was obtained was correct, because the computed curves differed from the true curves only in their relative position. We can convince ourselves of this by comparing graphs showing the value u for spectrometers with definite D, computed according to two generators of pseudorandom numbers (table 2). It should be pointed out that the selected model also made it possible to reduce the dispersion substantially and to obtain solutions with a substantially smaller consumption of computer time than in the case of the direct "physical" model.

Block Diagram of the Program

Figure 3 shows the principal block diagram of the program used to carry out the computation of the spectrometer characteristics described above. This diagram also shows the conditions for selecting the methods of processing the information.

Pseudorandom numbers of the type proposed by N. M. Korobov were used in the problem

$$\Xi_{\Gamma, l} = \left\{ \frac{q^{l}}{p} \right\},$$

where Γ is the trajectory number; q_l is the first type root of the modulus p; p, is a simple number; $\{\ \}$ is a symbol showing a split part; l, is the number of the random quantity. Calculations were carried out with two generators of the following numbers:

First generator:	p = 39,983,	q = 3,125.
Second generator:	p = 40,127,	q = 3,125.

The calculation of different versions were carried out using the same sequences of pseudorandom numbers.

TABLE 2. TWO VERSIONS OF THE CALCULATION OF SPECTROMETER EFFECTIVENESS FOR THE FIRST COMPOSITION (D = 80 mm).

Sensor No.	Energy in MeV		
	1	4	10
First.....	0.10355	0.02875	0.007542
Second.....	0.10789	0.03016	0.007696

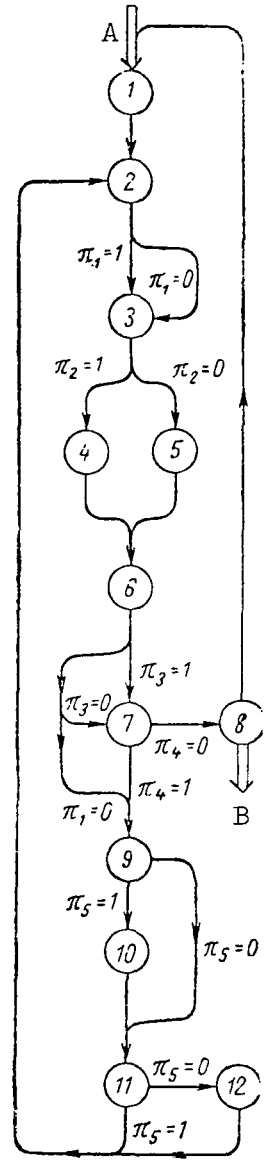

Figure 3. Block diagram of program (the arrows show signal paths); 1, computation of initial trajectory parameters; 2, generation of sequence of pseudorandom numbers; 3, computation of medium parameters and play-out of nucleus type involved in collision; 4, computation of escape probability and play out of mean free path length for spherical scintillator; 5, analogous calculations for cylindrical scintillator; 6, recalculation of functionals which do not depend on type of nucleus and on collision number; 7, recalculation of functionals which depend on

(Continued)

nucleus type and on number of collision as well as determination of trajectory end; 8, processing and readout of information, control of counting process; 9, preparation of numerical parameters for determining new directions and energy; 10, calculation of new energy; 11, calculation of new direction for general case of motion; 12, calculation of new direction for constant energy.

Conditions for selecting information processing paths:

$$\pi_1 = \begin{cases} 1 - n > 1; \\ 0 - n = 1; \end{cases} \quad \pi_2 = \begin{cases} 1 - \text{spherical geometry}; \\ 0 - \text{cylindrical geometry}; \end{cases}$$

$$\pi_3 = \begin{cases} 1 - n > 1, \text{ scattering by H nuclei}; \\ 0 - n > 1, \text{ scattering by H nuclei is absent}; \end{cases}$$

$$\pi_4 = \begin{cases} 1 - q_n > \epsilon; \\ 0 - q_n \leq \epsilon; \end{cases} \quad \pi_5 = \begin{cases} 1 - \text{energy} > \text{threshold} \\ 0 - \text{energy} < \text{threshold} \end{cases}$$

A - start of count; B - end of count.

Analysis of Calculation Results

The results of the calculations make it possible to clarify all of the laws characteristic of a spectrometer with a boron-hydrogen scintillator.

We found that the total effectiveness of the spectrometer (the total number of absorbed neutrons with respect to the neutron flux entering the scintillator) for neutron energies less than 4-5 MeV is described by the following simple relationship within the accuracy of the computations /296

$$\rho = C \frac{D^3}{E}, \tag{8}$$

where E is the neutron energy; D is the scintillator diameter (spherical geometry); C = const, which depends on the composition of the scintillator.

Relationship (8) shows that the effectiveness of the spectrometer is proportional to the scintillator volume. The true effectiveness of the spectrometer u for the same neutron energy, i.e., the ratio of the number of neutrons captured by boron nuclei after even one scattering by hydrogen nucleus to the total flux of neutrons, may be determined by means of equation

$$u = \frac{\Sigma_a D}{E} - (1 - e^{-\Sigma_a D}), \qquad (9)$$

where Σ_a is the macrascopic absorption cross section of neutrons by boron nuclei. Figure 4 shows this relationship for scintillators of two dimensions with different composition. As we can see from the figure, when the scintillator volume is given, the effectiveness increases with the concentration of boron and hydrogen nuclei in the scintillator. For large volume scintillators p differs little from u. Indeed, in this case the second term in the expression for u is of little significance.

For scintillators of smaller dimensions (diameter of 40 mm) the difference between p and u is greater for obvious reasons. At large energies (10 MeV) the discrepancy between p and u is greater than at small energies (1 MeV); in the specified energy interval the effectiveness varies approximately by a factor of 10, and the difference between p and u is obviously associated with a large leakage of neutrons from the volume of the scintillator.

As we can see from the figure, when neutron energies are greater than 4-5 MeV there is a departure from relationships (8) and (9) for all compositions of scintillators with a diameter of 80 mm and for compositions 1 and 3 of scintillators with small dimensions: the effectiveness of the spectrometer decreases with energy and the effectiveness of the scatter-capture process (u) decreases more sharply than p. Obviously this phenomenon is associated with the concentration of boron nuclei and possibly with the concentration of hydrogen nuclei. However, it is difficult to explain this effect without experimental verification.

Figure 4 also shows the results for computing p and u in the case of a cylindrical scintillator (diameter and height of 40 mm).

A comparison of the effectiveness of spectrometers with cylindrical and spherical scintillators shows that the proportionality of effectiveness to scintillator volume is retained so that $p_{cyl} = 1.5\ p_{sph}$ and $u_{cyl} = 1.5\ u_{sph}$, where the subscripts "cyl" and "sph" refer to a cylindrical and a spherical scintillator, respectively. We should note the following. The fact that the spectrometer effectiveness is proportional to the volume (for a given scintillator composition) makes it possible to extrapolate the obtained results very simply to other scintillator dimensions and to carry out computations for scintillators which have the form of a sphere. This is substantially simpler than calculations for cylinders.

The same relationships were obtained in the control calculations for a sphere with a diameter of 80 mm and for a cylinder with a diameter and height of 80 mm.

The results of the calculations have made it possible to clarify certain time relationships for processes in the scintillator, in particular they have made it possible to determine the energy dependence of the volume and concentration of boron nuclei, the value of the interval between the instant of the

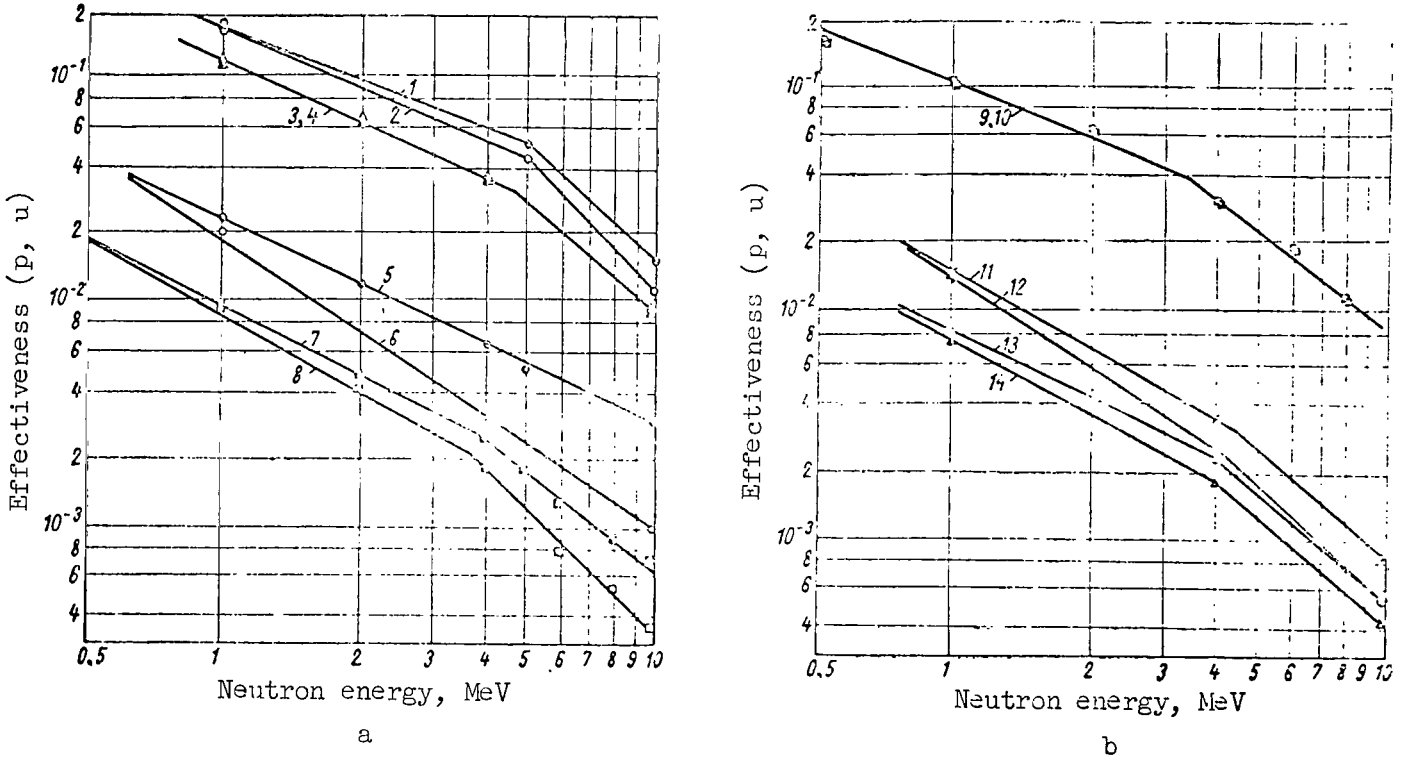

Figure 4. Variation in effectiveness of spectrometer as function of neutron energy:

Curve number, a	Effectiveness	Sphere diameter in mm	Composition number	Curve number, a, b	Effectiveness	Sphere diameter in mm	Composition number	Curve number, b	Effectiveness	Sphere diameter in mm	Composition number
1	p	80	2	6	u	40	2	11	p	Cylinder 40 x 40	1
2	u	80	2	7	p	40	1				
3	p	80	3	8	u	40	1	12	u	40 x 40	1
4	u	80	3	9	p	80	1	13	p	40	3
5	p	40	2	10	u	80	1	14	u	40	3

first scattering by hydrogen nucleus (t = 0) and the instant of such a neutron capture by a boron nucleus.

Thus it was established that for a given scintillator volume and composition the time distribution does not depend on the energy (fig. 5) when $t \leq 0.05$ μsec. (It is possible that the discrepancy at $t < 0.05$ μsec is explained by certain approximations made in the calculations.)

The time distribution varies depending on the scintillator volume (fig. 6) and for a scintillator of large dimensions the scatter-capture processes are separated more uniformly in time than for scintillators of small dimensions. /298

We note that from the point of view of the technical realization of a spectrometer with boron-hydrogen scintillator it is expedient to use a scintillator of large dimensions, because in this case, within the limits of a rational

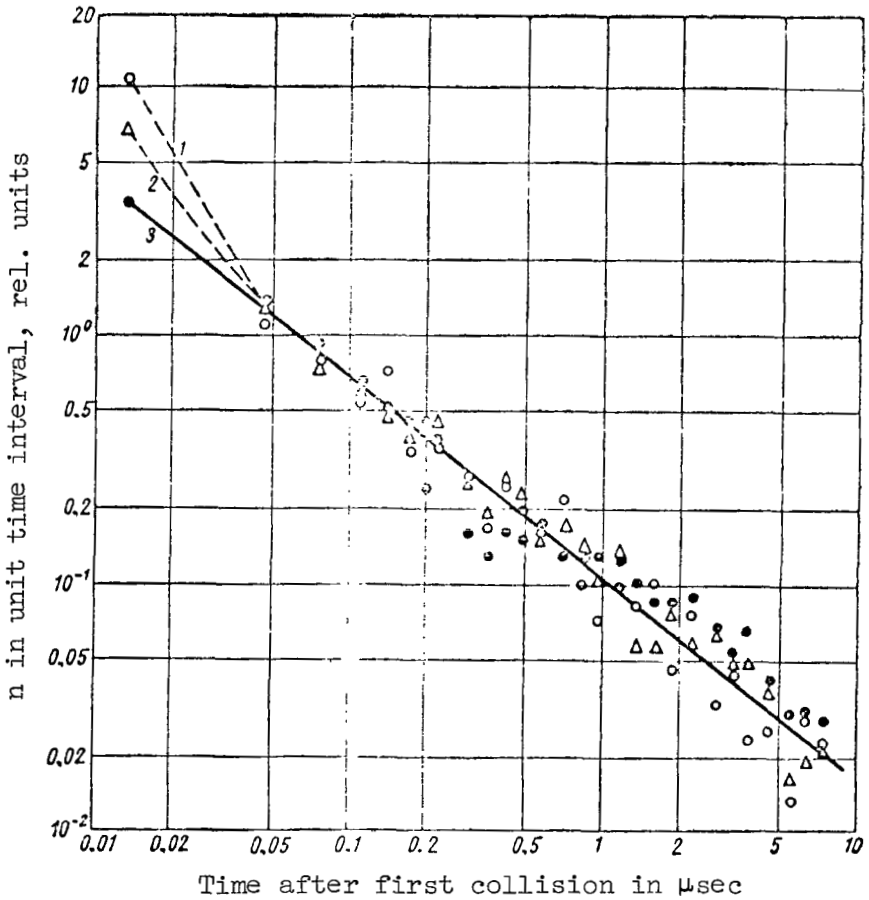

Figure 5. Time distribution of scatter-capture processes n as function of energy: 1, 1 MeV; 2, 4 MeV; 3, 10 MeV. Sphere diameter is 40 mm.

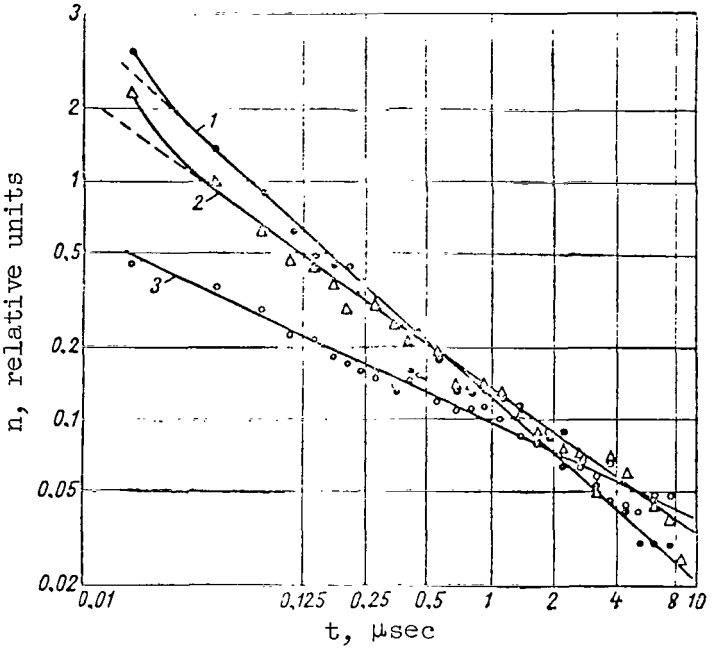

Figure 6. Time distribution of scatter-capture processes n as function of scintillator volume (E_n = 1 MeV): 1, sphere with diameter of 40 mm; 2, cylinder with dimensions 40 × 40 mm; 3, sphere with diameter of 80 mm.

value for the resolution time of the coincidence scheme, the variation in the number of scatter-capture processes as a function of time is less pronounced.

As the concentration of boron in the scintillator is increased, the number of scatter-capture processes in the small intervals of time after scattering increases (figs. 7 and 8), and this is observed for scintillators of small and large dimensions; however, according to the law for scintillators with a diameter of 80 mm, which has been noted earlier, the variation in the time distribution as a function of concentration is less noticeable.

For composition 2 (trimethyl borate with enriched boron) there is a deviation from the linear law for 2 μsec. Apparently this is associated with the high boron concentration and the sharp variation in the magnitude of the time interval.

Figure 9 shows the energy distribution of neutrons which have participated in the scatter-capture processes, normalized for an energy interval of 1 eV. As a rule the overwhelming number of neutrons captured by boron nuclei transmit their energy almost entirely to hydrogen or carbon nuclei before the capture. Consequently the energy resolution of the spectrometer, associated with the principle of its operation, is rather high, and the total /300

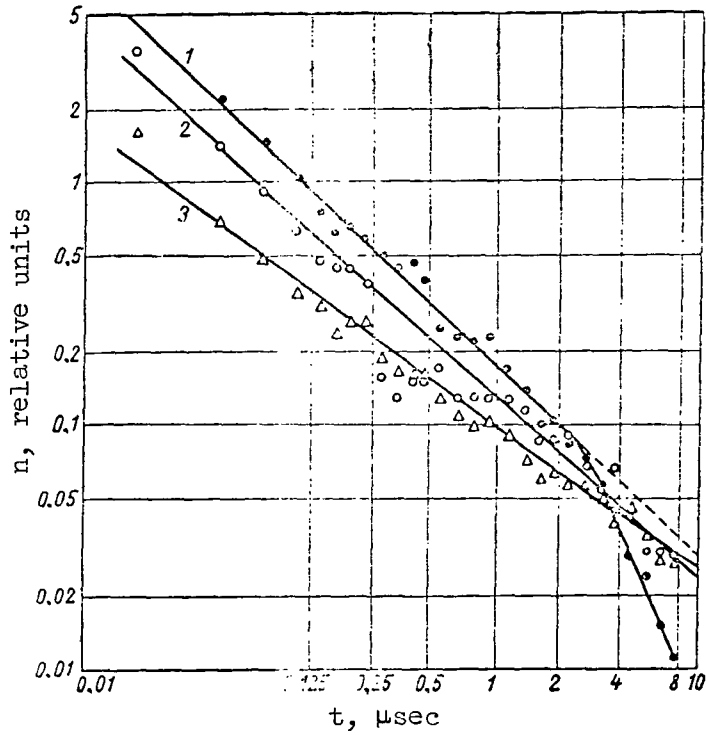

Figure 7. Time distribution of scatter-capture processes n as function of boron concentration in scintillator (sphere diameter of 40 mm): 1, second composition; 2, first composition; 3, third composition.

resolution of the spectrometer is determined by the resolution of the scintillator and of the photomultiplier.

Having clarified the general time characteristics of spectrometers, we shall attempt to evaluate the optimum resolution time of the coincidence circuit and the general electronic circuit of the spectrometer proceeding from real possibilities and from the achievement of maximum recording effectiveness of the scatter-capture events.

Let us assume that in order to achieve a reliable recording of true events the following relationship must exist between the number of false and useful coincidences

$$N_2 = aN_1 \qquad (a < 1). \tag{10}$$

It is known that

$$N_2 = \beta N^2 \tau, \tag{11}$$

where τ is the resolution time of the coincidence circuit; β is the probability that interactions are recorded; N_1 is the number of useful coincidences; N_2 is the number of false coincidences.

At the same time

$$N_1 = ZN, \tag{12}$$

where

$$Z = \sum_i u_i / u_\Sigma,$$

u_i is the number of recordings of the scatter-capture events in the i-th interval of time; summation is carried out from $t = t_0$ (t_0 is the delay time) in the intervals i_1; $i_1 + i_2$; $i_1 + i_2 + i_3$, etc.

As a result of simple transformations we obtain the following expression from equations (10), (11) and (12)

$$N_1 = AZ^2/\tau, \tag{13}$$

where A = const.

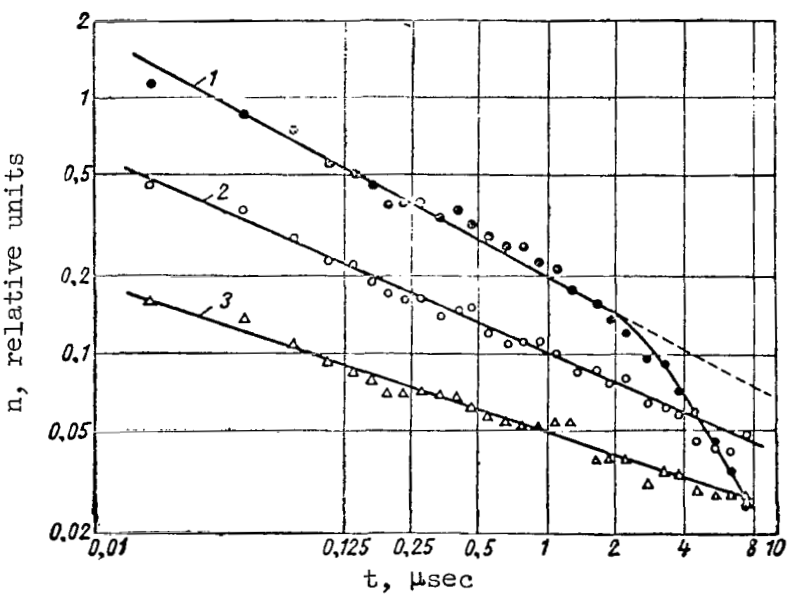

Figure 8. Time distribution of scatter-capture processes n as function of boron concentration in scintillator (sphere diameter of 80 mm): 1, second composition; 2, first composition; 3, third composition.

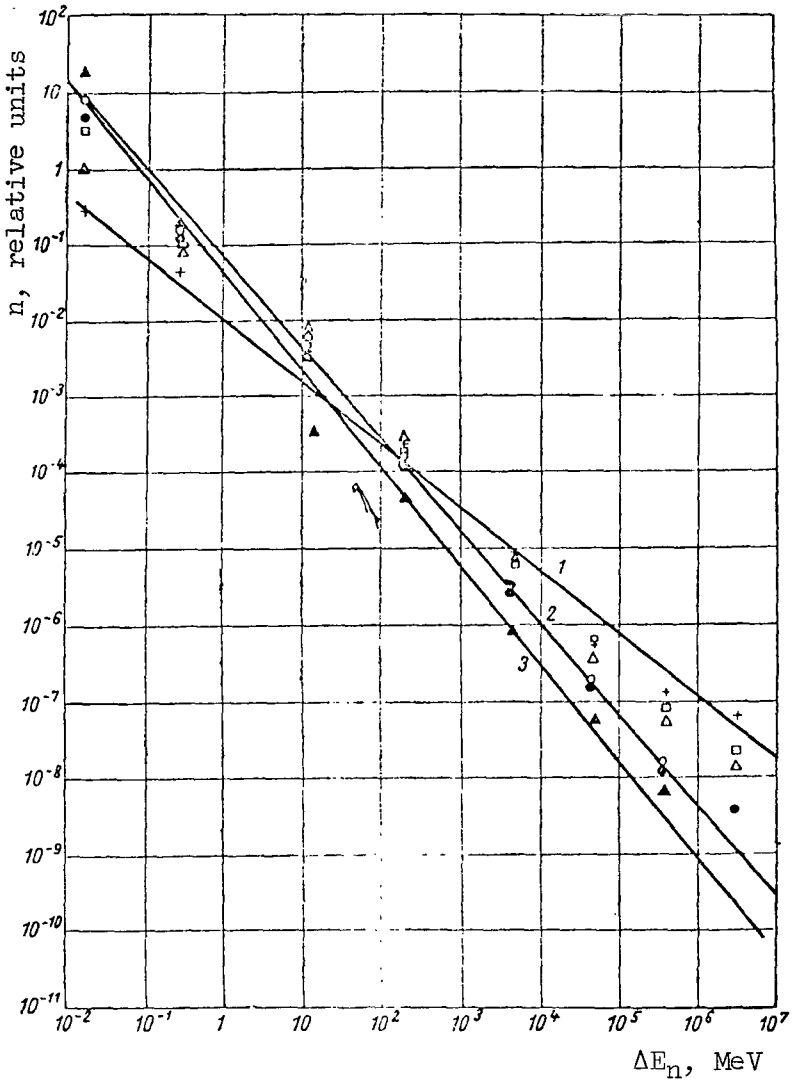

Figure 9. Energy distribution of neutrons n, captured by boron after scattering by hydrogen (normalized for energy interval of 1 eV): 1, second composition; 2, first composition; 3, third composition.

It is clear from this presentation that /301

$$\tau = \sum_{i=1}^{k} \Delta l_i, \quad k = 1, 2, 3, \ldots \tag{14}$$

Assuming that the delay time t_0 is approximately equal to 0.1 μsec, we have carried out calculations by means of equation (13) (fig. 10).

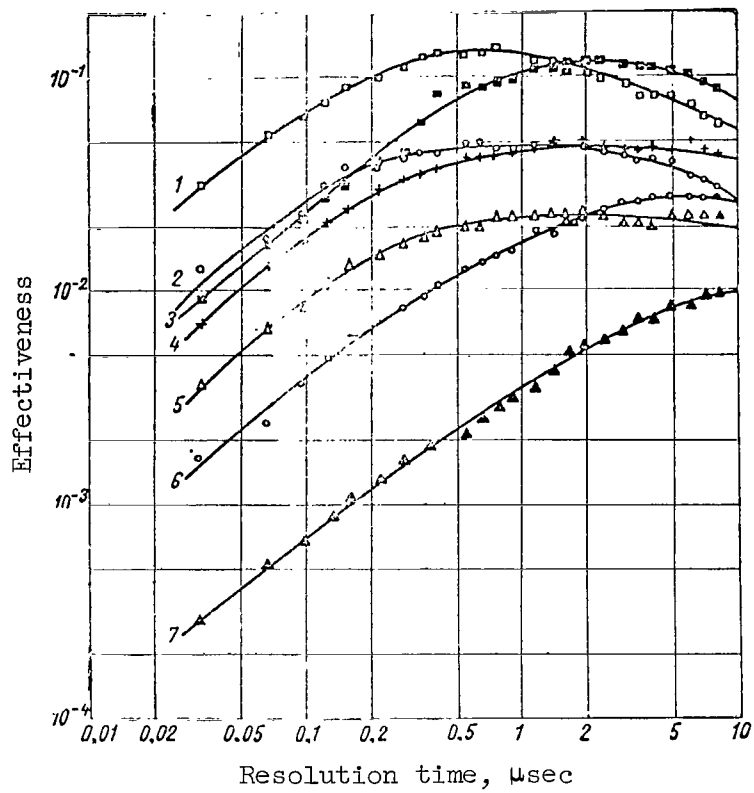

Figure 10. Effectiveness of spectrometer as function of coincidence circuit resolution time:

Curve number	Sphere diameter in mm	Composition number
1	40	2
2	40	1
3	80	2
4	Cylinder 40 × 40	1
5	40	3
6	80	1
7	80	3

By comparing the curves presented in figure 10 we can draw the following conclusions.

1. The effectiveness of the spectrometer as a function of the coincidence circuit resolution time has a maximum whose position is different for scintillators of various dimensions and compositions.

2. The effectiveness of the spectrometer is directly proportional to /302 the concentration of boron nuclei.

3. For scintillators with large boron nuclei concentrations the maximum value of the effectiveness is more clearly pronounced.

4. The maximum value of the effectiveness is less clearly pronounced for scintillators of large volumes.

5. For a cylindrical scintillator the maximum effectiveness is less pronounced than for a spherical one when the diameters of the sphere and the cylinder base are the same and are displaced in the direction of large coincidence circuit resolution time. However, the value of effectiveness at the maximum in this case is the same within the limits of computational error.

The data in figure 10 have been used to determine the maximum permissible fluxes of monochromatic neutrons and the corresponding numbers of useful coincidences. It was assumed in the calculation that A = 1 and that Z corresponds to the maximum value of the curves in figure 10. We found that the fast neutron scintillation spectrometer with boron-hydrogen scintillator can operate only in relatively small neutron fluxes. Thus, when E = 1 MeV, the flux /303 must not exceed (3-4) 10^4 sec^{-1} and when E = 10 MeV, it must not exceed 10^3 sec^{-1}.

Conclusions

The results of calculations and an analysis of characteristics associated with boron-hydrogen scintillator spectrometer have shown that of all the considered compositions the most suitable one is a mixture of equal quantities of

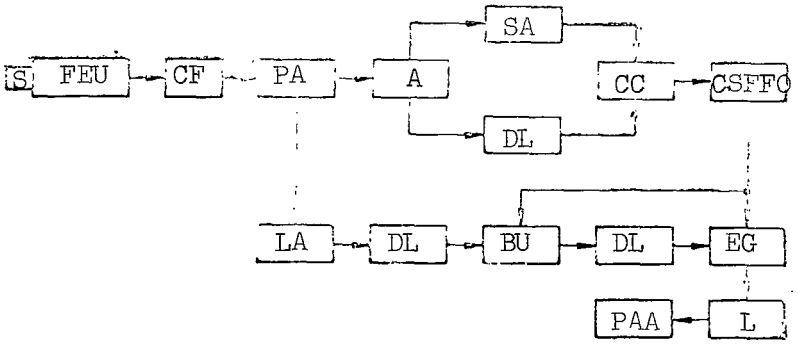

Figure 11. Proposed block diagram for spectrometer with boron-hydrogen scintillator: S, scintillator; CF, cathode follower; FEU, photomultiplier; PA, preamplifier; A, amplifier; LA, linear amplifier; DL, delay line; CC, coincidence circuit; BU, blocking units; EG, electronic gate; SA, single channel pulse amplitude analyzer; CSFFO, control single flip-flop oscillator; L, limiter; PAA, multichannel pulse amplitude analyzer.

xylene or phenylcyclohexane with trimethyl borate with enrichment of B^{10} up to 80 percent, poured into a vessel with a diameter and height of 80 mm. The resolving time of the coincidence circuit in this case must be equal to approximately 1.5 μsec.

Based on these facts the spectrometer block diagram shown in figure 11 has been adopted for developmental work. To decrease the number of random coincidences in the control circuit of the spectrometer a single channel pulse amplitude analyzer has been introduced.

REFERENCES

1. Rybakov, B. V. and Sidorov, V. A. Spectrometry of Fast Neutrons (Spektrometriya bystrykh neytronov). Moscow, Atomizdat, 1958.

2. Beghian, L. and Allen, R. Phys. Rev., Vol. 86, 1044, 1952.

3. Chagnon, P. R., Madancky, L. and Owen, G. E. Rev. Scient. Instrum., Vol. 24, 656, 1953.

4. Gusev, N. G., Yegorov, Yu. A. and Kovering, O. D. Scintillation Spectrometer of Neutrons. IN: Instruments and Methods of Analyzing Radiation (Stsintillyatsionnyy spektrometr neytonov. V sb.: Pribory i metody analiza izlucheniy). Moscow, MIFI, 1957.

5. Draper, J. E. Rev. Scient. Instrum., Vol. 25, 558, 1954.

6. Yegorov, Yu. A. Pribory i Tekhnika Eksperimenta, No. 3, 21, 1958.

7. Yegorov, Yu. A. and Orlov, Yu. V. P. 474 of this volume.

8. Owen, R. B. Trans. I.R.E. PGNS, Vol. 5, 198, 1958.

9. Brooks, F. D. Nucl. Instrum., Vol. 4, 151, 1959.

10. Yegorov, Yu. A. and Pankrat'yev, Yu. V. Inzh-fiz. zh. IV, 112, 1961.

11. Broek, H. W. Rev. Scient. Instrum., Vol. 31, 1063, 1960.

12. Dulin, V. A. et al. Pribory i Tekhnika Eksperimenta, No. 2, 35, 1961.

13. Yegorov, Yu. A., Orlov, Yu. V. and Pankrat'yev, Yu. V. P. 460 of this volume.

14. Marshall, J. Bull. Am. Phys. Soc., Vol. 27, 11, 1952.

15. Murray, R. B. Nucl. Instrum., Vol. 2, 237, 1958.

16. Avayev, V. N., Yegorov, Yu. A. and Orlov, Yu. V. P. 415 of this volume.

17. V'yugov, P. N. et al. Pribory i Tekhnika Eksperimenta, No. 3, 65, 1962.

18. Frolov, A. S. and Chentsov, N. N. The Application of Related Tests for Obtaining Smooth Curves. Report presented at the Fourth All Union Conference on the Theory of Probabilities (Primeneniye zavisimykh ispytaniy dlya polucheniya gladkikh krivykh. Doklady na IV Vsesoyuznom soveshchanii po teorii veroyatnostey). Vil'nyus, 1961.

SINGLE CRYSTAL FAST NEUTRON SPECTROMETER FOR MEASURING CONTINUOUS SPECTRA

Yu. A. Yegorov and Yu. V. Pankrat'yev

The method of recoil protons is widely used to measure the energy /304 of fast neutrons. This method is also used to measure neutron spectra by means of scintillation equipment. There are several types of fast neutron scintillation spectrometers (refs. 1-4), but the spectrometer with a single hydrogen-containing scintillator differs from the other types of scintillation spectrometers by its high effectiveness.

The sensitivity of such a spectrometer to γ-radiation has limited its possibilities to the present day. However, the possibility of detecting the difference in the dexcitation time of several organic scintillators when they are irradiated by protons and electrons (ref. 5) and the development of the method for discriminating against pulses due to γ-radiation (refs. 6 and 7) have made it possible to use the single crystal spectrometer extensively for various measurements.

If N_0 neutrons with energy E_0 enter a scintillator of thickness d, per unit time, the number of recoil protons N_p formed as a result of single neutron scatterings by protons, will be equal to

$$N_p = N_0(1 - e^{-\Sigma_p d}) \quad \text{when} \quad d < \frac{1}{\Sigma_p} \tag{1}$$

where $\Sigma_p = n\sigma_p(E_0)$; n is the concentration of hydrogen nuclei in the scintillator; σ_p is the effective scattering cross section of neutrons with energy E_0 by protons. The number of recoil protons with energy in the interval from E_p to $E_p + dE_p$ is equal to

$$N_p(E_p) = \begin{cases} N_0(E_0)\frac{dE_p}{E_0} & \text{when } E_p \leq E_0 \\ 0 & \text{when } E_p > E_0, \end{cases} \tag{2}$$

i.e., the distribution of recoil protons according to energy is a function which breaks off sharply when $E_p = E_0$. If a recoil proton with energy E_p produces a pulse with amplitude $h = h(E_p)$, the distribution of pulses according to amplitude will also be represented by a function which breaks off sharply at $h = h_0$, where h_0 is the amplitude of the pulse corresponding to the total absorbtion of neutron energy E_0. However, this result is only possible if the relationship between the absorbed energy and the light output of the scintillator is linear, when the statistical fluctuations in the magnitude of the pulse at the output of the photomultiplier are absent and the dimensions of the crystal, on the one hand, are sufficiently small (which eliminates the possibility of multiple neutron scattering), and, on the other hand, are sufficiently large so that the recoil proton energy is totally absorbed.

The amplitude distribution of pulses measured by means of a spectrometer differs radically from the distribution which breaks off: the boundary of the amplitude spectrum is somewhat diffuse, which is due to the simultaneous action of statistical fluctuations, the nonlinearity of light output and the incomplete absorption of recoil proton energy. In connection with this the amplitude distribution may be represented in the form of the function

$$N(h)\,dh = dh \int_0^{\infty} \frac{e^{-\left|\frac{h-h_0}{R(h_0)}\right|^2}}{\sqrt{\pi}R(h_0)}\,dh_0 \times \int_{E_{p0}}^{\infty} \frac{N(E_0)\,(1-e^{-\Sigma_p d})}{E_0}\,dE_0, \qquad (3)$$

where $R(h_0)$ is the width of the Gaussian distribution for $h = h_0$, obtained by differentiating the integral distribution. If in the processing of measurement results for the continuous fast neutron spectrum, for example, the spectrum of the nuclear reactor, we do not take into account the Gaussian spread, then expression (3) may be written in a simpler form and the spread effect may be taken into account by means of special corrections, /305

$$N(h)\,dh = \int_{E_p}^{\infty} \frac{N(E_0)\,(1-e^{-\Sigma_p d})}{E_0}\,dE_0. \qquad (4)$$

If the amplitude distribution corresponds to the recoil proton spectrum, then by differentiating expression (4) and solving it with respect to $N(E_0)$, we find

$$N(E_0)\,dE_0 = -\frac{E_0}{1-e^{-\Sigma_p d}} \left[\frac{dN(h)}{dE_p}\right]_{E_p=E_0}. \qquad (5)$$

However, expression (5) is valid only when the relationship between the light output of the scintillator and the recoil proton energy absorption is linear, because it is only when this condition is observed that the recoil proton spectrum coincides with the amplitude distribution. In order to take into account the variation in the light output of a crystal as a function of proton energy, it is necessary to introduce a correction into equation (5). As a result we obtain in place of equation (5) the relationship

$$N(E_0)\,dE_0 = -\frac{E_0}{1-e^{-\Sigma_p d}}\left[\frac{dL}{dE_p}\cdot\frac{dN(h)}{dL}\right]_{E_p=E_0}, \qquad (6)$$

where $L = L(E_p)$ is the variation in the light output as a function of proton energy.

As follows from a preceding consideration, equation (6) does not take into account the multiple scattering of neutrons in the crystal, the scattering of neutrons by carbon nuclei and also the effect of incomplete energy absorption by recoil protons. If we take into account the multiple scatterings in toluylene crystals of average dimensions (diameter of 30 mm and a height of 10-20 mm), then according to the data contained in references 8 and 9 this does not lead to a noticeable distortion of recoil proton spectrum, particularly since this effect is partially compensated by the incomplete absorption of proton energy.

According to the data in reference 10, the correction for the secondary scattering and leakage of recoil proton energy may be computed approximately by means of the equation

$$-0.78\frac{R_{\max}}{d}\frac{E_0}{} + 0.09\frac{d\Sigma_p(E_0)}{V} + 0.077\frac{D\Sigma_p(0.068E_0)}{2V}, \qquad (7)$$

where D is the crystal diameter; V is the crystal volume; $R_{max}(E_0)$ is the radius within whose limits the proton undergoes frontal scattering.

Equation (7) is obtained for a cylindrical crystal, assuming that the neutron flux falls perpendicular to its base. The first term in this equation determines the correction for secondary scattering, and the last two terms determine the correction for proton energy leakage. Equation (7) makes it possible to determine the optimum crystal thickness d for which the total action of both corrections is a minimum. According to the data of reference 10, the optimum crystal thickness varies from 1.4 mm at E_0 = 1 MeV to 18 mm when E_0 = 10 MeV. If, on the other hand, the spectrometer is designed to measure the continuous spectrum over a rather wide energy range, then apparently the optimum thickness is approximately 10 mm.

However, when measuring neutron spectra in the presence of intense background γ-radiation it is sometimes necessary to decrease the crystal thickness in order to decrease the sensitivity of the spectrometer to γ-quanta, even when a special scheme is used to discriminate against γ-pulses. For this reason a toluylene crystal with a thickness of 5 mm was used in the described spectrometer, which was designed for taking measurements on a nuclear reactor. Figure 1 shows the corrections for such a crystal as a function of neutron energy, computed by means of the equations presented above. As we can see from the figure, the correction for secondary scattering (curve 2) varies insignificantly, whereas the correction for incomplete proton energy absorption (curve 1) increases sharply with energy. These curves were used in processing the sults of measurements.

It is not necessary to take into account the effect of neutron scattering by carbon nuclei when processing the measurement results, because the /306
carbon recoil nuclei when this energy is the same as that of the recoil hydrogen nucleus, produce a light flash much smaller than that produced by the protons (ref. 11). At the same time, the carbon recoil nucleus receives approximately four times less energy than the recoil protons. The effect produced by the carbon reaction, which leads to the formation of charged particles, is negligibly small, because the cross sections of these reactions are much smaller than the (n, p)-interaction cross section.

Depending on the neutron energy, the effectiveness computed by means of equation (1) for a toluylene crystal of 5 mm thickness varies from 3 percent

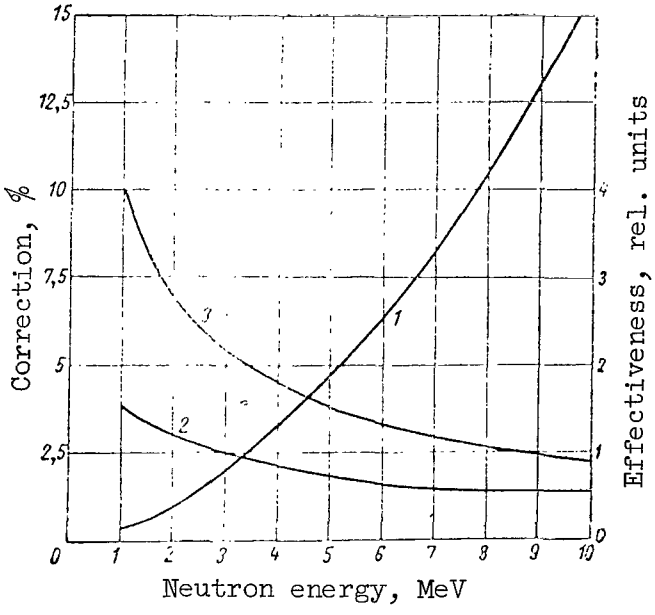

Figure 1. Corrections used for processing measurement results of continuous fast neutron spectra for toluylene crystal of 5 mm thickness: 1, correction for wall effect; 2, correction for secondary scattering; 3, effectiveness of recording neutrons.

for E_0 = 2 MeV to 1.3 percent when E_0 = 10 MeV (fig. 1). No other fast neutron scintillation spectrometer has such a high effectiveness. The single crystal spectrometer is designed to operate with the FEU-33 photomultiplier. To exclude the effect of background γ-radiation, a discrimination scheme is used as proposed in reference 6. The discrimination scheme is balanced by a /307 device whose block diagram is shown in figure 2. By means of this scheme every impulse on the screen of the oscilloscope is represented by a luminescent point (fig. 3). When the scheme is adjusted, an operating condition is achieved such that the pulses from electrons (the lower luminescent line) have a minimum amplitude.

The spectrometer for measuring the continuous fast neutron spectra is assembled according to the block diagram shown in figure 4. A pulse whose amplitude is proportional to the recoil proton energy is picked up from one dynode of the photomultiplier and is transmitted through the cathode follower to the linear pulse amplifier. The amplified pulse is transmitted through the delay line to the electronic gate. The operation of the spectrometer is controlled by a pulse from the output of the discrimination circuit, which is fed through the cathode follower to the amplifier and then to the integral discriminator. The integral discriminator also serves as a controlled single flip-flop oscillator and is adjusted so that it is triggered only by the proton pulses. A type USh-10 amplifier is used to amplify pulses in both channels; the pulse amplitude analyzer consists of the type AI-100-1 100-channel analyzer.

The quality of spectrometer operation was checked by measuring the neutron spectra from Po + Be, Po + B sources of a nuclear reactor and the deformation of the Po + Be source spectrum in water. The source spectra and reactor /308 measurements were carried out with a collimated flux; for this purpose the spectrometer sensor was placed into a cylindrical collimator made of paraffin with boron carbide and lead (fig. 5). The deformation of the spectrum was measured under conditions close to the conditions of "infinite" geometry.

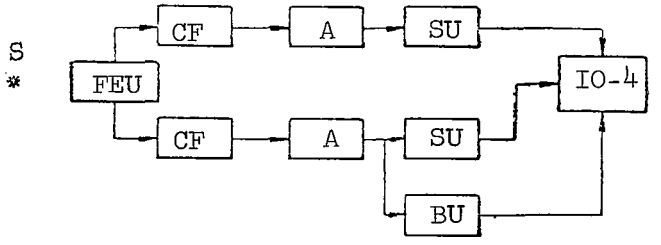

Figure 2. Block diagram of device for balancing discrimination circuit: S, source of fast neutrons or γ-quanta; FEU, spectrometer sensor with a discrimination circuit; CF, cathode follower; A, amplifier; SU, shaping unit; BU, bias lighting unit; IO-4, oscillograph (signals are fed directly to deflection plates of cathode ray tube).

Figure 3. Oscillogram of pulses observed on screen of IO-4 oscilloscope when crystal is irradiated by neutrons and by γ-quanta from Po + Be source and by γ-quanta from Co^{60} source.

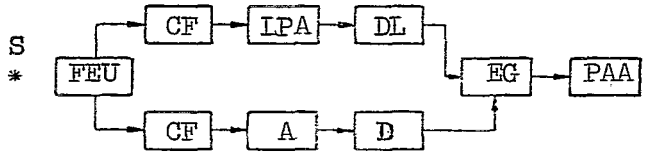

Figure 4. Block diagram of single crystal fast neutron spectrometer: S, radiation source; FEU, spectrometer sensor with discrimination circuit; CF, cathode follower; LPA, linear pulse amplifier; DL, delay line; EG, electron gate; A, amplifier; D, integral discriminator; PAA, pulse amplitude analyzer.

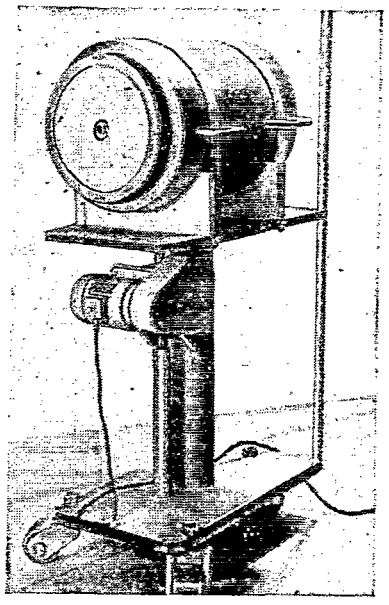

Figure 5. External view of spectrometer sensor in collimator on vertically adjustable stand.

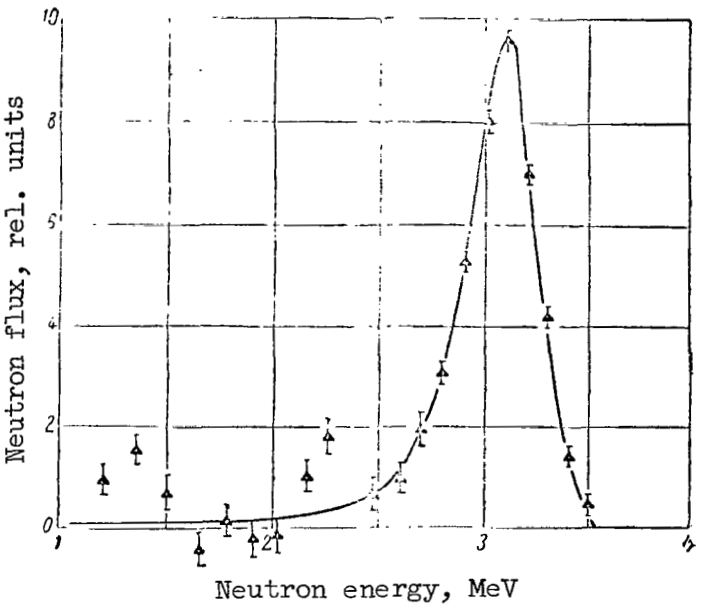

Figure 6. Spectrum of fast neutrons from source D (d, n) He^3.

In order to interpret the results which were obtained the spectrometer was previously calibrated by measuring the spectra of Compton electrons from Cs^{137}, Co^{60} and Po + Be source of γ-quanta. The data of reference 11 were used to make the transformation from electron energy to proton energy.

The results of measuring the spectrum of (d, n)-neutrons are shown in figure 6. In accordance with expression (5) the equipment spectrum of fast neutrons was obtained by graphic differentiation along channels beginning with the region of maximum amplitudes. The distribution obtained in this manner was transformed into an energy distribution by introducing a correction for the effectiveness. The measured spectrum of neutrons from the reaction D(d, n)He^3 coincided well with the known spectrum; the results of measuring the spectra of Po + Be, Po + B and other sources also agreed well with existing data. A good coincidence of the spectra was also confirmed by the correct calibration of the spectrometer by means of γ-radiation sources.

The spectrum of fast neutrons leaving the active zone of the nuclear reactor was measured at the lateral experimental channel of the reactor. The neutrons from the active zone travelled along a channel with a diameter of 100 mm and a length of 2.5 m in a concrete shielding and through a collimator (with an opening diameter of 20 mm) and entered the toluylene crystal. The results of the measurements are shown in figure 7. Within the limits of

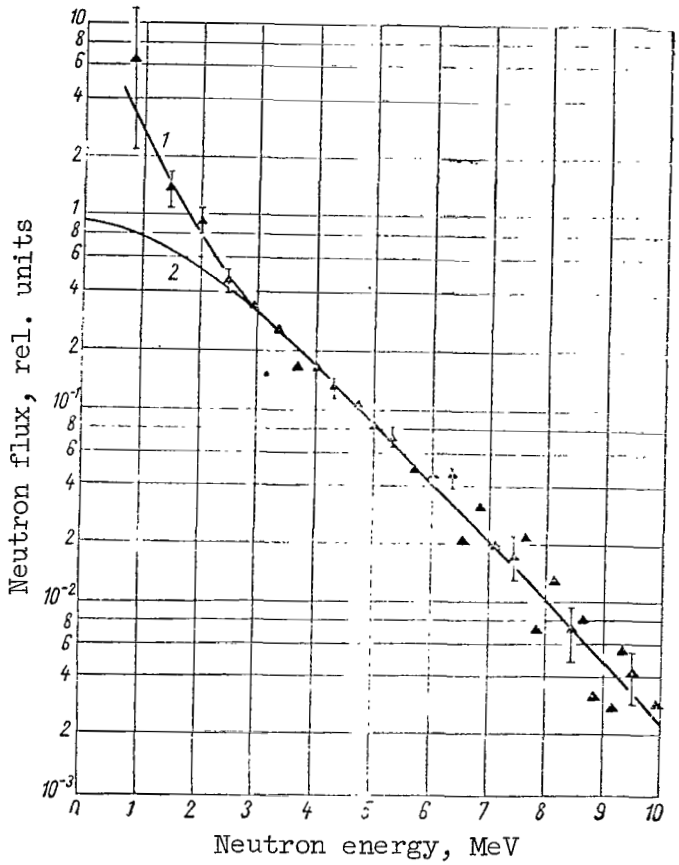

Figure 7. Neutron spectrum of nuclear reactor:

1, measured spectrum; 2, U^{235} fission neutron spectrum.

experimental error the measured spectrum coincides with the spectrum of U^{235} fission neutrons in the regions of energies greater than 3 MeV.

Measurements of the deformation of neutron spectrum from the Po + Be source were carried out in a tank with water. The source and the detector were placed in water and the distance between them was varied from 0 to 35 cm. The data obtained were used to compute the attenuation cross sections of neutrons in water as a function of energy. The results agreed with the data presented in reference 12.

Thus the control measurements showed that the spectrometer is reliable in operation. In the region of neutron energy greater than 0.9 MeV it is easy to process the results of the measurements; the spectrometer is practically insensitive to γ-radiation when the flux of γ-quanta is approximately 10^4 times greater than the neutron flux (ref. 13).

The author wishes to express his gratitude to Yu. G. Anisimov for his help in conducting the experiments and adjusting the spectrometer.

REFERENCES

1. Rybakov, B. V. and Sidorov, V. A. The Spectrometry of Fast Neutrons (Spektrometriya bystrykh neytronov). Moscow, Atomizdat, 1958.

2. Cleland, M. R. Bull. Am. Phys. Soc., Vol. 27, 5, 1952.

3. Khabakhpashev, A. G. Pribory i Tekhnika Eksperimenta, No. 1, 25, 1960.

4. Yegorov, Yu. A. Pribory i Tekhnika Eksperimenta, No. 3, 21, 1958.

5. Wright, G. T. Proc. Phys. Soc. B., Vol. 69, 358, 1956. /310

6. Brooks, F. D. Nucl. Instrum., Vol. 4, 3, 1959.

7. Owen, R. B. Trans. I. R. E. PGNS, Vol. 5, 198, 1958.

8. Chagnon, P. R. Rev. Scient. Instrum., Vol. 26, 1165, 1955.

9. Elliot, I. O. Phys. Rev., Vol. 93, 1348, 1954.

10. Broek, H. W. Rev. Scient. Instrum., Vol. 31, 1063, 1960.

11. Taylor, G. I. et al. Phys. Rev., Vol. 84, 1034, 1951.

12. Broeder, D. L., Kutuzov, A. A. and Kondrashov, A. P. Atomnaya Energya, Vol. 6, 578, 1959.

13. Yegorov, Yu. A., Orlov, Yu. V. and Pankrat'yev, Yu. V. P. 460 of this volume.

PERMISSIBLE GAMMA BACKGROUND RADIATION WHEN MEASURING FAST NEUTRONS WITH A SINGLE SENSOR SPECTROMETER

Yu. A. Yegorov, Yu. V. Orlov and Yu. V. Pankrat'yev

Scintillation spectrometers of fast neutrons with a single sensor, /310 which discriminate against the background γ-radiation on the basis of the time difference in the de-excitation of organic scintillators when these are irradiated by fast neutron fluxes and γ-quanta, do not record γ-quanta, if the dose power produced by them does not exceed a permissible value. When this permissible dose for the spectrometer is exceeded, discrimination against the background γ-radiation ceases to function and the spectrometer records γ-quanta along with the fast neutrons.

The value of the permissible dose power depends on the method used in the spectrometer to separate pulses due to neutrons and radiation: a method of achieving separation by means of electronic circuits (ref. 1) or a method based on the use of the space charge to saturate the region between the last dynode and anode of the photomultiplier (ref. 2). In addition, the value of the permissible dose power of γ-radiation depends on the value of the spectrometer energy threshold. It is obvious that as the energy threshold of the spectrometer becomes higher, the permissible dose power of γ-radiation also becomes greater. When the energy threshold is decreased the permissible dose power also decreases.

In order to study fast neutron spectra in the presence of background γ-radiation, the values of the permissible dose power for γ-radiation were determined for spectrometers with the background γ-radiation discrimination schemes proposed in references 1 and 2.[1] Both fast neutron spectrometers were assembled according to the same block diagram, and the sensors of both spectrometers utilized the FEU-33 photomultiplier with a toluylene crystal of 30 mm diameter and 20 mm height. The discrimination circuits for the background γ-radiation for both spectrometers were constructed in such a way that the energy threshold

[1]The schemes for differentiating against background γ-radiation proposed, for example, in references 5 and 6 may be used to measure fast neutron spectra when we have a substantially smaller background γ-radiation and therefore are not considered. The results reported in references 7 and 8 coincide with the results of the present work.

of the spectrometer was equal to 0.6 ± 0.1 MeV. The value of the energy threshold was determined from the results of measuring the spectra of fast neutrons from the D (d, n) He^3 reaction. To determine the sensitivity of the spectrometer to γ-radiation, its sensor was placed in a constant value neutron flux from the Po + Be source, and the dose power of γ-radiation was measured. The source of γ-radiation was Co^{60}.

The results obtained for a spectrometer with a separation scheme which compares the pulse of the total charge with the peak pulse are shown in figure 1. We can see from the figure that when the neutron count rate is approximately 200 min^{-1} the fast neutron spectrometer does not record γ-radiation with a maximum energy of 1.33 MeV, if the dose power γ-radiation does not exceed 4 μR/sec. As the dose power is increased, the count rate increases and by using a special circuit (ref. 3) we can clearly see on the oscilloscope screen that the pulses due to γ-radiation approach in amplitude the pulses produced by recoil protons.

The results obtained for the spectrometer in which a space charge scheme is used to discriminate against background γ-radiation are shown in figure 2. We can see that when the neutron recording level is approximately 300 min^{-1} the spectrometer begins to record the γ-radiation of Co^{60}, with the dose power 15-20 μR/sec. As the dose power of γ-radiation is further increased, /311

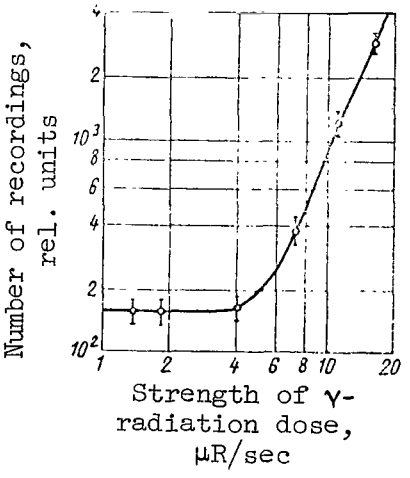

Figure 1. Calculated characteristics of fast neutron spectrometer with separation scheme which compares pulse of total charge with peak pulse.

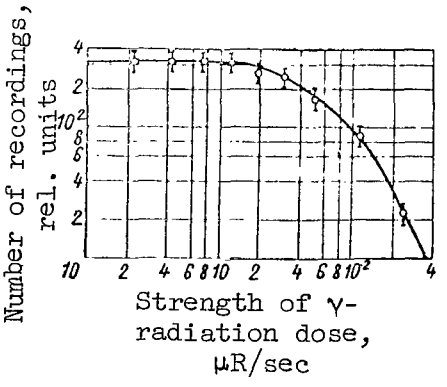

Figure 2. Calculated characteristics of fast neutron spectrometer with separation scheme of γ background and space charge.

the rate of count decreases and the recorded pulses include pulses produced by neutrons and by γ-radiation. Calculations carried out for this spectrometer show that when the dose power of γ-radiation is approximately 10 μR/sec the effectiveness of the spectrometer relative to fast neutrons from the Po + Be source is equal to 14 percent, and relative to the γ-radiation from the Co^{60} source it is equal to 0.005 percent.

The sensitivity of fast neutron spectrometers, utilizing the space charge scheme for discriminating against γ-radiation, was checked by measurements conducted on the nuclear reactor. Experiments have shown that the spectrometer records γ-radiation with energies greater than 3 MeV. In this case on the last dynode of the photomultiplier there are positive overshoots from the negative pulses produced by the electrons, in addition to the positive pulses due to the recoil protons. The amplitude of the positive overshoots increases with electron energy. Thus the background γ-radiation discrimination level established for Co^{60} γ-quanta is insufficient when $E_\gamma \geq 3$ MeV. The pulses produced by the Compton electrons were clearly seen in the amplitude distribution, and their presence was confirmed experimentally by using a filter of paraffin with a thickness of 20 cm. The amplitude distribution measured with the filter and without the filter, for $E_n > 6$ MeV, were almost unchanged, whereas for $E_n < 6$ MeV the number of pulses decreased approximately by a factor of 10. To eliminate the background γ-radiation produced by the reactor, the discrimination level in the spectrometer was increased from 0.6 to 2.1 MeV. When the energy threshold is 2.1 MeV it is possible to measure the spectrum of fast neutrons when the ratio of neutron flux to γ-quanta flux is 1:2000.

To measure the spectrum of reactor fast neutrons in the energy range from 0.8 to 10 MeV the experiment was conducted twice: for the energy threshold of 0.6 and 2.1 MeV, respectively, (ref. 4).

REFERENCES

1. Brooks, F. D. Nucl. Instrum., Vol. 4, 151, 1959.

2. Owen, R. B. Trans. I.R.E. PGNS, Vol. 5, 198, 1958.

3. Yegorov, Yu. A. and Pankrat'yev, Yu. V. Inzh.-fiz. zh., Vol. VI, 112, 1961.

4. Avayev, V. N., Vasil'yev, G. A. et al. Atomnaya Energiya, Vol. 15, 20, 1963.

5. Vyazemskiy, V. O., Gridnev, A. A. and Pisarevskiy, A. N. Pribory i Tekhnika Eksperimenta, No. 4, 149, 1961.

6. Brovchenko, V. G. and Gorlov, G. V. Pribory i Tekhnika Eksperimenta, No. 4, 49, 1961.

7. Funsten, H. O. and Cobb, G. C. Rev. Scient. Instrum., Vol. 31, 571, 1960.

8. V'yugov, P. M. et al. Pribory i Tekhnika Eksperimenta, No. 3, 65, 1962.

THE GAMMA-SPECTROMETER BASED ON THE FORMATION OF ELECTRON-POSITRON PAIRS

V. N. Avayev, Yu. A. Yegorov and Yu. V. Orlov

Annihilation γ-radiation consisting of two γ-quanta, each with an energy of 0.51 MeV, occurs when the substance of the scintillator absorbs the energy of γ-quanta due to the formation of the electron-positron pair. If the dimensions of the scintillator are small, the annihilation γ-quanta escape from it. In this case an energy $E_\gamma = E_{\gamma_0} - 1.02$ MeV is absorbed in the scintillator. /312

This makes it possible to design an electron-positron pair scintillation spectrometer with definite advantages over other spectrometers. The spectrometer system is designed to measure the amplitudes of only those pulses due to the absorption of γ-quanta energy as a result of the pair formation process. To achieve this, the sensors of the spectrometer, in addition to the scintillator illuminated by the flux of source γ-quanta, contain two auxiliary scintillators to record the annihilation γ-quanta.

When the amplitude distribution of pulses is measured when the central scintillator is illuminated with a flux of monochromatic γ-quanta, a single maximum is obtained and a relatively small low energy distribution. This distribution is due to the leakage of retardation radiation and of electrons from the central scintillator.

When complex γ-spectra are measured, a single maximum corresponds to each γ-line in the amplitude distribution.

Since the low energy background radiation is small, it is not necessary to introduce corrections for the low energy distribution in a series of cases when measuring the continuous γ-spectra.

These merits of a scintillation γ-spectrometer involving the electron-positron pairs may, indeed, distinguish it advantageously from other γ-spectrometers, particularly from spectrometers with a single scintillator of even large dimensions.

The difficulties associated with the interpretation of results, when measurements of complex γ-spectra are carried out by a spectrometer with a scintillator of relatively small dimensions are well known (for example, with a scintillator whose diameter and height are less than 40 mm). The measured distribution of pulse amplitudes may simultaneously contain three distributions:

a continuous Compton distribution for each γ-line, the peaks of the total γ-quanta energy absorption (due to the photoeffect or multiple scatterings) and peaks of energy absorption due to the effect of pair formation, where for a single energy of γ-quanta it is possible to have three peaks (ref. 1).

The situation is somewhat simpler, if the dimensions of the scintillator are sufficiently large (for example, a diameter and height of 80 mm). However, in this case the processing of measurement results for the continuous γ-spectra is rather difficult and requires a large number of preliminary calculations (ref. 2) or experiments (ref. 3).

The measurement of continuous γ-spectra by means of the Compton spectrometer is possible only for energies less than 2-3 MeV. For large energies the basic peak is accompanied by peaks due to the pair formation effect (refs. 4 and 5).

In addition it should also be pointed out that a spectrometer of pairs is practically insensitive to fast neutrons. The property of the pair scintillation spectrometer is particularly valuable, if the spectrometer is used to measure the γ-spectra in the presence of a neutron background, for example, when measurements are made on nuclear reactors.

However, the scintillation γ-spectrometer of pairs has two significant shortcomings: first, the effectiveness of the spectrometer is small and in its order of magnitude lies between the effectiveness of the spectrometer with a single scintillator and the effectiveness of the Compton spectrometer; in the second place, the electronic circuits of the spectrometer are rather complicated. /313

Nevertheless, the scintillation γ-spectrometer of pairs described below is successfully used to measure the deformation of nuclear reactor γ-spectra in a shielding for the region where the γ-quanta energy is greater than 1.5 MeV and for investigating the output of capture γ-radiation.

A block diagram of the scintillation γ-spectrometer of pairs is shown in figure 1. The central scintillator is mounted on the FEU-1 photomultiplier, and the signal from this photomultiplier passes through the cathode follower CF, is amplified by the amplifier A and is fed to the first delay line 1DL. Next the signal passes through the cathode follower CF and then follows 2 circuits: to the coincidence circuit CC and through the delay line 2DL to the input of the electronic gate EG.

The signals from the auxiliary sensors (FEU-2 and FEU-2') also pass through cathode followers CF to the single channel pulse amplitude analyzers AA, which select only those pulses due to the complete or almost complete absorption of annihilation γ-quanta energy in the scintillators of the auxiliary sensors.

The pulses from the amplitude analyzers are shaped by the shaping unit SU and fed to the input of the first coincidence circuit 1CC. If coincidence takes place, the pulse from the output is fed to the second coincidence circuit CC.

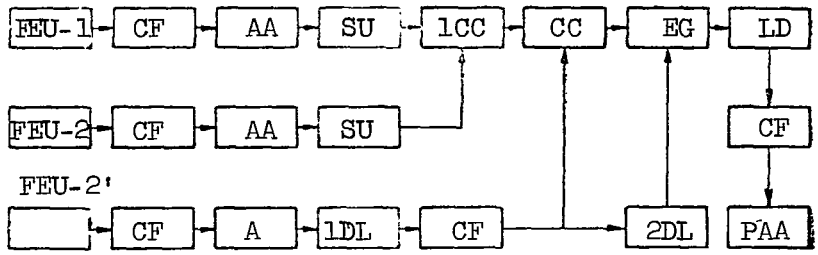

Figure 1. Block diagram of electron-positron pair γ-spectrometer. FEU-1, central spectrometer sensor; FEU-2 and FEU-2', auxiliary side sensors; CF, cathode follower; A, linear pulse amplifier; 1DL and 2DL, delay lines; AA, single channel amplitude analyzer; SU, shaping units; 1CC and CC, coincidence circuits; EG, electron gate; LD, limitor-discriminator; PAA, 100 channel amplitude analyzor.

If a pulse from the main spectrometer channel also appears at the CC circuit at this time, the second coincidence circuit opens an electronic gate and the pulse from the main channel passes through the limitor-discriminator LD to the pulse amplitude analyzer PAA.

In reality it is possible to have certain effects of greater complexity which cause all of the circuits to operate, even though energy absorption has occurred rather than the effect produced by pairs. However, these effects are insignificant and will be examined below.

The central sensor in this spectrometer consists of a type FEU-42 spectrometer photomultiplier, which also holds the NaJ(Tl) spectrometer crystal with a diameter and height of 40 mm. The auxiliary spectrometer sensors use the FEU-43 photomultiplier and CsJ(Tl) crystals with a diameter and height of /314 30 mm. The position of the sensor is shown schematically in figure 2.

The crystals and the photomultipliers are placed in a lighttight T-shaped case. This case also contains the cathode followers. The case is mounted on a special base with vertical guides (fig. 3) so that the position of the central sensor scintillator can be adjusted from 25 to 100 cm relative to the base.

In order to isolate pulses of definite amplitude, the control channel of the spectrometer contains standard AADO-1 single channel analyzers. The AADO analyzers are particularly useful in this application, because it is possible to control the threshold and channel width in them over wide limits.

The PAA amplitude analyzer consists of the 100 channel A1-100-1 analyzer.

The linear pulse amplifier A uses a simple circuit with feedback. Its gain is controlled and varied from 10-180. The remaining units of the block diagram form the commutation and signal shaping system.

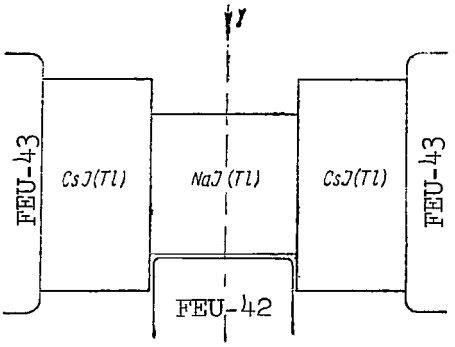

Figure 2. Position of spectrometer sensors.

The basic characteristics of the signal shaping and commutation system are as follows: the resolving time of the first coincidence circuit is 1×10^{-6} sec; the resolving time of the second coincidence circuit is 1.5×10^{-6} sec; the duration of the control pulses is 3.5 μsec; the transfer coefficient of the basic signal is approximately 0.2.

All of the electronic units of the spectrometer are assembled on two racks (fig. 4), which in addition to the units described above contain the high voltage rectifier (HVR) for feeding the photomultipliers and two counting systems used to control the operation of the coincidence circuits and to carry out the integral count at the output of the electronic gate.

Since the voltage stabilization coefficient of the type HVR rectifier is small, stabilization circuits similar to those described in reference 6 are used to feed the photomultipliers into the spectrometer.

In checking the operation of the spectrometers without the amplitude analyzers in the control channel of the spectrometer, it became clear that the low energy distribution, which accompanies the formation of pair peaks, is rather large (fig. 5) and is primarily due to the formation of false coincidences in the auxiliary sensors during the simultaneous absorption of the energy of source γ-quanta in the central sensor due to Compton scattering.

A contribution to the low energy distribution is also made by the processes of double Compton scattering: the source γ-quantum first undergoes Compton scattering in the scintillator of the central sensor, so that the secondary γ-quantum enters the scintillator of one of the lateral sensors and there undergoes Compton scattering. The scattered γ-quantum enters the scintillator of the second auxiliary sensor and is absorbed there. This effect is particularly noticeable when the energy of γ-quanta is slightly greater than 1.02 MeV.

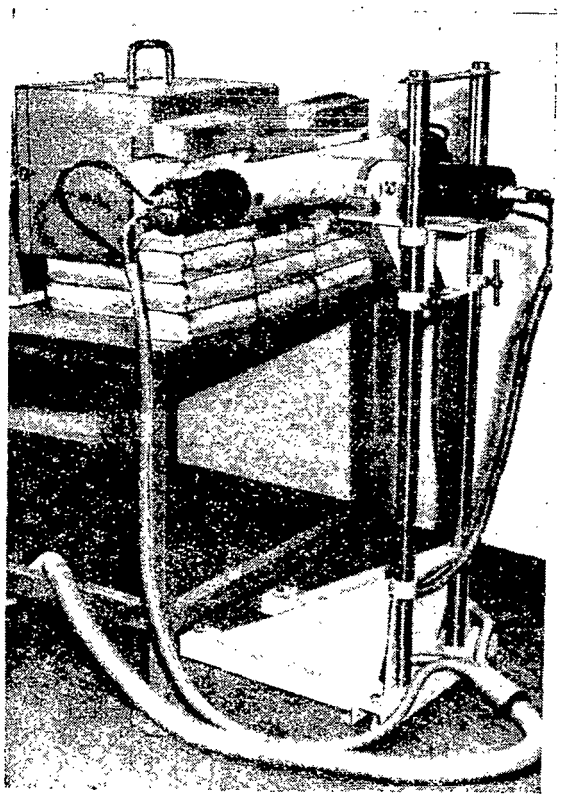

Figure 3. External view of unit containing spectrometer sensors.

The introduction of analyzers with a window width from 400 to 550 keV into the control channel (in order to select the thresholds and channels of amplitude analyzers, the amplitude distribution due to Hg^{203} and Cs^{137} γ-quanta was measured in the control channel of the spectrometer by means of these same analyzers) substantially reduces the number of false coincidences and completely eliminates the recording of double Compton scatterings, because the energy of the last γ-quantum in this process is close to 250 keV.

Indeed, while measuring the γ-spectrum of the Po + Be source, it has been noted that when analyzers are connected to the control channel, the low energy distribution decreases almost by a factor of 10 (fig. 5). The same /316 decrease in the low energy background radiation is observed when measuring the γ-spectrum of the Na^{24} source (fig. 6). The occurrence of low energy background radiation, when measurements are made with amplitude analyzers in the spectrometer control channel, is associated with the incomplete absorption of energy E_γ (1.02 MeV) in the scintillator of the central sensor, due to partial electron leakage and retardation radiation.

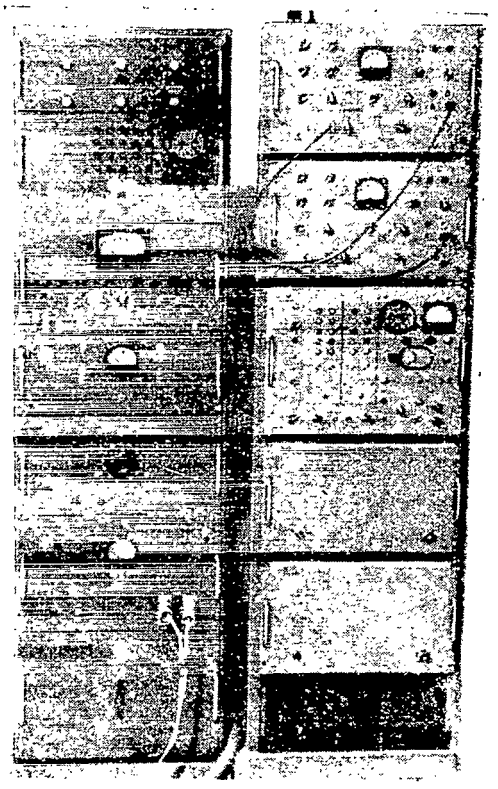

Figure 4. External view of racks with electronic units of spectrometer.

We can see from figures 5 and 6 that the low energy background radiation does not exceed 2-3 percent of the peak height, i.e., it lies within the accuracy of measurements. Therefore, when continuous γ-spectra are measured, it is not necessary to introduce a correction for the low energy distribution when processing the measurement results. This situation makes the pair spectrometer a rather useful device for measuring continuous γ-spectra.

Measurements of the Po + Be source γ-spectrum and the nuclear reactor γ-radiation spectrum were made to determine the sensitivity of the pair γ-spectrometer to neutrons. Measurements were carried out with bismuth filters with a thickness of 100 mm (ref. 7) and without filters.

The Po + Be source produces the same number of γ-quanta and neutrons, and it is not possible to note the distortion of the γ-spectrum due to the sensitivity of the spectrometer to neutrons. When the reactor γ-spectrum is /317 measured without a bismuth filter in the region of γ-radiation energies slightly less than 2.5 MeV, the distortion of the γ-spectrum by the neutron background is observed. However, this distortion, on the average, is equal to 2 percent of the measured distribution at these same energies and is somewhat greater at smaller energies.

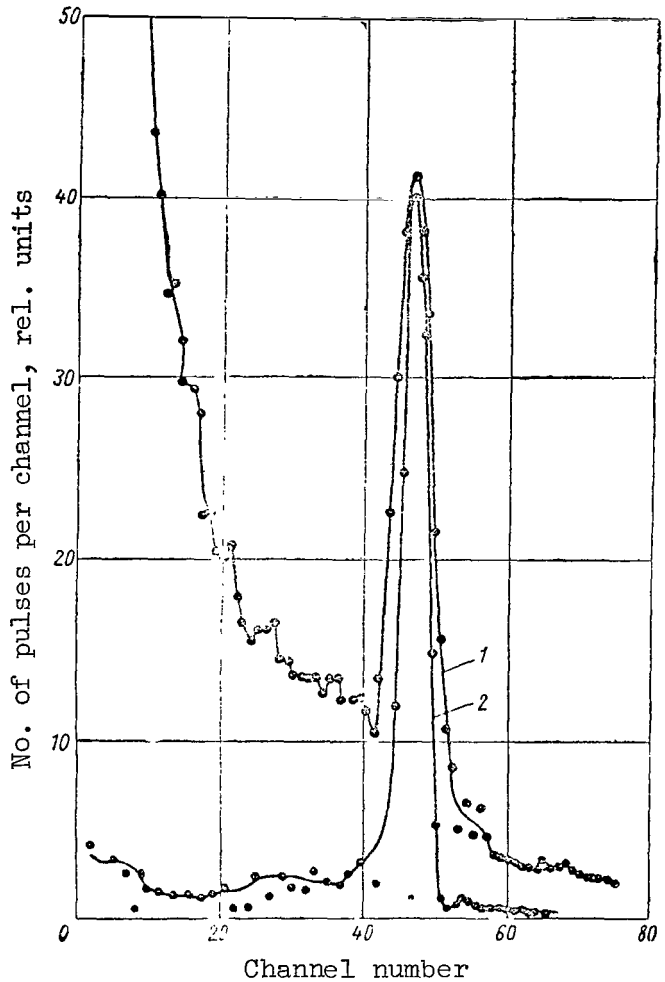

Figure 5. Gamma-spectrum of Po + Be source measured without amplitude analyzers in control channel of spectrometer (1) and measured with amplitude analyzers in control channel (2).

Thus the examination of pair γ-spectrometer sensitivity to neutrons has yielded the following results.

1. In the region of γ-quanta energies slightly less than 2.5 MeV it is possible to have some distortion in the γ-spectrum (not greater than 10 percent), which can be eliminated by auxiliary measurements with a bismuth filter of 100 mm thickness.

2. If the ratio of neutron fluxes to γ-quanta fluxes is approximately equal to unity, the distortion of the γ-spectrum is practically unobserved.

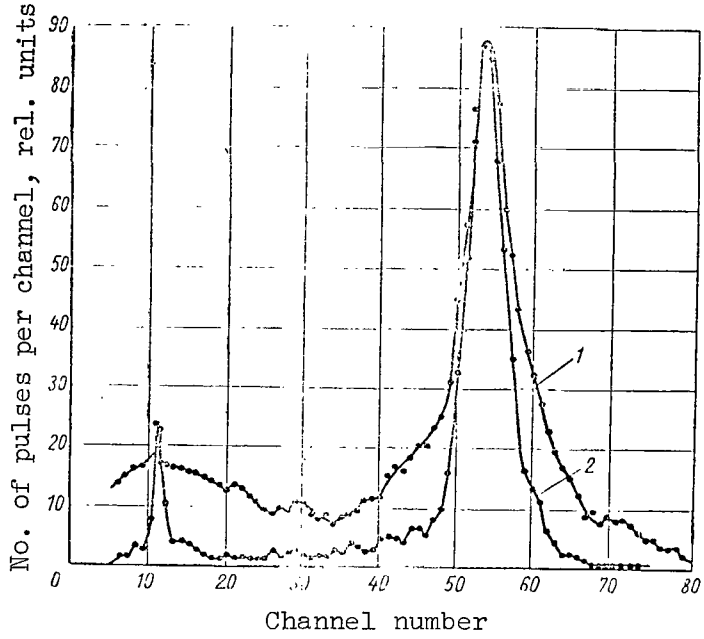

Figure 6. Na^{24} γ-spectrum measured by spectrometer with amplitude analyzers in control channel (2) and without analyzers (1).

3. When the energy of γ-quanta is greater than 2.5 MeV, the distortions of the γ-spectrum by the neutron background is also unobserved.

To make a quantitative evaluation of the relationships, the effectiveness of spectrometer ϵ is computed for the γ-spectrum

$$\varepsilon = \frac{\varkappa}{\mu}(1-e^{-\mu d})t^2\left(\frac{\alpha}{4\pi}\right)\left(\frac{E_\gamma}{E_\gamma - E'_\gamma}\right)^{-1}\xi,$$

where $\varkappa$ is the linear coefficient of γ-radiation energy absorption due to the formation of pairs in the crystal of the central sensors; μ is the total linear absorption coefficient for γ-radiation in the same crystal; d is the thickness of the crystal in the central sensor; $t = (1-e^{-\mu_1 R})k$ is the effectiveness of recording annihilation γ-quanta with the auxiliary crystals; μ_1 is the total linear attenuation coefficient for γ-radiation with an energy of 0.51 MeV by the auxiliary crystal; R is the average distance travelled by the annihilation γ-quanta in the auxiliary crystal; k is the coefficient which takes into account the analyzer channel widths in the spectrometer control channel; ξ is the correction for the absorption of annihilation γ-quanta in the scintillator of the central sensor; α is a solid angle covered by the auxiliary scintillators;

$\left(\frac{E_\gamma}{E_\gamma - E'_\gamma}\right)$ is a correction for the "threshold" of the spectrometer; E'_γ is the threshold energy of the spectrometer. /318

As the energy of γ-quanta increases, the correction for the spectrometer threshold rapidly decreases. For the spectrometer described above the magnitude of the threshold energy is approximately 250 keV and when $E_\gamma \geq 2$ MeV

$\frac{E_\gamma - E'_\gamma}{E_\gamma} \sim 1$.

We note that the value of t in the first approximation does not depend on the energy of the investigated γ-quanta, and it can be neglected when processing the measurement results.

To determine the true effectiveness of the spectrometer we computed the quantity $\varkappa/\mu\ (1-e^{-\mu d})$ as a function of energy and normalized it according to the results obtained by measuring the γ-spectrum of the Na^{24} source of known activity. The effectiveness obtained from measurements with the Po + Be source agreed sufficiently well with computed results (fig. 7).

As we can see from figure 7 the effectiveness of the pair γ-spectrometer varies approximately from 5×10^{-3} percent with $E_\gamma = 2$ MeV to 5×10^{-2} percent with $E_\gamma = 10$ MeV. The value of spectrometer effectiveness substantially exceeds the effectiveness of magnetic

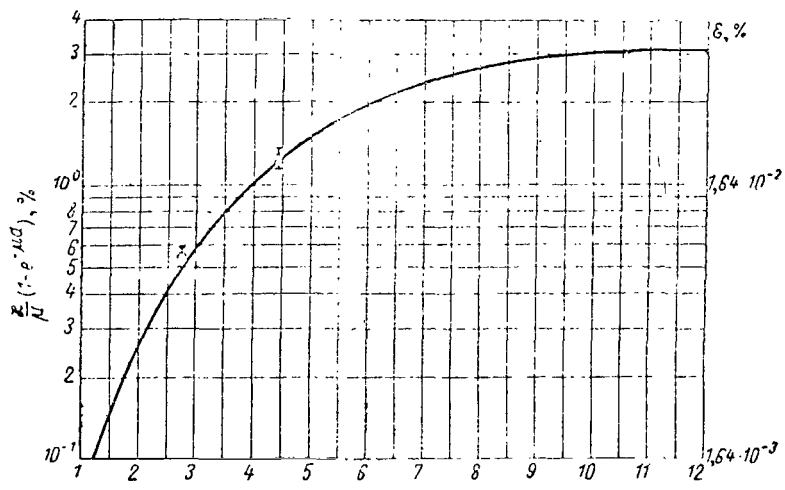

Figure 7. Variation in effectiveness of spectrometer as function of γ-quanta energy: ————, computed data; ●●●, experimental data.

pair γ-spectrometers. By using auxiliary scintillators of large dimensions and placing them in such a way that $\alpha \simeq 1$, the effectiveness of the spectrometer may be increased further. The increase in the effectiveness may also be achieved by controlling the quantity ξ, i.e., by selecting the optimum dimensions of the central scintillator.

REFERENCES

1. Stolyarova, Ye. L. and Konstantinov, I. Ye. Pribory i Tekhnika Eksperimenta, No. 1, 28, 1957.

2. Maeder, D. Muller, R. and Wintersteiger, V. Helv. phys. acta, Vol. 27, 3, 1954.

3. Kazanskiy, Yu. A. Pribory i Tekhnika Eksperimenta, No. 4, 32, 1959.

4. Konstantinov, I. Ye. The Application of Scintillation Spectrometers for Investigating the Continuous Spectra of γ-Radiation. IN: Some Problems of Engineering Physics (Primeneniye stsintillyatsionnykh spektrometrov dlya issledovaniya nepreryvnykh spektrov γ-izlucheniya. V sb.: Nekotoryye voprosy inzhenernoy fiziki). No. 3, Moscow, MIFI. 1958.

5. Burmistrov, V. R. and Kazanskiy, Yu. A. Pribory i Tekhnika Eksperimenta, No. 1, 32, 1957.

6. Keirim-Markus, I. B. and Lisitsina, V. P. Atomnaya Energiya, Vol. III, 157, 1957.

7. Yegorov, Yu. A. and Orlov, Yu. V. P. 474 of this volume.

APPLICATION OF A SINGLE CRYSTAL GAMMA-SPECTROMETER FOR TAKING MEASUREMENTS ON A NUCLEAR REACTOR

Yu. A. Yegorov and Yu. V. Orlov

In order to carry out a proper design of nuclear reactor shielding /319 it is necessary to know the spectrum of γ-radiation leaving the active zone of the reactor and the transmission spectra of primary and capture γ-radiation through materials used in the shielding.

The spectrum of γ-radiation leaving the active zone of the reactor may be computed approximately; however, it is not possible to compute the transmission spectra in practice when considering the capture γ-radiation, particularly if the shielding consists of several materials. For this reason in the experimental investigation of γ-spectra from reactors and of transmission spectra of γ-radiation it is the only presently available method of obtaining reliable data on γ-spectra from reactor shielding.

We can measure the spectra of γ-radiations leaving the active reactor zone and the transmission spectra of γ-radiations through shielding materials by applying various spectrometers. However, the most suitable spectrometer for such measurements is the single crystal scintillation spectrometer for the total absorption energy of γ-quanta, i.e., a spectrometer with a crystal of relatively large dimensions. Such a spectrometer has high effectiveness for recording γ-quanta and its electronic circuits are simple and stable in operation.

It has been shown in reference 1 that by using a spectrometer with a NaJ (Tl) crystal with dimensions of 130 x 200 mm it is possible to measure the γ-spectra in the energy interval from hundreds of keV to approximately 10 MeV, i.e., practically of the entire range of possible γ-quanta energies from a nuclear reactor. However, it is very difficult to obtain crystals of large dimensions with a high spectrometric property, and such crystals are not available to all experimentors.

The application of a single crystal scintillation spectrometer on nuclear reactors is complicated by the presence of a substantial neutron background.

We have made an effort to evaluate the possibility of measuring continuous γ-spectra in the presence of a neutron background by means of a spectrometer with a NaJ (Tl) crystal (diameter and height of 90 mm) and a CsJ (Tl) crystal (diameter and height of 80 mm). The spectrometer was assembled in accordance with a conventional block diagram. The crystal was mounted on the spectrometer type FEU-43 photomultiplier. A standard linear UlS-2 amplifier, which cannot

be overloaded, was used to amplify the pulses. The 100 channel type Al-100-1 amplitude analyzer was used to analyze the pulse amplitudes in the spectrometer. During the measurements the spectrometer sensor was placed into a lead collimeter. The diameter of the collimeter opening could be varied from 0.3 to 4 cm. The length of the collimation opening was 20 cm for any diameter.

The concept of "total γ-quanta energy absorption" has a relative meaning when applied to the spectrometer crystal: the dimensions of the crystal are always limited and a certain amount of leakage of γ-radiation energy from the crystal is possible. For this reason the amplitude distribution obtained from measurements with a monochromatic source of γ-radiation always consists of two parts: peaks of total energy absorption and a continuous low energy distribution due to the incomplete absorption of energy. The degree of energy absorption completeness is characterized by the value of the photocontribution, i.e., by the ratio of the area under the peak of total absorption in amplitude distribution to the area under the entire distribution. The magnitude of the photocontribution depends on the energy of γ-quanta, on crystal dimensions and on the density of crystal material.

For NaJ (Tl) and CsJ (Tl) crystals of given dimensions, when measurements are taken with a collimated beam of γ-quanta, the value of the photocontribution first decreases rapidly and then remains approximately constant as the energy of γ-quanta increases (ref. 2).

Thus for NaJ (Tl) crystal with a diameter of 12.5 cm and a height /320
of 10 cm the minimum value of the photocontribution takes place when the energy of γ-quanta is approximately 6 MeV (ref. 3). Consequently, if we were able to obtain a sufficiently high photocontribution with our crystal for $E_\gamma \cong 5$ MeV, we can assume that the NaJ (Tl) and CsJ (Tl) crystals with dimensions 80-90 x 80-90 mm can be used to measure γ-spectra in the energy range 0-10 MeV. The results of taking measurements by means of a spectrometer with NaJ (Tl) crystal are shown in figures 1 and 2. Measurements with sources Hg^{203}, Zr^{95}, Co^{60} and Na^{24} were carried out with a collimation opening of 0.8 cm in diameter; the sources were placed directly in front of the opening in the collimator.

Figure 3 shows the amplitude distribution for γ-quanta of the Po + Be source with an energy of 4.45 MeV. The diameter of the collimating opening in the measurements was 2 cm, whereas the source was placed at the distance of 20 cm from the collimator. The neutron background was excluded from the amplitude distribution by using the method described below.

As we can see from the presented figures, the peak of the total energy absorption is clearly defined on the background of low energy distribution for all measured γ-quanta energies.

We can see from the results of processing the amplitude distributions obtained during measurements by means of the spectrometer with radiation sources, that the amplitude resolution of the spectrometer decreases with γ-quanta energy

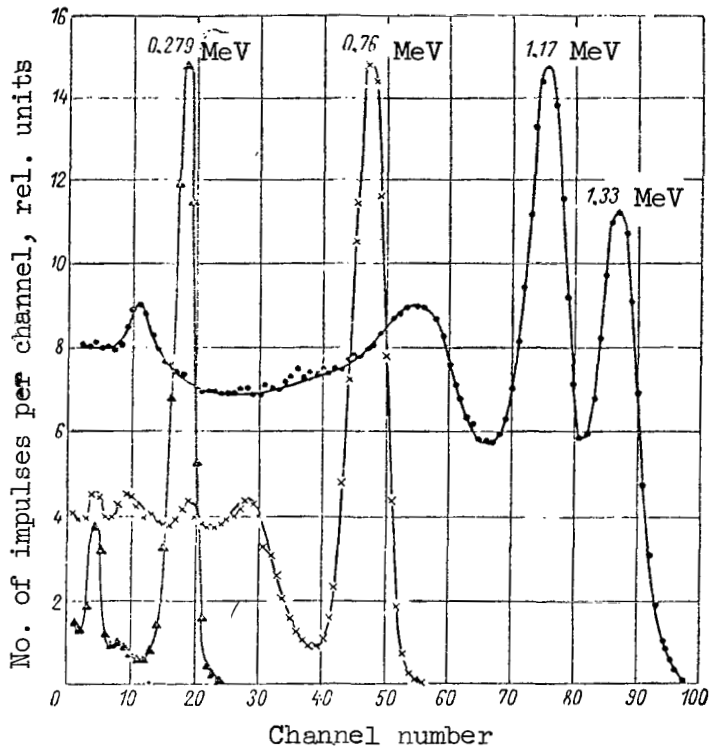

Figure 1. Amplitude distribution for γ-radiation produced by Hg^{203} (0.279 MeV). Zr^{95} (0.76 MeV) and Co^{60} (1.17 and 1.33 MeV), obtained by spectrometer with NaJ (Tl) crystal with diameter and height of 90 mm.

and for E_γ = 2.76 MeV, it is equal to 6.8 percent; the magnitude of the photocontribution also varies with energy increase; however, even for E_γ = 4.45 MeV, it remains sufficiently large--38 percent.

In recent times CsJ (Tl) crystals have been used in single crystal spectrometers in place of NaJ (Tl) crystals (refs. 4 and 5). The total coefficient of γ-radiation energy absorption by the CsJ (Tl) crystal is greater than /322 by the NaJ (Tl) crystal, and consequently, when all other conditions are equal, the spectrometer with the CsJ (Tl) must have a higher effectiveness and a larger value of photocontribution.

Figure 4 shows the variation and the total effectiveness of a spectrometer with a CsJ (Tl) crystal (with diameter and height of 80 mm) and with a NaJ (Tl) crystal (with a diameter and height of 90 mm) as a function of γ-quanta energy:

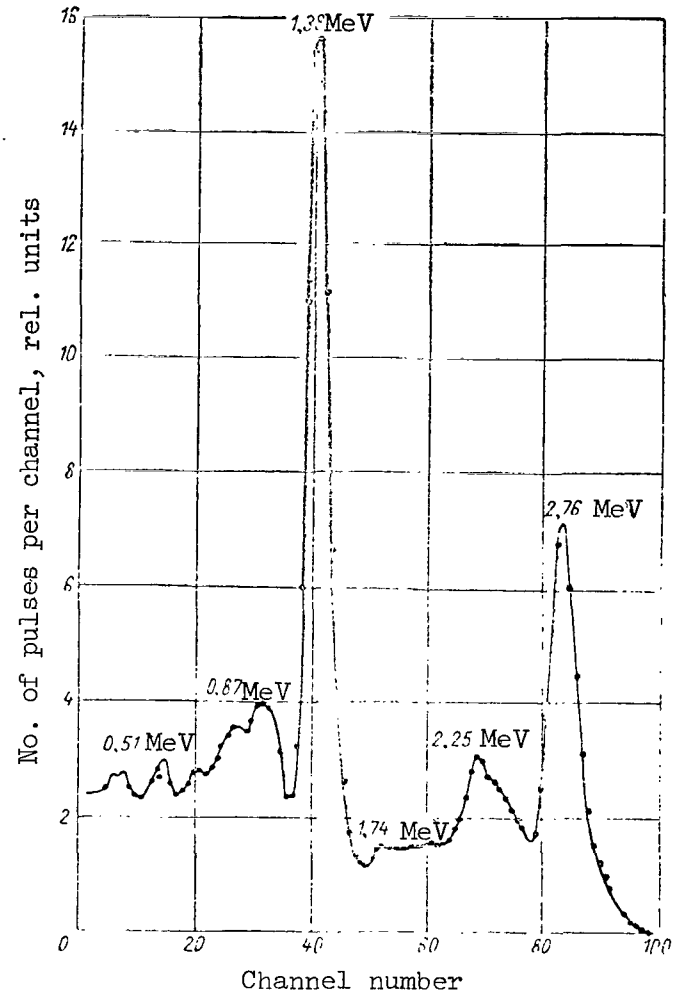

Figure 2. Amplitude distribution for Na^{24} γ-quanta (2.76 and 1.38 MeV), obtained by spectrometer with NaJ (Tl) crystal whose diameter and height are 90 mm.

even for smaller dimensions the effectiveness of the spectrometer with a CsJ (Tl) crystal is greater than that of the spectrometer with the NaJ (Tl) crystal. In order to compute the effectiveness of the spectrometer with the CsJ (Tl) crystal we utilize the absorption coefficients for the γ-quanta energy presented in reference 6 and recomputed for the CsJ (Tl) crystal.

The results of measurements taken with the CsJ (Tl) crystal spectrometer of Na^{24} γ-spectra and Po + Be γ-spectra are shown in figures 5 and 6. The measurements were made with a collimation opening diameter of 2 cm. In the Po + Be

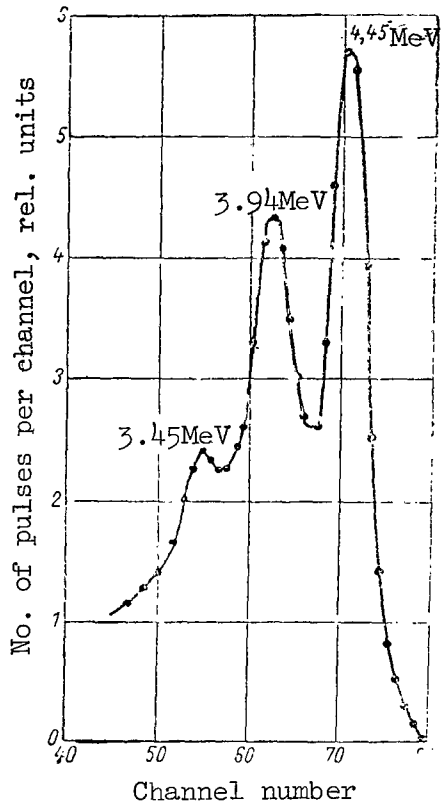

Figure 3. Amplitude distribution for γ-quanta with energies of 4.45 MeV from Po + Be source, obtained by spectrometer with NaJ (Tl) crystal whose dimensions are 90 x 90 mm.

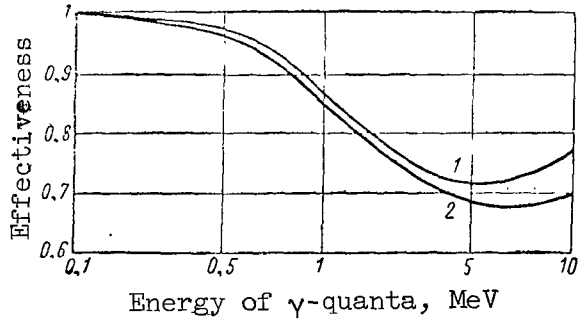

Figure 4. Variation in effectiveness of spectrometer as function of γ-quanta energy for following crystals: 1, CsJ (Tl) with diameter and height of 80 mm; 2, NaJ (Tl) with diameter and height of 90 mm.

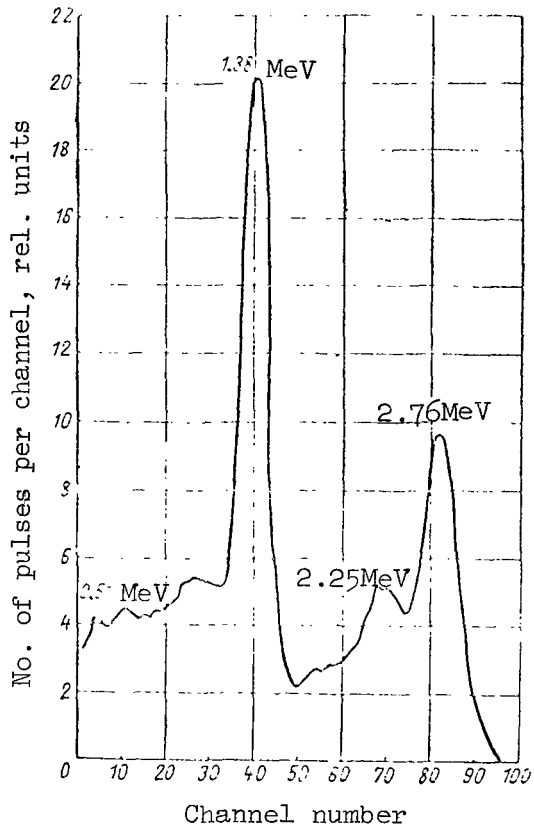

Figure 5. Amplitude distribution for Na^{24} (2.76 and 1.38 MeV) γ-quanta, obtained by spectrometer with CsJ (Tl) crystal whose diameter and height are 80 mm.

source γ-spectra (the neutron background is excluded), we can clearly see the 1.08 and 1.27 MeV lines due to capture γ-radiation from lead, and lines with energies of 0.8 MeV belonging to Po^{210}, as well as the 2.23 MeV line for the capture γ-radiation from hydrogen.

The energy resolution of the spectrometer with the CsJ (Tl) crystal is not quite as good as that of the spectrometer with the NaJ (Tl) crystal. However, when measuring continuous γ-spectra the resolution of the spectrometer is not very significant, because if necessary a corresponding correction can be easily introduced.

As was to be expected, the magnitude of the photocontribution for the CsJ (Tl) crystal turned out to be somewhat greater than for the NaJ (Tl) crystal. Therefore the results of measuring γ-spectra in the energy range of 0.28-4.45 MeV have shown that the spectrometer with the CsJ (Tl) crystal or NaJ (Tl) crystal with a diameter and height of 80-90 mm may be used for measuring continuous γ-spectra in the energy range from 0 to 10 MeV.

It has already been pointed out that operation with a single crystal γ-spectrometer during measurements on a nuclear reactor is complicated by the presence of a substantial neutron background. The neutron background can be excluded from the measurement results by introducing corresponding corrections obtained by repeating the measurements under the same conditions with a bismuth filter.

As we know, the capture cross section of bismuth is very small /324 (σ = 0.015 barn) over a wide range of neutron energies; however, because it has a high density (ρ = 9.8 g/cm^2) it is at the same time a good absorber of γ-quanta. Consequently, by subtracting the results of the second experiment from the results of the first experiment we can exclude the neutron background. In order to determine the required thickness of the bismuth filter, we recorded the γ-spectrum of the Po + Be source with filters of various thicknesses (from 0.8 to 15 cm). The results obtained are shown in figure 7 for filters with thickness of 0, 5, 10 and 15 cm (the diameter of the collimating hole was 2 cm).

The amplitude distributions which were obtained were used to construct attenuation curves for individual energy groups (or channel groups) as a function of filter thickness (fig. 8). The region of the attenuation curve with a sharp

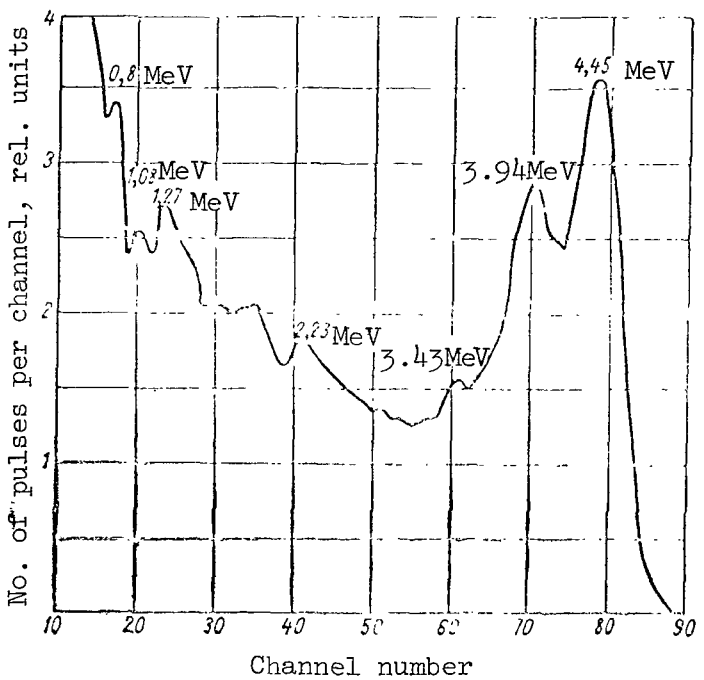

Figure 6. Amplitude distribution for Po + Be source γ-quanta obtained by spectrometer with CsJ (Tl) crystal whose dimensions are 80 x 80 mm.

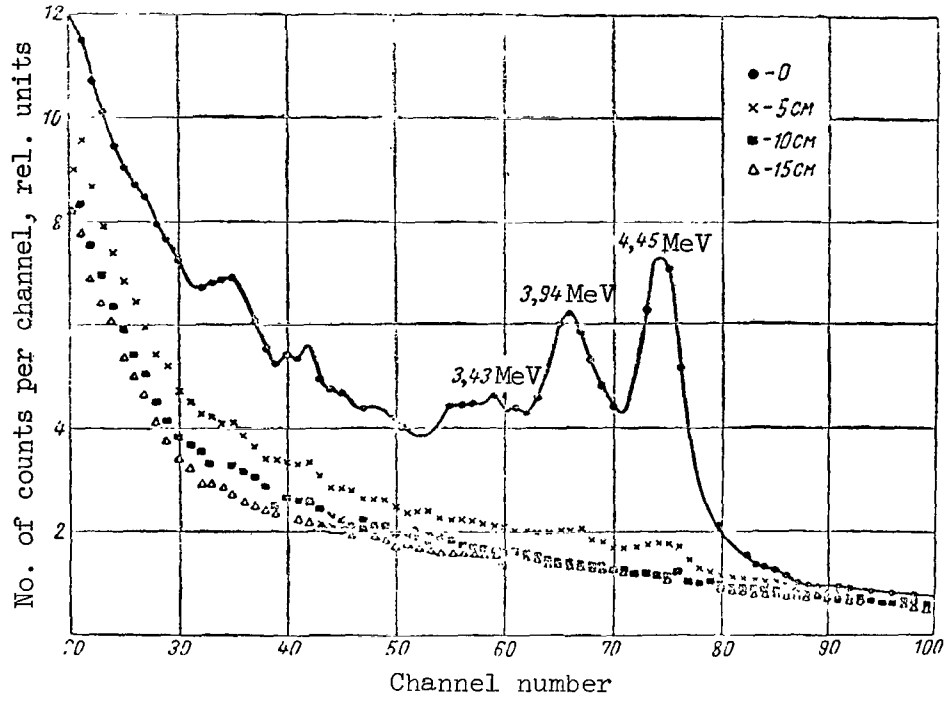

Figure 7. Amplitude distribution for Po + Be source γ-quanta obtained by measurements with bismuth filter of different thicknesses.

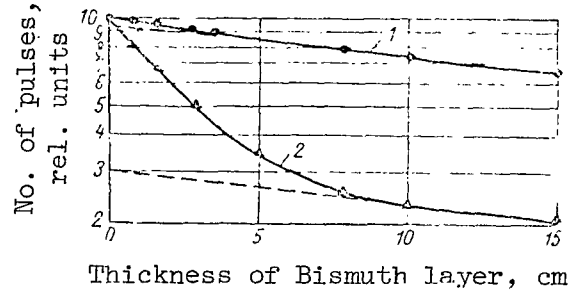

Figure 8. Attenuation curves for number of registrations in channels as function of bismuth filter thickness for Po + Be source: 1, for 20th channel (E_γ = 1.2 MeV); 2, for 71st channel (E_γ = 4.45 Mev).

incline corresponds to the attenuation law for γ-quanta flux, and a shallower region corresponds to the attenuation law for the neutron flux. The attenuation coefficient for γ-radiation agreed well with existing data for E_γ = 4.45 MeV. For all channel groups the neutron attenuation coefficient turned

out to be the same and equal to 0.029 cm^{-1}, within the limits of experimental error.

Analogous experiments were conducted in investigating the γ-spectra by means of a reactor. The coefficient of attenuation for reactor neutrons also turned out to be equal to 0.027 cm^{-1}, within the limits of experimental error.

We can see from the attenuation curves that the bismuth filter with /325 a thickness of approximately 10 cm, for all practical purposes, produces complete attenuation of the γ-quanta flux, and in the experiments it is not necessary to carry out measurements with an assembly of bismuth filters: it is sufficient to measure the spectrum either without a filter or with a filter of 10 cm thickness. When the γ-spectrum is measured in the presence of a neutron background, the number of γ-quanta registrations in each channel may be determined from the relationship

$$N_{\gamma} = N - 1.3N_{Bi},$$

where N is the total number of registrations in the channel during measurements without a filter; N_{Bi} is the number of registrations in the same channel when measurements are made with a filter.

The error made by excluding the neutron flux from the amplitude distribution obviously depends on the relationship between γ-quanta fluxes and neutron fluxes and increases with the neutron flux. The Po + Be source generates approximately the same number of neutrons and quanta, and, as we can see from figure 7, the contribution made by neutrons to the amplitude distribution is quite significant. Thus, in the region of the 20th channel (E_{γ} = 1.2 MeV) the number of pulses from the γ-quanta equals 5-7 percent of the total number of pulses. However, even for this case the error introduced by eliminating the neutron background does not exceed 15-20 percent.

When investigating the transmission of γ-radiation through shielding materials of the reactor, the flux of γ-quanta, as a rule, is substantially greater than the flux of neutrons. Consequently, the error produced by neutron contribution to the amplitude distribution is less: 5-7 percent in the region of small γ-quanta energies.

As an example of results obtained by measuring the γ-spectrum in the presence of a neutron background, figure 9 shows the instrument spectrum of γ-radiation which has left the active zone of the water-moderated, water-cooled experimental reactor and has passed through a layer with a thickness of 1 m. The γ-peak with an energy of 2.21 MeV is clearly seen. This peak is due to the capture γ-radiation from hydrogen, and the γ-peak with an energy of 7.8 MeV is due to the capture γ-radiation from aluminum (aluminum is the basic structural material of the reactor) and from iron (walls of the water vessel are made of steel and their total thickness is approximately 30 mm).

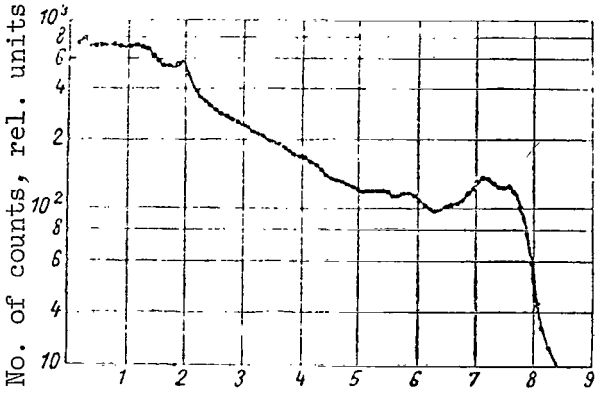

Figure 9. γ-spectrum (amplitude distribution) of γ-quanta leaving active zone of reactor behind layer of water with thickness of 1 m measured by spectrometer with CsJ(Tl) crystal whose dimensions are 80 x 80 mm.

For an energy of 7.1 MeV we can also see the peak which is apparently due to the leakage of a single annihilation γ-quanta from the crystal when the energy of γ-quantum, equal to 7.6 MeV, is absorbed due to the formation of the electron-positron pair. In this measurement the contribution made by neutrons to the amplitude distribution in the region of small γ-quanta energies ($E_\gamma \leq 2$ MeV) is approximately 15 percent.

In order to transform from the measured amplitude distribution to the energy distribution it is necessary to know the amplitude distribution for a series of γ-quanta energy values (refs. 3 and 7). It is not difficult to obtain such data for the range of energies below 3 MeV. However, when $E_\gamma > 3$ MeV, it is practically impossible to obtain the amplitude distributions experimentally due to the absence of suitable γ-radiation sources. The necessary information can be obtained only by calculations with the method of random tests (ref. 8). A comparison of experimental data with computed data in the /327 region of small γ-quanta energies (approximately up to 3 MeV) agrees sufficiently well (fig. 10), and we can hope that significant deviations do not exist at high energies.

Figure 11 shows the experimental and computed values of photocontributions for the NaJ(Tl) crystal whose diameter and height are 90 mm. The experimental points lie somewhat below the theoretical curve, and the reason for this apparently is the scattering of quanta at the source by surrounding objects, in the collimator, by the shell of the photomultiplier, by the crystal packing, etc.

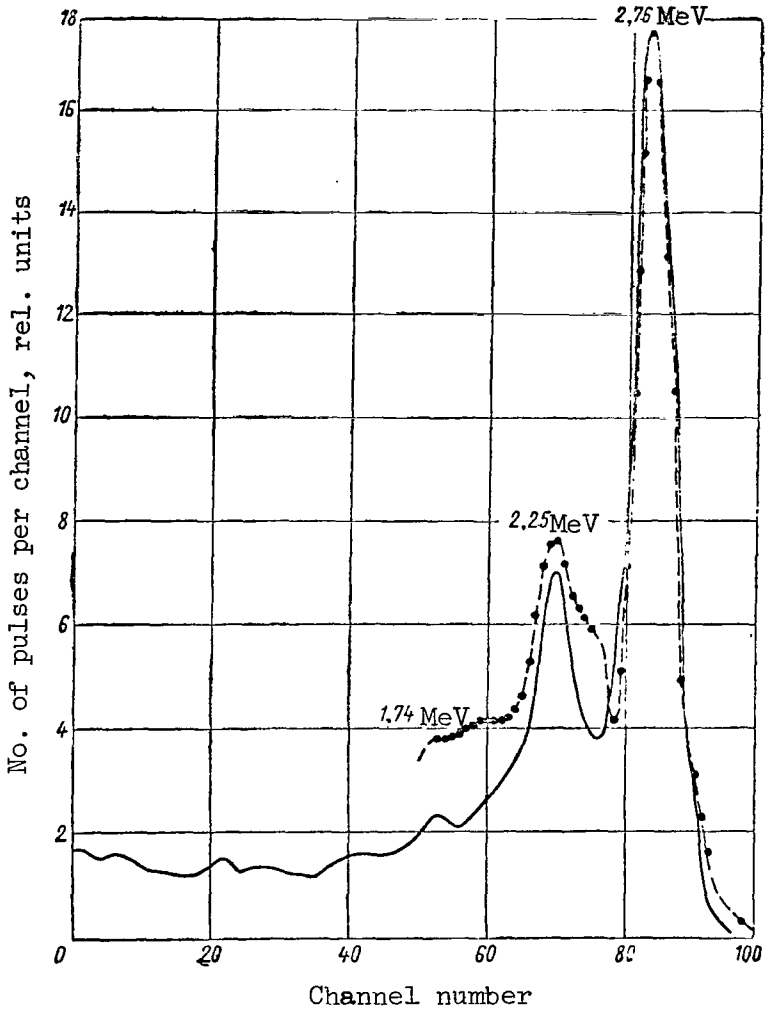

Figure 10. Amplitude distribution for NaJ(Tl) crystal with dimensions 90 X 90 mm: ———, theoretical data (ref. 8); – – – – –, experimental data.

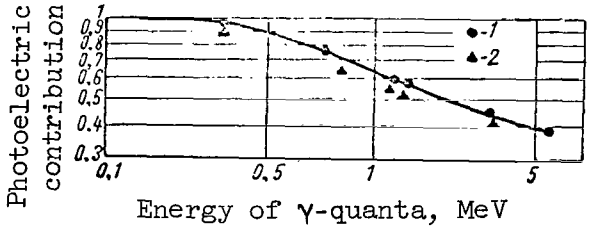

Figure 11. Photocontribution for NaJ(Tl) crystal with dimensions of 90 X 90 mm: 1, theoretical data (ref. 8); 2, experimental data.

Conclusions

The experiments have shown that a single crystal γ-spectrometer with a NaJ(Tl) or CsJ(Tl) crystal, whose diameter and height are 80-90 mm, may be used for measuring the continuous γ-spectra in the energy range from 0 to 10 MeV in the presence of a neutron background, i.e., for studying the γ-spectra on a nuclear reactor.

REFERENCES

1. Foote, P. S. and Koch, H. W. Rev. Scient. Instrum., Vol. 25, 746, 1954.

2. Miller, W. F. and Snow, W. J. Rev. Scient. Instrum., Vol. 31, 49, 1960.

3. Hubbell, J. H. Rev. Scient. Instrum., Vol. 29, 65, 1958.

4. Kazanskiy, Yu. A. Atomnaya Energiya, Vol. 8, 432, 1960.

5. Stolyarova, Ye. O. and Chukhin, S. G. Determination of the Sensitivity Function of a Single Crystal Spectrometer with CsJ(Tl) and NaJ(Tl) Crystals. IN: Instruments and Methods of Analyzing Radiation (Opredeleniye funktsii chustvitel'nosti odnokristal'nogo gamma-spektrometra s kristallami CsJ(Tl) i NaJ(Tl). V sb.: Pribory i metody analiza izlucheniy). No. 2, Moscow, Atomizat, 1960.

6. Beta and γ-Spectroscopy. Edited by K. Zigban. (Beta i gamma-spektroskopiya. Pod red. K Zigbana). Moscow, Fizmatgiz, 1959.

7. Kazanskiy, Yu. A. Pribory i Tekhnika Eksperimenta, No. 4, 32, 1959.

8. Avayev, V. N., Yegorov, Yu. A. and Orlov, Yu. V. P. 415 of this volume.

STRENGTH OF SPECIAL COMPOSITION CONCRETE AT HIGH TEMPERATURES (400-800°C)

I. A. Arshinov

As we know, concrete with special fillers is widely used as biological/327 shielding. Since the shielding may be subjected to high temperatures (up to 800°C) during the process of exploitation it is necessary, under these conditions, to use heat-resisting concretes with fillers which provide for satisfactory physical, mechanical and shielding properties.

This article presents the results of investigating the physical and mechanical properties of heat-resisting concretes with special fillers containing iron, carbon, hydrogen and boron. Test samples of the concrete were prepared from the following materials: chamotte, serpentine, hematite, graphite and iron powders and datolite ore. The binders consisted of the following: mark 500 Portland cement produced by the Voskresenkiy Plant, the aluminous cement from the Pashiyskiy Plant and water glass from the "Kleytuk" Plant with a modulus 2.47 density of 1.38 and with addition of sodium silicofluoride in the amount of 10-12 percent by weight of the water glass.

The properties of materials utilized in the experiments are shown in tables 1-6.

The concrete samples had dimensions of 10 X 10 X 10 cm; the vibration tests were conducted on a standard laboratory vibrating platform after two days. Samples which had undergone 7 and 28 days of normal hardening were also tested. Before heating the concrete was dried at a temperature of 100-110°C for a period of 32 hr. The heating temperature was increased at the rate of 150°C per hr up to 800°C. The test samples were held at this temperature for a period of 4 hr. After heating the test samples were cooled together with the furnace.

The samples were tested for compression strength 10 days after cooling, with the exception of samples made of water glass which were tested immediately after cooling.

Experiments have shown that after heating to 400°C the cube strength of concrete containing the Portland cement does not decrease or decreases by insignificant amounts (to 9 percent), regardless of the type of fillers used and the fineness of the additives. After heating above 400°C, the compression strength of the concrete decreases, and the extent of this decrease is not the same and depends on the fillers used.

TABLE 1. PHYSICAL AND MECHANICAL PROPERTIES OF BINDERS.

Properties	Portland cement from the Voskresenkiy plant	Aluminous cement from the Pashiyskiy plant
Activity, kg/cm^2	509	350
Normal viscosity of cement mass, percent	26.3	28.5
Hardening:		
Beginning	3 hr 20 min	2 hr 15 min
End	6 hr 31 min	4 hr 20 min
Volumetric weight, metric ton m/m^3	1.1	1.16
Specific weight, g/cm^3	3	3.1
Specific surface, cm^2/g	3097	2707
Fineness of grinding:		
Residue on sieve with 900 holes/cm^2, percent	1.34	8.44
Residue on sieve with 4900 holes/cm^2, percent	10.22	23.82
Quantity passing through sieve with 4900 holes/cm^2, percent	89.78	75.18

TABLE 2. GRANULOMETRIC COMPOSITION OF COARSE FILLER.

Type of filler	Total residue (%) on sieves with the specified number of holes per 1 mm^2			
	20	10	5	< 5
Chamotte	0.4	52.92	88.4	11.6
Serpentine	-	24.18	84.88	15.12
Datolite	87.7	98.8	99.2	0.8

As we can see from figure 1, the strength of the composite concrete which contains a mixture of graphite and iron powder with chamotte gravel, as well as of the concrete containing hematite sand and chamotte is greater than the strength of the dried control samples by 6-16 percent after heating to 600°C. The strength after heating to 800°C is 8-41 percent.

The serpentine concrete with addition of finely ground serpentine sand shows a 13 percent decrease in strength after heating to 600°C, and if the same quantity of chamotte powder is added, the strength decreases by 33 percent. After heating to 800°C the strength of serpentine concrete was substantially reduced (from 151 to 55 kg/cm^2).

TABLE 3. GRANULOMETRIC COMPOSITION OF FINE FILLER.

Type of filler	Total residues (%) on sieves with specified number of holes per 1 mm^2						
	5	2.5	1.2	0.6	0.3	0.15	< 0.5
Hematite	2	9	26	44	56.5	65	35
Serpentine	9.3	28.5	62.1	82	87.6	93.7	6.3
Graphite	10	22	45.5	70	84.5	91	9
Chromium-magnesite	0	2.3	43.3	74.1	89.6	99	1
Chamotte	5.2	15.2	40.6	65.6	77.4	96.6	5.4
Iron powder	-	-	-	0.08	0.2	15	85
Datolite	0.33	10	25	46.7	64	89	11

TABLE 4. VOLUMETRIC AND SPECIFIC WEIGHTS AND THE HOLLOWNESS OF FILLERS.

Type of filler	Volumetric weight, metric tons/m^3	Specific weight g/cm^3	Hollowness, %
Serpentine gravel	1.55	2.62	41
Datolite gravel	1.49	2.79	47
Chamotte gravel	1.20	2.39	49
Serpentine sand	1.35	2.62	49
Datolite sand	1.85	2.79	34
Chamotte sand	1.09	2.39	54
Hematite sand	2.55	4.1	38
Graphite	0.9	2.07	57
Chromium-magnesite	1.76	3.34	47
Iron powder	2.45	6.96	56

TABLE 5. GRANULOMETRIC COMPOSITION OF FINELY GROUND ADDITIVES.

Additive	Total residues (%) on sieves with the following number of openings per 1 cm^2		Number of additives which have passed through a sieve with 4900 holes/cm^2, %
	900	4900	
Chamotte	0.4	0.84	99.16
Serpentine	0.16	1.68	98.32
Datolite	6.72	19.8	80.20
Blast furnace dust	1.8	5	95

TABLE 6. CHEMICAL COMPOSITION OF FILLERS.

Form of filler	Composition, %							
	SiO_2	CaO	MgO	Fe_2O_3	Al_2O_3	B_2O_3	SO_3	Other Compounds
Chamotte.....	65.40	0.62	0.29	1.96	31.5	-	0.45	0.19
Datolite.....	33.70	33	0.96	2.52	4.60	13.01	0.36	12.23
Blast furnace dust.....	22.44	3.74	-	48.10	11.9	-	0.64	10.6
Hematite.....	16.34	2.68	1.45	78.4	-	-	0.63	-
Chamotte No. 31 containing boron...	30.15	2.02	1.50	0.94	49.10	15.3	0.2	0.48
Serpentine.....	44.61	2.3	29.87	6.44	3.26	-	1.16	11.98

When serpentine gravel is combined with hematite sand with additions of finely ground chamotte and serpentine powder, the relative strength of the /330 serpentine concrete after heating to 400-800°C does not decrease; the introduction of blast furnace dust into serpentine concrete as a fine filler together with a finely ground chamotte also causes the strength of serpentine concrete to remain constant after heating to 400-800°C. However, when the finely ground additive is replaced with serpentine sand, the strength after heating to a temperature of 600°C and above is sharply reduced (by 61-82 percent).

The strength of datolite concrete utilizing Portland cement increased by 17-35 percent after drying for 32 hr at a temperature of 100-110°C. Some increase in strength continued up to a temperature of 200°C. With a further increase in temperature the strength began to fall, although after 400°C the strength of 32-hr concrete was greater than the strength of the 28-day concrete. When datolite concrete was heated to a temperature of 600 and 800°C, the strength decreased rapidly and cracks developed on the surface of the samples.

The limiting temperature at which there is no decrease in strength is 500°C for concrete with serpentine fillers.

The datolite concrete with Portland cement is suitable for operation at a uniform temperature up to 300°C; the addition of boron carbide in the quantity of 0.75-1 percent by concrete weight (recomputed for elementary boron) does not have a negative effect on the strength of concrete in the temperature range 100-800°C.

The data obtained on concrete with boron containing Portland cement and boron containing chamotte fillers are of interest. The Portland cement contained 3.74 percent B_2O_3, and the chamotte fillers contained 15.3 percent B_2O_3. The boron content in the concrete was 3.44 percent. The strength of boron-containing concrete samples, which were 28 days old, was 383 kg/cm^2, and that of

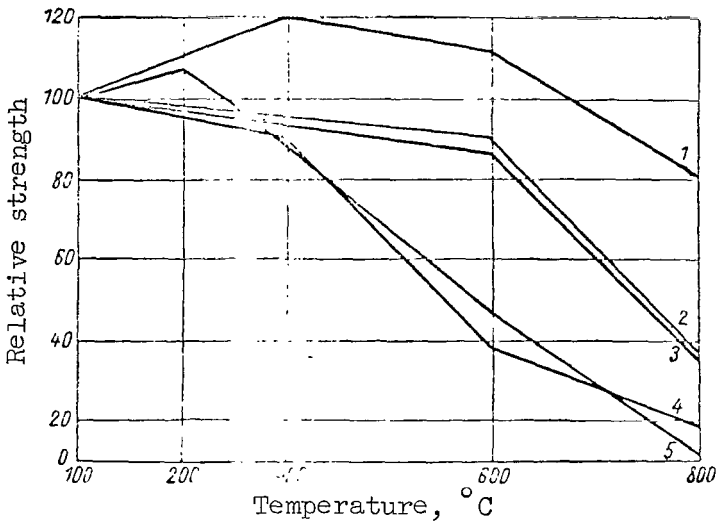

Figure 1. Effect of fillers on relative strength of concrete with Portland cement at temperatures of 400-800°C: 1, graphite + iron powder + chamotte; 2, hematite + serpentine; 3, serpentine; 4, blast furnace dust + serpentine; 5, datolite.

samples dried at 100°C was 488 kg/cm^2, i.e., 28 percent higher. For the conventional chamotte concrete the strength was 261 and 361 kg/cm^2, respectively. After heating at a temperature 800°C, the strength of boron-containing concrete decreased to 141 kg/cm^2 and was 29 percent, whereas the strength of conventional chamotte concrete was 37 percent of the dried control samples. The residual strength and the thermal stability of boron-containing concrete determined by the accelerated method (heating for a period of 4 hr at a temperature of 800°C and cooling with water for a period of 10-15 min were 43 percent and 14 cycles, respectively, and those of the conventional concrete were 53 percent and 12 cycles.

Thus, from the standpoint of strength and thermal stability, concrete with boron-containing cement and boron-containing chamotte fillers is no worse than the conventional chamotte concrete. /334

Aside from the Portland cement we utilized aluminous cement and water glass as binders in the experiments with the addition of sodium silicofluoride (10-12 percent of water glass weight).

As we can see from figure 2, concrete with aluminous cement behaves in a different manner than concrete with Portland cement in the temperature range of 400-800°C. Concrete samples heated to 400°C displayed a substantial decrease in strength; when the temperature was raised to 800°C there was, however, no decrease in strength.

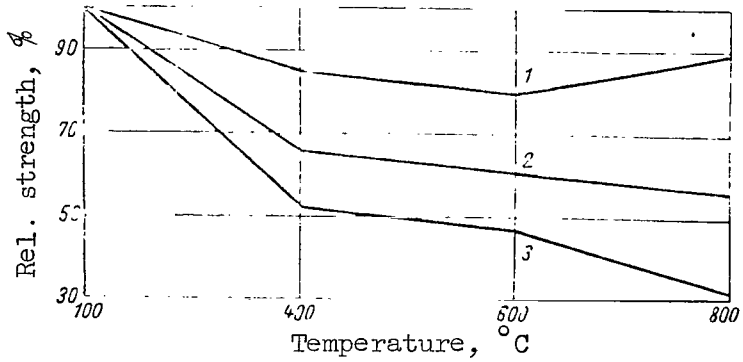

Figure 2. Effect of fillers on relative strength of concrete based on aluminous cement at temperatures of 400-800°C: 1, graphite + iron powder + chamotte; 2, hematite + chamotte; 3, blast furnace dust + chamotte.

The relative strength of composite concrete samples using a mixture of graphite powder with iron powder and chamotte gravel was only decreased by 11-29 percent after heating in the temperature interval 400-800°C.

Concrete based on water glass has high strength parameters during compression. As we can see from the comparative graphs (figs. 3-6), concrete based on water glass exhibits a relatively smaller decrease in strength in the temperature interval 400-800°C as compared with concretes based on alumina and Portland cement. The strength of water glass concrete after heating to 800°C decreases by only 20-37 percent. The greatest decrease in strength is characteristic of concrete which combines graphite powder with hematite sand. After heating to temperatures of 400, 600 and 800°C, the strength of this concrete was 66, 53 and 33 percent of the strength associated with the dried samples, respectively.

The best results were displayed by a composite concrete with chamotte gravel and hematite sand. After drying, its strength was 447 kg/cm^2 and after heating at a temperature of 800°C it was 350 kg/cm^2, i.e., 78 percent of the strength of the control samples.

It is peculiar that the serpentine concrete with water glass has better strength parameters in the temperature range of 400-800°C than the chamotte concrete (fig. 7). If, for example, the relative strength of the chamotte concrete after heating at temperatures of 400, 600 and 800°C was 72, 67 and 57 percent, respectively, the serpentine concrete had a strength which was 93, 77 and 67 percent of the control samples strength.

The introduction of boron carbide into concrete with aluminous cement does not produce a negative effect on the strength of the concrete, whereas its addition to concrete with water glass somewhat decreases the strength of the concrete, but has no effect on the nature of changes in the strength when the heating temperature is raised to 800°C (figs. 8 and 9).

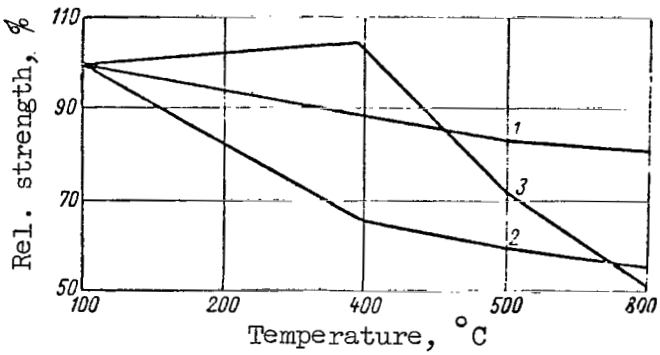

Figure 3. Effect of binder on relative strength of concrete (fillers consisted of chamotte gravel, and hematite ore sand: 1, concrete based on water glass; 2, concrete based on aluminous cement; 3, concrete based on Portland cement.

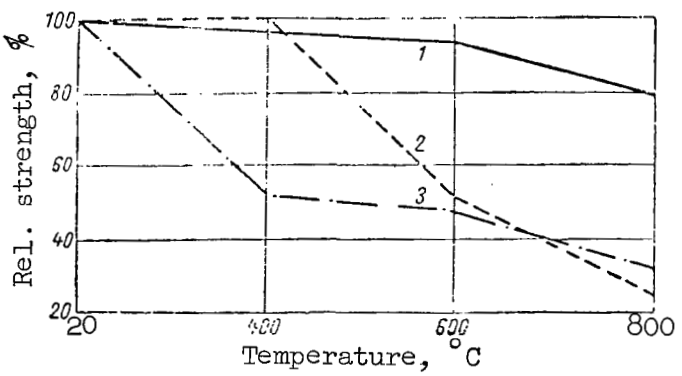

Figure 4. Effect of binder on relative strength of concrete at temperatures of 400-800°C (fillers were blast furnace dust + chamotte; microfiller was chamotte): 1, concrete based on water glass; 2, concrete based on Portland cement; 3, concrete based on aluminous cement.

Experiments have shown that the strength of chamotte concrete based on water glass increases during the period of seven days of hardening under dry air conditions and then begins to decrease. For example, the strength of 90-day concrete is 10 percent lower than the strength of 3-day concrete. However, the 90-day concrete heated to a temperature of 800°C showed only an 18 percent drop in strength, whereas the 3-day concrete lost more than half of its strength (fig. 10). Consequently, more prolonged aging of concrete with water glass before heating results in a substantially smaller drop in strength during its subsequent heating to 800°C.

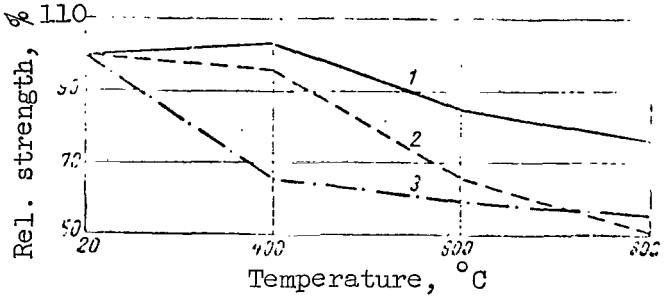

Figure 5. Effect of binder on relative strength of concrete (fillers were hematite + chamotte; the microfiller was chamotte): 1, concrete based on water glass; 2, concrete with Portland cement; 3, concrete with aluminous cement.

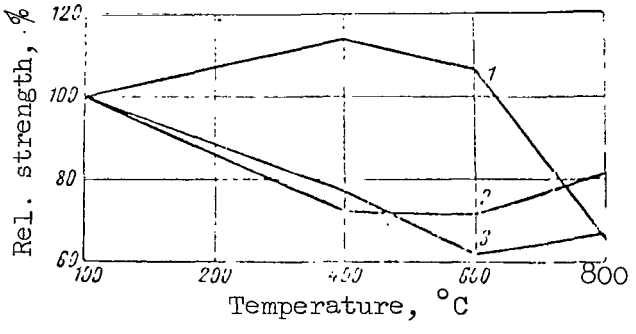

Figure 6. Effect of binder on relative strength of composite concrete (fillers were gravel and finely ground chamotte additive; fine fillers were graphite + iron powder): 1, concrete with Portland cement; 2, concrete with aluminous cement; 3, concrete with water glass.

The nature of changes in the strength of concrete based on Portland and aluminous cements during heating to 800°C is due, in particular, to the loss of chemically bound water and to the loosening of the concrete as a result of various deformation properties associated with its components.

Samples which were tested for compression strength after drying and heating at assigned temperatures of 400, 600 and 800°C were broken into pieces and ground into a fine powder. Five test samples weighing 2-4 g each were taken from the powder and were subjected to calcination at a temperature of 900-1000°C.

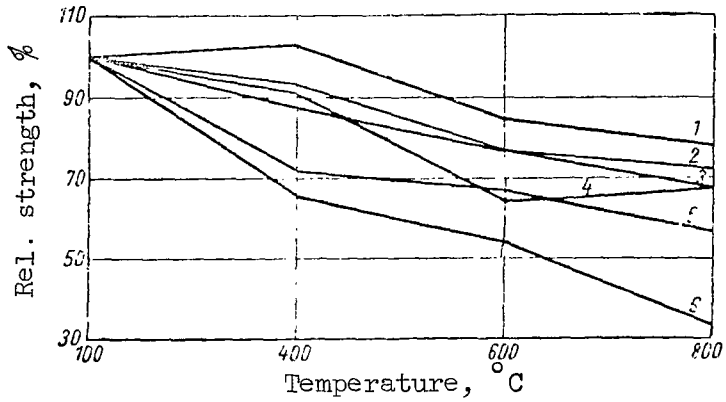

Figure 7. Effect of fillers on strength of concrete with water glass: 1, hematite + chamotte; 2, blast furnace dust + chamotte; 3, serpentine + serpentine; 4, graphite + iron powder + chamotte; 5, chamotte + chamotte; 6, graphite + hematite + chamotte.

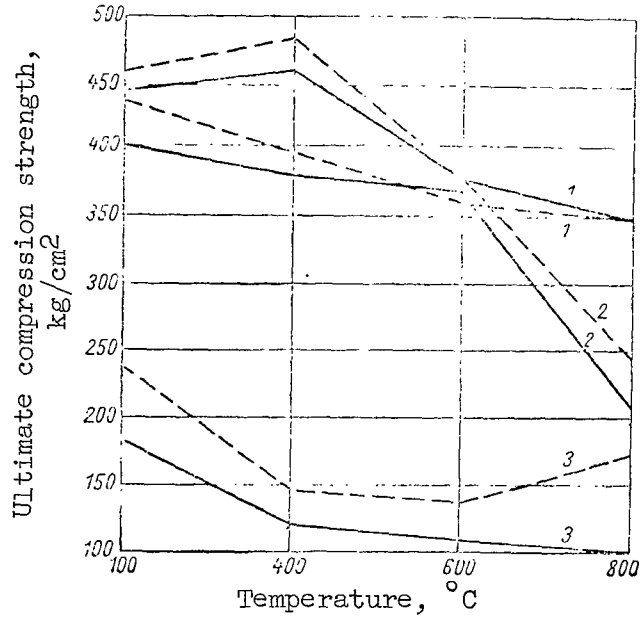

Figure 8. Effect of boron carbide on strength of hematite-chamotte concrete: 1, concrete with water glass; 2, concrete with Portland cement; 3, concrete with aluminous cement; ——— without chemical additives; – – – – – with addition of boron carbide.

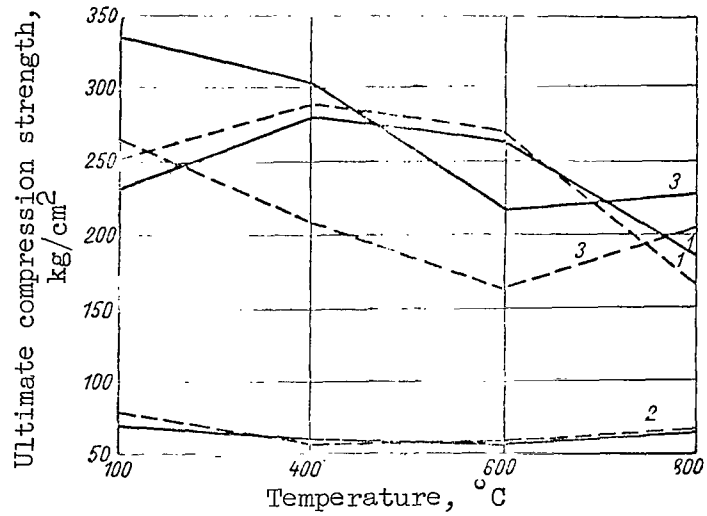

Figure 9. Effect of boron carbide on strength of concrete (fillers were graphite + iron powder + chamotte; microfiller was chamotte): 1, concrete with Portland cement; 2, concrete with aluminous cement; 3, concrete with water glass; ——— without chemical additives; – – – – – with addition of 1.7 percent boron carbide.

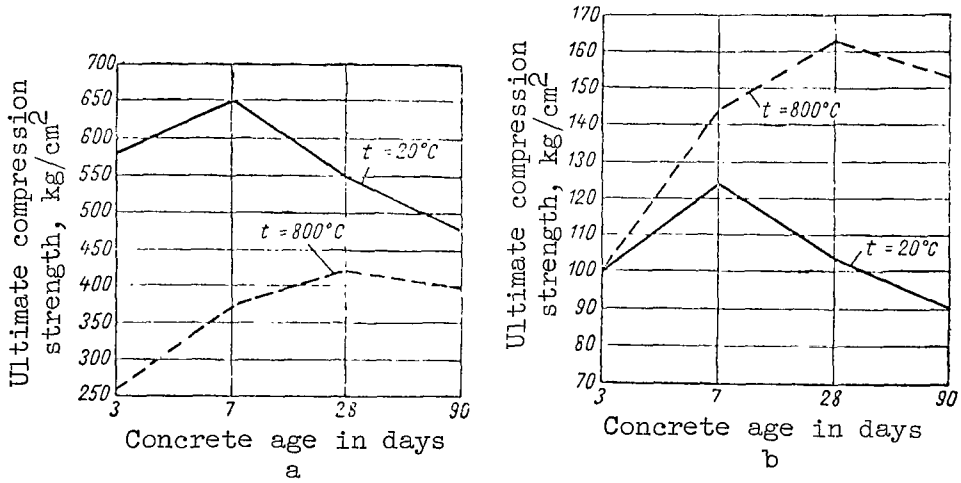

Figure 10. Effect of age and temperature on absolute (a) and relative (b) strengths of chamotte concrete with water glass.

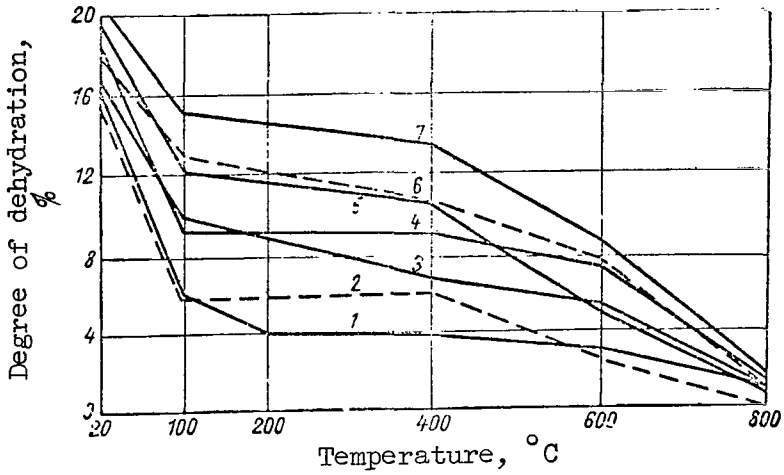

Figure 11. Variation in degree of dehydration for concrete based on Portland cement and containing various fillers as function of heating temperature: 1, chamotte + chamotte; 2, blast furnace dust + chamotte; microfiller-chamotte; 3, hematite + serpentine; microfiller-chamotte; 4, hematite + serpentine; microfiller-serpentine; 5, blast furnace dust + serpentine; microfiller-serpentine; 6, blast furnace dust + serpentine; microfiller-chamotte; 7, serpentine + serpentine; microfiller-serpentine.

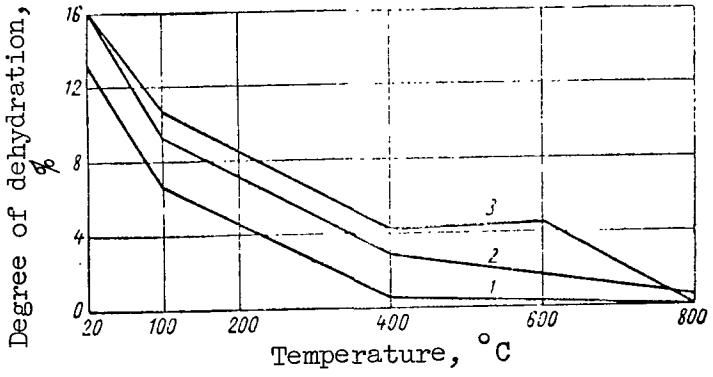

Figure 12. Variation in degree of dehydration for concrete with various fillers as function of heating temperature: 1, hematite + chamotte + chamotte + boron carbides; 2, blast furnace dust + chamotte + boron carbides; 3, same without addition of boron carbide.

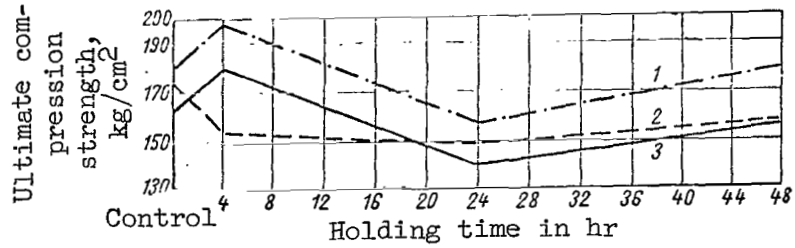

Figure 13. Effect of heating time at temperature of 400°C on strength of heat resisting serpentine concrete: 1, concrete based on water glass; 2, concrete based on Portland cement; 3, concrete based on aluminous cement.

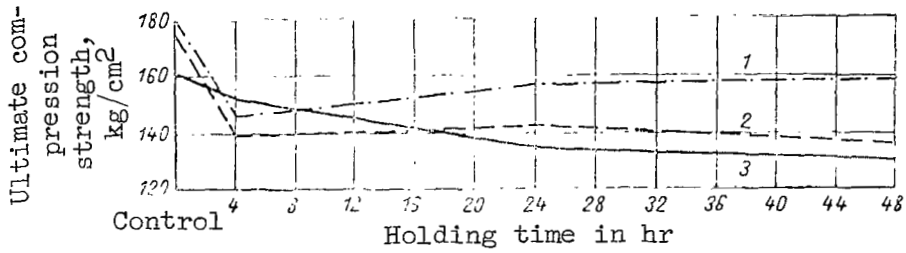

Figure 14. Effect of heating time at temperature of 500°C on strength of heat resisting serpentine concrete: 1, concrete based on water glass; 2, concrete based on aluminous cement; 3, concrete based on Portland cement.

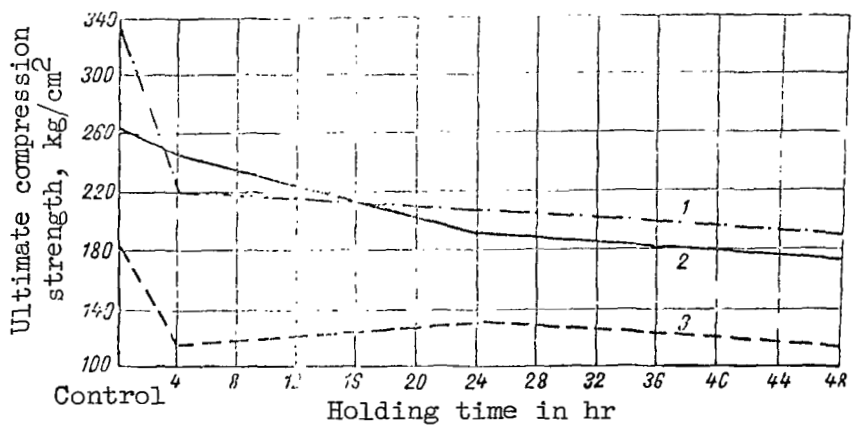

Figure 15. Effect of heating time at a temperature of 600°C on the strength of heat resisting concrete (fillers are graphite + iron powder + chamotte with addition of 1.7 percent boron carbide): 1, concrete based on water glass; 2, concrete based on Portland cement; 3, concrete based on aluminous cement.

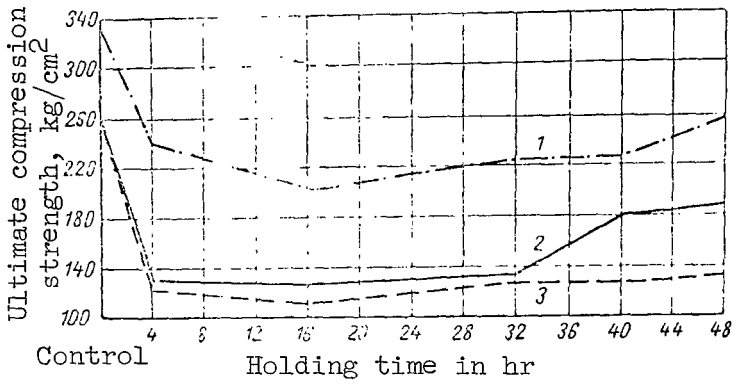

Figure 16. Effect of heating time at temperature of 800°C on strength of heat resisting concrete (fillers are graphite + iron powder + chamotte + 1.7 percent boron carbide): 1, concrete based on water glass; 2, concrete based on Portland cement; 3, concrete based on aluminous cement.

Figure 11 shows the water loss as a result of calcination at 400, 600 and 800°C (after a 32-hr drying period at 100°C).

It follows from the graph that the dry concrete samples based on Portland cement lost an insignificant quantity of chemically bound water when heated to 400°C. When the temperature was raised above 400°C, the loss of water increased, particularly for $t > 600°C$. (In this interval there is also a sharp drop in strength.) The nature of the curve showing the loss of water during calcination is different for concrete samples based on aluminous cement (fig. 12). When the dry samples are heated to 400°C, there is a loss in the main part of the chemically bound water, which agrees with the change in concrete strength. With a further increase of temperature from 400 to 800°C, the remnants of the water are removed. In this temperature range the strength of concrete based on aluminous cement decreases very little.

It is peculiar that the minimum water loss during heating in the specified temperature interval occurs in the serpentine concrete, whereas the maximum loss occurs in the chamotte concrete.

In addition to the short period 4-hr heating, the serpentine and composite concretes (involving a mixture of graphite and iron powders with chamotte gravel) were subjected to a 48-hr heating. Experiments have shown that during the 48-hr heating at a temperature of 400-500°C the compression strength of serpentine concrete remains practically unchanged, compared with its strength after a short-period heating (figs. 13 and 14).

The prolonged heating of composite concrete based on aluminous cement and water glass with the addition of boron carbide, at 600°C (fig. 15) did not produce a decrease in strength. Concrete based on Portland cement dropped its strength to 30 percent.

It is peculiar that during a 48-hr heating period at a temperature of 800°C (fig. 16) the strength of the composite cement did not decrease, but rather increased slightly compared with the strength during the short-period heating.

PHYSICAL AND MECHANICAL PROPERTIES OF CONCRETE WITH SERPENTINE FILLERS

I. A. Arshinov

The distinguishing property of serpentine is its capacity to retain /337
chemically bound water at high temperatures. The chemical composition of serpentine is as follows: $Mg_6[Si_4O_{10}](OH)_8$, in which 43 percent is MgO, 44.1 percent is SiO_2 and 12.9 percent is H_2O.

The amount of chemically bound water in serpentine may vary from /338
approximately 13 to 17 percent.

Serpentine is a mineral of the silicate class. Its crystalline structure is laminar. Its specific weight is 2.5-2.7 g/cm^3; its color varies from dark green to green-gray. It has a certain pliability which can be felt when it is hit with a hammer.

Serpentine rocks are prevalent in the Urals, North Caucasus, Transcaucasia, Siberia and Kazakhastan.

In our experiments we used serpentine from the Ural formation (town of Asbest) with a strength of 400-625 kg/cm^2, with a volumetric weight of 2.54-2.6 metric tons/m^3 in a chunk, with water absorption of 0.5 percent and containing 11.7 percent chemically bound water. As an example, figure 1 shows the granulometric composition of serpentine gravel. Serpentine cement was prepared by using Portland, aluminous, expanding, oxide-chloride ($MgO + MgCl_2$) cements and water glass with the addition of sodium silicofluoride. The compression strength of serpentine concrete was investigated over a large temperature range from 100 to 800°C, and the prismatic strength was studied in the range from 100 to 200°C. The loss of water at high temperatures was also investigated, both by serpentine and by serpentine concrete.

In the first series of experiments the physical and mechanical properties were investigated under normal temperatures, using test samples with dimensions of 15 X 15 X 15 cm. The results of testing samples which had undergone a 28-day period of normal hardening (table 1) have shown that the strength of

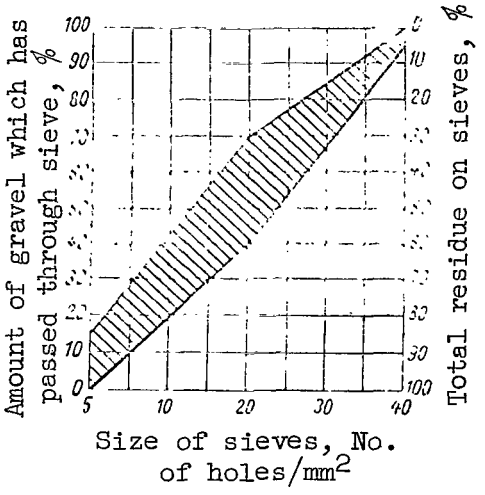

Figure 1. Granulometric composition of serpentine gravel.

TABLE 1. COMPRESSION STRENGTH OF SERPENTINE CONCRETE (1:9 COMPOSITION).

Type of cement	Consumption of materials per 1 m^3, kg				Water-cement ratio	Volumetric weight in metric tons/m^3	Settling of the cone, cm	Packing time, sec	Ultimate compression strength, kg/cm^2
	Cement	Sand	Gravel	Water					
Portland	216	660	1281	173	0.8	2.33	0.0	100	143
"	212	649	1258	191	0.9	2.33	0.0	90	127
"	210	641	1249	210	1.0	2.33	0.5	30	106
"	208	644	1219	239	1.1	2.33	1.0	25	101
"	205	627	1222	246	1.2	2.33	1.5	15	82
Aluminous	216	610	1281	173	0.8	2.33	0.0	103	109
"	212	649	1258	201	0.95	2.33	0.0	85	89
Expanding	216	660	1281	173	0.8	2.33	0.0	95	128
"	212	649	1258	212	1.0	2.33	0.0	40	69
Oxide-chloride	210	641	1247	202	0.96	2.33	0.0	87	284
($MgO + MgCl_2$)	205	625	1214	246	1.2	2.33	0.0	42	240

serpentine concrete with a mark 400 Portland cement in the amount of 205-216 kg/m^3 varies from 82 to 143 kg/cm^2 for a wide range of water-cement ratios; the volumetric weight is close to the volumetric weight of conventional concrete. The strength of the concrete based on the oxide-chloride cement is approximately 2 times greater than the strength of concrete with Portland cement.

The water demand for serpentine concrete is substantially higher, but the packing time is not as good as that of conventional concrete. For example, the

packing time of conventional concrete, with a 1:9 composition containing granite gravel and a water-cement ratio of 0.8-0.9, in our experiments varied from 7 to 17 sec, whereas for serpentine concrete it was from 90 to 100 sec.

Concrete samples were also tested in the hot state (100-300°C). The control samples were subjected to 28 days of normal hardening. The duration of heating was from 3 to 6 hr, of which 1 hr was taken up for reaching the specified temperature.

The cubic and prismatic strengths (table 2) of serpentine concrete using aluminous, expanding and oxide-chloride cements decrease when they are heated to a temperature of 300°C. The greatest decrease in cubic and prismatic strength is observed in concrete with the oxide-chloride binder at temperatures of 100-200°C (14-17 percent). When concretes with magnesite and aluminous cements are heated to 300°C, there is an insignificant decrease in the cubic strength (3-9 percent) which for the expanding cement is 19 percent.

The coefficient of prismatic strength for serpentine concrete for all of the utilized binders varies from 0.74 to 0.78. When heated to 200°C, the coefficient of prismatic strength of concrete with Portland cement is reduced to 0.55, whereas that of concretes with other binders increases from 0.78 to 0.8.

The investigation of serpentine concrete properties at high temperatures (up to 800°C) were carried out by using samples with dimensions of 10 X 10 X 10 cm. In this series of experiments, concrete samples which had been subjected to normal hardening for a period of 28 days were subjected to preliminary drying at a temperature of 100°C for a period of 32 hr. /341

Heating at the assigned temperature was carried on for a period of 4-16 hr with a temperature increase rate of 150°C per hr. The samples were tested 10 days after they were cooled together with the furnace.

Experiments have shown (table 3) that after heating at a temperature of 400°C the strength of the serpentine concrete as well as of concrete consisting of a mixture of serpentine gravel with hematite sand and blast furnace dust do not decrease; after heating at a temperature of 600°C there is an insignificant decrease in the strength in the range from 8 to 13 percent. The introduction of finely ground chamotte in place of the serpentine additive leads to a larger decrease in strength (33 percent). After heating to 800°C, the strength of serpentine and composite concretes decreases by 63-76 percent.

The application of water glass as a binder substantially improves the strength parameters of serpentine concrete. Thus, for example, the relative strength of concrete with water glass after heating at 800°C was 68 percent (135 kg/cm^2) of the strength of the dried control samples.

In addition to strength, after a 4-hr heating period at temperatures of 400, 600 and 800°C, the water residue was determined in samples of serpentine and composite concretes. For this purpose the samples which have been tested for strength were broken up into small pieces and ground into a fine powder. The water residue was determined from the weight loss during calcination.

TABLE 2. THE ULTIMATE VALUES OF CUBIC AND PRISMATIC STRENGTHS OF SERPENTINE CONCRETE DURING COMPRESSION (kg/cm^2) AT TEMPERATURES OF 100-300°C (THE CONCRETE COMPOSITION IS 1:9).

Type of concrete	Water-cement ratio	Control samples		100°C		150°C		200°C		300°C	
		Cubes	Prisms	Cubes	Prisms	Cubes	Prisms	Cubes	Prisms	Cubes	Prisms
Portland	0.8	143/100	—	130/91	—	152/106	—	180/126	—	200/140	—
"	0.9	127/100	100/100	126/99	89/89	123/97	89/89	148/117	82/82	178/140	—
Aluminous	0.8	120/100	89/100	104/87	82/92	—	—	110/92	86/97	—	—
"	0.9	109/100	—	87/80	—	89/82	—	107/98	—	99/91	—
Expanding	0.8	128/100	—	102/80	—	131/102	—	149/116	—	103/81	—
Oxide-chloride	0.7	284/100	—	241/85	—	177/62	—	204/72	—	274/97	—
" "	0.9	240/100	183/100	207/86	155/85	174/72	118/65	126/53	101/55	—	—

Remark 1. The control cubes are samples which have been dried at the temperature of 100°C for a period of 32 hr.

Remark 2. The denominator contains the relative strength in percent, compared with the strength of dried control samples.

TABLE 3. THE ULTIMATE CUBIC STRENGTH OF SERPENTINE CONCRETE AFTER HEATING AT TEMPERATURES OF 400-800°C (MARK 500 PORTLAND CEMENT, MANUFACTURED BY THE VOSKRESENSKIY PLANT).

Fillers (fine + coarse)	Finely ground additive	Consumption of materials per 1 m^3, kg					$\frac{W}{C+A}$	Volumetric weight in metric tons/m^3	Packing time in sec	Ultimate compression strength (kg/cm^2) after heating at following temperatures			
		Cement	Finely ground additive	Sand	Gravel	Water				Control samples	400°C	600°C	800°C
Serpentine + serpentine	Serpentine	230	230	600	847	243	0.55	2.2	65	151/100	142/94	131/87	55/36
Serpentine + serpentine	Chamotte	277	277	560	800	305	0.55	2.2	25	162/100	162/102	109/67	39/24
Hematite + serpentine	Serpentine	304	304	608	806	304	0.50	2.33	30	196/100	186/95	177/90	73/37
Hematite + serpentine	Chamotte	307	307	621	886	300	0.50	2.4	25	210/100	243/116	193/92	68/32
Blast furnace dust + serpentine	Chamotte	272	272	548	778	301	0.55	2.2	60	182/100	176/97	145/80	55/30

Remark 1. The control cubes consisted of samples dried at a temperature of 100°C for a period of 32 hr.
Remark 2. The denominator shows the relative strength in percent of the strength of dried control samples.
Remark 3. W/C + A, ratio of water to total amount of cement (C) + additive (A).

We can see in figure 2 that the greatest residue of chemically bound water was contained in the serpentine concrete. After a 4-hr heating period at 400°C the samples of serpentine concrete which had undergone preliminary drying retained almost all of their chemically bound water. Chamotte concrete, after heating at temperatures of 400 to 600°C, contained 3.8 and 3 percent of water, respectively, and the serpentine concrete contained 13.5 and 9 percent water in terms of the concrete weight.

Thermographic investigations with continuous weighing of the sample showed that during heating up to 578°C the serpentine sample loses approximately 20 percent of all the chemically bound water (11.7 percent), in the temperature interval 578-682°C it loses 4.4 percent and it loses the remaining 5 percent (or about half of the total water) at temperatures from 682 to 887°C.

This result radically differentiates serpentine from limonite. As /342 we can see from the comparative graph, prepared from the thermograms (fig. 3), limonite has lost more than 50 percent of all the chemically bound water at a temperature of 300°C.

Comparative data on the loss of water by serpentine, limonite and hematite were obtained by drying gravel test samples of the specified materials until their weight was constant. The size of the gravel was 5-20 mm and its weight was 0.5 kg. Test samples of gravel after thorough washing were first

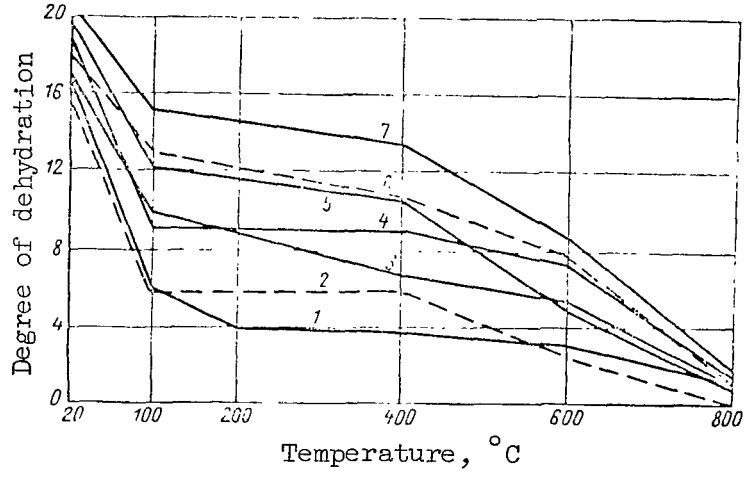

Figure 2. Variation in degree of dehydration for Portland cement concretes with various fillers as function of heating temperature: 1, Chamotte + chamotte, chamotte; 2, blast furnace dust + chamotte, chamotte; 3, hematite + serpentine, chamotte; 4, hematite + serpentine, serpentine; 5, blast furnace dust + serpentine; 6, blast furnace dust + serpentine, chamotte; 7, serpentine + serpentine, serpentine.

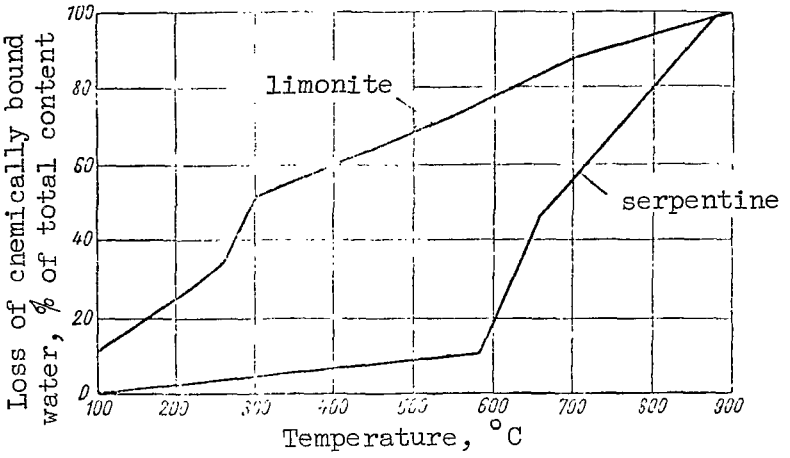

Figure 3. Loss of chemically bound water by limonite and serpentine at temperatures to 900°C.

TABLE 4. LOSS OF WATER BY SOME OF THE FILLERS DURING HEATING.

Type of filler	Dehydration, % of concrete weight at the following temperatures		
	100°C	200°C	300°C
Hematite	0.43	0.4	0.7
Serpentine	0.35	0.55	8
Limonite	1.01	2.63	7.27

dried at a temperature of 40-50°C and then dried at temperatures of 100, 200 and 300°C until their weight was constant.

The results of the experiments are shown in table 4.

The water loss during calcination was determined in test samples dried at three specified temperatures. In the case of serpentine the water residue after heating at 300°C was 10.5-10.9 percent, and for limonite water residue was equal to 5.63 percent or 46 percent of the entire quantity of water (12.3 percent). Thus these experiments have shown that for serpentine heated at 300°C to a constant weight there is practically no loss in the chemically bound water.

Reference 1 also investigated serpentine concrete with a composition of 1:1.8:4. The concrete and the serpentine rock were heated for a period lasting from several to 1,000 hours. Tests have shown (fig. 4) that the water of crystallization was liberated very slowly when the samples were heated up to 500°C. The authors of reference 1 assume that serpentine can be utilized at least up to a temperature of 480°C without losing the water of crystallization.

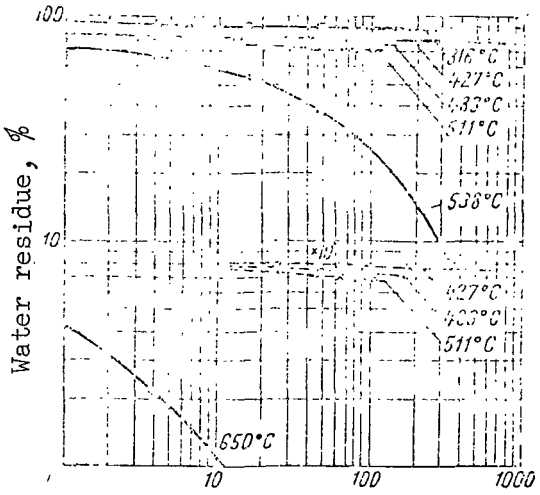

Figure 4. Water residue in serpentine rock and serpentine concrete as function of heating time and temperature (ref. 1): ● , serpentine rock; x, concrete with serpentine filler.

From an analysis of curves (fig. 5) the authors of reference 1 conclude that at a temperature of 430°C the loss of the water of crystallization during a period of 10 years will be only 5 percent of the water content which remained in the material after the first 10 hr of heating.

The temperature deformations of serpentine concrete were investigated /343 for four cements: Portland, aluminous, expanding and magnesite. When concrete containing expanding and magnesite binders is heated to a temperature of 250°C, its shrinkage is observed (fig. 5). The heating of concrete with magnesite cement to 500°C leads to an expansion of up to 0.2 percent, but further heating to 720°C produces no changes. For concrete with expanding cement, expansion takes place at a temperature above 250°C and ceases at 500°C; at 650°C it is replaced by shrinkage up to 0.3 percent.

Thus for serpentine concrete which uses expanding and magnesite cements, expansion is characteristic only in the temperature interval from 500 to 650°C: at other temperatures (100-150 and 650°C) shrinkage is characteristic.

Serpentine concrete with Portland and aluminous cements, when heated to 500°C, has the same value of expansion (0.2 percent); as the temperature is raised, concrete with aluminous cement continues to expand up to 0.4 percent, while at a temperature above 680°C the dimensions of the samples begins to decrease. Concrete with Portland cement contracts sharply when heated to temperatures greater than 680°C. The relative linear deformation due to shrinkage reaches 0.2 percent.

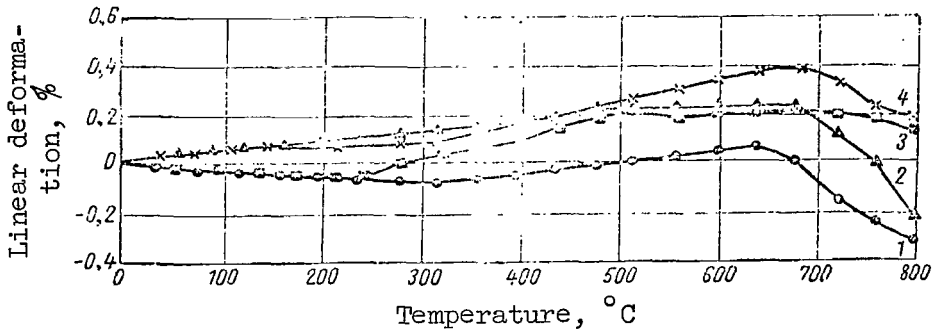

Figure 5. Relative linear deformation of serpentine concrete containing different cements: 1, expanding cement; 2, Portland cement; 3, magnesite cement; 4, aluminous cement.

It should be pointed out that compared with other special cements (containing metallic scrap, hematite, datolite, granite) serpentine cement has the smallest coefficient of expansion and relative linear deformation (table 5). Experiments on the investigation of high temperature effects on the shrinkage of serpentine concrete have shown that when a temperature increasing from 200 to 600°C is produced periodically, the shrinkage of concrete increases from 0.3 to 0.78 percent. In this case, after 4 hr of heating to 300°C and cooling together with the furnace, the shrinkage was 0.32 percent.

The heat conductivity of serpentine concrete at temperatures of 140, 200 and 340°C was 0.88, 0.84 and 0.66 kcal/m·hr·deg, respectively. /344

According to data presented in reference 1, the linear shrinkage of serpentine concrete after interrupted heating for a period of 1 hr at temperatures of 150 and 260°C and slow cooling to room temperature is 0.051-0.126 percent, and the volumetric shrinkage is 0.164-0.290 percent.

TABLE 5. COEFFICIENTS OF EXPANSION AND RELATIVE LINEAR DEFORMATION FOR CONCRETE WITH SERPENTINE FILLER.

Cement type	Coefficient of linear expansion at temperatures			Coefficient of relative linear deformation (%) at temperatures		
	up to 300°C	300-600°C	600-800°C	up to 300°C	300-600°C	600-800°C
Portland	4.14	4.1	1.3	0.07	0.19	0.074
Aluminous	2.9	4.1	3.8	0.05	0.2	0.25
Expanding	-2.4	-0.91	-1.3	-0.04	-0.03	-0.1
Magnesite	-1.75	2.57	2.56	-0.02	0.12	1.28

The Detroit Edison Company (ref. 2) has tested serpentine concrete for expansion and shrinkage (the standard consisted of stainless steel). At a temperature of 100°C the coefficient of expansion of concrete and of steel turned out to be the same. However, at higher temperatures the coefficient of expansion of concrete is unstable. When the temperature is raised from 100 to 150°C, the concrete expands faster than stainless steel, but in the temperature interval 150-250°C concrete contracts and then from 260 to 340°C it again begins to expand. At a temperature above 340°C, the process of concrete compression takes place. A secondary heating of the concrete leads only to its shrinkage. After two cycles of heating and cooling at different temperatures there is a constant linear shrinkage of concrete of the order of 0.05 percent.

Investigations have shown that concrete with serpentine fillers may be used to construct shielding to be used at temperatures to 500°C.

REFERENCES

1. Hangerford, H. Mantey, R. and Van-Mael, L. Atomnaya Tekhnika za rubezhom, Vol. 10, 20, 1960.

2. Detroit Edison Company Engineering Laboratory, Rept. No. 59D11, Aug. 22, 1958.

Translated for the National Aeronautics and Space Administration
by John F. Holman and Co. Inc.

"The aeronautical and space activities of the United States shall be conducted so as to contribute . . . to the expansion of human knowledge of phenomena in the atmosphere and space. The Administration shall provide for the widest practicable and appropriate dissemination of information concerning its activities and the results thereof."

—NATIONAL AERONAUTICS AND SPACE ACT OF 1958

NASA SCIENTIFIC AND TECHNICAL PUBLICATIONS

TECHNICAL REPORTS: Scientific and technical information considered important, complete, and a lasting contribution to existing knowledge.

TECHNICAL NOTES: Information less broad in scope but nevertheless of importance as a contribution to existing knowledge.

TECHNICAL MEMORANDUMS: Information receiving limited distribution because of preliminary data, security classification, or other reasons.

CONTRACTOR REPORTS: Scientific and technical information generated under a NASA contract or grant and considered an important contribution to existing knowledge.

TECHNICAL TRANSLATIONS: Information published in a foreign language considered to merit NASA distribution in English.

SPECIAL PUBLICATIONS: Information derived from or of value to NASA activities. Publications include conference proceedings, monographs, data compilations, handbooks, sourcebooks, and special bibliographies.

TECHNOLOGY UTILIZATION PUBLICATIONS: Information on technology used by NASA that may be of particular interest in commercial and other non-aerospace applications. Publications include Tech Briefs, Technology Utilization Reports and Notes, and Technology Surveys.

Details on the availability of these publications may be obtained from:

SCIENTIFIC AND TECHNICAL INFORMATION DIVISION

NATIONAL AERONAUTICS AND SPACE ADMINISTRATION

Washington, D.C. 20546